Topics in Current Chemistry 333

Pedro Cintas *Editor*

Biochirality

Origins, Evolution and Molecular Recognition

Springer

333
Topics in Current Chemistry

For further volumes:
http://www.springer.com/series/128

Aims and Scope

The series Topics in Current Chemistry presents critical reviews of the present and future trends in modern chemical research. The scope of coverage includes all areas of chemical science including the interfaces with related disciplines such as biology, medicine and materials science.

The goal of each thematic volume is to give the non-specialist reader, whether at the university or in industry, a comprehensive overview of an area where new insights are emerging that are of interest to larger scientific audience.

Thus each review within the volume critically surveys one aspect of that topic and places it within the context of the volume as a whole. The most significant developments of the last 5 to 10 years should be presented. A description of the laboratory procedures involved is often useful to the reader. The coverage should not be exhaustive in data, but should rather be conceptual, concentrating on the methodological thinking that will allow the non-specialist reader to understand the information presented.

Discussion of possible future research directions in the area is welcome.

Review articles for the individual volumes are invited by the volume editors.

Readership: research chemists at universities or in industry, graduate students.

Pedro Cintas
Editor

Biochirality

Origins, Evolution and Molecular Recognition

With contributions by

D.B. Amabilino · S.D. Banik · D.G. Blackmond · C. Blanco · P. Cintas · A.C. Evans · J. Gal · D. Gherase · C. Giri · F. Goesmann · A. González-Campo · J.E. Hein · D. Hochberg · U.J. Meierhenrich · C. Meinert · N. Nandi · V. Percec · C. Roche · B.M. Rosen

Springer

Editor
Pedro Cintas
Facultad de Ciencias-UEX
Dpto. Química Orgánica e
Inorgánica
Badajoz, Spain

ISSN 0340-1022 ISSN 1436-5049 (electronic)
ISBN 978-3-642-37625-2 ISBN 978-3-642-37626-9 (eBook)
DOI 10.1007/978-3-642-37626-9
Springer Heidelberg New York Dordrecht London

Library of Congress Control Number: 2013937201

Printed on acid-free paper

Springer is part of Springer Science+Business Media (www.springer.com)

Preface

Life and chirality have become invariably interlocked. This association is based on the assumption that key biological processes such as replication and translation would have been extremely difficult and inefficient in a racemic world. Conversely, enantiopure building blocks represent evolvable and self-replicating forms of life, an argument that has driven considerable experimental research since the early 1990s. With these exciting premises, it is not surprising that previous volumes of *Topics in Current Chemistry* were devoted to particular domains in the field such as asymmetric crystallization, amplification mechanisms, or chiral supramolecular architectures in an attempt to gain insights into the origin of chirality. The present volume constitutes a step forward, examining biochirogenesis from a multifaceted perspective. Far from being distracting, it is hoped that many readers will greatly appreciate the effort to cover the breadth of the origin and evolution of chirality through different scales and approaches.

An introductory chapter, the heading of which may certainly be *Retournons à Pasteur*, informs us about the seminal work of a few pioneers who discovered the molecular basis of enantiodiscrimination, often aided by no more than observation and intuition. Meierhenrich and associates then focus on the early incarnation of chirogenesis beyond our modest planet and the solar system itself. A collection of astrophysically relevant experiments opens the door to mechanisms capable of generating the small enantiomer imbalances found in interstellar bodies, thus serving as seeds of molecular diversity and, why not, life. Blackmond and co-workers have sought important answers from simple physico-chemical models, such as those involving attrition-enhanced deracemization, where the interplay of thermodynamic and kinetic factors exerts a decisive influence on enantioselection. González-Campo and Amabilino deal with mirror-symmetry breaking at surfaces and interfaces, unveiling potential routes to enantiodiscrimination in natural scenarios, leaving aside the impact of chirality on processes like biomineralization. Blanco and Hochberg move the discussion to their theoretical territory and provide a sound rationale that accounts for mirror-symmetry breaking and amplification in amino acid systems at the air/water interface and lattice-controlled formation of homochiral peptides.

Excursions into the biological machinery are well exemplified by two concluding chapters. Percec and co-workers use dendritic dipeptides as simplified models of larger peptide assemblies and show how the helical self-assembly of homochiral

sequences is thermodynamically more favorable than that of their heterochiral and racemic counterparts. Finally, Dutta Banik and Nandi shed light, with the aid of experimental and computational studies, on the enantiodiscrimination of protein biosynthesis, which involves aminoacylation in the active site of t-RNA synthetase coupled with peptide bond formation at the ribosome.

I am grateful to my esteemed colleagues who have contributed to this volume. They have filled the pages that follow with their unique approaches and achievements, all directed to the unveiling of the origin of enantioselection that characterizes living systems. Chirality certainly predates life, and, like the origin of life, no one was around to witness such historical events. Some hold that nothing regarding chirogenesis can ever be proven. However, science creates methods, interprets results, formulates mechanisms, and introduce strategies to mimic the ways of nature. Probably, Confucius (551–479 BC) put it better: *I hear and I forget, I see and I remember, I do and I understand.*

Badajoz Pedro Cintas
2013

Contents

Top Curr Chem (2013) 333: 1–40
DOI: 10.1007/128_2012_406

Published online: 29 December 2012

Early History of the Recognition of Molecular Biochirality

Joseph Gal and Pedro Cintas

Abstract This opening chapter recalls the history of the discoveries that led to the appreciation of the nature and importance of molecular chirality in biology, as well as the development of stereochemistry as an interdisciplinary field connecting chemistry and biology. The discoveries described cover roughly the period of ca. 1840–1940, although certain relevant events of earlier or later times are also addressed. A large number of chiral substances occur in nature in unichiral (i.e., single-enantiomer) form, and for centuries many such substances were used in crude extracts for relief from diseases. For the science of biochirality, the first milestone was the discovery of molecular chirality by Louis Pasteur in 1848. Thereafter, fundamental advances were made, beginning in 1857 with Pasteur's discovery of biological enantioselectivity, in the metabolism of (±)-tartaric acid. With the advances in organic chemistry during the second half of the nineteenth century, the structures of many organic molecules were elucidated and new chiral compounds synthesized, and by the turn of the twentieth century studies of stereoselectivity in the biological activity or enzymatic transformations of natural or synthetic substances were proliferating, and chiroselectivity was often found. Among the names associated with important discoveries in biochirality appear Pasteur, Piutti, Fischer, Cushny, Easson and Stedman, and others. The findings soon prompted attempts to explain the phenomenon of enantioselectivity in biological action, beginning with Pasteur's proposal to account for enantioselectivity in the metabolism of tartaric acid. In 1894 Fischer announced his "lock-and-key" metaphor to explain enantioselectivity in enzyme-substrate interactions and in 1933 Easson and Stedman

J. Gal (✉)
University of Colorado Hospital, 12401 East 17th Avenue, Mail Stop A-022, Aurora, CO-80045, USA
e-mail: Joe.Gal@ucdenver.edu

P. Cintas
Departamento de Química Orgánica e Inorgánica, Facultad de Ciencias-UEX, E-06006 Badajoz, Spain

advanced the first chemical-structure-based model, the three-point-attachment paradigm, to rationalize enantioselectivity at adrenergic receptors. This model has been generalized as the simplest basis for enantioselectivity in biological activity. Today molecular chirality is widely recognized as an important modulator of the effects of chiral substances in a variety of branches of biology and medicine.

Keywords Biological enantioselectivity · Chirality · Chiroselectivity · Drugs · History of chemistry pharmacology · Molecular recognition · Natural products

Contents

1 Introduction

Interest in the role of molecular chirality in biology is intense today [1–5]. It is abundantly clear by now that stereoisomeric chiral molecules often differ significantly – and at times drastically – in their biological effects and/or disposition. The most fascinating phenomenon in this domain is undoubtedly what is referred to as biological enantioselectivity, i.e., differences between enantiomerically related molecules in their biological effects or behavior. "Enantiomerically related molecules" refers, of course, to chiral molecules that are nonsuperposable-mirror-image forms of each other. Enantioselectivity has been observed in many areas of biology, e.g., biochemistry, physiology, pharmacology, toxicology, etc., and the phenomenon has important implications for these disciplines and the associated technologies. It is also true, however, that other types of stereoselectivity (i.e., collectively, diastereoselectivity) among chiral molecules in their biological effects exist and at times are important (for a brief discussion of the relevant terminology, see the following section in this chapter).

In this opening chapter the early history of the recognition of the role of molecular chirality in biology is examined. In this regard, some may ask "why should we pay attention to history"? Perhaps the most succinct answer to this question was given by the French writer and statesman André Malraux (1901–1976):

> Qui veut lire
> dans l'avenir
> doit feuilleter
> dans le passé.

(Whoever wants to read the future must peruse the pages of the past).

Although Malraux was not speaking in the science context, there is in fact little doubt that an examination of past scientific discoveries and the methods and thinking of scientists of the past can provide a perspective relevant and useful to current problems and future solutions. It is in this spirit, then, that we undertake in this chapter to "peruse the pages" of the rich history of molecular chirality in biology.

The chapter focuses on molecular aspects of biochirality, leaving aside issues related to left-right selection in embryogenesis and morphogenesis, even if these rely ultimately on molecular action. The emphasis will be on the interactions of small molecules with biological systems, and the history of the discoveries concerning the chirality per se of biological macromolecules (proteins, nucleic acids, etc.) will not be addressed here. Our approach in examining the history is to describe the important discoveries and their background and significance rather than provide an exhaustively comprehensive survey. After considering the millennia-old history of folk remedies based on chiral molecules, our analysis of the development of the science of molecular biochirality will cover the period of ca. 1840–1940, an era during which many of the fundamental observations were made. However, at times references will be made to earlier or more recent events relevant to the discussion.

2 Getting Started: A Semantic Touch

Stereochemistry, a complex and rich science, has a language that is therefore also rich and complex, and, naturally, a discussion of the stereochemical matters at hand requires the application of precise scientific language [6–11]. To state the obvious, accuracy in concepts requires accuracy in language. While a detailed discussion of the language of stereochemistry and its problems would be beyond the scope of this chapter, a few brief comments on some of the terminology essential to the topics included here would seem important.

Chiral was defined in one leading monograph on stereochemistry as follows: "Not superposable. . .with its mirror image, as applied to molecules, conformations, as well as macroscopic objects, such as crystals" [12]. Mislow gave a shorter but essentially equivalent definition: "An object is chiral if and only if it is not superposable on its mirror image; otherwise it is achiral" [13]. Thus, it is clear that *chiral* refers to a spatial property of objects, including molecules. Therefore, the term describes that nature of a molecule which makes it *non-superposable* on its mirror image, and *it does not refer to the stereochemical composition of bulk material,* i.e., *drugs, compounds, substances, etc*. Thus, "chiral compound" does not tell us whether the substance is racemic, a single enantiomer, or some other mixture of the stereoisomers. In the present chapter, therefore, *chiral* will be used strictly according to the definitions cited above, i.e., to refer to the chirality of individual molecules or other chiral *objects*. Thus, "chiral drug," "chiral

substance," etc., will be used to indicate that the compound in question is composed of chiral molecules, but the enantiomer composition is not specified by this terminology. This point needs to be emphasized because the literature contains other, often troubling, uses of the term; for example, some have applied *chiral* to indicate that the substance in question consists of only one of the two enantiomers, a usage that often leads to confusion. Similarly, the expression *chiral non-racemic* is entirely vague since it might allude either to a sample that consists of only one of the enantiomers or to one containing both enantiomers in undefined ratio but not racemic.

There is, however, a genuine and obvious need for a convenient term to refer to chiral substances that are composed of only one of the two enantiomers. Numerous terms for this purpose have been introduced over many years, but a consensus on this matter has not been reached. One of the present authors has discussed this issue in detail and introduced a new term for the purpose: *unichiral* [14]. In the present chapter *unichiral* will be used to specify the stereochemical composition of a chiral substance, compound, sample, etc., as stereochemically homogeneous, i.e., a single substance consisting of the same chiral molecules (single enantioform), in the context of use and within the limits of measurement [14]. "In the context of use" is an important element here, since "single-stereoisomer" identity is a variable concept, defined by the nature of the particular context in which it is used. To illustrate, a sample of levodeoxyephedrine [(*R*)-*N*,α-dimethylbenzeneethanamine], a "unichiral" over-the-counter medication used for the relief of nasal congestion, has been found to contain 1% contamination with the dextrorotatory enantiomer [15]. In the context of the use of this product, however, this level of enantiopurity is acceptable (the presence of 1% of the dextro enantioform has no pharmacological or clinical significance) and the drug is indeed considered "unichiral." On the other hand, when testing for the beta-adrenergic-antagonist activity of (+)-(*R*)-propranolol (a very weak antagonist), a 1% contamination with the levo enantiomer (which is 100 times more potent than (+)-propranolol as an antagonist) would distort the results of the testing and would thus be unacceptable. That is, the sample of (+)-propranolol containing 1% of the levo enantiomer could not be called "unichiral" in the context considered.

An important aspect of many chiral molecules from nature is their *homochirality*. This term, coined by Lord Kelvin in 1894 [16], indicates the same sense of chirality among chiral objects or molecules, i.e., their chirality is of the same direction or configuration. Thus, *D*-alanine and *D*-serine are homochiral, i.e., they have the same sense of chirality (configuration). Homochirality is a commonly seen phenomenon among chiral molecules from nature. This means that related chiral natural molecules often have the same configuration. For example, with relatively few exceptions α-amino acids occurring in nature consistently have the *L* configuration; similarly, most naturally occurring monosaccharides are of the *D* configuration, etc. Thus, both *unichirality* and *homochirality* are typical for compounds from nature: most of them occur in single-enantiomer form, and closely related molecules usually have the same sense of chirality. Unfortunately, the usage of *homochiral* (and *homochirality*) in the literature is fraught with inconsistencies

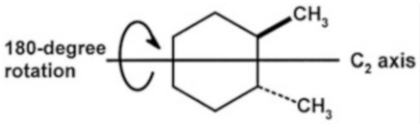

Fig. 1 *trans*-1,2-Dimethylcyclohexane and its C_2 axis of symmetry

and contradictions [14]. Above all, the most pernicious misuse of *homochiral* is as a synonym of *enantiomerically pure*. Be that as it may, in the present chapter *homochiral* will be used as defined above, i.e., indicating the same sense of chirality when comparing similar or related molecules.

Another term that needs to be addressed in the present context is *molecular asymmetry*. This expression is often employed to refer to *molecular chirality*, but such usage, in which "asymmetry" is equated with "chirality," is incorrect. To put it succinctly: an asymmetric object is necessarily chiral, but a chiral object is not necessarily asymmetric. An object or molecule is asymmetric if it has no symmetry element other than the identity operation (*E* or *I*), i.e., belonging to the (trivial) point group C_1. Such a structure is necessarily incongruent with (i.e., not superposable on) its mirror image, that is, chiral. However, the presence in a structure of some symmetry, namely, one or more simple axes of symmetry (i.e., proper rotation axis, C_n, $n > 1$), does not preclude chirality. For example, the enantiomers of *trans*-1,2-dimethylcyclohexane are chiral but not asymmetric since they contain a C_2 axis of symmetry. This means that 180° rotation of the molecule around the axis results in the same molecule, superposed on the original (Fig. 1).

Thus an object or molecule may be chiral without being asymmetric, and therefore "asymmetry" and "chirality" are not synonyms and should not be conflated [9]. Overall, "molecular asymmetry," when it is employed to refer specifically to the phenomenon of molecular chirality, should in fact be replaced with "molecular chirality."

Other relevant stereochemical vocabulary includes *stereoselective, enantioselective, enantiospecific*, and related terms. "Stereoselective" refers to selectivity concerning stereoisomers, i.e., a general term that does not identify the type of stereoisomers involved. "Enantioselective" and "enantiospecific" obviously refer to discrimination of or by enantiomerically related substances, but the distinction between the two terms is not clear. In this chapter "enantioselective" will be used.

Diastereoisomers are stereoisomers that are not related as object and mirror image, and may be chiral or achiral. Several significant examples of biological diastereoselectivity between chiral diastereoisomers will be discussed in this chapter. The terms "chiroselective" and "chiroselectivity" have appeared in the literature [17, 18] but are infrequently used. They refer to discrimination between chiral stereoisomers, be they enantiomers or diastereoisomers. Thus, they are useful terms when discrimination specifically between chiral stereoisomers is the intended meaning, without however limiting the phenomenon to enantioselectivity or diastereoselectivity.

3 Chiral Natural Products as Folk Remedies: The "Pre-science" Era

For thousands of years, substances obtained from vegetable, animal, or mineral sources were relied upon for relief from human diseases [19]. Such folk medicine was by its very nature inaccurate and unscientific and often had no rational basis. Moreover, toxicity of many of the products was a serious problem; indeed, some of the pharmacologically active preparations were used as poisons. The advent of the printing press in the fifteenth century resulted in the wide dissemination of knowledge about natural medications and this in turn produced a considerable increase in the use, and misuse, of such remedies. More rational therapy with purified natural products began only in the 1800s [19].

Despite the problems, however, some of the natural preparations were effective in relieving the symptoms and at times even eliminating the disease. In fact, we know today that the number of pharmacologically active substances produced by nature is large and the spectrum of biological activities of natural products is extraordinarily broad; for example, antimicrobial, antineoplastic, CNS-active, anti-inflammatory, cardiovascular, etc., are only a few of the therapeutic classes of drugs from nature.

Chirality is a hallmark of many molecules from nature. Indeed, the number of chiral natural molecules is very large and the structural variety they represent is vast. Among such substances – be they small molecules or macromolecules – an overwhelming majority occur in unichiral form. For example, in general, chiral α-amino acids and the peptides and proteins containing them, sugars and their polysaccharides, steroids, antibiotics, and many other compounds from nature are unichiral. It should be emphasized, however, that unichirality in natural products is not an absolute rule, and occasionally both enantiomers may be formed in the same or different genera/species. In particular, secondary metabolites may occur in both enantiomeric forms and are sometimes isolated as either the racemic or a scalemic mixture (i.e., enriched in one of the enantiomers) [20].

In light of the above, it is not surprising that many of the compounds used as therapeutic agents in natural remedies over the centuries and millennia have been chiral and that the vast majority of such substances occur in unichiral form. For centuries, until the beginning of the nineteenth century, most such natural remedies were used as crude plant extracts rather than purified active principles. Obviously, in that "pre-scientific" era, the remedies were used without any knowledge of the nature or identity of the active ingredient(s) within, let alone any understanding of the chirality of the molecules involved. Recognition of the existence of chirality in natural products had to await a better understanding of chemical structure, i.e., the advent of modern structural organic chemistry, and the discovery of molecular chirality (see below).

The number of pharmacologically active agents now known to be present in various old remedies is large [21] and many of these compounds are based on chiral molecules. Information about some of the earliest herbal remedies that today are

known to contain chiral active ingredients goes back nearly 5,000 years. A few examples of old therapies with chiral active ingredients are presented below.

In a book about herbs, the Chinese scholar-emperor Shen Nung described in 2735 B.C. the beneficial effects of *Ch'ang Shan* in the treatment of "fevers" [22]. This preparation is the powdered root of a plant, *Dichroa febrifuga* Lour. Modern medicinal chemistry has identified several alkaloids with *antimalarial* properties in the plant, and it is therefore clear that the ancient use of Ch'ang Shan in fevers was not entirely without basis. One of the antimalarial compounds from Ch'ang Shan is *februgine* (β-dichroine, 3-[3-[(2*R*,3*S*)-3-hydroxy-2-piperidinyl]-2-oxopropyl]- 4 (3*H*)-quinazolinone), a relatively simple unichiral compound. Modern attempts to develop these agents as antimalarial drugs failed due to significant toxicity [22].

Shen Nung also observed the stimulant properties of another Chinese plant, *Ma Huang*, now known as *Ephedra sinica* [23]. The chief active ingredient, *ephedrine* ((α*R*)-α-[(1*S*)-1-(methylamino)ethyl]benzenemethanol) is a unichiral levorotatory sympathomimetic amine, and therefore it is also clear in this case that the use of Ma Huang as a stimulant had a rational basis. Ephedrine was first isolated from Ma Huang in 1887 [24], i.e., more than 4,600 years after the effects of the compound were recorded. Ephedrine was introduced into medical practice during the 1920s [25] and for decades was widely used – as a CNS stimulant in narcolepsy, as a bronchodilator, in the treatment of Adams-Stokes syndrome with complete heart block, as a stimulant in some forms of depression, and in some other disorders – but more recently it has been largely replaced in most of these indications by other treatment modalities [26]. Ephedrine has also been widely available in "dietary supplements" for weight loss, increased energy, body building, etc. However, in the early 1990s concern arose over potentially serious adverse effects from such use of ephedrine, including cardiovascular, nervous-system, and other toxic effects, and in April 2004 the U.S. Food and Drug Administration (FDA) banned the sale in the United States of dietary supplements containing ephedrine or closely related compounds [27].

Another millennia-old unichiral drug is the opioid agent morphine. *Opioid* refers broadly to all compounds related to opium (a more recent definition states that the term *opioid* includes any compound that interacts with the brain's opioid receptors [28]). Opium powder is the dried juice from the unripe seed capsule of the poppy *Papaver somniferum* and its name is derived from the diminutive of the Greek word *ὀπός* (*opos*), i.e., vegetable juice. Opium has analgesic, euphoric, and other effects and contains many alkaloids, including morphine and codeine. Poppy juice is mentioned in the writings of the Greek philosopher and naturalist Theophrastus (ca. 371–287 B.C.), but evidence has been found suggesting that opium may have been known much earlier to ancient civilizations in Egypt and Mesopotamia [28, 29].

Within the Arab-Islamic civilization, whose rise began in the seventh century, opium came to be used mainly as a constipant to control dysentery [30]. The arrival of the Islamic armies and influence in Europe in the sixteenth century (Constantinople fell to the Ottoman Turks in 1453 and the first siege of Vienna by the Ottoman army took place in 1529) brought opium to Europe. *Laudanum,* a

somewhat purified opium concentrate, was compounded by Paracelsus (Theophrastus Bombastus von Hohenheim, 1493–1541), a Swiss alchemist and physician, and the smoking of opium became openly popular during the 1700s; however, opium may have been extensively but less openly used in Europe in earlier times [31].

The unichiral natural substance (−)-morphine, the most important alkaloid in opium, was obtained as a purified powder from opium in 1805 by Sertürner and he described his findings in detail in 1817 [32]. He named it *morphium* after Morpheus, the Roman god of dreams, so named by Ovid using a Greek word. Later, the eminent French chemist and physicist Joseph-Louis Gay-Lussac (1778–1850), who was a strong supporter of Sertürner in his priority claim for the isolation of the substance over French pretenders, renamed the drug *morphine*. The chemical structure of morphine (without the absolute configuration) was elucidated in 1923 [33].

The invention of the hypodermic needle and syringe in the middle of the nineteenth century resulted in the widespread use of morphine, and addiction became a common problem. An early – and false – hope to circumvent the addiction liability of morphine was provided by a most unlikely candidate, heroin. This compound, the diacetyl derivative of morphine, is a potent opiate narcotic first synthesized in 1874 via acetylation of morphine, and was introduced into medical practice in 1898 as a cough suppressant [24]. Heroin is a *semisynthetic* drug, i.e., a chemically modified derivative of a natural product, and retains the stereochemistry of morphine. Heroin may have been the first synthetic unichiral drug introduced in clinical medicine. Heroin was actively marketed to physicians by its manufacturer (Bayer).

Heroin was touted as a "non-addicting" morphine analog that could safely replace morphine and thereby eliminate the latter's addiction problem [34]. This claim turned out to be tragically mistaken and the abuse of heroin rapidly became widespread. A report in the *Journal of the American Medical Association* in 1912 warned of heroin abuse and called for strict legislation to prevent its sale in drugstores at a price of less than $1 per one hundred tablets (30 mg each) [35]. As is well known, such warnings had little effect, and today heroin is the most important abused opioid, with grave social, economic, and medical consequences.

Another chiral drug, methadone, a totally synthetic opiate agonist, has been recruited to fight heroin addiction. Methadone was first synthesized, in the racemic form, in Germany (at the IG Farbenindustrie company) just before WWII and was later shown to have stereoselective opioid agonist properties, concentrated nearly exclusively in the levorotatory enantiomer [36]. Methadone is widely used in the racemic form as an analgesic and in the treatment of opiate addiction, but in some other countries the pharmaceutical product is the unichiral *levo* form [37].

Perhaps the most fascinating old chiral drug, from a historical point of view, is the antimalarial agent quinine. Its earliest history is obscure, but it is known that by the early 1600s it was being used by South American natives in Peru, Ecuador, and neighboring regions as a crude preparation from the bark of a local tree for the treatment of "fevers." In 1633 Antonio de la Calancha (1584–1654), an Augustinian monk in Lima, Peru, wrote: "There is a tree of 'fevers' in the land of Loja, with cinnamon-colored bark of which the Lojans cast powders which are drunk in the

weight of two small coins, and [thereby] cure fevers and tertians; [these powders] have had miraculous effects in Lima" [38] (in some texts Loja is spelled Loxa). This appears to be the first recorded mention of the powers of the tree (later named *Cinchona* by the Swedish botanist Linnaeus) used by the natives to cure "fevers." By the middle of the 1600s the extract of "Jesuit's bark" (one of the names cinchona came to be known by) was being used in Europe indiscriminately for a variety of fevers. Cinchona was, however, effective only against malaria, an infectious disease widespread in many regions of Africa and Asia, and even in Europe and North America for centuries. Cinchona was the first effective treatment for malaria, and in 1820 the French pharmacists Pierre Joseph Pelletier (1788–1842) and Joseph Bienaimé Caventou (1795–1877) isolated quinine, the main antimalarial ingredient, from cinchona bark [39]. After its isolation in 1820, purified quinine quickly replaced the crude cinchona preparations in the treatment of malaria.

As mentioned above, the name *cinchona* was coined by the Swedish botanist Linnaeus (Carl von Linné, 1707–1778) in honor of Doña Francisca Henriquez de Ribera, the fourth *Condesa* (Countess) of Chinchón and wife of the viceroy of Peru, a Spanish colony at the time [40]. According to legend, in 1638 she was cured of malaria by the bark and, impressed with the cure, she took samples of cinchona to Spain, thereby launching the European career of the miracle remedy. However, as has been frequently pointed out, there are problems with Linnaeus' nomenclature. First, he misspelled *cinchona*, leaving out the first *h* present in the countess' name; second, she could not have taken the cinchona bark to Europe since she died in South America, in Cartagena de Indias (located today in Colombia) before she could return to Spain [40]. Be that as it may, cinchona has stuck in the official names of several species (e.g., *Cinchona officinalis* L and other species in the *Rubiaceae* family). As for *quinine*, this name is derived from *quina quina* ("bark of barks"), the Spanish spelling of a native Quechua name that was sometimes used for the cinchona tree in Peru, and was given by Pelletier and Caventou to their new substance [41].

After purified quinine became available during the first half of the nineteenth century, demand for the drug became intense, since malaria was widespread and quinine was needed in Europe, North America, and in various parts of Africa, Asia, and the Americas, where the major powers were engaged in establishing or strengthening their colonial control (indeed, quinine is tarnished with the infelicitous legacy of having facilitated colonization in some parts of the world). However, the supply of quinine was limited, and therefore the chemical synthesis of the substance became a topic of considerable interest to chemists. In England in 1856 an 18-year old chemistry student named William Henry Perkin (1838–1907), working with August Wilhelm von Hofmann (1818–1892), a German professor of chemistry and director of the Royal College of Chemistry in London, attempted to synthesize quinine by oxidizing *N*-allyltoluidine with potassium dichromate. The reaction, predictably in hindsight, did not produce quinine, but Perkin's further studies of the reaction led to the discovery of *mauveine*, a purple dye which in turn launched the "aniline" or "coal-tar" dyes and the synthetic-dye industry. Moreover, the invention of mauveine not only revolutionized the dye and textile industries but

also produced an intense stimulatory effect on chemical research in general, on the pharmaceutical industry, and on medicine [42] (Perkin's mauveine is a mixture of several achiral compounds).

Malaria was eventually eradicated in North America by the late 1940s and in Europe by the mid-1970s, as a result of better insect control, better construction and insulation of homes and buildings (to exclude mosquitoes), and the draining of swamps, marshes, and other bodies of stagnant water (where mosquitoes reproduce). However, malaria remains a rampant affliction in many other parts of the world, with nearly one million victims dying of the disease every year, the majority of them African children under the age of five [43].

The chemical structure of quinine (without the stereochemical details) was established at the beginning of the twentieth century [44]. The first (formal) synthesis of quinine was achieved by Woodward and Doering during World War II [45]. Their synthesis, although of no commercial value, nevertheless attracted a great deal of attention at the time, since during the war the Allies were suffering from a severe shortage of quinine, needed for the protection and treatment of troops fighting in malarious regions. The shortage was the result of the fact that large-scale cultivation of cinchona had by then shifted primarily to Java (now part of Indonesia), a Dutch colony occupied by Japan during the war. The first fully stereoselective synthesis of quinine appeared in 2001 [46]. However, for commercial purposes, quinine continues to be obtained from its natural source, since the chemical syntheses are complex and therefore unsuitable for the large-scale production of the substance. The chiroselectivity aspects of the biological properties of quinine and related substances will be discussed in a later section of this chapter.

Another chiral drug from the New World worthy of mention here is curare, whose known history spans several centuries. The first reference to the substance was made early in the 1500s by Pietro Martire d'Anghiera, a chronicler to King Charles V of Spain who described a soldier being lethally wounded by an arrow tipped with poison. For several centuries thereafter, travelers to South America wrote about the poison. For example, Laurence Keynes, serving with Sir Walter Raleigh on his expedition to the current region of Venezuela, listed numerous poisons used by the natives, including a herb known as "ourari" (from which the name curare emerged) which caused paralysis [47, 48]. French physician and physiologist Claude Bernard reported that curare prevented the ligated limb of a frog from responding to stimulation, even though both the nerve and muscle retained their function [49]. In 1936 it was shown that acetylcholine acts as neurotransmitter at the neuromuscular junction and that curare is an antagonist of that action [50]. Clinical applications of curare during the nineteenth and first-half of the twentieth centuries in the treatment of convulsive diseases were largely hindered by the poor quality of the curare extracts. The use of curare in combination with anesthetics emerged only in the early 1940s and permitted the use of low doses of the latter while attaining an appropriate muscle relaxation [51]. The bioactive substance of curare is a dextrorotatory macrocycle of the bis(benzylisoquinoline) alkaloid family. Chemists at the Squibb company isolated this substance in 1943 from a sample from the New York Botanical Gardens [52], and the compound

proved to be identical to a substance obtained earlier from a curare specimen stored in the British Museum [53]. Since the latter sample was packed in a bamboo tube, the drug was named tubocurarine.

The devastating disease scurvy is caused by insufficient amounts of *L*-ascorbic acid (vitamin C) in the diet. After the fifteenth century, exploration, expanding trade, and colonization by European powers required long sea voyages, usually undertaken without foods rich in vitamin C on board. The result was the decimation of ships' crews by scurvy. In a remarkable study in 1747 that can be described as the first serious clinical therapeutic trial, British physician James Lind (1716–1794), a surgeon in the Royal Navy and the "father of naval hygiene," demonstrated that fruits such as oranges and lemons can reverse and prevent the disease.

However, it was nearly 50 years later, in 1795, that the British Admiralty finally took notice of these findings and instituted an appropriate diet on board Royal Navy ships to prevent scurvy [54]. Ascorbic acid was isolated by the Hungarian biochemist Albert Szent-Györgyi (1893–1986) from fruit juices in 1928 and in part for this work he was awarded the Nobel Prize in Physiology or Medicine in 1937. In that same year one half of the Nobel Prize in Chemistry went to the English chemist Walter Norman Haworth (1883–1950) for the proof of structure and synthesis of ascorbic acid.

The above examples of old chiral drugs from natural sources are but a handful from a long list of many examples. Others include (some plant origins given in parentheses) tetrahydrocannabinol (marihuana, hashish), digoxin (foxglove, *Digitalis lanata* Ehrh.), cocaine (*erythroxylon*), cathinone (khat, *Catha edulis* Forsk.), nicotine (tobacco, *Nicotiana tabacum*), atropine (deadly nightshade, *Atropa belladonna* L.), reserpine (*Rauwolfia*), colchicine (autumn crocus, meadow saffron), and emetine (ipecac), to name only a few. Each of these chiral compounds has an interesting history but these accounts are beyond our scope here. The chemical structures encompassed by just these relatively few chiral molecules are highly varied. Stereochemically, atropine is an interesting case: this racemic substance is believed not to occur naturally, but its levorotatory form, (*S*)-(−)-hyoscyamine, occurs in several *Solanaceae* plant species and is racemized to atropine during isolation [55, 56].

The vast majority of chiral drugs present in the old remedies were unichiral substances: Mother Nature is not even-handed. All in all, chiral drugs have been of great importance in the development of pharmacotherapy, from the earliest plant remedies of millennia ago to the modern age. Many of these ancient chiral drugs are still in use today, and many new and important drugs have been developed by modifying the molecules of natural products identified in old remedies. The "pre-science" era of crude natural remedies came to an end as the nineteenth century was winding down. The birth of the modern era of therapeutics did not mean, however, the end of the therapeutic use of natural compounds, only that the science and technology became different.

At this stage, the development of the science of molecular biochirality required the recognition of the existence of the fundamental phenomenon of molecular chirality. This key discovery was made in the middle of the nineteenth century in France.

Fig. 2 Pasteur's official photograph as member of the *Académie française*. Reproduced from http://academie-francaise.fr/immortels/index.html, courtesy of the *Académie française*

4 Discovery of Molecular Chirality

The relevant background work that led to the recognition of the existence of molecular chirality was accomplished, mainly in France, during the first half of the nineteenth century [57]. *Hemihedrism* in crystals – those of quartz – was first reported by René-Just Haüy (1743–1822), a French priest and crystallographer, in 1801 [58]. Circularly polarized light (often referred to as plane-polarized light) was discovered in 1809 by Étienne Louis Malus (1775–1812), and the physicist François Arago (1786–1853) made the first observation of optical rotation by a substance when he studied the effects of quartz crystals on polarized light [57].

French physicist Jean-Baptiste Biot (1774–1862) discovered in 1815 that certain natural organic compounds rotate polarized light in the non-crystalline state, e.g., in the liquid or solution state. Among these compounds were sucrose, turpentine, camphor, and tartaric acid (TA) [57]. TA – obtained from tartar deposits produced by the fermenting juice of grapes during the wine-making process – had been discovered by the Swedish pharmacist Carl Wilhelm Scheele (1742–1786) in 1769 [59], and Biot showed that the compound was optically active [60]. Biot understood that optical rotation by substances in the non-crystalline state was the result of some *molecular* property, but the recognition of molecular chirality was arrived at later by Biot's younger colleague and protégé, Louis Pasteur (1822–1895) (Fig. 2).

Pasteur earned a doctorate in physical sciences in 1847 at the faculty of sciences of the University of Paris. For the doctorate he submitted two dissertations, one in chemistry and one in physics. After earning the doctorate, he continued research work in the laboratory of Antoine-Jérôme Balard (1802–1876), an eminent chemist of the time. Pasteur focused his attention on questions of crystallography and optical rotation. He was familiar with the work by Biot outlined above on optical rotation by natural organic compounds, and in 1848 he found that the crystals of sodium ammonium tartrate (from the natural *dextro*-TA, Fig. 3) were hemihedral, i.e., there were small facets at alternate corners of the crystals [61], and he recognized that these facets rendered the crystals chiral.

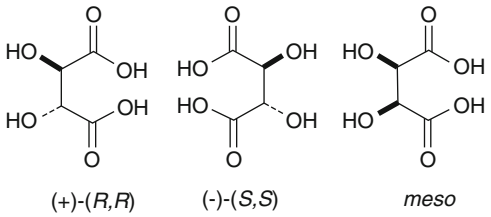

Fig. 3 (+)-, (−)-, and *meso*-tartaric acid

Pasteur then examined the sodium ammonium salt of another, related, acid. That acid had been obtained ca. 1819 – unexpectedly and on a single occasion – as a side-product during the manufacture of (+)-TA from tartar at a chemical plant in Thann in Alsace, France [62]. The mysterious new acid intrigued chemists. Gay-Lussac obtained a sample for study and showed it to have the same composition as "ordinary" (dextrorotatory) TA; he named it *racemic acid*, from the Latin *racemus*, i.e., cluster of grapes [63]. Another name used for the compound was *paratartaric* acid. In most of its properties racemic acid was found to be identical with (+)-TA, with the exception of its crystal morphology and that it did not rotate polarized light, a fact first shown by Biot [64].

Pasteur obtained a sample of paratartaric/racemic acid from Charles Kestner, owner of the Thann plant [62, 65], and found – to his initial dismay – that the crystals of sodium ammonium racemate, like those of the corresponding "ordinary" (dextrorotatory) tartrate, were hemihedral (he had predicted that the crystals of the optically inactive acid would not be hemihedral or chiral). To his surprise, however, he observed that there were two different crystals present in the salt of racemic acid. That is, in some of the crystals the hemihedral facets were inclined to the right while in the others to the left, and Pasteur recognized that the two tartrate crystals were related to each other as the two hands, i.e., they were *enantiomorphous* (by today's terminology). Pasteur then manually separated the two kinds of crystals and found that they rotated polarized light in solution, the rotations by the two being equal in absolute value (within experimental error) but opposite in direction. The dextrorotatory salt thus obtained was identical in all respects to the corresponding salt of the known (+)-TA and could be converted to a free acid that was identical in all respects to (+)-TA, while the levorotatory salt gave an acid that was identical to the natural acid except that it rotated polarized light in the opposite direction and its crystals were enantiomorphous with the natural acid. These results led Pasteur to realize that the molecules of the two substances in racemic acid must be chiral, due to some three-dimensional feature of their molecular structure, and that they are non-superposable-mirror-image (i.e., enantiomeric) molecules [61]. Pasteur, aged 25, announced his discovery in a lecture to the *Académie des sciences* in Paris on May 22nd, 1848 [61, 66]. Later he even proposed that a tetrahedral or helical arrangement of the atoms in the chiral molecules may be the basis of their chirality [67], proposals we now know to be correct.

Concerning Pasteur's term for handedness, he did not use *chirality* – this term was coined, by Lord Kelvin in 1894, nearly 50 years after Pasteur's discovery [16].

Pasteur did recognize the need for a specific term for handedness in molecules and objects and adapted the little-used French term *dissymétrie* (dissymmetry) to the phenomenon that today we call chirality [8].

Pasteur's discovery also opened the road toward an appreciation of the widespread existence of molecular chirality in natural products. The first steps on that road were in fact taken by Pasteur himself. In the early 1850s he went on to study many chiral natural compounds, and he recognized that these molecules were chiral and that the substances isolated from their natural sources were unichiral [68]. Later, Pasteur stated the essence of the matter: "...morphine, codéine, quinine, strychnine, brucine,...Tous ces principes immédiats sont moléculairement dissymétriques" (...morphine, codeine, quinine, strychnine, brucine,... All these natural compounds have molecular dissymmetry) [67].

It should be mentioned here that in 1820, i.e., well before Pasteur, there was a theoretical suggestion that some molecules may lack symmetry [69]. It came from Sir John Frederick William Herschel (1792–1871) [70, 71], an eminent English astronomer, physicist, and chemist. He proposed that such lack of symmetry may be the explanation for Biot's observation (see above) that some substances are optically active in the non-crystalline state. In 1827 Herschel repeated his suggestion, stating that such molecules "must be conceived as unsymmetrically constituted, i.e., as having a right and left side" [72]. This is, no doubt, a seed of the concept of molecular chirality. It must be recognized, however, that, insightful as it was, Herschel's proposal of "unsymmetrical molecules" was limited in scope and remained only a theoretical suggestion: he did not elaborate further on the subject and did not pursue any experimental studies on the phenomenon. Moreover, Herschel did not dispute Pasteur's claims for the discovery of molecular chirality. It was indeed Pasteur (whether he had been aware of Herschel's ideas or not) who placed the concept of molecular chirality on a solid experimental foundation in a series of studies that required a great deal of him: the recognition of the fundamental problem of the sodium ammonium tartrate/paratartrate crystals, the design and execution of crucial and difficult experiments, exceptional powers of observation, thorough familiarity with the literature, and superior scientific intuition. Ultimately, based on his tartrate work, Pasteur was able to elaborate a fundamental chemical phenomenon that his eminent predecessors, e.g., Biot, Mitscherlich, de La Provostaye, Hankel, etc., all of whom had worked with tartrate crystals and had access to Herschel's publications, had failed to recognize. All in all, it is therefore not inaccurate to speak of "*Pasteur's discovery* of molecular chirality." (Herschel's proposal was recently discussed in detail [8]).

Pasteur's preparation of *levo*-TA in 1848 produced the first known example of the existence of *both* enantiomers of a chiral substance. Shortly thereafter, in 1851, the isolation of (−)-camphor from a natural source by Chautard [73] created the second example [(+)-camphor had been known for a long time].

The next fundamental development in the history of molecular chirality occurred in 1874, when the asymmetric carbon atom was proposed as a basis for molecular chirality by the Dutch and French chemists Jacobus Henricus van't Hoff (1852–1911) [74] and Joseph Achille Lebel (1847–1930) [75], respectively,

independently and almost simultaneously. They also proposed that the four substituents connected to the carbon atom were arranged in the shape of a tetrahedron. The discovery of the "asymmetric carbon atom" (van't Hoff's terminology) finally provided the explanation for the existence of "optical isomers" and for the chiral nature of the molecules of optically active substances, including many naturally occurring substances.

5 Recognition of Biological Enantioselectivity

When in 1848 Pasteur began his experiments that led to the discovery of molecular chirality, all known optically active compounds were from natural sources. He recognized this fact and believed that optical activity is intimately connected to the genesis of such substances in nature, and ca. 10 years later he made a fundamental discovery relating the role of molecular chirality to biology.

Although he began his career as a chemist, Pasteur is primarily remembered today as the scientist who made revolutionary discoveries in microbiology and infectious diseases that have been of immense benefit to humanity. The circumstances and apparent reasons for his change of research direction from chemistry and crystallography to microbiology in the mid-to-late 1850s have recently been critically discussed and do not need to be further elaborated here [76]. Suffice it to state that in 1854, Pasteur, who was then professor of chemistry at Strasbourg, accepted an appointment as professor of chemistry and dean of the newly opened Faculty of Sciences at the University of Lille, in northern France. This was an industrial region where agricultural and food industries had considerable economic significance, and fermentation-based manufacturing, such as the production of ethanol from sugar beets and the production of beer, were of particular importance. It is highly likely that his move to Lille played a significant role in his shift to microbiology, including the study of fermentations [76].

After 3 years in Lille, Pasteur moved again, this time to Paris. On October 22nd, 1857, he was appointed Administrator of the École normale supérieure (ENS) and Director of Scientific Studies there. On December 21st, 1857, shortly after his arrival in Paris, he presented a communication to the *Académie* entitled "Memoir on Alcoholic Fermentation" which was published as a memoir in the proceedings of the *Académie*, the *Comptes rendus des séances de l'Académie des Sciences* (*Comptes rendus* henceforth) [77]. As its title indicates, the memoir dealt with certain aspects of alcoholic fermentation, but near the end of the communication Pasteur said the following:

> Before concluding, I ask for the permission of the Academy to present results to which I attach great importance. I have discovered a means of fermenting tartaric acid which readily affects ordinary right tartaric acid but involves left tartaric acid very poorly or not at all. Now, a remarkable thing, predictable from the preceding fact, is that when paratartaric acid, formed by the combination, molecule for molecule, of the two tartaric acids, right and left, is subjected to the same method of fermentation, it is resolved into the

> right acid which is fermented and left acid which remains intact, in such a way that the best means of obtaining left tartaric acid I know of today is to resolve paratartaric acid by fermentation.

The description of the fermentation of "paratartaric acid" in the memoir of December, 1857, constitutes the first published observation of enantioselectivity in a biological process [77]. Approximately 3 months after that brief announcement of the enantioselective microbial metabolism of TA, Pasteur presented to the *Académie* a communication devoted entirely to the subject. The new communication, bearing the title "Memoir on the Fermentation of Tartaric Acid," was presented to the *Académie* on March 29th, 1858, and, as usual, was published in the *Comptes rendus* [78]. Memoirs of original research appearing in the *Comptes rendus* were often relatively short, with few experimental details, and concentrated mainly on the essence and interpretation of the work. Pasteur sometimes followed up a presentation to the *Académie* with a full paper in another journal, but he did not publish a full paper on the fermentation of the TAs after his memoir of March, 1858, to the *Académie* [78]. For (±)-TA, in the 1858 memoir Pasteur abandoned the name "paratartaric acid" that he had used in the earlier communication [77] and employed instead the other common name for the compound at the time, "racemic acid" (see above) [78]. It should also be noted that while the stereochemical course of Pasteur's tartrate fermentation is described today as *enantioselective*, this (or any other) *enantio*-based term does not appear in his lectures and writings. The first *enantio*-based terms were introduced by Carl Friedrich Naumann (1797–1873), a German mineralogist, in 1856, but Pasteur did not adopt this terminology [79].

Pasteur's 1858 memoir is divided into two parts [78]. Part one dealt with the fermentation of (+)-TA and Pasteur pointed out that the spontaneous fermentation of this acid had been known for a long time as a result of manufacturing accidents. He also described some of the experimental details of the fermentation as conducted in his laboratory. The fermentation mixture contained ammonium (+)-tartrate, nitrogenous "albuminoid" material from plant or animal sources, and material from a previous active fermentation of TA.

In part two the analogous incubation of (±)-TA is described. The fermentation was carried out in the same manner as that of the dextrorotatory acid, and the key experimental tool was the monitoring of the optical rotation of the mixture as the fermentation proceeded. It was found that the reaction mixture, which showed no optical rotation at first, became levorotatory as the fermentation progressed over several days. The rotation continued to increase and eventually reached a maximum, at which point the fermentation stopped. The dextrorotatory acid was no longer present in the mixture, having been destroyed in the fermentation. (−)-TA, which was not affected by the "ferment," could then be readily isolated in pure form from the mixture. In the remainder of the memoir Pasteur proposed an explanation for the selective destruction of (+)-TA in the fermentation [76, 78] (see below).

Pasteur did not identify a specific microorganism in the memoir on the fermentation of TA [78], although he referred to the organism as "yeast." He also described it as resembling the lactic ferment, i.e., the microorganism he had identified as

responsible for lactic fermentation. In his scientific biography of Pasteur, Duclaux suggested that the microorganism of the tartrate fermentation may have been a species of *Penicillium,* a fungal microorganism [80]. In fact, in 1860 Pasteur reported in a brief note that *Penicillium glaucum,* a common mold, enantioselectively metabolized paratartaric acid in a manner very similar to the earlier fermentation: here too, (+)-TA was consumed and (−)-TA was left behind largely untouched [81].

The nature of the products of the fermentation of TA was not addressed by Pasteur in his memoir of March, 1858 [78]. He indicated in the memoir that he would soon publish information on this matter, but no such publication ever appeared. He did mention in the memoir an earlier report from the literature that identified *metacetonic acid* as a product of the fermentation of calcium (+)-tartrate. "Metacetonic acid" is an old name for propionic acid [82].

No indication is given in the memoir of March, 1858, whether (−)-TA was separately incubated under the conditions of the fermentation, although the brief statement in the first report (of December, 1857, [77]) suggests that such an experiment had in fact been carried out. In a related matter, in 1853 Pasteur had discovered the racemization of TA when he heated (+)-TA with a cinchona alkaloid, e.g., cinchonidine [83]. Among the products of the reaction he found not only (±)-TA but also *meso*-TA (Fig. 3). He recognized that this molecule, previously unknown, was inherently achiral and that therefore the substance was non-resolvable. Interestingly, however, he did not include the *meso* acid in the investigation of the tartrate fermentations.

Pasteur's discovery of biological enantioselectivity in 1857 was a key finding that formed the foundation stone of the science of molecular biochirality. However, nearly 30 years elapsed after Pasteur's discovery before the next landmark observation was made. That event and its significance will be detailed in the next section.

6 The First Finding of Enantioselectivity at a Biological Receptor

In 1886, Italian chemist Arnaldo Teofilo Pietro Piutti (1857–1928) (Fig. 4) discovered enantioselectivity in what is considered today receptor-mediated biological activity [84, 85].

Receptors are macromolecules "at the cell surface and within cells that mediate the effects of chemical messengers and hormones and the actions of many drugs in the body" [86]. The receptor concept was introduced at the dawn of the twentieth century, independently by the German physician and immunologist Paul Ehrlich (1854–1915) [87] and the British physiologist John Newport Langley (1852–1925) [88]. However, the concept of receptors was not widely accepted until the 1960s. More recently, the science of receptors has undergone an explosive growth and has assumed great importance in many areas of the biological sciences, including

Fig. 4 Arnaldo Piutti in the laboratory. Photograph and permission to reprint kindly provided to the authors by Dr. Claudia Piutti

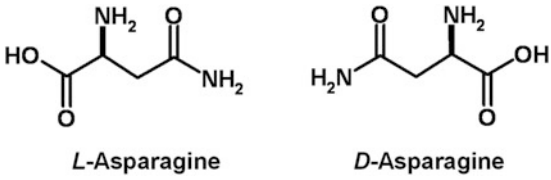

Fig. 5 The asparagine enantiomers

neuroscience, immunology, biochemistry, molecular biology, physiology, and pharmacology. Indeed, today receptors constitute one of the most intensively studied areas of biology.

Piutti completed his university education in chemistry at the University of Turin in 1879 and in 1881 moved to Florence to work with Ugo (Hugo) Schiff, an eminent professor of chemistry originally from Germany (he is mostly remembered today for "Schiff's bases" which he discovered). It was in 1886, while working in Schiff's laboratory, that Piutti made his discovery of enantioselectivity at receptors [85]. The discovery concerned the amino acid asparagine. In 1886 *L*-asparagine had already been known for 80 years. "Ordinary asparagine," as it was often referred to, is today's *L*-asparagine (Fig. 5); the latter name will be used in this chapter (and *D*-asparagine for its enantiomer). However, when quoting or discussing earlier writings in context, the original nomenclature (e.g., "ordinary asparagine" for *L*-asparagine) will be retained. The history of the first 125 years of asparagine has been described in detail by Vickery and Schmidt [89], and only a few relevant particulars will be provided here.

L-Asparagine (a non-essential amino acid) is thought to have been the first amino acid identified in natural sources and was first isolated in 1806 by the renowned French chemist and pharmacist Louis Nicolas Vauquelin (1763–1829) and his young assistant (and later a respected chemist and pharmacist in his own right) Pierre Jean Robiquet (1780–1840) [90]. They obtained the substance from the juice of the asparagus plant they indicated to be *Asparagus sativus*. Linn. *L*-Asparagine is now known to occur in the free state in many other plants as well, e.g., marshmallow, vetches, soybeans, and white lupino beans.

In the spring of 1885 Piutti assisted in the production on a large scale of ordinary asparagine in a factory producing the substance in Siena, Italy. From 6,500 kg of germinated vetch, 20 kg of crude levorotatory asparagine was obtained. The mother liquors remaining after this operation deposited, with time and natural evaporation, a mixture of two enantiomorphous crystal types, one being *L*-asparagine and the other a new species. Piutti mechanically separated the crystals and purified the material, obtaining in this manner 100 g of a substance whose crystals were enantiomorphous with the crystal habit of natural asparagine. The optical rotation of the new substance was found to be equal in absolute magnitude and opposite in direction to that of natural asparagine. In addition, the chemical properties and elemental composition of the new compound were the same as those of *L*-asparagine. No additional details on the isolation procedure are provided [84].

The chemical structure of asparagine was known in its major features at the time but not in all of its details. Specifically, the presence of the amino, carboxyl, and carboxamide groups was known, and it was understood that the latter two were separated by two saturated carbons. However, the position of the amino group was uncertain, i.e., it was not known whether the amino group is located α to the carboxyl group or α to the carboxamide function. Accordingly, Piutti asked the question whether the two asparagines (i.e., the "ordinary" form and the newly isolated compound) could be constitutional isomers, i.e., differing insofar as the position of the amino group is concerned, namely, that one of the two substances would have the structure $HO_2CCH(NH_2)CH_2CONH_2$ (an alpha-amino acid) while the other would correspond to $HO_2CCH_2CH(NH_2)CONH_2$.

In an attempt to answer this question, Piutti synthesized a series of derivatives of the two compounds and compared in each case the two analogous derivatives obtained from the two asparagines, respectively, for their chemical properties. He found no differences. However, when he compared the optical rotations of the two derivatives in each pair they were opposite in sign. He then reached the conclusion that his newly isolated compound was the "inverse" (i.e., the mirror-image form, in molecular terms) of *L*-asparagine [84]. Eventually Piutti settled the question of the exact structure of asparagine with an unequivocal synthesis that was imaginative and elegant for his time. He thus showed that asparagine is in fact an alpha-amino acid [91].

Even during the isolation and purification process leading to the new asparagine Piutti noticed that the mixture of the two asparagines tasted sweet. The pure *D*-asparagine obtained by Piutti retained the sweet taste and in this differed drastically from *L*-asparagine, which was without taste. Piutti stated that other

known amidated acids have a sweet taste, and, importantly, he pointed out that in other known examples of enantiomerically related substances the taste does not differ [84]. Thus, examination of the taste of *D*-asparagine vs that of the *L* enantiomer was the first example of a difference in taste found for enantiomerically related substances. In hindsight it was also the discovery of the first example of enantioselectivity at a biological (human) receptor.

Given the proportion of the two asparagines Piutti isolated from the same batch of vetches (20 kg *L* vs 100 g *D*), it is logical to ask whether the *D*-asparagine he obtained was the result of the actual presence of the substance in the plant or whether it was an artifact produced by the partial racemization of *L*-asparagine during the isolation procedure. This question was raised as early as 1910 by Hans Pringsheim (1876–1940), a professor of chemistry at Berlin, who then carried out experiments in search of the answer. He boiled aqueous solutions of *L*-asparagine under reflux for 12–16 h and demonstrated via fractional crystallization of the material obtained that partial racemization had occurred and thereby *D*-asparagine produced. He therefore concluded that Piutti's isolation of *D*-asparagine was the result of the partial racemization of *L*-asparagine during the extraction and isolation. Pringsheim also stated that no *D*-amino acid occurred naturally, at least based on the evidence available up to that time [92].

Piutti reacted to Pringsheim's claim by carefully examining the occurrence of the two enantiomers of asparagine in plants. To address Pringsheim's claims, Piutti first demonstrated that boiling aqueous solutions of *L*-asparagine does indeed cause, given enough time, detectable racemization. In the next step however he showed that if the temperature of the solution of *L*-asparagine is not allowed to rise above 55 °C no racemization takes place. He then extracted asparagine from lupines (*Lupinus albus*) while assuring that the temperature during the entire operation did not rise above 40 °C. Both *L*- and *D*-asparagine were found to be present in the plant extracts, proving that *D*-asparagine does in fact occur naturally in the plant and that his isolation of the substance was not the result of the racemization of *L*-asparagine. Piutti added that Pringsheim's conclusion that no *D*-amino acid occurred in nature was thus unjustified [93]. According to a standard source on amino acid chemistry, Piutti's isolation of *D*-asparagine in 1886 was one of the first two examples of the preparation of a *D*-amino acid [94].

In summary then, Piutti's discovery of a difference in the taste of *D*- and *L*-asparagine in 1886 was a milestone first observation of enantioselectivity at a biological (human) receptor. The discovery was also the first observation of stereoselectivity of any kind in taste, the first finding of biological enantioselectivity in an organism higher than microorganisms, the first example of biological enantioselectivity in an effect other than enzyme action, and one of the two earliest reports of the preparation of a *D*-amino acid. Piutti also proved the structure of asparagine with an elegant synthetic pathway and showed that *D*-asparagine occurs naturally by demonstrating that its isolation can be carried out without any racemization of *L*-asparagine which is also present in the plants. Overall, Piutti's investigations on asparagine addressed a series of challenging problems and were carried out with originality and imagination, and the result was a key discovery in the history of

molecular chirality in biology. Today chiroselectivity at biological receptors is recognized as an important aspect of ligand-receptor interactions and the phenomenon has substantial implications and consequences for the science and associated technologies, e.g., in new-drug development.

7 Early Studies of Chiroselectivity in the Biological Actions and Fate of Chiral Substances

Advances in organic chemistry during the second half of the nineteenth century began the era of the elucidation of the structures of organic molecules, including many chiral molecules, and by the end of the century the two-dimensional structures (i.e., the connectivity of the atoms) of many organic compounds were elucidated. As a result of these advances, many natural or synthetic chiral compounds of known structure became available. However, elucidation of the structures of more complex molecules remained a challenge. Thus, the structures of many compounds remained unknown or were formulated incorrectly. For example, the English edition of *Adolph Strecker's Short Text-Book of Organic Chemistry,* published in 1882 and authored by Johannes Wislicenus (1835–1902), a leading German chemist of the time, included many naturally occurring chiral substances, e.g., camphor, codeine, morphine, quinidine, quinine, etc., and optical rotation data were provided for many of them, but their chemical structures were not given since they were unknown.

Concerning the stereochemical aspects of chemical structures, the asymmetric carbon atom proposed in 1874 by van't Hoff and Lebel had solved the "mystery" of molecular chirality and provided an explanation for optical activity (see above). Thus, the stereochemistry could now be addressed (a good example in this regard was Piutti's determination of the molecular structure of asparagine and his recognition of the mirror-image relationship of his new asparagine to the known "ordinary" asparagine, as discussed above). However, it should be remembered that absolute stereochemical configurations were not known at the time and comparisons and chemical correlations of chiral molecules provided only relative configurations.

As a result of the advances in organic chemistry and despite the shortcomings in molecular-structure determination mentioned above, the chemical structures of many compounds became known by the final decades of the nineteenth century which in turn led to studies of potential chiroselectivity in the biological properties of many chiral substances. Since initially only in relatively few cases were both enantiomers available separately, at first only a small number of studies of enantioselectivity appeared (some of the investigations compared the activity of one of the enantiomers to that of the racemate). With time, however, the pace accelerated, and many studies were published on the role of molecular chirality in biology. Two general areas were addressed: (1) chiroselectivity in enzymatic reactions, as manifested in the metabolic fate or enzyme-catalyzed specific transformations of

substances and (2) chiroselectivity in the physiological, pharmacological, or toxicological effects of a variety of biologically active compounds.

The earliest studies investigated natural or physiological compounds, but eventually, with the advances in organic chemistry and pharmacology, synthetic substances of stereochemical interest became available and the role of chirality in the actions and disposition of such agents also began to receive attention. In this section some of the early studies of chiroselectivity are reviewed. Many of these investigations made important contributions to the budding field of the stereochemical aspects of biologically active compounds. Several reviews from that time period summarized and analyzed the early findings [95–99].

Concerning the first area of interest mentioned above, beginning at the end of the nineteenth and continuing into the first decades of the twentieth century, a great deal of work was carried out to examine the stereochemical course of enzyme-catalyzed reactions, i.e., metabolism or biochemical transformations by microorganisms, tissue preparations, crude enzyme extracts, or intact animals. Enantioselectivity was shown for many physiological compounds, e.g., amino acids, peptides, carbohydrates, lactic acid, etc., but some foreign compounds were also studied. Specific biochemical reactions were also studied, e.g., hydrolysis, oxidation, and reduction [98]. For example, pig liver esterase was found to catalyze enantioselectively the hydrolysis of mandelic acid esters [100]. These studies were carried out using the racemates, and, interestingly, when the esterase action on the separated individual enantiomers was examined, an enantiomeric interaction was revealed. Thus, when incubated separately, (−)-ethyl mandelate was hydrolyzed more rapidly than the dextrorotatory ester, while the latter was hydrolyzed faster than (−)-ethyl mandelate when the racemate was incubated [101].

Monumental work was carried out on the role of stereochemistry in biology, particularly on chiroselectivity in enzyme action (on sugars, amino acids, and peptides), by the eminent German chemist Emil Fischer (1852–1919) during ca. the last two decades of the nineteenth and early in the twentieth century. His ground-breaking work in a variety of chemical and biochemical areas has been amply chronicled [102], and only the relevant stereochemical aspects will be discussed here. Fischer began his work on carbohydrates in 1884 and pioneered the synthesis of sugars, including stereoisomeric forms, and the determination of their structures and stereochemical relationships. Indeed, Fischer's work on the synthesis of sugars qualifies him as a pioneer of asymmetric synthesis [103, 104] Fischer applied the fundamental concepts of van't Hoff and Lebel concerning the asymmetric carbon atom and its role in stereochemistry, and his work in this regard was a powerful validation of the ideas of the two chemists. Fischer's work also benefited from the great advances in structural organic chemistry, valence theory, etc., achieved during the second half of the nineteenth century.

Fischer studied both natural and synthetic sugars, and demonstrated that the microbial fermentation (e.g., by beer yeast) and other enzymatic reactions of sugars displayed considerable stereoselectivity. He found both diastereoselectivity and enantioselectivity in the action of enzymes on sugars. For example, he showed that natural glucose, fructose, and galactose were readily fermented by yeast but

their "optical antipodes" (i.e., the respective enantiomers) were left unchanged [105]. As for diastereoselectivity, he found, for example, that crude aqueous yeast extracts (which he named "invertin") hydrolyzed α-methyl-*D*-glucoside but not its diastereoisomer (epimer) β-methyl-*D*-glucoside, while a preparation obtained from almonds Fischer called "emulsin" hydrolyzed β-methyl-*D*-glucoside but not α-methyl-*D*-glucoside (the methyl-*L*-glucosides were entirely unaffected) [105]. Fischer also realized that "fermentation" by microorganisms is almost certainly the result of the action of enzymes within them, and his findings on the stereoselectivity of enzyme action prompted him to propose a model to rationalize the observations (his model will be discussed below, together with other early proposals to explain biological chiroselectivity). Fischer also made an important contribution to stereochemistry with his system of drawing stereochemically explicit and convenient structures using a convention now known as the Fischer projection [106].

Fischer was intrigued by nature's ability to synthesize sugars in unichiral form, and, as pointed out by Ramberg in his insightful analysis of Fischer's work on sugars, Fischer concluded that "asymmetric" chemical constituents within cells were responsible for this asymmetric synthesis, rather than external universal "dissymmetric forces" (e.g., sunlight or magnetism) believed by Pasteur to be the agents ultimately responsible for the unichiral character of natural compounds [107].

Today it is generally agreed that Fischer's work was revolutionary. His groundbreaking work was recognized in 1902 with the Nobel Prize in chemistry for "the extraordinary services he has rendered by his work on sugar and purine syntheses." In the award address, Professor Hj. Théel, President of the Swedish Royal Academy of Sciences, specifically discussed the revolutionary importance of Fischer's work on sugars, their stereochemistry, and the nature of enzymes and their interactions with sugars, and emphasized the overall impact of Fischer's work on the essential connections of chemistry and biology [108].

As attention began to be focused on enantioselectivity in biology at the end of the nineteenth century, metabolism in organisms higher than microorganisms was also investigated. For example, when racemic camphor was fed to dogs or rabbits, more of the *levo* enantiomer was converted to a glucuronyl conjugate than of the *dextro* enantiomer, and when (±)-malic acid was injected subcutaneously into rabbits, larger amounts of the unchanged dextrorotatory acid appeared in the urine, indicating that (−)-malic acid, the naturally occurring form, was more extensively metabolized; other compounds were also studied [109].

A complex picture of stereoselectivity emerged from the investigations of metabolic fate or enzymatic transformations, depending on the substrate, the microorganism, plant, animal species, or particular enzyme involved, and the biochemical reactions catalyzed. In some cases no enantioselectivity was found while in others only one of the enantiomers was acted upon; in some cases both enantiomers functioned as substrates for an enzyme (or were destroyed in vivo) but at different rates. Furthermore, in some cases the direction of enantioselectivity changed for the same substrate with the microorganisms or enzymes used. However, interpretation of the results of these studies is at times complicated by the fact that the nomenclature used was, in hindsight, confusing. The *d* and *l* descriptors, for

example, were originally introduced to indicate configuration, and later were used to refer to optical rotation [110], and this dual use renders the interpretation at times difficult indeed. To illustrate, Cushny wrote: "*d*-glucose is dextrorotatory. . .while *d*-fructose is laevorotatory." On the same page he also wrote: "in the same way a *l*-rotary [sic] substance may be destroyed by one enzyme in preference to the *d*-rotary isomer. . ." [111]. The potential confusion is obvious.

The other major area of interest, namely biological activity other than enzyme action, was also studied. As discussed above, the first observation of enantioselectivity in such activity was Piutti's finding of a difference in the taste of the asparagine enantiomers. Piutti's discovery prompted similar studies by others, and the taste of several amino acids was examined shortly thereafter. For example, in 1894 Menozzi and Appiani reported that the enantiomers of glutamic acid differed in their taste. The authors pointed out that their finding was not new, inasmuch as a difference in the taste of the enantiomers of asparagine had already been reported by Piutti [112]. Beginning during the end of the nineteenth century, many studies comparing the enantiomers of substances of pharmacological or toxicological interest were carried out, and many examples of enantioselective effects were observed.

The first clear example of enantioselectivity in a pharmacological action proper was the demonstration by Cushny that (−)-hyoscyamine was ca. 12–20 times more potent than the *dextro* enantiomer in a variety of pharmacological effects, e.g., mydriasis in the cat, salivary secretion in the dog, and at cardiac myoneural junctions. Interestingly, (+)-hyoscyamine was the more potent enantiomer in CNS-excitatory effects [113]. Cushny also found that the enantiomers of epinephrine (adrenalin) differ significantly in their ability to increase blood pressure, the levorotatory form being 12–15 times more potent than (+)-(*S*)-epinephrine [114]. Arthur Robertson Cushny (1866–1926), a Scottish pharmacologist, made important experimental contributions to the field of enantioselectivity in pharmacology; in 1926 he reviewed the studies of enantioselective pharmacology and enzyme action published during the previous ca. 40 years [115] and provided a detailed and critical discussion of enantioselectivity in biology that revealed a great deal of insight into the nature of chirality and its biological implications. Cushny was a leading figure in the discovery of the role of chirality in biology, particularly in pharmacology.

An interesting, complex, and important example of biological *diastereoselectivity* (with implications for *enantioselectivity*) between chiral molecules concerns the natural unichiral substances quinine and quinidine (Fig. 6), two important cinchona alkaloids (some aspects of the history and antimalarial, antiplasmodial effects of quinine were discussed in an earlier section of this chapter). Natural quinine is levorotatory and quinidine dextrorotatory.

The two alkaloids are diastereoisomerically related and differ in configuration at two of the five stereogenic centers. Thus, in quinine C8 and C9 are *S* and *R*, respectively, while in quinidine they are reversed, i.e., *R* and *S*, respectively (Fig. 6). (The literature shows some confusion concerning the stereochemical relationship of the two substances, with claims by some authors that the two substances are related as enantiomers [116].) In 1853 Pasteur recognized that

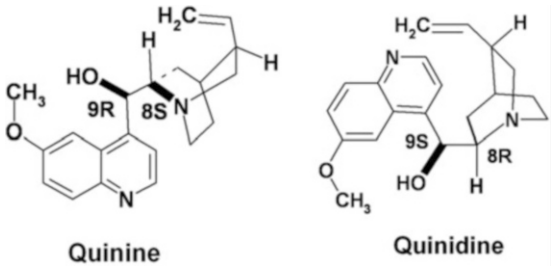

Fig. 6 The structures of quinine and quinidine

quinine and quinidine were "isomers" but not enantiomers, and studied the optical rotation, crystallographic properties, and some chemical reactions of the two substances [117]. However, the structures of quinine and quinidine were then unknown.

Today the main therapeutic use of quinine is as an antimalarial (other uses include the treatment of nocturnal leg cramps and application as a flavoring agent in food). Interestingly, quinidine is somewhat more potent as an antimalarial (against *Plasmodium falciparum*) than quinine and is used in that indication in some clinical settings [118]. Epiquinine and epiquinidine are the epimers at (the hydroxyl-bearing center) C9 of quinine and quinidine, respectively, with the configurations at C8 and C9 being *R,R* in epiquinidine and *S,S* in epiquinine. Epiquinine and epiquinidine, which are also present in cinchona, are essentially devoid of antimalarial activity, i.e., the antiplasmodial action is lost when the configuration at the C9 center *only* is inverted in quinine or quinidine [118]. It is clear therefore that the antimalarial activity requires the *R,S*/*S,R* relative configuration at C8,C9. Potential explanations of this radical change in biological properties produced by configurational change at C9, i.e., at only one of five stereogenic centers, are naturally of interest. Attempts have been made to discern conformational or physicochemical factors that may account for the difference between the antimalarial potencies of the two sets of alkaloids (i.e., quinine/quinidine vs epiquinine/epiquinidine). For example, a recent theoretical study of the conformational spaces of the cinchona alkaloids using a semiempirical method found significant conformational differences between the quinine/quinidine set on the one hand and the epiquinine/epiquinidine set on the other. Furthermore, it was also found that the conformational spaces of epiquinine and epiquinidine feature important conformers with an intramolecular hydrogen bond that is absent in quinine and quinidine [119]. It remains to be determined whether these conformational factors play a role in the profound difference in antimalarial activity between the two epimerically related sets of substances.

Quinidine has been mainly employed as a cardiac antiarrhythmic agent. The antiarrhythmic use of cinchona alkaloids goes back to the eighteenth century, when extracts of the cinchona bark were employed in the treatment of "rebellious palpitations" [120], and by the early 1920s quinidine was in clinical use as an antiarrhythmic agent. In 1922 Deschamps described his extensive studies comparing the cardiovascular properties and clinical effects of quinidine and quinine, and also gave a detailed review of previously published cardiovascular investigations of

the two drugs [121]. Deschamps concluded that the two substances are qualitatively similar in their cardiovascular effects but quinidine is considerably more potent. He also indicated that, of the two drugs, only quinidine was clinically useful as an antiarrhythmic agent since the therapeutic effects of quinine are weak and variable. Deschamps' analysis has been validated by the subsequent experience, and quinine is in fact not used as an antiarrhythmic drug. The difference between quinine and quinidine in this regard is a notable example of receptor-mediated chiroselectivity between diastereoisomers.

As indicated above, the configurations of the C8 and C9 centers in quinine are the opposite of those in quinidine, and in some systems the two compounds behave as if they were enantiomerically related, prompting some investigators to refer to the two molecules as "pseudoenantiomers" [119, 122]. In this light, it is of interest to recall that both quinine and quinidine are potent antimalarial agents, i.e., their "pseudoenantiomer" relationship does not result in a large difference in antiplasmodial potency. In antiarrhythmic effects and some other properties [123, 124], on the other hand, the two drugs do display considerable differences. These observations suggest that investigations of enantioselectivity in the biological actions of quinine and of quinidine may be instructive. However, the respective enantiomers of natural quinine and quinidine have not been described in the literature. Clearly, additional studies are needed to reveal the molecular, physiological, and pharmacological bases of the stereoselectivity in the actions of the cinchona alkaloids.

An important group of synthetic drugs is that of the barbituric acid derivatives. Such drugs ("the barbiturates") were introduced into pharmacotherapy as sedatives, hypnotics, anesthetics, or anticonvulsants beginning early in the twentieth century (e.g., phenobarbital, anticonvulsant; preparation patent 1911). Some of the early barbiturates were chiral and several of them are still in use (as racemates) in clinical medicine today, e.g., pentobarbital (sedative, hypnotic, anesthetic; preparation patent 1916), mephobarbital (anticonvulsant; preparation patent 1929), thiopental (ultra-short-acting anesthetic; preparation patent 1939), etc. The earliest investigation of enantioselectivity in the biological effects of a barbiturate appeared in 1928 and examined the properties of the enantiomers of 5-ethyl-5-α-methylheptylbarbituric acid [125]. The compounds were tested in albino rats, and no significant differences were found between the enantiomers in their hypnotic efficacy and acute toxicity. These results prompted the authors of the study to reaffirm the validity of the then prevailing view that anesthetic action is correlated with the lipophilicity (lipid solubility) of the drugs and is not influenced by their specific chemical-structural details, a view embodied in the Meyer–Overton theory [126]. Since the two enantiomers of a chiral substance do not differ in their lipid solubility (in an achiral environment), a lack of enantioselectivity would in fact be expected for the barbiturates.

However, it is now known that a number of chiral anesthetics, including several barbiturates, show significant enantioselectivity in their anesthetic and other effects [127, 128], a phenomenon which is incompatible with the Meyer–Overton correlation. It has in fact become clear in recent decades that anesthetic agents produce

anesthesia via interaction with specific receptors (proteins) such as ion channels [129], and therefore enantioselectivity is not unexpected for these drugs.

In a recent attempt to account for the lack of enantioselectivity in anesthetic effect observed in the 1928 study of 5-ethyl-5-α-methylheptylbarbituric acid, it was suggested that a possible explanation may be based on Pfeiffer's rule [130]. In 1956 Pfeiffer found a correlation between the average effective human dose of a series of racemic drugs and the ratio of the potencies of the two enantiomers of each drug [131]. It was found that the log values of the ratio of potency of the enantiomers plotted against the log of effective human dose of the racemate gave a linear relationship; as the effective racemic dose increased the ratio of the efficacy of the enantiomers decreased. Surprisingly, the correlation held for a variety of drugs, regardless of pharmacological class or effect, pharmacokinetic differences, etc. The interpretation offered was that when the effective dose is small, the affinity of the more active enantiomer for the receptor is high, which in turn means a tighter binding to the receptor, i.e., greater steric constraints in the binding of the drug to the receptor. Such steric constraints (tight binding) would of course magnify the difference between the enantiomers since the "wrong" enantiomer would have a lesser ability to bind productively to the receptor due to the tighter steric requirements. Therefore, it has been argued on the basis of Pfeiffer's rule that since the effective anesthetic dose of the racemic barbiturate (5-ethyl-5-α-methylheptylbarbituric acid) used in the 1928 study is particularly large (360 mg/kg) when compared to many other barbiturates, the anesthetic effect is in fact expected to display little if any enantioselectivity [131].

The complexities and limitations of Pfeiffer's rule have been discussed [132], but there is a puzzling detail in Pfeiffer's article that does not appear to have caught the attention of commentators. The issue is the fact that among the drugs included by Pfeiffer in the correlation were quinine and quinidine. As mentioned above, the respective enantiomers of natural quinine and quinidine have not been described in the literature, and therefore the ratios of the potency of the enantiomers for the two drugs could not have been available to Pfeiffer. Moreover, neither racemic quinine nor racemic quinidine has been used as a human drug. It is thus puzzling indeed that Pfeiffer included the two drugs in his correlation, since the data on these drugs needed for the correlation (i.e., the effective human doses of the two racemates and the ratios of the potencies of the enantiomers) were not available to him.

As the early examples of biological chiroselectivity (particularly enantioselectivity) began to unfold (as outlined above), it was to be expected that mechanistic explanations for the phenomenon would be sought. The first such efforts and proposed models will be described in the next section.

8 First Explanations of Biological Enantioselectivity

The first proposal of an explanation for the existence of biological enantioselectivity was provided by Pasteur himself in conjunction with his discovery (see above) of the enantioselective fermentation of TA by a microorganism [78]. He

proposed that a unichiral substance within the constitution of the microorganism is involved in the utilization of the tartrate molecules as nutrients, and stated the fundamental principle that two enantiomerically related molecules (the tartrate enantiomers in this case) interact differently (i.e., form different "combinations") with a third chiral molecule, i.e., a unichiral constituent of the microorganism, and explained that the latter does not "accommodate" equally well the left- and right-tartrate molecules. He recognized that the two "combinations" no longer had an enantiomeric relationship. This difference between the two complexes, he added, allows for different properties and behavior by the two combinations, i.e., the possibility of differences in biological effects by the two enantiomers [78].

It is noteworthy that Pasteur's fundamental explanation of enantioselective biological action is still considered valid today. The two complexes are indeed not related as enantiomers, and can therefore have different properties, i.e., the two enantiomers can produce different biological effects. Pasteur advanced the idea that a *diastereomeric relationship* (by today's terminology) between the ligand-mediator complexes exists and explains the discrimination between the enantiomers. Given that almost nothing was known at the time about organic chemical structure, enzymes, or microbial function, Pasteur's explanation was indeed far ahead of its time. He understood the fundamental stereochemical phenomenon that leads to biological enantioselectivity, and his words, "we see here the property of molecular dissymmetry possessed by natural materials intervening in a physiological phenomenon as a modifier of affinity," show a clear recognition of the essence of chirality as a modulator of molecular recognition in biology, as we would put it today.

The next proposal attempting to explain the chiroselectivity seen in the interaction of chiral molecules with biological systems came from Fischer and was the result of his extensive studies of enzymatic reactions of sugars and peptides using microorganisms or crude enzyme preparations. Fischer concluded that overall shape and stereochemical configuration strongly influence the suitability of a molecule to serve as substrate for an enzyme. He condensed these spatial requirements in the statement that for an enzyme to act on a substrate the two must fit like a lock and its key. Fischer used this metaphor ("Schlüssel-Schloss-Prinzip" in German) for the first time in a paper that appeared in 1894 [105]. Although the three-dimensional structure of enzymes was unknown at the time, their role as protein-like substances became quite apparent. In a comprehensive article on the significance of stereochemistry to physiology that appeared in 1898, Fischer summarized the basis of his analogy: "Although one does not know these substances [enzymes] in a pure state, their similarity with proteins is so close and their generation from these so probable, that they have undoubtedly to be considered as optically active, and, hence, asymmetric molecular forms. This had led to the hypothesis that there must be a similarity in the molecular configuration between the enzymes and their object of attack, if reaction is to take place. To make this thought more perspicuous, I have used the picture of lock and key" [99].

Fischer's model has become an enduring paradigm in enzyme-substrate interactions. Furthermore, the model clearly has a certain broader generality for interactions of molecules with biological systems in that it states simply that, for

productive contact, the two interacting components must fit according to some structural constraints. The concept is indeed broad, and not surprisingly therefore it has served as a rationale to account for complementarity in biological responses in contexts other than stereochemistry. For example, Paul Ehrlich (see above) harnessed the argument as a theoretical basis for his side chain theory [133]. To explain the immunological response, Ehrlich postulated that one of the side chains (or *receptors*, as he coined later) of the cell has an atomic grouping with a specific combining property for a toxin. He also distinguished between the so-called *toxophore* and *haptophore* groups of the toxin, the latter being the atomic group involved in binding the toxin to the side chain. As Ehrlich wrote in a 1900 publication, each cell possesses a number of side chains, which bind toxins in a lock-and-key type manner [87]. Furthermore, American zoologist Frank R. Lillie (1870–1947), a pioneer of embryology, invoked the lock-and-key analogy to describe the interaction between sperm and the egg receptor as a preliminary step in his theory of fertilization [134]. Overall, it appears clear today that on introducing the lock-and-key model for enzyme-substrate interactions, Fischer anticipated the field of molecular recognition and contributed to the intimate linkage of synthetic chemistry and biology, in the modern sense of interdisciplinary science.

It should be noted, however, that Fischer's conception of the lock-and-key model has also received some criticism. For example, Fruton [135] interpreted Fischer's view of his lock-and-key model as based on what Fischer believed to be the *chemical similarity* between the enzymes and their substrates, rather than on the *complementarity* between the interacting structures, the latter view being held today as the basis of phenomena of molecular recognition of the type Fischer encountered. However, Fischer's statement that "there must be a similarity in the molecular configuration between the enzymes and their object of attack" (see above) does not stress chemical similarity per se and focuses on similarity in "molecular configuration," i.e., the *geometric* aspects rather than *chemical* similarity.

A strong criticism of Fischer's lock-and-key paradigm came from Fajans, who in 1910 discussed Fischer's model and argued that it was too restrictive inasmuch as it held that one "antipode" of a chiral substrate fits the enzyme and is therefore acted upon by the enzyme, while its enantiomer does not fit and is accordingly left unaltered [95]. Fajans pointed out in contrast that considerable variability in enzymatic enantioselectivity had been reported in the literature, including many cases where both enantiomers of a substance serve as substrates for a given enzyme (albeit often the reaction rates differ). Fajans interpreted this state of affairs as incompatible with the lock-and-key model, pointing out that a key would not fit the mirror-image version of its lock, while an enzyme often catalyzes the reaction of both enantiomers as substrates [95]. However, Fajans' critique of Fischer's lock-and-key metaphor has not received significant support in the literature.

As we have seen, Pasteur's model focused on *enantioselectivity* in biology while Fischer's proposal had a broader character and included *diastereoselectivity*. However, neither Pasteur's nor Fischer's model invoked any specific molecular details or rules. The first specific chemical-structure-based proposal explaining

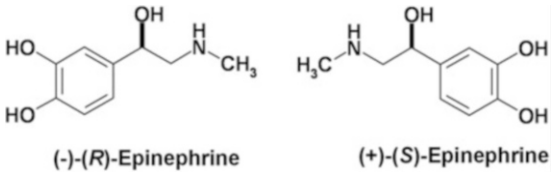

Fig. 7 The enantiomers of epinephrine

enantioselective biological effects was published in 1933 by Easson and Stedman [136]. They proposed a model for the differential binding of (−)- and (+)-epinephrine (Fig. 7) at the "adrenergic receptor" (the existence of multiple types of adrenergic receptors was unknown at the time) as the explanation for the considerable difference between the enantiomers in raising blood pressure. As mentioned above, the levorotatory enantiomer [(−)-(*R*)-epinephrine] had been shown to be ca. 12–15 times as potent as *dextro*-epinephrine [114].

The model advanced by Easson and Stedman was based on a paradigm of three points of interaction between the ligand and the receptor. It was proposed that the amino functionality, the benzylic hydroxyl group, and the electron-rich aromatic ring of epinephrine (Fig. 7) are groups that can interact with three respective complementary moieties strategically located on the (chiral) receptor. If one of the epinephrine enantiomers (i.e., *levo* form in this example) is able to bind fully with all three of its groups to the three complementary groups on the receptor (and thereby produce the full biological effect), then it can be readily demonstrated that *dextro*-epinephrine cannot interact fully in the same manner and at best only two of its three groups can bind simultaneously to their two respective complementary sites on the receptor. A two-point attachment means weaker binding than the full, three-point, connection, and this in turn produces a weaker biological effect. Such weaker binding would then account for the difference between the two epinephrine enantiomers in their pressor effects [136].

In support of this argument Easson and Stedman pointed out that if the benzylic hydroxyl group of epinephrine is replaced with a hydrogen atom, the resulting (achiral) molecule (epinine) would bind to the receptor in the same manner as (+)-epinephrine, i.e., only at two points (since in epinine one of the three binding groups, the benzylic hydroxyl, is no longer present). Therefore, epinine's effect on blood pressure should be weaker than that of (−)-epinephrine, i.e., epinine should be similar to (+)-epinephrine in its potency, a prediction borne out by the facts.

The differential attachment of the enantiomers to the receptor in this model is the result of simple three-dimensional-geometry considerations: two three-dimensional enantiomorphous structures (the epinephrine enantiomers here) in principle cannot attach in an identical manner to a third chiral structure (the receptor) if there are at least three points of binding (the fundamental assumption in this basic analysis is that the binding or attachment points are the only "interactions" between the two structures). This in turn implies that in three-dimensional space a minimum of three interaction points are required for potential enantioselectivity. Thus, fundamentally, the three-point-interaction model is not a biological concept but a geometry-dictated

paradigm. Indeed, the model has been successfully applied in non-biological contexts, e.g., to account for enantioselective chromatographic separations [137].

The three-point-interaction model is of course also applicable in biology, as in the present context to ligand-receptor binding, and can be extended to account for biological enantioselectivity in general. Such generalized adoption of the model has in fact spread in discussions and considerations of biological enantioselectivity. However, it is important to recognize that the theoretical three-point-interaction model is the minimal geometric paradigm and does not preclude the occurrence of ligand-to-mediator binding at more than three points (and associated enantioselective effects) in any given case – it simply states that, due to fundamental geometry principles, in three-dimensional space a minimum three points of interaction are required for potential enantioselectivity to occur.

In 1935 Bergmann et al. postulated three points of contact for enantioselective enzymatic reactions [138] but did not cite the earlier proposal by Easson and Stedman. In 1948 the three-point-interaction model was again proposed, this time by Ogston, in the context of *prochirality* in enzymatic reactions [139]. The issue concerned the tricarboxylic-acid (TCA, citric-acid, or Krebs) cycle in intermediary metabolism, and Ogston proposed the three-point-interaction model to explain the ability of one of the enzymes in the cycle to distinguish between two identical groups within the substrate, citric acid, an *achiral* molecule. The "identical" groups were the two $-CH_2COOH$ groups of citric acid. The stereochemical result of the reaction of citric acid catalyzed by the enzyme had confused biochemists, and Ogston's explanation using the three-point-attachment paradigm between the achiral substrate and the enzyme provided the answer to the stereochemical "puzzle" [139]. Today the two "identical" $-CH_2COOH$ groups (ligands) of citric acid are described as "enantiotopic," a term that is defined as referring to two groups "in constitutionally equivalent locations that are related by a symmetry plane (or center or alternating axis of symmetry) but not by a (simple) symmetry axis. Replacement of one or the other enantiotopic ligand by a new ligand produces enantiomers" [140]. In its essence, Ogston's three-point-interaction paradigm for the recognition of enantiotopic groups by an enzyme is equivalent to the three-point model proposed earlier by Easson and Stedman as an explanation of enantioselective binding by chiral molecules at receptors. Ogston cited neither the 1933 proposal by Easson and Stedman nor the 1935 article by Bergmann et al. on the three-point-attachment paradigm.

Some of the successes and limitations of the Easson–Stedman model have been discussed [141]. Although the model has been useful in accounting for the biological enantioselectivity of a variety of compounds, other studies [2] have shown that in certain cases the model needs refinements and additional elements. It has also been shown, not surprisingly, that in some systems that display enantioselectivity, more than three points of interaction can be demonstrated [142]. Some authors [143, 144] have questioned the fundamental validity of the three-point-attachment model, but such views have not received a great deal of support in the literature.

9 Final Reflections

The discovery of molecular chirality in the middle of the nineteenth century represents a watershed in the life sciences. The manual separation of enantiomorphous tartrate crystals by Pasteur has often been described as one of the most beautiful experiments in chemistry. In the subsequent ca. 100 years important discoveries concerning the role of molecular chirality in biology were made by, among others, Pasteur, Piutti, Fischer, Cushny, Easson and Stedman, etc., and their contributions paved the way to our modern understanding of chiroselectivity in biology and the intimate relationship between structure and function.

By the dawn of the twentieth century, studies of the stereochemical aspects of the biological activity, metabolism, or enzymatic transformations of natural or synthetic substances were proliferating and chiroselectivity was often found in these investigations. Overall, then, by the end of the 1930s a great deal of information on chiroselective biological phenomena had been amassed and the recognition had emerged that chiroselectivity is a common and important phenomenon in the interaction of chiral molecules with biological systems.

While this new knowledge on the biological role of molecular chirality was an enormous advance, it should also be pointed out that the information accumulated by the 1930s was not rapidly exploited for some of its possible benefits. In particular, the new understanding of the role of chirality in biology did not make an impact in the development and marketing of new chiral drugs for many decades after the 1930s. Indeed, during a long period the pharmaceutical industry and governmental drug-regulatory authorities largely ignored the implications and potential of molecular chirality for better and safer drugs. This neglect may have had its explanation, at least in part, in the lack of availability, certainly during the early part of the period in question, of scientific and technical tools essential for the research and development work needed to translate the accumulated scientific information into better and safer drugs (see below).

Be that as it may, it was only in the 1990s that this situation began to change. Thus, in 1992 the US FDA finally issued guidelines concerning the development of new drugs based on chiral molecules [145], and in the same time-frame other drug-regulatory authorities around the world also began to address the issue. The new regulations thus introduced required that during the development of new drugs the role and implications of molecular chirality in biology be taken into account. The impact of this change in the approach to chirality in new-drug development has been dramatic. For example, today the appearance of a new racemic drug on the market is a highly unlikely event (the significance of this change can be appreciated when we consider that at the time of the publication of the new FDA rules, in 1992, ca. 25% of all marketed drugs were racemic). The marketing of a racemic drug is justified in those cases where the drug is stereochemically labile, i.e., if there is in vitro or in vivo racemization or an in vivo stereochemical inversion on a time scale sufficiently fast to be relevant to the shelf-life of the drug or to its composition during the therapeutic treatment. A class of drugs where in vivo inversion of one of

the enantiomers is commonly seen is the "profens," i.e., the 2-arylproprionic-acid-based analgesic and anti-inflammatory agents [146].

Thus, in the 1990s, regulatory authorities and the pharmaceutical industry began to recognize that in many cases the racemic mixture is a combination of two biologically distinctly different substances. In most cases, in fact, the two enantiomers will differ in some aspects of their effects, and there are many examples where the enantiomers have been found to differ considerably – and at times drastically – in their pharmacology, toxicology, clinical efficacy, and/or pharmacokinetics, etc. Overall, it is generally believed today that a unichiral version of a therapeutic agent is likely to have advantages over the racemic or some other stereoisomeric mixture. For example, the pharmacology and toxicology profiles will be clearer for the single substance, the pharmacokinetics and the relationship between serum concentration and biological effects will be more readily interpretable, in some cases adverse effects or toxicity will be eliminated with the removal of the less-favorable stereoisomer(s), the dosage of the unichiral drug may be lower than that of the stereoisomer mixture, etc. A good example here is the case of racemic bupivacaine, an anesthetic agent. Both enantiomers possess anesthetic properties, but it has been demonstrated that levobupivacaine [(2*S*)-1-butyl-*N*-(2,6-dimethylphenyl)-2-piperidinecarboxamide] is a safer drug than the racemate (bupivacaine) due to the significant cardiotoxicity of the dextrorotatory enantiomer. As a result, levobupivacaine has been introduced as a drug with a better safety profile in anesthetic clinical practice in some countries [147].

However, a word of caution is in order here. In a few cases it has been shown that the racemic or some other mixture of the stereoisomers was a safer drug than a unichiral form [148]. Thus, each case should be considered on its own merits.

The question may be asked: what were the factors that finally produced, after a ca. 60-year delay, this change in attitude toward the role of chirality in new-drug development? In retrospect, it appears that advances in two chemical disciplines played a major role in focusing the attention on the importance of molecular chirality in new-drug development:

1. The considerable advances in stereoselective synthesis during the last several decades of the twentieth century. Such improvements in organic synthesis have allowed the preparation of a wide variety of unichiral drugs, drug metabolites, and related substances, including many with highly complex stereochemistry.
2. The advent, during the same period, of powerful methods for enantioselective analysis, i.e., the detection and quantification of enantiomerically related substances in the presence of each other, particularly via enantioselective chromatography. The benefits of such analytical methodology are multifold. For example, the new chromatographic analytical methods have allowed the convenient, rapid, precise, and accurate determination of the enantiomer composition or enantiopurity of chiral substances, even in cases of trace contamination of a unichiral compound with the enantiomer. Such enantioselective analytical capability is essential in the preparation of unichiral substances of high stereochemical purity and in the development of the necessary stereoselective synthetic

methods; such methods are also required to assure stereochemical purity during pharmacological testing, where even low levels of contamination of the *distomer* (the biologically less potent enantioform) with the *eutomer* (more potent enantiomer) may distort the results (see Sect. 2 for a discussion on propranolol); and, of course, the new analytical methodology has also allowed the study of enantioselectivity in the pharmacokinetics and metabolism of chiral substances. (An important additional advantage of some of the enantioselective chromatographic separations is that in the preparative mode they may rapidly provide sufficient amounts of the individual enantiomers for prompt initial pharmacological and toxicological evaluation, without the need to resort to enantioselective syntheses, whose development is often challenging and time-consuming.)

In conclusion, it is clear that a strong component of the interest in the role of molecular chirality in biology derives from the implications of the phenomenon for the development of new drugs and the corresponding needs of the pharmaceutical industry. However, in a more general sense, the often-seen distinctive properties of enantiomers at a biological level have fine-tuned key mechanisms, such as replication, transcription, biosynthesis, biological activity, metabolic fate, etc., in living organisms and produce profound consequences. All in all, it is widely recognized today that molecular chirality is a fundamentally important modulator of the effects and properties of chiral substances in a variety of branches of biology and medicine.

Acknowledgments Helpful information from Professors Andrew J. Hutt (University of Hertfordshire, UK), Michael Lämmerhofer (University of Tübingen, Germany), and Wolfgang Lindner (University of Vienna, Austria) is gratefully acknowledged. The authors are deeply indebted to Dr. Claudia and Pietro Piutti, great-granddaughter and grandson of Arnaldo Piutti, respectively, and to Pietro Piutti's spouse Caterina (née Rovetto), for permission to reproduce Arnaldo Piutti's photograph. In addition, permissions from Wiley and Taylor & Francis to reproduce text extracts from previous publications [8, 9, 14, 19, 76, 85] are gratefully acknowledged.

References

1. Simonyi M (1984) On chiral drug action. Med Res Rev 4:359–413
2. Patel BK, Hutt AJ (2004) Stereoselectivity in drug action and disposition: an overview. In: Reddy IK, Mehvar R (eds) Chirality in drug design and development. Marcel Dekker, New York
3. Crossley R (1992) The relevance of chirality to the study of biological activity. Tetrahedron 48:8155–8178
4. Guijarro A, Yus M (2009) The origins of chirality in the molecules of life. Royal Society of Chemistry, Cambridge
5. Brocks DR (2006) Drug disposition in three dimensions: an update on stereoselectivity in pharmacokinetics. Biopharm Drug Dispos 27:387–406
6. Cintas P (2007) Tracing the origins and evolution of chirality and handedness in chemical language. Angew Chem Int Ed 46:4016–4024
7. Cintas P (2004) The road to chemical names and eponyms: discovery, priority, and credit. Angew Chem Int Ed 43:5888–5894

8. Gal J (2011) Louis Pasteur, language, and molecular chirality–I. Background and dissymmetry. Chirality 23:1–16
9. Gal J (2011) Stereochemical vocabulary for structures that are chiral but not asymmetric: history, analysis, and proposal for a rational terminology. Chirality 23:647–659
10. Eliel EL (1997) Infelicitous stereochemical nomenclature. Chirality 9:428–430
11. Helmchen G (1997) Glossary of problematic terms in organic stereochemistry. Enantiomer 2:315–318
12. Eliel EL, Wilen SH (1994) Stereochemistry of organic compounds. Wiley, New York, p 1194
13. Mislow K (1999) Molecular chirality. Top Stereochem 22:1–82
14. Gal J (1998) Problems of stereochemical nomenclature and terminology. 1. The *homochiral* controversy. Its nature, origins, and a proposed solution. Enantiomer 3:263–273
15. Lee ED, Henion JD, Brunner CA, Wainer IW, Doyle TD, Gal J (1986) High-performance liquid-chromatographic chiral stationary phase-separation with filament on thermospray mass spectrometric identification of the enantiomer contaminant (*S*)-(+)-methamphetamine. Anal Chem 58:1349–1352
16. Kelvin L (1894) The molecular tactics of a crystal. The 2nd Robert Boyle lecture. J Oxford Univ Junior Sci Club 18:25
17. Kuhnert N, Le-Gresley A, Nicolau DC, Lopez-Periago A (2007) Synthesis, self-association and chiroselectivity of isotopically labeled trianglamine macrocycles in the ion trap mass spectrometer. J Label Compd Radiopharm 50:1215–1223
18. Wagner N, Rubinov B, Ashkenasy G (2011) β-Sheet-induced chirogenesis in polymerization of oligopeptides. Chemphyschem 12:2771–2780
19. Gal J (2006) Chiral drugs from a historical point of view. In: Francotte E, Lindner W (eds) Chirality in drug research. Wiley-VCH, Weinheim, pp 3–26
20. Finefield JM, Sherman DH, Kreitman M, Williams RM (2012) Enantiomeric natural products: occurrence and biogenesis. Angew Chem Int Ed 51:4802–4836
21. Burger A (1980) Introduction: history and economics of medicinal chemistry. In: Wolff ME (ed) Burger's medicinal chemistry, part I, 4th edn. Wiley, New York, pp 7–22
22. Burger A (1986) Drugs and people: Medications, their history and origins, and the way they act. University Press of Virginia, Charlottesville, p 4
23. Burger A (1986) Drugs and people: medications, their history and origins, and the way they act. University Press of Virginia, Charlottesville, pp 4–5
24. Burger A (1980) Introduction: history and economics of medicinal chemistry. In: Wolff ME (ed) Burger's medicinal chemistry, part I, 4th edn. Wiley, New York, p 8
25. Chen KK, Schmidt CF (1930) Ephedrine and related substances. Medicine (Baltimore, MD) 9:1–117
26. Hoffman BB (2001) Catecholamines, sympathomimetic drugs, and adrenergic receptor antagonists. In: Hardman JG, Limbird LE, Gilman AG (eds) Goodman and Gilman's the pharmacological basis of therapeutics, 10th edn. McGraw-Hill, New York, p 237
27. Newton GD, Pray WS, Popovich NG (2004) New OTC drugs and devices 2003: a selective review. J Am Pharm Assoc 44:211–225
28. Perrine DM (1996) The chemistry of mind-altering drugs – history, pharmacology, and cultural context. American Chemical Society, Washington, pp 44–45
29. Foye WO (1995) Medicinals of plant origins: historical aspects. In: Foye WO, Lemke TL, Williams DA (eds) Principles of medicinal chemistry, 4th edn. Lippincott Williams and Wilkins, Baltimore, p 8
30. Burger A (1986) Drugs and people: medications, their history and origins, and the way they act. University Press of Virginia, Charlottesville, p 15
31. Burger A (1980) Introduction: history and economics of medicinal chemistry. In: Wolff ME (ed) Burger's medicinal chemistry, part I, 4th edn. Wiley, New York, p 3
32. Sertürner FWA (1817) Ueber das Morphium, eine neue salzfähige Grundlage, und die Mekonsäure, als Hauptbestandtheile des Opiums. Ann Physik 55:56–89

33. Gulland JM, Robinson R (1923) Morphine group. I. Discussion of the constitutional formula. J Chem Soc 123:980–998
34. Johnson MR (1980) Analgetics. In: Wolff ME (ed) Burger's medicinal chemistry, part I, 4th edn. Wiley, New York, p 707
35. Phillips J (1912) Prevalence of the heroin habit: especially the use of the drug by snuffing. JAMA LIX:2146–2147
36. Johnson MR (1980) Analgetics. In: Wolff ME (ed) Burger's medicinal chemistry, part I, 4th edn. Wiley, New York, pp 708–709, 735
37. Eap CP, Finkbeiner T, Gastpar M, Scherbaum N, Powell K, Baumann P (1996) Replacement of (R)-methadone by a double dose of (R, S)-methadone in addicts: interindividual variability of the (R, S)-ratios and evidence of adaptive changes in methadone pharmacokinetics. Eur J Clin Pharmacol 50:385–389
38. Honigsbaum M (2001) The fever trail. In search of the cure for malaria. Farrar, Straus, and Giroux, New York, pp 24–25
39. Pelletier PJ, Caventou JB (1820) Suite: Des recherches chimiques sur les quinquinas. Ann Chim Phys 15:337–365
40. Honigsbaum M (2001) The fever trail. In search of the cure for malaria. Farrar, Straus, and Giroux, New York, pp ix–x
41. Honigsbaum M (2001) The fever trail. In search of the cure for malaria. Farrar, Straus, and Giroux, New York, pp x, xiii
42. Garfield S (2000) Mauve: how one man invented a color that changed the world. W. W. Norton & Co, New York
43. Tracy JW, Jr Webster LT (2001) Chemotherapy of parasitic infections. In: Hardman JG, Limbird LE, Gilman AG (eds) Goodman and Gilman's the pharmacological basis of therapeutics, 10th edn. McGraw-Hill, New York, p 1069
44. Seeman JI (2007) The Woodward-Doering/Rabe-Kindler total synthesis of quinine: setting the record straight. Angew Chem Int Ed 46:1378–1413
45. Woodward RB, Doering WE (1945) The total synthesis of quinine. J Am Chem Soc 67:860–865
46. Stork G, Niu D, Fujimoto A, Koft ER, Balkovec JR, Tata JR, Duke GR (2001) The first stereoselective total synthesis of quinine. J Am Chem Soc 123:3239–3242
47. Smith P (1969) Arrows of mercy. Doubleday, New York
48. Sneader W (2005) Drug discovery – a history. Wiley, New York, pp 99–100
49. Bernard C (1850) Action du curare et de la nicotine sur le système nerveux et sur le système musculaire. Compt Rend Séances Soc Biol (Paris) 2:195
50. Dale HH, Feldberg W, Vogt M (1936) Release of acetylcholine at voluntary nerve endings. J Physiol 86:353–380
51. McIntyre AR (1947) Curare. Its history, nature and clinical use. The University of Chicago Press, Chicago
52. Wintersteiner O, Dutcher JD (1943) Curare alkaloids from Chondodendron tomentosum. Science 97:467–470
53. King H (1935) Curare alkaloids. I. Tubocurarine. J Chem Soc 1381–1389
54. Weatherall M (1996) Drug treatment and the rise of pharmacology. In: Roy Porter R (ed) The Cambridge illustrated history of medicine. Cambridge University Press, Cambridge, p 256
55. Brown JH, Taylor P (2001) Muscarinic receptor antagonists. In: Hardman JG, Limbird LE, Gilman AG (eds) Goodman and Gilman's the pharmacological basis of therapeutics, 10th edn. McGraw-Hill, New York, p 164
56. Venturella VS (1985) Natural products. In: Gennaro AR (ed) Remingtons pharmaceutical sciences, 17th edn. Mack Publishing Company, Plainview, p 418
57. Eliel EL, Wilen SH (1994) Stereochemistry of organic compounds. Wiley-Interscience, New York, pp 2–4
58. Haüy R-J (1801) Traité de Minéralogie. Conseil des Mines, Paris

59. Findlay A (1948) A hundred years of chemistry, 3rd edn. Gerald Duckworth & Co Ltd, London, p 57
60. Mauskopf SH (1976) Crystals and compounds: molecular structure and composition in nineteenth-century French science. Trans Am Phil Soc 66:65
61. Pasteur L (1848) Mémoire sur la relation qui peut exister entre la forme crystalline et la composition chimique, et sur la cause de la polarisation rotatoire. C R Séances Acad Sci 26:535–538
62. Pasteur L (1850) Recherches sur les propriétés spécifiques des deux acides qui composent l'acide racémique. Ann Chim Phys, 3^{e} sér, 28:56–99
63. Delépine M (1941) Sur l'histoire de l'acide racémique et du mot racémique. Bull Soc Chim France 8:463–475
64. Biot J-B (1838) Sur l'emploie de la lumière polarisée pour manifester les differences des combinaisons isomérique. Ann Chim Phys 69:27
65. Pasteur L (1853) Notice sur l'origine de l'acide racémique. C R Séances Acad Sci 36:19–26
66. Gal J (2008) When did Louis Pasteur present his memoir on the discovery of molecular chirality to the Académie des Science? Analysis of a discrepancy. Chirality 20:1072–1084
67. Pasteur L (1922) Recherches sur la dissymétrie moléculaire des produits organiques naturels. In: Pasteur Vallery-Radot L (ed) Œuvres de Pasteur, vol 1. Masson et C^{ie}; Paris, pp 314–344
68. Pasteur L (1853) Nouvelles recherches sur les relations qui peuvent exister entre la forme crystalline, la composition chimique et le phénomène rotatoire moléculaire. Ann Chim Phys 38:437–483
69. Herschel JFW (1822) On the rotation impressed by plates of rock crystal on the planes of polarization of the rays of light, as connected with certain peculiarities of its crystallization. Trans Camb Phil Soc 1:45–100
70. Evans DS (1972) Herschel, John Frederick William. In: Gillispie CC (ed) Dictionary of scientific biography, vol VI. Charles Scribner's Sons, New York, pp 323–328
71. Schurig V (1997) On the origins of stereochemistry: the Herschel family – musicians, astronomers and natural scientists. Enantiomer 2:135–142
72. Herschel JFW (1827) Light. London, p 550 (taken from Encyclopedia Metropolitana, vol 4, 1849)
73. Chautard J (1853) Mémoire sur l'acide camphorique gauche et sur le camphre gaurche. Compt rend Acad Sci 37:166–167
74. Van't Hoff JH (1874) Sur le formules de structure dans l'espace. Arch Neerl 9:1–10
75. Le Bel JA (1874) Sur les relations qui existent entre les formules atomiques des corps organiques et le pouvoir rotatoire de leurs dissolutions. Bul Soc Chim Paris 22:337–347
76. Gal J (2008) The discovery of biological enantioselectivity: Louis Pasteur and the fermentation of tartaric acid – a review and analysis 150 years later. Chirality 20:5–19
77. Pasteur L (1857) Mémoire sur la fermentation alcoolique. C R Séances Acad Sci 45:1032–1036
78. Pasteur L (1858) Mémoire sur la fermentation de l'acide tartrique. C R Séances Acad Sci 46:615–618
79. Gal J (2007) Carl Friedrich Naumann and the introduction of *enantio* terminology: a review and analysis on the 150th anniversary. Chirality 19:89–98
80. Duclaux E (1896) Pasteur ─ Histoire d'un esprit. Masson et C^{ie}; Paris, p 63
81. Pasteur L (1922) Note relative au *Penicillium glaucum* et la dissymétrie moléculaire des produits organiques naturels. In: Pasteur Vallery-Radot L (ed) Œuvres de Pasteur, vol 2. Masson et C^{ie}, Paris, pp 129–130
82. Morley HF, Muir PMM (1892) Watt's dictionary of chemistry, vol 3. Longmans, Green, and Co, London, p 235
83. Pasteur L (1922) Transformation del l'acide tartrique en acide racémique. Découverte de l'acide tartrique inactif. Nouvelle méthode de séparation de l'acide racémique en acides tartriques droit et gauche. In: Pasteur Vallery-Radot L (ed) Œuvres de Pasteur, vol 1. Masson et C^{ie}; Paris, pp 258–262

84. Piutti A (1886) Ein neues Asparagin. Ber deutsch chem Ges 19:1691–1695
85. Gal J (2012) The discovery of stereoselectivity at biological receptors: Arnaldo Piutti and the taste of the asparagine enantiomers – history and analysis on the 125th anniversary. Chirality. doi:10.1002/chir
86. Prüll C-R, Maehle A-H, Halliwell RF (2009) A short history of the drug receptor concept. Palgrave MacMillan, Basingstoke, p 1
87. Ehrlich P, Morgenroth J (1900) Ueber Haemolysine. Dritte Mittheilung. Berliner klin Wochenschrift 37:453–458
88. Langley JN (1905) On the reaction of cells and nerve-endings to certain poisons, chiefly as regards the reaction of striated muscle to nicotine and to curare. J Physiol 33:374–413
89. Vickery H, Schmidt CLA (1931) The history of the discovery of the amino acids. Chem Rev 9:169–318
90. Vauquelin LN, Robiquet PJ (1806) La découverte d'un nouveau principe végétal dans le suc des asperges. Ann Chim 57:88–93
91. Piutti A (1888) Sintesi e costituzione delle asparagine. Gazz Chim Ital 18:457–472
92. Pringsheim H (1910) Notiz über das Vorkommen von Rechts-Asparagin in der Natur. Z Physiol Chem 65:89–95
93. Piutti A (1923) The simultaneous existence of optically active asparagines in germinated lupines. Atti congresso naz chim pura applicata 1923:384–386
94. Greenstein JP, Winitz M (1961) The chemistry of the amino acids, vol 3. Wiley, New York, p 1860
95. Fajans K (1910) Über die stereochemische Spezifizität der Katalysatoren (Optische Aktivierung durch asymmetrische Katalyse). Z physik Chem 73:25–96
96. Hirsch P (1918) Die Einwirkung von Mikroorganismen auf die Eiweiβkörper. Gebrüder Borntraeger, Berlin, pp 68–77
97. Cushny AR (1926) Biological relations of optically isomeric substances. The Williams and Wilkins Company, Baltimore, pp 18–37
98. Brockmann H (1933) Das biologische Verhalten stereoisomerer Verbindungen. In: Freudenberg K (ed) Stereochemie: eine Zusammenfassung der Ergebnisse, Grundlagen, und Probleme. Franz Deuticke, Leipzig, pp 921–961
99. Fischer E (1898) Bedeuting der Stereochemie für die Physiologie. Hoppe-Seyler's Z Physiol Chem 26:60–87
100. Dakin H (1904) The hydrolysis of optically inactive esters by means of enzymes. I. The action of lipase on esters of mandelic acid. The resolution of inactive mandelic acid. J Physiol 30:253–263
101. Brockmann H (1933) Das biologische Verhalten stereoisomerer Verbindungen. In: Freudenberg K (ed) Stereochemie: eine Zusammenfassung der Ergebnisse, Grundlagen, und Probleme. Franz Deuticke, Leipzig, pp 928–930
102. Farber E (1972) Fischer, Emil Hermann. Dictionary of scientific biography, vol 5. Charles Scribner's Sons, New York, pp 1–5
103. Lichtenthaler FW (1992) Emil Fischer's proof of the configuration of sugars. A centennial tribute. Angew Chem Int Ed 31:1541–1546
104. Kagan H, Gopalaiah K (2011) Early history of asymmetric synthesis: who are the scientists who set up the basic principles and the first experiments? New J Chem 35:1933–1937
105. Fischer E (1894) Einfluss der Konfiguration auf der Wirkung der Enzyme. Ber dtsch chem Ges 27:2985–2993
106. Fischer E (1891) Ueber die Configuration des Traubezuckers und seiner Isomeren. Ber dtsch chem Ges 24:1836–1845
107. Ramberg PJ (2003) Chemical structure, spatial arrangement. The early history of stereochemistry, 1874–1914. Ashgate Publishing Company, Burlington, p 275
108. http://www.nobelprize.org/nobel_prizes/chemistry/laureates/1902/press.html
109. Cushny AR (1926) Biological relations of optically isomeric substances. The Williams and Wilkins Company, Baltimore, pp 29–37

110. Hudson CS (1948) Historical aspects of Fischer's fundamental conventions for writing stereoformulas in a plane. Adv Carbohydr Chem 3:1–22
111. Cushny AR (1926) Biological relations of optically isomeric substances. The Williams and Wilkins Company, Baltimore, p 29
112. Menozzi A, Appiani G (1894) Derivatives of glutamic acid. Pyroglutamic acids and pyroglutamides. Gazz Chim Ital 24:370–391
113. Cushny AR (1920) On optical isomers. V. The tropeines. J Pharmacol 15:105–127
114. Cushny AR (1909) Further note on adrenalin isomers. J Physiol 38:259–262
115. Cushny AR (1926) Biological relations of optically isomeric substances. The Williams and Wilkins Company, Baltimore
116. Clement EM, Grahame-Smith D, Elliott JM (1998) Investigation of the presynaptic effects of quinine and quinidine on the release and uptake of monoamines in rat brain tissue. Neuropharmacology 37:945–951
117. Pasteur L (1853) Recherches sur les alcaloïdes des quinquinas. C R Séances Acad Sci 37:110–114
118. Karle JM, Karle IL, Gerena L, Milhous WK (1992) Stereochemical evaluation of the relative activities of the cinchona alkaloids against Plasmodium falciparum. Antimicrob Agents Chemother 36:1538–1544
119. Caner H, Biedermann PU, Agranat I (2003) Conformational spaces of Cinchona alkaloids. Chirality 15:637–645
120. Levy S, Azoulay S (1994) Stories about the origin of quinquina and quinidine. J Cardiovasc Electrophysiol 5:635–636
121. Deschamps PN (1922) La médication quinique et quinidique du coeur: Étude de l'action physiologique de la quinine et de la quinidine sur l'appareil circulatoire, et de leur emploi thérapeutique au cours des arythmies, et particulièrement au cours de l'arythmie complète. A Maloine, Paris
122. Zarbl E, Laemmerhofer M, Woschek A, Hammerschmidt F, Parenti C, Cannazza G, Lindner W (2005) Strong versus weak chiral cation exchangers: comparative evaluation for enantiomer separation of chiral bases by non-aqueous CEC. J Sep Sci 25:1269–1283
123. Hedman A, Meijer DKF (1998) The stereoisomers quinine and quinidine exhibit a marked stereoselectivity in the inhibition of hepatobiliary transport of cardiac glycosides. J Hepatol 28:240–249
124. Muralidharan G, Hawes E, Mckay G, Korchinski E, Midha K (1991) Quinidine but not quinine inhibits in man the oxidative metabolic routes of methoxyphenamine which involve debrisoquine 4-hydroxylase. Eur J Clin Pharmacol 41:471–474
125. Hsueh C, Marvel CS (1928) Optically active hypnotics. J Am Chem Soc 50:855–859
126. Maher TJ (2008) General anesthetics. In: Lemke TL, Williams DA, Roche VF, Zito SW (eds) Foye's principles of medicinal chemistry, 6th edn. Lippincott Williams & Wilkins, Baltimore, pp 493–494
127. Christensen HD, Lee IS (1973) Anesthetic potency and acute toxicity of optically active disubstituted barbituric acids. Toxicol Appl Pharmacol 26:495–503
128. Haley TJ, Gidley JT (1976) Pharmacological comparison of R(+), S(−) and racemic thiopentone in mice. Eur J Pharmacol 36:211–214
129. Yamakura T, Bertaccini E, Trudell JR, Harris RA (2001) Anesthetics and ion channels: molecular models and sites of action. Annu Rev Pharmacol Toxicol 41:23–51
130. Andrews PR, Mark LC (1982) Structural specificity for barbiturates and related drugs. Anesthesiology 57:314–320
131. Pfeiffer CC (1956) Optical isomerism and pharmacological action, a generalization. Science 124:29–31
132. Ariëns EJ (1983) Stereoselectivity of bioactive agents: general aspects. In: Ariëns EJ, Soudijn W, Timmermans PBMWM (eds) Stereochemistry and biological activity of drugs. Blackwell Scientific Publications, Oxford, pp 27–31

133. Parascandola J (1981) The theoretical basis of Paul Ehrlich's chemotherapy. J Hist Med 36:19–43
134. Lillie FR (1914) Studies of fertilization. VI. The mechanism of fertilizations in arbacia. J Exp Zool 16:523–590
135. Fruton JS (1999) Proteins, enzymes, genes – the interplay of chemistry and biology. Yale University Press, New Haven, p 152
136. Easson L, Stedman E (1933) Studies on the relationship between chemical constitution and physiological action. V. Molecular dissymmetry and physiological activity. Biochem J 27:1257–1266
137. Davankov V (1989) Introduction to chromatographic resolution of enantiomers. In: Krstulovic AM (ed) Chiral separations by HPLC. Ellis Horwood, Chichester, pp 183–186
138. Bergmann M, Zervas L, Fruton JS, Schneider F, Schleich H (1935) On proteolytic enzymes V. On the specificity of dipeptidase. J Biol Chem 109:325–346
139. Ogston AG (1948) Interpretation of experiments on metabolic processes, using isotopic tracer elements. Nature 162:963
140. Eliel EL, Wilen SH (1994) Stereochemistry of organic compounds. Wiley-Interscience, New York, p 1198
141. Ruffolo RR Jr (1983) Stereoselectivity in adrenergic agonists and adrenergic blocking agents. In: Ariëns EJ, Soudijn W, Timmermans PBMWM (eds) Stereochemistry and biological activity of drugs. Blackwell Scientific Publications, Oxford, pp 104–115
142. Mesecar AD, Koshland DE (2000) Structural biology – a new model for protein stereospecificity. Nature 403:614–615
143. Bentley R (1983) Three-point attachment: past, present, but no future. Trans N Y Acad Sci II 41:5–24
144. Topiol S (1989) A general criterion for molecular recognition: implication for chiral interactions. Chirality 1:69–79
145. Anonymous (1992) Fed Reg 5(102):22249
146. Caldwell J, Hutt AJ, Fournel-Gigleux S (1988) The metabolic chiral inversion and dispositional enantioselectivity of the 2-arylpropionic acids and their biological consequences. Biochem Pharmacol 37:105–114
147. Yun EM, Meadows W, Santos AC (1998) New amide local anaesthetics for obstetric use. Baillieres Clin Obstet Gynaecol 12:461–471
148. Shah RR, Midgley JM, Branch SK (1998) Stereochemical origin of some clinically significant drug safety concerns: lessons for future drug development. Adverse Drug React Toxicol Rev 17:145–190

Top Curr Chem (2013) 333: 41–82
DOI: 10.1007/128_2012_367

Published online: 14 September 2012

Synthesis and Chirality of Amino Acids Under Interstellar Conditions

Chaitanya Giri, Fred Goesmann, Cornelia Meinert, Amanda C. Evans, and Uwe J. Meierhenrich

Please note the erratum to this chapter at the end of the book.

Abstract Amino acids are the fundamental building blocks of proteins, the biomolecules that provide cellular structure and function in all living organisms. A majority of amino acids utilized within living systems possess pre-specified orientation geometry (chirality); however the original source for this specific orientation remains uncertain. In order to trace the chemical evolution of life, an appreciation of the synthetic and evolutional origins of the first chiral amino acids must first be gained. Given that the amino acids in our universe are likely to have been synthesized in molecular clouds in interstellar space, it is necessary to understand where and how the first synthesis might have occurred. The asymmetry of the original amino acid synthesis was probably the result of exposure to chiral photons in the form of circularly polarized light (CPL), which has been detected in interstellar molecular clouds. This chirality transfer event, from photons to amino acids, has been successfully recreated experimentally and is likely a combination of both asymmetric synthesis and enantioselective photolysis. A series of innovative

C. Giri
Max Planck Institute for Solar System Research, Max-Planck-Str. 2, 37191 Katlenburg-Lindau, Germany

Institut de Chimie de Nice, University of Nice-Sophia Antipolis, UMR 7272 CNRS, 28 Avenue Valrose, 06108 Nice Cedex 2, France

F. Goesmann
Max Planck Institute for Solar System Research, Max-Planck-Str. 2, 37191 Katlenburg-Lindau, Germany

C. Meinert and U.J. Meierhenrich (✉)
Institut de Chimie de Nice, University of Nice-Sophia Antipolis, UMR 7272 CNRS, 28 Avenue Valrose, 06108 Nice Cedex 2, France
e-mail: Uwe.Meierhenrich@unice.fr

A.C. Evans
Institut de Chimie de Nice, University of Nice-Sophia Antipolis, UMR 7272 CNRS, 28 Avenue Valrose, 06108 Nice Cedex 2, France

University of Cambridge, Murray Edwards College, Cambridge CB3 0DF, UK

studies have reported successful simulation of these environments and afforded production of chiral amino acids under realistic circumstellar and interstellar conditions: irradiation of interstellar ice analogues (CO, CO_2, NH_3, CH_3OH, and H_2O) with circularly polarized ultraviolet photons at low temperatures does result in enantiomer enriched amino acid structures (up to 1.3% ee). This topical review summarizes current knowledge and recent discoveries about the simulated interstellar environments within which amino acids were probably formed. A synopsis of the COSAC experiment onboard the ESA cometary mission ROSETTA concludes this review: the ROSETTA mission will soft-land on the nucleus of the comet 67P/Churyumov-Gerasimenko in November 2014, anticipating the first in situ detection of asymmetric organic molecules in cometary ices.

Keywords Amino acids · Chirality · Churyumov-Gerasimenko · Circularly polarized radiation · COSAC · GC–MS · Molecular clouds · PHILAE · ROSETTA

Contents

Abbreviations

Amu	Atomic mass unit
AU	Astronomical unit
A_V	Total visual extinction
DMF–DMA	Dimethylformamide–dimethylacetal

ECEE	*N*,*N*-ethoxycarbonyl ethyl ester
Kpc	Distance in kiloparsecs
$M_{\odot}$ pc^{-2} Gyr^{-1}	Mass loss rate per square parsec per gigayear
$M_{\odot}$ yr^{-1}	Mass loss rate
$n(H_2)$ yr	Accretion rate of hydrogen molecule
n_H	Condensate density
NIR	Near infrared
pcs	Parsecs
UV	Ultraviolet

1 Introduction to Interstellar Space

The universe is a boundless expanse inclusive of matter, energy, and the physical entities embodying them: cosmic dust, molecular clouds, stars, planets, nebulae, and the physicochemical signaling and self-replicating process known as life.

In terms of vastness of celestial bodies, galaxies are colossal clusters of millions of stars and their associated planets, asteroids, comets, icy bodies, and interstellar media (ISM). It is difficult to comprehend simultaneously every phenomenon concurrently occurring within such vast galactic systems. The interstellar medium (ISM) within a galaxy is defined as the portion of the galaxy where no stars and planets exist apart from matter and cosmic radiation. The chemistry that occurs in interstellar regions of different galaxies, and even within the same galaxy, can be highly diverse due to the variety of different environments in terms of the densities, temperatures, and masses of the systems involved. In this topical review we will focus on the ongoing interstellar chemistry towards the formation of prebiotic molecules, the origins of their stereochemistry, and thus the potential molecular origins of today's homochiral evolving life systems.

1.1 Interstellar Medium

A star system identical to our solar system would include a star, planets revolving around it in their orbits, asteroids, interplanetary dust, and icy bodies. Beyond the sphere of influence of any star, known as the heliosphere, exists the ISM. The term "interstellar" refers to any object occupying the space that exists between two or more stars. The interstellar boundary of our solar system is a region within the heliosphere where solar wind speeds decline from supersonic to subsonic levels due to an interfacing with the immediate ISM – this phenomenon is called termination shock [1]. Interstellar space exists beyond this termination shock. The ISM is consequently indigenous and beyond the physical influence of the heliosphere.

The ISM is primarily composed of particulate dust, hydrogen, helium, and heavier elements which are present in ionized, non-ionized, molecular gaseous

Table 1 Elemental abundance in interstellar medium [4]

Elements	Abundance by number (%)	Abundance by mass (%)
Hydrogen	90.8	70.4
Helium	9.18	28.1
Heavier elements (metals)	0.12	1.5

Table 2 Temperature-density values of neutral medium [2]

Medium	Temperature (K)	Density (cm^{-3})
WNM	8,000	0.5
CNM	80	50

phases or in solid-states [2]. The density of these various states ranges from ~1.5×10^{-26} g/cm^3 in hot medium to ~2×10^{-19} g/cm^3 in dense molecular clouds [3]. The elemental composition of the ISM is comparable to the cosmic elemental composition; this is contingent upon the abundance measurements of these elements in disk-like stars, sun, and meteorites. Hydrogen is the most abundant element in the ISM followed by helium and other heavier elements (Table 1) [4].

One possible justification for the low abundances of heavier elements seen to be present in the ISM can be inferred from the interstellar absorption lines observed in the far-ultraviolet spectra of hot stars. A large fraction of heavier elements are depleted from the ISM but might be captured and accumulated by the interstellar dust (ISD) grains [5]. Commonly detected Period Two elements like C, O, and N have been observed to be depleted by an average factor of ~1.2–3, while heavier elements resistant to very high temperatures, such as Fe, Si, and Mg, are depleted by an average factor of ~10–100 from the ISM. These observations indicated that although ISD comprises 0.5–1% of the total interstellar mass, it could well play a pivotal role in dictating the dynamic chemical composition of the ISM [6].

1.2 Objects in ISM

The majority of the ISM exists in the gaseous phase. Various gases tend to accumulate within regions of ISM as ionized, neutral, or molecular clouds, depending on their constituent expanse, temperature, and density (Table 2). Hydrogen, the most abundant element in the universe, is found in gaseous neutral state, gaseous ionized state, or in molecular gaseous form within these clouds. The objects/clouds formed from each of these three compositions respectively are known as H I cloud regions, H II cloud regions, and molecular clouds. The H I and H II cloud regions are also referred to as diffuse clouds, while molecular clouds are also known as dense clouds.

1.2.1 H I Regions

Due to the low density of hydrogen in some regions of ISM, particle collision frequency is correspondingly low; hence most hydrogen atoms in these low density regions exist in ground state electronic level, $n = 1$. These low density regions are called H I cloud regions. It is difficult to observe H I regions at visual light wavelengths but it is relatively easy to observe them in the UV and it is also possible to visualize characteristic optical absorption lines of metallic elements in the field of view of bright background stars. The neutral hydrogen extant in H I regions is commonly observed by radio telescopes using an H 21 cm absorption line. Temperature and density are interdependent in these H I regions (Table 2) and are observed in the form of both the diffuse cold neutral medium (CNM) and the less dense warm neutral medium (WNM) [2].

1.2.2 H II Regions

In these larger, low-density cloud regions the formation of massive and extremely luminous stars, being bluish in appearance, has recently occurred. The so-called O-type and B-type main sequence stars are the largest and hottest of this type of luminous stars known to exist in the Milky Way Galaxy. These blue giants emit highly energetic UV radiation below 912 Å (corresponding to an energy input of 13.6 eV) that is strong enough to ionize neutral gases such as hydrogen. The hydrogen atoms in these H II regions are therefore almost fully ionized but their thermal electrons and protons readily recombine and are then reionized by the emitted UV radiation. The degree of hydrogen ionization remaining in equilibrium state in these regions is affected by variations in UV ionization and subsequent recombination. Any superfluous radiation that is not used by the system for ionization is then converted by thermally-excited electrons into kinetic energy. The density of H II cloud regions ranges between 1 and 10^5 atoms/cm^3 and the temperature is 10^4 K: thus these regions are denser and thermally more active than the H I regions [3]. H II regions exhibit diverse morphologies from filamentous (e.g., Cygnus nebula) to clump-like (e.g., Carina nebula, Fig. 1), owing to large density gradients within their structures.

1.2.3 Molecular Clouds

Molecular clouds are large dense clouds within which a variety of molecules are known to be generated, particularly molecular hydrogen (H_2). Shock waves due to supernovae, collisions between clouds, and magnetic interactions can all trigger the collapse of portions of the molecular cloud and subsequently lead to star formation. It is difficult to probe the dense dusty interiors of these molecular clouds using optical and UV absorption lines. Radio waves provide an alternative method for

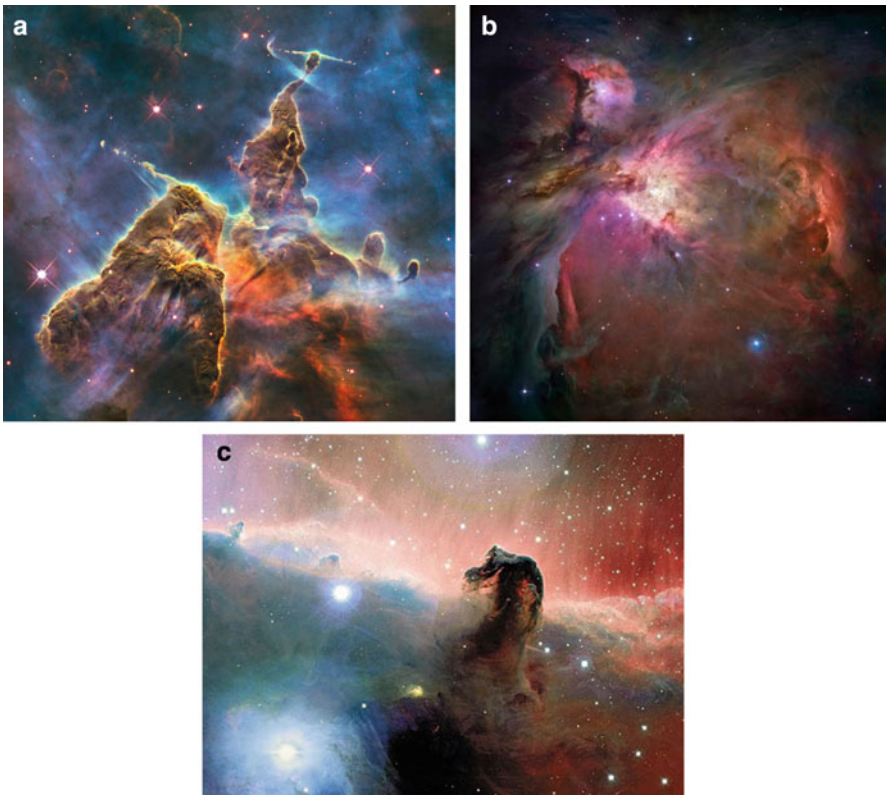

Fig. 1 (**a**) Optical image of a stellar nursery pillar from Carina Nebula taken from the NASA/ESA Hubble's Space Telescope. The Carina Nebula is located 7,500 light years away from Earth in the constellation Carina. The pillar observed above is approximately 3 light years tall and consists of densely packed gases and dust [image credits: NASA, ESA, M. Livio and the Hubble twentieth Anniversary Team (STScI)]. (**b**) Optical image of the Orion Nebula taken from the NASA/ESA Hubble's Space Telescope. The Orion Nebula is 1,500 light years away from the Earth and is the nearest star formation region to our solar system [image credits: NASA, ESA, M. Robberto (Space Telescope Science Institute/ESA) and the Hubble Space Telescope Orion Treasury Project Team]. (**c**) Representative-color image of the Horsehead Nebula taken from the Canada–France–Hawaii Telescope (CFHT) in Hawaii. The Horsehead Nebula is entrenched in the enormous Orion Nebula. It is a dark molecular cloud of dust that is particularly visible due to a brighter background creating a silhouette. The distinct horsehead structure is an extension of a large, dark and dusty molecular cloud [image credits: Jean-Charles Cuillandre (CFHT), Hawaiian Starlight, CFHT]

chemically characterizing the contents of these dense cloud regions as they are able to penetrate these dense clouds without extinction. This discovery has led to wide applications of radio spectroscopy in astronomy.

Stable H_2 molecules possess no electric dipole moments and have negligible moments of inertia: their permitted transitions lie outside the radio domain of the electromagnetic spectrum and hence H_2 is not directly observed at radio wavelengths [7]. Another molecule commonly found in these molecular cloud

regions, carbon monoxide (CO), is therefore used by astronomers as a primary tracer molecule for interstellar molecular clouds [8]. CO is easy to trace using radio spectroscopy due to its rotational transition of $J = 1 \rightarrow 0$ at radio wavelengths of 2.6 mm and also possesses a strong electric dipole moment [9]. The dense packing of matter within molecular cloud regions can lead to extensive gas-phase chemistry driven by the cosmic ray ionization that can penetrate within the cloud. Molecular clouds have cooler temperatures (10 K) than H I and H II regions, and this characteristic serves to enhance molecular accretion onto ISD grains and the formation of icy mantles on the surfaces of ISD grains. Such enhanced gas–grain interactions can result in a greater diversity of chemical species that can exist in these clouds.

2 Origin and Abundance of Organics in Interstellar Space

Interstellar space contains an abundant collection of dispersed organic compounds. Observations at infrared, radio, millimeter, and sub-millimeter frequencies have detected more than 160 different molecular species in both gas and condensed phases in star-forming regions [10, 11]. These comprise both simple and complex species and stable or transient molecules. In addition to large abundances of H_2 and He, a host of other molecules (nitriles, aldehydes, alcohols, acids, ethers, ketones, amines, amides, long-chain hydrocarbons) have been identified in the ISM. These more complex organic molecules that pervade interstellar clouds constitute an important fraction of the available carbon in the universe. Some of these organics are considered to be fundamental precursor molecules of the basic building blocks for carbon-based cellular life on Earth. However, an understanding of how basic building blocks evolve into the complex self-replicating organic systems remains elusive [12, 13]. Additionally, the events that originally resulted in the exogenous delivery of organic matter to Earth in terms of time and volume have yet to be elucidated.

2.1 Origin of Carbon–Carbon Stars

The origin of organic molecules in the universe is directly linked to the origin of carbon in the universe. Carbon is the sixth most abundant element in the universe [14]. The origin of carbon itself can be traced to the fusion reactions that are known to occur within stellar interiors – the products of these fusion reactions are believed to be ejected into far away interstellar space during stellar collapse and supernova bursts. This mechanism is conceivable as it can both generate and disperses stellar material. However, there is another major source of carbon production in the universe – carbon stars.

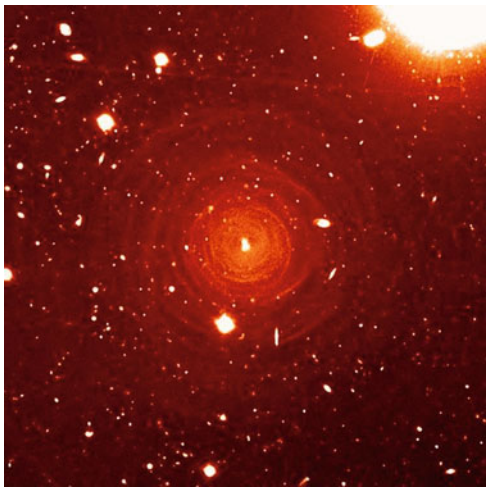

Fig. 2 Optical image of carbon star IRC +10216 taken from Focal Reducer and low dispersion Spectrograph (FORS1) on the Very Large Telescope of European Space Observatory. The concentric layers around the central star form the dusty astrosphere of IRC +10216. The astrosphere radius is approximately 84,000 AU and is a distinct source of organic molecules and dust [20, 21] (image credits: Izan Leao, Universidade Federal do Rio Grande do Norte, Brazil)

Classical carbon stars are late-type stars similar to red giants. They have a carbon/oxygen (C/O) ratio greater than unity that is characterized by an exceptionally strong C_2 absorption band in addition to CN and CH absorption bands. The high C/O ratio at the surface of these red giants can be due to CNO processing, helium-core flash, or helium shell flash. As carbon stars are main-sequence stars, they eject large quantities of surface matter slowly into space [15].

IRC +10216 is the closest carbon star to Earth: it is located at a distance of 120–250 pcs within the Milky Way Galaxy [16–19] and was first discovered by Eric Becklin and his team while using the Caltech Infrared Telescope at the Mount Wilson Observatory in 1969 (Fig. 2) [18]. The Herschel Space Observatory instrument HIFI has measured a mass loss rate of $4.0 \times 10^{-8}\ M_{\odot}\ \mathrm{yr}^{-1}$ from IRC +10216 [22]. This mass-loss suggests an interesting reason for the observed sooty appearance of the regions surrounding around carbon stars. Within the optically thick and dusty astrosphere of IRC +10216, more than 70 different chemical species have been detected. The Sub-millimeter Wave Astronomy Satellite – a NASA project studying the chemical composition of interstellar gas clouds – has also detected circumstellar water vapor in the astrosphere of IRC +10216. These observed water vapor spectral lines have been detected in a highly excited state, which indicates the presence of much warmer water molecules at temperatures of 1,000 K [23].

Carbon is observed to be the main constituent of ISD grains, which will be discussed in detail in Sect. 3 of this review. In 1969, Gilman suggested that graphite, an allotrope of carbon, should be the first species to condense from low-temperature carbon-rich gas into ISD grains [19]. Once formed, these ISD grains are capable of accreting molecules in the gas phase on their surfaces to form surrounding mantles of organic ices. Numerous dust species of this nature have been detected in the astrosphere of IRC +10216. It is currently thought that these ISD grains might act as reactive surfaces for driving solid phase organic chemistry in interstellar space.

Table 3 Inventory of astrosphere of carbon star IRC +10216

Chemical functional group	Chemical species	References
Cyanopolyynes	HC_3N, HC_5N, HC_7N, HC_9N, $HC_{11}N$	[25]
Acetylenic compounds	C_2H, C_3H, C_4H, C_5H, C_6H	[26]
Carbenes	H_2CCC, H_2CCCC	[27]
Carbon chain molecules	C_2, C_3, C_5, C_3N	[28]
Simple organics	HCN, CN, C_2H_2, CH_4, C_2H_4, CH_3CN, HC_2N	[21]

2.2 *Interstellar Dispersion and Abundance of Organic Molecules*

Carbon is mainly present in interstellar space in the form of CO, which is commonly used by astronomers as a primary tracer for molecular clouds within the ISM. The next most abundant carbon-containing molecule observed is acetylene. As CO is less reactive and more stable than acetylene, it is generally assumed that complex interstellar organic chemistry usually utilizes acetylene as a primary substrate [24]. The astrosphere of the carbon star IRC +10216 has been propagating at a speed of $\geq$91 km/s over the past 69,000 years and current predictions estimate the radius of its astrosphere to be 84,000 AU [20]. These data suggest that a carbon star could be a dominant source of organic species and possibly possess the ability to disperse these organic species into distant interstellar space in a non-destructive manner (Table 3).

In addition to having been observed in the nebulae formed around carbon stars, organics are observed in the various interstellar cloud structures. These clouds are characterized by their visual extinction into three individual cloud groups: diffuse clouds ($A_V \leq 1$ mag), dense clouds ($A_V > 5$ mag), and translucent clouds (1 mag $\leq A_V \leq 5$ mag) [29].

As already outlined in Sect. 1.2.3, dense molecular clouds are considered to be the stellar nurseries of the universe and are abundant in both organic molecular species and ISD grains. The density of these clouds results from the gravity exerted by constituent cloud matter that acts inwardly upon the cloud structure. The high density and low temperatures of these molecular clouds assist in promoting molecular synthesis on the ISD grain surfaces.

Dense clouds can be further broken down into three sub-regions in which distinct chemical processes occur [30, 31]. In one type of sub-region, organic molecules are generated within the condensed phase existing on ISD grain substrates. At low temperatures these dust grains thus acquire an icy mantle of molecules that have accreted from the gaseous phase. Interaction with interstellar radiation can activate numerous chemical processes that subsequently yield organic molecules, depending on the energy of the radiation and the system itself [30, 31].

In another type of sub-region of dense molecular clouds, ISD grains tend to shield interior regions that are largely made up of gaseous matter; radiation thus does not reach these gaseous shielded inner regions. However the ISD grains here permit penetration of low intensity cosmic rays that can initiate and drive ion-rich molecular reactions along with neutral molecule processes that are known to result in the formation of a number of organic species [32].

A third typology of dense cloud sub-regions is known as "hot molecular cores" – these are cloud regions of high temperature in which sputtering and evaporation of icy grain mantles have recently occurred [33]. Due to their highly thermodynamic natures, these regions are rich with the synthesis of organic molecules of diverse complexity.

3 The Requisite for a Substrate: Interstellar Dust

Robert J. Trumpler was a prominent Swiss-American astronomer of the early twentieth century. He was interested in observing galactic open clusters – a group of co-evolved stars formed from the same parent molecular cloud. He observed that remote galactic open clusters appear to be roughly twice the size of closer ones. Failing to find an observational inaccuracy he assumed that this size difference could be due to the existence of an unknown absorbing medium extant between the galactic open clusters and the observer on Earth. Trumpler also assumed that the quantity of absorbing medium would increase with distance from the observer, thereby causing more distant open clusters to appear dimmer and resulting in an overestimation of their size and distance. He later calculated that the luminosity of a star is decreased by this absorbing medium by a factor of 1.208 for every 1,000 light-years the starlight travels toward Earth [34]. This absorbing medium that Trumpler postulated was later found to be ISD.

ISD is a fundamental substrate for the synthesis of complex molecules in interstellar space. The low temperatures (~3–90 K) and densities (~10^6 H atoms/cm^3) observed in dense molecular clouds favor the condensation of volatile molecules from the gas phase onto the surface of ISD grains and thus lead to diverse molecular products. Of these molecular products, the formation of amino acids and the chemical processes involved in their interstellar synthesis are of primary importance for the purposes of this review. Amino acids are the basic building blocks used for the majority of life's structural and functional processes and are therefore considered to be key prebiotic molecules.

There are a number of important factors necessary for the generation of amino acids onto ISD grain surfaces. These are: (1) the source of ISD; (2) the density and diversity of volatile molecules present in the icy mantle; (3) the radiation dosage to which the icy mantle surface of the ISD grain is exposed; (4) the evolutionary lifespan of the organic icy mantle on the ISD grain.

3.1 Sources of ISD

It is commonly said that "we are all made of stardust." This statement may be spiritually inspiring but provides very little scope for understanding the origin of ISD in the universe. Stars late in their lives do donate their innate matter into space

Fig. 3 Infrared image of Cassiopeia A taken by Spitzer Space Telescope. The region in *blue* contains matter expelled during the supernova explosion and energized by a forward shock wave; this region is now composed of stars born from this matter (see *blue dots*). The regions of *red*, *green*, and *yellow* contain the same matter which is heated by a reverse shock wave (image credits: NASA/ JPL-Caltech/Rudnick L, University of Minnesota, USA)

either tranquilly or destructively, but this material donation does not itself constitute the only source of ISD.

Cosmic dust is a collective term for dust present in interplanetary, interstellar, and intergalactic space. However, the amorphous silicate and carbon-based submicron-sized dust grains in the above three dimensions vary depending on their origin, chemical composition, and morphology. ISD is believed to act as a substrate for a wide variety of gas-grain chemical reactions. It is thus also known to influence the chemical, thermal, and ionization states of matter actively participating in the chemical evolution of the universe. Mass loss from the evolved stars in the asymptotic giant branch (AGB) phase is one of the main sources of ISD grains. These evolved stars of intermediate mass emit dust at a rate of 5.3×10^{-3} to 6.5×10^{-3} $M_{\odot}$ pc^{-2} Gyr^{-1} [35]. The chemical composition of the ISD grains produced depends upon the type of the giant star producing them, and these composition differences are usually observed with reference to C/O ratios. Oxygen rich M-type giants have C/O ratios less than unity, whereas carbon-rich C-type stars have a C/O ratio greater than unity and are thus much more likely to be producing ISD [36]. The carbon-rich Mira type star IRC +10216 has proven itself capable of ejecting carbon-rich dust over quite a long span of time – 4.0×10^{-8} $M_{\odot}$ yr^{-1} [22]. Such a long, gradual, and non-destructive dust emission process can ensure the transportation of ISD over vast distances (~84,000 AU in this instance) [20].

Another common source of ISD is the rapid breakdown and violent explosion of the massive stars known as type II supernovae. Vast amounts of dust, as much as ~2–4 $M_{\odot}$, have been observed in the galactic supernova remnant Cassiopeia A (Fig. 3) and have also been detected using the SCUBA array on the James Clerk Maxwell Telescope in Hawaii. These type II supernovae explosions can contribute significantly to the dust inventory of a galaxy with an estimated dust production rate of 7–18 $\times 10^{-3}$ $M_{\odot}$ yr^{-1} [37], relative to stellar production rates of ~5 $\times 10^{-3}$ $M_{\odot}$ yr^{-1} [38].

3.2 Density and Diversity of Molecules

It has often been observed that after dense molecular clouds are formed, the physical conditions within them become more favorable for the production of complex molecular species in the gas phase relative to the conditions present in the diffuse ISM. Additionally, due to the low temperatures present within dense molecular clouds (~20 K), any polyatomic molecules bombarding the dust grains inside them tend to condense on the grain surfaces [39]. The accretion of simple polyatomic molecules on the ISD grain surface can lead to the formation of an icy mantle. This condensed mantle of accreted molecules is a chemically active region that can support numerous ionic and radical reaction processes within it. A large portion of this complex solid-state chemistry is driven by cosmic radiation, stellar shock waves, thermal stimulation, and UV photons (Fig. 4). Hydrogen also tends to play a key role in enhancing the molecular diversity present on grain surfaces [40]. This overall enhanced degree of reactivity within the mantle could be responsible for the observed abundance of simple interstellar polyatomic molecules in the condensed phase as compared to their gas phase counterparts within these cloud regions (Table 4).

As the most abundant element within the icy mantle (followed by carbon, nitrogen, and oxygen), hydrogen regulates gas-grain chemistry in a manner based upon the H/H_2 ratios present in the gas. Regions with greater H/H_2 ratios yield hydrogenated/reduced species like NH_3, CH_4, and H_2O, forming a hydrogen-rich polar mantle. Regions with lower H/H_2 ratio yield species like N_2, O_2, CO_2, and CO, subsequently forming a more hydrogen-deficient, oxidized non-polar mantle [48].

During the gradual warm up in regions of massive star formation known as hot cores, where temperatures can rise to 200 K, the more strongly bound heavy radicals can become mobile on grain surfaces: this is thought to be the most crucial step for the formation of complex organic molecules within the mantle [49]. Ice evaporation in these hot, dense regions enriches the gas phase abundances of molecules, and the formation of many hot-core molecules has been attributed to this [50]. It is assumed that thermo-chemical processes occurring within the ice layers accreted on inorganic dust particles may also form a macromolecular organic residue that contains amino acid precursor structures.

3.3 Radiation Dosage on the Icy Grain Mantle Surface

Interstellar grains are produced and evolve under continual exposure to cosmic radiation. The radiation dosage to which the surface of ISD grains is exposed depends upon surrounding interstellar environments. The ISD grains found within the interiors of dense clouds are protected from intense galactic cosmic radiation by the outer cloud structure but are exposed to more deeply penetrating UV/IR

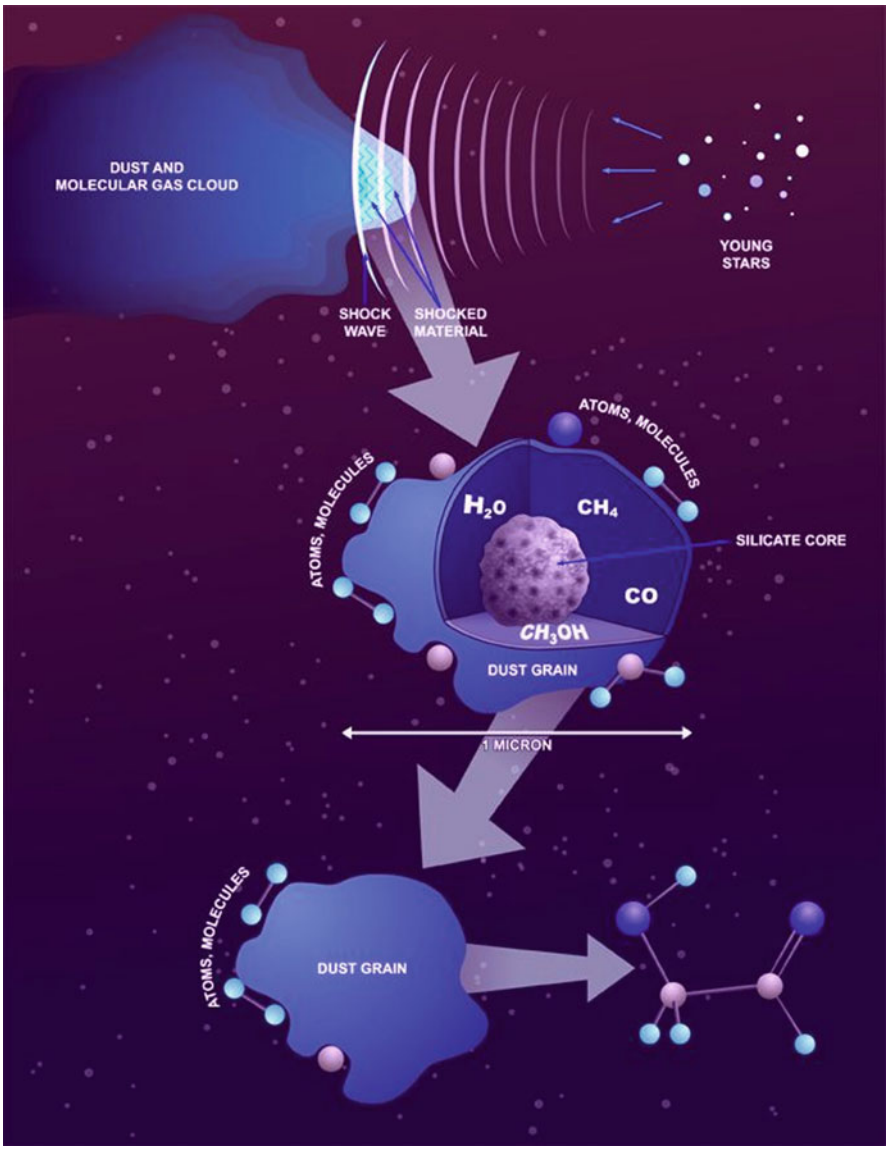

Fig. 4 Artistic impression of the synthesis of complex organic molecules on an interstellar dust grain surface. Young stars emit radiation and shock waves to liberate matter from molecular clouds. These molecular clouds are usually composed of dust and simple polyatomic molecules. At very low temperatures, simple molecules tend to accrete on the grain surface and develop into an icy mantle. The development of an icy mantle occurs at the same time that the IDPs are exposed to the radiation and stellar shock waves that ultimately assist in the interstellar synthesis of complex organic molecules (image credits: Bill Saxton, NRAO/AUI/NSF)

Table 4 Comparison between condensed and gas phase abundances of polyatomic molecules[a,b,c]

	Condensed phase				Gas phase		
Molecule	TMC-1[a,d]	OMC-1[a,e]	ρ Oph-A[a,f]	NGC 7538 IR9[b]	TMC-1[c]	OMC-1[a]	ρ Oph-A[a]
CH_4	–	–	–	6×10^{-7}	–	–	–
CO_2	37	10	22	8×10^{-6}	5×10^{-8}	$3–7 \times 10^{-7}$	$<6 \times 10^{-8}$
CO	19	0	5.6	6×10^{-6}	8×10^{-5}	1×10^{-4}	5×10^{-5} [c]
CH_3OH	–	–	–	6×10^{-6}	2×10^{-9}	1×10^{-7}	–
H_2O	100	100	100	6×10^{-5}	$<7 \times 10^{-8}$	$1–8 \times 10^{-8}$	3×10^{-9}
NH_3	–	–	–	6×10^{-6}	2×10^{-8}	–	–

[a]Condensed phase abundances are relative to water being 100%; gas phase abundances are relative to hydrogen [41]
[b]Condensed phase mantle abundances [42]; CH_4 [43]; CO_2 [44] (units: molecules cm^{-2})
[c]Gas phase abundances: TMC-1 [45]; H_2O [46]; OMC-1 [47] (units: molecules cm^{-2})
[d]Condensed phase mantles are not observed in TMC-1. They are approximated from the Taurus source Elias 18 that has an approximately same declination and ascension [46]
[e]Data measured from the ISO spectra for the source Orion IRc2 [41]
[f]Data obtained for the line of sight to Elias 29, a protostar with low mass [43]

radiation. Here, larger and more complex organic molecules can occur within the bulk material of the mantle and/or larger clusters [51].

Grains present in the exterior of dense clouds or in diffuse interstellar regions can experience heavy doses of cosmic and X-ray radiation and solar winds: this exposure can actually result in disruption of the structural integrity of the grain itself. Numerous interstellar simulation experiments have been conducted to study the effect of various wavelengths and types of radiation on the chemical evolution of icy grain mantles. The chemical effects of radiation exposure on a parent set of molecules and the subsequent synthesis of new molecular species have been studied extensively over the past two decades. The parent set of molecules in these simulations remains well-defined (CO, CO_2, NH_3, CH_3OH, and H_2O), as the effects of defined radiation doses on organic substrates during interstellar simulation experiments have proven difficult to analyze. Thus the effects of particular radiations onto a well-defined interstellar ice analogue, with defined frequencies and wavelengths, have been the foci of most previous studies. However in the real world the icy mantle experiences radiation of varying intensities often simultaneously.

In regions of high atomic hydrogen abundance, the most dominant species present within the icy mantles of interstellar dust particles (IDPs) has been observed to be condensed water. Water ice is known to exist in up to 17 different phases within the icy mantles, and these phases can be amorphous and/or crystalline in nature. Crystalline water ice is usually formed at temperatures above 130 K and hence is not abundantly present on interstellar icy grain mantles [52]. One experiment studying the effect of soft X-ray radiation on water ice has been reported by a research team from Laboratoire de Chimie-Physique, Université Pierre et Marie Curie and Laboratoire des Collisions Atomiques et Moléculaires, Université Paris Sud 11 in France. A porous amorphous solid water film composed of ultrapure

water and of a thickness of 120 monolayers was prepared by isotropically doping from a background pressure of 1.2×10^{-4} Torr, and considering the sticking co-efficient of water as unity. This film was grown on a clean Pt(1 1 1) single crystal and was then mounted on a rotatable sample holder maintained at 20 K in a thermally-controlled helium cryostat. Films were irradiated with a monochromatic X-ray radiation and with an unmonochromatized white beam at the synchrotron Lure SuperACO, Orsay on the bending magnet beamline SA22. Using near-edge X-ray fine absorption spectroscopy (NEXAFS) measurements, the team observed irradiation radical and molecular species such as OH, O_2, O, HO_2, and H_2O_2 [53]. However, H_2 and H were not detected. The species HO_2, H_2O_2, and O_2 were likely evolved during the annealing process occurring between 20 and 50 K, and their formation was possibly catalyzed by the presence of OH radical:

$$OH + OH \rightarrow H_2O_2 \tag{1a}$$

$$H_2O_2 + OH \rightarrow HO_2 + H_2O \tag{1b}$$

$$HO_2 + OH \rightarrow O_2 + H_2O \tag{1c}$$

A similar experiment was conducted with another abundant interstellar molecule, CO. This CO ice simulation sample was prepared within a novel ultra-high vacuum interstellar astrochemistry chamber (ISAC) at the Centro de Astrobiología, Madrid [54]. The CO ice used was of 99% purity and was deposited on a CsI window maintained at 8 K on a cold-finger within a closed-cycled He-cryostat. Numerous irradiations investigating the effects of different ice layer thicknesses and irradiation times were conducted. The observed irradiation products of these CO ices were CO_2, C_2O, C_3O_2, C_3, C_4O, and CO_3/C_5 [55]. The possible evolution of these molecules can be represented in the following reactions:

$$CO + CO \rightarrow C_2O + O \tag{2a}$$

$$CO + CO \rightarrow CO_2 + C \tag{2b}$$

$$5\ C \rightarrow C_5 \tag{2c}$$

$$4\ C + O \rightarrow C_4O \tag{2d}$$

$$CO_2 + O \rightarrow CO_3 \tag{2e}$$

$$C_2O + CO \rightarrow C_3O_2 \tag{2f}$$

The soft X-ray irradiation of CO and H_2O in ice grain simulation experiments provides insight into the possible ionization products that could be present on the mantle surface as well as within its vicinity. Hard X-rays in interstellar space are

highly penetrative and can ionize the grain through to its core. Such complete ionization would make it very difficult to observe higher order molecules on grain surfaces in regions with highly ionizing radiation.

Water-dominated ices yield the first order product $OH^{\cdot}$ and higher order products such as $HO_2^{\cdot}$ and H_2O_2 upon exposure to UV radiation, a condition widely presumed to exist in dense media. However addition of CO to a water-dominated UV-irradiated system can also yield species like CO_2, H_2CO, HCO, and HCOOH [55]. There is little evidence for the formation of any higher mass polymeric molecules in the ISM. The presence of ISD, rich in organic molecules itself, makes detection of fine spectroscopic signatures from interstellar space even more difficult. This is indeed one of the main reasons why it has been difficult to date to detect amino acids and similar molecules in interstellar space. This limiting factor of detecting more complex organics is a limitation inherent to astronomical spectroscopy and has led to the development of simplified laboratory interstellar simulation experiments to understand and recreate those physico-chemical processes that are currently largely undetectable by astronomical technology to date.

3.4 Accretion of Organics on Icy Mantles

An interstellar grain with an icy mantle is not a stable substrate. It is indeed chemically dynamic and there is much to consider in terms of the possible physico-chemical processes occurring within IDPs. The polarity attained by an icy mantle, which is dictated by H_2/H ratios, should allow separation of the grains within the mantle into polar mantle grains and non-polar mantle grains [56]. Even if layer thickness is standardized, the time required for the development of each new layer can vary. Accretion of layers is considered to occur efficiently at the low temperatures extant in interstellar space (~15 K). This accretion of layers facilitates chemical reactivity within IDPs, with layer accretion occurring on a timescale of $\sim 2 \times 10^9/n(H_2)$ yr, if the sticking efficiency is assumed as unity [56]. If the simplified scenario of accretion within generic dense cloud media is considered, the formation of ices on IDPs can be considered to result from either of two separation mechanisms: diverse condensation (DC) and diverse desorption (DD) [57].

The DC model proposes that the polar and non-polar components of interstellar ice mantles are affiliated with dense regions of varying visual extinction and densities. The model asserts that condensation at densities 2×10^3 cm^{-3} $< n_H <$ 2×10^4 cm^{-3} yields water-dominated ice mantles with diverse volatile inclusions of species such as CO, CO_2, O_2, N_2, and CH_3OH. Each of these inclusions are condensed at their respective condensation densities; for example, mantles with CO, O_2, and N_2 are obtained at condensation densities $n_H > \sim 10^5$ cm^{-3}[57].

Within the DD model, the differential composition of H_2O-dominated ices and non-polar ices indicate a difference in their volatility. This model states that initial condensation produces homogenous ice with abundant volatile inclusions like those

mentioned above. Selective desorption would deplete volatile inclusions from within the mantle and allow these volatiles to recondense on top of the original ice. Thus in the DD model the H_2O-dominated ice is the "original" ice and the recondensed volatile inclusions are considered to be the "non-polar" ice. This model predicts the formation of recondensed non-polar ice mantles of diverse molecular and elemental composition [57].

4 The Formation of Amino Acids and the Origin of Homochirality in Interstellar Space

The search for the origin of the universe's biomolecules continues to capture the human imagination. However, there are many physicochemical conditions that would have had to be necessary in order for amino acid synthesis to have originally occurred in interstellar space. Some of these necessary conditions would likely have included a dusty environment, appropriate radiation dosage, appropriate stoichiometry of molecules, and appropriate sources for molecular asymmetry.

4.1 Asymmetry Propagates Asymmetry

Asymmetry is observed in all of the biomolecular molecules that constitute life: proteins, carbohydrates, RNA, and DNA. For the purposes of biological organics, a molecule is asymmetric if at least one carbon atom within the molecular structure, called the stereogenic center, has four different atoms or groups attached to it. If a molecule is asymmetric, or chiral, this necessarily also implies that it has a mirror image, known as an "enantiomer." If one enantiomer is present in larger quantities in a given environment than the other enantiomer, an enantiomeric excess (ee), or asymmetrical bias, occurs. However, in order for a molecule to be enantioenriched, it must have been synthesized in an asymmetric environment (Fig. 5).

There currently exist two main accepted models for the creation of asymmetry in our universe: (1) parity-violation by the weak nuclear force; and (2) the presence of chiral fields such as circularly polarized light (CPL).

The parity-violating weak force, mediated by the Z^0 boson, can influence molecules either (1) by altering the energies and energy levels imparting a parity violating energy difference (PVED) between enantiomers [58] or (2) by the interaction of spin-polarized electrons with matter following β-decay. In 1966, Yamagata reported that there exists a small difference in energy between enantiomers due to parity violation and addressed possible consequences both for molecular chirality and biomolecular homochirality [59]. Consideration of the parity-violating weak interaction indicates that L-amino acids are stabilized with respect to D-amino acids [60–62]. However, recent quantum-chemical ab initio

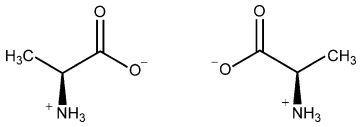

Fig. 5 The zwitterionic enantiomers of the amino acid alanine: L-alanine (*left*) and D-alanine (*right*). Alanine is the simplest chiral amino acid

calculations, particularly those of Quack and co-workers [63] and Schwerdtfeger et al. [64], have shown that the magnitude and indeed the sign of the PVED depend upon the exact molecular conformation of the species being considered. Moreover, parity violation leads to energy differences between enantiomers in the femtojoule to picojoule per mole range – this makes experimental observation of these differences difficult to perform. The small values of PVED for biological molecules composed only of light atoms have prompted chemists to doubt that the parity violating term could give rise to the distinct chirality of molecules observed in living nature.

The use of spin-polarized electrons as a source of chiral asymmetry has scarcely been employed in chemical reactions, even though this radiation might also have played an important role in the origin of molecular chirality [65]. Spin-polarized electrons can be generated as a result of parity violation in nuclear β-decay products [66]. A chiral molecule will be ionized at different rates by longitudinally spin-polarized electrons, as proposed by Vester and Ulbricht in 1962 [67]. Upon passing through matter, spin-polarized electrons decelerate and this deceleration results in the emission of circularly polarized electromagnetic radiation. These "chiral photons" can then interact with racemic or prochiral organic molecules via asymmetric photoreactions in order to induce an enantiomeric excess. However, again due to laboratory limitations in the detection of the very small asymmetry inducible by the Vester-Ulbricht process [68], experimental verification of this phenomenon remains inconclusive.

Currently the most promising external physical agent to induce optical activity in molecules appears to be CPL. The potential use of either *right*-handed or *left*-handed CPL (*r*-CPL or *l*-CPL) to induce enantiomeric enrichment into originally racemic mixtures was recognized by the end of the nineteenth century by van't Hoff and Le Bel. When a racemic mixture of molecules with sufficiently small and excited electronic state barriers to enantiomer inversion is irradiated with CPL at wavelengths of significant circular dichroism (CD), the initial equality of the enantiomers in the ground state will change. The concentration of the more strongly absorbing enantiomer will decrease, and that of the other will increase, resulting in a measurable enantiomeric excess (ee). From a mechanistic viewpoint, photochemical induction of optical activity with CPL can occur via different pathways: (1) absolute asymmetric photolysis (preferential decomposition of one enantiomer of a racemic mixture); (2) absolute asymmetric photosynthesis; or (3) photoisomerization between enantiomers [69–71]. A number of enantio-differentiating photoreactions initiated by CPL have already been successfully achieved [72–79]; thus the

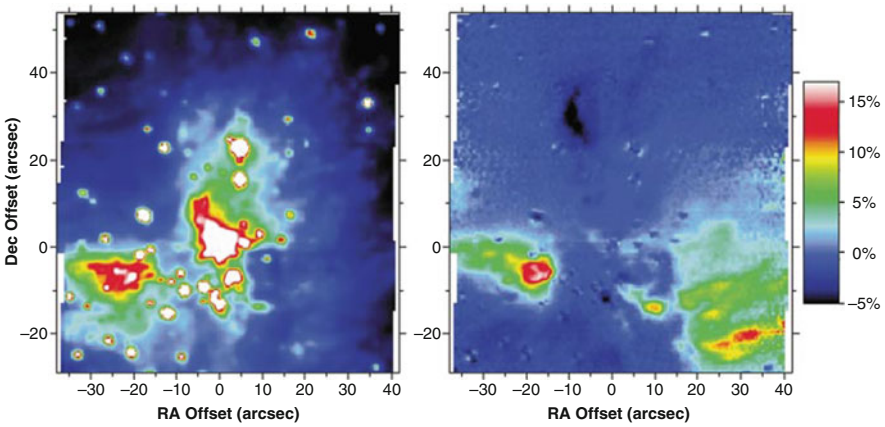

Fig. 6 Circular polarization (CP) map of the Orion Molecular Cloud-1 star formation region at 2.2 μm. *Left*: total infrared intensity of CP map of OMC-1. The typical size of the protostellar disk is much smaller than the observed structure of polarization. *Right*: percentage circular polarization at IR wavelength is observed to vary from 17% (*dark region*) to +5% (*white region*) [81]. Reproduced by permission of AAAS

observation of interstellar CPL and the role it could play in determining interstellar asymmetric molecules is therefore of great interest.

Although neutron stars were originally thought to be a source of CPL in interstellar space, this theory has since been discarded due to the fact that CPL has not been observed within the UV and visible wavelengths of light that they emit [80]. It is currently thought that star-formation regions, particularly those regions containing solar-mass stars and their planetary systems, were and continue to be the main source of CPL in the universe. This theory has been substantiated by the detection of CPL at IR wavelengths using the 3.9 mm Anglo-Australian Telescope along with a polarimetry system within the Orion Molecular Cloud Complex (OMC-1) [81]. The OMC-1 is a massive star-forming region at a distance of approximately 1,500 light years from Earth. Near IR circular polarization images of OMC-1 depict a quadrupolar distribution of left-handed and right-handed CPL, with the majority of light emission centered on a young luminous star known as IRc2 [82, 83]. The largest amount of CPL observed was from a region of a reflection nebula that scatters light from the Orion IRc2 region. The percentage of CPL observed in this region was as high as 17% at IR wavelengths (Fig. 6). These values of CPL detection are much larger than those previously observed from low mass stars emitting CP of around 1–2% [84]. Yet it is UV-CPL and not IR-CPL that is capable of inducing enantiomeric excesses in the molecules within the mantle being synthesized/degraded by it. It is thought that no UV-CPL has yet been detected from OMC-1 for this very reason: UV-CPL is readily absorbed by ISD and therefore does not make its way to astronomical detection systems [81].

Non-spherical ISD grains are, however, also thought to contribute to the CPL produced by star-forming regions via a process called dichroic scattering of linearly

polarized light (LPL). During this process, non-spherical dust grains become aligned to the direction of the LPL, and the axis of the dust's greatest rotational angular momentum rotates about the surrounding magnetic field to create a dichroic scattering phenomenon [85]. Whether these aligned dust grains produce CPL as well as produce asymmetric organic molecules within their icy mantles remains debatable.

The scientific community is now investigating the history of how and when our solar system might have been exposed to asymmetric CPL. Our sun is a low-mass star like those found in star-forming regions such as the OMC-1. The confirmed presence of ^{60}Fe in meteorites suggests the occurrence of a supernova explosion near our solar system and further implies that the solar system was formed in a huge star-forming region that would have continuously been emitting CPL. ^{60}Fe is a radioisotope with a half-life of 1.5 Myr and can provide a means for dating these explosions. Recently the rate of occurrence of supernovae explosions in the solar vicinity ($<$0.85 kpc) has been studied, and it would appear that the Earth was exposed to supernovae explosions around 372.6, 269.1, 140.6, and 17.3 Myr before the present day [86].

Although close proximity to supernovae would result in destruction of any ice grain chemistry, studies conducted by ESA's Integral Observatory have indicated that supernovae explosions occur every 50 years in the Milky Way galaxy and likely play a crucial role in catalyzing interstellar chemistry [87]. Supernovae are one of the main sources of ISD in the universe. It is thus possible that dust from remnant supernovae that had been strewn far away from its explosion source originally accreted polyatomic molecules within an icy mantle that was simultaneously irradiated by UV-CPL emitted from a moderately proximal star-forming region.

4.2 The Detection of Amino Acids in Interplanetary Space

Amino acids form an integral part of all structural and functional biomolecular processes occurring in all living organisms. However, the origin of amino acids and their role in the evolution of life remain questions unanswered within the scientific community, despite decades of investigation. It still remains uncertain whether amino acids were originally formed terrestrially or extra-terrestrially, and the origin of their homochirality is also currently unknown.

Amino acids can be readily formed from precursor molecules such as formic acid and acetic acid. These small volatile molecules are detected in abundance in the ISM even though amino acids remain undetected in interstellar space. However, the observation of glycine in the cometary samples collected by the Stardust space-probe [88] indicates that amino acids could potentially be found in interplanetary space. The discovery of nearly 90 monoamino and diamino acids in the Murchison meteorite that fell to Earth in 1969 in Murchison, Australia [89] suggests the possibility that amino acids formed extraterrestrially could have originally been

delivered to Earth by interstellar bodies. Meteorites are fragments of extraterrestrial matter – mostly propelled from asteroids into Earth-crossing orbits – that eventually fall to Earth's surface. The insoluble organic matter of the Murchison meteorite is significantly enriched in deuterium and ^{15}N [90]. Similar bulk isotopic enrichments have been found in chondritic IDPs and comet Wild 2 samples, suggesting that there is an evolutionary link between organics in meteorites and comets. Analyses of Murchison meteorite samples have been found to contain several natural and non-natural amino acids among the carbonaceous fragments, with a slight preponderance of L-enantiomers relative to D-enantiomers [91–94]. Interestingly, there was an even higher occurrence (up to 18.5%) of the L-form of several α-methyl substituted amino acids such as isovaline and α-methylnorleucine [94]. The fact that only L-amino acid excesses have been found in carbonaceous meteorites analyzed so far may indicate an extraterrestrial origin for life on Earth and that this life was biased toward L-amino acid homochirality from the very beginning.

5 Production of Amino Acids in Laboratory Simulation Experiments

Numerous laboratory interstellar ice mantle simulation experiments dedicated to the synthesis of amino acids have been conducted in hope of furthering understanding how amino acids might have been synthesized in the ISM. The experimental set-ups commonly used for these investigations involve standardized low pressures (10^{-7} mbar) and low temperatures (10–100 K) to simulate realistic interstellar conditions. The condensed gas mixtures used are chosen to be representative of ices formed near protostellar sources and are mostly deposited on a metal or inert metal-salt window mounted on an icy finger to form a condensed film of prespecified dimensions. During the experiment, the condensed gas mixture is irradiated with UV light of particular wavelengths. After irradiation exposure, the sample is warmed slowly to room temperature and is derivatized and analyzed using different analytical techniques – the most common of these are GC–MS, GC × GC–MS, HPLC, and IR spectroscopy. Contamination of samples can be excluded with the use of isotopic labeling [95].

5.1 Laboratory Studies on Amino Acid Formation in Interstellar Ice Analogues

Two independent simulation experiments were conducted by Bernstein et al. [96] and Muñoz Caro et al. [95] in 2002 where they irradiated their respective samples with non-polarized UV light. Bernstein et al. [96] used an ice mixture containing H_2O:NH_3:CH_3OH:CH_3CN = 20:2:1:1 (molar composition); the ice mixture after

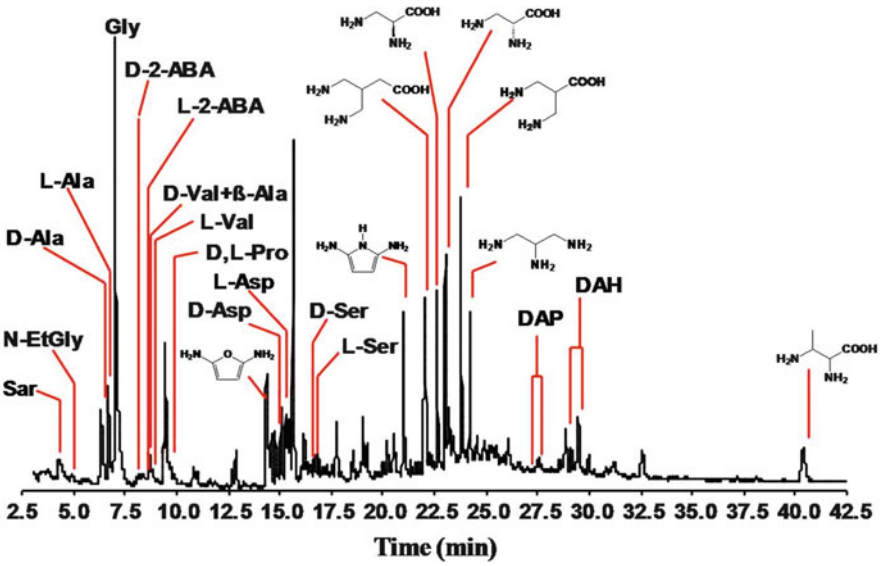

Fig. 7 Gas chromatogram of an ice mixture H_2O:NH_3:CH_3OH:CH_3CN = 2:1:1:1 (molar composition) prepared under realistic circumstellar/interstellar conditions by Munoz Caro et al. [95]. The ice mixture was irradiated, warmed to room temperature, hydrolyzed with acid, and derivatized. Sixteen product amino acids were observed as racemates using enantioselective gas chromatography mass spectrometry (GC–MS). Two diamino acids were also detected: DAP (diaminopentanoic acid) and DAH (diaminohexanoic acid)

irradiation was warmed to room temperature and compositionally analyzed using GC–MS and HPLC. The amino acids serine, glycine, and alanine were detected as products from this interstellar ice simulation.

Munoz Caro et al. [95] used another ice mixture that specifically avoided preformed carbon-nitrogen bonds in the precursor gas molecules. This condensed gas mixture contained H_2O:$^{13}CH_3OH$:NH_3:^{13}CO:$^{13}CO_2$ = 2:1:1:1:1 (molar composition). CO is a dominant interstellar molecule relative to acetonitrile and both CO and CO_2 are thought to play a crucial role in enhancing the diversity of amino acid production. In order to exclude any terrestrial contamination, isotopic ^{13}C-labeled reactants were used in this interstellar ice simulation experiment. After irradiation, the sample was allowed to warm to room temperature, hydrolyzed, derivatized using ECEE, and further analyzed by enantioselective GC–MS. From this simulation, 16 amino acids out of which 6 were proteinogenic amino acids were detected. Although the numbers of amino acids formed in both these experiments differ, one common result in both simulations was the high amount of glycine detected (Fig. 7). Thus both of these investigations would appear to indicate that glycine should be abundantly formed in ISM [97, 98].

Both teams further indicated that the identified amino acids are likely originally parts of peptidic or oligomeric structures that form within the organic residue of interstellar ice analogues and are released as free molecules after additional acid

hydrolysis. The UV-photoprocessed interstellar residue may form exothermically from recombined radicals which are able to diffuse and react within complex radical chain reactions in the slow melting ice [99]. The precise reaction pathways and channels, however, are not yet fully understood (see Sect. 5.4).

A more recent experiment by Meinert et al. [100] has involved the exposure of an interstellar ice analogue containing H_2O:$^{13}CH_3OH$:NH_3 = 2:1:1 (molar composition) to UV light at 121 nm. The mixture was deposited on MgF_2 window and simultaneously irradiated for a period of 10 days. After irradiation the sample was extracted in H_2O, hydrolyzed using 6 M HCl, derivatized, and analyzed using enantioselective two-dimensional gas chromatography coupled to time-of-flight mass spectrometry (GC × GC–TOFMS). A total of 20 amino acids and 6 diamino acids have been identified in the organic residue, including proteinogenic amino acids such as serine, proline, aspartic acid, alanine, glycine, and the diamino acid *N*-(2-aminoethyl) glycine.

5.2 *Asymmetric Photochemistry and Anisotropy Spectra of Amino Acids*

Given that amino acids are abundantly present in living organisms in predominantly one enantiomeric form, the simulated synthesis of amino acids in interstellar environments must inevitably incorporate the induction of asymmetry. Thus, the next step in designing interstellar ice simulation experiments of amino acids was to consider the effect of CPL on both the synthetic and photolytic chemistry that might be occurring in the ice mantle of IDPs. The first of these investigations exploring photosynthesis was performed at the DESIRS beamline of the SOLEIL synchrotron facility in France [101, 102]. A condensed gas mixture was irradiated with UV-CPL radiation under simulated interstellar conditions. The condensed gas mixture used consisted of H_2O:$^{13}CH_3OH$:NH_3 = 2:1:1; the methanol carbon was isotopically labeled in order to ensure that any contamination that might have occurred during the experiment could be accounted for during analysis. The condensed gas mixture was irradiated with VUV-CPL of either right helicity (*r*-CPL) or left helicity (*l*-CPL) at low temperature (T = 80 K) for 36 h. The sample was then warmed slowly to room temperature and analyzed using GC × GC–TOFMS. Enantiomeric excesses of either L-alanine or D-alanine (up to 1.34% ee) were observed, depending on the handedness of the CPL, and these enantiomeric excesses were found to be proportional to the number of photons absorbed per ice molecule. Encouragingly, the enantiomeric excesses detected approximate those observed for alanine detected previously in meteoritic sample extracts (1.2% ee).

This research, however, does not address the mechanism for amino acids synthesis in extraterrestrial environments and how they continued to exist while associated with larger interstellar bodies prior to their descent to Earth. It is thought that upon formation on their parent bodies, amino acids might have agglomerated

into polymeric states that would have rendered them invisible to astronomical spectroscopic detection [103]. The circumstantial evidence of the detection of monoamino and diamino acids in meteorite samples [104] and the ability of amino acids to form peptides and extended polymeric structures might support this theory; however amino acids in interstellar space, either in monomeric or polymeric form, remain undetected.

In order to understand the asymmetric photochemistry of amino acids and how UV-CPL might have facilitated the transfer of asymmetry from chiral massless photons to organic molecules, it has been necessary to attempt to characterize the interaction between CPL and amino acids. Enantiomers of a given amino acid absorb CPL differentially. This differential absorption (ΔA) is a function of CPL wavelength and can be expressed as CD. The CD spectra of a series of prebiotic amino acids have now been recorded in order to begin to characterize this interaction. Measurements of CD spectra ranging from 130 to 330 nm have demonstrated that the highest degree of effect of CPL on amino acids occurs in the vacuum UV (VUV) range between 130 and 190 nm where intense CD bands have been observed [105, 106] and calculated [107]. This VUV spectral range is not accessible if aqueous solutions of the amino acids are analyzed because water absorbs UV light below 200 nm. Therefore, in order to extend the range of CD measurements obtained, solid amorphous amino acid films were analyzed instead. The use of these films, of a pre-specified thickness, more accurately models the solid state in which amino acids would likely exist in interstellar environments.

More recently, an additional means of characterization of the interaction of CPL with chiral small molecules such as amino acids has been reported. In 2012 Meinert et al. [100] reported a series of characterizing anisotropy spectra of amino acids, stating that it is not exclusively the CD signal that influences chirality transfer from photons to amino acids. The anisotropy factor g, the ratio between CD signal and absorption, can be used to describe more accurately the behavior of the interaction between a chiral small molecule and CPL. Anisotropy factors of amino acids were previously only known for a few specific wavelengths. Anisotropy spectra have now been recorded for various isotropic amorphous amino acid enantiomers such as alanine and valine (Fig. 8) in the UV and VUV spectral regions: anisotropy factor g is described as a function of CPL wavelength. Use of anisotropy spectra to characterize the CPL-chiral molecule interaction will allow for prediction of reaction rates and the extent of ee achievable when conducting photochemical reactions of amino acids using CPL. Given that anisotropy spectra can be used to characterize asymmetric photochemical behavior, these data will certainly be used to investigate other families of chiral small molecules.

Using the data obtained from both CD and anisotropy spectroscopy of amino acids, a series of experiments has been performed investigating the photolysis mechanism for the generation of asymmetry in amino acids. Thin amorphous films of racemic amino acids in their solid state (e.g., alanine and leucine) have been subjected to CPL of given handedness and predetermined wavelengths. The irradiation wavelengths were chosen on the basis of the maxima and minima for ee generation as determined from CD and anisotropy spectra. Enantiomeric

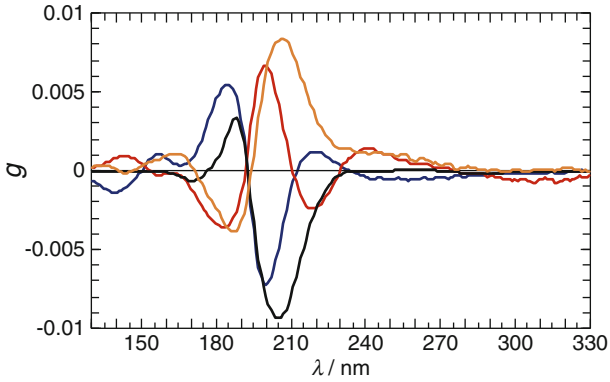

Fig. 8 Anisotropy spectra in the vacuum UV and UV spectral region of isotropic amorphous D-alanine (*red*), L-alanine (*blue*), D-valine (*orange*), and L-valine (*black*) enantiomers

enrichments of up to 5.2% ee have now been reported for the enantioselective photolysis of leucine by CPL [108–110]. The results of these systematic photochemical studies demonstrate that asymmetric photochemistry does have the potential to induce enantiomeric excesses of up to a few percent into amino acids in environments of high vacuum and low temperature.

5.3 Asymmetric Amplification Processes

To date, only small excesses of asymmetry in proteinaceous amino acids have been observed during analyses of both cometary ice simulation experiments and chondritic meteorite samples. How could these small excesses have evolved into the overwhelming enantiomeric preference for L-amino acids in all of today's living organisms? Several authors have addressed ways in which a small enantiomeric bias can be amplified. The Frank autocatalytic kinetic model for asymmetric synthesis suggests that even a slight excess of one enantiomer will influence and favor the synthesis of that enantiomer over the other. Over time, such a slight excess would thereby evolve into a dominant preference for one enantiomer over its opposite in a given system [111]. Kondepudi, et al. [112, 113] have demonstrated this concept within a number of autocatalytic systems to demonstrate its effectiveness (Fig. 9). Morowitz proposed that this model could be applied to the evolution of asymmetry in prebiotic amino acids in 1969, given the fact that most racemates of amino acids are less soluble than the crystals of either the D-enantiomers or the L-enantiomers. The reductive Zn-mediated alkylation reported by Soai, et al. in 1995 was the first truly autocatalytic asymmetric amplification, with greater than 99.5% ee observed [114]. Both Breslow and Blackmond have reported successful enantiomeric enhancement of amino acids by differential crystallization processes and autocatalytic asymmetry amplification [115–118]. Further research is certainly

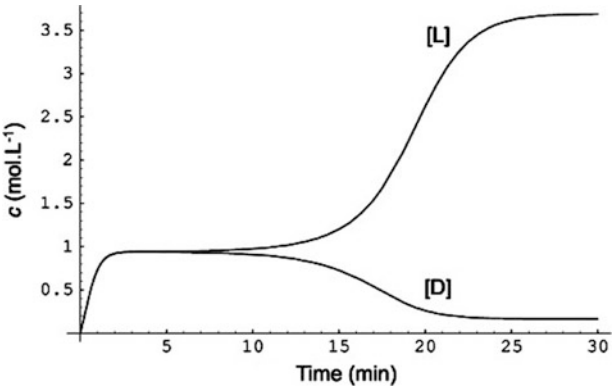

Fig. 9 Concept of autocatalytic amplification – autocatalytic amplification of the L-enantiomer (*upper branch*) over the D-enantiomer (*lower branch*) in the Kondepudi–Prigogine reaction sequence [112, 113]. A tiny ee of the L-enantiomer at $t = 0$ is increased to a high ee after only 30 min of reaction time

required in this field of asymmetric autocatalysis in order to provide a logical explanation of the evolution from achiral condensed gaseous mixtures to the asymmetric amino acids used in all biological processes today.

5.4 The Higher Order Structures of Amino Acids

In 2004 both monoamino and diamino acids were discovered in the CM type Murchison meteorite [104]. CM type carbonaceous chondritic meteorites have very high carbon content relative to other types of meteorites; hence these meteorites can provide a significant amount of information about what kinds of organic molecules might have been synthesized extraterrestrially and how these compounds might have been delivered to Earth. The meteorite analysis that afforded the detection of diamino acids in 2004 involved the extraction of a fresh sample of the Murchison meteorite using hot water hydrolysis and further analysis using an enantioselective chromatographic column on a GC–MS instrument. Efficient derivatization of the sample with ECEE resulted in the identification of six diamino acids of the type diaminoalkanoic acids. This finding correlated well with the identification of similar diamino acids (diaminopentanoic acid and diaminohexanoic acid) from the UV-irradiated interstellar ices simulations using a condensed gas mixture of H_2O:$^{13}CH_3OH$:NH_3:CO:CO_2 = 2:1:1:1:1 [95]. Recently, six diamino acids including the two enantiomers of D,L-2,4-diaminobutyric acid and, for the first time, the achiral *N*-(2-aminoethyl)glycine were detected after a similar interstellar ice experiment using enantioselective GC × GC–TOFMS analysis (Fig. 10) [100]. These diamino acids are of particular interest given that they can participate in the formation of peptide nucleic acid

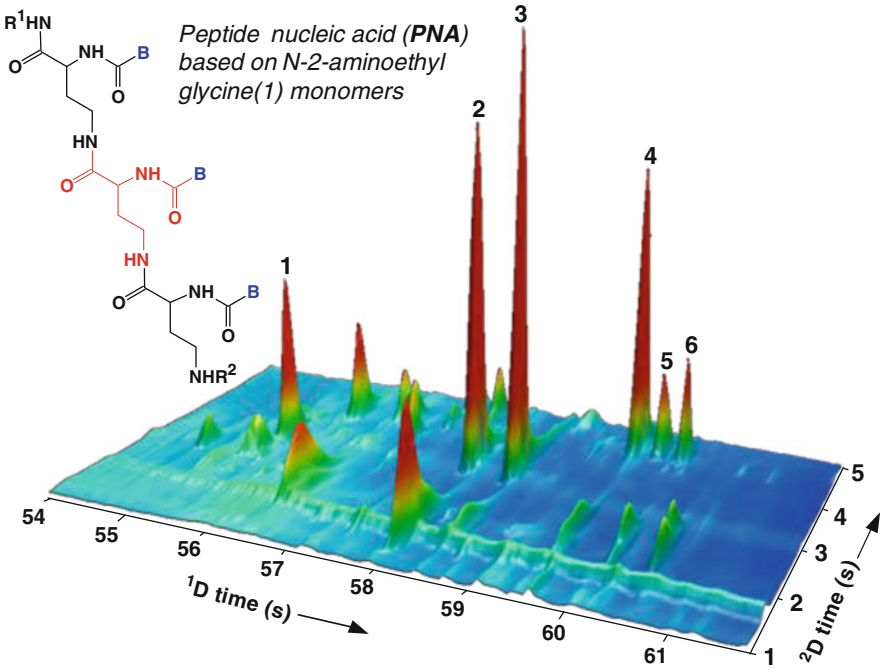

Fig. 10 Close-up view of the two-dimensional enantioselective gas chromatogram depicting derivatives of ^{13}C-labelled diamino acids (**1**) *N*-(2-aminoethyl) glycine, (**2**) L-2,3-diaminopropanoic acid (DAP), (**3**) D-2,3-DAP, (**4**) 3-amino-2-(aminoethyl) propionic acid, (**5**) L-2,4-diaminobutyric acid (DAB), and (**6**) D-2,4-DAB generated under simulated interstellar pre-cometary conditions [100]

(PNA) which might have served as the primordial genetic material [119]. PNA has been proposed to be a possible pre-RNA structure, whereby the sugar-phosphate molecular backbone of RNA and DNA evolved from an uncharged peptide backbone. [119]. This peptide-based backbone could have either been composed of *N*-(2-aminoethyl)glycine (aeg) (leading to aegPNA molecules) or of 2,4-di-aminobutyric acid (da) (leading to daPNA structures). PNA can form stable double helices with complementary molecules of RNA or DNA, and this stability might indicate that PNA could have served as an initial evolutionary template.

The observation of amino acids, diamino acids, and other organic molecules [120–122] in interstellar ice analogues and in meteoritic samples indicates that there exist mechanisms via which exogenous organic molecules could have been delivered to Earth (Fig. 11). It is difficult to relate icy bodies and meteorites; both may carry amino acids formed by different mechanisms, or perhaps the meteorites analyzed to date that contain amino acids could have been remnants of an icy comet. Thus the next step in understanding the origin and evolution of amino acids in extraterrestrial environments is to attempt the search for amino acids on actual interstellar bodies. The COSAC instrument on the ESA mission ROSETTA is

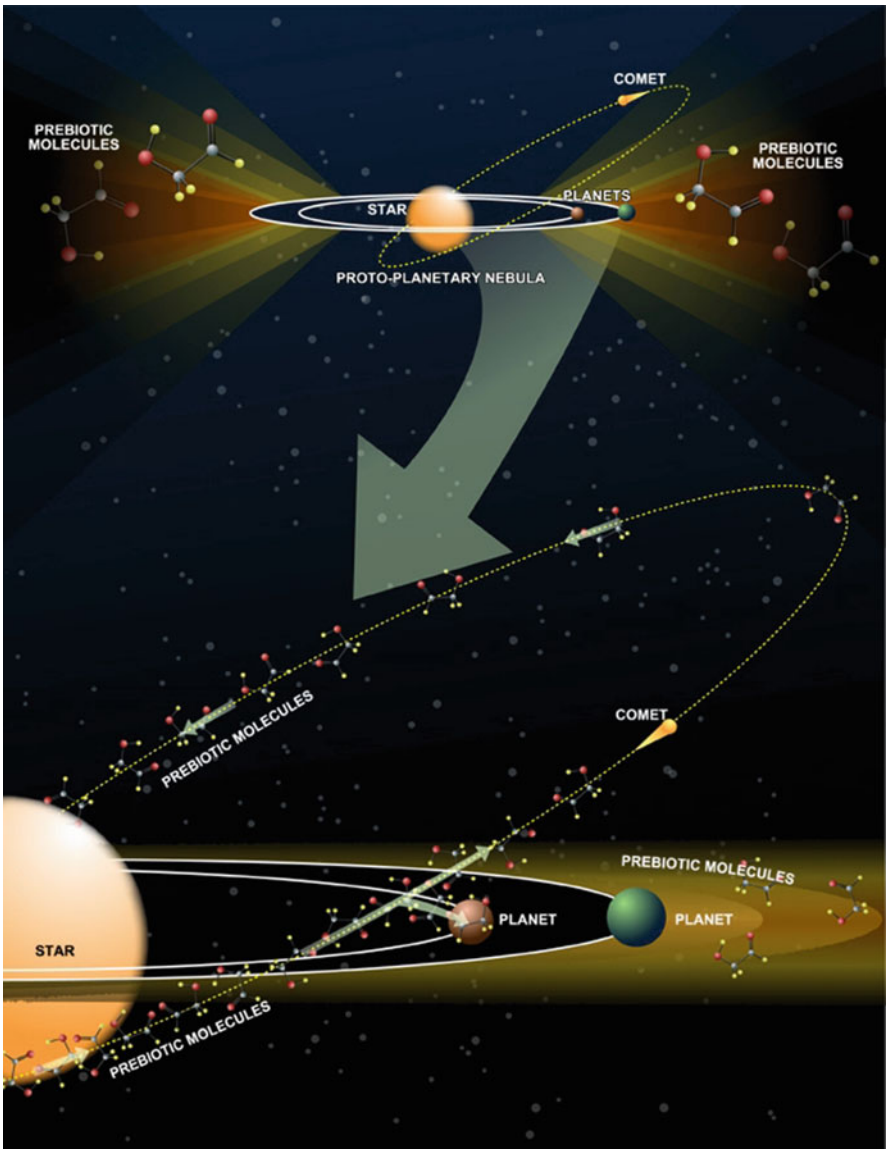

Fig. 11 Artistic impression of the possible journey of prebiotic molecules from comets to planets. Comets and meteorites are important delivery agents of interstellar organic molecules to Earth and other planets (image credits: Bill Saxton, NRAO/AUI/NSF)

intended to achieve this goal and conduct thorough chemical analyses on the surface of the comet 67P/Churyumov-Gerasimenko in order to determine the existence of interstellar amino acids and other chiral organics.

6 The COSAC Experiment on ROSETTA: The First Advances

In the mid-twentieth century astronomers began studying comets using ground based telescopes, analyzing multiple electromagnetic spectral regions. However remote observations cannot always afford certain desired answers. Thus with advances in space exploration the European Space Agency (ESA) envisioned an in situ exploration of a cometary nucleus.

In the late 1970s the ESA proposed a close fly-by of the comet 1P/Halley (Halley's comet), due to approach its perihelion in 1986 [123, 124]. This fly-by mission was called GIOTTO after the famous Italian renaissance painter Giotto di Bondone. GIOTTO was launched on an Ariane 1 rocket on 22 July 1985. It successfully flew past 1P/Halley on 14 March 1986 and was later commanded to fly past another comet, 26P/Grigg-Skjellerup, on 10 July 1992 [125]. This significant mission was the first to afford close analysis of the shape and size of both of these two comets, providing accurate dimensions and compositional and velocity estimates of the dust particles and the gases emitted. The GIOTTO mission was considered a technological landmark and changed the perception of comets as proposed by the earlier cometary sandbank model. It actually confirmed that comets do possess a solid and cohesive structure and lent hope to the prospect of landing on a cometary nucleus [126]. This cometary nuclear landing is the envisioned goal of the first ESA cometary surface exploration mission ROSETTA.

ROSETTA was approved in the year 1993 as a Planetary Cornerstone Mission of ESA in its Horizon 2000 long-term program. A successor to GIOTTO, ROSETTA's principal objective is to study the origin of comets and to understand the origin of the solar system by attempting a landing on Comet 67P/Churyumov-Gerasimenko [125, 126]. The ROSETTA mission physically consists of two mission elements – the lander PHILAE and the orbiter ROSETTA. The mission was originally designed to study the comet 46P/Wirtanen but a launch failure of an ESA rocket Ariane 5 in December 2002 led to a postponement of the mission and a new target comet was required. The comet 67P/Churyumov-Gerasimenko was identified and the mission was redesigned for this new target. ROSETTA was finally launched on 2 March 2004 by an Ariane G + rocket from the Guyana Space Center in Kourou, French Guyana [127]. ROSETTA's journey includes four planetary gravity assist maneuvers in the sequence Earth–Mars–Earth–Earth in order to acquire sufficient thrust to reach 67P. It is planned to reach comet 67P in November 2014 after 10 years of flight time through the Solar System.

6.1 PHILAE Lander and COSAC

The PHILAE Lander is an ambitious indigenous element of the ROSETTA mission that will be detached from the orbiter to land on the cometary nucleus (Fig. 12). The Lander, previously known as ROLAND, was proposed by a team of scientists led

Fig. 12 Artistic impression of Philae Lander on the surface of comet 67P/Churyumov-Gerasimenko. Philae is planned to soft land on the cometary nucleus in November 2014. The landing site will be determined by the Rosetta team after a close approach to the comet (image credit: ESA)

by Dr. Helmut Rosenbauer from the Max Planck Institute for Solar System Research in Katlenburg Lindau, Germany. The Lander system has integrated within it ten scientific instruments and sub-systems provided by various space agencies and research laboratories from six European nations; its landing and the analytical study of the cometary surface is overseen by ESA. A complete description of the PHILAE Lander system can be found in "The ROSETTA Lander ('PHILAE') Investigations" [128]. Apart from a wide range of instruments targeted to study the various aspects of the comet 67P, the cumulative activity of sample drilling and acquisition is of particular importance to analyze the composition of the cometary nucleus. The drilling and sample acquisition activity has been assigned to the Sampler, Drill, and Distribution (SD-2) system. Analysis of the acquired surface sample will be performed by (1) the cometary sampling and composition (COSAC) experiment to investigate the molecular and stereoselective composition; (2) PTOLEMY for isotopic measurements composition; and (3) the comet infrared and visible analyzer (CIVA) for infrared imaging and microscopic measurement of the sample (Table 5). The sample collected by SD-2 will be first measured by CIVA prior to delivery to PTOLEMY and COSAC [129].

The COSAC Experiment consists of an instrumental suite of a gas chromatograph (GC), a time-of-flight mass spectrometer (TOFMS), and an allied electronic system allowing remote operation of the suite (Fig. 13). The GC–TOFMS instrument performs the separation, identification and quantification of the individual components from a mixture of volatile molecules.

The COSAC Experiment is designed to meet payload specifications since there are strict limitations of size, power, mass, and resources involved in a space mission. The GC detectors, valves, and carrier tanks have been miniaturized to

Table 5 The sample acquisition and analysis instrumental suite onboard PHILAE

Instrument	Purpose	Contributing organization
SD−2	Sample drilling and acquisition	Politecnico di Milano, Milan, Italy
COSAC	Molecular and chirality analysis of sample	Max-Planck-Institut für Sonnensystemforschung, Katlenburg-Lindau, Germany
PTOLEMY	Isotopic analysis of sample	Planetary and Space Science Research Institute, The Open University, Milton Keynes, England
CIVA	Optical imaging, infrared spectral imaging and microscopic analysis	IAS, Institut d'Astrophysique Spatiale, Orsay, France

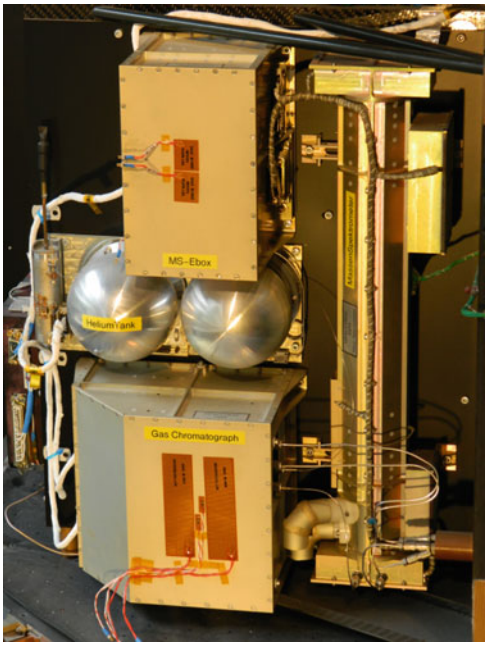

Fig. 13 The COSAC Experiment on the Philae Lander that will land on the nucleus of comet 67P/Churyumov-Gerasimenko. COSAC will receive cometary sample from the Sample Drill and Distribution System and analyze them for organic composition and homochirality. The image shows two helium tanks (each of volume 330 cm^3); the gas chromatograph box at the *bottom* contains the GC hardware frame and its affiliate electronics; the MS-Ebox (electronic box) contains the affiliate electronics for the mass spectrometer. The TOFMS seen here is arranged vertically on the *right*. The flight instrument is protected from radiation and cometary debris by the solar panels of the Philae unit. The entire instrumental suite is 500 mm tall and 400 mm wide

adhere to the payload requisites. Helium will be used as a carrier gas in the GC component as it is chemically inert, has a higher thermal conductivity relative to many organic molecules, and is not likely to be found on the cometary nucleus. The

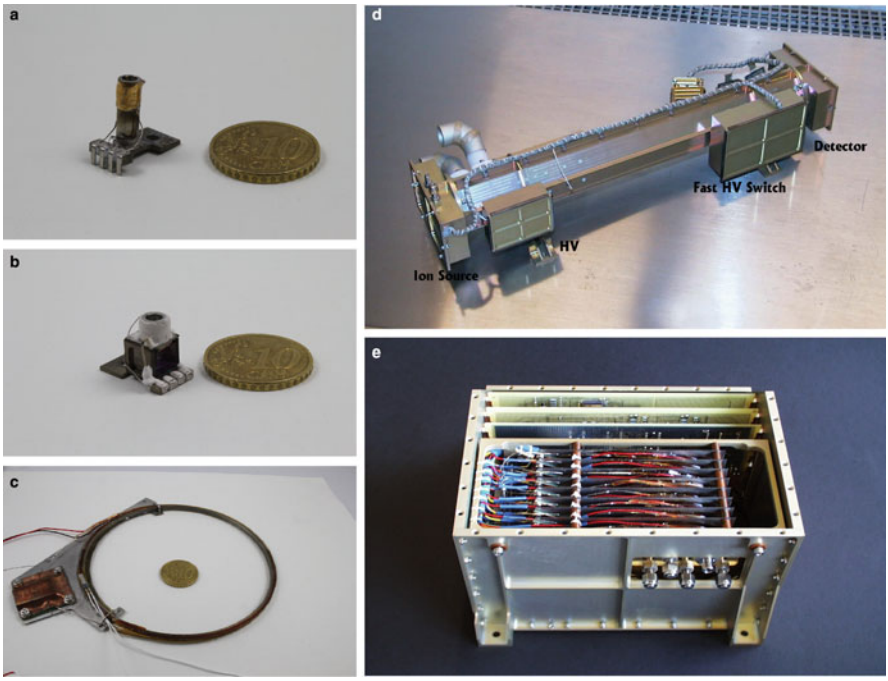

Fig. 14 (**a**) COSAC high temperature oven (heats up to 600°C). (**b**) COSAC medium temperature oven (heats up to 180°C). (**c**) Typical COSAC capillary chromatographic column arranged in a ring formation along with the thermal conductivity detector below the copper plate (inner diameter 100 mm). (**d**) COSAC time-of-flight mass spectrometer (460 mm long). (**e**) Pneumatic gas chromatography hardware mounting frame (80 mm width, 120 mm length, 105 mm height). The frame consists of eight different chromatographic columns and their respective TCDs connected to the incoming gas supply as well as the exhaust via thermally operated valves

carrier gas has been packed in two spherical tanks each of volume 330 cm^3 that are filled to a pressure of 40 bar.

The calibration gas that will be used during the COSAC Experiment is a mixture of noble gases of the following composition: 24% Ne, Ar, Kr, Xe, and 4% He. The pressure regulation for the gas flow will be performed using thermally operated valves that run on the principle of thermal expansion. The thermally operated valve is a patented technology developed and produced at the Max Planck Institute for Solar System Research, Germany. The gas distribution system in the GC is controlled by 28 indigenously developed on-off switching valves. These valves work in the temperature range from −60°C to +200°C.

The COSAC–GC possesses two different types of pyrolysis ovens in which the samples will be vaporized (Fig. 14). The medium temperature oven heats the sample to 180°C and allows real-time sample monitoring in the visible and infrared region by CIVA through a window at the bottom of the oven. The other type of pyrolysis oven is the high temperature oven that can heat samples to 600°C without

Table 6 Chromatographic columns in the COSAC–GC

Column	Length (m)	Inner diameter (mm)	Stationary phase thickness(μm)
Enantioselective columns			
Chirasil L Val	12.5	0.25	0.12
Chirasil Dex CB	10	0.25	0.25
Cyclodextrin G-TA	10	0.25	0.125
General columns			
MXT 1	10	0.18	0.1
MXT 20	15	0.18	1.0
MXT 1701	15	0.18	1.2
MXT U-PLOT	10	0.18	1.0
CarboBond	15	0.25	10

any provision for real-time inspection [130]. The chromatographic columns and detectors are the analytical heart of the COSAC–GC (Fig. 14). There are a total of eight columns of varying stationary phase thicknesses, diameters, and lengths: five of these are standard GC columns aiming to separate substantially different molecules and the other three are enantioselective columns that will be used to detect chiral organic molecules (Table 6).

Each of these eight columns is fitted with a micro-machined thermal conductivity detector (TCD) manufactured by Varian. This TCD is in principle a Wheatstone bridge of four filaments that are supplied with a constant voltage and are cooled by two parallel, symmetrical, and opposite flows of gas. A signal is obtained when an analyte, which has a lower thermal conductivity relative to the carrier gas, enters the gas flow. This increases the temperature of the filament and, due to the temperature co-efficient of resistance of filament, this temperature change yields a differentiating output voltage.

The COSAC–TOFMS is a high-resolution multi-pass time-of-flight instrument. It can be used in either stand-alone or GC–TOFMS mode. The gas molecules entering the mass spectrometer will be ionized by a beam of electrons. These ionized molecules, depending on their m/z ratio, will travel towards a multi-sphere detector to produce a characteristic spectral signal.

At lower resolutions only a single-flight path, 370 mm distant from the source, will be used. For higher resolution runs, the TOFMS is to be used in multiple-turn mode, which is accomplished using two gridless reflectors, one near the source, the other on the opposite side of the source. The resolution of COSAC–MS is 200 and it can measure masses from 1 to 1,500 amu [131].

6.2 *The Scientific Vision of COSAC*

The GC–MS unit of the COSAC Experiment will be the first of its kind to conduct in situ compositional analysis of a cometary nucleus. Numerous interstellar ice simulation experiments and analyses of meteoritic samples have afforded many

Table 7 Organic molecules separated by the chirality module of COSAC

Enantioselective columns of COSAC	Directed chiral analytes
Chirasil Dex CB	Hydrocarbons
Chirasil-L-Val	Carboxylic acids; amino acids
Cyclodextrin G-TA	Alcohols; diols

theories about the mechanisms that afforded (and continue to afford) the delivery of exogenous material to Earth. These theories will be put to the test as COSAC explores the nucleus of Comet 67P.

Comets have been long considered "dirty icy bodies" due to their high organic and aqueous content. These adjectives were originally used based on data from ground-based observations of numerous cometary missions like GIOTTO, STARDUST, and DEEP IMPACT. The detection of the amino acid glycine from the strewn dust of comet 81P/Wild-2 by STARDUST [132] supports the possibility of discovering larger organic molecules on Comet 67P; however it should be noted that all comets do not necessarily have similar chemical compositions. The orbit of a comet, its radiation dosage, the age of the comet in a particular orbit, its size, volume, and other physical factors all govern their respective compositions. Comet 67P will only provide initial data towards a more complete understanding of the chemical composition of comets.

The search for amino acids and other organic chiral molecules is of fundamental interest to the ROSETTA mission. The COSAC experiment's enantioselective columns were carefully selected to allow for resolution of simple enantiomers and to initiate potentially an understanding of the origin of biomolecular homochirality within the solar system [131, 133]. The use of different enantioselective chromatographic columns (Table 7) will ensure resolution of a wide range of chiral molecules that could be encountered, including amino acids, amines, diols, alcohols, hydroxy carboxylic acids, and hydrocarbons such as *R*,*S*-3-methylhexane and its higher homologues [134].

The polar nature of amino acids requires their derivatization in order to transform them into more volatile and less reactive analytes prior to gas chromatographic analysis. Bulky, non-polar silyl groups or different esterification methods are traditionally used to convert the polar functional groups on OH, NH_2, and SH into nonpolar moieties. These conventional methods cannot be used during the COSAC experiment: sample analysis will be conducted in vacuum, at low temperatures, and under low gravity, excluding any solvent chemistry. An alternative dry derivatization method using DMF–DMA has therefore been selected for the COSAC experiment [135]. This method entails simultaneously exposing the sample to pyrolysis and a suitable gas phase derivatization agent. Pyrolysis is preferred in this instance over the conventional procedure of acid hydrolysis because pyrolysis does not require wet chemistry and reduces the complexity of the experimental set-up. Capsules of DMF–DMA have been placed within the COSAC assembly in the pyrolysis oven, where they will melt and release DMF–DMA once temperatures of 100°C are reached within the oven-injector

system of the COSAC experiment [135]. Derivatized amino acids (and other small molecules) will then be resolvable on the GC module and can also be transferred into the mass spectrometer for identification via characteristic mass fragmentation analysis.

Within the first few hours of landing, the COSAC Experiment will first perform an initial set of experiments known as the first science sequence (FSS). This FSS will be powered by a set of on-board batteries. The long-term science phase (LTS) will be then be conducted until the end of the mission and these experiments will be powered by the solar panels on PHILAE. The data generated will be uplinked to the orbiter and then to Earth for analysis.

7 Outlook

There are numerous proposed mechanisms via which amino acids could have been generated in interstellar space. It is currently thought that the substrates supporting amino acid synthesis were likely to have been IDPs that could then have been incorporated into comets, asteroids, and planets. The likely mechanism of homochiral amino acid synthesis suggests photochemical triggering by circularly polarized photons that subsequently induced asymmetric amino acid formation on icy grains and comets. The presence of liquid water on comets or meteorites may have served to enhance amino acid production and homochirality via Strecker processes. At the same time, photochemistry may also have induced amino acid synthesis on icy grains and comets via chemistry involving radical mechanisms. It is likely that the COSAC experiment will provide some insight into which of these mechanisms might have afforded amino acid synthesis in interstellar contexts.

The science of the origin of life does not fall strictly into the domain of biology and chemistry – rather it is cross-disciplinary and involves additional fields such as astronomy, geology, and physics for a complete appreciation of how life in our universe may have come into existence. Thus the discoveries of the roles that carbon stars, supernovae, and any other astrophysical phenomena play in the creation of prebiotic molecules could significantly contribute to a scientific understanding of life's origins. Continued ice simulation experiments on Earth and meteorite analyses, combined with exploration missions into interstellar space, will likely yield further answers. The successful landing of ROSETTA on comet 67P/Churyumov-Gerasimenko in November 2014 will open a new chapter in the history of space exploration. This first attempt to detect large quantities of organic molecules in situ on a cometary nucleus will hopefully yield clues for the presence and diversity of prebiotic molecules and homochirality in the universe and further insight into the origin of life itself.

Acknowledgements We thank the generous support provided by the Max Planck Institute for Solar System Research, Deutsches Zentrum für Luft- und Raumfahrt, Centre National d'Etudes Spatiales, the RSC JWT Jones Fellowship (for A.C.E.), the European Space Agency, as well as the synchrotron centers SOLEIL, Gif-sur-Yvette, France, and the Institute for Storage Ring Facilities at Aarhus University, Denmark.
Author contributions: C.G., C.M., and A.C.E. wrote the manuscript. F.G. is the principal investigator of ROSETTA's COSAC instrument and led the writing of Sect. 6. U.J.M. initiated research programs on biomolecular asymmetry and defined major science subjects as written in Sects. 4 and 5.

References

1. Suess ST (1990) The heliosphere. Rev Geophys 28:97–115
2. Tielens AGGM (2005) The physics and chemistry of the interstellar medium. Cambridge University Press, Cambridge
3. Ferrière KM (2001) The interstellar environment of our galaxy. Rev Mod Phys 73:1031–1066
4. Spitzer L (1978) Physical processes in the interstellar medium. Wiley, New York
5. Morton DC, Drake JF, Jenkins EB, Rogerson JB, Spitzer L, York DG (1973) Spectrophotometric results from the Copernicus satellite II. Composition of interstellar clouds. Astrophys J 181:103–109
6. Savage BD, Sembach KR (1996) Interstellar abundances from absorption-line observations with the Hubble Space Telescope. Annu Rev Astron Astrophys 34:279–329
7. Field GB, Somerville WB, Dressler K (1966) Hydrogen molecules in astronomy. Annu Rev Astron Astrophys 4:207–244
8. Sanders DB, Scoville NZ (1991) Molecular gas in luminous infrared galaxies. Astrophys J 370:158–171
9. Wilson RW, Jefferts KB, Penzias AA (1970) Carbon monoxide in the Orion nebula. Astrophys J 161:43–44
10. Irvine WM (1991) The molecular composition of dense interstellar clouds. In: Greenberg JM, Pirronello V (eds) Chemistry in space – NATO ASI Series C 323:89–121
11. Herbst E, van Dishoeck EF (2009) Complex organic interstellar molecules. Annu Rev Astron Astrophys 47:427–480
12. Meierhenrich UJ, Filippi J-J, Meinert C, Vierling P, Dworkin JP (2010) On the origin of primitive cells: from nutrient intake to elongation of encapsulated nucleotides. Angew Chem Int Ed 49:3738–3750
13. Meierhenrich UJ, Filippi J-J, Meinert C, Vierling P, Dworkin JP (2010) Die Entstehung erster Zellen – von der Nährstoffaufnahme hin zur Verlängerung eingeschlossener Nucleotide. Angew Chem 122:3826–3839
14. Suess HE, Urey HC (1956) Abundances of the elements. Rev Mod Phys 28:53–74
15. Castor JI, Abbott DC, Klein RI (1975) Radiation-driven winds in Of stars. Astrophys J 195:157–174
16. Loup C, Forveille T, Omont A, Paul JF (1993) CO and HCN observations of circumstellar envelopes. A catalogue – mass loss rates and distributions. Astron Astrophys Suppl Ser 99:291–377
17. Cernicharo J, Goicoechea JR, Caux E (2000) Far-infrared detection of C_3 in Sagittarius B2 and IRC +10216. Astrophys J 534:199–202
18. Becklin EE (1969) The unusual infrared object IRC +10216. Astrophys J 158:133–137
19. Gilman RC (1969) On the composition of circumstellar grains. Astrophys J 159:185–187
20. Sahai R, Chronopoulos CK (2010) The astrosphere of asymptotic giant branch star IRC +10216. Astrophys J 711:53–56

21. Ehrenfreund P, Charnley SB (2000) Organic molecules in the interstellar medium, comets, and meteorites: a voyage from dark clouds to the early Earth. Annu Rev Astron Astrophys 38:427–483
22. De Beck E, Lombaert R, Agúndez M, Daniel F, Decin L, Cernicharo J, Müller HSP, Min M, Royer P, Vandenbussche B, de Koter A, Waters LBFM, Groenewegen MAT, Barlow MJ, Guélin M, Kahane C, Pearson JC, Encrenaz P, Szczerba R, Schmidt MR (2012) On the physical structure of IRC +10216 – ground-based and Herschel observations of CO and C_2H. http://arxiv.org/pdf/1201.1850.pdf. Accessed 9 Mar 2012
23. Gustaffson B (2010) Astrophysics: unexpected warm water. Nature 467:35–36
24. Tielens AGGM, Charnley SB (1997) Circumstellar and interstellar synthesis of organic molecules. In: Whittet DCB (ed) Origins of life evolution of the biosphere. Kluwer Academic, Dordrecht
25. Bell MB, Avery LW, MacLeod JM, Matthews HE (1992) The excitation temperature of HC_9N in the circumstellar envelope of IRC +10216. Astrophys J 400:551–555
26. Cernicharo J, Guélin M (1996) Discovery of C_8H radical. Astron Astrophys 309:27–30
27. Langer WD, Velusamy T, Kuiper TB, Peng R, McCarthy MC, Travers MJ, Kovács A, Gottlieb CA, Thaddeus P (1997) First astronomical detection of the cumulene carbon chain molecule H_2C_6 in TMC-1. Astrophys J 480:63–66
28. Guélin M, Cernicharo J, Travers MJ, McCarthy MC, Gottlieb CA, Thaddeus P, Ohishi M, Saito S, Yamamoto S (1997) Detection of a new linear carbon chain radical: C_7H. Astron Astrophys 317:1–4
29. Spaans M, Ehrenfreund P (1999) In: Ehrenfreund P, Krafft C, Kochan H, Pirronello V (eds) Laboratory astrophysics and space research. Kluwer Academic, Dordrecht
30. Evans NJ II (1999) Physical conditions in regions of star formation. Annu Rev Astron Astrophys 37:311–362
31. Greenberg JM (1986) The role of grains in molecular chemical evolution. Astrophys Space Sci 128:17–31
32. Herbst E (1987) In: Hollenbach DJ, Thronson HA (eds) Interstellar processes. Riedel, Dordrecht
33. Millar TJ, Hatchell J (1998) Chemical models of hot molecular cores. Faraday Discuss 109:15–30
34. Trumpler RJ (1930) Absorption of light in the galactic system. Publ Astron Soc Pac 42:214–227
35. Jones AP, Tielens AGGM (1994) In: Montmorle T, Lada CJ, Mirabel IF, Tran Than Van J (eds) The cold universe. Editions Frontieres, Gif-sur-Yvette
36. Henning T (1999) Grain formation and evolution in the interstellar medium. In: Le Seargent d'Hendecourt L, Joblin C, Jones A (eds) Solid interstellar matter: the ISO revolution. EDP Science/Springer, Les Ulis/Heidelberg
37. Dunne L, Eales S, Ivison R, Morgan H, Edmunds M (2003) Type II supernovae as a significant source of interstellar dust. Nature 424:285–287
38. Morgan HL, Edmunds MG (2003) Dust formation in early galaxies. Mon Not R Astron Soc 343:427–442
39. Sandford SA, Allamandola LJ (1993) H_2 in interstellar and extragalactic ices: infrared characteristics, ultraviolet production, and implications. Astrophys J 409:65–68
40. Greenberg JM (1978) Interstellar dust. In: McDonnell JAM (ed) Cosmic dust. Wiley-Interscience, New York
41. Charnley SB, Rogers SD, Ehrenfreund P (2001) Gas-grain chemical models of star forming molecular clouds as constrained by ISO and SWAS observations. Astron Astrophys 378:1024–1036
42. Allamandola LJ, Sandford SA, Tielens AGGM, Herbst TM (1992) Infrared spectroscopy of dense clouds in the C-H stretch region: methanol and "diamonds". Astrophys J 399:134–146
43. Boogert ACA, Ehrenfreund P, Gerakines PA, Tielens AGGM, Whittet DCB, Schutte WA, van Dishoeck EF, de Graauw T, Decin L, Prusti T (2000) ISO-SWS observations of

interstellar solid $^{13}CO_2$: heated ice and the galactic $^{12}C/^{13}C$ abundance ratio. Astron Astrophys 353:349–362
44. de Graauw T, Whittet DCB, Gerakines PA, Bauer OH, Beintema DA, Boogert ACA, Boxhoorn DR, Chiar JE, Ehrenfreund P, Feuchtgruber H, Helmich FP, Heras AM, Huygen R, Kester DJM, Kunze D, Lahuis F, Leech KJ, Lutz D, Morris PW, Prusti T, Roelfsema PR, Salama A, Schaeidt SG, Schutte WA, Spoon HWW, Tielens AGGM, Valentijn EA, Vandenbusshe B, van Dishoeck EF, Wesselius PR, Wieprecht E, Wright CM (1996) SWS observations of solid CO_2 in molecular clouds. Astron Astrophys 315:345–348
45. Ohishi M, Irvine WM, Kaifu N (1992) In: Singh PD (ed) Astrochemistry of cosmic phenomena. Kluwer, Dordrecht
46. Nummelin A, Whittet DCB, Gibb EL, Gerakines PA (2001) Solid carbon dioxide in regions of low mass star formation. Astrophys J 558:185–193
47. Blake GA, Sutton EC, Masson CR, Phillips TG (1987) Molecular abundances in OMC-1 – the chemical composition of interstellar molecular clouds and the influence of massive star formation. Astrophys J 315:621–645
48. Le Sergeant d'Hendecourt L, Allamandola LJ, Greenberg JM (1985) Time dependent chemistry in dense molecular clouds I. Grain surface reactions, gas/grain interactions and infrared spectroscopy. Astron Astrophys 152:130–150
49. Garrod RT, Weaver SLW, Herbst E (2008) Complex chemistry in star-forming regions: an expanded gas-grain warm-up chemical model. Astrophys J 682:283–302
50. Millar TJ (2001) Molecules in high-mass star-forming regions – theory and observation. Astron Soc Pac Conf Ser 235:45–58
51. Duley WW (2000) Chemical evolution of carbonaceous material in interstellar clouds. Astrophys J 528:841–848
52. Mason NJ, Dawes A, Holtom PD, Mukerji RJ, Davis MP, Sivaraman B, Kaiser RI, Hoffman SV, Shaw DA (2006) VUV spectroscopy and photo-processing of astrochemical ices: an experimental study. Faraday Discuss 133:311–329
53. Laffon C, Lacombe S, Bournel F, Parent P (2006) Radiation effects in water ice: a near edge X-ray absorption fine structure study. J Chem Phys 125:204714
54. Muñoz Caro GM, Jiménez-Escobar A, Martín-Gago JÁ, Rogero C, Atienza C, Puertas S, Sobrado JM, Torres-Redondo J (2010) New results on thermal and photodesorption of CO ice using the novel InterStellar Astrochemistry Chamber (ISAC). Astron Astrophys 522:108–122
55. Ciaravella A, Jiménez-Escobar A, Muñoz Caro GM, Cecchi-Pestellini C, Candia R, Giarrusso S, Barbera M, Collura A (2012) Soft X-ray irradiation of pure carbon monoxide interstellar ice analogues. Astrophys J Lett 746:L1
56. Ehrenfreund P, Fraser H (2003) Ice chemistry in space. In: Pirronello V, Krelowski J, Manicò G (eds) Proceedings of the NATO advanced study institute on solid state astrochemistry, Kluwer Academic, Dordrecht
57. Schutte WA (1999) Ice evolution in the interstellar medium. In: Le Seargent d'Hendecourt L, Joblin C, Jones A (eds) Solid interstellar matter: the ISO revolution. EDP Science/Springer, Les Ulis/Heidelberg
58. Hegstrom RA, Rein DW, Sandars PGH (1979) Parity non-conserving energy difference between mirror-image molecules. Phys Lett A 71:499–502
59. Yamagata Y (1966) A hypothesis for the asymmetric appearance of biomolecules on Earth. J Theor Biol 11(3):495–498
60. Mason S, Tranter G (1984) The parity violating energy difference between enantiomeric molecules. Mol Phys 53:1091–1111
61. Tranter G (1987) Parity violation and the origins of biomolecular handedness. Biosystems 20:37–48
62. Tranter GE, McDermott AJ (1989) Electroweak bioenantioselection. Chem Phys Lett 163:1–4
63. Berger R, Quack M (2000) Electroweak quantum chemistry of alanine: parity violation in gas and condensed phases. ChemPlusChem 1:57–60

64. Laerdahl JK, Wesendrup R, Schwerdtfeger P (2000) D- or L-alanine: that is the question. Chemphyschem 1:60–62
65. Rosenberg RA (2011) Spin-polarized e-induced asymmetric reactions in chiral molecules. Top Curr Chem 298:279–306
66. Bonner WA, Van Dort MA, Yearian MR (1975) Asymmetric degradation of DL-leucine with longitudinally polarized electrons. Nature 258:419–421
67. Ulbricht TLV, Vester F (1962) Attempts to induce optical activity with polarized beta radiation. Tetrahedron 18:629–637
68. Bonner WA, Flores JJ (1975) Experiments on the origins of optical activity. Orig Life Evol Biosph 6:187–194
69. Inoue Y (1992) Asymmetric photochemical reactions in solution. Chem Rev 92:741–770
70. Buchard O (1974) Photochemistry with circularly polarized light. Angew Chem Int Ed Engl 13:179–185
71. Rau H (1983) Asymmetric photochemistry in solution. Chem Rev 83:535–547
72. Kuhn W, Braun E (1929) Photochemical preparation of optically active substances. Naturwissenschaften 17:227–228
73. Kuhn W, Knopf E (1930) The preparation of optically active compounds by the aid of light. Z Phys Chem 7:292–310
74. Flores JJ, Bonner WA, Massey GA (1977) Asymmetric photolysis of (RS)-leucine with circularly polarized ultraviolet light. J Am Chem Soc 99:3622–3625
75. Balavoine G, Moradpour A, Kagan HB (1974) Preparation of chiral compounds with high optical purity by irradiation with circularly polarized light, a model reaction for the prebiotic generation of optical activity. J Am Chem Soc 96:5152–5158
76. Norden B (1997) Was photoresolution of amino acids the origin of optical activity of life? Nature 266:567–568
77. Nishino H, Kosaka A, Hembury GA, Shitomi H, Onuki H, Inoue Y (2001) Mechanism of pH-dependent photolysis of aliphatic amino acids and enantiomeric enrichment of racemic leucine by circularly polarized light. Org Lett 3:921–924
78. Meierhenrich UJ, Nahon L, Alcaraz C, Bredehöft JH, Hoffmann SZ, Barbier B, Brack A (2005) Asymmetric vacuum UV photolysis of the amino acid leucine in the solid state. Angew Chem Int Ed 44:5630–5634
79. Meierhenrich UJ, Nahon L, Alcaraz C, Bredehöft JH, Hoffmann SZ, Barbier B, Brack A (2005) Asymmetrische Vakuum-UV Photolyse der Aminosäure Leucin in fester Phase. Angew Chem 117:5774–5779
80. Bailey J (2001) Astronomical sources of circularly polarized light and the origin of homochirality. Orig Life Evol Biosph 31:167–183
81. Bailey J, Chrysostomou A, Hough JH, Gledhill TM, McCall A, Clark S, Ménard F, Tamura M (1998) Circular polarization in star-formation regions: implications for biomolecular homochirality. Science 281:672–674
82. Buschermöhle M, Whittet DCB et al (2005) An extended search for circularly polarized infrared radiation from the OMC-1 region of Orion. Astrophys J 624:821–826
83. Fukue T, MetM T et al (2009) Near-infrared circular polarimetry and correlation diagrams in the Orion Becklin-Neugebauer/Kleinman-low region: contribution of dichroic extinction. Astrophys J 692:88–91
84. Minchin NR, Hough JH, Burton MG, Yamashita T (1991) Near-infrared imaging polarimetry of bipolar nebulae – IV. GL490, GL 2789 and GL 2136. Mon Not R Astron Soc 251:522–528
85. Lucas PW, Hough JH, Bailey J, Chrysostomou A, Gledhill TM, McCall A (2005) UV circular polarisation in star formation regions: the origin of homochirality? Orig Life Evol Biosph 35:29–60
86. Svensmark H (2012) Evidence of nearby supernovae affecting life on Earth. Mon Not R Astron Soc 423:1234–1253
87. Diehl R, Halloin H, Kretschmer K et al (2006) Radioactive ^{26}Al from massive stars in the galaxy. Nature 439:45–47

88. Sandford SA, Aléon J et al (2006) Organics captured from comet 81P/Wild 2 by the Stardust Spacecraft. Science 314:1720–1724
89. Oro J, Gibert J, Lichtenstein H, Wikstrom S, Flory DA (1971) Amino-acids, aliphatic and aromatic hydrocarbons in the Murchison meteorite. Nature 230:105–106
90. Robert F, Epstein S (1982) The concentration and isotopic composition of hydrogen, carbon and nitrogen in carbonaceous meteorites. Geochim Cosmochim Acta 46:81–95
91. Kvenvolden KA, Lawless JG, Ponnamperuma C (1971) Non-protein amino acids in the Murchison meteorite. Proc Natl Acad Sci USA 68:486–490
92. Cronin JR, Pizzarello S (1997) Enantiomeric excesses in meteoritic amino acids. Science 275:951–955
93. Pizzarello S, Cronin JR (2000) Non-racemic amino acids in the Murray and Murchison meteorites. Geochim Cosmochim Acta 64:329–338
94. Glavin DP, Dworkin JP (2009) Enrichment of the amino acids L-isovaline by aqueous alteration on CI and CM meteorite parent bodies. Proc Natl Acad Sci 106:5487–5492
95. Muñoz Caro GM, Meierhenrich UJ, Schutte WA, Barbier B, Arcones Segovia A, Rosenbauer H, Thiemann WH-P, Brack A, Greenberg JM (2002) Amino acids from ultraviolet irradiation of interstellar ice analogues. Nature 416:403–406
96. Bernstein MP, Dworkin JP, Sandford SA, Cooper GW, Allamandola LJ (2002) Racemic amino acids from the ultraviolet photolysis of interstellar ice analogues. Nature 416:401–403
97. Holtom PD, Bennett CJ, Osamura Y, Mason NJ, Kaiser RI (2005) A combined experimental and theoretical study on the formation of the amino acid glycine (NH_2CH_2COOH) and its isomer ($CH_3NHCOOH$) in extraterrestrial ices. Astrophys J 626:940–952
98. Briggs R, Ertem G, Ferris JP, Greenberg JM, McCain PJ, Mendoza-Gomez CX, Schutte W (1992) Comet Halley as an aggregate of interstellar dust and further evidence for the photochemical formation of organics in the interstellar medium. Orig Life Evol Biosph 22:287–307
99. d'Hendecourt LB, Allamandola LJ, Baas F, Greenberg JM (1982) Inter-stellar grain explosions – molecule cycling between gas and dust. Astron Astrophys 109:12–14
100. Meinert C, Fillipi J-J, de Marcellus P, Seargent L, d'Hendecourt L, Meierhenrich UJ (2012) *N*-(2-Aminoethyl)glycine and amino acids from interstellar ice analogues. Chempluschem 77:186–191
101. Nahon L, de Oliveira N, Garcia G, Gil JF, Pilette B, Marcouille O, Lagarde B, Polack F (2012) DESIRS: a state-of-the-art VUV beamline featuring high resolution and variable polarization for spectroscopy and dichroism at SOLEIL. J Synchrotron Radiat 19:508–520
102. Nahon L, Alcaraz C (2004) SU5: a calibrated variable-polarization synchrotron radiation beam line in the vacuum-ultraviolet range. Appl Opt 43:1024–1037
103. Meierhenrich UJ (2008) Amino acids and the asymmetry of life – caught in the act of formation. Springer, Heidelberg
104. Meierhenrich UJ, Muñoz Caro GM, Bredehöft JH, Jessberger EK, Thiemann WH-P (2004) Identification of diamino acids in the Murchison meteorite. Proc Natl Acad Sci USA 101:9182–9186
105. Meierhenrich UJ, Filippi J-J, Meinert C, Bredehöft JH, Takahashi J, Nahon L, Jones NC, Hoffmann SV (2010) Circular dichroism of amino acids in the vacuum-ultraviolet region. Angew Chem Int Ed 49:7799–7802
106. Meierhenrich UJ, Filippi J-J, Meinert C, Bredehöft JH, Takahashi J, Nahon L, Jones NC, Hoffmann SV (2010) Circulardichroismus von Aminosäuren im Vakuum-Ultravioletten. Angew Chem 122:7966–7970
107. Adrian-Scotto M, Antonczak S, Bredehöft JH, Hoffmann SV, Meierhenrich UJ (2010) Chiroptical properties of amino acids: a density functional theory study. Symmetry 2:935–949
108. Meierhenrich UJ, Filippi J-J, Meinert C, Hoffmann SV, Bredehöft JH, Nahon L (2010) Photolysis of rac-Leucine with circularly polarized synchrotron radiation. Chem Biodivers 7:1651–1659

109. Meierhenrich UJ, Filippi J-J, Meinert C, Hoffmann SV, Bredehöft JH, Nahon L (2011) Photolysis of rac-leucine with circularly polarized synchrotron radiation. In: Brückner H, Fujii N (eds) D-Amino acids in chemistry, life sciences, and biotechnology. Wiley-VCH, Weinheim
110. Evans AC, Meinert C, Giri C, Goesmann F, Meierhenrich UJ (2012) Chirality, photochemistry and the detection of amino acids in interstellar ice analogues and comets. Chem Soc Rev 41:5447–5458
111. Frank FC (1953) On spontaneous asymmetric synthesis. Biochim Biophys Acta 11:459–463
112. Kondepudi DK, Prigogine I (1998) Modern thermodynamics: from heat engines to dissipative structures. Wiley, New York
113. Kondepudi DK, Asakura K (2001) Chiral autocatalysis, spontaneous symmetry breaking, and stochastic behavior. Acc Chem Res 34:946–954
114. Soai K, Shibata T, Morioka H, Choji K (1995) Asymmetric autocatalysis and amplification of enantiomeric excess of a chiral molecule. Nature 378:767–768
115. Breslow R, Levine M (2006) Amplification of enantiomeric concentrations under credible prebiotic conditions. Proc Natl Acad Sci USA 103:12979–12980
116. Klussmann M, Iamura H, Mathew S, Wells D, Pandya U, Armstrong A, Blackmond D (2006) Thermodynamic control of asymmetric amplification in amino acid catalysis. Nature 441:621–623
117. Noorduin W, Izumi T, Millemaggi A, Leeman M, Meekes H, Van Enckevort W, Kellogg R, Kaptein B, Vlieg E, Blackmond D (2008) Emergence of single solid chiral state from a nearly racemic amino acid derivative. J Am Chem Soc 130:1158–1159
118. Viedma C, Ortiz J, de Torres T, Izumi T, Blackmond D (2008) Evolution of solid phase homochirality for a proteinogenic amino acid. J Am Chem Soc 130:15274–15275
119. Nielsen PE (1993) Peptide nucleic-acid (PNA) – a model structure for the primordial genetic material. Orig Life Evol Biosph 123:323–327
120. Muñoz Caro GM, Meierhenrich UJ, Schutte WA, Greenberg JM, Thiemann W (2004) UV-photoprocessing of interstellar ice analogs: detection of hexamethylenetetramine-based species. Astron Astrophys 413:209–216
121. Meierhenrich UJ, Muñoz Caro GM, Schutte WA, Thiemann WH-P, Barbier B, Brack A (2005) Precursors of biological cofactors from ultraviolet irradiation of circumstellar/interstellar ice analogs. Chemistry 11:4895–4900
122. Nuevo M, Bredehöft JH, Meierhenrich UJ, d'Hendecourt L, Thiemann WH-P (2010) Urea, glycolic acid, and glycerol in an organic residue produced by ultraviolet irradiation of interstellar/precometary ice analogs. Astrobiology 10:245–256
123. Bonnet RM (1985) The new mandatory scientific programme for ESA. ESA Bull 43:8–13
124. Huber MCE, Schwehm G (1991) Comet nucleus sample return: plans and capabilities. Space Sci Rev 56:109–115
125. Schwehm G, Schulz R (1999) ROSETTA goes to comet Wirtanen. Space Sci Rev 90:313–319
126. Weismann PR, Asphaug E, Lowry SC (2004) Structure and density of cometary nuclei. In: Festou MC, Keller HU, Weaver HA (eds) Comets II. University of Arizona Press, Tucson
127. Glassmeier K-H, Boehnhardt H, Koschny D, Kührt E, Richter I (2008) The ROSETTA mission: flying towards the origin of the solar system. In: Schulz R, Alexander C, Boehnhardt H, Glassmeier K-H (eds) ROSETTA ESA's mission to the origin of the solar system. Springer, New York
128. Bibring J-P, Rosenbauer H, Boehnhardt H, Ulamec S, Biele J, Espinasse S, Feuerbacher B, Gaudon P, Hemmerich P, Klestzkine P et al (2007) The ROSETTA lander ("PHILAE") investigations. Space Sci Rev 128:205–220
129. Goesmann F, Rosenbauer H, Roll R, Boehnhardt H (2005) COSAC onboard Rosetta: a bioastronomy experiment for the short-period comet 67P/Churyumov-Gerasimenko. Astrobiology 5:622–631

130. Goesmann F, Rosenbauer H, Roll R, Szopa C, Raulin F, Sternberg R, Israel G, Meierhenrich UJ, Thiemann W, Muñoz Caro GM (2007) COSAC, the cometary sampling and composition experiment on PHILAE. Space Sci Rev 128:257–280
131. Meierhenrich U, Thiemann WH-P, Rosenbauer H (1999) Molecular parity violation via comets? Chirality 11:575–582
132. Elsila JE, Glavin DP, Dworkin JP (2009) Cometary glycine detected in samples returned by Stardust. Meteorit Planet Sci 44:1323–1330
133. Thiemann WH-P, Rosenbauer H, Meierhenrich UJ (2001) Conception of the 'chirality-experiment' on ESA's mission ROSETTA to comet 46P/Wirtanen. Adv Space Res 27:323–328
134. Meierhenrich UJ, Thiemann WH-P, Goesmann F, Roll R, Rosenbauer H (2001) Enantiomer separation of hydrocarbons in preparation of Rosetta's 'chirality-experiment'. Chirality 13:454–457
135. Meierhenrich U, Thiemann WH-P, Rosenbauer H (2001) Pyrolytic methylation assisted enantioseparation of chiral hydroxycarboxylic acids. J Anal Appl Pyrolysis 60:13–26

Top Curr Chem (2013) 333: 83–108
DOI: 10.1007/128_2012_397

Published online: 28 December 2012

Chemical and Physical Models for the Emergence of Biological Homochirality

Jason E. Hein, Dragos Gherase, and Donna G. Blackmond

Abstract The past several decades have witnessed the development of a number of different experimental approaches to help understand how the homochirality of biological molecules might have evolved in a prebiotic world. This chapter reviews chemical and physical models with a special focus on recent developments in attrition-enhanced deracemization of conglomerates, a process that combines solution phase chemical interconversion of enantiomers with thermodynamic and kinetic considerations of solubility, crystal growth, and dissolution.

Keywords Asymmetric amplification · Autocatalysis · Conglomerate · Enantiomeric excess · Enantiomorph · Eutectic composition · Homochirality · Racemic compound · Solubility

Contents

J.E. Hein and D. Gherase
Chemistry and Chemical Biology University of California Merced, CA 95343 USA
e-mail: jhein2@ucmerced.edu; gherase@scripps.edu

D.G. Blackmond (✉)
Department of Chemistry, The Scripps Research Institute, La Jolla, CA 92037, USA
e-mail: blackmond@scripps.edu

1 Introduction

Homochirality is a characteristic of biological molecules that has intrigued scientists for more than 150 years [1]. Experimental studies aimed at probing the plausibility of different hypotheses for how molecular single-handedness may have emerged have increased in number and diversity over the past several decades, complementing earlier theoretical models [2, 3]. Several of the most popular approaches that have been reported are illustrated in Fig. 1. These include chemical models such as the Soai autocatalytic reaction [4] (Fig. 1a) and physical models based on the physical phase behavior of chiral molecules, exploiting different features of how enantiomers crystallize, as illustrated in Fig. 1b–d [5–8]. One of the most recent and arguably most intriguing of these physical models is the attrition-enhanced deracemization of chiral conglomerates discovered by Viedma [8] (Fig. 1d). The process of attrition-enhanced solid-phase deracemization has received significant attention in both experimental [9–19] and theoretical [20–26] studies. After a brief discussion of the models in Fig. 1a–c, the main part of this chapter focuses on the model of Fig. 1d. We discuss and assess proposed explanations for this phenomenon based on results reported to date and we present additional experimental findings to help shed further light on this intriguing route to homochirality.

2 Asymmetric Autocatalysis

The Soai autocatalytic reaction [4] provided the first experimental proof-of-concept that amplification of enantiomeric excess could arise from a small initial imbalance via autocatalysis (Fig. 1a). As outlined by Frank in a classic 1953 theoretical paper [2], an autocatalytic reaction, in which the product acts as a catalyst to produce more of itself, can lead to the emergence of homochirality if this reaction is coupled

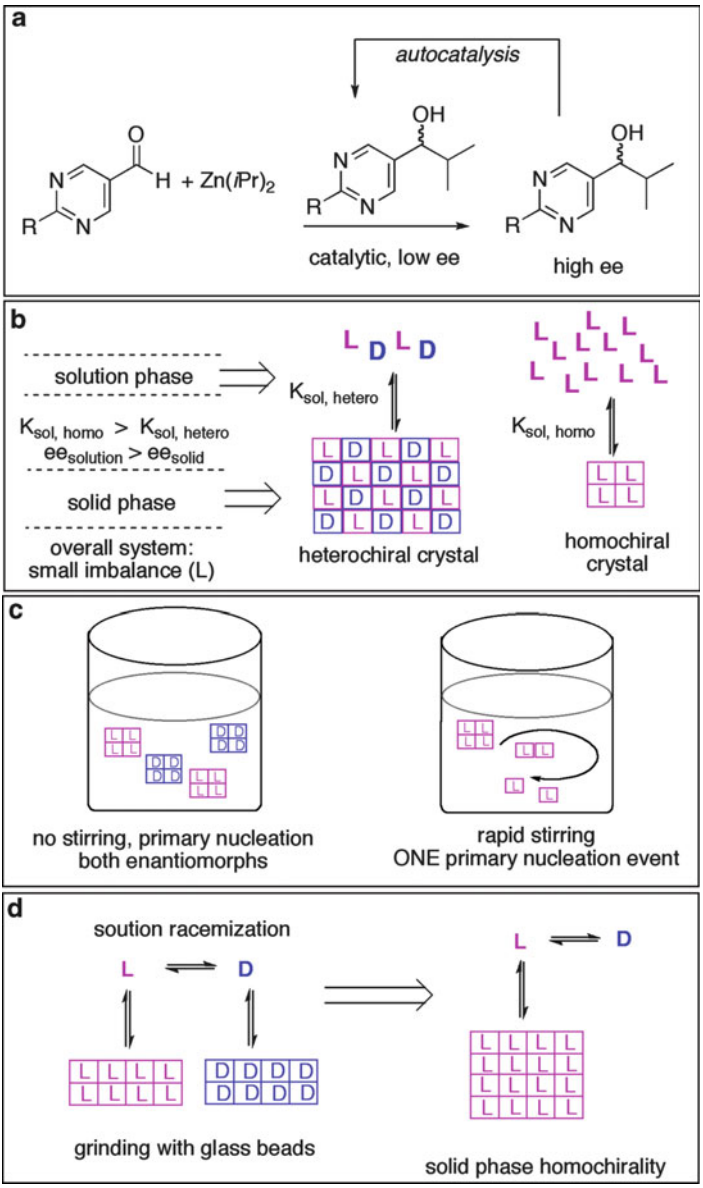

Fig. 1 Models for the emergence of homochirality. (**a**) the Soai asymmetric autocatalytic reaction [4] that amplifies a small initial imbalance in the product (catalyst) ee [5]; (**b**) the eutectic model that exploits differences in solubility of homo- and heterochiral crystals to create solution-phase enantioenrichment [6]; (**c**) Kondepudi's crystallization of enantiomorphic solids via rapid secondary nucleation of a single "Eve" crystal [7]; (**d**) conversion of one chiral enantiomorph to the other via solution phase racemization based on Viedma's model for $NaClO_3$ [8]

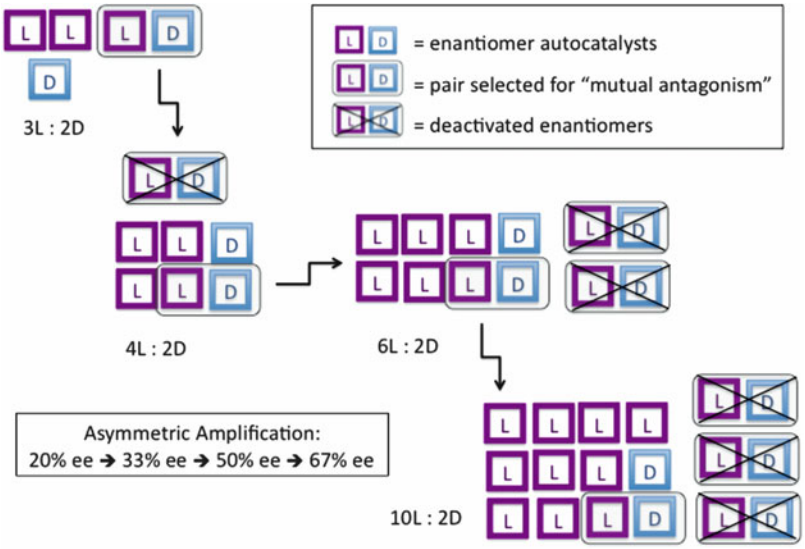

Fig. 2 Illustration of the Frank model for the evolution of homochirality based on self-replication of like and mutual antagonism of opposite enantiomers. Redrawn from [4]

with inhibition of production of the other enantiomer (a process called "mutual antagonism" by Frank). In its simplest form, the Frank model dictates that when opposite enantiomers interact, they "deactivate" one another and prevent each other from undergoing further self-replication. Because equal numbers are siphoned off from each enantiomer pool, a small initial imbalance of enantiomers will grow over time. The amplification achieved in this scenario may be illustrated by the example in Fig. 2. For each autocatalytic cycle in the illustration shown in Fig. 2 we assume that one L:D pair is selected for deactivation by mutual antagonism, while the remaining enantiomers of both hands replicate themselves. Figure 2 shows an initial ratio of L:D = 3:2, or 20% ee. This system contains one deactivated L:D pair along with one D and two L active enantiomers. These enantiomers replicate to yield 4 L and 2 D, giving an ee value of 33%. Repetition of the mutual antagonism and self-replication processes leads to 50% ee and 67% ee over the next two cycles.

This simple example illustrates the mathematical roles of both the self-replication and the inhibition processes in the emergence of homochirality, but it does not offer chemical insight into the mechanism of a reaction that might follow its precepts [27, 28]. The first mechanistic studies to shed light on the Soai reaction were carried out by Blackmond, Brown, and coworkers [29–33] who demonstrated, from in situ kinetic studies, NMR spectroscopy, and computational work, the manner in which the Soai reaction adheres to the Frank model: the alkoxide reaction product is driven to dimerize, forming homo- and heterochiral dimers in equal proportions. The formation of higher order species may also occur as suggested by more recent experiments. The active catalyst is thought to be a homochiral aggregate, while

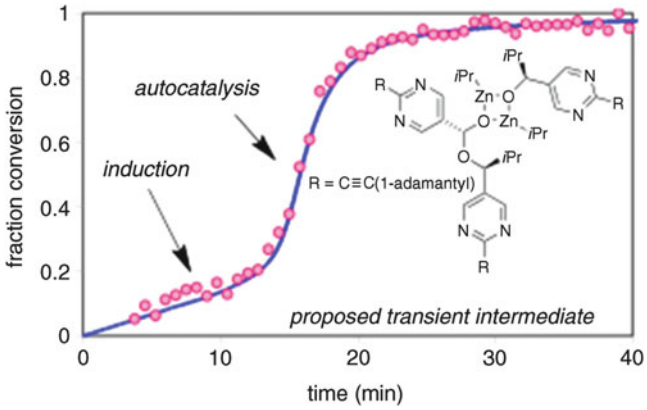

Fig. 3 Kinetic profile (Gehring T, Blackmond DG, unpublished results) of the Soai reaction from reaction calorimetry (*blue line*) and FTIR spectroscopy (*pink circles*), with the proposed transient species observed by NMR [33]

heterochiral species are inactive as catalysts, providing the "mutual antagonism" component. Blackmond [34] demonstrated mathematically how this inhibition feature is critical to achieving amplification of enantiomeric excess in this application of the Frank model.

Since its initial discovery, experimental studies of the Soai reaction have revealed a number of intriguing details that demonstrate the power of this reaction to amplify enantiomeric excess. Extremely low levels of low ee catalysts can cause amplification to extremely high product ee values over many reaction cycles [35]. Amplification may be reproducibly initiated using a variety of chiral sources to create a small imbalance, including circularly polarized light or chiral solids such as quartz [36, 37]. Recent studies show that the minute energy difference provided by isotopically chiral molecules is sufficient to direct the chirality of the reaction product over repeated autocatalytic cycles [38–40].

Even given all these striking results, details about the structure of the active species in the Soai reaction have remained elusive. A number of attempts to model the reaction have been made based on available kinetic data, but direct observation of reactive species has been a challenge. Most recently, however, Gehring et al. reported the first NMR observation of a transient intermediate in the Soai reaction during reaction turnover [33]. The species is identified as an alkoxyacetal, suggested to be comprised of one reactant aldehyde and two product alkoxides. Reaction calorimetric and FTIR spectroscopic monitoring of the kinetic profile shown in Fig. 3 support these NMR observations (Gehring T, Blackmond DG, unpublished results). The structure of the intermediate was computed from DFT studies based on a square dimer species found in previous computational work. The precise role of this transient species in construction of the active autocatalyst during the critical induction period is still unknown and is the subject of further experimental and computational study.

The Soai reaction has inspired a wealth of studies – experimental, theoretical, and computational – aimed at understanding the processes of symmetry breaking and asymmetric amplification. However, this most prominent experimental example of asymmetric autocatalysis exhibits significant constraints on substrates and reaction conditions. The search for further examples, in particular for reactions exhibiting chemistry of greater prebiotic relevance, continues apace but has proved inconclusive to date.

3 Eutectic Model

3.1 Application to Racemic Compounds

The phase behavior of chiral molecules may be exploited to effect enantioenrichment starting from a small overall imbalance of enantiomers partially dissolved in water or other liquids as solvent. The equilibrium-driven partitioning that occurs between solid and liquid phases provides the basis for what is commonly called the eutectic model for homochirality (Fig. 1b) applied to racemic compounds, which are chiral molecules that crystallize preferentially as heterochiral crystals [5, 6, 41–46]. Similar behavior has also been demonstrated for selective partitioning between solid and gas phases via sublimation [47–49]. In both cases, enantioenrichment relies on differences in the solubility and stability (as measured by the heat of fusion) of crystals that form in a heterochiral (L–D) array compared to those that form homochirally (L–L or D–D). When a non-racemic, non-enantiopure chiral molecule partially dissolved in solvent attains equilibrium between the solution and solid phases at a given temperature and pressure, the Gibbs phase rule dictates that its solution composition is fixed at what is commonly called the eutectic point. Typically, heterochiral crystals are less soluble than homochiral crystals, and at equilibrium the solution will be enriched in the enantiomer that is overall in excess in the system. As early as 1969, Morowitz [41] recognized that this selective partitioning could lead to solution-phase amplification of enantiomeric excess, demonstrated in studies of phenylalanine and isoleucine. Breslow corroborated this phenomenon for phenylalanine [42] and reported high eutectic ee values for several nucleosides of prebiotic importance [43]. Blackmond and coworkers surveyed eutectic compositions for a wide range of proteinogenic amino acids [6, 44, 45]. A recent theoretical treatment based on a two-dimensional lattice model successfully predicts the ternary phase behavior of amino acids based on the interactions that stabilize the racemic crystal, providing molecular level insight into enantiomer partitioning [46].

Blackmond and coworkers also demonstrated how enantioenriched solutions that resulted from eutectic partitioning could be used to extend enantioenrichment to other molecules by exploiting amino acids in solution as asymmetric catalysts [6]. For example, the product enantiomeric excess in an aldol reaction catalyzed by

serine was observed to be identical for a partially dissolved system of overall 1% ee serine and an enantiopure homogeneous solution. Such strong amplification is possible because serine exhibits a high eutectic ee of 99% and the solution phase serine effects the catalytic reaction.

3.2 Comparison to Asymmetric Autocatalysis

It is important to note that this amplification mechanism differs in a significant way from asymmetric autocatalysis as described by the Frank model [2]. While the formation of less soluble heterochiral crystals may be considered analogous to the "mutual antagonism" component of the Frank model, the eutectic model provides no means of increasing the major enantiomer analogous to autocatalytic self-replication. The maximum possible level of amplification is dictated by the molecule's eutectic value, which is a characteristic property of that substance. Amplification cannot be made to increase exponentially over repetitive cycles of equilibrium evaporation, unlike in repetitive autocatalytic cycles as illustrated in Fig. 2. While it is possible to produce nearly enantiopure solutions starting from nearly racemic mixtures for some amino acids, as was observed with serine, for many amino acids the level of solution enantioenrichment is much lower. For example, isoleucine, proline, and alanine are limited by their eutectic compositions to maximum solution ee values of ca. 50–60% ee [6].

3.3 Eutectic Tuning

Thus the eutectic model cannot directly rationalize homochirality for all of the proteinogenic amino acids. However, Blackmond and coworkers discovered a means by which eutectic ee values may be enhanced by a modification to the eutectic model which exploits characteristics of amino acids co-crystallized with achiral additives. If the intrinsic relative stability/solubility of L–D vs D–D or L–L crystals is modified when additives are incorporated in the crystal, enhanced solution enantioenrichment may be possible for a range of molecules, including amino acids that naturally exhibit low eutectic ee values [44, 45]. An example is valine (val), with a eutectic of 47% ee, meaning that the homochiral and heterochiral crystals are approximately equally soluble. When fumaric acid (FA) co-crystallizes with val, the solubility of the heterochiral crystals incorporating the additive is suppressed nearly tenfold relative to that of the homochiral crystals, resulting in solution phase enantioenrichment to 99% ee. Fumaric acid co-crystallizes with phenylalanine, phe, altering relative solubility to produce nearly enantiopure solutions. The extended crystal structure of the 1:1 DL phe:FA is shown in Fig. 4. Hydrogen bonding between the additive and the amino acid enantiomers effectively

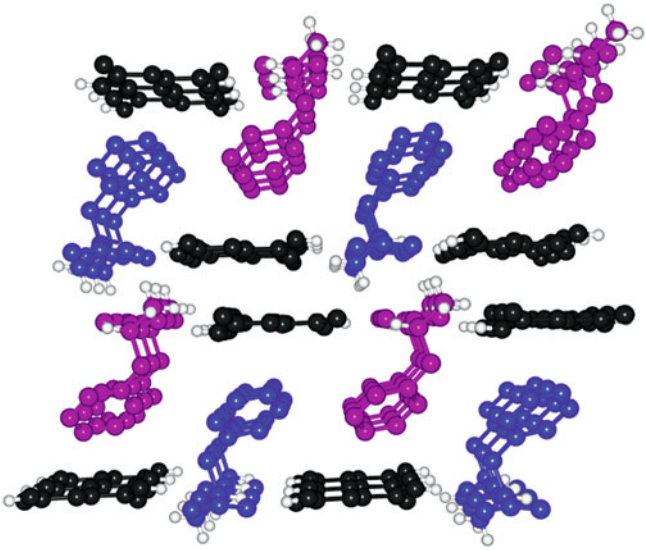

Fig. 4 Extended crystal structure for racemic phenylalanine with fumaric acid as a 1:1 co-crystal. Phe enantiomers are shown in *magenta* and *blue*, fumaric acid in *black* [45]

Table 1 Solution ee at the eutectic for amino acids in aqueous solution in the presence of carboxylic acid additives [45]

	Amino acid % ee at the eutectic						
Additive	Thr	Val	Ile	Met	Phe	Leu	His
None	0	47	52	85	88	88	94
Oxalic acid	50	66	82	43	23	98	63
Malonic acid	11	50	51	69	86	91	91
Succinic acid	2	93	52	42	79	89	56
Maleic acid	34	69	71	55	7	81	82
Fumaric acid	24	99	59	72	99	92	98
Adipic acid	0	46	51	66	94	92	77

enrichment

depletion

stabilizes the heterochiral co-crystal, decreasing its solubility. An illustration of how this concept of "eutectic tuning" can alter the eutectic composition is shown in Table 1 for a variety of amino acids with dicarboxylic acid additives [45].

The concept that equilibrium solution ee values for partially dissolved amino acids and other chiral molecules may be "tuned" by the presence of achiral additives broadens the potential scope of the eutectic model for the emergence of homochirality. Equilibrated, enantioenriched solutions of a wide range of chiral molecules may be envisioned, serving as "warm little ponds" that undergo further reactions either as chiral catalysts or as chiral building blocks, providing enantioenriched reaction products.

4 Solid Phase Homochirality for Conglomerate Crystals of Achiral Molecules

4.1 "Eve Crystal" Model

Enantioenrichment by the eutectic approach outlined above may be possible for a wide variety of chiral molecules. However, ca. 10% of chiral compounds do not form heterochiral crystals, including several proteinogenic amino acids. Molecules that crystallize as separate L–L and D–D crystals are called conglomerates. A route to homochirality for such conglomerate crystals was first hinted at in studies of the crystallization of $NaClO_3$, a molecule that is itself not chiral but which forms mirror-image conglomerate crystals. Kondepudi showed that supersaturated solutions of $NaClO_3$ could be induced under rapid stirring to crystallize as a single solid enantiomorph, without any pre-existing chiral bias [7]. The process is random, with an equal chance of producing either enantiomorph in a given experiment. Rationalization of this intriguing finding led to what is called the "Eve crystal" model. Upon impact of a stirring blade, the first nucleated ("Eve") crystal disintegrates into many small crystals of that same handedness. The resulting increased crystal surface area leads to rapid secondary nucleation where molecules from solution rapidly add on to these crystals before another primary crystal is formed [7, 50].Primary nucleation events, which could result in formation of crystals of the opposite handedness, are further suppressed because of the rapid decrease in solution concentration that occurs as molecules add to the daughter crystals (Fig. 1c).

4.2 Viedma Ripening for $NaClO_3$

The $NaClO_3$ system was also the original focus of a further mechanism for the evolution of homochirality that involves near-equilibrium physical and chemical processes. In a striking experiment, Viedma [8] showed that a mixture of equal amounts of left- and right-handed crystals could be transformed completely to one or to the other – randomly – when a saturated solution of the crystals is subjected to attrition. Strictly speaking, this process does not involve crystallization at all. Dynamic changes occur – some crystals dissolve and others grow – but under these attrition conditions the level of supersaturation is never high enough for new crystals to nucleate from solution.

This result was unexpected, because a racemic mixture of left- and right-handed crystals in equilibrium with its achiral liquid phase appears to have no driving force for the net movement of molecules from one hand to the other. Because the proposed explanation calls upon the concept of Ostwald ripening, as discussed in the next section, this phenomenon has earned the term "Viedma ripening."

5 Application to Intrinsically Chiral Molecules

5.1 *Proof of Concept*

Viedma's remarkable report inspired a quest to apply this phenomenon to intrinsically chiral molecules (Fig. 1d). When the enantiomers of a chiral molecule undergo rapid interconversion in solution via racemization they may emulate the behavior of an achiral molecule such as $NaClO_3$ – that is, an enantiomer dissolving from a left- or right-hand crystal can exchange its chiral "identity" while in solution and ultimately add to a crystal of the opposite hand. Attrition-enhanced deracemization was ultimately demonstrated for a number of chiral conglomerates, including a proteinogenic amino acid [10] (Fig. 5). In fact, it was shown that the phenomenon is also driven by heating, even in the absence of attrition. Key to the process is the imparting of thermal or mechanical energy to the system.

5.2 *Comparison to Eutectic Model*

It is important to note the fundamental differences between Viedma ripening and the eutectic model. Both exploit the phase behavior of chiral molecules to achieve enantioenrichment, which occurs in the solution phase for the eutectic model but in the solid phase for Viedma ripening. The eutectic model is applied to racemic compounds, which form heterochiral crystals preferentially, and Viedma ripening applies to conglomerates that prefer homochiral arrays in the solid phase. Both models rely on thermodynamic or near-thermodynamic equilibrium conditions. Viedma ripening incorporates both chemical reactions and physical phase transfer processes, while the eutectic model involves purely physical phase behavior. Most importantly, however, is the fact that Viedma ripening achieves not simply a selective *partitioning* of enantiomers as in the eutectic model but a net *conversion* of molecules from one hand of the solid enantiomorph to the other in a process driven and mediated by chemical interconversion in the solution phase.

5.3 *Dimroth's Principle*

Viedma ripening involves both chemical reactions in solution and physical mass transfer between phases. The interplay between these different rate processes has been studied for over a century since the development of Dimroth's principle [51], which today is routinely applied in the pharmaceutical industry for the separation and interconversion of diastereomers [52]. It is worthwhile to explain Dimroth's principle here because of its implications for Viedma ripening, as will be discussed. The mechanism is illustrated in Fig. 6 for an example taken from Dimroth's classic work. Isomer **A** is less soluble than isomer **B**, resulting in a sixfold higher

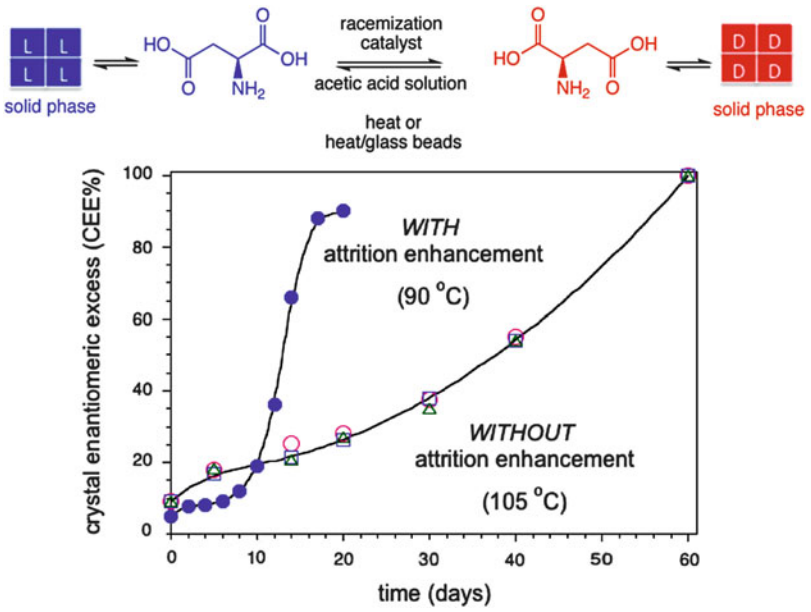

Fig. 5 Emergence of solid-phase homochirality for the amino acid aspartic acid in acetic acid with salicylaldehyde added as racemization catalyst. Redrawn from [10]

concentration of **B** in solution at equilibrium. When a catalyst is added to this system under its physical equilibrium, the driving force for chemical equilibrium must also be taken into account, because interconversion between **A** and **B** in solution proceeds at an enhanced rate. It happens that in this case the chemical equilibrium for **A** and **B** lies far towards **A**. This means that the chemical and physical equilibria are at odds with one another: solubility considerations dictate an excess of **A** in solution, while chemical equilibrium dictates an excess of **B** in solution. Isomerization driving **B** towards **A** in solution disturbs the physical equilibria, which the system attempts to re-establish by dissolving molecules from solid **B** to replenish solution saturation in **B**; at the same time, solution molecules of **A** are driven to add to solid **A** to relieve super-saturation in **A**. Key to this concept is the opposition of the isomerization equilibrium position to that of the physical phase equilibria. Thus the imbalance between the chemical and physical equilibria reinforce the net movement of molecules from **B** to **A** that continues until all of solid **B** has dissolved.

5.4 Application of Dimroth's Principle to Enantiomers

At first glance, applying the concepts of Dimroth's principle to the net conversion of enantiomers appears to be problematic, since the physical and chemical processes in question should be perfectly balanced: the racemization equilibrium

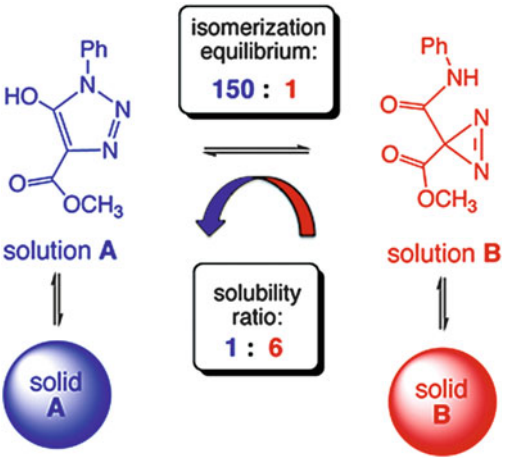

Fig. 6 Illustration of Dimroth's principle [51]: an imbalance between concentration driving forces dictated by chemical (isomerization) and physical (solubility) equilibria leads to the net movement of molecules from solid phase **B** to solid phase **A** through the conduit of solution phase isomerization

constant is unity, and enantiomers exhibit identical solubilities. Under these circumstances, how can a net driving force be constructed to move molecules from one solid enantiomorph to the other?

The earliest explanations of Viedma's results for $NaClO_3$ invoked a combination of well-known physical processes for crystal growth by Ostwald ripening and crystal dissolution according to the Gibbs–Thomson rule, given in (1). These theories tell us that, as a consequence of the dependence of crystal size on solubility, big crystals tend to grow bigger and small crystals tend to dissolve more readily. Because crystals of different sizes exhibit different solubilities, a solubility driving force may be established if a difference in average crystal size exists between the two enantiomorphs. The key to rationalizing Viedma ripening lies in understanding how a crystal size imbalance between L and D crystals, present in the same pot under the same attrition or thermal conditions, might occur:

$$C_{sol} = C_{\infty} \cdot \exp\left(\frac{\sigma}{R}\right) \tag{1}$$

C_{sol} = crystal solubility (M)
C_{∞} = solubility of infinite planar surface (M)
R = crystal radius (m)

$$\sigma = \frac{2\gamma V_{\mathrm{m}}}{K_{\mathrm{B}} T}$$

γ = surface tension (N/m)
V_{m} = molecular volume (m^3)
K_{B} = Boltzmann's constant (J/K)
T = absolute temperature, K

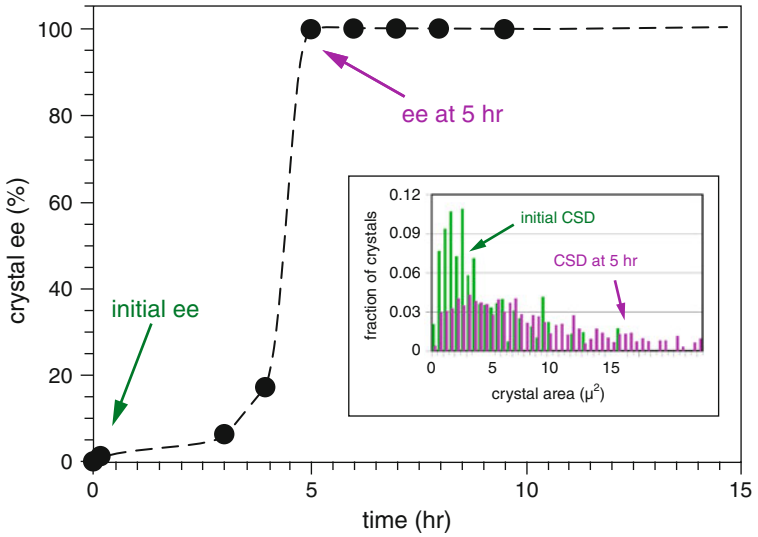

Fig. 7 Crystal ee and crystal size distribution as a function of time during attrition-enhanced deracemization of **1** (redrawn from [19])

A recent study [19] demonstrated a clear correlation between the evolution of homochirality and the transient, temporal broadening of the crystal size distribution in attrition-enhanced deracemization studies of **1** (2), the chiral component of the blockbuster drug Clopidogrel (Plavix) as shown in Fig. 7.

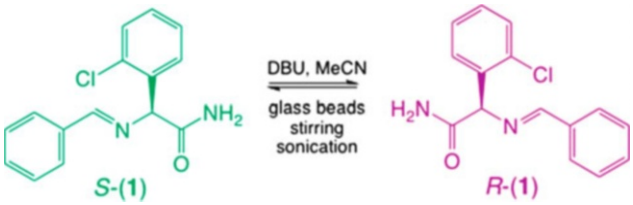

(2)

5.5 *Stochastic Behavior*

The randomness of the deracemization process starting from seemingly racemic mixtures of enantiomorphic solids is highlighted by the results shown in Fig. 8. Of 24 separate runs carried out under identical conditions, the number trending towards *R* and towards *S* was similar, and a similar number did not move away from racemic at all over the course of the experiment. Interestingly, runs that did not evolve away from the racemic state also did not show an increase in crystal size.

Movement of molecules from one solid enantiomorph to the other via the conduit of solution phase racemization must occur even in runs where the system remains racemic, i.e., when there is no *net* movement of molecules resulting in solid

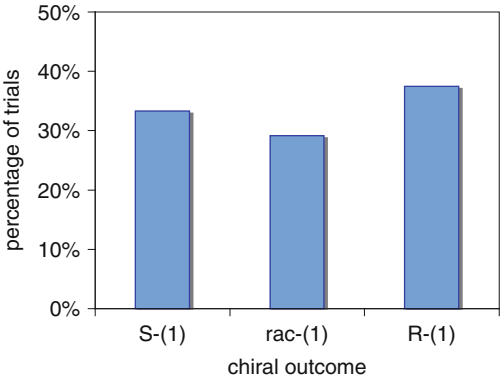

Fig. 8 Probability of different chiral outcomes for racemic mixtures of solid (**1**) attrition-enhanced deracemization. Redrawn from data in [19]

phase homochirality. This overall mass transfer rate between solids may be monitored by isotopic labeling of one enantiomorph [19]. Compound **1** was synthesized with ^{15}N label in the amide group. Racemic mixtures of labeled solid *R*-(**1**) and unlabeled solid *S*-(**1**) (and the reverse case) were subjected to attrition under racemizing conditions, allowing the rate of movement of the label between the solids to be compared to the rate of evolution of homochirality. Figure 9 shows that after less than 3 h, molecules that started out in the *R*-solid have an equal probability of being found in the *S*-solid. Even more strikingly, this reversible mass transfer occurs reproducibly even in cases where the system remains racemic. Thus mass transfer of molecules between the solids occurs freely and apparently independently of the process of the emergence of homochirality.

5.6 A Role for Subcritical Clusters

The results in Figs. 7, 8, and 9 show that the evolution to solid phase homochirality correlates with a sudden, if randomly and not reproducibly triggered, increase in crystal size of one enantiomorph. Under attrition conditions it might be envisioned that occasionally a crystal that avoids contact with glass beads could serve as a "seed" for attracting deposition of molecules, resulting in cycles of further growth and then further deposition. Such cycles could lead to the emergence of homochirality via a crystal size-induced net flux of molecules from one enantiomorph to the other. However, some researchers have argued that solubility considerations of the Gibbs–Thomson driving force are insufficient to rationalize the exponential form of the deracemization profiles [18, 22]. They propose that crystal growth such as that observed during deracemization of **1** is aided by addition of nascent "clusters" of molecules that are too small to be considered as crystals in their own right and are not observable under the conditions of the experiment. Kinetic models of the

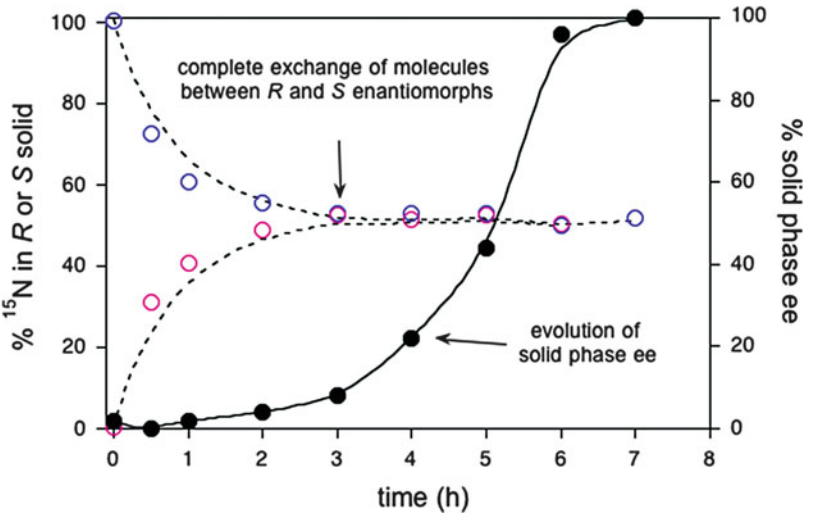

Fig. 9 Monitoring movement of molecules between solid *R* and *S* enantiomorphs by isotopic labeling starting from equal amounts of ^{15}N-labeled *R*–(**1**) (*open blue circles*) and ^{14}N-labeled *S*-(**1**) (*open pink circles*) under racemizing attrition conditions. Evolution of solid phase ee shown as *filled black circles*. Redrawn from [19]

agglomeration of such clusters onto same-handed crystals treat these physical rate processes in mathematical analogy to elementary chemical reaction rates, with higher order concentration dependences resulting when clusters interact with crystals than when single molecules interact with crystals [24]. It has been shown that for amplification of ee in autocatalytic reactions, the rate of production must exhibit a greater than linear dependence on concentration [53]. This provides an empirical description of the physical processes of crystal growth and dissolution, in contrast to chemical kinetic models, which are founded on the fundamental behavior of molecules engaged in elementary chemical reaction steps.

5.7 *Crystal Size and Solubility*

The relationship between crystal size and solubility dictated by the Gibbs–Thomson rule was probed further by carrying out careful solubility measurements of separate *R*-(**1**) and *S*-(**1**) fractions with different median crystal sizes. These samples were prepared by stirring separate slurries of each enantiomorph under different attrition conditions, which alters both the crystal size distribution and the solubility. Equal portions by weight of the two enantiomorphs were then taken from the two preparations and mixed together (in the absence of a racemization catalyst). The solution phase ee for the combined slurry was found to be ca. 5% ee towards *S*, the sample exhibiting smaller crystals, even though the total number of *S* and *R*

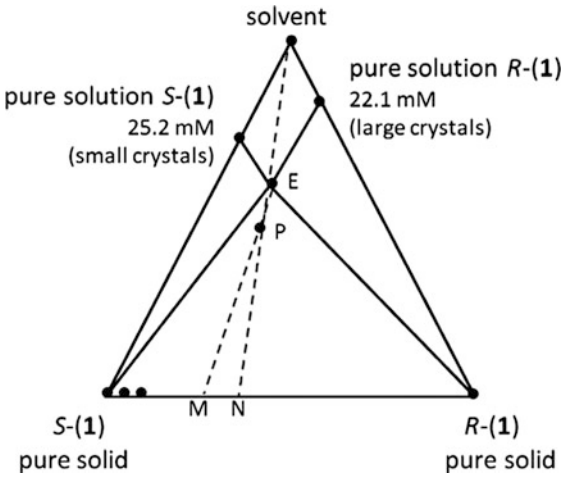

Fig. 10 Transient ternary phase diagram, providing a kinetic snapshot of a system where larger *S* and smaller *R* particles are mixed. Point E is the "kinetic eutectic" composition measured from a racemic mixture of the two enantiomorphs at their respective crystal sizes (Hein JE, Blackmond DG, unpublished results)

molecules was identical. Identical behavior was confirmed for the opposite case of large *S*-crystals and small *R*-crystals (Hein JE, Blackmond DG, unpublished results). These results may be reconciled with the expected behavior of racemic conglomerates, which exhibit 0% solution phase ee under equilibrium conditions, by taking into account the solubility difference between different average sizes for *S* and *R* crystals. This allows us to construct the modified ternary phase diagram of Fig. 10 that deviates from the equilibrium solubility behavior predicted for the ideal case of infinitely planar particles of a conglomerate. The observed solution enantiomeric excess at **E** represents what may be thought of as a "kinetic eutectic" composition and is located slightly skewed from the vertical racemic line (ca. 5% ee in *S*-**1**) due to the unequal *R*-(**1**) and *S*-(**1**) solubilities represented by the points on the left and right sides of the diagram. The diagram describes a theoretical mixture of large *R*-(**1**) and small *S*-(**1**) crystals of composition **M** (with *S*-(**1**) in excess) mixed with solvent to attain the composition **P**, for which the solution phase composition will be given by **E** and the final solid phase composition under these conditions is given by **N**.

Figure 10 does not describe equilibrium phase behavior but instead provides a convenient way to characterize non-equilibrium crystal-size induced solubility differences. In many practical examples of preferential crystallization of non-racemizable conglomerates, the attainment of equilibrium solubility conditions can be slow, especially for highly concentrated solutions, and a "kinetic window" of solubility such as is described by Fig. 10 may be observed. Stirring the mixture of large *R*-**1** and small *S*-**1** crystals over time in the absence of a racemization catalyst causes evolution to a common crystal size distribution and a steady-state solubility whose value is dictated by the prevailing stirring conditions. The solution phase ee returns to racemic, and the ternary phase diagram reverts to the classic symmetrical case for enantiomers that form conglomerates, with the eutectic composition centered on the racemic line and the pure enantiomer solubilities at equal horizontal

positions. Figure 10 demonstrates that the solution may become enriched in either the major or the minor enantiomorph, depending on which exhibits the smaller average crystal size.

In contrast, a curious result was recently reported in which it was found that the solution-phase ee for slurries of *R* and *S* crystals of a compound related to **1** subjected to attrition consistently showed enrichment in the minor enantiomer. This inverse relationship increased with increasing solid phase ee. In addition, it was shown that, paradoxically, solubility increased when slurries were diluted under attrition conditions. Both observations were suggested as evidence for the role of clusters: solution concentration will remain elevated, and clusters will have a lower probability of encountering a crystal, under dilute conditions, which occur for the minor enantiomorph at high solid phase ee and for either enantiomorph when solvent is added.

5.8 Kinetic Solubility Considerations

We reproduced the reported observations [18] of an inverse relationship between solution ee and solid phase ee in studies of **1**, as shown in Fig. 11 (Hein JE, Blackmond DG, unpublished results). The picture from these data is somewhat more complex: it is interesting to note that a non-racemic solution ee towards the minor solid enantiomorph is obtained under attrition conditions only when the solid phase ee is very high and when very small amounts of solid are present. Both of these conditions occur when dilution is very high for the minor enantiomorph, in keeping with the results of [18]. However, we found a further correlation to dilution for systems undergoing attrition. Our studies point to a role for the *kinetics* of solubilization that has not previously been noted. Solubilities were measured for two samples differing in total weight of solid by a factor of 10. After 2 h of attrition, the more dilute sample exhibits a ca. 10% higher solubility. This difference disappears after 12 h of grinding/sonication. Thus a steady-state in solubility is approached more rapidly when smaller amounts of solid are subjected to attrition. A similar kinetic effect was observed in our studies of solution vs solid phase ee. Figure 11 shows solution phase ee as a function of dilution for a solid phase sample initially at 75% CEE (Hein JE, Blackmond DG, unpublished results). The observed solution excess in the enantiomer increases with dilution, but this excess erodes over time, even during continued attrition. This suggests that the kinetic solubility advantage of the smaller crystals is overcome with time as the larger amount of the major enantiomorph approaches its steady-state solubility. Together, the results in Figs. 10, 11, and 12 highlighting the non-steady-state kinetics of solubilization and crystal growth suggest that the experimental observations for the reverse dilution effect may be rationalized without invoking the presence of clusters.

As was shown in Fig. 11, systems with larger amounts of solid equilibrate to give a racemic solution phase under sonication/grinding conditions. However, the persistence of a solution phase excess in the enantiomer of the minor solid phase shown

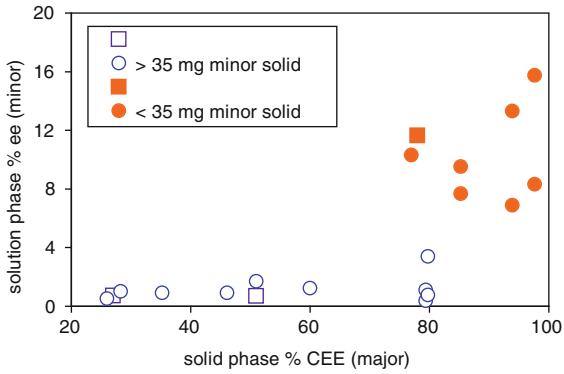

Fig. 11 Solution phase enantiomeric excess towards the minor enantiomer as a function of the solid phase crystal enantiomeric excess in the major enantiomorph. *Squares*: *R* as major enantiomorph; *circles*: *S* as major enantiomorph (Hein JE, Blackmond DG, unpublished results)

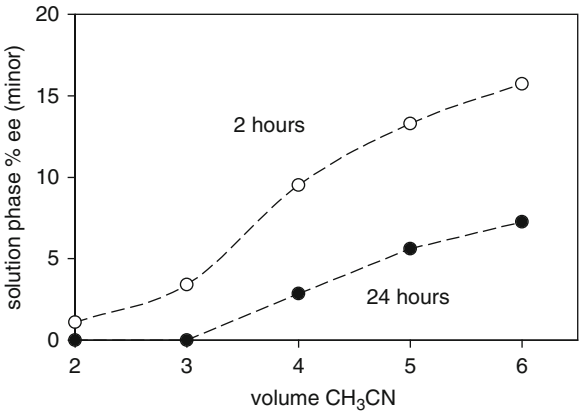

Fig. 12 Solution phase enantiomeric excess towards the minor enantiomer as a function of the dilution with solvent for systems initially with solid phase CEE of 75%. *Open circles*: after 2 h grinding/sonication; *filled circles*: after 24 h grinding/sonication (Hein JE, Blackmond DG, unpublished results)

in Fig. 11 for highly dilute systems even after 24 h grinding/sonication implies that a crystal size-induced enhanced *kinetic solubility* can be sustained under these attrition conditions in cases where only a small amount of that solid remains. It is interesting to note that these are conditions that mimic those occurring during attrition-enhanced deracemization such as the experiments shown in Figs. 7 and 9. During the regime of accelerated evolution of solid phase enantiomeric excess, the amount of the minor enantiomer's solid phase necessarily decreases rapidly as the system approaches solid-phase homochirality. A "kinetic window" afforded by an increasingly smaller amount of the minor enantiomer solid that exhibits an increasingly higher transient solubility provides a driving force for its conversion to the major enantiomer through solution phase racemization, ultimately driving the evolution of solid phase ee. Thus the more rapid kinetics of solubilization exhibited by smaller amounts of solids under enhanced attrition conditions may be a significant promoter of the deracemization process.

5.9 Dueling Crystals: Size vs Number

In their studies of the relationship between solubility and attrition-enhanced deracemization, Noorduin et al. stated that the inverted enantiomeric excess in the solution phase (higher solution ee for the minor enantiomorphic solid) provides the driving force for conversion of the minor to the major enantiomorph [18]. However, as some of these authors have previously shown, attrition-enhanced deracemization can proceed with conversion to the (originally) minor enantiomorph when its crystal size is large enough to overcome the larger number of molecules of the other enantiomorph [17]. In other words, greater size may win out against greater number. Figures 13 and 14 show experimental results where this effect is reproduced in a case where both crystal size and solubility were quantified (Hein JE, Blackmond DG, unpublished results). Samples of the larger and smaller crystals were prepared by stirring at different speeds in the presence and absence of glass beads to produce different initial crystal size distributions of *S*-(**1**) and *R*-(**1**)as shown in Fig. 13. The slurry with the larger crystals exhibits a ca. 5% lower solubility value. The organic base DBU was added to each slurry to initiate solution phase racemization. Different relative amounts of the slurries of the two enantiomorphs were combined to institute a bias in crystal size towards one enantiomer with a bias in enantiomeric excess towards the other. Figure 12 shows the evolution of solid-phase homochirality for two cases with excess *S*-(**1**) at two different % CEE values, while the minor enantiomer *R*-(**1**) exhibits the larger initial crystal size. The left figure shows that homochirality was achieved favoring the hand of the initially larger (*R*) crystals even when these crystals represented the minor enantiomer in a ratio 53.6:46.4, or 7.2% CEE (*S*). The right figure shows that larger crystals ultimately lose out in favor of homochirality toward the hand of the smaller crystals, when these latter represent the major enantiomer at a greater excess of 57.5:42.5, or 15% CEE (*S*). The trends for size vs CEE were confirmed for the opposite case with larger *R* crystals representing the minor enantiomer.

These results confirm the results of [17]. Although the Gibbs–Thomson rule states that the driving force is greater for solution phase molecules to add to larger crystals, these results show that a larger *number* of smaller *size* crystals can provide a surface area sufficient to counteract this solubility driving force. Thus either larger crystal size or greater total surface area can become the critical factor in ultimately determining the sense of the solid phase homochirality.

6 Pasteur's Tweezers Revisited: From Deracemization to Separation

Interplay between the thermodynamics of crystal growth and dissolution, manifested by the Gibbs–Thomson rule, and kinetic considerations of crystal size-dependent solubility both contribute to the attrition-enhanced deracemization

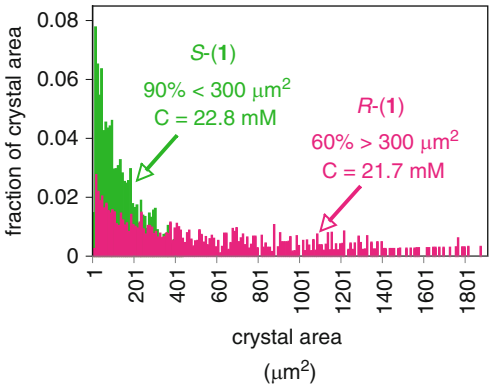

Fig. 13 Crystal size distributions and solubilities for *R*-(**1**) and *S*-(**1**) samples employed in the attrition-enhanced deracemization experiments of Fig. 14 (Hein JE, Blackmond DG, unpublished results)

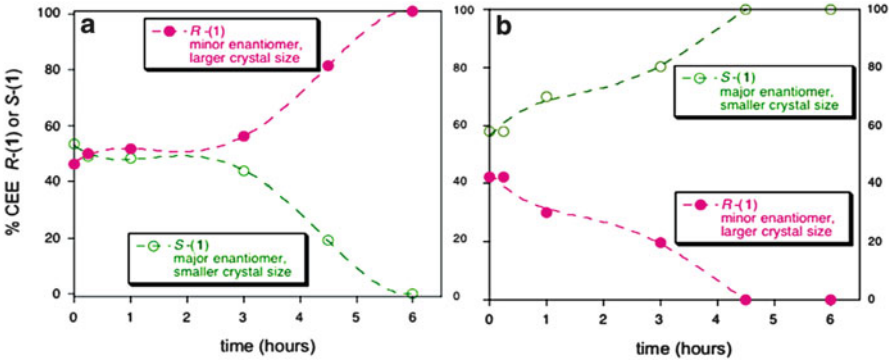

Fig. 14 Experimental crystal enantiomeric excess (% CEE) of **1** in the deracemization process carried out using mixtures of *R*-(**1**) and *S*-(**1**) samples of different crystal size distributions as shown in Fig. 10. Initial % CEE values are (**a**) 7.2% (*S*), and (**b**) 16% (*S*) (Hein JE, Blackmond DG, unpublished results)

process. These results demonstrate the ease with which molecules move between solution and solid phases under attrition enhanced stirring, and at the same time they highlight the randomness of the overall *net* conversion from one solid enantiomorph to the other in the deracemization process. This makes it difficult to control or predict if and when such a crystal growth/solubility driving force will be sustained long enough for the evolution of solid phase ee to commence.

6.1 Crystal Size-Induced Emergence of Homochirality

We reasoned that the process triggering the evolution of solid phase ee would be reliably reproducible if a means could be found to maintain the crystal size-induced solubility gradient. Sustaining a population of larger crystals of one of the

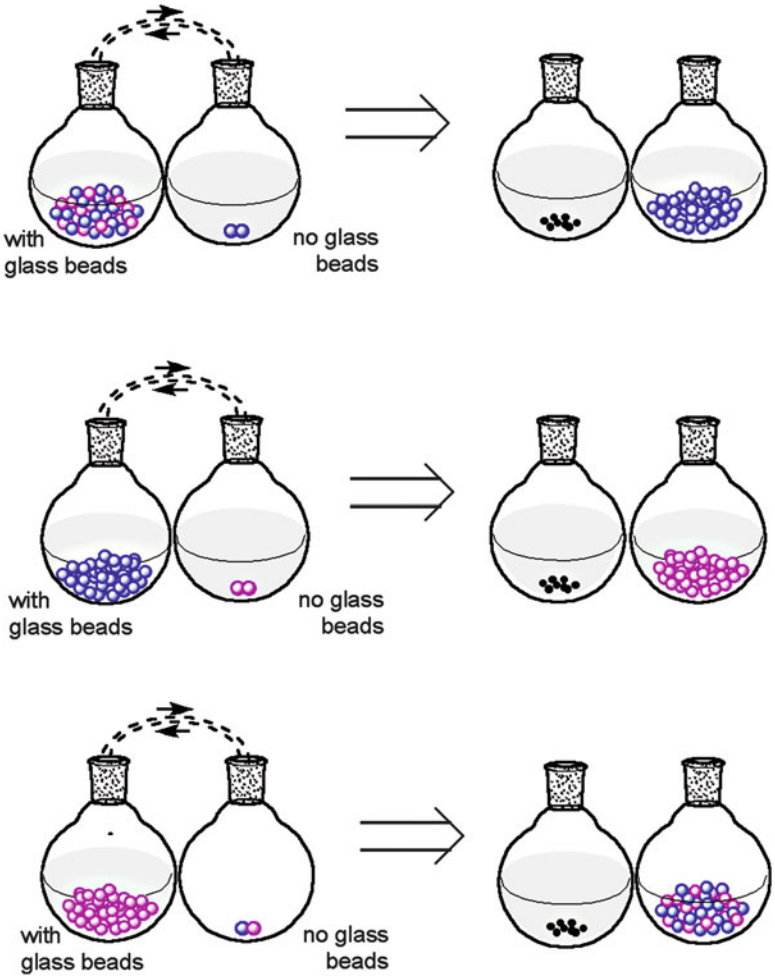

Fig. 15 Attrition enhanced deracemization under solution-phase racemizing conditions in a two-vessel setup held under isothermal conditions with solution phase circulation between the left and right vessels while movement of solids is prevented [17]. *Top left*: vessel contains solid *rac*-**1** and glass beads in saturated CH_3CN solution under high solubility conditions; *right*: vessel contains large seed crystals of *S*-**1** under low solubility conditions. *Middle*: glass beads are added to vessel containing *S*-**1** from Step 1, which is connected to a new, mildly stirred vessel on the left containing large seed crystals of *R*-**1**. *Bottom*: glass beads are added to vessel containing *R*-**1** from Step 2, which is connected to a new, mildly stirred vessel on the right containing larger seed crystals of *rac*-**1**. In each step, total conversion of solid towards the seed vessel occurred after ca. 24 h. Redrawn from [19]

enantiomorphs requires a reliable means of preventing their attrition, which is difficult to control in the presence of crystals of the other enantiomorph. A discussion of what was termed "stochastic sorting" by Welch [54] inspired a modification of the Viedma ripening process. Welch argued that simple sorting processes in a prebiotic environment, involving winds, waves, or similar forces, might act to

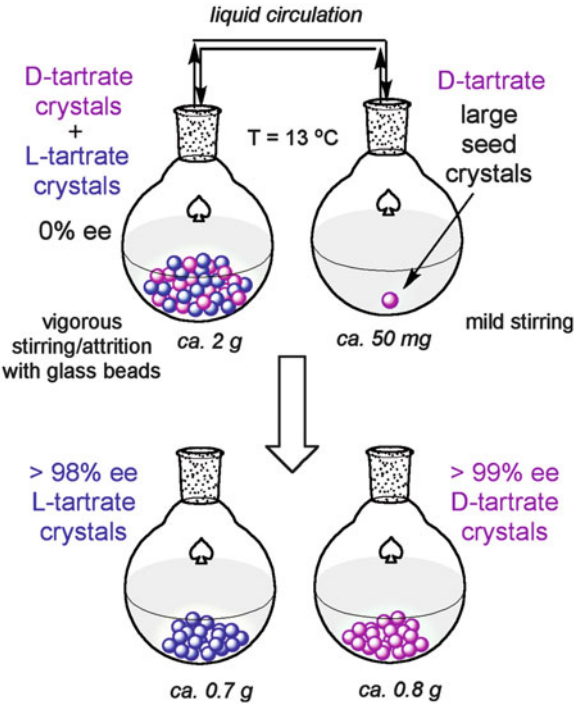

Fig. 16 Extension of crystal size-induced solubility driving force to the separation of non-racemizing conglomerate crystals. Redrawn from [19]

"sort" or deposit individual crystals into separate environments. We reasoned that this partial physical separation of enantiomorphic solids might be the basis for a new mode of attrition-enhanced deracemization that overcomes the problem of irreproducibility in the formation of the larger crystals that trigger the net movement of molecules from one enantiomorph to another. Figure 15 illustrates this process: a racemic slurry of crystals under attrition-enhanced solubility conditions is connected via solution phase to a mildly stirred, lower solubility enantiopure "seed" population of single handed crystals in a separate vessel. The two vessels communicate without movement of solids, solely by circulation of the liquid phase between the vessels. The crystal-size induced solubility gradient is sufficient to induce the complete transformation of solid from the high solubility environment to that of the low solubility environment.

6.2 Crystal Size-Induced Enantiomer Separation

The majority of chiral molecules that form enantiomorphic solids do not undergo solution racemization in a facile manner. For example, sodium ammonium tartrate, the conglomerate system separated manually by Pasteur using tweezers, does not racemize in the presence of acid or base. We envisioned that the concept of crystal

size-induced solubility differences might be extended to the *separation* of, rather than *conversion* between, enantiomers in such cases [19]. Figure 16 demonstrates this protocol for an initially racemic mixture of enantiomorphic crystals of Pasteur's tartrate. This net movement of mass via the liquid phase results ultimately in the quantitative physical separation of the enantiomorphic crystals. A crystal size-induced solubility gradient serves the role of Pasteur's tweezers.

These results add weight to Welch's "stochastic sorting" mechanism [54] for the evolution of homochirality both for molecules that racemize easily as well as those that do not. In the absence of further driving forces to promote enantiomer separation, it might be imagined that such sorting processes might face competing processes driving re-equilibration to a locally racemic environment, thus hindering enantioenrichment. The crystal size-induced solubility gradient acting as a separation driving force as described here could enhance these simple stochastic sorting processes towards the establishment of regions exhibiting a single solid enantiomorph.

7 Conclusions

The implications of the single chirality of biological molecules may be viewed in this context of complexity. Whether or not we will ever know how this property developed in the living systems represented on Earth today, studies of how single chirality might have emerged will aid us in understanding the much larger question of how life might have emerged, and might emerge again, as a complex system.

References

1. Heilbronner E, Dunitz JD (1993) Reflections on symmetry in chemistry. . .and elsewhere. Verlag Helvetica Chimica Acta, Basel
2. Frank FC (1953) On spontaneous asymmetric synthesis. Biochim Biophys Acta 11:459–463
3. Calvin M (1969) Molecular evolution. Oxford University Press, Oxford
4. Blackmond DG (2010) The origin of biological homochirality. In: Deamer D, Szostak JW (eds) The origin of life. Cold Spring Harbor Lab Press, 2: a002147
5. Soai K, Shibata T, Morioka H, Choji K (1995) Asymmetric autocatalysis and amplification of enantiomeric excess of a chiral molecule. Nature 378:767–768
6. Klussmann M, Iwamura H, Mathew SP, Wells DH Jr, Pandya U, Armstrong A, Blackmond DG (2006) Thermodynamic control of asymmetric amplification in amino acid catalysis. Nature 441:621–623
7. Kondepudi DK, Kaufman RJ, Singh N (1990) Chiral symmetry breaking in sodium chlorate crystallization. Science 250:975–976
8. Viedma C (2005) Chiral symmetry breaking during crystallization: complete chiral purity induced by nonlinear autocatalysis and recycling. Phys Rev Lett 94:065504–1–065504–4
9. Noorduin WL, Izumi T, Millemaggi A, Leeman M, Meekes H, Van Enckevort WJ, Kellogg RM, Kaptein B, Vlieg E, Blackmond DG (2008) Emergence of a single solid chiral state from a nearly racemic amino acid derivative. J Am Chem Soc 130:1158–1159

10. Viedma C, Ortiz JE, de Torres T, Izumi T, Blackmond DG (2008) Evolution of solid phase homochirality for a proteinogenic amino acid. J Am Chem Soc 130:15274–15275
11. Viedma C (2007) Chiral symmetry breaking and complete chiral purity by thermodynamic-kinetic feedback near equilibrium: implications for the origin of biochirality. Astrobiology 7:312–319
12. Leeman M, de Gooier JM, Boer K, Zwaagstra K, Kaptein B, Kellogg RM (2010) Attrition-enhanced total resolution leads to homochiral families of amino acid derivatives. Tetrahedron Asymmetry 21:1191–1193
13. Noorduin WL, van der Asdonk P, Bode AA, Meekes H, van Enckevort WJ, Vlieg E, Kaptein B, van der Meijden M, Kellogg RM, Deroover G (2010) Scaling up attrition-enhanced deracemization by use of an industrial bead mill in a route to clopidogrel (Plavix). Org Process Res Dev 14:908–911
14. Maarten W, van der Meijden M, Leeman M, Gelens E, Noorduin WL, Meekes H, van Enckevort WJ, Kaptein B, Vlieg E, Kellogg RM (2009) Attrition-enhanced deracemization in the synthesis of clopidogrel – a practical application of a new discovery. Org Process Res Dev 13:1195–1198
15. Noorduin WL, Bode AA, van der Meijden M, Meekes H, van Etteger AF, van Enckevort WJ, Christianen PC, Kaptein B, Kellogg RM, Rasing T, Vlieg E (2009) Complete chiral symmetry breaking of an amino acid derivative directed by circularly polarized light. Nat Chem 1:729–732
16. Noorduin WL, Meekes H, van Enckevort WJ, Millemaggi A, Leeman M, Kaptein B, Kellogg RM, Vlieg E (2008) Complete deracemization by attrition-enhanced Ostwald ripening elucidated. Angew Chem Int Ed 47:6445–6447
17. Kaptein B, Noorduin WL, Meekes H, van Enckevort WJ, Kellogg RM, Vlieg E (2008) Attrition-enhanced deracemization of an amino acid derivative that forms an epitaxial racemic conglomerate. Angew Chem Int Ed 47:7226–7229
18. Noorduin WL, van Enckevort WJ, Meekes H, Kaptein B, Kellogg RM, Tully JC, McBride JM, Vlieg E (2010) The driving mechanism behind attrition-enhanced deracemization. Angew Chem Int Ed 49:8435–8438
19. Hein JA, Cao BH, Viedma C, Kellogg RM, Blackmond DG (2012) Pasteur's tweezers revisited: on the mechanism of attrition-enhanced deracemization and resolution of chiral conglomerate solids. J Am Chem Soc 134:12629–12636
20. Crusats J, Veintemillas-Verdaguer S, Ribo JM (2006) Homochirality as a consequence of thermodynamic equilibrium? Chem Eur J 12:7776–7781
21. Blackmond DG (2007) "Chiral amnesia" as a driving force for solid-phase homochirality. Chem Eur J 13:3290–3295
22. McBride JM, Tully JC (2008) Did life grind to a start? Nature 452:161–162
23. Meekes H, Noorduin WL, Bode AAC, van Enckevort WJP, Kaptein B, Kellogg RM, Vlieg E (2008) Explanation for the emergence of a single chiral solid state during attrition-enhanced Ostwald ripening: survival of the fittest. Cryst Growth Des 8:1675–1681
24. Uwaha MJ (2004) A model for complete chiral crystallization. J Phys Soc Jpn 73:2601–2603
25. Skrdla P (2011) Kinetics and thermodynamics of efficient chiral symmetry breaking in nearly racemic mixtures of conglomerate crystals. Cryst Growth Des 11:1957–1965
26. Iggland M, Mazzotti M (2011) A population balance model for chiral resolution via Viedma ripening. Cryst Growth Des 11:4611–4622
27. Feringa B, van Delden RA (1999) The origin, control, and amplification of chirality. Angew Chem Int Ed 38:3418–3438
28. Mislow K (2003) Absolute asymmetric synthesis: a commentary. Collect Czechoslov Chem Commun 68:849–864
29. Blackmond DG, Mcmillan CR, Ramdeehul S, Schorm A, Brown JM (2001) Asymmetric amplification in autocatalytic alkylzinc additions. J Am Chem Soc 123:10103–10104
30. Buono FG, Blackmond DG (2003) Kinetic evidence for a tetrameric transition state in the asymmetric autocatalytic alkylation of pyrimidyl aldehydes. J Am Chem Soc 125:8978–8979

31. Gridnev ID, Serafimov JM, Brown JM (2004) Solution structure and reagent binding of the zinc alkoxide catalyst in the Soai asymmetric autocatalytic reaction. Angew Chem Int Ed 43:4884–4887
32. Quaranta M, Gehring T, Odell B, Brown JM, Blackmond DG (2010) Unusual inverse temperature dependence on reaction rate in the asymmetric autocatalytic alkylation of pyrimidyl aldehydes. J Am Chem Soc 132:15104–15107
33. Gehring T, Quaranta M, Odell B, Blackmond DG, Brown JM (2012) Observation of a transient intermediate in Soai's asymmetric autocatalysis: insights from 1H NMR turnover in real time. Angew Chem Int Ed 51:9539–9542
34. Blackmond DG (2002) Description of the condition for asymmetric amplification in autocatalytic reactions. Adv Synth Catal 344:156–158
35. Sato I, Urabe H, Ishiguro S, Shibata T, Soai K (2003) Amplification of chirality from extremely low to greater than 99.5% ee by asymmetric autocatalysis. Angew Chem Int Ed 42:315–317
36. Shibata T, Yamamoto J, Matsumoto N, Yonekubo S, Osanai S, Soai K (1998) Amplification of a slight enantiomeric imbalance in molecules based on asymmetric autocatalysis. The first correlation between high enantiomeric enrichment in a chiral molecule and circularly polarized light. J Am Chem Soc 120:12157–12158
37. Soai K, Osanai S, Kadowaki K, Yonekubo S, Shibata T, Sato I (1999) D- and L-quartz-promoted highly enantioselective synthesis of a chiral compound. J Am Chem Soc 121: 11235–11236
38. Kawasaki T, Matsumura Y, Tsutsumi T, Suzuki K, Ito M, Soai K (2009) Asymmetric autocatalysis triggered by carbon isotope ($^{13}C/^{12}C$) chirality. Science 324:492–495
39. Kawasaki T, Okano Y, Suzuki E, Takano S, Oji S, Soai K (2011) Asymmetric autocatalysis: triggered by chiral isotopomer arising from oxygen isotope substitution. Angew Chem Int Ed 50:8131–8133
40. Kawasaki T, Ozawa H, Ito M, Soai K (2011) ChemInform abstract: enantioselective synthesis induced by compounds with chirality arising from partially deuterated methyl groups in conjunction with asymmetric autocatalysis. Chem Lett 40:320–321
41. Morowitz M (1969) A mechanism for the amplification of fluctuations in racemic mixtures. J Theor Biol 25:491–494
42. Breslow R, Levine MS (2006) Amplification of enantiomeric concentrations under credible prebiotic conditions. Proc Natl Acad Sci USA 103:12979–12980
43. Breslow R, Cheng ZL (2009) On the origin of terrestrial homochirality for nucleosides and amino acids. Proc Natl Acad Sci USA 106:9144–9146
44. Klussmann M, White AJP, Armstrong A, Blackmond DG (2006) Rationalization and prediction of solution enantiomeric excess in ternary phase systems. Angew Chem Int Ed 47:7985–7989
45. Klussmann M, Izumi T, White AJP, Armstrong A, Blackmond DG (2007) Emergence of solution-phase homochirality via crystal engineering of amino acids. J Am Chem Soc 129:7657–7660
46. Lombardo TG, Stillinger FH, Debenedetti PG (2009) Thermodynamic mechanism for solution phase chiral amplification via a lattice model. Proc Natl Acad Sci USA 106:15131–15135
47. Perry RH, Wu C, Nefliu M, Cooks RG (2007) Serine sublimes with spontaneous chiral amplification. Chem Commun 1071–1073
48. Fletcher SP, Jagt RBC, Feringa BL (2007) An astrophysically-relevant mechanism for amino acid enantiomer enrichment. Chem Commun 2578–2580
49. Klussmann M, Blackmond DG (2007) Spoilt for choice: assessing phase behavior models for the evolution of homochirality. Chem Commun 3990–3996
50. McBride JM, Carter RL (1991) Spontaneous resolution by stirred crystallization. Angew Chem Int Ed Engl 30:293–295
51. Dimroth O (1910) Über intramolekulare Umlagerung, 5th Abhandlung. Der Einfluss des Lösungsmittels auf Reaktionsgeschwindigkeit und Gleichgewicht (On intramolecular

rearrangement, Part 5. The influence of solvent on reaction rate and equilibrium). Justus Liebigs Ann Chem 377:127–163
52. Brands KMJ, Davies AJ (2006) Crystallization-induced diastereomeric transformations. Chem Rev 106:2711–2733
53. Blackmond DG (2009) 'If pigs could fly' chemistry: a tutorial on the principle of microscopic reversibility. Angew Chem Int Ed 48:2648–2654
54. Welch CR (2001) Formation of highly enantioenriched microenvironments by stochastic sorting of conglomerate crystals: a plausible mechanism for generation of enantioenrichment on the prebiotic earth. Chirality 13:425–427

Top Curr Chem (2013) 333: 109–156
DOI: 10.1007/128_2012_405

Published online: 5 March 2013

Biomolecules at Interfaces: Chiral, Naturally

Arántzazu González-Campo and David B. Amabilino

Abstract Interfaces are a most important environment in natural and synthetic chemistries for a wide variety of processes, such as catalysis, recognition, separation, and so on. Naturally occurring systems have evolved to one handedness and the study of interfaces where biomolecules are located is a potentially revealing pursuit with regard to understanding the reasons and importance of stereochemistry in these environments. Equally, the spontaneous resolution of achiral and chiral compounds at interfaces could lead to explanations regarding the emergence of single handedness in proteins and sugars. Also, the attachment of biomolecules to surfaces leads to systems capable of stereoselective processes which may be useful for the applications mentioned above. The review covers systems ranging from small biomolecules studied under ultrapure conditions in vacuum to protein adsorption to surfaces in solution, and the techniques that can be used to study them.

Keywords Nanoscience · Spontaneous resolution · Stereochemistry · Surfaces · Symmetry breaking

Contents

A. González-Campo and D.B. Amabilino (✉)
Institut de Ciència de Materials de Barcelona (ICMAB-CSIC), Campus Universitari de Bellaterra, 08193 Cerdanyola del Vallès, Catalonia, Spain
e-mail: amabilino@icmab.es

Abbreviations

CD	Cyclodextrin
DFT	Density functional theory
LEED	Low energy electron diffraction
NPs	Nanoparticles
QDs	Quantum dots
Rac	Racemic
RAIRS	Reflection absorption infrared spectroscopy
SAM	Self-assembled monolayer
STM	Scanning tunnelling microscopy
UHV	Ultrahigh vacuum

1 Introduction

1.1 Preamble: Homochirality and Mirror Symmetry in Natural Chemical Systems

Biological systems contain a variety of materials and interfaces which are more often than not chiral, and which perform a variety of functions. From the collagen in our bodies which is ubiquitous in connective tissue, where interfaces and the bonding between them is so important [1], to relatively fragile membranes through which ions and molecules bind and pass and where chiral molecules can exert bending forces [2]. Because of the staggeringly common single handedness in living things, it is often argued that homochirality is the "signature of life" [3]. The exclusive presence of L-amino acids in proteins active during translation in the ribosome and of the predominance of D sugars in natural systems are impelling evidence for this argument. Yet homochirality is not an essential situation; rather, at least in the

case of amino acids, metabolites can be produced in enantiomeric forms, so the enantiomers take on different roles. It has been known for some time that D-amino acids are present in invertebrates [4]; more recently it has been found that they are also important in higher mammals [5] and the presence of D-amino acids in soil is documented [6]. They enter it from a variety of sources as well as by racemisation of the more naturally abundant enantiomer and it is known that they inhibit plant growth. The soil interface is therefore another place where chirality is influential. Thus, chirality at interfaces is irrefutably determining in the function of complex biological systems in our present day world.

The way in which this chiral bias arose is enigmatic and a continuing matter of intriguing debate [7–12], but a frequently cited candidate for the emergence of a chiral preference in terrestrial nature is the interaction of organic molecules with inorganic surfaces [13–16]. The examples we shall present in this review show compelling support for this kind of hypothesis, and the reasons behind the special characteristics of interfaces will be discussed in the coming sections. The interest in chirality at interfaces involving biological and other molecules is not only because of scientific curiosity regarding the origin and passage of handedness in living things, but is also potentially useful for a number of other areas such as catalysis [17–19], sensing [20] and materials with a variety of properties [21–27].

The understanding of function of chemical systems is intimately linked to their structural arrangement, and the description of chirality at surfaces requires consideration of several aspects which are particular to this environment; these are made in the following section.

1.2 Surfaces and Interfaces and Their Chirality

A surface and interface are good places for dissymmetry to arise, because the border between two continua results in particular characteristics very different from those of the two phases they divide. Considering a bulk solid material, the atoms or molecules at its surface are available to interact in more or less specific ways with a complementary adsorbent molecule, because their coordination sphere or non-covalent interaction sphere are incomplete. Similarly, molecules in a liquid may accumulate at the surface to reduce the global energy of the system. The occurrence of chirality in these environments is frequent, and we shall now consider different situations which lead to this phenomenon.

Chiral surfaces are not only evident on intrinsically chiral solids but can also be present on bulk achiral solids [28, 29]. Chirality can arise on the faces of crystals for three reasons (represented in Fig. 1): (1) the two-dimensional structure at the surface is intrinsically chiral because the way the surface plane cuts the bulk structure, (2) a step between terraces of atoms or molecules forms an angle with the main symmetry axes of the surface leading to a chiral step and (3) a kink on a step edge leads to the formation of a local chirality of the surface atoms. The occurrence of chirality at step edges between terraces is particularly interesting in principle,

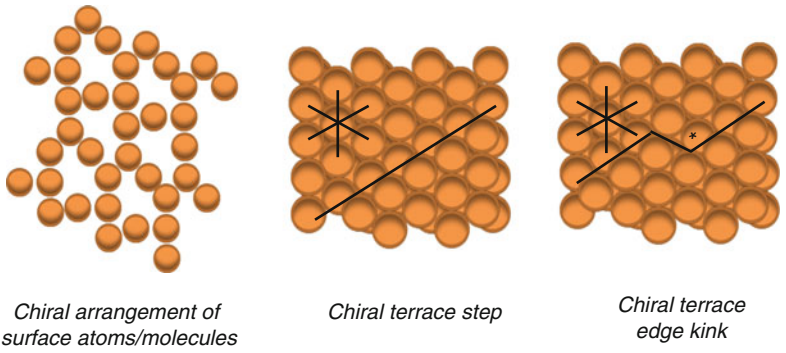

Fig. 1 Illustration of three chiral surfaces, whose dissymmetry lies at different sources. *Left*: a periodic arrangement of atoms or molecules which is chiral when laid on a surface. *Middle*: the step in terraces which is chiral along the edge (*long line*, which makes a slight angle with one of the *crossed lines* showing three symmetry directions). *Right*: a stereogenic centre at a surface atom (*asterisk*) at a kink site

because adsorbed molecules tend to adhere best to step edges where the surface atoms have highest energy.

The first case can be controlled by cutting a crystal, and may occur naturally. The faces of a crystal can be thought of as a plane which runs across the three-dimensional periodic structure of the solid formed by the molecule(s) or atom(s). The Miller indices are three integers which correspond to the orientation of the face of the crystal with respect to the three crystallographic axes of the bulk solid. All possible faces of a crystal with a given unit cell has a unique set of Miller indices describing it. The chiral structure is generally recognised easiest when the surface unit cell is drawn: an oblique unit cell on a surface is the signature of a chiral interface structure.

The chirality of inorganic materials has been shown for both metals and oxides. Hazen has written an excellent review concerning the chiral faces of naturally-occurring minerals [30], which are perhaps prime candidates for chiral discrimination and induction phenomena because of their great abundance, while other inorganic surfaces are also naturally chiral [31]. It is clear that any achiral molecule landing on a chiral mineral surface may have a chiral structure induced upon it upon its interaction with the surface.

While we have considered only crystalline solids up to this point, non-periodic structures can equally well possess chiral surfaces locally, on a small scale, on the order of nanometres. Perhaps some of the best examples are solids used as supports for the separation of enantiomers, where a surface can be imprinted with organic molecules [32] as in polymer imprinting [33–36]. However, their precise characterisation is far more challenging than flat surfaces of crystalline samples (non-trivial in itself), and presently techniques which allow an accurate description and characterisation of uneven chiral surfaces are lacking; this shortcoming is a very real challenge and an area where much is to be discovered.

Fig. 2 Illustration representing glycine – the simplest and achiral amino acid – adsorbed on a surface (underneath the molecule as observed here), where the mode on the *left* would be regarded as *pro-S* (because the groups turn anticlockwise when viewed from the surface using the Cahn–Ingold–Prelog rules) and the *right*, *pro-R*

Now let us consider the interaction of molecules adsorbing to surfaces. Consider an achiral, but prochiral, molecule attaching to a surface, glycine for example (Fig. 2). Fixing the orientation of the nitrogen to carbon bond, one can appreciate that the carbon to carbon bond may either veer to the left or the right relative to it, the angle being determined by the interactions of the different groups with the surface and the hybridisation of the atoms. The orientation of the molecule is perhaps best defined using the prochirality descriptors *pro-R* (for attachment of the face which gives a hypothetical *R* enantiomer) and *pro-S* (using an analogous argument). In the case of glycine, we would assign the hydrogen atom in contact with the surface as the third priority ligand, and therefore the adsorbed configuration on the left hand side of Fig. 2 would be the *pro-S* arrangement. For the sake of this argument, the surface need only be non-crystalline, although clearly a similar situation may occur on an ordered surface.

In fact, one can extend the argument to any molecule which has three or more different groups. The molecule will randomly attach through either its *pro-S* or *pro-R* face when adsorbed on a surface, but subsequent molecules might then attach randomly – in which case a racemate is formed – or in the same sense – in which case symmetry breaking takes place (Fig. 3). Packing of the molecules in the monolayer must take place according to the packing arrangements described in the next section.

In the discussion up to now, we have considered the surface to which the molecule adsorbs as an amorphous continuum. However, when the surface is crystalline the molecules and their assemblies can form well defined angles with respect to the symmetry axes of the solid. In this case, the orientation of the molecule and its layers can be defined using the helical chirality descriptors *M* (for minus) and *P* (for plus), where this direction corresponds to the angle formed by some axis of the molecule and a symmetry axis of the surface (Fig. 4). It should be noted, however, that this situation does not necessarily arise, and depends on the orientation of the functional groups of the adsorbate with respect to the surface and the non-covalent interactions between the adsorbate molecules, modulated by the symmetry requirements of the surface and its interaction with the adsorbate.

To summarise, there are four contrasting situations one could consider for the expression of molecular chirality in larger scale effects in monolayers: (1) the case

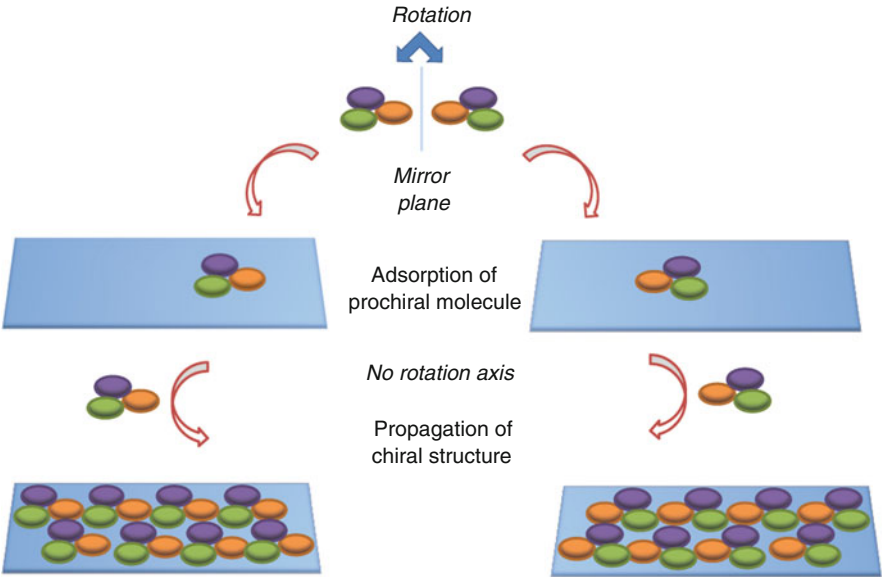

Fig. 3 A representation of an achiral but prochiral molecule – the object formed by three differently coloured lobes, which can ideally realised be inter-converted when in its free state at the *top* of the picture – which, when adsorbed to a surface, one of the two possible enantiomers are formed by attachment through one face of a molecule. When more of the same species is attached, provided the first-anchored molecule propagates its chirality in a dense crystal-like form, a homochiral structure can be generated

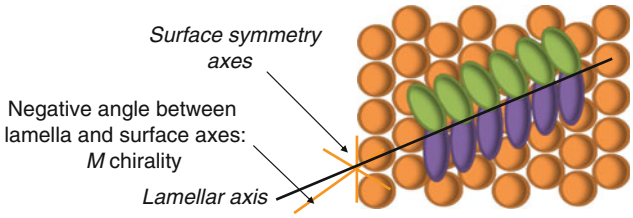

Fig. 4 A representation of a lamella of a molecule (represented by the two *ellipses*) on a single crystalline surface – atoms represented by *spheres* – showing the angle that is formed between the axes of the two

where chirality is generated by spontaneous symmetry breaking whereby an achiral molecule attaches to an achiral surface, and this symmetry breaking is propagated throughout the monolayer, (2) the situation where one of the components – surface or adsorbate – is achiral and the other component is chiral, that is the "trivial" case of inherent chirality by adsorption and induction, (3) the case where a diastereoselective adsorption takes place because of the exposure of a chiral surface to a mixture of enantiomers and (4) the case where one or both components are chiral and yet no chiral structure is observed.

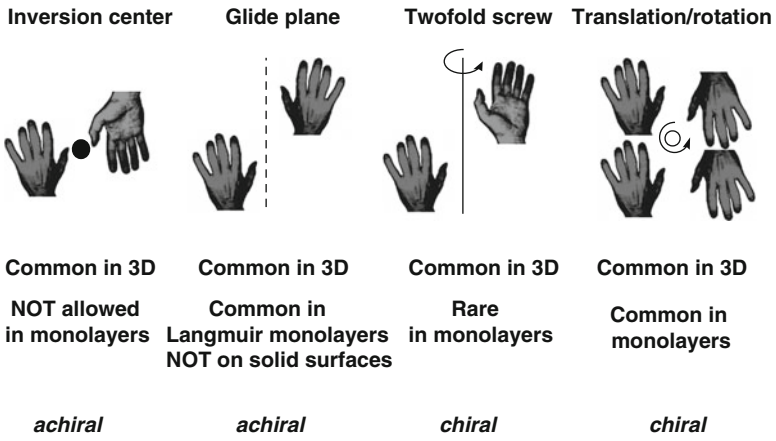

Fig. 5 Common symmetry operators in three-dimensional and two-dimensional ordered systems, their relative propensity, and their outcomes in terms of dissymmetry

In the preceding arguments one might have assumed virtually flat two-dimensional systems, but interfaces in general could be in a flat plane or curved away from it. In purely biological systems the vast majority of systems are non-crystalline and curved, be they at cell walls, in filaments and so on [37]. Despite this curvature, the arguments relating to chiral adsorption apply, although their molecular level characterisation can be very difficult. Minerals, on the other hand, generally present flat crystallographic surfaces, albeit with the possibility of chiral defects as we discussed. The combination of the two types of material leads to nanocomposites in which chirality has a potentially important role in the compatibility of the two components, which is determined in great measure by the interface between them.

1.3 Symmetry Limitations in a Plane

Having considered schematically the chirality of surfaces and adsorbed molecules forming the interface, it is important to delve into the detail of the symmetry conditions that apply in these systems when compared with bulk materials in order to understand the special conditions that apply at interfaces. It has been observed frequently that in three-dimensional systems the inversion centre is one of the most common symmetry elements [38]. On a surface, this symmetry operator is denied the system [39]. Similarly, the glide plane with its plane parallel to a surface and the twofold screw axis whose vector is parallel to a surface are not favoured in many cases. Therefore, some symmetry elements are not viable options in packing, as shown for some cases in Fig. 5.

But how *can* the molecules adsorb and organise? As pointed out by Raval [40], an adsorbate isolated from its neighbours on a surface has point group symmetry defined by the geometry both of the adsorbed molecule and of the region of the surface which constitutes the adsorption site. The restrictions in allowed symmetry elements of surfaces leave the point groups C_n and C_{nv}, which gives ten allowed crystallographic point groups. Chirality arises when adsorption creates a discrete molecule–surface entity with one of the five chiral point group symmetries C_1, C_2, C_3, C_4 or C_6, which by definition have no local mirror planes, but can exist as two enantiomorphous forms.

The packing of the chiral adsorbed molecules can lead to one of the five chiral two-dimensional space groups (C_1, C_2, C_3, C_4 or C_6). Again, mirror-related space groups exist. There are a total of 17 two-dimensional space groups. Although the amount of chiral space groups as a proportion of the total possible is not so different to three-dimensional crystals (65 of 230), the restrictions in symmetry operators pointed out above means that chiral two-dimensional systems are more commonly observed than in three-dimensional systems, especially when the molecules lie in the plane of the surface rather than perpendicular to it (where the glide plane with its symmetry operator perpendicular to the interface becomes common) [41].

The fact that both point groups and space groups exist as enantiomorphous pairs means that in a totally achiral starting system either outcome could be possible – in the case where a single point which acts as a nucleus is grown up to a full layer – or the surface could comprise domains of the enantiomers – in the case where multiple nucleation points arise. The latter case corresponds to the conglomerate phase, where enantiomers exist in different areas of the sample as they do in different crystals in a bulk sample displaying spontaneous resolution. The former case corresponds to spontaneous mirror symmetry breaking.

1.4 Interfaces in Biologically Derived Systems

Biological systems are highly compartmental [42]. The interaction between interfaces is therefore of prime importance for the huge variety of functions that these natural systems display, including sensing odours [43], transferring charges [44], adhering components to one another [45] and the motion of the molecular machines [46] in them. Indeed, in molecular recognition operating within biological systems, handedness is inherent. Consider that the cell membranes are formed by chiral amphiphiles, and collagen is formed from helical fibres, without the need to mention the more widely cited double helix in genetic material. In all the chemistry taking place at interfaces in biological systems, stereospecific and stereoselective processes are operational.

The interaction of chiral surfaces with biological material has been reviewed [47, 48], albeit with a distinct complementary focus to the hierarchical vision given here. It is clear from both viewpoints that macroscopic effects are seen and are

evident, yet the difficulty in many of the studies in large scale and functioning systems is to trace the point at which chiral discrimination takes place. For this reason, studies on model systems in low dimensions and which can be probed with great precision are very important. These studies are usually performed on atomically flat surfaces to avoid the experimental complications implicit in the molecular level study of rough surfaces and interfaces, such as those present in most biological systems.

Many studies of chiral interface reactions in biologically derived systems have focussed on the simplest chiral building blocks, the amino acids and their derivatives, as we shall see. The charge and relative orientation are always important when considering the ability of these simple components to break symmetry, as calculations have revealed [49]. The use of theoretical science is particularly helpful in the interpretation of all surface-based systems, even when high resolution techniques are used for structural observation. In the following sections we shall take a hierarchical approach to the subject matter of this review, showing illustrative examples but in the knowledge that this cannot be a completely comprehensive review, and we refer the expert reader to the more specific articles which we have cited for a complete coverage of the subject matter.

2 Self-assembly of Biomolecules on Surfaces: Origins of Chirality

We shall now discuss specific examples of the adsorption of biologically relevant molecules to surfaces. Those most widely studied are the amino acids [50] because of their availability and ease of handling. In particular, the possibility of subliming the compounds makes them a boon for the surface scientist who can study adsorbates very precisely with a variety of analytical techniques [51]. As we shall see though, they do present great challenges because of their limited size and lack of functionality which can be identified.

2.1 Adsorption of Prochiral Molecules on Achiral Surfaces

The adsorption of prochiral molecules on surfaces can lead to symmetry breaking at the molecular level, which in turn can give rise to spontaneous resolution over large areas of a substrate, as we have discussed theoretically in the preceding sections and which does indeed take place commonly on substrates with a weak interaction with synthetic adsorbates where the latter lie parallel to the surface [52]. However, the cases where the spontaneous resolution of achiral compounds related to biology is observed in a clear cut way are few and far between. Perhaps the simplest case is that of the achiral amino acid glycine, which in principle should form enantiomeric

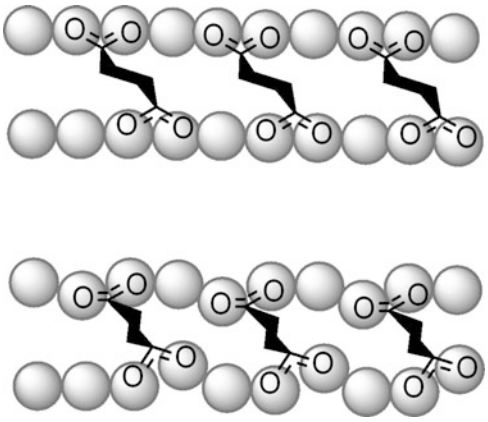

Fig. 6 Possible sources of chiral structure in succinic bis-carboxylate assemblies on copper (1,1,0). In the *top* schematic structure, the two carboxylate groups are coordinated to consecutive copper rows but consecutive pairs of copper atoms because of the kink in the organic backbone which leads to chirality. In the *lower* schematic structure, the orientation of the organic adsorbate and a restructuring of the copper atoms at the surface lead to a chiral interface

adsorbates as a result of attachment through pro-*R* or pro-*S* faces [53]; yet at least on achiral copper surfaces it appears unlikely that homochiral domains of glycine exist [54], possibly because of its mode of interaction with the surface. The difficulty in assigning a definitive molecular structure lies in the nature of the structure formed (3×2) which can be fitted to achiral and chiral situations, although modelling and X-ray photoelectron diffraction experiments indicated a racemic compound. Subsequently, low energy electron diffraction (LEED) data have suggested glide-line symmetry in the layers, supporting an achiral structure [55].

Succinic acid (Fig. 6) – a compound involved in the biochemical citric acid cycle which can be extracted from amber – does show spontaneous resolution on a copper surface [56]. The Cu (1,1,0) surface was used for the formation of an intriguing assembly in ultrahigh vacuum (UHV) and scanning tunnelling microscopy (STM) and LEED showed that the dianionic form of the compound forms mirror image domains (as seen by their deviation from the main metal surface axes). The reason for the propagation of the chiral structure could be explained either by a kink in the backbone of the succinate, which leads to a chiral adsorbed species, or by a twisted adsorption accompanied by a movement of the copper atoms at the surface of the metal (Fig. 6). In any case, a chiral structure is formed unequivocally. Reflection absorption infrared spectroscopy (RAIRS) is particularly powerful for determining the adsorbate nature. At high coverage (the amount of molecule per unit area of the surface) the monosuccinate form of the adsorbate prevails and here the structure is apparently achiral, any kink in the molecule not being able to provide a long range chiral structure because of the packing of the standing up mode on the surface. The emergence of a chiral structure from the succinate system which is devoid of stereogenic centres arises from adsorption-induced symmetry breaking. Point

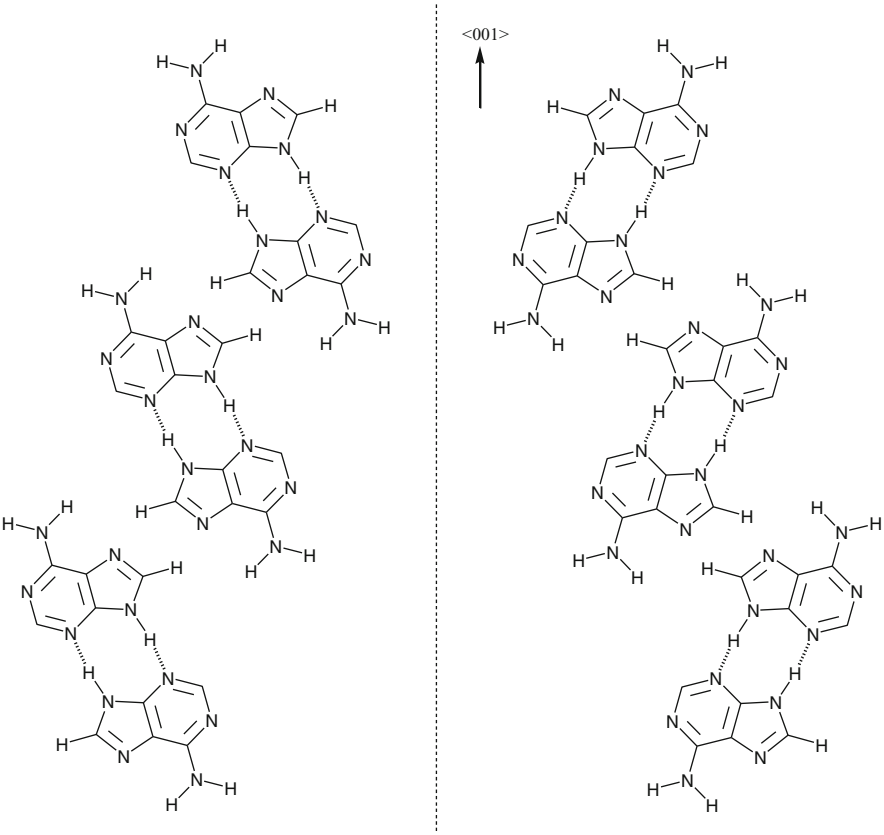

Fig. 7 Representations of the enantiomeric chiral chains of molecules formed by adenine on the copper (1,1,0) single crystal surface, with the axis of the substrate indicated

chirality is induced through molecular conformational distortion and/or metal reconstruction in the vicinity of the adsorption site. Through-space and through-metal interactions then lead to a chiral organisation by packing of the homochiral pieces. Overall, the system is a racemic conglomerate consisting of mirror image domains because of the equal probability of the growth of either enantiomeric domain at any nucleation point on the surface.

When the nucleic acid base adenine was adsorbed on the same Cu (1,1,0) single crystal surface a remarkable spontaneous resolution of chains of molecules was observed by STM and LEED [57]. When a little of the material was evaporated to the metal (high area available per molecule), STM revealed ordered one-dimensional molecular chains propagating along (± 1, 2) directions of the surface. When the amount of molecule on the surface was increased, and the sample annealed at 430 K, ordered chiral domains were formed, showing that the chirality of the chains can be transferred effectively to domains. High resolution electron energy loss spectroscopy (HREELS) showed that the molecular plane is parallel to

the substrate, but that the C–NH_2 bond was a tilted towards the copper, indicating a coordinative bond (an idea supported by ab initio calculations which suggest an sp_3 hybridisation on this nitrogen atom). The STM imaging and other data suggest the kind of packing illustrated in Fig. 7, in which the prochiral adenine separates into domains in which *pro-R* or *pro-S* faces are adsorbed and propagate thanks to intermolecular interactions between the molecules leading to homochiral chains, and eventually domains. The packing is favoured by the fact that it is commensurate with the substrate, an important factor in this kind of metal–molecule interface assembly with strong bonds between substrate and adsorbate. The adenine rows have also been shown to be stable on graphite under ambient conditions [58], and at a liquid–graphite interface the homochiral packing situation lies very close in energy to the racemic compound: The two phases are observed simultaneously [59]. In the latter case, the primary amine group is involved in intermolecular hydrogen bonds which could play a role in this delicate equilibrium between phases. In contrast, adenine has been shown to resolve spontaneously into mirror image monolayer domains on the naturally occurring mineral molybdenite [60]. STM was used to observe the chiral areas which possess clearly oblique unit cells of opposite handedness, and the occurrence of chiral domains on a terrestrially abundant surface might infer their candidacy as a place for templating biomolecular assembly.

Spontaneous resolution at surfaces has also been shown for xanthine [61, 62], another purine base which is an intermediate in the degradation of nucleic acids arising from the de-amination of guanine and found in high concentrations in meteorites, indicating its presence in the ancient solar system. For both graphite and molybdenum sulphide, STM imaging of monolayers formed by evaporation of solutions of the base to the substrates afforded a structure which could be consistent with chirality in the interface [61]. On the other hand, evaporation of the base to the gold (1,1,1) surface gave layers which, when imaged by high-resolution STM, produced clear evidence of homochiral domains. The xanthine molecules self-assembled on the noble metal to give two extended homochiral networks incorporating two kinds of di-pentamer units which were stabilised by intermolecular double hydrogen bonding [62].

A very nice example of the formation of chiral domains in a quite dynamic system is that of simple achiral thioethers which lack C_2 symmetry and are prochiral and become chiral upon adsorption to the gold (1,1,1) surface in vacuum, as revealed by the formation of chiral domains [19]. This case is interesting in that the size of the chiral domains that are formed increases with increasing coverage of these simple molecules on the surface. Perhaps the dynamics assists the formation of the large domains ($>10^3$ nm^2), unlike in other systems where the molecules are held more rigidly by the surface. It should be pointed out that thioethers are more mobile than the related thiolate systems on gold because of their slightly weaker binding.

Apart from molecules devoid of stereogenic centres, meso compounds are an interesting case where chirality can arise. This idea is demonstrated nicely for meso tartaric acid on the copper (1,1,0) surface [63]. The compound clearly displays three

phases, one of which has chiral domains and was assigned to the bistartrate species. LEED showed the coexistence of domains in which the skeleton of the molecule is distorted in one direction or another. Interestingly, the surface interaction overcomes the chirality of the stereogenic centres, as each should "push" the structure in the opposite direction with regard to distortion of the backbone. The chemisorbed nature of the layer and the packing forces at the interface are sufficient to induce symmetry breaking.

Thus far in the review we have discussed molecules adsorbed to surfaces wherein the molecules lie in parallel to the substrate principally. Langmuir–Blodgett layers of achiral calcium arachidate seem to show spontaneous symmetry breaking, as indicated by atomic force microscope images. Chiral packing structures of opposite handedness were observed, and were attributed to an interplay between the molecular-area requisites of the calcium ions and the packing constraints of the alkyl chains in the anion [64].

Apart from all these studies on biological molecules on surfaces, there are a great number of examples of spontaneous resolution in purely synthetic achiral systems on surfaces [65–77], from which much can be learned, and the reader is encouraged to explore these fascinating cases. They demonstrate the power of surface science techniques, as well as optical techniques such as nonlinear optical phenomena to look at orientation of molecules at interfaces [78].

Despite all the beautiful work done in these surface systems, a very real challenge is to be able to prove spontaneous mirror symmetry breaking, that is, the formation of just one of the chiral forms from achiral materials. The nature of the interfaces formed by the adsorption of molecules on inorganic materials perhaps makes this process less favourable than in solution-based systems, but there is no doubt that this experiment would be of interest. In an ideal Ostwald ripening experiment on a surface, this could occur. Reaching this goal would shed light on the spontaneous emergence of chirality in three-dimensional bulk systems, in which minor impurities apparently induce large scale chirality, because the surface science techniques (most notably STM) allow molecule by molecule tracking of the processes taking place.

2.2 Adsorption of Chiral Molecules on Achiral Surfaces

A chiral molecule when adsorbed on an achiral surface will, more often than not, form a chiral monolayer structure [79]. While this statement holds true generally for monocrystal surfaces, the number of ways the molecule can attach to the surface – leading to diastereomeric adsorbate forms – can affect the order within a monolayer. Just as the molecule can rearrange to adsorb in different ways, to think of adsorption having a unique outcome is not realistic; many adsorption sites can exist – equivalent to different recognition sites – and molecules can interact with these different sites in varying ways as a function of coverage (the number of molecules per unit area) and temperature. This idea led scientists to

develop adsorption phase diagrams, which are useful for understanding the phenomenon of attachment of a molecule to a surface and its possible arrangements upon it [80]. Another potential complication in the formation of chiral monolayers involving spontaneous resolution is that, in a domain minority, enantiomers can be incorporated into regions dominated by one [81]. Therefore, while the following examples show beautifully chiral structures, the sensitivity of the layers to thermodynamic and kinetic factors must be remembered.

Amino acids are the biomolecules which have perhaps received the most attention regarding surface studies, largely because of the availability (in the biological and commercial sense), relevance to the proteins [82], and as their simplicity which aids in precise studies using the tools of surface science, as reviewed comprehensively by Barlow and Raval [80]. Here we provide a brief historical perspective of this area and highlight the most recent advances.

The formation of chiral monolayers by tryptophan was revealed using LEED and reported by Atanasoska et al. in 1978 [83]. The presence of enantiomorphous layers was also proven for the enantiomers of the amino acid. Diffraction techniques have limited resolution, however, and incredible insight has been provided by the combination of STM and theory tools for structural evaluation and image simulation. For example, the high coverage phase of enantiomeric alanine on Cu (1,1,0) when annealed at 400 K and imaged by STM shows large chiral domains wherein the amino acids are packed in groups of six or eight molecules [84]. Because the symmetry axes of these groups do not coincide with the major symmetry directions of the metal surface, mirror symmetry is not present. Phenyl glycine also shows chiral packing [85] because of the bulkiness of the phenyl group which theory shows to favour a chiral arrangement [86].

Cysteine is a particularly beautiful example of chiral self-assembly on metal surfaces. When the molecule was evaporated to the gold (1,1,0) surface, pairs of molecules self-assemble [87]. Deposition of the racemic sample to the surface leads to homochiral dimers, partially as a result of local surface structure reordering. Simulation approaches to the adsorbed system using density functional theory (DFT) imply that the selective formation of the homochiral dimer is a result of three bonds at each cysteine molecule, and analogies were made to the three point model for stereoselective binding in biological systems. In addition, when the racemic example was deposited an excess of one type of enantiomer dimer was observed at the gold surface [88], for which there is yet to be an explanation, although we should point out the tiny amount of material on the surface which might arise from an undetectable scalemic mixture. Finally, the same racemic mixture leads to apparent spontaneous resolution of larger chiral clusters on the same surface, again witnessed by STM with remarkable resolution [89].

Proline converts into prolate upon adsorption to the copper (1,1,0) surface, with the oxygen atoms of the carboxylate bound to metal atoms on the same row of metal atoms [90]. The STM images of the monolayer show different contrast for different molecules on the surface, because one enantiomer of the amino acid can actually form two adsorbate structures because the nitrogen atom of the compound also adsorbs to copper atoms on adjacent rows to give two diastereomeric conformations

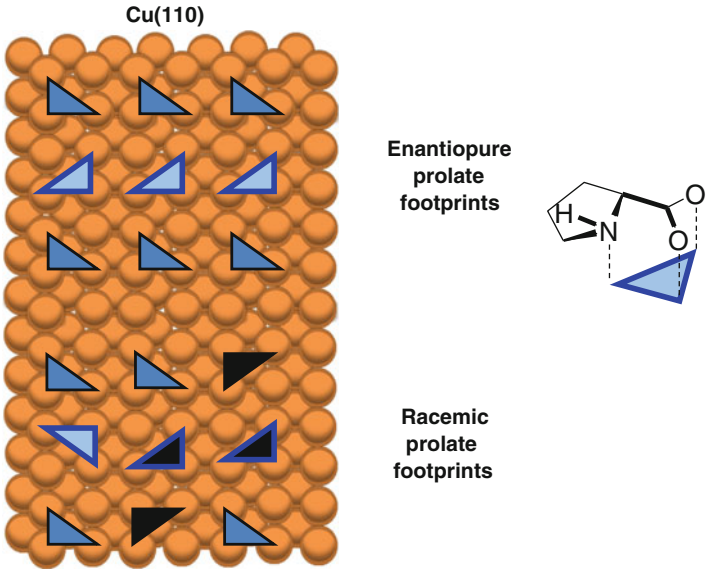

Fig. 8 Representations of the adsorption of enantiomeric prolate on the copper (1,1,0) single crystal surface, where two footprints are evident (one of them is indicated schematically on the *right*) and the footprint pattern of the racemate of the same molecule

(Fig. 8). When the racemate of proline was adsorbed at the copper (1,1,0) surface a very complex monolayer is formed, with no long range order, but in which the enantiomers and diastereomers can be identified [91]. The handedness and footedness which the enantiomers have lead to four distinct contrasts in the STM images. However, while handedness is random, the footedness is ordered in rows (alternating double – carboxylate – and single – nitrogen – coordination on a copper row). Remarkably, when the heterocyclic ring is rigidified in the form of 3-pyrroline-2-carboxylic acid, while the enantiomers independently show very well ordered monolayers, the racemic compound shows a totally random packing on the surface [92].

This intriguing situation implied to Raval and coworkers that the "handedness" of a molecular adsorbent is not necessarily correlated with the molecule's "footedness" [93]. This group created the monster they dubbed "Frankenfoot" (Fig. 9)[1] in order to convey the idea of the intrinsic chirality of an organic component in terms of its stereogenic centre(s) and the induced chirality on the surface through the footprint the molecule makes when adhered. The apparently minor differences between proline and 3-pyrroline-2-carboxylic acid mean that the latter forms an ordered two-dimensional footprint at the copper surface [94].

[1] This nomenclature was used in lectures and we feel it illustrative. We thank the Raval group for permission to use the term in press.

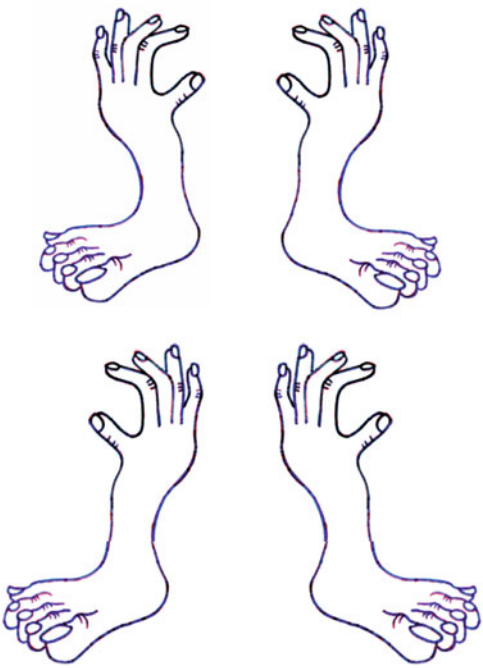

Fig. 9 The diastereomers of "Frankenfoot": a representation of the handedness of molecules and their possible footedness when they adsorb on a surface

The adsorption of these amino acids on surfaces has been highlighted here for gold and copper, although other metals and oxidised versions of them have been used. The choice of the material used as the surface and the single crystal face that is used can influence greatly the bonding between it and the adsorbate as well as the subsequent organisation. The bonding between histidine and gold or copper is illustrative of the different binding [95]. We should also reiterate that thermal treatment can cause passage from a part of the phase diagram devoid of true interface chirality to one where the organisational disymmetry is evident [80].

The adsorption of oligo- and poly-aminoacids – peptides and proteins – to metal and oxide surfaces has been elegantly discussed by Pradier and co-workers [96]. As they point out, studies can be largely divided into the adsorption of oligopeptides to surfaces and those of proteins. For the purposes of this section of the review, we shall concentrate on the expression of chirality by oligopeptides, because when proteins are adsorbed on surfaces their chirality is usually evident through diastereoselective interactions with other entities (as we shall see in a subsequent section of this review).

The combination of amino acids into oligomers provides a considerable combinatorial library to wade through on different surfaces and under differing conditions, and perhaps for this reason the first studies on this type of compound have been on homopeptides (made of the same amino acid in each monomer unit) and a vast – if apparently daunting – area for research lies ahead in this area. For example, di-L-alanine was observed to form chiral rows on copper [97]. On the same surface, diphenylalanine enantiomers adsorb, diffuse and generate homochiral chains [98].

Video STM shows how enantiomers do not interact significantly with one another, while like enantiomers join and form chiral chains. Modelling confirmed that conformational rearrangement is necessary in order for this recognition process to take place [99]. Thus, on this surface, the molecules act as if they are enantiophobic [52]. Interestingly, the order in these chains could be improved by co-depositing terephthalic acid on the surface, leading to a two-dimensional co-crystal [100]. This case is an example of how addition of an achiral adsorbate can lead to more well defined chirality in the monolayer.

Beyond this size, little is known at the molecular level concerning the chirality of higher peptides, spectroscopic data being determined which implies modes of adsorption [101–103] but no precise information concerning the chirality obtained. Specific segments have been studied in order to gain insight into their action in biological systems and on the path remarkable discoveries have been made. For example, with insulin growth factor tripeptide, when adsorbed in the (1,1,1) surface of gold, a truly dramatic restructuring of the surface takes place [104]. STM shows that lines of gold atoms are formed which are grown from step edges and kinks of the initial metal surface when the peptide is adsorbed, even without annealing. The process is dynamic and can even affect areas of the metal where no apparent defects are present at the outset. Other excellent works concerning the assembly of peptides on surfaces include those of a gold binding peptide on gold (1,1,1) [105] and the self-assembly on graphite of dodecapeptides selected by phage display [106]. In the latter case the peptide was further engineered by mutations so that intermolecular interactions, initial binding, surface aggregation and growth kinetics were modified. Yet again, the role of chirality in these examples is not established.

Up to this point in the review we have concentrated on amino acids and peptides binding to essentially flat crystalline metal surfaces, but a great body of work also exists on the formation of layers of these molecules on a variety of inorganic nanoparticles. These studies open the way to spectroscopic studies in solution, but offer a less precise "molecule by molecule" visualisation of the interfaces. Both silver [107, 108] and gold [109] nanoparticles are readily prepared with amino acids on their surfaces, giving them particular properties regarding their dispersion. In an analysis of the chirality of one amino acid in one of these systems, the conformation of *N*-acetyl-L-cysteine on gold nanoparticles has been determined by vibrational circular dichroism spectroscopy [110]. Gold nanoparticles coated with *N*-isobutyryl-L-cysteine and *N*-isobutyryl-D-cysteine of sizes less than 2 nm were prepared and separated into well defined clusters in which spectroscopy and calculation implied that the carboxylate as well as the thiol were coordinated to the surface [111]. Some of the separated clusters showed high optical activity as a result of metal-based transitions, and a chiral footprint of the adsorbed thiol on the metal core was suggested. This is a non-trivial conclusion, because in principle the optical activity could arise either from chiral metal structure or from an induction of a chiroptical signal from the stereogenic centres in the ligand [112, 113].

While the symmetry breaking experiment with chiral ligands on metal nanoparticles has not yet been reported to our knowledge (although the separation of chiral clusters with achiral ligands has been achieved [114]), the replacement of one enantiomer for another – so-called thiolate-for-thiolate ligand exchange – has

been observed [115]. In the experiment, well-defined gold nanoparticles with one enantiomer of a ligand were replaced with the opposite enantiomer with no significant modification of the number of metal atoms. The optical activity of the product had the same order and characteristics as the starting material but opposite sign, implying that the metal atoms at the surface can be reorganised under the influence of the ligands.

The chirality of the cysteine stabilisers used for the preparation of CdTe nanocrystals was correlated with the outer structure of the inorganic core [116]. Using either enantiomer of the amino acid produced nanocrystals in water which had the opposite optical activity. The growth rate and product structure in the inorganic part of the particles were affected by the stabiliser, and the spectroscopic data backed up by molecular modelling suggested that surface chirality is present because of the tetrahedral environment of the metals which is reminiscent of carbon stereochemistry. The authors hypothesised that this discovery might aid in finding applications for chiral nanomaterials in optics and medicine.

The functionalisation of gold nanoparticles with peptides of random coil or α-helix secondary structures led to optical activity through peptide−nanoparticle interactions [117]. Circular dichroism spectroscopy showed a plasmon resonance signal at 520 nm from the peptide − nanoparticle complex. Addition of metal ions to the nanoparticles dispersions caused their aggregation and a red-shifted plasmonic CD effect.

While research into ensembles of surfactant-protected nanoparticles in solution is relatively accessible for noble metals, the study of the adsorption of chiral molecules on the surfaces of all but the noblest of single crystal metal surfaces in solution is difficult because of atmospheric damage. Yet electrochemical STM (ECSTM) is an interesting and versatile (if challenging) technique for this purpose. A particularly nice example is that of the enantiomers and racemic modification of tyrosine on the copper (1,1,1) surface [118]. The ECSTM images show clearly that the enantiomers of the compound form mirror image space groups. The bent shape of the molecule was inferred in which it lies quasi-planar to the metal surface with carboxyl and phenol oxygen atoms coordinated to the metal, a conformation which was consistent with the measured unit cell. When the racemic mixture was adsorbed on the surface, domains showing unit cells consistent with either one or the other enantiomer of tyrosine were observed, suggesting spontaneous resolution of the molecule.

Moving away from amino acids and peptides, tartaric acid is an important natural product historically because of Louis Pasteur's famous discovery of enantiomorphous crystals of its sodium ammonium mixed salt [119]. The acid also shows remarkable chirality on achiral metal surfaces when deposited from the gas phase and studied by scanning tunnelling microscopy and low energy electron diffraction in vacuum. The (*R*,*R*)-tartaric acid forms chiral motifs in the form of the monotartrate monomer, the monotartrate dimer and the bistartrate monomer at different parts of its adsorption phase diagram corresponding to the adsorbed species the on the Cu (1,1,0) surface [120]. These can be interconverted by changing conditions, and can lead to extended surface chirality thanks to the supramolecular interactions taking place between them [121]. The monolayer contains chiral "channels" where metal atoms are exposed, and the enantioselectivity in catalysis by this surface is believed to arise from docking into

these sites. A detailed study of the low-coverage phases thought to be important for the enantioselective reaction using surface science techniques revealed a subtle balance between them depending on adsorption temperature, coverage and the time taken for each process. The relative stabilities of the phases depend on coverage (they can be inverted) and significant molecular mass transport is a key factor [18].

In an interesting recent paper, chiral copper oxide films were reportedly grown by epitaxial electrodeposition from copper(II) complexes of malic acid to a single crystal copper surface [122]. Alkaline solutions of copper malate were used to deposit anodically the CuO to the (1,1,1) and (1,1,0) single crystal surfaces to give chiral epitaxial layers in the case of the enantiopure complexes, as indicated using X-ray diffraction pole figures and stereographic projections. The layers formed from the racemic metal complex did not yield the chiral phases obtained from the enantiopure complexes. The bulk crystal structures of the enantiopure and racemic crystals showed that, while the former generate coordination polymer chains in the crystal, the racemate did not, pointing, perhaps, to a possible packing explanation for the formation of the unique structures in the case of the homochiral compounds.

Films of biological relevance formed at the air–water interface can show the emergence of chiral structures [123–127]. Since the observation of spontaneous separation of chiral phases by Eckhardt et al. [128], where monolayers of a rigid amphiphile were transferred to mica and imaged by atomic force microscopy and the subsequent explanation for the separation of enantiomers in the layer [129], the requirements for symmetry breaking at the water surface have become clearer [130]. The glide plane with its plane perpendicular to the water surface is a favoured packing arrangement for the alkyl chains often present in molecules which order at the interface with air, giving the compounds the herringbone packing associated with a non-chiral space group. To avoid this packing, translation symmetry only has to be favoured. So amphiphiles based on amino acid head groups with amide spacers before an alkyl chain pack with translation symmetry only at the air–water interface and resolve spontaneously [131]. The observation of the separation of enantiomers was achieved using grazing incidence X-ray diffraction, which showed clearly that the mixture of enantiomers had an oblique unit cell characteristic of chirality. This family of compounds can also undergo spontaneous resolution into apparent domains of pure enantiomers when spread in a monolayer with phospholipids [132], a fact which shows that the phenomenon can occur outside the pure system. Of crucial importance is the length of the spacer in between the amino acid head group and the amide unit, which helps the molecules self-assemble at the water–air interface. In any case, the amphiphiles of this nature are held at the interface and while segregation can take place, different areas of the surface contain opposite enantiomers.

2.3 Adsorption of Achiral Molecules on Chiral Surfaces

An interesting possibility regarding the emergence of chirality in the natural world is that achiral but prochiral molecules adsorbed to the chiral surfaces of

naturally-occurring minerals and were modified there by diastereoselective reactions to afford chiral molecules [133]. Yet there is very little work being done in this area, and many opportunities exist. An example which exemplifies adsorption of one prochiral face of an achiral molecule is that of glycine on copper. The structures of dense glycine and alanine monolayers on a chiral copper surface were studied using density functional theory calculations [134]. They showed that the monolayer's overall stability is due to a combination of chemical bonds of the molecules with the Cu surface, deformation of the organic residue while attaching to the metal and intermolecular hydrogen bonds between the molecules. Adsorbate-induced surface reconstruction leads to the facets of the chiral metal surface when glycine or alanine are adsorbed and annealed on Cu (1,0,0).

Interestingly, surfaces of aggregates of chiral biomolecules can induce chirality on growing inorganic materials. When gold nanoparticles were grown on either enantiomer of diphenylalanine peptide nanotubes the nanocomposite showed a circular dichroism spectrum with significant intensity at the surface plasmon absorption of the metal [135]. The optical activity was assigned to an asymmetric organisation of the metal atoms in the nanoparticles on the peptide nanotubes. Mirror image relationship in the circular dichroism spectra clearly indicates that the chiral molecules on the nanotubes drive the organisation of nanoparticles in two different ways. It seems probable that similar growth phenomena will be observed in other systems with biomolecules of relevance in the emergence of chirality in natural systems.

3 Evolution of Chirality at Interfaces

Once the enantiomers of a compound have landed on a surface, and may even have organised themselves in some way, there remains the possibility that the chirality of the surface can evolve under certain conditions. That is, that the handedness of the system develops so that dissymmetry is generated. There are a limited number of examples of this kind of phenomenon at interfaces for biomolecules, and therefore representative examples of synthetic molecules will be given to act as an inspiration for the development of this area. This phenomenon is most easily seen in non-surface systems in nonlinear amplification of handedness in a scalemic mixture (the imbalance created artificially) by the majority rules effect [136–142], as well as in mixtures where chiral agents induce chirality on achiral chains, the sergeants and soldiers effect [143–154].

Evaporation of heptahelicene to the Cu (1,1,1) crystal face results in a layer which displays enantiomorphism on a mesoscopic length scale that is readily amplified, despite the fact that the compound does not resolve spontaneously on the surface [155]. Domains of the heptahelicene in the racemate are non-superimposable mirror-like lattice structures. A small excess of one of the enantiomers of the molecule results in the presence of just one domain chirality. An apparent enantiomeric excess of only 0.1 gives an almost total induction of chirality in the ordered domains, while the

so-called "residual" areas – which contain small clusters and short rows – are more predominant than in the pure enantiomers, and increase with increasing ee. Proof that the domains contained both enantiomers of the heptahelicene was provided by high resolution STM images where the two could be inferred in the same area. The driving force for the phenomenon was hypothesised to be the removal of domain boundaries, which are energetically unfavourable.

Slight imbalances in the proportion of enantiomers of tartaric acid on copper (1,1,0) can lead to "drastic symmetry breaking" [156]. The transmission of chirality was skewed from the molecular to the supramolecular level so that single-handed superstructures were created from mixed enantiomer systems where a slight enantiomer enrichment was enforced. This effect was achieved because of flipping the conformational chirality (not the chirality of the stereogenic centres) of all the molecules to the same orientation with respect to the metal surface. LEED measurements indicated that all of the crystalline domains were a single handedness at an enantiomeric excess of approximately 0.2, so clearly the majority enantiomer organises into its preferred superstructure. STM imaging shows the nonlinear symmetry breaking is partially caused by the fact that the minority enantiomer is located in disordered domains on the surface and simulations indicated that the effect was caused by configurational entropy effects. It was hypothesised that the fact that such a small imbalance can lead to such a dramatic change in supramolecular order implies a possible route to amplification of broken symmetry, whereby the separated areas could behave in different ways towards an enantiospecific process.

The study of small amino acids adsorbed on Cu surfaces under ultraclean UHV conditions allows precise correlation between molecular chirality and the surface interface structure, as we have seen in many of the previous examples. The transfer of chirality from the stereogenic centres to the surface can be a result of the reorganisation of the metal atoms at the interface between the bulk metal and the organic adsorbent. The study of alanine overlayers on Cu (3,1,1) surfaces helps one to understand the interplay between different manifestations of chirality, especially footprint chirality, at the interface. On the other hand, the same compound adsorbed to the intrinsically chiral Cu (5,3,1) shows an enantiospecific amino acid-induced restructuring of the surface [157]. The different effects that chiral adsorption can have on the arrangement of the molecules and on the way in which the single crystal surfaces adapt to the adsorption process is likely to indicate ways in which the inverse process – the transfer of surface order into chiral organisation of prochiral organic molecules – could have taken place.

The transmission of chirality in monolayers at an air–water interface is a particularly intriguing possibility given the abundance of this environment on Earth. Two recent papers show the emergence of chirality upon some influence from the system. In one, thermal annealing of Langmuir–Blodgett films of a tetraphenylporphyrin bearing one carboxylate at the 4-position of one of the phenyl rings prepared by spreading, compression and horizontal lifting showed an amplification of chirality [158]. The as-formed layers revealed weak circular dichroic signals, but after heating up to 120°C for 10 h under vacuum a very strong CD

signal was observed. It is important to note that the acid group is important for the chiral organisation because the corresponding methyl ester does not show any optical activity. This situation is perhaps reminiscent of the formation of a metastable phase in gel materials formed by intrinsically chiral porphyrins [159], with the important exception that here no chiral influence is present in principle and both chiralities are observed from different batches [158]. Therefore, symmetry breaking takes place at the surface, also observed in solution for other porphyrins [160–162]. The other recent example of symmetry breaking at the air–water interface is that of an achiral ligand which forms chiral layers and can also form chiral structures in silver coordination complexes [163].

4 Stereoselective Molecular Recognition at Interfaces

The functionalisation of the surfaces of different materials with chiral biomolecules and the use of the resulting surfaces for molecular recognition of solution borne compounds or systems has received considerable attention, and the literature dealing with the topic is abundant and diverse. The most explored approach in this area is the preparation of chiral monolayer-protected surfaces. Upon surface functionalisation the stereoselective molecular recognition between the monolayer and chiral biomolecules such as cells, proteins and aminoacids has been studied. In this section we shall only consider cases in which the stereoselectivity takes place in the vicinity of the surface. There are numerous examples where stereogenic centres are decoupled from any interface by a long spacer [164–166] which favours interaction with the surrounding medium but which isolates the true interface from the molecular recognition event and essentially gives a similar environment to a purely solution based situation, except that molecules can be caught from solution and immobilised. Our interest here is related to the interface where substrate and adsorbate can influence one another.

4.1 Self-assembled Monolayers

One of the most developed strategies to study the stereoselective molecular recognition at the interfaces is the preparation of self-assembled monolayers (SAMs) on surfaces, which are the result of the formation of organic assemblies by the adsorption of the molecules from solution or gas phase to an inorganic (metallic or semiconductor) substrate [167, 168]. SAMs on gold or other metallic surfaces have been widely applied in surface chemical modification thanks to their easy functionalisation and manipulation and their potential applications in biosensors, biomolecular electronics and nanotechnology [168]. Among all the metallic surfaces, gold films are by far the most used substrates for the preparation of SAMs thanks to their ease of preparation, low toxicity and good stability of the

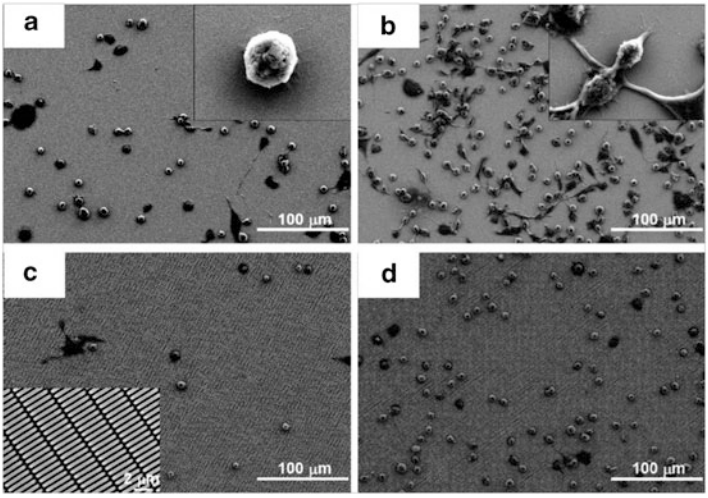

Fig. 10 Scanning electron microscopic images of macrophages cells adhesion on chiral NIBC SAMs, D-NIBC SAMs (**a**, **c**) and L-NIBC SAMs (**b**, **d**). Reprinted with permission from [169]. Copyright © 2007 American Chemical Society

gold in air and habitual solvents, the utilisation of gold films as substrates for several spectroscopies and analytical techniques, together with the formation of stable and reproducible SAMs on gold by the spontaneous adsorption of organo-sulphur compounds. Various strategies have been followed for the preparation of chiral functionalised SAMs for stereoselective molecular recognition between the monolayer and the biomolecules in order to control the specific binding and to minimise the steric hindrance between the molecules. Preparation of functionalised SAMs of thiols with desired bio-functionality is sometimes difficult. Amino acids are good candidates to prepare chiral bio-functionalised surfaces and to study recognition processes close to the interface. The –SH group and the –S–S– bond in the cysteine (Cys) and cystine residues, respectively, present in proteins have been used to prepare chiral bio-derived SAMs. The stereospecific interaction between immune cells and Cys-derivative functionalised SAMs showed that immune cells had different adhesion behaviour to the surface depending on the enantiomer of *N*-isobutyryl-L(D)-cysteine (NIBC) used to prepare the SAMs [169]. When cells were incubated with the L-modified surfaces a good adhesion to the surfaces was observed, while with D-modified surfaces less adhesion and activation of the cells was observed and different shapes were obtained (Fig. 10). The different biocompatibility depending on the enantiomorphous surfaces indicates the importance of the chirality in the design of new biomaterials and the way they influence cell behaviour.

The same L/D-NIBC enantiomers were used to explore the interaction between the functionalised surfaces and single-stranded DNA (ssDNA) and plasmid DNA molecules [170, 171]. The importance of the hydrogen bonding interactions in the

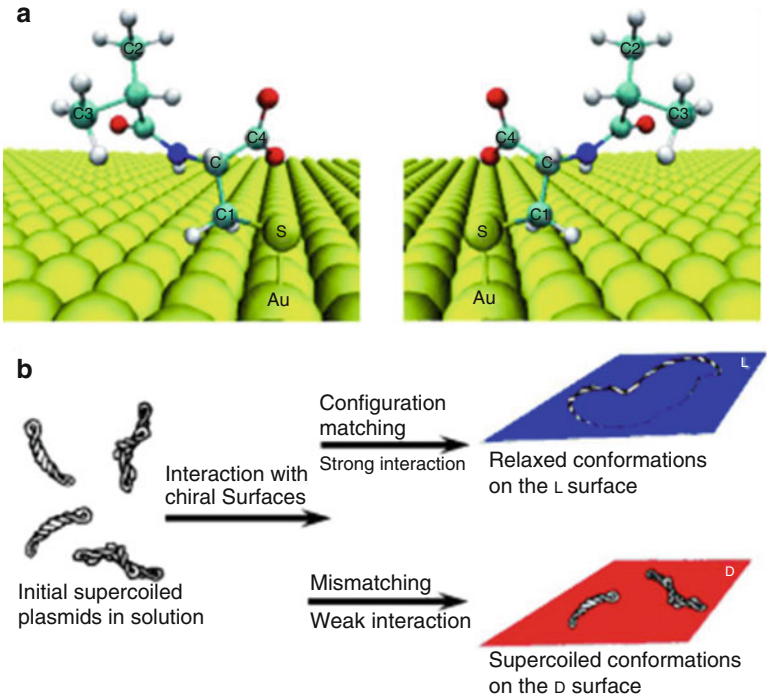

Fig. 11 Simulation of NIBC molecules on gold surfaces (**a**) and schematic representation of the stereospecific interaction between DNA and chiral modified surfaces with L/D-NIBC enantiomers (**b**). Reprinted with permission from [171]. Copyright © 2009 Wiley-VCH

final physical and chemical behaviours of the ssDNA and its interaction with other molecules explains the different behaviour depending on the chirality of the surface. The NIBC structure contains –COOH and –NH groups, which can form strong hydrogen bonds with the DNA chains. Then, depending on the arrangement of these groups of the NIBC in the immobilised molecules on the surfaces, a different stereoselective interaction between the L/D-surfaces and the DNA occurred. When L surfaces were used, a stronger interaction with the ssDNA chains was expected because of the orientation and environment of the hydrogen bonds, inducing a higher DNA adsorption and a more relaxed state of the chains (Fig. 11). Furthermore, when a plasmid DNA molecule (pcDNA3) was used, the same stereoselective adsorption on the chiral NIBC modified surfaces was observed. Again the amount of the DNA adsorbed on the L-surface was higher than for the D-surface. Furthermore, another chiral-induction effect was observed because of the stereoselective adsorption. The higher interaction between the plasmids and the L-surface resulted in a change of the conformation of the molecules from the supercoiled to the relaxed conformations, while for the D-surfaces the supercoiled conformation was preferred. It is worth noting that, although the utilisation of NIBC enantiomers induces stereoselective interaction with DNA molecules, the presence of the large isopropyl side group can also influence

the adsorption process. Nevertheless, when pure cysteine enantiomers were used to study protein and cell adhesion, a higher amount of both on the L-cysteine surfaces than on the D-cysteine surfaces was also observed [172].

In a different approach based on the use of chiral molecules which can interact with or have a selective response to biomacromolecules, 1,2-diphenylethylenediamine (DPEN) enantiomers were used in SAMs [173]. In this case, DPEN enantiomers were attached to the surfaces through an amide linkage with SAMs of 3-mercaptopropionic acid on gold electrodes. The stereoselective interaction of alpha-fetoprotein antibody and antigen (anti-AFP and AFP), which is an important tumour marker, with (1*R*,2*R*)-DPEN or (1*S*,2*S*)-DPEN surfaces was studied by cyclic voltammetry. Different amperometric responses were obtained depending on the chirality of the surface. The greater change of the current peak acquired from the (1*S*,2*S*)-DPEN modified electrode indicated better recognition for the antibody anti-AFP and better arrangement of the molecules for the antigen/antibody reaction. The chiral-induced arrangement of the $–NH_2$, –NH– and phenyl groups of the different enantiomers of DPEN – which control the hydrogen bonding and π–π interactions between the surfaces and the biomacromolecules – explained the different response of the modified electrodes.

4.2 Nanoparticles

Preparation and application of biofunctionalised monolayer-protected nanoparticles (NPs) has emerged as an important field of research because of their size and tunable properties which allow their spectroscopic observation. Furthermore, when particles are used in recognition processes an enhancement of the sensing signals is obtained. The huge possibilities for tuning the properties of the particles have meant their widespread use in sensing studies with biomolecules. An interesting example is the employment of gold functionalised nanoparticles as "noses" for protein, bacteria and cells sensing [174, 175]. The type of NPs particles used is also extensive due to the broad range of properties they show and includes metal NPs (Au, Ag), quantum dots (QDs) and SiO_2 NPs and magnetic particles such as Fe_2O_3 [176]. The charge, hydrophobicity, surface topology, solubility, stability, toxicity and of course chirality of the particles can be modified by changing their surface coating layer. However, the origin of optical activity in chiral metal NPs is still not clear (see above) and research to understand this phenomenon is attracting great attention to develop new biological sensors. One of the strategies followed is to tune and induce chiroptical activity to metal NPs and QDs by the use of chiral biomolecules as capping agents such as cysteine, penicillamine and gluthathione amongst others [111, 113, 177–180].

A second strategy to induce intense optical activity with metal NPs is the creation of chiral nanoparticle assemblies by using biomolecule scaffolds [181, 182]. DNA is by far the most used biomolecule to prepare these chiral assemblies. Chiral pyramidal assemblies of Au NPs by single-stranded DNA hybridisation, growing Ag NPs assemblies on DNA templates and DNA-guided assembly of

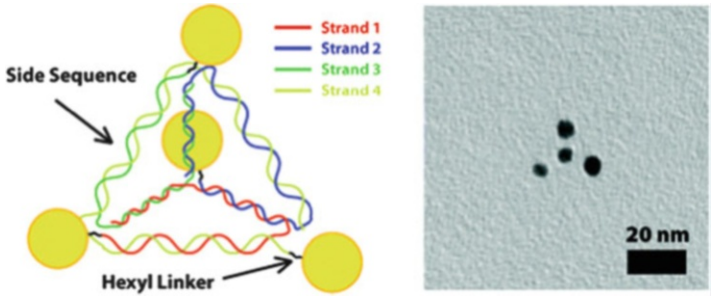

Fig. 12 Schematic representation of pyramidal chiral organisation of Au NPs and the corresponding transmission electronic microscopic image. Reprinted with permission from [183]. Copyright © 2009 American Chemical Society

Au NPs into crystallisation structures are just some examples that can be found in the literature [183–185]. Figure 12 shows a pyramidal case in which DNA strands bring together four nanoparticles.

In spite of all the fundamental studies to explain the chirality and all the approaches to prepare chiral NPs and control their optical properties, few examples can be found where they have been used for an enantioselective recognition process. Polarimetry, fluorescence, electrochemistry or surface plasmon resonance of the particles were used to determinate the enantioselectivity of the interactions and to develop new sensors. Chiral cysteine-capped CdSe(ZnS) QDs were used to quantify carnitine enantiomers by following the emission spectra of QDs upon the selective interaction [186]. The isomers of carnitine are of interest because they present different biological activities. A quenching of the L-Cys-capped QDs fluorescence was observed upon the addition of D-carnitine. However, when D-carnitine was added to the D-Cys-capped QDs solution the fluorescence of the QDs was not affected, indicating a chiral selectivity of each type of chiral cysteine-capped QD with only one enantiomer of carnitine. The decrease of the fluorescence was a consequence of the reorganisation of the Cys molecules on the QDs when the selective interaction occurred.

Modified D- or L-Cys AuNPs were also used to study enantioselective and enantiospecific interactions with *R*- and *S*-propylene oxide (PO) enantiomers by polarimetry. The different optical rotation measurements of the modified AuNPs with (*R*)-PO and (*S*)-PO enantiomers indicated a selective adsorption of one enantiomer. Then the AuNps modified with L-cysteine selectively adsorbed the (*R*)-propylene oxide while D-cysteine modified NPs adsorbed the (*S*)-propylene oxide enantiomer. Moreover, enantiospecific interactions were observed when a *rac*-PO solution was used. The detection of optical rotations by *rac*-PO in solutions containing chiral Au NPs showed the adsorption of one of the enantiomers of the PO leaving an excess of the other in solution. Therefore, enantioselective separation of the PO enantiomers on the chiral AuNPs was hypothesised [187]. In a bulk system attached to a surface, electrochemical sensors were developed using penicillin modified AuNPs [188]. The gold electrodes were modified with D- and L-penicillin AuNPs, respectively,

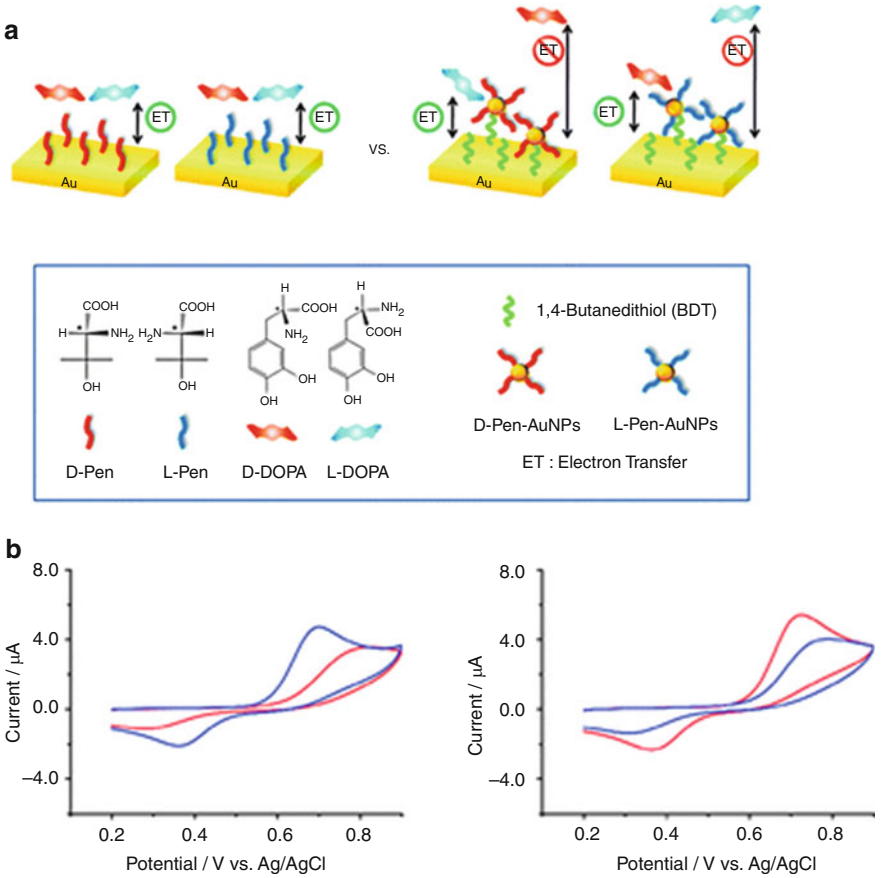

Fig. 13 (**a**) Schematic representation of the modified gold electrodes with L- or D-Pen and L- or D-Pen AuNPs. (**b**) Cyclic voltammograms for DOPA on L- or D-Pen AuNPs-immobilised electrodes. Reprinted with permission from [188]. Copyright © 2010 Royal Society of Chemistry

and the enantioselective recognition of 3,4-dihydroxyphenylalanine (DOPA) was demonstrated. The cyclic voltammetry curves of the modified gold electrodes with L- or D-penicillin AuNPs showed a preferential diastereomeric interaction with D- or L-DOPA, respectively, (Fig. 13). Moreover, the use of the penicillin-modified chiral AuNPs allowed greater values of differences of anodic peak potential between D- and L-DOPA than on penicillin-modified gold electrodes, highlighting the benefits of nanostructuring on the diastereoselective interaction.

Chiral recognition of enantiomers by colorimetric enantiomeric discrimination was employed to separate and quantify L- and D-Cys in aqueous solution [189]. Ag NPs were capped with uridine 5′-triphosphate (UTP) nucleotide and the colour change of the selectively induced aggregates was used for enantioselective recognition identification. D-Cys selectively induced the aggregation of AgNPs and a shift of the colour of the modified AgNPs, whereas with L-cys no changes were

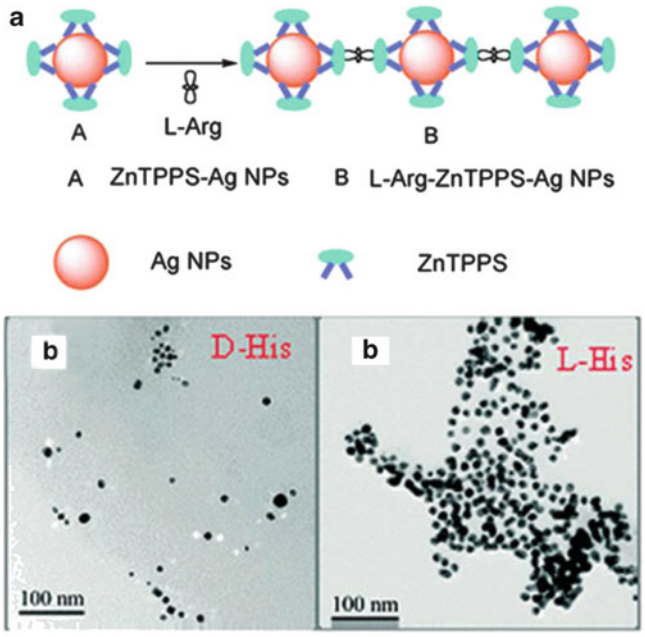

Fig. 14 Schematic representation of zinc tetraphenylporphyrin-modified Ag NPs (**a**) and transmission electron microscopy images of the aggregates after incubation with D-His and L-His (**b**). Reprinted with permission from [190]. Copyright © 2012 Royal Society of Chemistry

observed. When the same experiment was done with a *rac*-cys solution and because of the precipitation of the D-cys induced aggregates after centrifugation, an enantioselective separation of the cys-enantiomers was obtained. However, when other nucleotides were used, such as ATP, only quantitative determination of cys-enantiomers was possible. Other chiral amino acids were also developed to prepare chiral colorimetric sensors for stereoselective recognition of D/L-histidine based on the formation of aggregation of the Ag NPs [190]. The design of the sensor consisted of the preparation of modified Ag NPs with zinc tetraphenylporphyrin (ZnTPPS) and the formation of assemblies of the particles by introducing chiral L-arginine ligands (Fig. 14). The exposure of the L-arginine NPs assemblies with D/L-histidine solutions showed a selective response to L-histidine together with an amplification of the chiral signal. The difference response to D/L-histidine solution was attributed to the different ability of L-histidine to induce the formation of large aggregates of the Ag NPs, as seen clearly in the transmission electron microscopy images. The same strategy was used to develop a new colorimetric sensor based on *N*-acetyl-L-cysteine (NALC) capped Au NPs for the enantioselective detection of tyrosine (Tyr) [191]. As a result of the formation of aggregates, when NALC AuNPs interacted with L-Tyr, a change of the colour of the solution was observed and by centrifugation the aggregates were separated from the solution. The different response depending on the enantiomer of tyrosine used indicated a different chiral

conformation of L-Tyr and D-Tyr on the particles in their interaction with NALC through the carboxylic, amino and hydroxyl groups of the NP covering.

One of the most important applications to which biofunctionalised NPs can be made is in living systems, and their biocompatibility is a particularly important aspect which must be taken into account, especially in the case of QDs because of the toxicity of the heavy metals that form the core of the particles. QDs capped with tripeptide glutathione were examined to determine the influence of the conformation of the capping ligands on the cytoxicity and autophagy of QDs in cells [192]. The cell viability in human cells showed higher cytoxicity and induced autophagy for L-glutathione QDs than for the corresponding D-glutathione QDs, highlighting the importance of the NP coating on activity in natural systems.

4.3 Polymer Surfaces

One of the widest uses of the phenomenon of stereoselective recognition at polymer surfaces is that of chiral separation in chromatography or in membranes, and readers are directed to authoritative reviews on this subject [193–195]. Polymers of biological origin, often suitably modified chemically, or synthetic polymers modified with chiral layers of molecules from biologically derived compounds (notably the cyclodextrins), are frequently used for this purpose. Just as an example, the biopolymer chitosan can be immobilised in nanoparticulate form – functionalised with glycidyl methacrylate – using methacrylamide to give an efficient stationary phase in the form of a capillary for electrochromatography [196]. The materials exhibited favourable surface-to-volume ratios and were able to separate the enantiomers of tryptophan and catechin effectively. The nature of the immobilisation of the chitosan is important for analytical application, although presumably the diastereoselective interaction is always present.

Chiral biodegradable polymers such as polylactides are used in many biomedical applications. However, the study of the influence of the chirality of those polymers is still a challenge. Different stereoisomers of polylactide polymer were used to study the influence of the chirality of the chains to interact with proteins and cells [197]. The different studies of protein absorption, cell morphology, cell proliferation and protein activity revealed better results with poly(L-lactide) than with poly (D-lactide) polymers films. Besides, when a racemic mixture (poly(L/D-lactide) was used the films showed favourable cell proliferation probably because of the higher stability of the film.

For the development of interfaces based on polymers, chiral polymer brushes have been used as an alternative to SAMs. The use of the polymer brushes allows perfect control of the surface properties thanks to their easy modulation of composition and functions. Moreover, the layers obtained are thicker than for the corresponding chiral SAMs, which is important for practical applications. The main strategy followed has been to graft the polymer brushes to surfaces by surface-initiated polymerisation. For that, chiral monomers based on chiral amino acids linked to achiral polymeric units

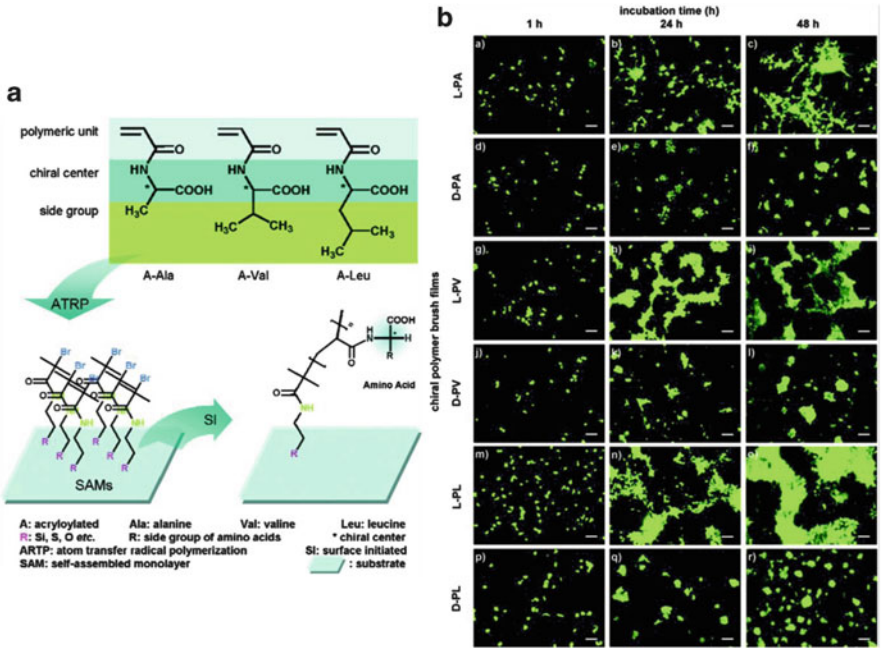

Fig. 15 (**a**) Preparation of chiral polymer brush films of chiral amino acids and (**b**) fluorescence images of cells incubated on the chiral polymer brush film. Reprinted with permission from [199]. Copyright © 2012 American Chemical Society

were prepared and reacted with functionalised SAMs. To apply the chiral polymer brushes as new biomaterials the stereoselective recognition with cells and proteins has also been demonstrated. L(D)-Valine based polymer films with achiral backbone were used to study the influence of chirality on cell behaviour [198]. The results concluded that different cell adhesion and spreading and assembly behaviour on L-valine and D-valine polymer films were caused by the different chirality of the films. For L-valine films higher adhesion, growth, spread and assembly of the two types of cells studied – fibroblast-like cell line (COS-7) and type-endothelial cells (bEnd.3) – were observed (Fig. 15). Because of the different cytocompatibility of the enantiomeric valine based synthetic macromolecules, other chiral amino acids with different sizes and hydrophobic side groups such as alanine and leucine were used to modulate cell behaviour on polymer films. It was demonstrated, using the same COS-7 and bEnd.3 cells, that in general all L-surfaces showed better cytocompatibility regardless of the amino acid used. Nevertheless, the size of the side groups was highly important and L-amino acids with larger hydrophobic side groups exhibited different cell adhesion and behaviour [199]. The influence of hydrophobic interactions between L(D)-valine grafted polymers and proteins were also explored due to their influence in the protein-guest interactions [200].

The use of stereoselective recognition to prepare chiral-responsive polymers is a fascinating possibility which has been reviewed recently [201]. An example of this

phenomenon is shown by a three-component copolymer based on chiral dipeptides grafted to silicon surfaces for chiral recognition of monosaccharide enantiomers [202]. Use of the three-component copolymer, which consisted of chiral recognition units (L-dipeptides), functional switching units (poly(*N*-isopropylacrylamide) and mediating units (phenylthiourea derivatives), allowed monitoring of the stereoselective recognition of the monosaccharide enantiomers by the different wettability of the films upon incubation with L(D)-monosaccharide solutions. Furthermore, the chiral-selective wettability response was reversible when the films were treated with pure water and monosaccharide solutions.

4.4 Cyclodextrins

Cyclodextrins (CDs) are natural products (made by enzymatic conversion from starch) which are extensively used as stereoselective ligands in chiral separation because of their ready availability and their toroidal structure which invites guest inclusion [193]. Chemical modification of the CDs structure is also widely explored in order to improve their properties and to immobilise them on different surfaces. Modification of the CDs structure was used, for example, to prepare a new cationic chiral selector to improve the chiral recognition and separation of the enantiomers of dansyl-amino acids by capillary electrophoresis [203]. The use of CDs as receptors for chiral sensing at interfaces is also an important field of research and different sensing methodologies such as potentiometric, surface plasmon resonance, cyclic voltammetry and quartz crystal microbalance among others have been applied [204].

The properties of QDs have driven researchers to perform the modification of their surface with CDs with the aim of developing new chiral fluorescent sensors. This is the case for CDs-capped CdSe/ZnS QDs, which were used for chiral recognition of L/D-tyrosine and L/D-methionine amino acids. The different response depending on the enantiomer was revealed in the luminescence properties of the QDs. For L-tyrosine and L-methionine an enhancement of the fluorescence was observed, whereas for the corresponding D-enantiomers the luminescence was barely changed when compared with the nanoparticles bearing the host element. The different fluorescent response was attributed to a different binding strength of each enantiomer with the CDs and the influence of this interaction to the structure of the QDs [205].

Signal-response devices for enantioselective recognition of amino acids and in particular for L-histidine were developed by the immobilisation of βCDs into biomimetic artificial nanochannels [206]. The nanochannels were fabricated using polyethylene terephthalate (PET) membrane and modified with NH_2-βCDs covalently attached. Upon the modification, the channels were exposed to a solution of L-histidine and changes in the ionic current were observed, indicating a correct binding of the amino acid to the channel. However, this change of the ionic current was insignificant when D-histidine was flow through the channel. Moreover, when

other amino acids such L/D-phenylalanine and L/D-tyrosine were used no changes were observed, although βCDs are also chiral receptors for those amino acids. The selectivity of the system to histidine derivatives was attributed to the working pH 7.2. At this pH only histidine amino acids are not negatively charged and therefore no electrostatic repulsion happened with the negatively charged nanochannels.

Modified thermoresponsive membranes have also been explored to develop systems in which the chiral selectivity is induced by the recognition of CDs together with signal response materials. To this end, poly(*N*-isopropylacrylamide) (PNIPAM) – which has a phase transition with low critical solution temperature – was grafted to nylon-6-membrane and modified with βCDs and used for the chiral resolution of L/D-tryptophan [207]. Adjusting the operating temperature, the structure of the polymer and the binding constant between βCDs and tryptophan could be modulated. When the membrane was operating below the phase transition, the responsive part of the polymer was swollen and hydrophilic and the βCDs were able to enantioselectively host L-tryptophan molecules and therefore the membrane became permeable to D-tryptophan. Moreover, it was possible to recover the L-tryptophan and regenerate the membrane by increasing the temperature above the transition temperature. The polymer became more hydrophobic and a decomplexation process of the L-tryptophan from the βCDs occurred, leaving the membrane ready for another chiral resolution cycle.

4.5 Langmuir Layers

The air–water interface is a highly relevant place to look for diastereoselective noncovalent interactions, because the environment is very similar to that of any cell in aqueous media [125, 208, 209]. The Langmuir technique is highly appropriate for these studies because the surface pressure isotherms give a direct reading of any additional interactions in a monolayer, and molecular recognition in this area can even be enhanced over bulk systems [210]. There are several examples highlighting the effectiveness of the stereoselectivity in this air–water interface, which have been reviewed in the cited articles, and therefore we give only some of the most recent cases to show the principles. In general, the formation of stable and reproducible Langmuir layers which form clear single molecule thick films require a molecular anisotropy, with a relatively polar head group which contacts the water and a non-polar section which orients towards the air. This condition usually involves the preparation of molecules which contain long alkyl chains and some sort of ionisable head group like carboxylic acid or amine. Clearly, amino acid derivatives are prime candidates for studies of this sort.

The surface-pressure isotherms – where the average molecular area at the interface can be calculated and where the kind of curve indicates the stability of the monolayer – were used to establish the stereoselectivity of interaction of a Langmuir film of *N*-hexadecanoyl-L-proline with the enantiomers of ditryptophan [211]. In this system only very small differences were observed in the isotherms,

yet a clear indication of enantiodiscrimination was obtained from Brewster angle microscopy images taken of the interface. There is really a necessity to look at Langmuir monolayers with several techniques, be it the isotherms, microscopy, diffraction techniques or even the more recent use of second harmonic generation of laser light [78].

A hybrid biomolecule-synthetic amphiphile system has been shown to exhibit enantioselective recognition [212]. Nucleobase head groups were attached to diacetylene chains which were polymerised with circularly polarised light to give crystalline domains, as shown by grazing incidence X-ray diffraction. A cytosine-containing monolayer showed stereoselective binding toward oligonucleotides containing the guanine base. Also, when the films were polymerised in the presence of the oligobase in the subphase during compression, the structure of the resulting film was very different when the reaction was performed using either right or left handed circularly polarised light, supporting the suggestion that enantiomeric forms of the monolayer are formed using the oppositely handed light.

An intriguing example of the emergence of homochiral peptide sequences with an air–water interface is that of the oligomerisation of racemic mixtures of amphiphilic peptide derivatives [213, 214]. In solution these compounds form the expected atactic polymer, in which both enantiomers are incorporated. However, in the ordered monolayer – and where crystalline domains are present – the reaction takes place between like molecules related in the periodic structure by a translation axis, even though the crystal as a whole is racemic. The preference for homochiral reaction can be further taken advantage of when a non-racemic mixture is used, where the excess is converted into the homochiral peptide sequence [132].

4.6 Crystal Surfaces of Achiral Materials

The interaction of the chiral surface of achiral materials with molecules containing elements of dissymmetry seems a plausible route for the selective adsorption of compounds, and therefore for generating an excess of one enantiomer of a species either on a surface or in solution [215]. Calcite is a common rock-forming mineral (the most stable polymorph of calcium carbonate) whose mirror-related surfaces exhibit enantioselective adsorption of aspartic acid from solution [216]. The surfaces of the inorganic crystals which had more terraces were found to show greater selectivity between enantiomers of the acid, an indication that the adsorbate is recognised best at the step edges rather than the plane. The authors hypothesised that a posterior polycondensation would lead to homochiral peptides, which could then express their chirality in biological systems.

As in the studies of adsorption on achiral surfaces, the adsorption of chiral compounds on the chiral faces of metallic copper has been researched relatively widely, with remarkable results being obtained. The adsorption of (*R*)-3-methylcyclohexanone to the kinked chiral surfaces of copper followed by temperature-programmed desorption showed that the molecule desorbed enantioselectively from chiral kink sites on the Cu (6,4,3) surfaces [217].

The difference in the desorption energies of the enantiomers of the adsorbate were used to prove enantioselective, kinetic separation of the racemate into its enantiomers by adsorption followed by desorption on either enantiomer of the copper (6,4,3) surface. Subsequently, on different copper surfaces with kink sites, the desorption was shown to be comprised of three processes, assigned as evaporation from the flat terrace, the close-packed step and the kink sites [218]. It was found that the difference in desorption temperature of one enantiomer of the compound from the *R*- and *S*-chiral kink sites on Cu (13,9,1) is 2.4 ± 0.8 K, equivalent to a difference in desorption energy of 0.7 ± 0.2 kJ/mol. The (*R*)-3-methylcyclohexanone adsorbed preferentially at the *R* kink site.

Another beautiful recent example is the Cu (5,3,1) surface, which exhibits the adsorption of serine in two different geometries [219]. At low coverage (far below a monolayer) the molecule is bound to the substrate through the amino group, the two oxygen atoms of the carboxylate group and the deprotonated beta-OH group, and the enantiomers show very different orientations. When a full monolayer is formed, the latter bond is not formed and the diastereoselectivity is not evident. The work shows that the three point interaction, at least in this case, is far more effective than two in diastereoselective discrimination on a surface.

Achiral crystals can act as intermediate auxiliaries in absolute asymmetric transformations [220]. Pairs of homochiral surfaces of opposite handedness are common among organic crystals of the triclinic, monoclinic, orthorhombic or tetragonal space groups. The chiral surfaces of this kind of crystal exhibit enantiomeric selectivity in the adsorption of chiral compounds to their faces, and in subsequent crystal growth. This phenomenon leads to crystals with unique properties [220].

4.7 Crystal Surfaces of Chiral Materials

Crystal surfaces of chiral materials can be used as interfaces to study the stereoselectivity and enantioselectivity of recognition towards antibodies, cells and amino acids [221]. The enantiomers of tartrate were used to prepare crystals with the same morphology, calcium (*R*,*R*) and (*S*,*S*)-tartrate, but with different recognition results after incubation with cells. The incubation of A6 cells with the enantiomorphous calcium tartrate tetrahydrate crystals revealed a different attachment on the (0,1,1) faces of the crystals. Only a short incubation time was necessary to observe cells covering the faces of the (*R*,*R*) crystals while almost nothing was adsorbed on the (*S*,*S*)-crystals after the same spell (Fig. 16). Moreover, using a racemic mixture of the enantiomorphous crystals, the same results were obtained [222].

With the aim of understanding the different recognition process and adhesion of the cells on the crystal surfaces, adsorption of possible molecules responsible for cell recognition processes, such as hyaluronan, dextran and fibronectin, were studied by their incubation with calcium (*R*,*R*) and (*S*,*S*)-tartrate crystals. Neither dextran nor fibronectin showed different recognition behaviour. However, when

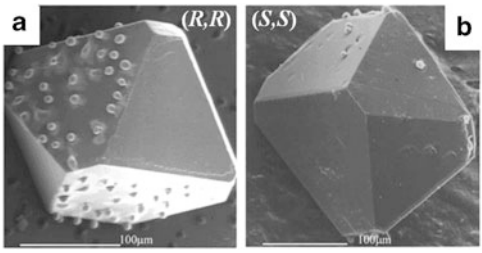

Fig. 16 Scanning electron micrographs of the crystals of calcium (*R*,*R*)- and (*S*,*S*)-tartrate tetrahydrate (**a** and **b**, respectively) after incubation with cells. Reprinted with permission from [221]. Copyright © 2012 Royal Society of Chemistry

hyaluronan was used the same results as for the cells were obtained, and therefore the molecule responsible for the chiral recognition of the selective adhesion seems to be this [223].

Antibodies are widely used in recognition processes and important to the development of the biosensors field. Chiral surface recognition of different antibodies on surfaces of crystals has also been explored [221]. Antibodies such as 48E and 602E, 36A1 and 23C1 were chosen to study the recognition and interaction with crystals of (L/D)leu-(L/D)-leu-(L/D)-tyr and cholesterol monohydrate, respectively, showing different levels of stereoselectivity and enantioselectivity for each antibody. For example, while 48E antibodies interacted with (L/D)leu-(L/D)-leu-(L/D)-tyr crystals with high stereoselectivity and enantioselectivity, antibodies 602 presented low stereoselectivity for the same crystals [224]. In order to measure the thermodynamic parameters associated with chiral interactions, crystal surfaces and isothermal titration calorimetry have been combined. Using this technique it was possible to determine the chiral interaction between crystal surfaces of L- and D-tyrosine and L-threonine and L-phenylalanine molecules. Thus, it was shown that L-threonine interactions with L-tyrosine crystals were 1.25 times stronger than with D-tyrosine crystal surfaces. Nevertheless, for L-phenylalanine the results were the opposite and stronger chiral interactions were observed with D-tyrosine crystal surfaces [225]. This kind of study will continue to give important insight into the stereoselective interactions taking place at interfaces thanks to the precision of the conformational chirality at the crystal surface.

4.8 Chiral Expression During Crystal Growth

Enantioselective crystallisation on nanochiral surfaces is receiving close attention due to the application of chiral crystalline surfaces in different fields such as nanotechnology and biosensors, among others [226]. Previously it has been shown that crystal surfaces of chiral materials can be used to study stereoselective recognition processes with biomolecules. Also of interest is the preparation of crystals with chiral morphology as a result of specific recognition between

biomolecules and achiral compounds [227]. The interphase between a nucleating and growing crystal and a solution phase is a place where stereochemical phenomena can often be expressed. The biomineralisation processes whereby on a self-ordered structure one constructs the solid form of inorganic materials is a prime example [228].

Calcium oxalate nonohydrate crystals are an example of morphological chirality induced during crystal growth [229]. When the crystals were extracted from tobacco or tomato leaves they showed chirality while from solution their morphology was achiral. The chiral morphology was attributed to a selective nucleation of the crystals arising from specific recognition interactions between a protein and different faces of the same crystallographic plane. Moreover, the same enantiomorph was always obtained, although the crystals were extracted from different plants.

In a more synthetic environment, chiral inorganic surfaces can be generated on achiral metals as is the case of the electrochemical growth of tartaric acid-directed copper(I) oxide formation on the gold (0,0,1) surface [230]. When the enantiopure acid was present during the deposition process a homochiral CuO surface was seen. On the other hand, films prepared in the presence of the racemic tartaric acid were completely symmetric. The copper oxide grows along specific directions of the substrate in the presence of enantiopure tartaric acid, giving a well defined surface orientation. When CuO was deposited from a solution containing racemic tartaric acid to a preformed homochiral film of the metal oxide, the same enantiomer deposited on top, showing how, once nucleated, growth of the chiral oxide perpetuates.

5 Conclusions and Outlook

We have discussed a wide variety of techniques and systems where remarkable symmetry breaking and propagation of chirality have taken place at interfaces where biomolecules are involved, and perhaps some of these shed light on some of the routes which have been put forward for the origin of biological chirality [231, 232]. Indeed, we have seen many times that the tools of nanoscience have been used to probe the emergence of chirality down to the molecular level, and in this sense the development of this discipline remains a tremendous opportunity for the study of systems which might be behind the emergence of a dominant chirality in terrestrial biological systems [233]. The application of the increasingly powerful tools of theoretical chemistry and physics to the understanding of experimental results will become increasingly common. Theory is already predicting new mechanisms as well as explaining experimental observations [234–236]. The advancement of analytical techniques for the determination of chiral phases is sure to aid understanding and identification of spontaneous mirror symmetry breaking. For example, circular dichroism in angle-resolved valence photoelectron spectroscopy has been used recently to observe transfer of chirality from alaninol to the copper surface to which it is adsorbed [237].

On the other hand, the control of chirality in certain supramolecular structures which must interact through interfaces could aid therapeutic benefits. The understanding and treatment of amyloidoses such as Alzheimer's and Parkinson's disease might well benefit from consideration of chirality of interfaces, as stereochemistry is certainly a player in the construction of the fibres [238].

Some of the possible applications of chiral surfaces have been outlined and a few challenges presented in this chapter and elsewhere [239], and there are surely many more. The manner in which well defined surfaces adapt to the adsorption process is likely to indicate ways in which the inverse process – the transfer of surface order into chiral organisation of prochiral organic molecules – could have occurred. But perhaps just as exciting are the possibilities that biomolecules at interfaces could provide for novel properties, such as the spin polarisation of electrons [240, 241]. In the coming years we predict increased attraction to these and related applications [242] benefiting from chirality at interfaces on the nanoscale.

Acknowledgements We thank warmly our colleagues from the RESOLVE project from the European Community's Seventh Framework Programme under grant agreement n° NMP4-SL-2008-214340, and in particular Prof. Rasmita Raval, Dr. Andrew Mark and Matthew Forster for Frankenfoot. We acknowledge the CSIC for a JAE-Doc grant (AGC) and funding for our research through projects 2009 SGR 158 and CTQ2010-16339.

References

1. van der Rest M, Garrone R (1991) Collagen family of proteins. FASEB J 5:2814–2823
2. Helfrich W, Prost J (1988) Intrinsic bending force in anisotropic membranes made of chiral molecules. Phys Rev A 38:3065–3068
3. MacDermott AJ, Barron LD, Brack A, Buhse T, Drake AF, Emery R, Gottarelli G, Greenberg JM, Haberle R, Hegstrom RA, Hobbs K, Kondepudi DK, McKay C, Moorbath S, Raulin F, Sandford M, Schwartzman DW, Thiemann WHP, Tranter GE, Zarnecki JC (1996) Homochirality as the signature of life: the SETH cigar. Planetary Space Sci 44:1441–1446
4. Corrigan JJ (1969) D-Amino acids in animals. Science 164:142–149
5. Fuchs SA, Berger R, Klomp LWJ, de Koning TJ (2005) D-Amino acids in the central nervous system in health and disease. Mol Gen Met 85:168–180
6. Vranova V, Zahradnickova H, Janous D, Skene KR, Matharu AS, Rejsek K, Formanek P (2012) The significance of D-amino acids in soil, fate and utilization by microbes and plants: review and identification of knowledge gaps. Plant Soil 354:21–39
7. Pályi G, Zucchi C, Caglioti L (eds) (2004) Progress in biological chirality. Elsevier, Amsterdam
8. Blackmond DG (2010) The origin of biological homochirality. Cold Spring Harb Perspect Biol 2:a002147. doi:10.1101/cshperspect.a002147
9. Managadze G (2010) Plasma and collision processes of hypervelocity meteorite impact in the prehistory of life. Int J Astrobiol 9:157–174
10. Wallace R (2011) On the evolution of homochirality. Comptes Rendus Biol 334:263–268
11. Caglioti L, Micskei K, Palyi G (2011) First molecules, biological chirality, origin(s) of life. Chirality 23:65–68

12. Viedma C, Cintas P (2011) On the chiral homogeneity of nature: from atoms to small molecules. Isr J Chem 51:997–1006
13. Bonner WA (1991) The origin and amplification of biomolecular chirality. Orig Life Evol Biosph 21:59–111
14. Orgel LE (1998) Polymerization on the rocks: theoretical introduction. Orig Life Evol Biosph 28:227–234
15. Bielski R, Tencer M (2007) A possible path to the RNA world: enantioselective and diastereoselective purification of ribose. Orig Life Evol Biosph 37:167–175
16. Fuss W (2009) Biological homochirality as result from a single event. Colloids Surf B Biointerfaces 74:498–503
17. Blaser HU (1991) Enantioselective synthesis using chiral heterogeneous catalysts. Tetrahedron 2:843–866
18. Lorenzo MO, Humblot V, Murray P, Baddeley CJ, Haq S, Raval R (2002) Chemical transformations, molecular transport, and kinetic barriers in creating the chiral phase of (R, R)-tartaric acid on Cu(110). J Catal 205:123–134
19. Jewell AD, Tierney HL, Zenasni O, Lee TR, Sykes ECH (2011) Asymmetric thioethers as building blocks for chiral monolayers. Top Catal 54:1357–1367
20. Ariga K, Richards GJ, Ishihara S, Izawa H, Hill JP (2010) Intelligent chiral sensing based on supramolecular and interfacial concepts. Sensors 10:6796–6820
21. Amabilino DB, Veciana J (2006) Supramolecular chiral functional materials. Top Curr Chem 265:253–302
22. Diaz-Diaz D, Cid JJ, Vazquez P, Torres T (2008) Strength enhancement of nanostructured organogels through inclusion of phthalocyanine-containing complementary organogelator structures and in situ cross-linking by click chemistry. Chemistry 14:9261–9273
23. Zhang Y, Zheng L (2010) Towards chirality-pure carbon nanotubes. Nanoscale 2:1919–1929
24. Cao H, Jiang J, Zhu X, Duan P, Liu M (2011) Hierarchical co-assembly of chiral lipid nanotubes with an azobenzene derivative: optical and chiroptical switching. Soft Matter 7:4654–4660
25. Mori T, Kyotani M, Akagi K (2011) Horizontally and vertically aligned helical conjugated polymers: comprehensive formation mechanisms of helical fibrillar morphologies in orientation-controlled asymmetric reaction fields consisting of chiral nematic liquid crystals. Chem Sci 2:1389–1395
26. Danila I, Riobé F, Piron F, Puigmartí-Luis J, Wallis JD, Linares M, Ågren H, Beljonne D, Amabilino DB, Avarvari N (2011) Hierarchical chiral expression from the nano- to meso-scale in synthetic supramolecular helical fibers of a non-amphiphilic C3-symmetrical π-functional molecule. J Am Chem Soc 133:8344–8353
27. Avinash MB, Govindaraju T (2012) Amino acid derivatized arylenediimides: a versatile modular approach for functional molecular materials. Adv Mater 24:3905–3922
28. Pratt SJ, Jenkins SJ, King DA (2005) The symmetry and structure of crystalline surfaces. Surf Sci 585:L159–L165
29. Jenkins SJ, Pratt SJ (2007) Beyond the surface atlas: a roadmap and gazetteer for surface symmetry and structure. Surf Sci Rep 62:373–429
30. Hazen RM (2004) Chiral crystal faces of common rock-forming minerals. In: Palyi G, Zucchi C, Caglioti L (eds) Progress in biological chirality. Elsevier, Oxford
31. Horvath JD, Gellman AJ (2003) Naturally chiral surfaces. Top Catal 25:9–15
32. Zhao XY, Perry SS, Horvath JD, Gellman AJ (2004) Adsorbate induced kink formation in straight step edges on Cu(533) and Cu(221). Surf Sci 563:217–224
33. Wulff G (1995) Molecular imprinting in cross-linked materials with the aid of molecular templates – a way towards artificial antibodies. Angew Chem Int Ed Engl 34:1812–1832
34. Kempe M, Mosbach K (1995) Molecular imprinting used for chiral separations. J Chromatogr A 694:3–13
35. Sellergren B (2001) Imprinted chiral stationary phases in high-performance liquid chromatography. J Chromatogr A 906:227–252

36. Pernites RB, Venkata SK, Tiu BDB, Yago ACC, Advincula RC (2012) Nanostructured, molecularly imprinted, and template-patterned polythiophenes for chiral sensing and differentiation. Small 8:669–1674
37. Fuhrhop J-H (1996) Synkinetic micellar and vesicular fibres made of amphiphilic lipids and porphyrins. In: Atwood JL, Davies JED, Vögtle F (eds) Comprehensive supramolecular chemistry, vol 9. Elsevier, Pergamon, pp 407–450
38. Brock CP, Dunitz JD (1994) Towards a grammar of crystal packing. Chem Mater 6:1118–1127
39. Weissbuch I, Kuzmenko I, Berfeld M, Leiserowitz L, Lahav M (2000) Stereochemical studies on chiral systems in two dimensions. J Phys Org Chem 13:426–434
40. Raval R (2009) Chiral expression from molecular assemblies at metal surfaces: insights from surface science techniques. Chem Soc Rev 38:707–721
41. Pérez-García L, Amabilino DB (2002) Spontaneous resolution under supramolecular control. Chem Soc Rev 31:42–356
42. Duarte NC, Becker SA, Jamshidi N, Thiele I, Mo ML, Vo TD, Srivas R, Palsson BO (2007) Global reconstruction of the human metabolic network based on genomic and bibliomic data. Proc Natl Acad Sci USA 104:1777–1782
43. Laska M, Shepherd GM (2007) Olfactory discrimination ability of CD-1 mice for a large array of enantiomers. Neuroscience 144:295–301
44. Mamedov MD, Kurashov VN, Cherepanov DA, Semenov AY (2010) Photosysem II: where does the light-induced voltage come from? Front Biosci 15:1007–1017
45. Anselme K (2000) Osteoblast adhesion on biomaterials. Biomaterials 21:667–681
46. Vale RD (2003) The molecular motor toolbox for intracellular transport. Cell 112:467–480
47. Sun T, Qing G, Su B, Jiang L (2011) Functional biointerface materials inspired from nature. Chem Soc Rev 40:2909–2921
48. Zhang M, Qing G, Sun T (2012) Chiral biointerface materials. Chem Soc Rev 41:1972–1984
49. Thirumoorthy K, Nandi N (2006) Comparison of the intermolecular energy surfaces of amino acids: orientation-dependent chiral discrimination. J Phys Chem B 110:8840–8849
50. Xu LP, Liu Y, Zhang X (2011) Interfacial self-assembly of amino acids and peptides: scanning tunnelling microscopy investigation. Nanoscale 3:4901–4915
51. Barlow SM, Raval R (2008) Nanoscale insights in the creation and transfer of chirality in amino acid monolayers at defined metal surfaces. Curr Opin Colloid Interface Sci 13:65–73
52. Pérez-García L, Amabilino DB (2007) Spontaneous resolution, whence and whither: from enantiomorphic solids to chiral liquid crystals, monolayers and macro- and supra-molecular polymers and assemblies. Chem Soc Rev 36:941–967
53. Booth NA, Woodruff DP, Schaff O, Giessel T, Lindsay R, Baumgartel P, Bradshaw AM (1998) Determination of the local structure of glycine adsorbed on Cu(110). Surf Sci 397:258–269
54. Rankin RB, Sholl DS (2004) Assessment of heterochiral and homochiral glycine adlayers on Cu(110) using density functional theory. Surf Sci 548:301–308
55. Zheleva ZV, Eralp T, Held G (2012) Complete experimental structure determination of the p(3 x 2)pg phase of glycine on Cu{110}. J Phys Chem C 116:618–625
56. Humblot V, Lorenzo MO, Baddeley CJ, Haq S, Raval R (2004) Local and global chirality at surfaces: succinic acid versus tartaric acid on Cu(110). J Am Chem Soc 126:6460–6469
57. Chen Q, Frankel DJ, Richardson NV (2002) Self-assembly of adenine on Cu(110) surfaces. Langmuir 18:3219–3225
58. Bald I, Weigelt S, Ma XJ, Xie PY, Subramani R, Dong MD, Wang C, Mamdouh W, Wang JG, Besenbacher F (2010) Two-dimensional network stability of nucleobases and amino acids on graphite under ambient conditions: adenine, L-serine and L-tyrosine. Phys Chem Chem Phys 12:3616–3621
59. Mamdouh W, Dong MD, Kelly REA, Kantorovich LN, Besenbacher F (2007) Coexistence of homochiral and heterochiral adenine domains at the liquid/solid interface. J Phys Chem B 111:12048–12052

60. Sowerby SJ, Heckl WM, Petersen GB (1996) Chiral symmetry breaking during the self-assembly of monolayers from achiral purine molecules. J Mol Evol 43:419–424
61. Sowerby SJ, Petersen GB (1999) Scanning tunnelling microscopy and molecular modelling of xanthine monolayers self-assembled at the solid–liquid interface: relevance to the origin of life. Orig Life Evol Biosph 29:597–614
62. Yu M, Wang JG, Mura M, Meng QQ, Xu W, Gersen H, Laegsgaard E, Stensgaard I, Kelly REA, Kjems J, Linderoth TR, Kantorovich LN, Besenbacher F (2011) Homochiral xanthine quintet networks self-assembled on Au(111) surfaces. ACS Nano 5:6651–6660
63. Parschau M, Kampen T, Ernst KH (2005) Homochirality in monolayers of achiral meso tartaric acid. Chem Phys Lett 407:433–437
64. Viswanathan R, Zasadzinski JA, Schwartz DK (1994) Spontaneous chiral symmetry breaking by achiral molecules in a Langmuir–Blodgett film. Nature 368:440–443
65. Dmitriev A, Spillmann H, Stepanow S, Strunskus T, Woll C, Seitsonen AP, Lingenfelder M, Lin N, Barth JV, Kern K (2006) Asymmetry induction by cooperative intermolecular hydrogen bonds in surface-anchored layers of achiral molecules. Chemphyschem 7:2197–2204
66. Bohringer M, Morgenstern K, Schneider WD, Berndt R (1999) Separation of a racemic mixture of two-dimensional molecular clusters by scanning tunnelling microscopy. Angew Chem Int Ed 38:821–823
67. Bohringer M, Morgenstern K, Schneider WD, Berndt R, Mauri F, De Vita A, Car R (1999) Two-dimensional self-assembly of supramolecular clusters and chains. Phys Rev Lett 83:324–327
68. Schonherr H, Crego-Calama M, Vancso GJ, Reinhoudt DN (2004) Spontaneous resolution of racemic hydrogen-bonded nanoassemblies on graphite revealed by atomic force microscopy. Adv Mater 16:1416–1420
69. Blum MC, Cavar E, Pivetta M, Patthey F, Schneider WD (2005) Conservation of chirality in a hierarchical supramolecular self-assembled structure with pentagonal symmetry. Angew Chem Int Ed 44:5334–5337
70. Katsonis N, Lacaze E, Feringa BL (2008) Molecular chirality at fluid/solid interfaces: expression of asymmetry in self-organised monolayers. J Mater Chem 18:2065–2073
71. In't Veld M, Iavicoli P, Haq S, Amabilino DB, Raval R (2008) Unique intermolecular reaction of simple porphyrins at a metal surface gives covalent nanostructures. Chem Commun 1536–1538
72. Zhang J, Li B, Cui XF, Wang B, Yang JL, Hou JG (2009) Spontaneous chiral resolution in supramolecular assembly of 2,4,6-tris(2-pyridyl)-1,3,5-triazine on Au(111). J Am Chem Soc 131:5885–5890
73. Iavicoli P, Xu H, Feldborg LN, Linares M, Paradinas M, Stafström S, Ocal C, Nieto-Ortega B, Casado J, López-Navarrete JT, Lazzaroni R, De Feyter S, Amabilino DB (2010) Tuning the supramolecular chirality of one- and two-dimensional aggregates with the number of stereogenic centers in the component porphyrins. J Am Chem Soc 132:9350–9362
74. Cun HY, Wang YL, Yang B, Zhang L, Du SX, Wang Y, Ernst KH, Gao HJ (2010) Homochiral recognition among organic molecules on copper(110). Langmuir 26:3402–3406
75. Stohr M, Boz S, Schar M, Nguyen MT, Pignedoli CA, Passerone D, Schweizer WB, Thilgen C, Jung TA, Diederich F (2011) Self-assembly and two-dimensional spontaneous resolution of cyano-functionalized [7]helicenes on Cu(111). Angew Chem Int Ed 50: 9982–9986
76. Iavicoli P, Xu H, Keszthelyi T, Telegdi J, Wurst K, Van Averbeke B, Saletra WJ, Minoia A, Beljonne D, Lazzaroni R, De Feyter S, Amabilino DB (2012) Organisation of the enantiomeric and racemic forms of an amphiphilic resorcinol derivative at the air-water and graphite-1-phenyloctane interfaces. Chirality 24:155–166
77. Song YH, Wang Y, Wan LL, Ye SH, Hou HQ, Wang L (2012) Scanning tunneling microscopy study of alpha, omega-dihexylsexithiophene adlayers on Au(111): a chiral separation induced by a surface. Microsc Microanal 18:885–891

78. Benichou E, Derouet A, Russier-Antoine I, Jonin C, Lascoux N, Liu MH, Brevet PF (2011) Supramolecular chirality at the air/water interface. Opt Express 1:17–26
79. Ernst KH (2006) Supramolecular surface chirality. Top Curr Chem 265:209–252
80. Barlow SM, Raval R (2003) Complex organic molecules at metal surfaces: bonding, organisation and chirality. Surf Sci Rep 50:201–341
81. Ahn S, Henssler JT, Matzger AJ (2011) Conglomerate with periodic enantiomer inclusion: a mechanism for homochirality erosion. Chem Commun 47:11432–11434
82. Lambert JF (2008) Adsorption and polymerisation of amino acids on mineral surfaces: a review. Orig Life Evol Biosph 38:211–242
83. Atanasoska LL, Buchholz JC, Somorjai GA (1978) Low-energy electron diffraction study of surface structures of adsorbed amino-acid monolayers and ordered films deposited on copper crystal surfaces. Surf Sci 72:189–207
84. Barlow SM, Louafi S, Le Roux D, Williams J, Muryn C, Haq S, Raval R (2004) Supramolecular assembly of strongly chemisorbed size-and shape-defined chiral clusters: S- and R-alanine on Cu(110). Langmuir 20:7171–7176
85. Chen Q, Lee CW, Frankel DJ, Richardson NV (1999) The formation of enantiospecific phases on a Cu{110} surface. Phys Chem Comm 2:41–44
86. Blankenburg S, Schmidt WG (2007) Steric effects and chirality in the adsorption of glycine and phenylglycine on Cu(110). Nanotechnology 18:424030, 5 pp
87. Kuhnle A, Linderoth TR, Hammer B, Besenbacher F (2002) Chiral recognition in dimerization of adsorbed cysteine observed by scanning tunnelling microscopy. Nature 415:891–893
88. Kuhnle A, Linderoth TR, Besenbacher F (2011) Chiral symmetry breaking observed for cysteine on the Au(110)-(1x2) surface. Top Catal 54:1384–1391
89. Kuhnle A, Linderoth TR, Besenbacher F (2003) Self-assembly of monodispersed, chiral nanoclusters of cysteine on the Au(110)-(1 x 2) surface. J Am Chem Soc 125:14680–14681
90. Forster M, Dyer MS, Persson M, Raval R (2009) Probing conformers and adsorption footprints at the single-molecule level in a highly organized amino acid assembly of (S)-proline on Cu(110). J Am Chem Soc 131:10173–10181
91. Forster M, Dyer MS, Persson M, Raval R (2010) 2D random organization of racemic amino acid mono layers driven by nanoscale adsorption footprints: pro line on Cu(110). Angew Chem Int Ed 49:2344–2348
92. Forster M, Dyer MS, Barrett SD, Persson M, Raval R (2011) Mapping complex chiral adlayers: a truly random 2-D solid solution of (RS)-3-pyrroline-2-carboxylic acid on Cu (110). J Phys Chem C 115:1180–1185
93. Mark AG, Forster M, Raval R (2011) Recognition and ordering at surfaces: the importance of handedness and footedness. Chemphyschem 12:1474–1480
94. Forster M, Dyer MS, Persson M, Raval R (2011) Tailoring homochirality at surfaces: going beyond molecular handedness. J Am Chem Soc 133:15992–16000
95. Mateo-Marti E, Quash A, Méthivier C, Dubot P, Pradier C-M (2004) Interaction of S-histidine, an amino acid, with copper and gold surfaces, a comparison based on RAIRS analyses. Colloids Surf A 249:85–89
96. Vallee A, Humblot V, Pradier CM (2010) Peptide interactions with metal and oxide surfaces. Acc Chem Res 43:1297–1306
97. Stensgaard I (2003) Adsorption of di-L-alanine on Cu(110) investigated with scanning tunneling microscopy. Surf Sci 545:L747–L752
98. Lingenfelder M, Tomba G, Costantini G, Colombi-Ciacchi L, De Vita A, Kern K (2007) Tracking the chiral recognition of adsorbed dipeptides at the single-molecule level. Angew Chem Int Ed 46:4492–4495
99. Tomba G, Lingenfelder M, Costantini G, Kern K, Klappenberger F, Barth JV, Ciacchi LC, De Vita A (2007) Structure and energetics of diphenylalanine self-assembling on Cu(110). J Phys Chem A 111:12740–12748
100. Wang Y, Lingenfelder M, Classen T, Costantini G, Kern K (2007) Ordering of dipeptide chains on cu surfaces through 2D cocrystallization. J Am Chem Soc 129:15742–15743

101. Barlow SM, Haq S, Raval R (2001) Bonding, organization, and dynamical growth behavior of tripeptides on a defined metal surface: tri-L-alanine and tri-L-leucine on Cu{100}. Langmuir 17:3292–3300
102. Vallee A, Humblot V, Methivier C, Pradier CM (2008) Adsorption of a tripeptide, GSH, on Au(111) under UHV conditions; PM-RAIRS and low T-XPS characterisation. Surf Sci 602:2256–2263
103. Vallee A, Humblot V, Methivier C, Pradier CM (2009) Adsorption of di- and tripeptides on Au(110) under ultrahigh vacuum conditions. 1. Polarization modulation reflection absorption infrared spectroscopy and X-ray photoelectron spectroscopy characterization. J Phys Chem C 113:9336–9344
104. Humblot V, Vallee A, Naitabdi A, Tielens F, Pradier CM (2012) Drastic Au(111) surface reconstruction upon insulin growth factor tripeptide adsorption. J Am Chem Soc 134:6579–6583
105. So CR, Tamerler C, Sarikaya M (2009) Adsorption, diffusion, and self-assembly of an engineered gold-binding peptide on Au(111) investigated by atomic force microscopy. Angew Chem Int Ed 48:5174–5177
106. So CR, Hayamizu Y, Yazici H, Gresswell C, Khatayevich D, Tamerler C, Sarikaya M (2012) Controlling self-assembly of engineered peptides on graphite by rational mutation. ACS Nano 6:1648–1656
107. Mandal S, Gole A, Lala N, Gonnade R, Ganvir V, Sastry M (2001) Studies on the reversible aggregation of cysteine-capped colloidal silver particles interconnected via hydrogen bonds. Langmuir 17:6262–6268
108. Li TH, Park HG, Lee HS, Choi SH (2004) Circular dichroism study of chiral biomolecules conjugated nanoparticles. Nanotechnology 15:S660–S663
109. Selvakannan PR, Mandal S, Phadtare S, Pasricha R, Sastry M (2003) Capping of gold nanoparticles by the amino acid lysine renders them water-dispersible. Langmuir 19:3545–3549
110. Gautier C, Burgi T (2005) Vibrational circular dichroism of N-acetyl-L-cysteine protected gold nanoparticles. Chem Commun 5393–5395
111. Gautier C, Burgi T (2006) Chiral N-isobutyryl-cysteine protected gold nanoparticles: preparation, size selection, and optical activity in the UV–vis and infrared. J Am Chem Soc 128:11079–11087
112. Noguez C, Garzon IL (2009) Optically active metal nanoparticles. Chem Soc Rev 38:757–771
113. Gautier C, Burgi T (2009) Chiral gold nanoparticles. Chemphyschem 10:483–492
114. Knoppe S, Dolamic I, Dass A, Burgi T (2012) Separation of enantiomers and CD spectra of $Au_{40}(SCH_2CH_2Ph)_{24}$: spectroscopic evidence for intrinsic chirality. Angew Chem Int Ed 51:7589–7591
115. Gautier C, Burgi T (2008) Chiral inversion of gold nanoparticles. J Am Chem Soc 130:7077–7084
116. Zhou Y, Yang M, Sun K, Tang Z, Kotov NA (2010) Similar topological origin of chiral centers in organic and nanoscale inorganic structures: effect of stabilizer chirality on optical isomerism and growth of CdTe nanocrystals. J Am Chem Soc 132:6006–6013
117. Slocik JM, Govorov AO, Naik RR (2011) Plasmonic circular dichroism of peptide-functionalize gold nanoparticles. Nano Lett 11:701–705
118. Wang D, Xu Q-M, Wan L-J, Bai C-L, Jin G (2003) Adsorption of enantiomeric and racemic tyrosine on Cu(111): a scanning tunnelling microscope study. Langmuir 19:1958–1962
119. Pasteur L (1848) Sur les relations qui peuvent existir entre la forme crystalline, la composition chimique et le sense de la polarisation rotoatoire. Ann Chim Phys 24:442–459
120. Lorenzo MO, Haq S, Bertrams T, Murray P, Raval R, Baddeley CJ (1999) Creating chiral surfaces for enantioselective heterogeneous catalysis: R, R-tartaric acid on Cu(110). J Phys Chem B 103:10661–10669
121. Lorenzo MO, Baddeley CJ, Muryn C, Raval R (2000) Extended surface chirality from supramolecular assemblies of adsorbed chiral molecules. Nature 404:376–379

122. Gudavarthy RV, Burla N, Kulp EA, Limmer SJ, Sinn E, Switzer JA (2011) Epitaxial electrodeposition of chiral CuO films from copper(II) complexes of malic acid on Cu(111) and Cu(110) single crystals. J Mater Chem 21:6209–6216
123. Arnett EM, Harvey NG, Rose PL (1989) Stereochemistry and molecular recognition in "two dimensions". Acc Chem Res 22:131–138
124. Nandi N, Vollhardt D (2003) Effect of molecular chirality on the morphology of biomimetic Langmuir monolayers. Chem Rev 103:4033–4075
125. Weissbuch I, Leiserowitz L, Lahav M (2008) Molecular recognition in chiral and non-chiral amphiphilic self-assemblies at interfaces. Curr Opin Colloid Interface Sci 13:12–22
126. Ariga K, Michinobu T, Nakanishi T, Hill JP (2008) Chiral recognition at the air-water interface. Curr Opin Colloid Interface Sci 13:23–30
127. Ariga K, Hill JP (2011) Monolayers at air-water interfaces: from origins-of-life to nanotechnology. Chem Record 11:199–211
128. Eckhardt CJ, Peachey NM, Swanson DR, Takacs JM, Khan MA, Gong X, Kim JH, Wang J, Uphaus RA (1993) Separation of chiral phases in monolayer crystals of racemic amphiphiles. Nature 362:614–616
129. Iwamoto M, Wu CX, Zhong-Can OY (1998) Separation of chiral phases by compression: kinetic localization of the enantiomers in a monolayer of racemic amphiphiles viewed as mixing cholesteric liquid crystals. Chem Phys Lett 285:306–312
130. Weissbuch I, Leiserowitz L, Lahav M (2009) Structure and function of chiral molecules at the air/water interface. In: Amabilino DB (ed) Chirality at the nanoscale: nanoparticles, surfaces, materials and more. Wiley-VCH, Weinheim
131. Weissbuch I, Berfeld M, Bouwman WG, Kjaer K, Als-Nielsen J, Lahav M, Leiserowitz L (1997) Separation of enantiomers and racemate formation in two-dimensional crystals at the water surface from racemic alpha-amino acid amphiphiles: design and structure. J Am Chem Soc 119:933–942
132. Weissbuch I, Rubinstein I, Weygand MJ, Kjaer K, Leiserowitz L, Lahav M (2003) Crystalline phase separation of racemic and nonracemic zwitterionic alpha-amino acid amphiphiles in a phospholipid environment at the air/water interface: a grazing-incidence X-ray diffraction study. Helv Chim Acta 86:3867–3874
133. Hazen RM, Sholl DS (2003) Chiral selection on inorganic crystalline surfaces. Nat Mater 2:367–374
134. Rankin RB, Sholl DS (2006) Structures of dense glycine and alanine adlayers on chiral Cu (3,1,17) surfaces. Langmuir 22:8096–8103
135. George J, Thomas GK (2010) Surface plasmon coupled circular dichroism of Au nanoparticles on peptide nanotubes. J Am Chem Soc 132:2502–2503
136. Green MM, Garetz BA, Munoz B, Chang HP, Hoke S, Cooks RG (1995) Majority rules in the copolymerisation of mirror-image isomers. J Am Chem Soc 117:4181–4182
137. Cheon KS, Selinger JV, Green MM (2004) Counterintuitive influence of microscopic chirality on helical order in polymers. J Phys Org Chem 17:719–723
138. Lohr A, Wuerthner F (2008) Evolution of homochiral helical dye assemblies: involvement of autocatalysis in the "majority-rules" effect. Angew Chem Int Ed 47:1232–1236
139. Zhu XF, Li YG, Duan PF, Liu MH (2010) Self-assembled ultralong chiral nanotubes and tuning of their chirality through the mixing of enantiomeric components. Chemistry 16:8034–8040
140. ten Eikelder HMM, Markvoort AJ, de Greef TFA, Hilbers PAJ (2012) An equilibrium model for chiral amplification in supramolecular polymers. J Phys Chem B 116:5291–5301
141. Cantekin S, ten Eikelder HMM, Markvoort AJ, Veld MAJ, Korevaar PA, Green MM, Palmans ARA, Meijer EW (2012) Consequences of cooperativity in racemizing supramolecular systems. Angew Chem Int Ed 51:6426–6431
142. Veling N, van Hameren R, van Buul AM, Rowan AE, Nolte RJM, Elemans JAAW (2012) Solvent-dependent amplification of chirality in assemblies of porphyrin trimers based on benzene tricarboxamide. Chem Commun 48:4371–4373

143. Green MM, Reidy MP, Johnson RJ, Darling G, OLeary DJ, Willson G (1989) Macromolecular stereochemistry – the out-of-proportion influence of optically-active co-monomers on the conformational characteristics of polyisocyanates – the sergeants and soldiers experiment. J Am Chem Soc 111:6452–6454
144. Gu H, Nakamura Y, Sato T, Teramoto A, Green MM, Jha SK, Andreola C, Reidy MP (1998) Optical rotation of random copolyisocyanates of chiral and achiral monomers: sergeant and soldier copolymers. Macromolecules 31:6362–6368
145. Prince RB, Moore JS, Brunsveld L, Meijer EW (2001) Cooperativity in the folding of helical m-phenylene ethynylene oligomers based upon the 'sergeants-and-soldiers' principle. Chemistry 7:4150–4154
146. Prins LJ, Timmerman P, Reinhoudt DN (2001) Amplification of chirality: the "sergeants and soldiers" principle applied to dynamic hydrogen-bonded assemblies. J Am Chem Soc 123:10153–10163
147. Ajayaghosh A, Varghese R, Mahesh S, Praveen VK (2006) From vesicles to helical nanotubes: a sergeant-and-soldiers effect in the self-assembly of oligo(p-phenyleneethynylene)s. Angew Chem Int Ed 45:7729–7732
148. Jain V, Cheon KS, Tang K, Jha S, Green MM (2011) Chiral cooperativity in helical polymers. Isr J Chem 51:1067–1074
149. Anderson TW, Pantos GD, Sanders JKM (2011) Supramolecular chemistry of monochiral naphthalenediimides. Org Biomol Chem 9:7547–7553
150. Mikami K, Daikuhara H, Inagaki Y, Yokoyama A, Yokozawa T (2011) Chiral amplification based on sergeants and soldiers effect in helically folded poly(naphthalenecarboxamide). Macromolecules 44:3185–3188
151. Goto H, Yokochi Y, Yashima E (2012) Chirality induction in metal-induced achiral polythiophene aggregates assisted by optically active amines and polythiophene. Chem Commun 48:3291–3293
152. Ohsawa S, Sakurai S, Nagai K, Maeda K, Kumaki J, Yashima E (2012) Amplification of macromolecular helicity of dynamic helical poly(phenylacetylene)s bearing non-racemic alanine pendants in dilute solution, liquid crystal and two-dimensional crystal. Polym J 44:42–50
153. van Houtem MHCJ, Benaskar F, Fitie CFC, Martin-Rapun R, Vekemans JAJM, Meijer EW (2012) Helical self-assembly and co-assembly of fluorinated, preorganized discotics. Org Biomol Chem 10:5898–5908
154. Ho RM, Li MC, Lin SC, Wang HF, Lee YD, Hasegawa H, Thomas EL (2012) Transfer of chirality from molecule to phase in self-assembled chiral block copolymers. J Am Chem Soc 134:10974–10986
155. Fasel R, Parschau M, Ernst KH (2006) Amplification of chirality in two-dimensional enantiomorphous lattices. Nature 439:449–452
156. Haq S, Liu N, Humblot V, Jansen APJ, Raval R (2009) Drastic symmetry breaking in supramolecular organization of enantiomerically unbalanced monolayers at surfaces. Nat Chem 1:409–414
157. Clegg ML, de la Garza LM, Karakatsani S, King DA, Driver (2011) Chirality in amino acid overlayers on Cu surfaces. Top Catal 54:1429–1444
158. Rong Y, Chen P, Wang D, Liu M (2012) Porphyrin assemblies through the air/water interface: effect of hydrogen bond, thermal annealing, and amplification of supramolecular chirality. Langmuir 28:6356–6363
159. Nieto-Ortega B, Ramirez FJ, Amabilino DB, Linares M, Beljonne D, Lopez-Navarrete JT, Casado J (2012) Electronic and vibrational circular dichroism spectroscopies for the understanding of chiral organisation in porphyrin aggregates. Chem Commun 48:9147–9149
160. D'Urso A, Fragala ME, Purrello R (2012) From self-assembly to noncovalent synthesis of programmable porphyrins' arrays in aqueous solution. Chem Commun 48:8165–8176
161. Micali N, Engelkamp H, van Rhee PG, Christianen PCM, Scolaro LM, Maan JC (2012) Selection of supramolecular chirality by application of rotational and magnetic forces. Nat Chem 4:201–207

162. Sorrenti A, El-Hachemi Z, Arteaga O, Canillas A, Crusats J, Ribo JM (2012) Kinetic control of the supramolecular chirality of porphyrin J-aggregates. Chemistry 18:8820–8826
163. Liu L, Li T, Lee M (2012) Chiral assemblies of achiral rigid-flexible molecules at the air/water interface induced by silver(I) coordination. Chemphyschem 13:578–582
164. You C-C, Agasti SS, Rotello VM (2008) Isomeric control of protein recognition with amino acid- and dipeptide-functionalized gold nanoparticles. Chemistry 14:143–150
165. El-gind J, Benson K, de Cola L, Galla H-J, Kehr NS (2012) Cell adhesion behavior on enatiomerically functionalized zeolite L monolayers. Angew Chem Int Ed 51:3716–3720
166. Bandyopadhyay D, Prashar D, Luk Y-Y (2011) Anti-fouling chemistry of chiral monolayers enhancing biofil resistance on racemic surface. Langmuir 27:6124–6131
167. Ulman A (1996) Formation and structure of self-assembled monolayers. Chem Rev 96:1533–1554
168. Love JC, Estroff LA, Kriebel JK, Nuzzo RG, Whitesides GM (2005) Self-assembled monolayers of thiolates on metals as form of nanotechnology. Chem Rev 105:1103–1169
169. Sun T, Han D, Rhemann K, Chi L, Fuchs H (2007) Stereospecific interaction between immune cells and chiral surfaces. J Am Chem Soc 129:1496–1497
170. Tang K, Gan H, Li Y, Chi L, Sun T, Fuchs H (2008) Stereoselective interaction between DNA and chiral surfaces. J Am Chem Soc 130:11284–11285
171. Gan H, Tang K, Sun T, Hirtz M, Li Y, Butz LS, Fuchs H (2009) Selective adsorption of DNA on chiral surface supercoiled or relaxed conformation. Angew Chem Int Ed 48:5882–5886
172. Zhou F, Yuan L, Li D, Huang H, Sun T, Chen H (2012) Cell adhesion on chiral surface: the role of protein adsorption. Colloids Surf B Biointerfaces 90:97–101
173. Zhou J, Wang L, Chen Q, Wang Y, Fu Y (2011) Selective response of antigen-antibody reactions on chiral surfaces modified with 1,2-diphenylethylenediamine enantiomers. Surf Interface Anal 44:170–174
174. Moyano DF, Rotello VM (2011) Nano meets biology: structure and function at the nanoparticle interface. Langmuir 27:10376–10385
175. Rana S, Yeh Y-C, Rotello VM (2010) Engineering the nanoparticle-protein interface: applications and possibilities. Curr Opin Chem Biol 14:828–834
176. Ding L, Ju H (2011) Biofunctionalization of nanoparticles for cytosensing and cell surface carbohydrate assay. J Mater Chem 21:18154–18173
177. Liu H, Ye Y, Chen J, Lin D, Jiang Z, Liu Z, Sun B, Yang L, Liu J (2012) In situ photoreduced silver nanoparticles on cysteine: an insight into the origin of chirality. Chemistry 18:8037–8041
178. Zhou Y, Zhu Z, Huang W, Liu W, Wu S, Liu X, Gao Y, Zhang W, Tang Z (2011) Optical coupling between chiral biomolecules and semiconductor nanoparticles: size-dependent circular dichroism absorption. Angew Chem Int Ed 50:11456–11459
179. Moloney MP, Gun'ko YK, Kelly JM (2007) Chiral highly luminescent Cds quantum dots. Chem Commun 38:3900–3902
180. Huang P, Pandoli O, Wang X, Wang Z, Li Z, Zhang C, Chen F, Lin J, Cui D, Chen X (2012) Chiral guanosine 5′-monoposphate-capped gold nanoflowers controllable synthesis, characterization, surface-enhanced Raman scattering activity, cellular imaging and phothermal therapy. Nano Res 5:630–639
181. Guerrero-Martínez A, Alonso-Gómez JL, Auguié B, Cid MM, Liz-Marzán LM (2011) From individual to collective chirality in metal nanoparticles. Nano Today 6:381–400
182. Govorov AO, Gun'ko YK, Slocik JM, Gérard VA, Fan Z, Naik RR (2011) Chiral nanoparticle assemblies:circular dichroism, plasmonic interactions and exciton effects. J Mater Chem 21:16806–16818
183. Mastroianni AJ, Claridge SA, Alivisatos AP (2009) Pyramidal and chiral groupings of gold nanocrystals assembled using DNA scaffolds. J Am Chem Soc 131:8455–8459
184. Shemer G, Krichevski O, Markovich G, Molotsky T, Lubitz I, Kotlyar AB (2006) Chirality of silver nanoparticles synthesized on DNA. J Am Chem Soc 128:11006–11007

185. Park SY, Lytton-Jean AKR, Lee B, Weigand S, Schatz GC, Mirkin CA (2008) DNA-programmable nanoparticle crystallization. Nature 451:553–556
186. Carillo-Carrión C, Cárdenas S, Simonet BM, Valcárcel M (2009) Selective quantification of carnitine enantiomers using chiral cysteine-capped CDSe(ZnS) quantum dots. Anal Chem 81:4730–4733
187. Shukla N, Bartel MA, Gellman AJ (2010) Enantioselective separation on chiral Au nanoparticles. J Am Chem Soc 132:8575–8580
188. Kang Y, Oh J-W, Kim Y-R, Kim JS, Kim H (2010) Chiral gold nanoparticle-based electrochemical sensor for enantioselective recognition of 3,4-dihydroxyphenylalanine. Chem Commun 46:5665–5667
189. Zhang M, Ye B-C (2011) Colorimetric chiral recognition of enantiomers using the nucleotide-capped silver nanoparticles. Anal Chem 83:1504–1509
190. Sun Y, Zhang L, Li H (2012) Chiral colorimetric recognition of amino acids based on silver nanoparticle clusters. New J Chem 36:1442–1444
191. Su H, Zheng Q, Li H (2012) Colorimetric detection and separation of chiral tyrosine based on N-acetyl-L-cysteine modified gold nanoparticles. J Mater Chem 22:6546–65548
192. Li Y, Zhou Y, H-Y W, Perrett S, Zhao Y, Tang Z, Nie G (2011) Chirality of glutathione surface coating affects the cytotoxicity of quantum dots. Angew Chem Int Ed 50:5860–5864
193. Ward TJ, Ward KD (2011) Chiral separations: a review of current topics and trends. Anal Chem 84:626–635
194. Sancho R, Minguillon C (2009) The chromatographic separation of enantiomers through nanoscale design. Chem Soc Rev 38:797–805
195. Higuchi A, Tamai M, Ko YA, Tagawa YI, Wu YH, Freeman BD, Bing JT, Chang Y, Ling QD (2010) Polymeric membranes for chiral separation of pharmaceuticals and chemicals. Polym Rev 50:113–143
196. Chen J-L, Hsieh K-H (2011) Nanochitosan crosslinked with polyacrylamide as the chiral stationary phase for open-tubular capillary electrochromatography. Electrophoresis 32: 398–407
197. Yi Q, Wen X, Li L, He B, Nie Y, Wu Y, Zhang Z, Gu Z (2009) The chiral effects on the responses of osteoblastic cells to the polymeric substrates. Eur Polym J 45:1970–1978
198. Wang X, Gan H, Sun T, Fuchs H, Vestweber D, Butz S (2010) Stereochemistry triggered differential cell behaviours on chiral polymer surfaces. Soft Matter 6:3851–3855
199. Wang X, Gan H, Zhang M, Sun T (2012) Modulating cell behaviours on chiral polymer brush films with different hydrophobic side groups. Langmuir 28:2791–2798
200. Wang X, Gan H, Sun T (2011) Chiral design for polymeric biointerface: the influence of surface chirality on protein adsorption. Adv Funct Mater 21:3276–3281
201. Quing G, Sun T (2012) The transformation of chiral signal into macroscopic properties of materials using chirality-responsive polymer. NPG Asia Materials 4:e4. doi:10.1038/am.2012.6.
202. Quing G, Sun T (2011) Chirality-triggered wettability switching on a smart polymer surface. Adv Mater 23:1615–1620
203. Liu P, He W, Qin X, Sun X, Chen H, Zhang S (2010) Synthesis and application of a novel single-isomer mono-6-deoxy-6((2S,3S)-(+)-2, 3-O-isopropylidiene-1,4-tetramethylenediamine)-β-cyclodextrin as chiral selector in capillary electrophoresis. Chirality 22:914–921
204. Shahgaldian P, Pieles U (2006) Cyclodextrin derivatives as chiral supramolecular receptors for enantioselective sensing. Sensors 6:593–615
205. Han C, Li H (2008) Chiral recognition of amino acids based on cyclodextrin-capped quantum dots. Small 4:1344–1350
206. Han C, Hou X, Zhang H, Guo LG, Jiang L (2011) Enantioselective recognition in biomimetic single artificial nanochannels. J Am Chem Soc 133:7644–7647
207. Yang M, Chu L-Y, Wang H-D, Xie R, Song H, Niu CH (2008) A thermoresponsive membrane for chiral resolution. Adv Funct Mater 18:652–663
208. Leblanc RM (2006) Molecular recognition at Langmuir monolayers. Curr Opin Chem Biol 10:529–536

209. Kitano H, Ringsdorf H (1985) Surface behaviours of nucleic base-containing lipids in monolayer and bilayer systems. Bull Chem Soc Japan 58:2826–2828
210. Onda M, Yoshihara K, Koyano H, Ariga K, Kunitake T (1996) Molecular recognition of nucleotides by the guanidinium unit at the surface of aqueous micelles and bilayers. A comparison of microscopic and macroscopic interfaces. J Am Chem Soc 118:8524–8530
211. Sorrenti A, Diociaiuti M, Corvaglia V, Chistolini P, Mancini G (2009) Chiral recognition of dipeptides in Langmuir monolayers. Tetrahedron 20:2737–2741
212. Sigal-Batikoff I, Konovalov O, Singh A, Berman A (2010) Enantioselective recognition between polydiacetylene nucleolipid monolayers and complementary oligonucleotides. Langmuir 26:16424–16433
213. Zepik H, Shavit E, Tang M, Jensen TR, Kjaer K, Bolbach G, Leiserowitz L, Weissbuch I, Lahav M (2002) Chiral amplification of oligopeptides in two-dimensional crystalline self-assemblies on water. Science 295:1266–1269
214. Weissbuch I, Bolbach G, Zepik H, Shavit E, Tang M, Frey J, Jensen TR, Kjaer K, Leiserowitz L, Lahav M (2002) Oligopeptides with homochiral sequences generated from racemic precursors that spontaneously separate into enantiomorphous two-dimensional crystalline domains on water surface. J Am Chem Soc 124:9093–9104
215. Hazen RM, Sverjensky DA (2010) Mineral surfaces, geochemical complexities and the origins of life. Cold Spring Harb Perspect Biol 2:a002162
216. Hazen RM, Filley TR, Goodfriend GA (2001) Selective adsorption of L- and D-amino acids on calcite: implications for biochemical homochirality. Proc Natl Acad Sci USA 98:5487–5490
217. Horvath JD, Koritnik A, Kamakoti P, Sholl DS, Gellman AJ (2004) Enantioselective separation on a naturally chiral surface. J Am Chem Soc 126:14988–14994
218. Huang Y, Gellman AJ (2011) Enantiospecific adsorption of (R)-3-methylcyclohexanone on naturally chiral surfaces vicinal to Cu(110). Top Catal 54:1403–1413
219. Eralp T, Ievins A, Shavorskiy A, Jenkins SJ, Held G (2012) The importance of attractive three-point interaction in enantioselective surface chemistry: stereospecific adsorption of serine on the intrinsically chiral Cu{531} surface. J Am Chem Soc 134:9615–9621
220. Weissbuch I, Leiserowitz L, Lahav M (2011) Achiral organic, inorganic, and metal crystals as auxiliaries for asymmetric transformations. Isr J Chem 51:1017–1033
221. Addadi L, Geva M (2003) Molecular recognition at the interface between crystals and biology: generation, manifestation and detection of chirality at crystal surfaces. Cryst Eng Comm 5:140–146
222. Hanein D, Geiger B, Addadi L (1994) Differential adhesion of cells to enantiomorphous crystal surfaces. Science 263:1413–1416
223. Zimmerman E, Geiger B, Addadi L (2002) Initial stages of cell-matrix adhesion can be mediated and modulate by cell-surface hyaluronan. Biophys J 82:1848–1857
224. Geva M, Frolow F, Eisenstein M, Addadi L (2002) Antibody recognition of chiral surfaces. Enantiomorphous crystals of leucine-leucine-tyrosine. J Am Chem Soc 125:696–704
225. Shval A, Mastai Y (2011) Isothermal titration calorimetry as a new tool to investigate chiral interactions at crystal surfaces. Chem Commun 47:5735–5737
226. Mastai Y (2009) Enantioselective crystallization on nanochiral surfaces. Chem Soc Rev 38:772–780
227. Oaki Y, Imai H (2004) Amplification of chirality from molecules into morphology of crystals through molecular recognition. J Am Chem Soc 126:9271–9275
228. Mann S (1996) Self-assembly in biomineralisation and biomimetic materials chemistry. In: Atwood JL, Davies JED, Vögtle F (eds) Comprehensive supramolecular chemistry, vol 9. Pergamon, Elsevier, pp 529–564
229. Levy-Lior A, Weiner S, Addadi L (2003) Achiral calcium-oxalate crystals with chiral morphology from the leaves of some Solanacea plants. Helv Chim Acta 86:4007–4017
230. Widmer R, Haug FJ, Ruffieux P, Groning O, Bielmann M, Groning P, Fasel R (2006) Surface chirality of CuO thin films. J Am Chem Soc 128:14103–14108

231. Percec V, Leowanawat P (2011) Why are biological systems homochiral? Isr J Chem 51:1107–1117
232. Weissbuch I, Leiserowitz L, Lahav M (2005) Stochastic "mirror symmetry breaking" via self-assembly, reactivity and amplification of chirality: relevance to abiotic conditions. Top Curr Chem 259:123–165
233. Sowerby SJ, Holm NG, Petersen GB (2001) Origins of life: a route to nanotechnology. Biosystems 61:69–78
234. Paci I, Szleifer I, Ratner MA (2007) Chiral separation: mechanism modeling in two-dimensional systems. J Am Chem Soc 129:3545–3555
235. Linares M, Minoia A, Brocorens P, Beljonne D, Lazzaroni R (2009) Expression of chirality in molecular layers at surfaces: insights from modelling. Chem Soc Rev 38:806–816
236. Szabelski P, Kasperski A (2011) Two-dimensional chiral molecular networks from achiral building blocks: a computational study. Top Catal 54:1368–1377
237. Contini G, Turchini S, Sanna S, Catone D, Fujii J, Vobornik I, Prosperi T, Zema N (2012) Transfer of chirality from adsorbed chiral molecules to the substrate highlighted by circular dichroism in angle-resolved valence photoelectron spectroscopy. Phys Rev B 86:035426
238. Ouberai M, Dolphin GT, Dumy P, Garcia J (2011) Amyloidogenesis highlighted by designed peptides forming supramolecular self-assemblies. Chem Sci 2:1293–1300
239. Gellman AJ (2010) Chiral surfaces: accomplishments and challenges. ACS Nano 4:5–10
240. Göhler B, Hamelbeck V, Markus TZ, Kettner M, Hanne GF, Vager Z, Naaman R, Zacharias H (2011) Spin selectivity in electron transmission through self-assembled monolayers of double-stranded DNA. Science 331:894–897
241. Xie Z, Markus TZ, Cohen SR, Vager Z, Gutierrez R, Naaman R (2011) Spin specific electron conduction through DNA oligomers. Nano Lett 11:4652–4655
242. Naaman R, Beratan D, Waldeck D (eds) (2011) Electronic and magnetic properties of chiral molecules and supramolecular architectures. Top Curr Chem 298

Top Curr Chem (2013) 333: 157–212
DOI: 10.1007/128_2012_362

Published online: 6 September 2012

Stochastic Mirror Symmetry Breaking: Theoretical Models and Simulation of Experiments

Celia Blanco and David Hochberg

Please note the erratum to this chapter at the end of the book.

Abstract This chapter provides a review of recently elaborated mathematical models for explaining the salient features of two experimental studies selected for their relevance to the problem of stochastic mirror symmetry breaking and amplification. The first experiment modeled treats the phenomena of mirror symmetry breaking via the autocatalytic crystallization of the glycine and α-amino acid system at the air-water interface. The second experiment deals with the lattice-controlled generation of homochiral oligopeptides, which we model based on a kinetic scheme for copolymerization in a closed reaction system. Since the fundamental paradigm of mutual inhibition lies at the core of both these models, we review how the final asymptotic states in the Frank model depend crucially on whether the system is open or closed, and emphasize the importance of temporary chiral excursions, which can and do arise in more complex reaction schemes during their approach to chemical equilibrium in closed systems.

Keywords Amino acids · Homochiral polymers · Mathematical models · Mirror symmetry breaking · Nonlinear kinetics · Stability analysis

Contents

C. Blanco and D. Hochberg (✉)
Centro de Astrobiología (CSIC-INTA), Carretera Ajalvir Kilómetro 4, 28850 Torrejón de Ardoz, Madrid, Spain
e-mail: blancodtc@cab.inta-csic.es; hochbergd@cab.inta-csic.es

1 Introduction

Theoretical proposals for prebiotic chemistry suggest that homochirality emerged in nature in abiotic times via deterministic or chance mechanisms [1]. The abiotic scenario for the emergence of single homochirality in the biological world implies that single asymmetry could have emerged provided a small chiral fluctuation with respect to the racemic state can be amplified to a state useful for biotic evolution. For this reason, experiments that can demonstrate the feasibility of stochastic mirror symmetry breaking involving the self assembly of molecular clusters, and possibly in conjunction with interface effects, are particularly important. This is because, once generated by chance or an initial chiral fluctuation, the chirality can then be preserved and transmitted to the rest of the system provided that the symmetry breaking step is coupled to a sequential step of efficient amplification via self-replication reactions. Some relevant features common to such systems are that they take into account the small fluctuations about the racemic state and that they display nonlinear kinetic effects. Stochastic scenarios are theoretically well understood on general grounds [2, 3] and, equally important, are experimentally feasible in the laboratory [4].

The observed bias in biopolymers composed from homochiral L-amino acids and D-sugars towards single handedness or chirality is undoubtedly a remarkable feature of Nature. A stochastic surmise suggests that spontaneous mirror symmetry breaking (SMSB) might have occurred in systems that were far from equilibrium. A number of successful experiments dealing with the random or chance supposition have been reported over the years, and in this review we select two for detailed consideration and theoretical modeling. We discuss a mathematical model for achieving resolution of racemic solutions of α-amino acids and glycine into enantiomeric territories based on a chemical scheme proposed by the Rehovot group some years ago. Their crystallization experiments provide a simple chemical model for the generation and amplification of optically active amino acids in prebiotic conditions. The glycine and α-amino acid system may be relevant to the origin of optical activity as it involves compounds that are among the simplest building blocks of life: indeed, prebiotic synthesis of "protobiopolymers" in Miller-type experiments and their variants typically yields a variety of amino acids with achiral glycine always being the most abundant.

The experiment itself involves a slow evaporation of racemic mixtures of α-amino acids in the presence of large quantities of glycine in aqueous solutions. Oriented crystals of glycine attached with one of the enantiotopic faces – either (0 1 0)-oriented or (0 $\bar{1}$ 0)-oriented – were formed at the air-solution interface which occlude only one of the enantiomers of the α-amino acids: the L-amino acids when

the glycine crystals are (0 1 0) oriented towards solution and the D-amino acids when the crystals are $(0\,\bar{1}\,0)$-oriented. The overall process comprises the following steps. (1) Mirror symmetry breaking via enantioselective occlusion of one of the enantiomers of the racemic α-amino acids within crystals of glycine grown at the air-solution interface. (2) The crystal formed at the interface operates as a seed for further occlusion of amino acids of the same handedness. (3) The amplification experiments comprise self-aggregation of hydrophobic α-amino acids into chiral clusters that operate as templates for an oriented crystallization of fresh crystals of glycine. (4) Enantioselective inhibition (akin to the Frank model) of embryonic nuclei of glycine generated at the air-solution interface by the water soluble-amino acids formed in excess during the process.

Given the relevance of the experiment, we review a recent mathematical model for the experimentally established processes outlined above. The model is suitable for numerical simulation, and the results can be contrasted against the main qualitative aspects and features of the basic experiment. The quantitative model leads to the generation and amplification of optical activity via the enantioselective occlusion of chiral amino acid additives through the chiral surfaces of glycine crystals. The full experimental account is given in two papers [5, 6] and is further reviewed [4, 7], together with the references cited therein.

One scenario for the transition from prebiotic racemic chemistry to chiral biology suggests that homochiral peptides must have appeared before the appearance of the primeval enzymes. Polymerization reactions of racemic mixtures of monomers in solution are however expected to yield polymers composed of random sequences of the left-handed and right-handed repeat units following a binomial distribution. This statistical problem can be overcome by catalyzed polymerization of amphiphilic amino acids, in racemic and nonracemic forms, which self-assemble into two-dimensional ordered crystallites at the air-water interface.

Based on a process involving self-assembly followed by lattice controlled polymerization, Lahav and coworkers have proposed a general scenario for the generation of homochiral oligopeptides of a single handedness from non-racemic mixtures of activated α-amino acids. The initial non-racemic mixtures undergo a phase separation by self-assembly into a 2D racemic crystalline phase and a separate enantiomorphous 2D phase of the enantiomer in excess. Each of these crystalline phases has markedly different chemical properties, thus yielding products that differ in the composition of the oligomers. So polymerization within the enantiomorphous crystalline phase yields homochiral oligopeptides of one handedness whereas the reaction controlled by the racemic crystallites yields racemic mixtures and heterochiral products. The combination of the two routes leads to an overall chiral amplification process.

We also review an effective mathematical description of the experimentally measured relative abundances. The model takes as given the prior formation of the self-assembled 2D crystallites at the air-water interface and is concerned exclusively with the subsequent polymerization reactions. We model the latter via a copolymerization scheme where the independent reaction rates effectively account for the different chemical properties of the crystalline phases (the racemic 2D crystallites

and the pure enantiomorphous 2D crystallites) that lead to the formation of racemic mixtures, heterochiral products, and isotactic oligopeptides. We contrast the numerical fits from our model with those assuming a purely random binomial process. This correlation between experimental and numerical data is greater for our copolymerization model than for the binomial distribution, except for the single chemical system composed of γ-stearyl-glutamic thioacid, which provides the experimental reference system for random polymerization. Overall, the mathematical model succeeds rather well in the task and provides a further example of how experiments aimed at shedding light on the origins of biochirality can be *effectively* modeled with a minimum of assumptions.

Before introducing the experiments and their mathematical descriptions, we give some consideration to the emergence of chirality in reversible autocatalytic reactions as the result of temporary asymmetric amplification. We focus our attention on the elementary Frank model, not only because of its fundamental role as the paradigmatic model of mirror symmetry breaking in chemistry, but also because it has recently been shown to lie at the heart of the well-known and spectacular Soai reaction [8]. Frank's concept of enantiomeric mutual or cross inhibition is moreover operative in the two chemical/mathematical models reviewed below. In the case of the glycine plus α-amino acid system, it is clearly manifested through the enantioselective occlusion process as well as through the kinetic inhibition effect. In the case of the chiral copolymerization model for lattice-controlled chiral amplification, the inhibition is expressed via the process of heteropolymerization. We therefore discuss, from the combined perspectives afforded by numerical simulation, phase-plane analysis and linear stability analysis, the influence that partial or total matter in-flow and out-flow can have on the onset of temporary or permanent asymmetric amplification. Conditions leading to temporary amplification give rise to what we denote as chiral excursions [9] which are not generally expected for reversible reactions taking place in systems closed to matter flow and under thermodynamic control. The interest in these excursions lies in the fact that the racemization time scale can be much longer than that of mirror symmetry breaking.

2 Frank Model: Permanent Vs Temporary Broken Mirror Symmetry

In 1953, Frank proposed a homogeneous open flow reactor system with a continuous input of an achiral substrate A from which both enantiomers L and D are formed. This model [10, 11] and a diverse number of variations on a theme [3, 12–21] have been invoked over the years to justify theoretically the emergence of biological homochirality [21, 22]. Most of the schemes that have been proposed are usually analyzed as a reaction network in open flow systems for which matter and energy are exchanged with the surroundings. These are typically composed of an irreversible

enantioselective autocatalysis coupled to an irreversible mutual inhibition reaction between the product enantiomers. The model shows how homochirality is achieved as a stationary state when the mutual inhibition product (the heterodimer LD) is removed from the system and when the concentration of the achiral substrate A is held constant. By marked contrast, for reversible transformations and when the mutual inhibition product remains in the system, *the final* asymptotic stable state can only be the racemic one. As a consequence, a thermodynamically controlled SMSB cannot be expected to take place. In particular, SMSB is not expected for reversible reactions taking place in systems closed to matter and energy flow.

In spite of this expectation, and as was recently demonstrated [23] for systems closed to matter flow, the Frank model is actually the prime candidate for the fundamental reaction network necessary for reproducing the key experimental features reported on absolute asymmetric synthesis in the absence of any chiral polarization [8]. Most importantly, when reversible steps in all the reactions are allowed, it is capable of [23] (1) amplification of the initially tiny statistical enantiomeric excesses from ee $\sim 10^{-8}\%$ to practically 100%, leading to (2) long duration chiral *excursions* or chiral pulses away from the racemic state at nearly 100% ee, followed by (3) the final and inevitable approach to the stable racemic state for which ee $= 0$, i.e., the mirror symmetry is recovered permanently. Understanding this temporary asymmetric amplification is important because the racemization time scale can be much longer than that required for the complete conversion of the achiral substrate into enantiomers.

Long duration chiral excursions have also been reported recently in closed chiral polymerization models with reversible reactions [24] where constraints implied by micro-reversibility have been taken into account. These results are important because they suggest that temporary SMSB in experimental chiral polymerization can take place, and with observable and large chiral excesses, without the need to introduce chiral initiators [25] or large initial chiral excesses [26].

The specific reaction scheme we consider consists of a straight non-catalyzed reaction (1) and an enantioselective autocatalysis (2), where A is a prechiral starting product and L and D are the two enantiomers of the chiral product. We allow for reversible heterodimerization step in Eq. (3) where LD is the achiral heterodimer. $k_{\pm i}$ denote the forward/reverse reaction rate constants.

Production of chiral compound:

$$\mathrm{A} \underset{k_{-1}}{\overset{k_1}{\rightleftharpoons}} \mathrm{L}, \quad \mathrm{A} \underset{k_{-1}}{\overset{k_1}{\rightleftharpoons}} \mathrm{D}. \tag{1}$$

Auto catalytic amplification:

$$\mathrm{L} + A \underset{k_{-2}}{\overset{k_2}{\rightleftharpoons}} \mathrm{L} + \mathrm{L}, \quad \mathrm{D} + \mathrm{A} \underset{k_{-2}}{\overset{k_2}{\rightleftharpoons}} \mathrm{D} + \mathrm{D}. \tag{2}$$

Hetero-dimerization or mutual inhibition:

$$\mathrm{L} + D \underset{k_{-3}}{\overset{k_3}{\rightleftharpoons}} \mathrm{LD}. \tag{3}$$

Focusing our attention on chiral excursions as defined above, we make a careful distinction between open, semi-open, or semi-closed systems. These system constraints or boundary conditions are crucial for determining both the intermediate dynamics and the asymptotic final stationary states of the chemical system. Temporary chiral excursions are observed for semi-closed and semi-open systems and the corresponding behavior can be appreciated graphically by means of phase space analysis, in conjunction with linear stability analysis and direct numerical simulations. Such chiral excursions may be experimentally observed and are the long sought goal of the experimentalist. It is therefore important to understand the basic processes and constraints responsible for this phenomenon.

2.1 Open Systems: Permanent Mirror Symmetry Breaking

We first consider the original Frank scenario [10]. There, steady and stable chiral states can be achieved, since the system is permanently held out of equilibrium. See [27] for more details derived from applying linear stability analysis. An important question is whether the system can support chiral excursions even if the final asymptotic state is racemic. That is, can it pass through temporary chiral states before its approach to the final racemic state?

2.1.1 Kinetic Rate Equations

In the original Frank model there is an incoming flow of achiral compound A and the elimination of the heterodimer LD from the system [21]. A mathematically convenient way to account for the inflow of achiral matter is to assume that the concentration of the prechiral component [A] is constant, and then we need not write the corresponding kinetic equation for it. For the outflow, the heterodimer leaves the system at a rate $\bar{\gamma}$. We assume that the heterodimer formation step is irreversible, and set $k_{-3} = 0$. Note that the elimination of LD from the system can actually be neglected as long as the heterodimerization step is irreversible [22]. We retain this product outflow, however, since it is needed to obtain *stationary* asymptotic values of all three concentrations [L], [D], and [LD]; see the explicit fixed points below. Otherwise, the concentration of heterodimer would build up and overwhelm the system. So with [A] = const and replacing (3) by

$$\mathrm{L} + \mathrm{D} \xrightarrow{k_3} \mathrm{LD}, \tag{4}$$

$$\mathrm{LD} \xrightarrow{\bar{\gamma}} \emptyset, \tag{5}$$

we obtain the corresponding kinetic rate equations governing the time development of the concentrations:

$$\frac{\mathrm{d}}{\mathrm{d}t}[\mathrm{L}] = k_1[\mathrm{A}] + (k_2[\mathrm{A}] - k_{-1})[\mathrm{L}] - k_{-2}[\mathrm{L}]^2 - k_3[\mathrm{L}][\mathrm{D}], \tag{6}$$

$$\frac{\mathrm{d}}{\mathrm{d}t}[\mathrm{D}] = k_1[\mathrm{A}] + (k_2[\mathrm{A}] - k_{-1})[\mathrm{D}] - k_{-2}[\mathrm{D}]^2 - k_3[\mathrm{D}][\mathrm{L}], \tag{7}$$

$$\frac{\mathrm{d}}{\mathrm{d}t}[\mathrm{LD}] = k_3[\mathrm{L}][\mathrm{D}] - \bar{\gamma}[\mathrm{LD}]. \tag{8}$$

The key variable throughout the subsequent analysis is the chiral polarization

$$\eta = \frac{[\mathrm{L}] - [\mathrm{D}]}{[\mathrm{L}] + [\mathrm{D}]}, \tag{9}$$

also called enantiomeric excess ee, which obeys $-1 \leq \eta \leq 1$ and which represents the order parameter for mirror symmetry breaking. That is $1 \geq |\eta| > 0$ iff mirror symmetry is broken.

To simplify the analysis, we define a dimensionless time parameter $\tau = (k_2[\mathrm{A}]–k_{-1})t$ and dimensionless concentrations that scale as $[\widetilde{L}] = k_3(k_2[\mathrm{A}] - k_{-1})^{-1}[\mathrm{L}]$, $[\widetilde{\mathrm{D}}] = k_3(k_2[\mathrm{A}] - k_{-1})^{-1}[\mathrm{D}]$, $[\widetilde{\mathrm{LD}}] = k_3(k_2[\mathrm{A}] - k_{-1})^{-1}[\mathrm{LD}]$. It is convenient to define the sums and differences of concentrations: $\chi = [\widetilde{\mathrm{L}}] + [\widetilde{\mathrm{D}}], y = [\widetilde{\mathrm{L}}] - [\widetilde{\mathrm{D}}]$, and for the heterodimer put $P = [\widetilde{\mathrm{LD}}]$. The chiral polarization $\eta = y/\chi$; remains unchanged by this rescaling.

In terms of the new variables, Eqs. (6)–(8) read

$$\frac{\mathrm{d}\chi}{\mathrm{d}\tau} = 2u + \chi - \frac{1}{2}(g+1)\chi^2 - \frac{1}{2}(g-1)\chi^2\eta^2, \tag{10}$$

$$\frac{\mathrm{d}\eta}{\mathrm{d}\tau} = \eta(1 - g\chi) - \frac{\eta}{\chi}\left(\frac{\mathrm{d}\chi}{\mathrm{d}\tau}\right), \tag{11}$$

$$\frac{\mathrm{d}P}{\mathrm{d}\tau} = \frac{1}{4}\chi^2(1 - \eta^2) - \gamma P. \tag{12}$$

The three dimensionless parameters appearing here are

$$u = \frac{k_1 k_3[\mathrm{A}]}{(k_2[\mathrm{A}] - k_{-1})^2}, \; g = \frac{k_{-2}}{k_3}, \; \gamma = \frac{\bar{\gamma}}{(k_2[\mathrm{A}] - k_{-1})}. \tag{13}$$

The parameter g plays a privileged role as we will see below. The system is described by three equations (10–12). Since P does not enter into the equations

for χ and η, the three equations actually decouple and the dynamical system to study is effectively two-dimensional. The onset of SMSB cannot depend on whether the heterodimer is removed from the system when $k_{-3} = 0$, although the *fixed points* will (see Sect. 2.1.3).

2.1.2 Phase Plane Representation

In the two-dimensional phase space of the dynamical system defined by Eqs. (10) and (11), there are a few curves with a special significance. These are the known as the null-clines, defined by

$$\frac{\mathrm{d}\chi}{\mathrm{d}\tau} = 0, \tag{14}$$

$$\frac{\mathrm{d}\eta}{\mathrm{d}\tau} = 0. \tag{15}$$

The intersections of these curves give all the possible steady states (or fixed points) of the dynamical system. The condition $\mathrm{d}\chi/\mathrm{d}t = 0$ leads to the two curves

$$\chi_{\pm}^{(1)} = \frac{1 \pm \sqrt{1 + 4u(g(1+\eta^2) + 1 - \eta^2)}}{g(1+\eta^2) + 1 - \eta^2}, \tag{16}$$

whereas $\mathrm{d}\eta/\mathrm{d}\tau = 0$ implies the three curves

$$\eta = 0, \quad \chi_{\pm}^{(2)} = \pm\sqrt{\frac{4u}{1 - g + (g-1)\eta^2}}. \tag{17}$$

For $u > 0$ the solutions denoted $\chi_{-}^{(1,2)}$ correspond to negative total enantiomer concentrations so we discard them. The three remaining physically acceptable null-clines are plotted in Fig. 1. Which of the two different intersection configurations or topologies pertains depends only on the single parameter $g = \frac{k_{-2}}{k_3}$ which gives the relative rate of *inverse* enantioselective autocatalysis to mutual inhibition. We emphasize that, despite the similar appearance, the nullcline graphs should not be confused with the classic bifurcation diagrams that have often been discussed in the past [3, 28, 29].

2.1.3 Fixed Points and Stability

The system has several steady states or fixed points: besides an unphysical state that we disregard, there is a Z_2 pair of chiral solutions $Q\pm$, and a racemic state R:

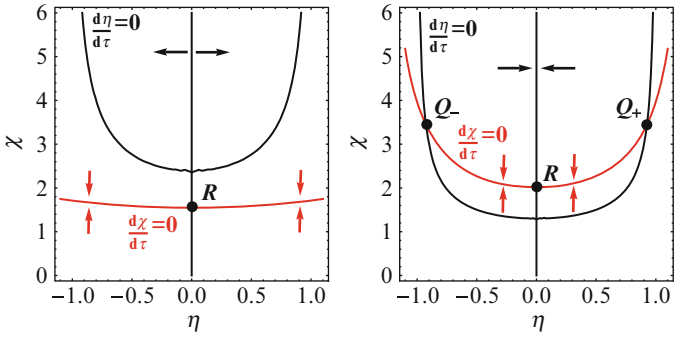

Fig. 1 Nullclines for the open system (10, 11). These curves correspond to $u = 0.3$ implying $g_{\text{crit}} = 0.59$. The $d\eta/d\tau = 0$ and $d\chi/d\tau = 0$ nullclines are plotted in *black* and *red*, respectively. The *black* (*red*) *arrows* indicate the regions of phase space where η (χ) increases or decreases in time. *Left*: $g = 0.79 > g_{\text{crit}}$. The nullclines intersect in only the one point R representing the asymptotic stable racemic state. *Right*: $g = 0.29 < g_{\text{crit}}$. In this case there are three intersections, $Q_{\pm}$ and R representing the Z_2 equivalent stable chiral states and the unstable racemic state, respectively. From Eq. (22) the enantiomeric excess at $Q_{\pm}$ is $\eta = \pm 0.93$

$$R = \left(P = \frac{2(g+1)u + \sqrt{4(g+1)u+1}+1}{2(g+1)^2\gamma}, \chi = \frac{1+\sqrt{4(g+1)u+1}}{g+1}, \quad y = 0 \right), \tag{18}$$

$$Q_{\pm} = \left(P = \frac{u}{\gamma - g\gamma}, \ \chi = \frac{1}{g}, \ y = \pm \frac{\sqrt{((g-1)/g^2)+4u}}{\sqrt{g-1}} \right). \tag{19}$$

Linear stability is provided by calculating the Jacobian of the linearized fluctuation equations. The eigenvalues of that Jacobian are given by [27]

$$\lambda_{1,2,3}(R) = \left(-\sqrt{4(g+1)u+1}, \ \frac{1 - g\sqrt{4(g+1)u+1}}{g+1}, -\gamma \right), \tag{20}$$

$$\lambda_{1,2,3}(Q_{\pm}) = \left(\frac{-\sqrt{16g^3u + 4g^2 - 4g + 1} - 1}{2g}, \frac{\sqrt{16g^3u + 4g^2 - 4g + 1} - 1}{2g}, -\gamma \right). \tag{21}$$

This is one of the few models for which explicit and reasonably manageable expressions can be derived in closed form. Note that $\lambda_1(R) < 0$ and $\lambda_1(Q) < 0$ are always negative whereas $\lambda_2(R) > 0$ and $\lambda_2(Q) < 0$ for $g < g_{\text{crit}}$, otherwise $\lambda_2(R) < 0$ and $\lambda_2\ (Q) > 0$ for $g > g_{\text{crit}}$, where $g_{\text{crit}} = \left(\sqrt{1+16u} - 1\right)/8u$ is the critical value for this parameter. Note that $g_{\text{crit}}\ (u) \leq 1$ for all $u \geq 0$. For small u we can write $g_{\text{crit}} = 1\text{–}4u$, while for large u, $g_{\text{crit}} \to 1/2u^{1/2}$. Thus the direct monomer

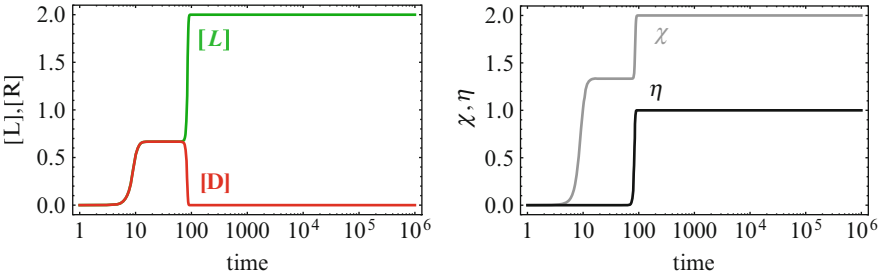

Fig. 2 $g < g_{\text{crit}}$: chiral symmetry breaking in the open chemical system (6–8). Temporal behavior (logarithmic scale) of the individual enantiomer concentrations [L] and [D] (*left*), and the chiral polarization η; and total monomer concentration χ; (*right*). Initial concentrations: $[\text{L}]_0 = (1 \times 10^{-6} + 1 \times 10^{-15})$ M, $[\text{D}]_0 = 1 \times 10^{-6}$ M ($\eta_0 = 5 \times 10^{-8}\%$) and [A] = 1 M. Rate constants: $k_1 = 10^{-4}\ \text{s}^{-1}$, $k^{-1} = 10^{-6}\ \text{s}^{-1}$, $k_2 = 1\ \text{s}^{-1}\ \text{M}^{-1}$, $k_{-2} = 0.5\ \text{s}^{-1}\ \text{M}^{-1}$ and $k_3 = 1\ \text{s}^{-1}\ \text{M}^{-1}$, These values correspond to $g = 0.5$ and $u = 10^{-4}$. In figures of simulations, we always display original concentration variables [L], [D], [LD], etc., as functions of the time t

production step [$\propto k_1$ in (1)] tends to racemize the system leading to final η values strictly less than unity:

$$\eta = \pm\sqrt{1 - \frac{4ug^2}{1-g}}, \tag{22}$$

which holds when $g < g_{\text{crit}}$. The monomer production step thus reduces the range of g for which stable mirror symmetry breaking can occur, and the chiral solutions themselves are no longer 100% chiral, but only fractionally chiral.

If more information is required we must resort to a numerical integration of the coupled nonlinear rate equations. Their solution gives the entire temporal history of the system evolution from initial conditions to the final asymptotic state. Figure 2 shows the temporal evolution of the L and D chiral monomers starting from an extremely dilute total monomer concentration and the very small statistical chiral deviations from the ideal racemic composition. The right hand side of this figure shows the evolution in terms of the quantities χ and η. Note that the mirror symmetry breaking is signaled by the enantiomeric excess η.

Are there chiral excursions to be found in the open system model? A chiral excursion holds when the enantiomeric excess η departs from a small initial value, evolves to some maximum absolute value, and then decays to the final value of zero. To ensure a final racemic state we must set $g > g_{\text{crit}}$, but then we find no numerical evidence for such temporary chiral excursions or chiral pulses. This can be understood qualitatively from inspection of the left hand side of Fig. 1. The initial conditions (dilute monomer concentration and statistical chiral fluctuation) correspond to an initial point located at tiny values of χ and close to the vertical nullcline, well below the point labeled as R. The system is attracted to the black curve and moves up the curve to R. In this situation, it is impossible for the chiral excess to increase, even temporarily. Note the time scales for χ and η are of the

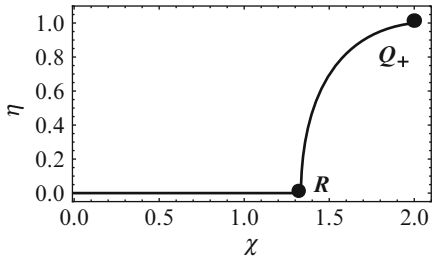

Fig. 3 Phase space: parametric plot of the solution pair $[\chi(t), \eta(t)]$ for the initial conditions and rate constants as in the previous Fig. 2. Compare to *right hand sides* of Figs. 1 and 2

same order. On the other hand, if $g < g_{\text{crit}}$, then we have the situation depicted on the right hand side of the figure. Here the same initial point moves towards the vertical nullcline and up towards R, but once past the locally horizontal black curve, is attracted to one of the two chiral fixed points $Q_{\pm}$ where it stays forever, provided the system is maintained out of equilibrium. The chiral symmetry is permanently broken, and there is no excursion such as we have defined it. This solution represented parametrically in phase space in Fig. 3.

2.2 Semi-Closed Systems: Chiral Excursions

2.2.1 Kinetic Rate Equations

To elucidate the temporal evolution of χ and η for a more general setting, we do not remove the heterodimer from the system (and also allow for the back reaction or dissociation to monomers), although we still keep [A] constant for mathematical convenience. The corresponding rate equations are now given by

$$\frac{\mathrm{d}}{\mathrm{d}t}[\mathrm{L}] = k_1[\mathrm{A}] + (k_2[\mathrm{A}] - k_{-1})[\mathrm{L}] - k_{-2}[\mathrm{L}]^2 - k_3[\mathrm{L}][\mathrm{D}] + k_{-3}[\mathrm{LD}], \tag{23}$$

$$\frac{\mathrm{d}}{\mathrm{d}t}[\mathrm{D}] = k_1[\mathrm{A}] + (k_2[\mathrm{A}] - k_{-1})[\mathrm{D}] - k_{-2}[\mathrm{D}]^2 - k_3[\mathrm{D}][\mathrm{L}] + k_{-3}[\mathrm{LD}], \tag{24}$$

$$\frac{\mathrm{d}}{\mathrm{d}t}[\mathrm{LD}] = k_3[\mathrm{L}][\mathrm{D}] - k_{-3}[\mathrm{LD}]. \tag{25}$$

After performing the same change of variables and rescaling as in the open case above, we arrive at

$$\frac{\mathrm{d}\chi}{\mathrm{d}\tau} = 2u + \chi - \frac{1}{2}(g+1)\chi^2 - \frac{1}{2}(g-1)\chi^2\eta^2 + 2rP, \tag{26}$$

$$\frac{\mathrm{d}\eta}{\mathrm{d}\tau} = \eta(1 - g\chi) - \frac{\eta}{\chi}\left(\frac{\mathrm{d}\chi}{\mathrm{d}\tau}\right), \tag{27}$$

$$\frac{\mathrm{d}P}{\mathrm{d}\tau} = \frac{1}{4}\chi^2(1 - \eta^2) - rP. \tag{28}$$

The three dimensionless parameters appearing here are

$$u = \frac{k_1 k_3[\mathrm{A}]}{(k_2[\mathrm{A}] - k_{-1})^2}, \qquad g = \frac{k_{-2}}{k_3}, \qquad r = \frac{k_{-3}}{(k_2[\mathrm{A}] - k_{-1})}. \tag{29}$$

The system is described by three nonlinear equations (26–28) which do not decouple.

2.2.2 Phase Plane Representation

In order to obtain an *approximate* two-dimensional phase plane representation of the above dynamical system, we will invoke the dynamic steady state approximation for the heterodimer P. Such approximations are usually justified a priori when there exists a clear separation of *time scales* in the problem, thus allowing one to identify changing concentrations rapidly and slowly [30]. Here, however, no such time scales are evident, all concentration variables evolving on a similar time scale. Nevertheless, we will see a posteriori that this approximation can be reasonably good over a wide range of time scales. We therefore assume that the heterodimer is in a dynamic steady state P_{stat} relative to the monomer concentrations and chiral polarization, so setting (28) to zero yields

$$P_{\mathrm{stat}} \approx \frac{\chi^2}{4r}(1 - \eta^2). \tag{30}$$

Substituting this P_{stat} into Eqs. (26) and (27) leads to the differential equation pair

$$\frac{\mathrm{d}\chi}{\mathrm{d}\tau} = 2u + \chi - \frac{g}{2}\chi^2(1 + \eta^2), \tag{31}$$

$$\frac{\mathrm{d}\eta}{\mathrm{d}\tau} = \eta\left(-g\chi - \frac{2u}{\chi} + \frac{g}{2}\chi(1 + \eta^2)\right). \tag{32}$$

As above, we study the phase space of the two-dimensional system by means of the nullclines. The condition $\mathrm{d}\chi/\mathrm{d}\tau = 0$ implies the two curves

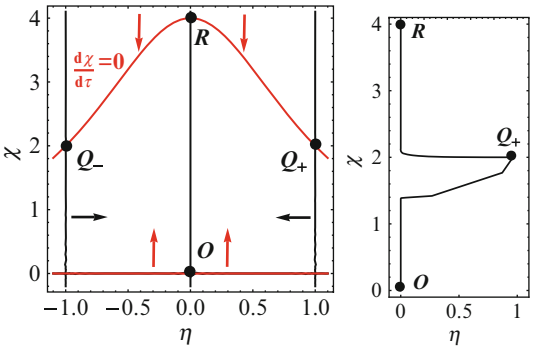

Fig. 4 Nullclines for the semi-open case (31, 32) in the steady state approximation for P. The nullclines (33, 34) are plotted in *red* and *black*, respectively. *Red* and *black arrows* indicate the phase-space regions of increasing or decreasing χ and η. The four stationary solutions $O, R, Q_{\pm}$ are indicated by the *black dots*. These *curves* are illustrated for $u = 0$ and $g = 0.5$. *Right*: actual dynamic path in phase space, clearly indicating the chiral excursion or "pulse" in η, calculated for the initial concentrations and rate values indicated in Fig. 5. The time flows from O to Q_+ to R

$$\chi_{\pm} = \frac{1 \pm \sqrt{1 + 4gu(1+\eta^2)}}{g(1+\eta^2)}, \tag{33}$$

whereas the condition $\mathrm{d}\eta/\mathrm{d}\tau = 0$ implies the three curves

$$\eta = 0, \quad \eta_{\pm} = \pm\sqrt{1 + \frac{4u}{g\chi^2}}. \tag{34}$$

These are plotted on the left hand side of Fig. 4.

2.2.3 Fixed Points and Stability

We next solve the rate equations (26–28) looking for steady states (the fixed points). To keep the algebra manageable, we also take $u = 0$ as in [27]. There are four solutions, namely, the empty O solution, the racemic R, and the two mirror-symmetric chiral $Q_{\pm}$ solutions:

$$O = (P = 0,\ \chi = 0, y = 0), \tag{35}$$

$$R = \left(P = \frac{1}{g^2 r}, \chi = \frac{2}{g}, y = 0\right), \tag{36}$$

$$Q_{\pm} = \left(P = 0,\, \chi = \frac{1}{g}, y = \pm\frac{1}{g} \right). \tag{37}$$

Note that the final heterodimer concentration P is *zero* in the chiral states $Q_{\pm}$. Note also that the steady state approximation (30) implies the same result since $|\eta| = 1 \rightarrow P_{\text{stat}} = 0$. In order to study the linear stability of the four possible homogeneous solutions O, R, and $Q_{\pm}$, we calculate the eigenvalues of the 3×3 Jacobian array M_{open} as described in [27]. The eigenvalues corresponding to these fixed point solutions are given by (recall we set $u = 0$)

$$\lambda_{1,2,3}(O) = (1, 1, -r), \tag{38}$$

$$\lambda_{1,2,3}(R) = \left(-1, -\frac{2 + g(1+r) + \sqrt{4 + g^2(-1+r)^2 + 4g(1+r)}}{2g}, \right.$$
$$\left. \frac{-2 - g(1+r) + \sqrt{4 + g^2(-1+r)^2 + 4g(1+r)}}{2g} \right) \tag{39}$$

$$\lambda_{1,2,3}(Q_{\pm}) = \left(-1, -\frac{1 + g(-1+r) + \sqrt{1 + 2g(-1+r) + g^2(1+r)^2}}{2g}, \right.$$
$$\left. \frac{-1 + g(1-r) + \sqrt{(1 + g(-1+r))^2 + 4g^2 r)}}{2g} \right) \tag{40}$$

As $\lambda_{1,2}(O) > 0$, the empty state is always unstable. An inequality analysis shows that both $\lambda_2(R) < 0$ and $\lambda_3(R) < 0$ for all $r > 0$ and $g > 0$. Since $\lambda_1(R) = -1$ this demonstrates that the racemic state R is always stable. As an independent check, we can also verify that $\lambda_3(Q) > 0$ is positive for all $r > 0$ and $g > 0$, so the chiral solutions $Q_{\pm}$ are always unstable. The final outcome will therefore always be the racemic state. There is no stable mirror symmetry broken solution when the heterodimer dissociates back into the chiral monomers. Nevertheless, the system can undergo temporary chiral excursions. To see this, we perform a numerical integration of the coupled rate equations.

In Fig. 5 we plot the temporal evolution of the L and D chiral monomers starting from an extremely dilute total monomer concentration and the very small statistical chiral deviations from the ideal racemic composition. The right hand side of this figure shows the evolution in terms of the quantities χ and η. Note the chiral excursion in η for the time interval between $t \simeq 100$ s and $t \simeq 1{,}000$ s.

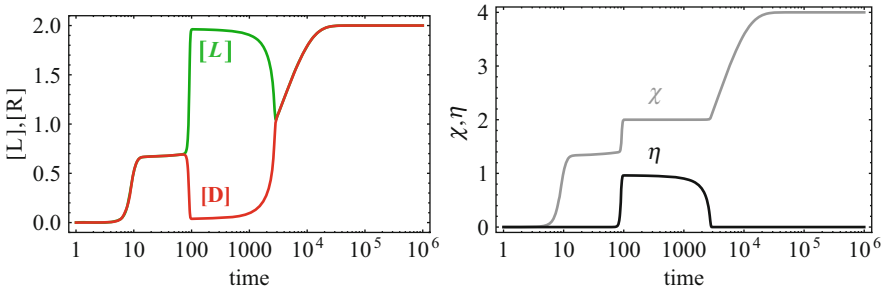

Fig. 5 Temporary chiral symmetry breaking and chiral excursions in the semi-open system (23–25). Temporal behavior (logarithmic scale) of the individual enantiomer concentrations [L] and [D] (*left*) and the chiral polarization η and total monomer concentration χ (*right*). Initial concentrations: $[\text{L}]_0 = (1 \times 10^{-7} + 1 \times 10^{-15})$ M, $[\text{D}]_0 = 1 \times 10^{-7}$ M ($\eta_0 = 5 \times 10^{-8}$%) and [A] = 1 M. Rate constants: $k_1 = 10^{-4}\ \text{s}^{-1}$, $k_{-1} = 10^{-6}\ \text{s}^{-1}$, $k_2 = 1\ \text{s}^{-1}\ \text{M}^{-1}$, $k_{-2} = 0.5\ \text{s}^{-1}\ \text{M}^{-1}$, $k_3 = 1\ \text{s}^{-1}\ \text{M}^{-1}$ and $k_{-3} = 10^{-3}\ \text{s}^{-1}$. These rate constants imply $g = 0.5$ and $u = 10^{-4}$

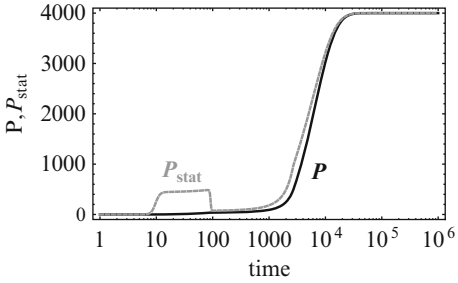

Fig. 6 Semi-open system: comparison of direct numerical solution [LD] and the steady state approximation $[\text{LD}]_{\text{stat}}$ in Eq. (30) for the heterodimer concentration (after rescaling from P to [LD])

Finally, we compare the heterodimer concentration from direct numerical simulation with the steady state approximation in Fig. 6. While $[\text{LD}]_{\text{stat}}$ appears to overestimate [LD] at earlier times, it provides a reasonably good approximation to the actual heterodimer concentration P right after chiral symmetry is broken, at about $t \simeq 100$ s, and coincides perfectly after chiral symmetry is recovered, and when χ reaches its asymptotic value, after approximately $t \simeq 10^4$ s.

In summary, the main lesson learned can be succinctly stated as follows:

- *Systems open* to matter and energy exchange: the *final* state can be chiral or racemic. There are no chiral excursions.
- *Systems closed* to matter and energy exchange: for reversible reactions the *final* state can *only* be racemic. There can be chiral excursions.

3 Mirror Symmetry Breaking at Interfaces: Glycine + α Amino Acids

Among the experiments dedicated to exploring chance mechanisms in chirality, a particularly noteworthy laboratory study with a marked relevance for prebiotic chemistry was reported some years ago by the Rehovot group. They dealt with an autocatalytic process for the resolution of racemic α-amino acids within crystals of glycine grown at the air-solution interface [5, 6]. They used cooperative crystallization processes for the spontaneous separation of racemic mixtures of α-amino acids rich with glycine into optically pure enantiomers. Their experimental model involves slow evaporation (an open system) of aqueous solutions of the centrosymmetric form of glycine containing racemic mixtures of α-amino acids. Due to the unique crystal structure of glycine, all chiral D-amino acids except for proline are occluded within the crystal through the (0 1 0) face, whereas the L-amino acids are occluded through the $(0\,\bar{1}\,0)$ face. Glycine crystals float in solution so that only one face is available for growth. Thus when glycine crystals are grown at the air-water interface in the presence of DL-amino acids, only one of its enantiotopic faces, say (0 1 0), is exposed to the solution and so picks up only the D-amino acid together with glycine. By symmetry, crystals exposing their $(0\,\bar{1}\,0)$ face towards solution occlude only the L-enantiomers. Now, if by *chance* a single or small number of oriented glycine crystals grow initially at the interface, the bulk solution will be enhanced with the amino acid of one handedness. The preservation and transmission of the chirality generated by chance of the original "Adam" crystal means that new crystals grown at later stages at this interface must adopt the same orientation. There are two proven ways this is achieved [5, 6]: (1) by means of a hydrophobic effect and (2) by a kinetic inhibition effect. Regarding the first effect, if the solution contains hydrophobic amino acids these tend to accumulate at the interface forming two-dimensional domains acting as templates for the oriented crystallization of the glycine crystals. Thus, the L-amino acids induce crystallization of floating glycine crystals exposing their (0 1 0) face towards solution and these faces occlude only the D-amino acids. This asymmetric induction has been established experimentally [5, 31]. As for the second effect, this comprises an enantioselective inhibition (qualitatively akin to Frank's mutual inhibition) of the glycine nuclei by the amino acids present in solution (these can be both partially dissolved hydrophobic as well as hydrophilic amino acids). This independent effect was proven experimentally by achieving complete orientation of the floating glycine nuclei when grown in the presence of hydrophobic DL-leucine and hydrophilic L-amino acids. The presence of the DL-leucine is to ensure nucleation of floating glycine crystals exposing either enantiotopic face towards solution in a 1:1 ratio whereas increasing the concentration of the hydrophilic amino acid additives inhibited the glycine nuclei exposing their $(0\,\bar{1}\,0)$ face and so prevented their further growth. These hydrophilic amino acids inhibit the crystal nuclei from growing and developing into macroscopic crystals [32]. Both the hydrophobic and kinetic effects act

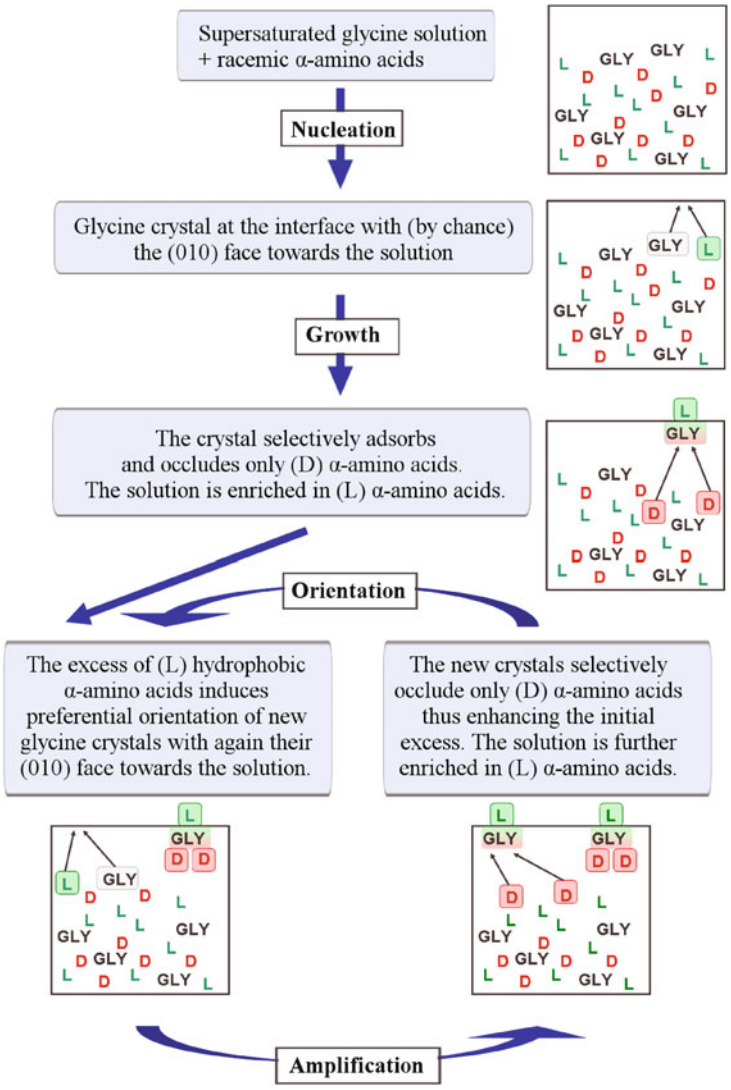

Fig. 7 The overall process of mirror symmetry breaking and amplification. Scheme adapted from [4, 6]. Glycine is denoted by GLY while the two amino-acid enantiomers are L and D

cooperatively in the same direction in that they both contribute to the territorial segregation of the enantiomers.

The overall experimental process can be summarized by the following steps (Fig. 7) [4, 6]: (1) mirror symmetry breaking via the enantioselective occlusion of one of the enantiomers of the racemic α-amino acids within crystals of glycine grown at the air-solution interface, (2) the oriented crystal formed at the interface operates as a seed for further occlusion of amino acids of the same handedness,

(3) the amplification experiments comprises self-aggregation of hydrophobic α-amino acids into chiral clusters that operate as templates for an oriented crystallization of fresh crystals of glycine. (i.e., the hydrophobic effect), and (4) enantioselective inhibition of embryonic nuclei of glycine generated at the air-solution interface by the water soluble α-amino acids formed in excess during the process. (i.e., the kinetic effect). We illustrate graphically each key step of the overall process in Fig. 7 by a simplified caricature of the associated reaction involving the glycine (GLY) and the two enantiomers (L) and (D). The only gross pictorial oversimplification is that dealing with the orientation of the glycine at the interface by the hydrophobic amino acid monomer: realistically this step requires several dozens of hydrophobic amino acids to form a monolayer template. Building in this realism however only affects the model quantitatively, not qualitatively.

The fundamental relevance of this experiment is that it provides a simple chemical model for the generation and amplification of optically active amino acids in prebiotic conditions. It employs the centrosymmetric crystal structure of glycine, which is the only achiral amino acid and is the major component found in modern prebiotic synthesis experiments [33]. The enantiomeric resolution and symmetry breaking is achieved without the need to input mechanical energy: in particular there is need for neither mechanical stirring [34] nor grinding with glass beads [35], and it involves only amino acids which have an immediate relevance for prebiotic chemistry. We next discuss the model of the overall processes involved.

3.1 Differential Reaction Rate Model

3.1.1 Preliminary Considerations

Following the experiment, we assume a supersaturated solution of glycine and racemic α amino acids. The glycine monomers and clusters in solution will be denoted by A_1 and A_r, respectively, the cluster being made up from r-monomer units. A typical glycine cluster size should exist $\langle r \rangle = M$ for M glycine monomer units. This is the average size of the primary nucleation or glycine seed crystal which can then precipitate at the air-water interface where it will, in the presence of hydrophobic D- and L-amino acids, assume one of two possible orientations [6]. X_M and Y_M will denote these two possible enantiotopic orientations of the glycine crystal floating at the interface: X for the (0 1 0) enantiotopic face exposed to solution and Y for the other $(0\ \bar{1}\ 0)$ enantiotopic face exposed to solution. The D and L denote the two amino acid enantiomers.

The enantioselective occlusion of the amino acid into the host glycine crystals will be fairly straightforward to represent mathematically. Recall that only the (0 1 0) face of the glycine crystal can occlude the D-amino acid whereas only the $(0\ \bar{1}\ 0)$ face can occlude the L-amino acid; see Fig. 7. To begin, we first write down a "microscopic" model which contemplates all kinds of crystal aggregations growing

from both glycine take-up and the amino acid occlusion and with cluster size dependent rates and then simplify things by taking the reaction rates independent of cluster size, assuming only cluster-monomer aggregation. We will not consider fragmentation in any case. Since the hydrophobic effect dominates over the kinetic effect [6], we will consider this mechanism first.

3.1.2 Modeling the Hydrophobic Crystal Orientating Effect

The goal in the following is to transcribe the scheme in Fig. 7 into explicit reaction steps. Additional simplifications will follow later in order to obtain a minimal model leading to mirror symmetry breaking which can then be contrasted with experimental data.

The Formation of Glycine Aggregates/Clusters in Solution

The achiral molecules of glycine in solution combine pairwise to yield achiral glycine clusters in solution, where r, s denote number of monomers in the cluster and $\delta_{r,\,s}$ is the cluster size dependent rate constant:

$$\mathrm{A}_r + \mathrm{A}_s \overset{\delta_{r,s}}{\longrightarrow} \mathrm{A}_{r+s}. \tag{41}$$

We simplify this below so that only dimers are formed ($r = 1$, $s = 1$) [36].

Nucleation of Oriented Glycine Crystals at the Air-Water Interface in Presence of Hydrophobic LD-Amino Acids

The hydrophobic amino acid at the interface acts as a nucleator or seed:

$$\begin{aligned} \mathrm{A}_r + \mathrm{L}_1 &\overset{\mu_r}{\longrightarrow} \{\mathrm{L}_1\mathrm{X}_r\}, \\ \mathrm{A}_r + \mathrm{D}_1 &\overset{\mu_r}{\longrightarrow} \{\mathrm{D}_1\mathrm{Y}_r\}. \end{aligned} \tag{42}$$

Here, and henceforth, the brackets denote the solid phase. This process occurs at the rate μ_r. The two enantiotopic crystal faces exposed to the solution are denoted by X_r and Y_r, respectively. Realistically, a single leucine or valine molecule cannot serve as a nucleus for the glycine crystallization; instead, several dozen arranged in self-assembly are usually required. However, for the sake of simplicity (and limitations on computational time), we assume that a single hydrophobic amino acid monomer is sufficient to trigger the nucleation. We note that HPLC analysis of the crystals indicates that only minute amounts of the orienting hydrophobic amino acids are occluded through the upward pointing face [5], so our single monomer

"template" assumption is not entirely unreasonable and results in a welcome mathematical simplification. Varying the size of the template can only have quantitative but not qualitative effects in so far as mirror symmetry breaking is concerned. Below, we will assume a transition regime, that is, only dimer glycine clusters $r = 2$, get nucleated in this way to form oriented host seeds.

Enantioselective Occlusion of the Amino Acid Monomers from Solution

As per the experiment [5], we assume that the X face exposed to solution occludes only the D-amino acids, whereas the Y face occludes only the L-amino acids:

$$\begin{aligned} \{\mathrm{L}_1\mathrm{X}_r\mathrm{D}_n\} + \mathrm{D}_1 &\overset{\xi_{r,n}}{\rightarrow} \{\mathrm{L}_1\mathrm{X}_r\mathrm{D}_{n+1}\}, \\ \{\mathrm{D}_1\mathrm{Y}_r\mathrm{L}_n\} + \mathrm{L}_1 &\overset{\xi_{r,n}}{\rightarrow} \{\mathrm{D}_1\mathrm{Y}_r\mathrm{L}_{n+1}\}. \end{aligned} \tag{43}$$

The corresponding rate $\xi_{r,n}$ could depend both on the size r of the glycine host and on the number n of previously occluded enantiomers. We assume the oriented host glycine crystal occludes one amino-acid monomer at a time. Crystallographic models suggest that single molecules, not clusters, are incorporated one at a time into the growing crystal. The notation in $\{\ldots\}$ is, reading from left to right, the orienting hydrophobic amino acid attached to the face exposed to air, the enantiotopic crystal face exposed to solution (composed of r-glycine monomers), and the number n of occluded amino acids from solution.

Growth of the Oriented Host Glycine Crystal

Growth of the enantiotopic face exposed to solution by take-up of the achiral glycine monomers from the solution is

$$\begin{aligned} \{\mathrm{L}_1\mathrm{X}_r\mathrm{D}_n\} + \mathrm{A}_1 &\overset{\alpha_{r,n}}{\rightarrow} \{\mathrm{L}_1\mathrm{X}_{r+1}\mathrm{D}_n\}, \\ \{\mathrm{D}_1\mathrm{Y}_r\mathrm{L}_n\} + \mathrm{A}_1 &\overset{\alpha_{r,n}}{\rightarrow} \{\mathrm{D}_1\mathrm{Y}_{r+1}\mathrm{L}_n\}. \end{aligned} \tag{44}$$

The newly acquired glycine monomers adopt the same orientation as their host-face. It is assumed that take-up involves one glycine monomer at a time. Here the rate $\alpha_{r,n}$ could in principle depend on r and n.

The above steps give a specific articulation of the scheme represented in Fig. 7 in terms of chemical transformations.

The next task is to transcribe the above processes into the corresponding differential rate equations. To this end, we introduce concentration variables $a_r(t) = [\mathrm{A}_r]$, $\mathrm{L}_1(t) = [\mathrm{L}_1]$, $\mathrm{D}_1(t) = [\mathrm{D}_1]$ and for the two host-plus-guest crystal orientations exposed towards the solution $f_{r,n}(t) = \{\mathrm{L}_1\mathrm{X}_r\mathrm{D}_n\}$ and $\bar{f}_{r,n}(t) = \{\mathrm{D}_1\mathrm{Y}_r\mathrm{L}_n\}$, respectively. We consider separately the kinetic equations for $f_{r,0}$, $f_{2,n}$, and then $f_{r,n}$ and

similarly for the other enantiotopic face orientation. That is, we can treat the growth of pure host crystal, growth of guest on minimal host substrate and then the general *mixed* growth of both host and guest. Remember $f_{r,k} = f_{\text{host,guest}}$, so there must be a minimum host size r to accommodate the occluded guests.

3.1.3 Some Simplifications of the Model

The main problem with the model as it stands is the large number of parameters that have been introduced, namely $\delta_{r,n}$, μ_r, $\alpha_{r,n}$, and $\xi_{r,n}$. It is thus clear that we need to make several simplifications already at this stage. We assume that only the coalescence of two glycine monomers A_1 to form an A_2 dimer needs to be retained, and only A_2 dimer clusters are used to form new oriented host crystals when they encounter a hydrophobic amino acid monomer. We also assume that all rates are independent of cluster size, so that

$$\delta_{1,1} = \delta, \quad \delta_{r,k} = 0 \quad (\text{otherwise}) \tag{45}$$

$$\mu_2 = \mu, \quad \mu_r = 0 \quad (r = 1 \text{ and } r \geq 3) \tag{46}$$

$$\alpha_{r,n} = \alpha, (r \geq 2), \quad \alpha_{1,n} = 0 \tag{47}$$

$$\xi_{r,n} = \xi, (r \geq 2), \quad \xi_{1,n} = 0. \tag{48}$$

3.2 *Complete Simplified Model*

There is a fundamental physical limitation imposed by the fact that the air-water interface used in the experiments is of finite area: the experiments are carried out in a bounded reaction domain which means only a finite air-water interface is available for the crucial orientation/amplification processes to take place. We thus need to model the effect of a bounded (finite area) interface. Once the interface is *covered* by floating glycine crystals, no more hydrophobic amino acids can diffuse up to the surface, and the remaining reactions from this point on can only be the glycine up-take from the solution and the enantioselective occlusion of the amino acids in solution. The finite size of the interface area implies that these latter two processes must be limited as well; we will thus consider how to truncate both the host growth as well as the number of occluded guests per host. The reactions will thus stop at some point: there must be maximum values of both R and N such that $2 \leq r \leq R$ and hosts $0 \leq n \leq N(R)$. Each instantaneous size r of the host crystal will be allowed to occlude up to maximum number $n(r)$ of guests. We can account for all of these limiting features by implementing certain truncations or cut-offs that we apply to the underlying model. At the same time, we complete the final model by including the kinetic inhibition effect.

3.2.1 Hydrophobic and Kinetic Effects Vs Hydrophobic and Hydrophilic Additives

The experiment demonstrates that the glycine crystals at the interface are oriented via two distinct effects: (1) hydrophobic and (2) kinetic. The former is due to the induction by hydrophobic amino acids while the latter is achieved through the inhibition of nucleation and growth of the oriented glycine crystals. The hydrophobic effect is confined to hydrophobic amino acids but the kinetic effect applies to all α-amino acid *additives*, both hydrophobic and hydrophilic. It is important to bear in mind that there is hence not a one-to-one correspondence between effects and additives. For this reason, in the full model below, we introduce the two kinds of additives and talk about the effect of the additives rather than the hydrophobic or kinetic effects per se, since the latter are not easily separable. The two effects, however, do act in the same direction. The inclusion of both types of additive leads to only a minor modification and leads to a complete model. As per the above discussion, we also implement a consistent truncation where R is maximum size of the glycine host crystal and $n = n(r)$ is a maximum number of occluded amino acid guest monomers for any instantaneous host size r. We summarize the effect of each type of additive in the table below.

Amino acid additive	Effect	
Hydrophobic	Hydrophobic orientation	Kinetic inhibition
Hydrophilic	–	Kinetic inhibition

For completeness, we list the full set of chemical reactions defining the final model. Formation of glycine crystals/clusters in solution:

$$\mathrm{A}_1 + \mathrm{A}_1 \xrightarrow{\delta} \mathrm{A}_2. \tag{49}$$

Diffusion of amino acids in bulk solution to interface implying nucleation of *oriented* glycine crystals at the air-water interface in presence of hydrophobic LD-amino acids is represented by

$$\begin{aligned} \mathrm{A}_2 + \mathrm{L}_1 &\xrightarrow{\mu(f_c)} \{\mathrm{L}_1\mathrm{X}_2\}, \\ \mathrm{A}_2 + \mathrm{D}_1 &\xrightarrow{\mu(f_c)} \{\mathrm{D}_1\mathrm{Y}_2\}. \end{aligned} \tag{50}$$

The effective conversion rate of bulk amino acids to amino acids at the interface will depend on a critical glycine crystal interface concentration f_c. Beyond this concentration, no more hydrophobic amino acids will diffuse up to the surface, and consequently no more fresh glycine crystals can nucleate at the surface. To implement this we will take a step-function dependence:

$$\mu(f_c) = \mu_0 \Theta(f_c - f(t)), \tag{51}$$

where $f(t)$ is the instantaneous concentration of glycine crystals, with and without occluded amino acids, at time t, and f_c is a critical surface concentration which is supposed to mimic effectively the finite area interface. Here

$$\mu(t) = \mu_0 \Theta\left(f_c - \sum_{r=2}^{R} \sum_{n=0}^{\Gamma} \left(f_{r,n}(t) + \bar{f}_{r,n}(t) \right) \right), \tag{52}$$

where the unit step function is defined as

$$\Theta(x) = \begin{cases} 1, & x>0 \\ 0, & x<0. \end{cases} \tag{53}$$

Once the instantaneous concentration of glycine crystals reaches f_c then reaction (50) shuts off, from which point on the hydrophobic orienting effect ceases to act. This is an effective way of implementing the finite interface area constraint without adding complicated spatial dependence to the model (i.e., diffusion, Laplacians, spatial boundary conditions, etc.).

In keeping with the above remarks and experimental facts, we must allow for hydrophobic amino acids to inhibit those glycine nuclei exposing their enantiotopic faces towards the solution from further growth. We also introduce a second species of hydrophilic amino acids $\overline{\mathrm{L}}, \overline{\mathrm{D}}$, which can only participate in the kinetic effect.

Inhibition of the fresh glycine seeds by kinetic effect due to the *hydrophobic* additives is as follows:

$$\begin{aligned} \{\mathrm{L}_1\mathrm{X}_2\} + \mathrm{D}_1 &\xrightarrow{\xi} \{\mathrm{L}_1\mathrm{X}_2\mathrm{D}_1\}, \\ \{\mathrm{D}_1\mathrm{Y}_2\} + \mathrm{L}_1 &\xrightarrow{\xi} \{\mathrm{D}_1\mathrm{Y}_2\mathrm{L}_1\}. \end{aligned} \tag{54}$$

Inhibition of the fresh glycine seeds by kinetic effect due to the *hydrophilic* additives:

$$\begin{aligned} \{\mathrm{L}_1\mathrm{X}_2\} + \overline{\mathrm{D}}_1 &\xrightarrow{\beta} \{\mathrm{L}_1\mathrm{X}_2\overline{\mathrm{D}}_1\}, \\ \{\mathrm{D}_1\mathrm{Y}_2\} + \overline{\mathrm{L}}_1 &\xrightarrow{\beta} \{\mathrm{D}_1\mathrm{Y}_2\overline{\mathrm{L}}_1\}. \end{aligned} \tag{55}$$

and the total inert product of inhibited crystal seeds (via either the hydrophobic or hydrophilic additives) will be denoted as $P(t)$. An excess of $\mathrm{L} > \mathrm{D}$ in solution inhibits glycine nuclei exposing their $(0\,\bar{1}\,0)$ towards solution [4], preventing their further growth, and analogously for $\mathrm{D} > \mathrm{L}$. We have opted to model this kinetic effect as a cross-inhibition reaction, in the spirit of the Frank model, except here we form a small tetramer unit with a glycine dimer trapped between the hydrophobic

templater and the hydrophilic growth inhibitor. The templater and growth inhibitor have opposite handedness. So, if the glycine host crystal occludes an amino acid having the opposite chirality of the nucleator amino and located on the opposite enantiotopic face, then the seed glycine crystal has been inhibited and cannot grow further. Otherwise, if the seed grows by incorporating a glycine monomer, it can escape this inhibition "bottleneck," and will continue to grow via glycine up-take and/or by amino acid occlusion.

The remainders of the reactions are unchanged, except that now we impose the finite size truncations (bounds on r and on n) mentioned above, as follows.

Growth of the oriented fresh glycine hosts:

$$\begin{aligned} \{\mathrm{L}_1\mathrm{X}_2\} + \mathrm{A}_1 &\xrightarrow{\alpha} \{\mathrm{L}_1\mathrm{X}_3\}, \\ \{\mathrm{D}_1\mathrm{Y}_2\} + \mathrm{A}_1 &\xrightarrow{\alpha} \{\mathrm{D}_1\mathrm{Y}_3\}. \end{aligned} \tag{56}$$

Growth of the oriented host glycine crystal:

$$\begin{aligned} \{\mathrm{L}_1\mathrm{X}_r\mathrm{D}_n\} + \mathrm{A}_1 &\xrightarrow{\alpha} \{\mathrm{L}_1\mathrm{X}_{r+1}\mathrm{D}_n\}, \\ \{\mathrm{D}_1\mathrm{Y}_r\mathrm{L}_n\} + \mathrm{A}_1 &\xrightarrow{\alpha} \{\mathrm{D}_1\mathrm{Y}_{r+1}\mathrm{L}_n\}, \\ (3 \le r \le R-1,\ \ 0 \le n \le \Gamma(r)). & \end{aligned} \tag{57}$$

Enantioselective occlusion of the amino acid monomers from solution:

$$\begin{aligned} \{\mathrm{L}_1\mathrm{X}_r\mathrm{D}_n\} + \mathrm{D}_1 &\xrightarrow{\xi} \{\mathrm{L}_1\mathrm{X}_r\mathrm{D}_{n+1}\}, \\ \{\mathrm{D}_1\mathrm{Y}_r\mathrm{L}_n\} + \mathrm{L}_1 &\xrightarrow{\xi} \{\mathrm{D}_1\mathrm{Y}_r\mathrm{L}_{n+1}\}, \\ (3 \le r \le R,\ \ 0 \le n \le \Gamma(r)-1). & \end{aligned} \tag{58}$$

Each host glycine crystal can grow by incorporating achiral glycine monomers from the solution, so we must impose a maximum number R of glycine monomers forming the host crystal. By the same token, we impose a maximum number of guest chiral monomers N to be occluded in the host crystal. The maximum number of guests that a crystal can occlude depends on the number of host monomers of the crystal, so we define a function $\Gamma(r)$ that simply rounds the elements of γr to the nearest integer less than or equal to γr and $0 < \gamma \le 1$ is a free parameter that allows us to vary the percentage of occluded amino acids. The full set of reaction steps is summarized in Fig. 8. Note that the processes in steps (3) and (4) in Fig. 8 are akin to Frank's mutual inhibition: the two enantiomers are joined together indirectly through the host glycine crystal. See also Fig. 9.

With these truncations and limits and for both types of additives, the final set of model kinetic equations reads as follows:

(1) Formation of glycine dimers in solution

$$A_1 + A_1 \xrightarrow{\delta} A_2$$

(2) Nucleation of oriented glycine crystals at the air/water interface in the presence of hydrophobic amino acids

$$A_2 + L_1 \xrightarrow{\mu(\vec{r}_i)} \{L_1X_2\}$$
$$A_2 + D_1 \xrightarrow{\mu(\vec{r}_i)} \{D_1Y_2\}$$

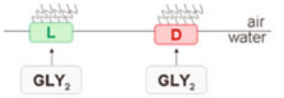

(3) Kinetic orienting effect which inhibits crystal growth:

- Inhibition of fresh glycine nuclei by kinetic effect due to hydrophobic additives

$$\{L_1X_2\} + D_1 \xrightarrow{\xi} \{L_1X_2D_1\}$$
$$\{D_1Y_2\} + L_1 \xrightarrow{\xi} \{D_1Y_2L_1\}$$

- Inhibition of fresh glycine nuclei by kinetic effect due to hydrophilic additives

$$\{L_1X_2\} + \overline{D}_1 \xrightarrow{\beta} \{L_1X_2\overline{D}_1\}$$
$$\{D_1Y_2\} + \overline{L}_1 \xrightarrow{\beta} \{D_1Y_2\overline{L}_1\}$$

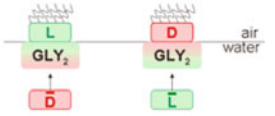

(4) Enantioselective occlusion of amino acid monomers from solution

$$\{L_1X_rD_n\} + D_1 \xrightarrow{\xi} \{L_1X_rD_{n+1}\}$$
$$\{D_1Y_rL_n\} + L_1 \xrightarrow{\xi} \{D_1Y_rL_{n+1}\}$$

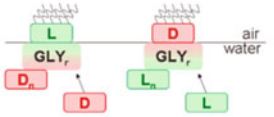

(5) Growth of oriented host glycine crystals at the interface:

- Growth of fresh glycine nuclei by up-take (escape the kinetic effect bottleneck)

$$\{L_1X_2\} + A_1 \xrightarrow{\alpha} \{L_1X_3\}$$
$$\{D_1Y_2\} + A_1 \xrightarrow{\alpha} \{D_1Y_3\}$$

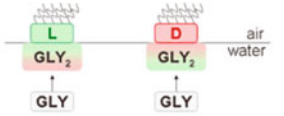

- Growth of oriented host glycine crystal (up-take)

$$\{L_1X_rD_n\} + A_1 \xrightarrow{\alpha} \{L_1X_{r+1}D_n\}$$
$$\{D_1Y_rL_n\} + A_1 \xrightarrow{\alpha} \{D_1Y_{r+1}L_n\}$$

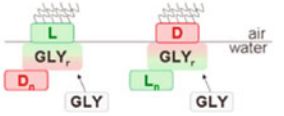

Fig. 8 The complete simplified model. Each of the five key steps is illustrated by a corresponding picture representing the chemical reaction taking place, where GLY denotes the glycine, $(\overline{\text{L}}, \overline{\text{D}})$ and (L, D) the enantiomers of the hydrophilic and hydrophobic amino acids, respectively

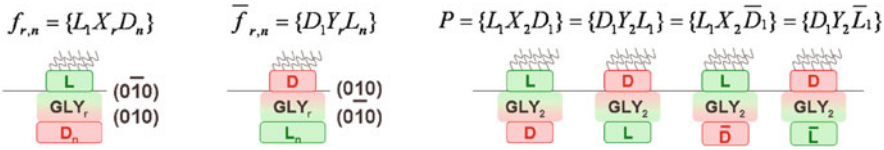

Fig. 9 Notation: the oriented glycine host plus occluded guest structures at the interface $(f_{r,n}, \bar{f}_{r,n})$, for r glycine monomers and n occluded guests. The crystals P that do not survive the kinetic inhibition "bottleneck." The *wiggly lines* represent the template formed by the hydrophobic amino acids that orient the glycine crystal at the air-solution interface

$$\frac{da_1}{dt} = -2\delta a_1^2 - \alpha a_1 \left(f_{2,0} + \bar{f}_{2,0} + \sum_{r=3}^{R-1} \sum_{n=0}^{\Gamma(r)} (f_{r,n} + \bar{f}_{r,n}) \right), \tag{59}$$

$$\frac{da_2}{dt} = \delta a_1^2 - \mu a_2 (\mathrm{L}_1 + \mathrm{D}_1), \tag{60}$$

$$\frac{d\mathrm{L}_1}{dt} = -\mu \mathrm{L}_1 a_2 - \xi \mathrm{L}_1 \left(\bar{f}_{2,0} + \sum_{r=3}^{R} \sum_{n=0}^{\Gamma(r)-1} \bar{f}_{r,n} \right), \tag{61}$$

$$\frac{d\mathrm{D}_1}{dt} = -\mu \mathrm{D}_1 a_2 - \xi \mathrm{D}_1 \left(f_{2,0} + \sum_{r=3}^{R} \sum_{n=0}^{\Gamma(r)-1} f_{r,n} \right), \tag{62}$$

$$\frac{d\overline{\mathrm{L}}_1}{dt} = -\beta \bar{f}_{2,0} \overline{\mathrm{L}}_1, \tag{63}$$

$$\frac{d\overline{\mathrm{D}}_1}{dt} = -\beta f_{2,0} \overline{R}_1, \tag{64}$$

$$\frac{dP}{dt} = \xi (\mathrm{D}_1 f_{2,0} + \mathrm{L}_1 \bar{f}_{2,0}) + \beta (\overline{\mathrm{D}}_1 f_{2,0} + \overline{\mathrm{L}}_1 \bar{f}_{2,0}), \tag{65}$$

$$\begin{aligned} \frac{df_{r,n}}{dt} =& \mathrm{A}(r,n) \mu \mathrm{L}_1 a_2 + \mathrm{B}(r,n) \xi \mathrm{D}_1 f_{r,n-1} - \mathrm{C}(r,n) \xi \mathrm{D}_1 f_{r,n} \\ &+ \mathrm{D}(r,n) \alpha a_1 f_{r-1,n} - \mathrm{E}(r,n) \alpha a_1 f_{r,n} - \mathrm{F}(r,n) \beta \overline{\mathrm{D}} f_{r,n}, \\ &(2 \le r \le R,\ 0 \le n \le \Gamma(r)) \end{aligned} \tag{66}$$

$$\begin{aligned}\frac{\mathrm{d}\bar{f}_{r,n}}{\mathrm{d}t} =& \mathrm{A}(r,n)\mu \mathrm{D}_1 a_2 + \mathrm{B}(r,n)\xi \mathrm{L}_1 \bar{f}_{r,n-1} - \mathrm{C}(r,n)\xi \mathrm{L}_1 \bar{f}_{r,n} \\ &+ \mathrm{D}(r,n)\alpha a_1 \bar{f}_{r-1,n} - \mathrm{E}(r,n)\alpha a_1 \bar{f}_{r,n} - \mathrm{F}(r,n)\beta \overline{\mathrm{L}} \bar{f}_{r,n}, \\ &(2 \le r \le R,\ 0 \le n \le \Gamma(r)). \end{aligned} \tag{67}$$

The oriented glycine host plus occluded guest structures at the interface are denoted by $(f_{r,n},\bar{f}_{r,n})$ for r glycine monomers and n occluded guests. The crystals that do not survive the kinetic inhibition "bottleneck" are denoted by P; see Fig. 9.

We have written a single differential equation for the $f_{r,n}$ and another for the $\bar{f}_{r,n}$, whose individual terms are switched on or off depending on the values of r,n. To this end, we define the following functions A, B, C, D, E and F:

$$\begin{aligned} A(r,n) &= 1 \quad \text{if} \quad r = 2 \text{ and } n = 0 \\ B(r,n) &= 1 \quad \text{if} \quad r \ge 3 \text{ and } n \ge 1 \\ C(r,n) &= 1 \quad \text{if} \quad (r = 2 \text{ and } n = 0)\,||\, \\ &\qquad\qquad (r \ge 3 \ \text{ and } \ n \le \Gamma(r) - 1) \end{aligned} \tag{68}$$

$$\begin{aligned} D(r,n) &= 1 \quad \text{if} \quad (r \ge 3 \text{ and } n \le \Gamma(r-1)) \\ E(r,n) &= 1 \quad \text{if} \quad (r = 2 \text{ and } n = 0)\,||\, \\ &\qquad\qquad (3 \le r \le R - 1) \end{aligned} \tag{69}$$

$$F(r,n) = 1 \quad \text{if} \quad r = 2 \text{ and } n = 0. \tag{70}$$

The above set of kinetic equations obeys the overall mass conservation condition monitored and verified in all the numerical simulations:

$$\begin{aligned} &\mathrm{L}_1 + \mathrm{D}_1 + \overline{\mathrm{L}}_1 + \overline{\mathrm{D}}_1 + 4P \\ &+ a_1 + 2a_2 + \sum_{r=2}^{R} \sum_{n=0}^{\Gamma(r)} (r + n + 1)(f_{r,n} + \bar{f}_{r,n}) = \text{const.} \end{aligned} \tag{71}$$

3.3 Simulation of the Model: Numerical Results

Numerical results are calculated in terms of a number of experimentally relevant chiral measures. The percent enantiomeric excess of the hydrophobic additives in solution is

$$\text{ee}\ (\%) = \frac{[\mathrm{L}_1] - [\mathrm{D}_1]}{[\mathrm{L}_1] + [\mathrm{D}_1]} \times 100. \tag{72}$$

When hydrophilic amino acids are added, a corresponding percent enantiomeric excess can also be defined:

$$\mathrm{ee}_h\ (\%) = \frac{[\overline{\mathrm{L}_1}] - [\overline{\mathrm{D}_1}]}{[\overline{\mathrm{L}_1}] + [\overline{\mathrm{D}_1}]} \times 100. \tag{73}$$

We consider the percent excess of the occluded amino acids via

$$\mathrm{ee}_{\mathrm{occlude}}\ (\%) = \frac{\mathrm{L}_{\mathrm{occluded}} - \mathrm{D}_{\mathrm{occluded}}}{\mathrm{L}_{\mathrm{occluded}} + \mathrm{D}_{\mathrm{occluded}}} \times 100. \tag{74}$$

In keeping with the experimental reports, this counts the amino acids occluded in the host crystal enantiotopic faces exposed to the solution. An important aspect of the experiment is the degree of crystal orientation at the interface. The following parameter measures the orientation degree (od) of the crystals at the interface:

$$\mathrm{od}\ (\%) = \frac{f - \bar{f}}{f + \bar{f}} \times 100, \tag{75}$$

and gives us a direct measure of the orientation. Here f and $\bar{f}$ are the total amount of crystal of each type (i.e., pyramids and plates [6]) at the surface (omitting the floating inhibited seeds):

$$f = \sum_{r=3}^{R} \sum_{n=0}^{\Gamma(r)} f_{r,n} \quad \bar{f} = \sum_{r=3}^{R} \sum_{n=0}^{\Gamma(r)} \bar{f}_{r,n}. \tag{76}$$

The main results are presented in terms of the types of additives employed, that is, hydrophobic and/or hydrophilic amino acids.

3.3.1 Hydrophobic Additives

In the following cases, only hydrophobic additives have been added to the saturated glycine solution. We maintain zero concentration of the hydrophilic additives $[\overline{\mathrm{L}_1}]_0 = [\overline{\mathrm{D}_1}]_0 = 0$ throughout the following set of simulations. All the numerical results have been obtained for the values $R = 50$, $\gamma = 0.1$, $\alpha = 10^{-3}$, $\delta = 10^{-6}$, $\xi = 1$, $\mu_0 = 10^{-6}$, and $f_c = 0.01$ M. The experiment reports that only a small fraction of the α-amino acids (0.02−0.2%) is subsequently occluded into the bulk of the growing glycine crystals. We therefore try to maximize the host crystal size R so as to be able to achieve small fractions of occluded guests. Computational limitations (essentially memory and time) forced us to compromise and we thus choose $R = 50$ and $\gamma = 0.1$ (for the desired values $\gamma = 0.0002 - 0.002$, the corresponding host size R is so great as to exceed available computational

Table 1 Orientation of floating glycine crystals in the presence of mixtures of (L, D)-hydrophobic additives

(L, D)-Hydrophobic (w/w_{gly})	$f + \bar{f}$ (mol L^{-1})	P (mol L^{-1})	od (%)	ee (%)	ee_{oc} (%)
10^{-4}	8.15×10^{-5}	4.38×10^{-6}	0	0	0
10^{-3}	6.33×10^{-4}	3.54×10^{-4}	0	0	0
10^{-2}	2.38×10^{-3}	1.51×10^{-2}	0	0	0
10^{-1}	3.48×10^{-3}	2.12×10^{-1}	0	0	0

resources). Next, we aimed to reproduce as closely as possible the reported details concerning the growth of crystals at the air-solution interface. The first step was to find reactions rates satisfying these conditions, as shown in Table 1. Since we do not have spatial information (and thus cannot distinguish between pyramids and plates), we tried to find the reaction rates (at least the relation between them) reproducing this behavior (supposing that pure platforms were the pyramids and the product of the inhibition yields the plates). This strategy led us to employ the values of α, γ, ξ and μ cited above.

We have used the same glycine concentrations as reported in the experiments [6]. Thus, in a typical experiment 10 g of glycine ($m_{gly} = 10$ g) were dissolved in 30 mL (Vol = 0.03 L) of double distilled water, where its molar mass $Mm_{gly} = 75.07$ g mol^{-1}. Following this, the initial glycine concentration should therefore be $[a_1]0 = m_{gly}/(Mm_{gly} \times Vol) = 4.44$ mol L^{-1}, and this is the value of initial glycine monomer concentration used in all the simulations. For the glycine dimers we initially set $[a_2]_0 = 0$, and zero initial concentrations of the oriented glycine crystals at the interface: $(f_{r,n})_0 = 0$ and $(\bar{f}_{r,n})_0 = 0$, respectively. Finally, from the initial enantiomeric excess ee_0 and the relative weight of additive to glycine, (w/w_{gly}), we can deduce the initial concentrations $[L]_0$ and $[D]_0$ straightforwardly from the pair of equations in (77):

$$[L]_0 = \frac{(w/w_{gly})m_{gly}(1 + ee_0)}{2Mm_{gly} \times Vol},$$
$$[D]_0 = \frac{(w/w_{gly})m_{gly}(1 - ee_0)}{2Mm_{gly} \times Vol}. \tag{77}$$

We ignore the molar mass differences Mm between glycine and the α-amino acid molar masses (Mm(Ala) = 89.09 g mol^{-1}, Mm(Leu) = 131.17 g mol^{-1}, Mm (Val) = 117.15 g mol^{-1}, Mm(Val) = 105.09 g mol^{-1}).

3.3.2 Racemic Mixtures of Hydrophobic Additives

The composition of the complete solution is obtained by adding a racemic hydrophobic additive to the supersaturated solution of glycine. We start with zero initial excess of chiral hydrophobic monomers, $ee_0 = 0$. We want to observe the effect of varying the relative mass of the chiral monomers with respect to the amount of

glycine (w/w_{gly}). The numerical results obtained in these simulations are shown in Table 1. For each relative initial concentration of additives (w/w_{gly}) we evaluate the total concentration $f + \bar{f}$ of the oriented mixed host plus guest crystals at the interface summed over both orientations, and P, the total concentration of nuclei or seed crystals killed by the kinetic inhibition effect and their associated chiral polarizations or excesses. Recall that *both* the hydrophobic and kinetic effects are operative for the hydrophobic amino acid additives.

From inspection of Table 1, for all cases the interface is covered with crystals of both orientations. This is not surprising, since we start from a racemic composition, but no initial "Adam" crystal; this must therefore lead to an equal ratio $f : \bar{f} = 1 : 1$ of the enantiotopic faces exposed to the solution, thus od(%) = 0. By the same token, the ee of the solution and the net ee_{oc} of occluded monomers must also be zero. There is no symmetry breaking in this idealized situation. In the actual experiments, floating glycine crystals can exhibit two distinct morphologies, either pyramidal or plates [5, 6]. The former are the result of the hydrophobic orienting effect, while the latter morphology results from the kinetic inhibition effect. Because of this, we can infer the crystal morphologies implicit in our simulations: indeed, the concentrations f and $\bar{f}$ correspond to the pyramidal form (resulting from the hydrophobic effect) whereas the concentration P corresponds to the plate-like form (resulting from the kinetic effect).

Thus for values of w/w_{gly} as low as 10^{-4} we found enantiomorphous pyramids showing no macroscopic evidence for the kinetic retardation of growth by, for example, leucine. By increasing the additive concentration, a *morphological change* of the floating glycine crystals is numerically observed, from pyramids $f + \bar{f}$ to plates P (inhibited seeds). The concentration of the pyramids decreases while that of the plates increases as we increase the concentration of the racemic additive. This simulation result is in qualitative accord with the experiment where an evident morphological change from pyramids to plates was observed upon increasing the leucine concentration (i.e., the hydrophobic additive employed there) [6]. The initially racemic amino acid solution remains racemic at all later times, no matter how large the initial amount of additives.

3.3.3 Racemic Mixture of Hydrophobic Additives + an Initial Oriented Glycine Crystal

The reaction scheme in Fig. 7 starts from a *first random crystallization*, so we include this feature in the initial conditions. We consider the previous situation ($ee_0 = 0$) and suppose that there is one single crystal of glycine exposing, say, the (0 1 0) face toward the solution at an initial time; this means starting with a small initial concentration of $(f_{2,0})_0$. Since only one initial crystal cannot be taken, it can be "modeled" taking by a fraction of the critical interface concentration f_c of glycine crystals: $(f_{2,0})_0 = x\,fc$, where $x \ll 1$ is given in the first column of Table 2. There we display the numerical results for this particular situation, starting from an initial concentration of (LD)-hydrophobic amino acids $w/w_{gly} = 0.01$. The simulation results

Table 2 Orientation of floating glycine crystals in the presence of mixtures of (L, D)-hydrophobic additives and "one" initial oriented crystal

$(f_{2,0})_0/fc$	$f + \bar{f}$ (mol L^{-1})	P (mol L^{-1})	od (%)	ee (%)	ee_{oc} (%)
0.01	3.02×10^{-3}	1.51×10^{-2}	30.04	100	7.10
0.05	4.59×10^{-3}	1.47×10^{-2}	62.46	100	21.55
0.1	6.11×10^{-3}	1.42×10^{-2}	76.32	100	33.60

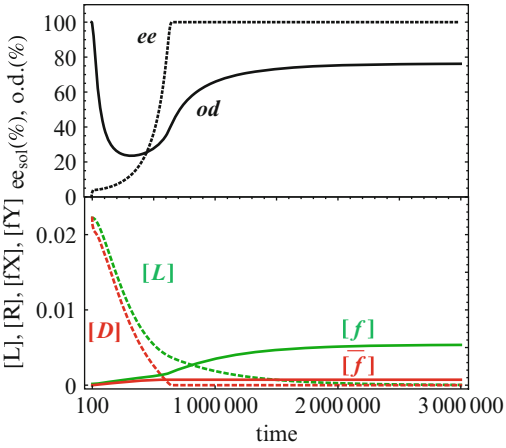

Fig. 10 Racemic mixture hydrophobic additives + an initial oriented glycine crystal. Initial conditions: $ee_0 = 0$, $w/w_{gly} = 0.01$, $[f_{2,0}]_0 = 10^{-3} f_c$, $ee_{h0} = 0$, and $w_h/w_{gly} = 0$. *Upper figure*: *the dotted line* represents the enantiomeric excess ee of solution and the *solid line* the orientation degree (od). *Lower figure*: *the dotted lines* represent the concentrations of the hydrophobic enantiomers (where [L] is the *upper dotted curve*), *the solid lines* represent the total concentration of oriented crystals (where [*f*] is the *upper solid curve*)

show a preferential (0 1 0) orientation of the glycine crystals at the surface induced by the initial (0 1 0) crystal. Even if this preferential orientation is not exclusively od $< 100\%$, an optically active solution is still generated, ee $= 100\%$.

The single crystal occludes the D enantiomers enantioselectively, thus enriching the aqueous solution with the L monomers. If this small excess can induce preferential orientation of the further growing crystals of glycine, again with the (0 1 0) face pointing toward the solution, replication will ensue by the cascade mechanism, finally leading to a separation of enantiomeric territories [6]. From Table 2 we see that increasing the initial concentrations of the first oriented Adam crystals leads to increased degree of orientation od, and to increased enantiomeric excesses of both the amino acids in solution, ee, and of those that have been occluded by the pyramidal crystals, ee_{oc}. Dynamical time-dependent aspects of the symmetry breaking can be appreciated from the time evolution of the concentrations and chiral excesses as displayed in Fig. 10.

Table 3 Orientation of floating glycine crystals induced by resolved L-hydrophobic additives (see Table 3) of [6])

(L)-Hydrophobic (w/w_{gly})	$f + \bar{f}$ (mol L^{-1})	P (mol L^{-1})	od (%)	ee (%)	ee_{oc} (%)
0.01	10^{-2}	0	100	100	–
0.05	10^{-2}	0	100	100	–
0.1	1.01×10^{-2}	0	100	100	–
0.5	1.02×10^{-2}	0	100	100	–

3.3.4 Chiral Hydrophobic Additives

Instead of racemic hydrophobic additives we next consider adding a chiral hydrophobic compound (i.e., L-α-amino acids) to the supersaturated solution of glycine. This means we now start with an initial excess of the chiral hydrophobic monomers in solution so that $ee_0 = 1$. Table 3 shows the results for different concentrations in terms of the quoted w/w_{gly} values. As expected, in the presence of a resolved hydrophobic α-amino acid, the system achieves exclusive orientation at the interface: od = 100% and the excess ee of the remaining amino acids in solution is 100%. In this situation, there can be no amino acids occluded by the oriented crystals at the interface since the system lacks the D-monomer, hence ee_{oc} is not defined. Moreover, without D monomers the kinetic effect is inoperative and so $P = 0$: no plates can be formed, only pyramidal crystals. When L-α-amino acids are used, these pyramids are exclusively (0 1 0) oriented (the face exposed towards the solution). By symmetry, D-amino acids would induce the enantiomorphous $(0\,\bar{1}\,0)$ oriented pyramids [6].

3.3.5 Hydrophilic Additives

We now treat the general situation where both hydrophobic and hydrophilic additives are added to the supersaturated glycine solution. As before, the following numerical results have been obtained for the values $R = 50$, $\gamma = 0.1$, $\alpha = 10^{-3}$, $\delta = 10^{-6}$, $\beta = \xi = 1$, $\mu_0 = 10^{-6}$, and $f_c = 0.01$ M. The initial glycine monomer concentration is $[a_1]0 = 4.44$ mol L^{-1} and for the initial glycine dimer concentration we set $[a_2]_0 = 0$ and zero initial concentrations of the oriented glycine crystals at the interface: $(f_{r,n})_0 = 0$, $(\bar{f}_{r,n})_0 = 0$. Controlling the amount of hydrophilic additives gives us an independent control of the kinetic inhibition effect.

3.3.6 Racemic Mixtures of Hydrophilic Additives

The complete amino acid solution is now composed of a mixture of both *racemic* hydrophobic α-amino acids and *racemic* hydrophilic α-amino acids. Here the role of the hydrophobic additive is merely to induce oriented crystallization at the air-water interface. Since its composition is racemic, this leads to an equal ratio

Table 4 Orientation of floating glycine crystals in the presence of racemic mixtures of hydrophilic additives and 1% hydrophobic (L, D) amino acids

(L, D)-Hydrophobic (w/w_{gly})	$f + \bar{f}$ (mol L^{-1})	P (mol L^{-1})	od (%)	ee (%)	ee_{oc} (%)
0	2.38×10^{-3}	1.51×10^{-2}	0	0	0
0.01	1.08×10^{-3}	2.86×10^{-2}	0	$0 \sim 10^{-8}$	0
0.05	3.44×10^{-4}	3.89×10^{-2}	0	$\sim 10^{-7}$	0
0.1	1.86×10^{-4}	4.14×10^{-2}	0	$\sim 10^{-5}$	0
0.5	3.99×10^{-5}	4.38×10^{-2}	0	$\sim 10^{-7}$	0

$f : \bar{f} = 1 : 1$ of enantiotopic faces exposed to the solution, and for this we use a concentration corresponding to $w/w_{gly} = 0.01$. Thus the corresponding initial excesses of chiral hydrophobic and hydrophilic monomers are $ee_0 = 0$ and $ee_{h0} = 0$, respectively. There is no initial Adam crystal. We then observe what effect, if any, varying the amount of the hydrophilic additives has on this initial orientation.

Numerical results showing the effect of varying the relative mass of hydrophilic chiral monomers (w/w_{gly}) are shown in Table 4. No matter how large the amount of hydrophilic monomers, in the presence of racemic additives of both types the surface is still covered with crystals of both orientations which immediately implies that the net excess of occluded monomers is zero. Note the solution achieves an extremely feeble optical activity. In fact these excesses are only slightly greater or at the same level as the enantiomeric excess expected from pure statistical fluctuations. Just as reported in the experiment, we observe how the amount of plates is much greater than the amount of enantiomorphous pyramids: $P > (f + \bar{f})$ [6]. The kinetic inhibition effect is clearly manifested.

3.3.7 Chiral Hydrophilic Additive

Just as in the previous simulation, the amino acid solution is composed of a racemic mixture of hydrophobic α-amino acids merely to induce the X:Y = 1:1 crystallization at the air-water interface and again we use $w/w_{gly} = 0.01$. However, in this case we add *chiral* hydrophilic additives, and without loss of generality we take the L enantiomer. This is then a situation described by the initial excesses of hydrophobic and hydrophilic monomers given by $ee_0 = 0$ and $ee_{h0} = 1$, respectively. Here we are interested in the effect of varying the relative mass of hydrophilic chiral monomers (w/w_{gly}). Table 5 presents the numerical results for this situation. As can be seen, the presence of a chiral hydrophilic additive induces a preferential orientation; it is an indirect mechanism since the kinetic effect inhibits the growth of the crystal nuclei that would otherwise expose the Y-face towards solution. Even if the orientation is not exclusive but only preferential, the solution becomes optically active for low concentrations of the hydrophilic additive. And from Table 5 we see that territorial separation of the enantiomers is achieved.

The hydrophilic additives have an indirect orienting effect upon the floating glycine crystals in that they inhibit or kill the glycine nuclei so that these are unable

Table 5 Orientation by kinetic effect of floating glycine crystals in the presence of resolved hydrophilic additives and 1% hydrophobic (L, D)

(L, D)-Hydrophobic (w/w_{gly})	$f + \bar{f}$ (mol L^{-1})	P (mol L^{-1})	od (%)	ee (%)	ee_{oc} (%)
0	2.38×10^{-3}	1.51×10^{-2}	0	0	0
10^{-6}	2.38×10^{-3}	1.51×10^{-2}	0.51	100	0.08
10^{-5}	2.51×10^{-3}	1.51×10^{-2}	8.43	100	1.56
10^{-4}	3.28×10^{-3}	1.52×10^{-2}	38.88	100	9.21
10^{-3}	6.10×10^{-3}	1.52×10^{-2}	79.03	100	33.36
10^{-2}	1.00×10^{-2}	1.51×10^{-2}	96.26	100	76.09
10^{-1}	1.00×10^{-2}	1.51×10^{-2}	99.51	100	96.60

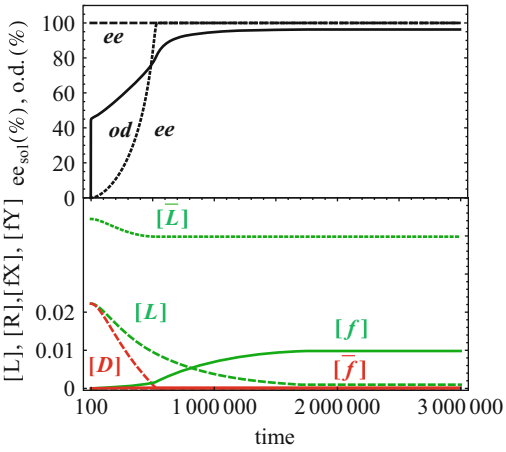

Fig. 11 Chiral hydrophilic additive. Initial conditions: $ee_0 = 0$, $w/w_{gly} = 0.01$, $ee_{h0} = 1$, $w_h/w_{gly} = 0.01$. *Upper figure*: *the dotted line* represents the enantiomeric excess ee of the hydrophobic additives in solution, the *solid line* the orientation degree (od), and the *dashed line* is the ee_h of the hydrophilic additive. *Lower figure*: *dotted lines* represent the concentrations of the hydrophobic additives (where [L] is the *upper dotted curve*), the *solid lines* represent the total amount of oriented crystals of each type ([f] is the *upper solid curve*), and *dashed line* represents the hydrophilic monomer concentration: [$\bar{L}$]

to occlude. Only the hydrophobic additives can directly induce orientation. A typical time evolution of the symmetry breaking in this situation is depicted in Fig. 11.

3.3.8 Hydrophobic Vs Hydrophilic Additives

Next we study how hydrophobic and hydrophilic additives of *opposite* chirality compete to induce a preferential orientation of the glycine crystals at the interface. To emphasize this competition, the amino acid solution will be composed of strictly

Table 6 Orientation of floating glycine crystals by hydrophobic effect in the presence of resolved hydrophilic additives and 1% (w/w_{gly}) hydrophobic amino acids of the opposite configuration

(D)-Hydrophilic (w/w_{gly})	$f + \bar{f}$ (mol L^{-1})	P (mol L^{-1})	od (%)	ee (%)	ee_{oc} (%)
0.01	1.86×10^{-3}	4.26×10^{-2}	100	100	0
0.05	2.15×10^{-4}	4.42×10^{-2}	100	100	0
0.1	1.04×10^{-4}	4.43×10^{-2}	100	100	0
0.5	2.04×10^{-4}	4.44×10^{-2}	100	100	0

(L)-hydrophobic and (D)-hydrophilic α-amino acids. So initially we have $ee_0 = 1$, $ee_{h0} = -1$. Take the (L)-hydrophobic additive concentration to be $w/w_{gly} = 0.01$, and we vary the (D)-hydrophilic additive concentration. Table 6 shows there is a clear ability of the resolved hydrophobic α-amino acids to induce a specific orientation of the floating glycine crystals, even in the presence of large excesses of the hydrophilic α-amino acids of the opposite absolute configuration [6]. This can be compared with Table 4 of [6], which established experimentally the *dominance* of the hydrophobic effect over the kinetic inhibition effect. Note: in our model, ee_{oc} is zero in this situation since there are no D hydrophobic monomers that would otherwise be occluded.

3.3.9 The Amplification Step

The hydrophobic resolved α-amino acids are advantageous for such a study with respect to the hydrophilic ones because both the kinetic inhibitory effect and the stabilization of the nuclei by hydrophobic effect act in the same direction for orientation of the growing floating crystals of glycine. For this reason, we next study the crystallization of glycine in the presence of partially enriched mixtures of (L, D)-hydrophobic amino acids at various concentrations.

The presence of an excess of hydrophobic (D)-amino acids will favor the (0 1 0) oriented nucleation at the interface while at the same time preventing the growth of (0 $\bar{1}$ 0) oriented crystals from the solution. The experimental [6] correlation between the initial enantiomeric excess of the solution with the total concentration needed to obtain complete orientation of the floating glycine crystals is reproduced in Fig. 12 for comparison.

The correlation between the initial enantiomeric excess of the solution and the total concentration needed to obtain *maximum* orientation of the floating glycine crystals is shown in Fig. 13. The point we wish to make here is simply that our model succeeds in capturing the general *trend* observed in the experiment, namely that smaller initial enantiomeric excesses require greater initial hydrophobic amino acid concentrations in order to achieve a (maximal) crystal orientation. Figure 14 shows the temporal evolution of this situation.

Experimental proof that hydrophobic effect plays a dominant role in the orientation of the glycine crystals can be deduced from Table 4 of [6]. Nevertheless, both effects are always present for the hydrophobic amino acids: those in solution contribute to the

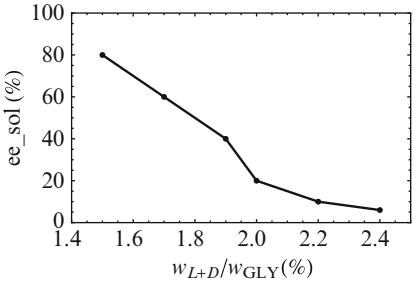

Fig. 12 Correlation between the initial leucine enantiomeric excess in solution and the total concentration needed for the complete $(0\,\bar{1}\,0)$ orientation of the floating glycine crystals. Adapted from [6]

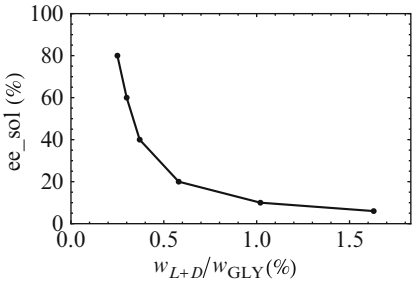

Fig. 13 Correlation between the initial enantiomeric excess of the hydrophobic additive in solution and the total concentration needed for the *maximal* $(0\,\bar{1}\,0)$ orientation of the floating glycine crystals. See text for discussion

inhibitory kinetic effect; this is depicted in Fig. 12. This also explains why, at higher concentrations, the glycine plates observed in the experiment are so thin. At lower initial ee, the higher concentrations needed appear to forbid formation of floating plates altogether [6].

4 Homochiral Oligopeptides by Lattice Controlled Chiral Amplification

In the transition from prebiotic racemic chemistry to chiral biology, one scenario suggests that homochiral peptides must have appeared before the appearance of the primeval enzymes [37, 38]. While several stochastic synthetic routes for mirror symmetry breaking that convert racemates into nonracemates have been described [39, 40], the generation of long bio-like polymers [37] made up of repeating units of the same handedness requires elaboration of new synthetic routes. Polymerization reactions of racemic mixtures of monomers in solution are typically expected to

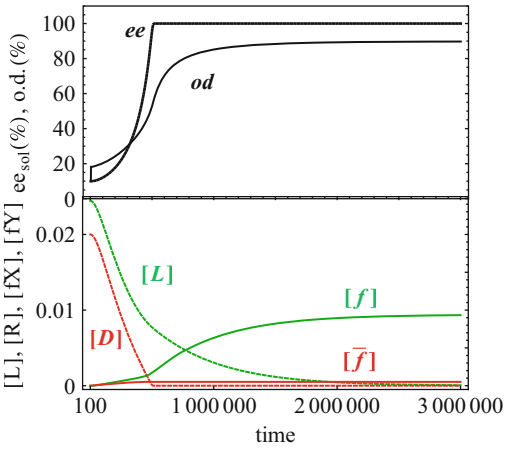

Fig. 14 Partially enriched mixtures of (L, D)-hydrophobic amino acids. Initial conditions: $ee_0 = 0.1$, $w/w_{gly} = 0.01$, $ee_{h0} = 0$, $w_h/w_{gly} = 0$. *Upper figure*: the orientation degree (od; *solid line*) and the enantiomeric excess ee in solution (*dotted line*). *Lower figure*: concentration of the hydrophobic monomers (the *upper dotted curve* is [L]). *Solid lines* represent the concentration of oriented crystals ([*f*] is the *upper solid curve*)

yield polymers composed of random sequences of the left-handed and right-handed repeat units following a binomial or Bernoulli distribution. Thus the probability for obtaining oligomers with homochiral sequence becomes negligible with increasing chain length [37].

Recent investigations have proposed that *N*-carboxyanhydride (NCA) [41, 42] and thioester derivatives [43] of amino acids might have operated as relevant precursors for the formation of the early peptides [44]. Results on the polymerization of NCA monomers in organic solvents [45–50], in water [51–53], and in the solid state [54, 55] have been published. Luisi and coworkers [26, 56–58] have reported the polymerization of racemic α-amino acids in solution which yields small amounts of oligopeptides of homochiral sequence whose abundances with respect to the heterochiral chains exhibit a slight departure from the binomial distribution.

This problem of random distribution can be overcome by catalyzed polymerization of amphiphilic amino acids, in racemic and nonracemic forms, which self-assemble into two-dimensional ordered crystallites at the air-water interface [59, 60]. Based on a process involving self-assembly followed by lattice controlled polymerization, Lahav and coworkers recently proposed a general scenario for the generation of homochiral oligopeptides of a single handedness from non-racemic mixtures of activated α-amino acids [59, 60]. Initial non-racemic mixtures undergo a phase separation by self-assembly into a 2D racemic crystalline phase and a separate enantiomorphous 2D phase of the enantiomer in excess. Each of these crystalline phases has markedly different chemical properties, thus yielding products that differ in the composition of the oligomers. So, polymerization within the enantiomorphous

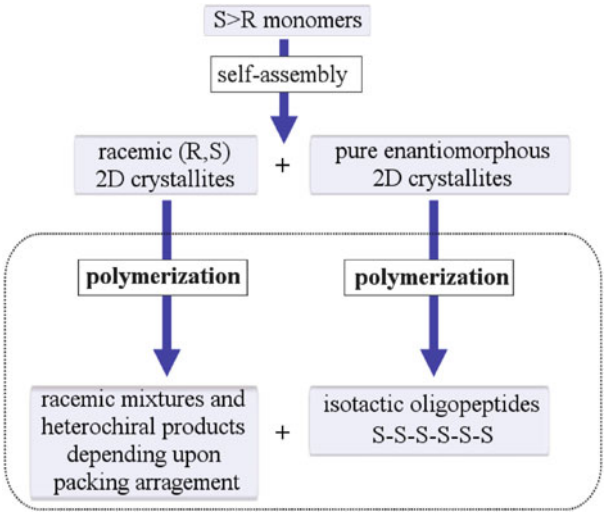

Fig. 15 Scheme for the chiral amplification process starting from non-racemic mixtures of monomers undergoing a phase separation by self-assembly at the air-water interface, as originally proposed by the authors of [60]. Our model is concerned with the effective polymerization controlled by each of the two crystalline phases, the processes outlined by the box

crystalline phase yields homochiral oligopeptides of one handedness whereas the reaction controlled by the racemic crystallites yields racemic mixtures and heterochiral products. The combination of the two routes leads to an overall chiral amplification process; see Fig. 15.

It is important to clarify at the outset what specific aspect of the overall experimental mechanism we want to model here and the way we aim to do so. The proposed experimental scheme starts from an initial excess, say $S > R$, of monomers which undergoes an initial self-assembly process into two types of two-dimensional crystallites at the air-water interface. Once formed, each of these two crystal phases participates in the control of a subsequent type of polymerization. Thus, the racemic crystallites polymerize racemic mixtures of oligomers and the heterochiral products, whereas the other pure enantiomorphous crystallite controls the polymerization of the isotactic chains (see Fig. 15); these are formed from the monomer in excess (S in this example). However, the details of the polymerizations depend in a complicated way upon the specific *packing arrangements* of the crystal monomers and the possible *reaction pathways* taken within each crystallite phase. Below we review a model that can account for these complications in an indirect effective way.

4.1 The Chiral Copolymerization Model

Our starting point is a simple model for the copolymerization of two chemically distinct monomers displaying a wide variety of product sequence compositions.

The model discussed here [61] is an appropriately modified, corrected, and extended version of the model considered by Wattis and Coveney [62].

The main important differences compared to prior and related models are that (1) we consider polymerization in *closed* systems [24], so that no matter flow is permitted with an external environment and (2) we allow for reversible monomer association steps. We also correctly include the formation (and dissociation) of the heterodimer [24], an important detail that was overlooked in [62]. It turns out that this must be treated on a separate basis in order to avoid double counting which, if left unchecked, would lead to a violation in the constant mass constraint. Once the heterodimer is treated correctly, this implies that the hetero-trimer must also be treated separately. Beyond this, the remainder of the hetero-oligomers can be treated in a collective and uniform way.

We introduce the notation to be used. Polymers are classified by three quantities: the number of A monomers of which it is composed (subscript r), the number of B monomers which it contains (subscript s), and the final or terminal monomer in the chain, denoted by a superscript. In this scheme the monomers are denoted by $\mathrm{A} = \mathrm{C}^{\mathrm{A}}_{1,0}$ and $\mathrm{B} = \mathrm{C}^{\mathrm{B}}_{0,1}$; pure homopolymers are denoted by $\mathrm{C}^{\mathrm{A}}_{r,0}$ and $\mathrm{C}^{\mathrm{B}}_{0,s}$; all copolymer chains $\mathrm{C}^{\mathrm{A}}_{r,s}$ or $\mathrm{C}^{\mathrm{B}}_{r,s}$ with $r,s \geq 1$ are heteropolymers. Note also that chains of the form $\mathrm{C}^{\mathrm{A}}_{0,s}$ and $\mathrm{C}^{\mathrm{B}}_{r,0}$ are forbidden. The corresponding time-dependent concentrations are denoted by lower case variables, e.g., $c^{\mathrm{A}}_{r,s}(t)$ and $c^{\mathrm{B}}_{r,s}(t)$. The model is then defined by the following reactions, in which equilibrium is maintained between the finite monomer pool and the ensemble of copolymers:

$$\mathrm{C}^{\mathrm{A}}_{r,s} + \mathrm{A} \underset{k^*_{aa}}{\overset{k_{aa}}{\rightleftharpoons}} \mathrm{C}^{\mathrm{A}}_{r+1,s}, \tag{78}$$

$$\mathrm{C}^{\mathrm{A}}_{r,s} + \mathrm{B} \underset{k^*_{ab}}{\overset{k_{ab}}{\rightleftharpoons}} \mathrm{C}^{\mathrm{B}}_{r,s+1}, \tag{79}$$

$$\mathrm{C}^{\mathrm{B}}_{r,s} + \mathrm{A} \underset{k^*_{ba}}{\overset{k_{ba}}{\rightleftharpoons}} \mathrm{C}^{\mathrm{A}}_{r+1,s}, \tag{80}$$

$$\mathrm{C}^{\mathrm{B}}_{r,s} + \mathrm{B} \underset{k^*_{bb}}{\overset{k_{bb}}{\rightleftharpoons}} \mathrm{C}^{\mathrm{B}}_{r,s+1}. \tag{81}$$

This model can accommodate any two chemically distinct monomers. For the purpose of this review, we consider the case when $\mathrm{A} = R$ and $\mathrm{B} = S$ are two enantiomers.

The overall basic scheme must be broken down into several special subcases, especially important so as to avoid the undesired double counting of the heterodimer and heterotrimer reactions; see Fig. 16. Once we treat these special cases, we can then pass to the corresponding set of differential rate equations for the concentrations [61].

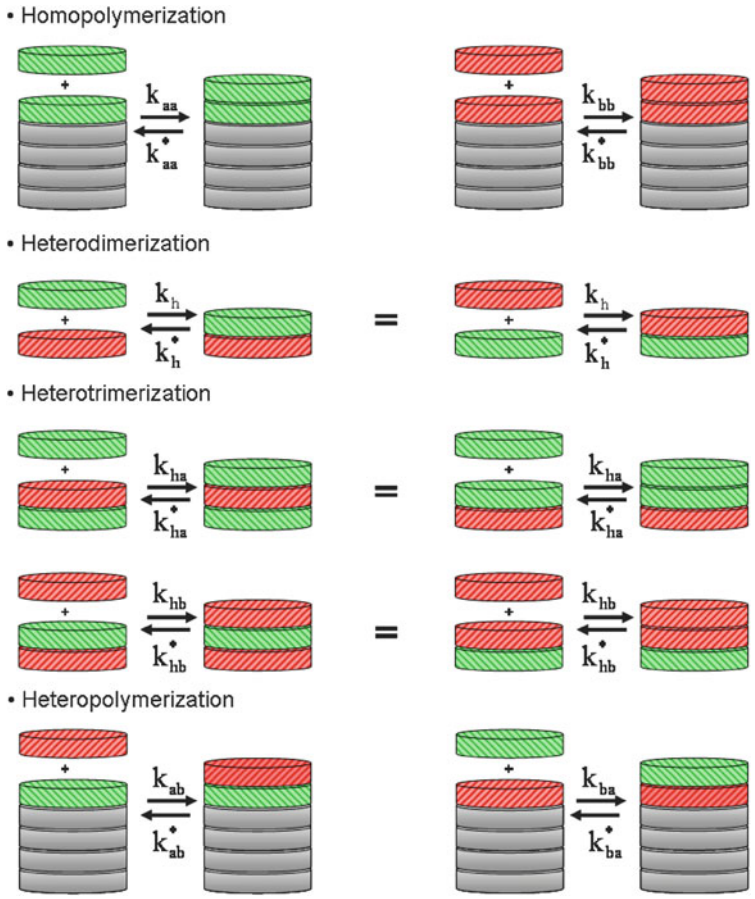

Fig. 16 The copolymerization model. The (*R*)-chiral (*red*) and (*S*)-chiral (*green*) monomers reversibly associate into the growing homochiral (*top*) or heterochiral (*bottom*) copolymer chains. Because the system is *closed*, both the heterodimer (*second line*) and hetero-trimer (*third* and *fourth lines*) reactions must be treated separately to avoid double counting and thus ensure that the total system mass is conserved in a closed system (see text for an explanation)

The formation of chirally pure polymer chains denoted by $c^{\mathrm{A}}_{n,0}$ and $c^{\mathrm{B}}_{0,n}$ for $1 \leq n \leq N$–1 is described by the homo-polymerization reactions

$$C^{\mathrm{A}}_{n,0} + \mathrm{C}^{\mathrm{A}}_{1,0} \underset{k^*_{aa}}{\overset{k_{aa}}{\rightleftharpoons}} \mathrm{C}^{\mathrm{A}}_{n+1,0} \quad \mathrm{C}^{\mathrm{B}}_{0,n} + \mathrm{C}^{\mathrm{B}}_{0,1} \underset{k^*_{bb}}{\overset{k_{bb}}{\rightleftharpoons}} \mathrm{C}^{\mathrm{B}}_{0,n+1}. \tag{82}$$

N is the maximum chain length permitted. In our recently reported work [24] we considered that once a monomer has been added to a homopolymer of the opposite chirality (that is, "the wrong" monomer), the polymer is inhibited and further growth is halted. This polymer could not directly react anymore and could only

lose its wrong terminal monomer through the inverse reaction. In the present model, we assume that such a chain can continue to grow by adding monomers of both configurations. So, for $2 < n < N - 1$, the heteropolymerization or inhibition-like reactions are as follows:

$$\mathrm{C}^{\mathrm{A}}_{n,0} + \mathrm{C}^{\mathrm{B}}_{0,1} \underset{k^*_{ab}}{\overset{k_{ab}}{\rightleftharpoons}} \mathrm{C}^{\mathrm{B}}_{n,1} \quad \mathrm{C}^{\mathrm{B}}_{0,n} + \mathrm{C}^{\mathrm{A}}_{1,0} \underset{k^*_{ba}}{\overset{k_{ba}}{\rightleftharpoons}} \mathrm{C}^{\mathrm{A}}_{1,n}. \tag{83}$$

For both homo-polymerization and heteropolymerization reactions, represented by Eqs. (82) and (83), the upper limits specified for n ensure that the *maximum* length for all oligomers produced (or consumed) by these reaction sets, both the homochiral and heterochiral ones, is never greater than N. For the remainder of this discussion we will consider the natural and chiral symmetric reaction rate assignments $k_{aa} = k_{bb}, k_{ab} = k_{ba}$ and likewise for the inverse rates, $k^*_{aa} = k^*_{bb}$ and $k^*_{ab} = k^*_{ba}$, reducing the number of independent rate constants to just four.

Even if we have the information about the composition, we can only know the chirality of the last monomer attached to the chain; we have no information regarding the specific *sequence*. This implies that the following two reactions are indistinguishable:

$$\mathrm{C}^{\mathrm{A}}_{1,0} + \mathrm{C}^{\mathrm{B}}_{0,1} \underset{k^*_{ab}}{\overset{k_{ab}}{\rightleftharpoons}} \mathrm{C}^{\mathrm{B}}_{1,1} \quad \mathrm{C}^{\mathrm{B}}_{0,1} + \mathrm{C}^{\mathrm{A}}_{1,0} \underset{k^*_{ba}}{\overset{k_{ba}}{\rightleftharpoons}} \mathrm{C}^{A}_{1,1}. \tag{84}$$

Thus for all practical purposes, $\mathrm{C}^{\mathrm{A}}_{1,1} \equiv \mathrm{C}^{\mathrm{B}}_{1,1}$, and this suggests using the following notation: $\mathrm{C}_{1,1} \equiv \mathrm{C}^{\mathrm{A}}_{1,1} \equiv \mathrm{C}^{\mathrm{B}}_{1,1}$ and defining a unique direct constant rate $k_h = \frac{k_{ab}+k_{ba}}{2}$ and an inverse one $k^*_h = \frac{k^*_{ab}+k^*_{ba}}{2}$. Note that if $k_{ab} = k_{ba}$, then $k_h = k_{ab} = k_{ba}$. Due to these characteristics, we will treat the heterodimer in a different way compared with the other heteropolymers. The reaction of the heterodimer formation is therefore

$$\mathrm{C}^{\mathrm{A}}_{1,0} + \mathrm{C}^{\mathrm{B}}_{0,1} \underset{k^*_h}{\overset{k_h}{\rightleftharpoons}} \mathrm{C}_{1,1}. \tag{85}$$

As before, the reactants and products in Eq. (85) are the same, so the differences in the free energy between initial and final states should be the same in all the reactions in these equations, implying the following thermodynamic constraint on the reaction rates:

$$\frac{k_{ab}}{k^*_{ab}} = \frac{k_{ba}}{k^*_{ba}}. \tag{86}$$

If the heterodimer formation were not to be treated in the separate way as we have done, and were to be included, e.g., in Eq. (83) by merely changing the lower limits for n ($2 \leq n \leq N - 1$) by $1 \leq n \leq N - 1$, we would be making the mistake of double counting it. The same occurs for the heteropolymers formed from the

addition of a monomer to a heterodimer. The two reactions of each pair of the following equations are also indistinguishable:

$$\mathrm{C}_{1,1} + \mathrm{C}^{\mathrm{A}}_{1,0} \underset{k^*_{aa}}{\overset{k_{aa}}{\rightleftharpoons}} \mathrm{C}^{\mathrm{A}}_{2,1} \quad \mathrm{C}_{1,1} + \mathrm{C}^{\mathrm{A}}_{1,0} \underset{k^*_{ba}}{\overset{k_{ba}}{\rightleftharpoons}} \mathrm{C}^{\mathrm{A}}_{2,1} \tag{87}$$

$$\mathrm{C}_{1,1} + \mathrm{C}^{\mathrm{B}}_{0,1} \underset{k^*_{bb}}{\overset{k_{bb}}{\rightleftharpoons}} \mathrm{C}^{\mathrm{B}}_{1,2} \quad \mathrm{C}_{1,1} + \mathrm{C}^{\mathrm{B}}_{0,1} \underset{k^*_{ab}}{\overset{k_{ab}}{\rightleftharpoons}} \mathrm{C}^{\mathrm{B}}_{1,2}. \tag{88}$$

Again, it is convenient to define the following direct reaction rates for these steps, $k_{ha} = \frac{k_{aa}+k_{ba}}{2}$, $k_{hb} = \frac{k_{bb}+k_{ab}}{2}$, and inverse $k^*_{ha} = \frac{k^*_{aa}+k^*_{ba}}{2}$, $k^*_{hb} = \frac{k^*_{bb}+k^*_{ab}}{2}$ Note that if $k_{aa} = k_{bb}$ and $k_{ab} = k_{ba}$, then $k_{ha} = k_{hb}$, and if $k^*_{aa} = k^*_{bb}$ and $k^*_{ab} = k^*_{ba}$, then $k^*_{ha} = k^*_{hb}$.

The reactions to consider are then

$$\mathrm{C}_{1,1} + \mathrm{C}^{\mathrm{A}}_{1,0} \underset{k^*_{ha}}{\overset{k_{ha}}{\rightleftharpoons}} \mathrm{C}^{\mathrm{A}}_{2,1} \quad \mathrm{C}_{1,1} + \mathrm{C}^{\mathrm{B}}_{0,1} \underset{k^*_{hb}}{\overset{k_{hb}}{\rightleftharpoons}} \mathrm{C}^{\mathrm{B}}_{1,2}. \tag{89}$$

As we have already remarked, in our model, as in the earlier one for open systems [62], the polymeric chains that have taken up the "wrong" chirality monomer can continue to grow. Thus, we allow for the further growth of these chains by adding monomers of either chirality. This kind of polymerization reaction for $2 \leq n \leq N-2$ is given by

$$\mathrm{C}^{\mathrm{A}}_{1,n} + \mathrm{C}^{\mathrm{A}}_{1,0} \underset{k^*_{aa}}{\overset{k_{aa}}{\rightleftharpoons}} \mathrm{C}^{\mathrm{A}}_{2,n} \quad \mathrm{C}^{\mathrm{B}}_{n,1} + \mathrm{C}^{\mathrm{B}}_{0,1} \underset{k^*_{bb}}{\overset{k_{bb}}{\rightleftharpoons}} \mathrm{C}^{\mathrm{B}}_{n,2} \tag{90}$$

$$\mathrm{C}^{\mathrm{A}}_{1,n} + \mathrm{C}^{\mathrm{B}}_{0,1} \underset{k^*_{ab}}{\overset{k_{ab}}{\rightleftharpoons}} \mathrm{C}^{\mathrm{B}}_{1,n+1} \quad \mathrm{C}^{\mathrm{B}}_{n,1} + \mathrm{C}^{\mathrm{A}}_{1,0} \underset{k^*_{ba}}{\overset{k_{ba}}{\rightleftharpoons}} \mathrm{C}^{\mathrm{A}}_{n+1,1}. \tag{91}$$

and for $2 \leq r \leq N-2, 1 \leq 1 \leq s \leq N-1-r$,

$$\mathrm{C}^{\mathrm{A}}_{r,s} + \mathrm{C}^{\mathrm{A}}_{1,0} \underset{k^*_{aa}}{\overset{k_{aa}}{\rightleftharpoons}} \mathrm{C}^{\mathrm{A}}_{r+1,s} \quad \mathrm{C}^{\mathrm{B}}_{r,s} + \mathrm{C}^{\mathrm{B}}_{0,1} \underset{k^*_{bb}}{\overset{k_{bb}}{\rightleftharpoons}} \mathrm{C}^{\mathrm{B}}_{r,s+1}. \tag{92}$$

$$\mathrm{C}^{\mathrm{A}}_{r,s} + \mathrm{C}^{\mathrm{B}}_{0,1} \underset{k^*_{ab}}{\overset{k_{ab}}{\rightleftharpoons}} \mathrm{C}^{\mathrm{B}}_{r,s+1} \quad \mathrm{C}^{\mathrm{B}}_{r,s} + \mathrm{C}^{\mathrm{A}}_{1,0} \underset{k^*_{ba}}{\overset{k_{ba}}{\rightleftharpoons}} \mathrm{C}^{\mathrm{B}}_{r+1,s}. \tag{93}$$

Note that in the elementary reaction steps, in the rate constants, and in the corresponding differential rate equations (see Appendix), the left-right symmetry of the model is manifest, that is, possesses a discrete Z_2 symmetry. This symmetry can be broken spontaneously by the dynamical solutions of the differential rate equations, and thus this model is suitable for studying SMSB. The complete

transcription from the individual reactions to corresponding kinetic equations employed in the simulations is spelled out in full detail in [61] and collected in the Appendix for completeness.

4.2 Fitting the Copolymerization Model to the Data

We apply our copolymerization model to fit the experimental data measured by the Rehovot group, so our primary goal is to reproduce as closely as possible the details reported concerning the experiments on chiral amplification of oligopeptides. For this purpose, the first step is to determine the initial monomer concentrations to be employed in the simulations. The actual experiments were carried out for 0.5 mM solutions of monomers; thus we have employed for each case: (1) $R{:}S = 1{:}1$ which corresponds to an initial enantiomeric excess $\mathrm{ee}_0 = 0\%$, so $c^{\mathrm{A}}_{1,0}(0) = 0.25\,\mathrm{mM}$ and $c^{\mathrm{B}}_{0,1}(0) = 0.25\,\mathrm{mM}$; (2) $R{:}S = 4{:}6$ corresponding to $\mathrm{ee}_0 = 20\%$, so $c^{\mathrm{A}}_{1,0}(0) = 0.2$ mM and $c^{\mathrm{B}}_{0,1}(0) = 0.3\,\mathrm{mM}$; (3) $R{:}S = 3{:}7$ which corresponds to $\mathrm{ee}_0 = 40\%$, so $c^{\mathrm{A}}_{1,0}(0) = 0.15\,\mathrm{mM}$ and $c^{\mathrm{B}}_{0,1}(0) = 0.35\,\mathrm{mM}$. The remainder of the initial concentrations (the dimers and on up) are taken to be strictly zero. Next, we systematically search for the reaction rates leading to the best fit to the given data.

Four different chemical model systems were used in the experiments, namely γ-stearyl-glutamic thioethyl ester (C_{18}–TE–Glu), N^{ε}-stearoyl-lysine thioethyl ester (C_{18}–TE–Lys), γ-stearyl-glutamic acid *N*-carboxyanhydride (C_{18}–Glu–NCA), and γ-stearyl-glutamic thioacid (C_{18}–thio–Glu), varying both their initial compositions and choices of catalyst. The composition of the oligopeptides formed was analyzed by matrix-assisted laser desorption/ionization time-of-flight mass spectroscopy (MALDI-TOF) with enantio-labeled samples. The experimental relative abundances of the oligopeptides was inferred from the ion intensity. These are the relative abundances that we aim to interpret vis-à-vis our copolymerization model.

Since only the experiments with racemic mixtures of the starting compounds required a catalyst, it is reasonable to expect that the racemic and the chiral enriched cases will follow different dynamics for a given chemical model system. That is, the presence or absence of a specific catalyst affects the rate constants for a given chemical system. First we will find the reaction rates for the racemic case, and afterwards those for the enriched chiral case, allowing us to compare both. The a priori nine free parameters we must set to run the numerical integrations [61] are comprised by the four direct and the four inverse rate constants k_{aa}, k_{bb}, k_{ab}, k_{ba}, and k^*_{aa}, k^*_{bb}, k^*_{ab}, k^*_{ba}, plus the maximum polymer chain length, *N*. We set all the inverse reaction rates to a unique value, $k^*_{aa} = k^*_{bb} = k^*_{ab} = k^*_{ba} = 10^{-10}(\mathrm{s}^{-1})$, implying an almost irreversible scheme, and we determine the remainder of the parameters from fitting the copolymerization model to the relative abundance data. This required numerical integration of the set of differential equations which follow after transcribing the above transformation steps [61].

Results from fitting the model to the data indicate that the maximum chain length N does not play a significant role and the calculated Pearson product–moment correlation coefficient, r, remains the same for $N = 12, 14, 16, 18, 20$, so we will set $N = 12$ for all compounds and cases treated below. Since the number of independent equations grows as N^2, this represents an important reduction of computer time and memory used. We note that one is free to scale out the dependence of one pair of reaction constants from the rate equations by a suitable redefinition of the time variable. Thus, without loss of generality, we set the cross inhibition rates equal to unity, $k_{ab} = k_{ba} = 1\ \mathrm{s}^{-1}\ \mathrm{mol}^{-1}$, and then search for the reaction rates $k_{aa} = k_{bb}$ leading to the best fits.

4.2.1 Racemic Mixtures

In one set of experiments, the authors reported MALDI-TOF analysis of the oligopeptides formed at the air-water interface from racemic mixtures $R{:}S = 1{:}1$ of the monomers for the various model systems and catalysts. We first fit the copolymerization model to this data.

The best correlation data for the racemic C_{18}–TE–Glu system, with the I_2/KI catalyst are found for $k_{aa} = k_{bb} = 1.7\ \mathrm{s}^{-1}\ \mathrm{mol}^{-1}$. In this case, the best fit obtains for the time scale $t = 10^{11}$ (s). Exactly by the same process, the best correlation data for the racemic C_{18}–TE–Lys are found for $k_{aa} = k_{bb} = 2.3\ \mathrm{s}^{-1}\ \mathrm{mol}^{-1}$ and for $k_{aa} = k_{bb} = 1.3\ \mathrm{s}^{-1}\ \mathrm{mol}^{-1}$ when adding I_2/KI and $AgNO_3$ as catalyst, respectively. For the simulations, we took the times $t = 10^{10}$ (s) and $t = 10^{11}$ (s) in the racemic cases with I_2/KI and $AgNO_3$, respectively. Finally, we fit our copolymerization model to the C_{18}–thio–Glu experimental relative abundances. The authors of the experiments affirmed that this compound undergoes a truly random polymerization, so fits from our model are expected to be slightly less satisfactory than those for the binomial distribution function. Setting the inverse reaction rates and the cross inhibition as indicated above, the best correlation coefficients are found for $k_{aa} = k_{bb} = 0.4\ \mathrm{s}^{-1}\ \mathrm{mol}^{-1}$. The instant or time-scale leading to these numerical values is $t = 10^{10}$ (s).

The corresponding (experimental and numerical) relative abundances for the four compounds cited above corresponding to these values are shown in Fig. 17. The histograms show the relative abundance of each experimentally obtained oligopeptide compared to the best fit from our copolymerization model (Table 7). We emphasize that we fit the model to the complete family of stereoisomer subgroups (that is, a global fit).

In the case of the C_{18}–Glu–NCA model system with catalyst $Ni(CH_3CO_2)_2$, the best fit is obtained for $k_{aa} = k_{bb} = 0.2\ \mathrm{s}^{-1}\ \mathrm{mol}^{-1}$.

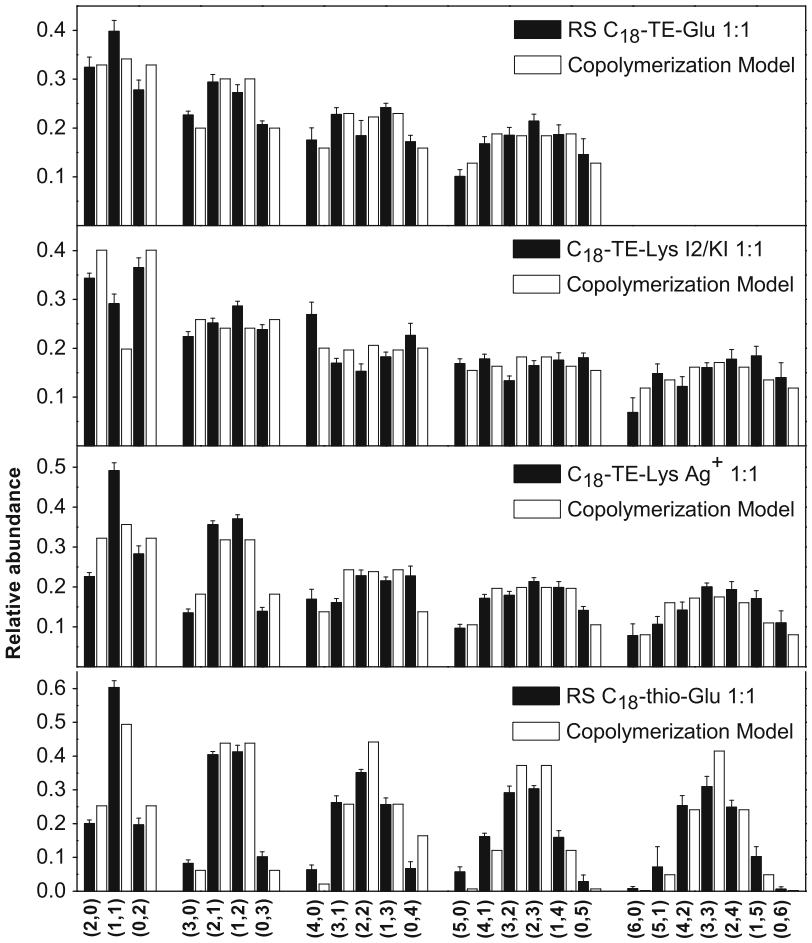

Fig. 17 Relative abundance vs number of repeat units (r, s) of the oligopeptides obtained from fitting the model (*white*) to the experimental data (*black*) from racemic mixtures R:S = 1:1 of monomers. The four chemical models are indicated by the *insets*

Table 7 Comparative fits between the copolymerization model and the binomial distribution (Bin.) to the experimental relative abundances: racemic mixtures R:S = 1:1 of monomers of the four model chemical systems as indicated in the leftmost column

	Copolymerization model						Bin.
	Fits for each subgroup n						
r	di	tri	tetra	penta	hexa	Global fit	Global fit
C_{18}–TE–Glu	0.92	0.96	0.80	0.84	–	0.93	0.75
C_{18}–TE–Lys(I_2/KI)	0.96	−0.82	−0.11	−0.73	0.45	0.85	0.32
C_{18}–TE–Lys(Ag)	0.98	1	0.03	0.88	0.76	0.84	0.8
C_{18}–thio–Glu	1	1	1	0.98	0.97	0.95	0.98

Only in the case of C_{18}–thio–Glu does the binomial distribution give a better global fit than the copolymerization model: this latter system provides an experimental reference system for random polymerization [60]

Table 8 Comparative fits between the copolymerization model and the binomial distribution (Bin.) to the experimental relative abundances measured for non-racemic mixtures of C_{18}–TE–Glu

	Copolymerization model						Bin.
	Fits for each subgroup *n*						
r	di	tri	tetra	penta	hexa	Global fit	Global fit
(*R*:*S*) 4:6	0.86	0.89	0.93	0.99	–	0.94	0.75
(*R*:*S*) 3:7	0.95	0.94	0.96	0.99	0.99	0.95	0.85

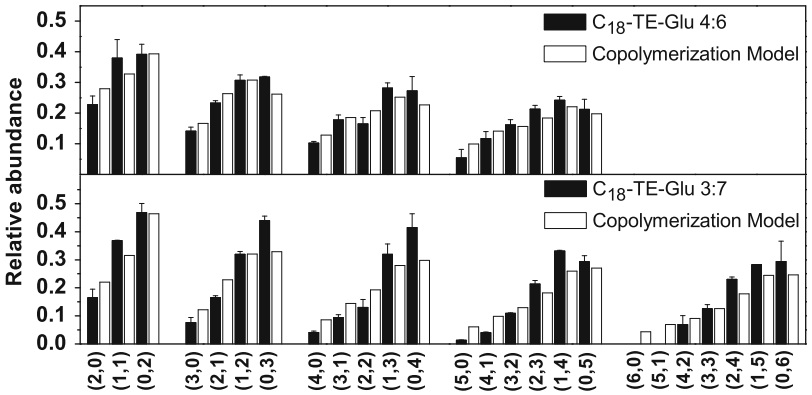

Fig. 18 Relative abundance vs number of chiral repeat units (*r*, *s*) of the oligopeptides obtained from fitting the model (*white*) to the experimental data (*black*) from non-racemic mixtures of monomers for the C_{18}–TE–Glu system

Table 9 Enantiomeric excesses, ee*:* numerical results from the copolymerization model (experimental data) for the relative abundances of the homochiral oligopeptides for the C_{18}–TE–Glu system

ee (%)	di	tri	tetra	penta	hexa
(*R*:*S*) 4:6	18 (26)	24 (39)	30 (46)	35 (59)	–
(*R*:*S*) 3:7	37 (48)	48 (71)	57 (82)	66 (92)	73 (>99.8)

4.2.2 Chirally Enriched Mixtures

In a second set of experiments the authors reported MALDI-TOF analysis of the oligopeptides formed at the air-water interface from non-racemic mixtures of the monomers for the same model systems. No catalysts were employed there. We next consider fits of our copolymerization model to these data sets.

The best correlations factors for both chiral enriched mixture cases (20% and 40% excesses) in the case of the C_{18}–TE–Glu system are found for the same rates, that is for $k_{aa} = k_{bb} = 2\ s^{-1}\ mol^{-1}$. The results for these values are shown in Table 8. In Fig. 18 we display the relative abundances of the homochiral oligopeptides and in Table 9 both the calculated and experimental enantiomeric

Table 10 Results for the copolymerization model and experimental data correlations for non-racemic mixtures of C_{18}–TE–Lys

	Copolymerization model							Bin.
	Fits for each subgroup n							
r	di	tri	tetra	penta	hexa	hepta	Global fit	Global fit
(R:S) 4:6	0.78	1	0.87	0.90	0.84	0.97	0.89	0.46
(R:S) 3:7	0.93	1	0.95	0.97	0.99	–	0.94	0.65

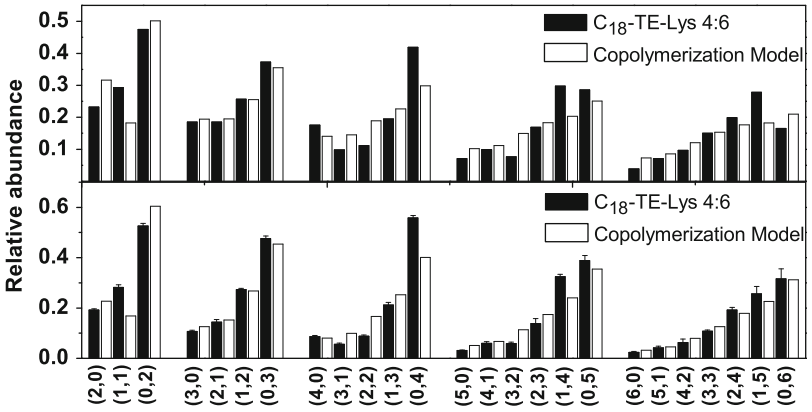

Fig. 19 Relative abundance vs number of repeat units (r, s) of the oligopeptides obtained from fitting the model (*white*) to the experimental data (*black*) from non-racemic mixtures of monomers of C_{18}–TE–Lys

Table 11 Enantiomeric excesses: numerical results from the copolymerization model (experimental data in parenthesis) for the relative abundances of the homochiral oligopeptides for C_{18}–TE–Lys

ee (%)	di	tri	tetra	penta	hexa	hepta
(R:S) 4:6	23 (34)	30 (34)	36 (41)	42 (60)	49 (62)	54 (>99.8)
(R:S) 3:7	45 (46)	57 (63)	66 (73)	75 (85)	81 (86)	–

excesses for the 4:6 and 3:7 (R:S) mixtures. Numerical results for the non-racemic case have been found for the time scale $t = 10^{11}$ (s).

For the chiral mixtures of C_{18}–TE–Lys we found the best fits for the dynamics corresponding to $k_{aa} = k_{bb} = 2.5\ \mathrm{s}^{-1}\ \mathrm{mol}^{-1}$. The results for these values are shown in Table 10. The relative abundances results for these values are shown in Fig. 19 and the enantiomeric excesses obtained for 4:6 and 3:7 (R:S) mixtures are presented in Table 11. For the simulations here we took $t = 10^{10}$ (s) for the chirally enriched mixtures.

Table 12 Results for the copolymerization model and experimental data correlations for non-racemic mixtures of C_{18}–thio–Glu

	Copolymerization model							Bin.
	Fits for each subgroup *n*							
r	di	tri	tetra	penta	hexa	hepta	Global fit	Global fit
(*R*:*S*) 4:6	0.93	0.98	0.93	0.92	0.92	0.91	0.91	0.93
(*R*:*S*) 3:7	0.89	1	0.99	0.99	0.98	–	0.96	0.97

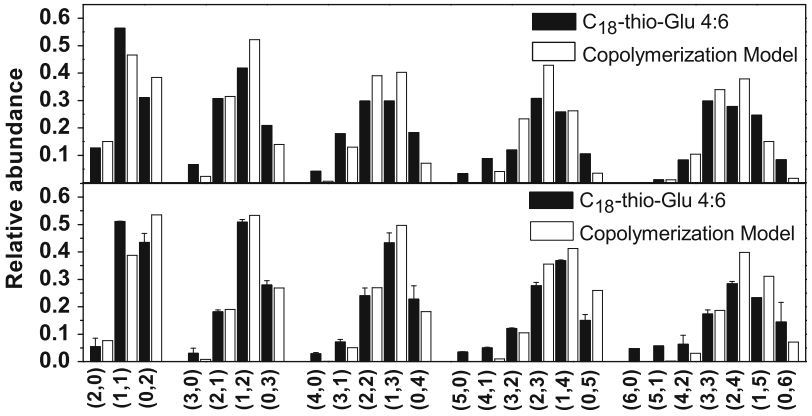

Fig. 20 Relative abundances vs number of repeat units (*r*, *s*) of the oligopeptides obtained from fitting the model (*white*) to the experimental data (*black*) for the non-racemic mixtures of C_{18}–thio–Glu

In the case of nonracemic C_{18}–thio–Glu, the best correlation coefficients are found for the same values of the reaction rates that we found in the racemic case, namely for $k_{aa} = k_{bb} = 0.4\ s^{-1}\ mol^{-1}$. Results for the chiral cases are shown in Table 12. As is to be expected and as shown there, the correlation factors for the global fit to the binomial distribution function are slighter better than those for any simulation we could perform with the copolymerization model, so we reconfirm what was claimed by the authors of the experimental work: namely that the C_{18}–thio–Glu system polymerizes randomly. In Fig. 20 the relative abundances of the oligopeptides are shown.

To summarize, the main features of the fitted model are as follows:

- The correlation factor between experimental and numerical data is greater for the copolymerization model than for the binomial distribution.
- The correlation is also greater for the non-initially racemic situations, and the higher the initially chiral enrichment of the mixture, the better the copolymerization model reproduces the chemical data.
- The results obtained lead us to affirm that the system is undergoing a non-random polymerization (except for the C_{18}–thio–Glu), as was originally argued by the authors of the experiments.

5 Summary and Discussion

A recent kinetic analysis of the Frank model in systems *closed* to matter and energy flow applied to the Soai reaction [8] indicates that, in actual chemical scenarios, reaction networks that exhibit SMSB are extremely sensitive to chiral inductions due to the presence of inherent tiny initial enantiomeric excesses [23]. This amplification feature is also operative in much more involved reaction networks such as chiral polymerization [24]. When the system is subject to a very small perturbation about an extremely dilute racemic state, the initial chiral fluctuation does not immediately decay but becomes amplified and drives the system along a long-lived chiral excursion in phase space before final and inevitable approach to the stable racemic solution. We have reviewed the nature of such chiral excursions within the setting of the Frank model, combining methods from phase space, linear stability analysis, and direct numerical simulation. Despite its relative simplicity, the Frank model lies at the heart of more involved schemes of chiral symmetry breaking and amplification, including the two experimental processes modeled here. In the case of the glycine plus α-amino acid system, the mutual inhibition comes into play through the enantioselective occlusion as well as through the kinetic inhibition effect. In the case of the lattice controlled polymerization, cross inhibition is manifest in the steps leading to formation of the hetero-oligomers. We further note in this regard that Mauksch and Tsogoeva have also previously indicated that chirality could appear as the result of a temporary asymmetric amplification [63, 64].

We have reviewed a mathematical model we developed recently for achieving resolution of racemic solutions of α-amino acids and glycine into enantiomeric territories based on a chemical scheme proposed some years ago by the Rehovot group. Those crystallization experiments provide a simple and elegant model for the generation and amplification of optically active amino acids in prebiotic conditions. Our mathematical model results from translating this proposed chemical scheme into basic reaction steps and then into a corresponding system of coupled nonlinear differential rate equations which we then integrate numerically to test out the hypothesized mechanisms and to underscore the salient features of the original experiment.

The glycine and α-amino acid system may be relevant to the origin of optical activity as it involves compounds that are among the simplest building blocks of life. In this vein it is interesting to point out that a recent prebiotic synthesis of "proto-biopolymers" under alkaline ocean conditions has yielded a variety of amino acids with glycine being the most abundant [33]. In addition, in an astrophysical context, amino acids have been detected in room-temperature residues of UV-irradiated interstellar ice analogs, and again glycine was found to be the most abundant amino acid [65].

The polymerization within two-dimensional crystallites composed of racemic compounds appropriately packed can lead to the enhanced generation of oligopeptides with homochiral sequences via lattice controlled reactions between

molecules of the same handedness. We have reviewed the key aspects of a copolymerization model we introduced recently for explaining the relative abundances of the oligomers observed in these experiments.

The authors of these experiments stated that the connection between the monomer packing arrangements in the crystallites and the resultant composition of the various diastereoisomeric products is "not straightforward" [60]. We therefore strove for a simple model for interpreting the data. This led us to consider a copolymerization model for the interpretation of the experimental data. The model may be termed *effective* in the sense that it presupposes or takes as given the *prior* formation of the self-assembled 2D crystallites at the air-water interface and is concerned exclusively with the *subsequent* co-polymerization reactions. Thus the complicated microscopic details referring to the monomer packing arrangements and reaction pathways within the crystallite self-assemblies are treated implicitly with our rate constants. Our fitted copolymerization reaction rates satisfactorily account for the different chemical properties of the two crystalline phases (racemic 2D crystallites and pure enantiomorphous 2D crystallites) that lead to the formation of racemic mixtures, heterochiral products, and isotactic oligopeptides. We contrast the fits from our model with those assuming a purely random process that obeys a binomial distribution. The final justification for considering such an effective model rests on its ability to yield good fits to the data. The goodness of the fits obtained demonstrates that the experimental data can be fit convincingly as if the simple scheme depicted graphically in Fig. 16 was the sole mechanism leading to the observed relative abundances. This then gives additional meaning to term "effective," and in the operational sense. We believe this effective nature of relatively simple mathematical models is a guiding principle that can be profitably exploited for modeling many other chemical systems.

Finally, it has been proposed that self assemblies of amphiphilic molecules have played a role in the earliest stages of evolution in the formation of primitive membranous minimum protocells [66, 67]. The lattice controlled polymerization scheme whose mathematical modeling is reviewed here suggests that ordered self assembled architectures of appropriate amphiphiles in aqueous media or on mineral surfaces might have been crucial in the formation of the first optically active biopolymers.

Acknowledgements The authors are grateful to Professor Josep M. Ribó (University of Barcelona) and to Professor Meir Lahav (Weizmann Institute of Science) for collaboration and for many useful discussions over the past few years which have helped to shape and temper our own perspectives on the subject of chiral symmetry breaking and chiral amplification at the molecular level. DH acknowledges the Grant AYA2009-13920-C02-01 from the Ministerio de Ciencia e Innovación (Spain) and forms part of the COST Action CM07030: *Systems Chemistry*. CB acknowledges a Calvo-Rodés graduate student contract from the Instituto Nacional de Técnica Aeroespacial (INTA).

Appendix

The differential rate equations for the chiral copolymerization scheme [61] are collected here. We begin with the rate equations for the two enantiomers:

$$\begin{aligned}
\frac{\mathrm{d}c^{\mathrm{A}}_{1,0}}{\mathrm{d}t} =& -k_{aa}c^{\mathrm{A}}_{1,0}\left(2c^{\mathrm{A}}_{1,0}+\sum_{n=2}^{N-1}c^{\mathrm{A}}_{n,0}+\sum_{n=2}^{N-2}c^{\mathrm{A}}_{1,n}+\sum_{r=2}^{N-2}\sum_{s=1}^{N-1-r}c^{\mathrm{A}}_{r,s}\right)\\
&-k_{ba}c^{\mathrm{A}}_{1,0}\left(\sum_{n=2}^{N-1}c^{\mathrm{B}}_{0,n}+\sum_{n=2}^{N-2}c^{\mathrm{B}}_{n,1}+\sum_{s=2}^{N-2}\sum_{r=1}^{N-1-s}c^{\mathrm{B}}_{r,s}\right)\\
&-k_{h}c^{\mathrm{A}}_{1,0}c^{\mathrm{B}}_{0,1}-k_{ha}c^{\mathrm{A}}_{1,0}c_{1,1}+k^{*}_{aa}\left(2c^{\mathrm{A}}_{2,0}+\sum_{n=3}^{N}c^{\mathrm{A}}_{n,0}+\sum_{n=2}^{N-2}c^{\mathrm{A}}_{2,n}+\sum_{r=3}^{N-1}\sum_{s=1}^{N-r}c^{\mathrm{A}}_{r,s}\right)\\
&+k^{*}_{ba}\left(\sum_{n=2}^{N-1}c^{\mathrm{A}}_{1,n}+\sum_{n=2}^{N-2}c^{\mathrm{A}}_{2,n}+\sum_{r=3}^{N-1}\sum_{s=1}^{N-r}c^{\mathrm{A}}_{r,s}\right)+k^{*}_{h}c_{1,1}+k^{*}_{ha}c^{\mathrm{A}}_{2,1},
\end{aligned}$$

$$\begin{aligned}
\frac{\mathrm{d}c^{\mathrm{B}}_{0,1}}{\mathrm{d}t} =& -k_{bb}c^{\mathrm{B}}_{0,1}\left(2c^{\mathrm{B}}_{0,1}+\sum_{n=2}^{N-1}c^{\mathrm{B}}_{0,n}+\sum_{n=2}^{N-2}c^{\mathrm{B}}_{n,1}+\sum_{s=2}^{N-2}\sum_{r=1}^{N-1-s}c^{\mathrm{B}}_{r,s}\right)\\
&-k_{ab}c^{\mathrm{B}}_{0,1}\left(\sum_{n=2}^{N-1}c^{\mathrm{A}}_{n,0}+\sum_{n=2}^{N-2}c^{\mathrm{A}}_{1,n}+\sum_{r=2}^{N-2}\sum_{s=1}^{N-1-r}c^{\mathrm{A}}_{r,s}\right)\\
&-k_{h}c^{\mathrm{A}}_{1,0}c^{\mathrm{B}}_{0,1}-k_{hb}c^{\mathrm{B}}_{0,1}c_{1,1}+k^{*}_{bb}\left(2c^{\mathrm{B}}_{0,2}+\sum_{n=3}^{N}c^{\mathrm{B}}_{0,n}+\sum_{n=2}^{N-2}c^{\mathrm{B}}_{n,2}+\sum_{s=3}^{N-1}\sum_{r=1}^{N-s}c^{\mathrm{B}}_{r,s}\right)\\
&+k^{*}_{ab}\left(\sum_{n=2}^{N-1}c^{\mathrm{B}}_{n,1}+\sum_{n=2}^{N-2}c^{\mathrm{B}}_{n,2}+\sum_{s=3}^{N-1}\sum_{r=1}^{N-s}c^{\mathrm{B}}_{r,s}\right)+k^{*}_{h}c_{1,1}+k^{*}_{hb}c^{\mathrm{B}}_{1,2}.
\end{aligned}$$

The equations describing the concentration of the homopolymers, for $2 \leq n \leq N-1$:

$$\begin{aligned}
\frac{\mathrm{d}c^{\mathrm{A}}_{n,0}}{\mathrm{d}t} &= k_{aa}c^{\mathrm{A}}_{1,0}\left(c^{\mathrm{A}}_{n-1,0}-c^{\mathrm{A}}_{n,0}\right)-k_{ab}c^{\mathrm{A}}_{n,0}c^{\mathrm{B}}_{0,1}+k^{*}_{aa}\left(c^{\mathrm{A}}_{n+1,0}-c^{\mathrm{A}}_{n,0}\right)+k^{*}_{ab}c^{\mathrm{B}}_{n,1},\\
\frac{\mathrm{d}c^{\mathrm{B}}_{0,n}}{\mathrm{d}t} &= k_{bb}c^{\mathrm{B}}_{0,1}\left(c^{\mathrm{B}}_{0,n-1}-c^{\mathrm{B}}_{0,n}\right)-k_{ba}c^{\mathrm{B}}_{0,n}c^{\mathrm{A}}_{1,0}+k^{*}_{bb}\left(c^{\mathrm{B}}_{0,n+1}-c^{\mathrm{B}}_{0,n}\right)+k^{*}_{ba}c^{\mathrm{A}}_{1,n}.
\end{aligned}$$

It is necessary to treat the kinetic equations of the maximum length N homopolymers individually. Since these do not elongate further, they cannot directly react, and cannot be the product of an inverse reaction involving a longer chain:

$$\frac{\mathrm{d}c^{\mathrm{A}}_{N,0}}{\mathrm{d}t} = k_{aa}c^{\mathrm{A}}_{1,0}c^{\mathrm{A}}_{N-1,0} - k^{*}_{aa}c^{\mathrm{A}}_{N,0},$$
$$\frac{\mathrm{d}c^{\mathrm{B}}_{0,N}}{\mathrm{d}t} = k_{bb}c^{\mathrm{B}}_{0,1}c^{\mathrm{B}}_{0,N-1} - k^{*}_{bb}c^{\mathrm{B}}_{0,N}.$$

The differential equations describing the concentration of each type of heteropolymer (included the heterodimer), for $2 \leq n \leq N-2$:

$$\frac{\mathrm{d}c_{1,1}}{\mathrm{d}t} = k_h c^{\mathrm{A}}_{1,0}c^{\mathrm{B}}_{0,1} - k_{ha}c_{1,1}c^{\mathrm{A}}_{1,0} - k_{hb}c_{1,1}c^{\mathrm{B}}_{0,1} - k^{*}_{h}c_{1,1} + k^{*}_{ha}c^{\mathrm{A}}_{2,1} + k^{*}_{hb}c^{\mathrm{B}}_{1,2},$$
$$\frac{\mathrm{d}c^{\mathrm{A}}_{1,n}}{\mathrm{d}t} = -k_{aa}c^{\mathrm{A}}_{1,0}c^{\mathrm{A}}_{1,n} - k_{ab}c^{\mathrm{B}}_{0,1}c^{\mathrm{A}}_{1,n} + k_{ba}c^{\mathrm{B}}_{0,n}c^{\mathrm{A}}_{1,0} + k^{*}_{aa}c^{\mathrm{A}}_{2,n} + k^{*}_{ab}c^{\mathrm{B}}_{1,n+1} - k^{*}_{ba}c^{\mathrm{A}}_{1,n},$$
$$\frac{\mathrm{d}c^{\mathrm{B}}_{n,1}}{\mathrm{d}t} = -k_{bb}c^{\mathrm{B}}_{0,1}c^{\mathrm{B}}_{n,1} - k_{ba}c^{\mathrm{A}}_{1,0}c^{\mathrm{B}}_{n,1} + k_{ab}c^{\mathrm{A}}_{n,0}c^{\mathrm{B}}_{0,1} + k^{*}_{bb}c^{\mathrm{B}}_{n,2} + k^{*}_{ba}c^{\mathrm{A}}_{n+1,1} - k^{*}_{ab}c^{\mathrm{B}}_{n,1}.$$

It is useful to treat individually the maximum length polymers N:

$$\frac{\mathrm{d}c^{\mathrm{A}}_{1,N-1}}{dt} = k_{ba}c^{\mathrm{B}}_{0,N-1}c^{\mathrm{A}}_{1,0} - k^{*}_{ba}c^{\mathrm{A}}_{1,N-1},$$
$$\frac{\mathrm{d}c^{\mathrm{B}}_{N-1,1}}{\mathrm{d}t} = k_{ab}c^{\mathrm{A}}_{N-1,0}c^{\mathrm{B}}_{0,1} - k^{*}_{ab}c^{\mathrm{B}}_{N-1,1}.$$

Each kind of trimer $c^{\mathrm{A}}_{2,1}$ and $c^{\mathrm{B}}_{1,2}$ must have its own differential equation in terms of k_{ha}, k_{hb}:

$$\frac{\mathrm{d}c^{\mathrm{A}}_{2,1}}{\mathrm{d}t} = -k_{aa}c^{\mathrm{A}}_{1,0}c^{\mathrm{A}}_{2,1} - k_{ab}c^{\mathrm{B}}_{0,1}c^{\mathrm{A}}_{2,1} + k_{ha}c_{1,1}c^{\mathrm{A}}_{1,0} + k^{*}_{aa}c^{\mathrm{A}}_{3,1} + k^{*}_{ab}c^{\mathrm{B}}_{2,2} - k^{*}_{ha}c^{\mathrm{A}}_{2,1},$$
$$\frac{\mathrm{d}c^{\mathrm{B}}_{1,2}}{\mathrm{d}t} = -k_{bb}c^{\mathrm{B}}_{0,1}c^{\mathrm{B}}_{1,2} - k_{ba}c^{\mathrm{A}}_{1,0}c^{\mathrm{B}}_{1,2} + k_{hb}c_{1,1}c^{\mathrm{B}}_{0,1} + k^{*}_{bb}c^{\mathrm{B}}_{1,3} + k^{*}_{ba}c^{\mathrm{A}}_{2,2} - k^{*}_{hb}c^{\mathrm{B}}_{1,2}.$$

For $2 \leq n \leq N-3$:

$$\frac{\mathrm{d}c^{\mathrm{A}}_{2,n}}{\mathrm{d}t} = k_{aa}c^{\mathrm{A}}_{1,0}\left(c^{\mathrm{A}}_{1,n} - c^{\mathrm{A}}_{2,n}\right) - k_{ab}c^{\mathrm{B}}_{0,1}c^{\mathrm{A}}_{2,n} + k_{ba}c^{\mathrm{B}}_{1,n}c^{\mathrm{A}}_{1,0} + k^{*}_{aa}\left(c^{\mathrm{A}}_{3,n} - c^{\mathrm{A}}_{2,n}\right) + k^{*}_{ab}c^{\mathrm{B}}_{2,n+1} - k^{*}_{ba}c^{\mathrm{A}}_{2,n},$$

$$\frac{\mathrm{d}c^{\mathrm{B}}_{n,2}}{\mathrm{d}t} = k_{bb}c^{\mathrm{B}}_{0,1}\left(c^{\mathrm{B}}_{n,1} - c^{\mathrm{B}}_{n,2}\right) - k_{ba}c^{\mathrm{A}}_{1,0}c^{\mathrm{B}}_{n,2} + k_{ab}c^{\mathrm{A}}_{n,1}c^{\mathrm{B}}_{0,1} + k^{*}_{bb}\left(c^{\mathrm{B}}_{n,3} - c^{\mathrm{B}}_{n,2}\right) + k^{*}_{ba}c^{\mathrm{A}}_{n+1,2} - k^{*}_{ab}c^{\mathrm{B}}_{n,2}.$$

As before, the equations corresponding to the maximum length N homopolymers are

$$\frac{\mathrm{d}c^{\mathrm{A}}_{2,N-2}}{\mathrm{d}t} = k_{aa}c^{\mathrm{A}}_{1,0}c^{\mathrm{A}}_{1,N-2} + k_{ba}c^{\mathrm{B}}_{1,N-2}c^{\mathrm{A}}_{1,0} - k^{*}_{aa}c^{\mathrm{A}}_{2,N-2} - k^{*}_{ba}c^{\mathrm{A}}_{2,N-2},$$
$$\frac{\mathrm{d}c^{\mathrm{B}}_{N-2,2}}{\mathrm{d}t} = k_{bb}c^{\mathrm{B}}_{0,1}c^{\mathrm{B}}_{N-2,1} + k_{ab}c^{\mathrm{A}}_{N-2,1}c^{\mathrm{B}}_{0,1} - k^{*}_{bb}c^{\mathrm{B}}_{N-2,2} - k^{*}_{ab}c^{\mathrm{B}}_{N-2,2}.$$

For $3 \leq r \leq N-2$ and $1 \leq s \leq N-1-r$:

$$\frac{\mathrm{d}c^{\mathrm{A}}_{r,s}}{\mathrm{d}t} = k_{aa}c^{\mathrm{A}}_{1,0}\left(c^{\mathrm{A}}_{r-1,s} - c^{\mathrm{A}}_{r,s}\right) - k_{ab}c^{\mathrm{B}}_{0,1}c^{\mathrm{A}}_{r,s} + k_{ba}c^{\mathrm{B}}_{r-1,s}c^{\mathrm{A}}_{1,0},$$
$$+ k^{*}_{aa}\left(c^{\mathrm{A}}_{r+1,s} - c^{\mathrm{A}}_{r,s}\right) + k^{*}_{ab}c^{\mathrm{B}}_{r,s+1} - k^{*}_{ba}c^{\mathrm{A}}_{r,s}.$$

For $3 \leq s \leq N-2$ and $1 \leq r \leq N-1-s$:

$$\frac{\mathrm{d}c^{\mathrm{B}}_{r,s}}{\mathrm{d}t} = k_{bb}c^{\mathrm{B}}_{0,1}\left(c^{\mathrm{B}}_{r,s-1} - c^{\mathrm{B}}_{r,s}\right) - k_{ba}c^{\mathrm{A}}_{1,0}c^{\mathrm{B}}_{r,s} + k_{ab}c^{\mathrm{A}}_{r,s-1}c^{\mathrm{B}}_{0,1}$$
$$+ k^{*}_{bb}\left(c^{\mathrm{B}}_{r,s+1} - c^{\mathrm{B}}_{r,s}\right) + k^{*}_{ba}c^{\mathrm{A}}_{r+1,s} - k^{*}_{ab}c^{\mathrm{B}}_{r,s}.$$

For $3 \leq n \leq N-1$:

$$\frac{\mathrm{d}c^{\mathrm{A}}_{n,N-n}}{\mathrm{d}t} = k_{aa}c^{\mathrm{A}}_{1,0}c^{\mathrm{A}}_{n-1,N-n} + k_{ba}c^{\mathrm{B}}_{n-1,N-n}c^{\mathrm{A}}_{1,0} - k^{*}_{aa}c^{\mathrm{A}}_{n,N-n} - k^{*}_{ba}c^{\mathrm{A}}_{n,N-n,}$$
$$\frac{\mathrm{d}c^{\mathrm{B}}_{N-n,n}}{\mathrm{d}t} = k_{bb}c^{\mathrm{B}}_{0,1}c^{\mathrm{B}}_{N-n,n-1} + k_{ab}c^{\mathrm{A}}_{N-n,n-1}c^{\mathrm{B}}_{0,1} - k^{*}_{bb}c^{\mathrm{B}}_{N-n,n} - k^{*}_{ab}c^{\mathrm{B}}_{N-n,n}.$$

The complete reaction scheme must satisfy mass conservation in a closed system, implying that the mass variation rate must be strictly zero:

$$0 = 2\dot{c}_{1,1} + 3\left(\dot{c}^{\mathrm{A}}_{2,1} + \dot{c}^{\mathrm{B}}_{1,2}\right) + \sum_{n=1}^{N} n\left(\dot{c}^{\mathrm{A}}_{n,0} + \dot{c}^{\mathrm{B}}_{0,n}\right) + \sum_{n=2}^{N-1}(n+1)\left(\dot{c}^{\mathrm{A}}_{1,n} + \dot{c}^{\mathrm{B}}_{n,1}\right)$$
$$+ \sum_{n=2}^{N-2}(n+2)\left(\dot{c}^{\mathrm{A}}_{2,n} + \dot{c}^{\mathrm{B}}_{n,2}\right) + \sum_{r=3}^{N-1}\sum_{s=1}^{N-1}(r+s)\left(\dot{c}^{\mathrm{A}}_{r,s} + \dot{c}^{\mathrm{B}}_{r,s}\right),$$

where the overdot stands for the time-derivative.

References

1. Guijarro A, Yus M (2009) The origin of chirality in the molecules of life. RSC, Cambridge
2. Kondepudi D, Prigogine I, Nelson G (1985) Phys Lett A 111:29
3. Avetisov V, Kuz'min V, Anikin S (1987) J Chem Phys 112:179

4. Weissbuch I, Leiserowitz L, Lahav M (2005) Top Curr Chem 259:123
5. Weissbuch I, Addadi L, Berkovitch-Yellin Z, Gati E, Lahav M, Leiserowitz L (1984) Nature 310:161
6. Weissbuch I, Addadi L, Leiserowitz L, Lahav M (1988) J Am Chem Soc 110:561
7. Weissbuch I, Lahav M (2011) Chem Rev 111(5):3236
8. Soai K, Shibata KT, Morioka H, Choji K (1995) Nature 378:767
9. Blanco C, Stich M, Hochberg D (2011) Chem Phys Lett 505:140
10. Frank FC (1953) Biochim Biophys Acta 11:459
11. Mason S (1985) Nature 314:400
12. Seelig FF (1971) J Theor Biol 31:355
13. Decker P (1974) J Mol Evol 4:49
14. Hochstim AR (1975) Orig Life 6:317
15. Fajszi F, Czëgë J (1981) Orig Life 11:143
16. Tennakone K (1984) Chem Phys Lett 105:444
17. Gutman I, Babović V, Jokić S (1988) Chem Phys Lett 144:187
18. Gutman I, Todorović D (1992) Chem Phys Lett 195:62
19. Gutman I, Todorović D, Vučković M (1993) Chem Phys Lett 216:447
20. Todorović D, Gutman I, Radulović M (2003) Chem Phys Lett 372:464
21. Mason SF (1991) Chemical evolution. Oxford University Press, Oxford
22. Plasson R, Kondepudi DK, Bersini H, Commeyras A, Asakura K (2007) Chirality 19:589
23. Crusats J, Hochberg D, Moyano A, Ribó JM (2009) Chemphyschem 10:2123
24. Blanco C, Hochberg D (2011) Phys Chem Chem Phys 13:12920
25. Weissbuch I, Illos RA, Bolbach G, Lahav M (2009) Acc Chem Res 42:1128
26. Hitz T, Luisi PL (2003) Helv Chim Acta 86:1423
27. Ribó JM, Hochberg D (2008) Phys Lett A 373:111
28. Morozov LL, Kuzmin VV, Goldanskii VI (1983) Orig Life 13:119
29. Kondepudi DK, Nelson GW (1984) Physica A 125:465
30. Scott SK (1994) Oscillations, waves, and chaos in chemical kinetics. Oxford University Press, Oxford
31. Landau E, Wolf SG, Levanon M, Leiserowitz L, Lahav M, Sagiv J (1989) J Am Chem Soc 111:1436
32. Weissbuch I, Lahav M, Leiserowitz L (2003) Cryst Growth Des 3:125
33. Ruiz-Bermejo M, Rivas L, Palancin A, Menor-Salvan C, Osuna-Esteban S (2011) Orig Life Evol Biosph 41(4):331
34. Kondepudi D, Kaufman R, Singh N (1990) Science 250:975
35. Viedma C (2005) Phys Rev Lett 94:065504
36. Weissbuch I, Torbeev VY, Leiserowitz L, Lahav M (2005) Angew Chem Int Ed 44:3226
37. Joyce G, Visser G, van Boeckel C, van Boom J, Orgel L, van Westrenen J (1984) Nature 310:602
38. Avetisov V, Goldanskii V (1996) Proc Natl Acad Sci USA 93:11435
39. Kondepudi D, Asakura K (2001) Acc Chem Res 34:946
40. Cintas P (2002) Angew Chem Int Ed 41:1139
41. Huber C, Eisenreich W, Hecht S, Wachtershauser G (2003) Science 301:938
42. Leman L, Orgel L, Ghadiri M (2004) Science 306:283
43. Huber C, Wachtershauser G (1997) Science 276:245
44. Pascal R, Boiteau L, Commeyras A (2005) Top Curr Chem 259:69
45. Lundberg R, Doty P (1957) J Am Chem Soc 79:3961
46. Idelson M, Blout E (1957) J Am Chem Soc 79:3948
47. Akaike T, Inoue S (1976) Biopolymers 15:1863
48. Blair N, Bonner W (1980) Orig Life Evol Biosph 10:255
49. Blair N, Bonner W (1981) Orig Life Evol Biosph 11:331
50. Kricheldorf K (2006) Angew Chem Int Ed 45:5752
51. Ehler K, Orgel L (1976) Biochim Biophys Acta 434:233

52. Hill A, Bohler C, Orgel L (1998) Orig Life Evol Biosph 28:235
53. Brack A (1987) Orig Life Evol Biosph 17:367
54. Kanazawa H (1992) Polymer 33:2557
55. Kanazawa H, Ohashi Y (1996) Mol Cryst Liq Cryst 277:45
56. Hitz T, Blocher M, Walde P, Luisi P (2001) Macromolecules 34:2443
57. Hitz T, Luisi P (2002) Helv Chim Acta 85:3975
58. Blocher M, Hitz T, Luisi P (2001) Helv Chim Acta 84:842
59. Zepik H, Shavit E, Tang M, Jensen T, Kjaer K, Bolbach G, Leiserowitz L, Weissbuch I, Lahav M (2002) Science 295:1266
60. Weissbuch I, Zepik H, Bolbach G, Shavit E, Tang M, Jensen T, Kjaer K, Leiserowitz L, Lahav M (2003) Chem Eur J 9:1782
61. Blanco C, Hochberg D (2012) Phys Chem Chem Phys 14:2301
62. Wattis JAD, Coveney PV (2007) J Phys Chem B 111:9546
63. Mauksch M, Tsogoeva SB, Wei S-W, Martinova IM (2007) Chirality 19:816
64. Mauksch M, Tsogoeva SB (2008) Chemphyschem 9:2359
65. Muñoz Caro G, Meierheinrich U, Schutte W, Barbier B, Arcones Segovia A, Rosenbauer H, Thiemann WHP, Brack A, Greenberg J (2002) Nature 416:403
66. Deamer DW (1997) Microb Mol Biol Rev 61:239
67. Segre D, Ben-Eli D, Deamer DW, Lancet D (2001) Orig Life Evol Biosph 31:119

Top Curr Chem (2013) 333: 213–254
DOI: 10.1007/128_2012_398

Published online: 11 January 2013

Self-Assembly of Dendritic Dipeptides as a Model of Chiral Selection in Primitive Biological Systems

Brad M. Rosen, Cécile Roche, and Virgil Percec

Abstract Biological macromolecules are homochiral, composed of sequences of stereocenters possessing the same repeated absolute configuration. This chapter addresses the mechanism of homochiral selection in polypeptides. In particular, the relationship between the stereochemistry (L or D) of structurally distinct α-amino acids is explored. Through functionalization of Tyr–Xaa dipeptides with self-assembling dendrons, the effect of stereochemical sequence of the dipeptide on the thermodynamics of self-assembly and the resulting structural features can be quantified. The dendritic dipeptide approach effectively isolates the stereochemical information of the shortest sequence of stereochemical information possible in polypeptide, while simultaneously allowing for dendron driven tertiary and quaternary structure formation and subsequent transfer of chiral information from the dipeptide to the dendritic sheath. This approach elucidates a mechanism of selecting a homochiral relationship between dissimilar but neighboring α-amino acids through thermodynamic preference for homochirality in solution-phase and bulk supramolecular helical polymerization.

Keywords Chirality · Dendrimers · Self-assembly

B.M. Rosen
DuPont Central Research & Development, Experimental Station, Wilmington, DE 19880, USA

C. Roche and V. Percec (✉)
Roy & Diana Vagelos Laboratories, Department of Chemistry, University of Pennsylvania, Philadelphia, PA 19104-6323, USA
e-mail: percec@sas.upenn.edu

Contents

Abbreviations

Boc	*tert*-Carbonyl butoxy
CD-UV	Circular dichroism/UV–vis spectroscopy
DSC	Differential scanning calorimetry
ED	Electron diffraction
SFM	Scanning force microscopy
TEM	Transmission electron microscopy
TMV	Tobacco mosaic virus
XRD	X-Ray diffraction

1 Introduction

Life is an emergent system. Small changes to gene sequence can cascade to new productive phenotypes or with unfortunate frequency lead to morbidity. Justifiably, vigorous research has been aimed at reducing organism-level complexity to understandable, predictable, and medically applicable models. Despite these efforts, life itself is an emergent and arguably beneficial property [1] of the abiotic chemical environment of the young Earth. To understand the conditions and driving forces of the complex chemical system that give rise to life would simultaneously illuminate the evolutionary path from the primordial uninhabited world to the rise of nucleic acid coded organisms, but moreover could render scientists capable of producing de novo systems that exhibit similarly rich, complex, and potentially useful functionality to that of our living world.

Unlike modern living organisms, which we are now able to modify and probe at the genetic level, we do not have access to or detailed records of the complex system from which life emerged. Therefore, in order to gain an understanding of the rules that governed its function, we must develop suitable model systems based on rudimentary understandings of the primordial Earth provided by geochemists [2].

One of the most conspicuous chemical *and geometric* features of modern life is its lack of symmetry. The three main biomacromolecules encompassed by *the central dogma of molecular biology* "DNA makes RNA makes PROTEIN" exhibit hierarchical asymmetry. Proteins, which possess the greatest structural and functional diversity, are, at their core, linear polymers constructed via the templated condensation polymerization of relatively simple building blocks, a library of 20 standard α-amino acids. All of these α-amino acids, except for Gly which is achiral, possess a single stereocenter on their main chain at the α-carbon (Ile and Thr possess a second along their side-chains). Each amino acid is produced through a separate biosynthetic pathway [3], yet all of the translationally incorporated amino acids have the same absolute *sinister* (S) configuration.[1] Synthetic organic chemists yearn for high enantioselectivity but seldom reach the level achieved by the natural world. While the Miller–Urey experiment demonstrated that mixtures of α-amino acids such as alanine, aspartic acid, and glycine could be produced under "possible primitive Earth conditions" in the absence of enzymes or other organocatalysts [4], these mixtures were racemic.

It has been hypothesized that, in order to achieve the homochirality observed for α-amino acids and other biological molecules and macromolecules, three fundamental steps [5] must occur: (1) mirror-symmetry breaking, (2) chiral amplification, and (3) chiral transmission.

Mirror-symmetry breaking (Step 1) is the formation of an enantiomeric imbalance of a specific molecule. This multi-disciplinary field spanning particle physics, statistical thermodynamics, and astrobiology has been extensively reviewed [5–8]. Several compelling theories predict at least a slight enantiomeric excess on Earth. Parity violation in the electroweak field suggests femtojoule to picojoule per mole differences in ground state energy of enantiomers, with the imbalance favoring L amino acids and D sugars [9]. The enantiomeric excess on Earth may also have extraterrestrial origins, as suggested by the slight chiral imbalances of organic molecules in meteorites, which could be due to the effect of polarized light [6]. Another theory states that mirror-symmetry breaking originates from stochastic imbalance in the racemic state. Racemism is, indeed, a macroscopic notion; the probability of having a truly racemic mixture at the molecular level is extremely small [5]. Amplification of an initial chiral imbalance to achieve enantiopurity of a single molecule (Step 2) is an area that has captivated mechanistic chemists and has also been extensively reviewed [10, 11]. Theories of chiral amplification have focused largely on autocatalytic reactions – where a chiral adduct catalyzes its own formation according to the Frank model – and chiral partitioning between solution and the solid state. Chiral transmission (Step 3) from one molecule to another is a less frequently discussed component of the process. Some might dismiss chiral transmission as an inevitable consequence of chiral amplification.

[1] Cysteine technically contains a *rectus* (R) stereocenter, but this is only due to the higher priority given to the sulfur atom. It otherwise possesses the same configuration as the other 18 chiral standard α-amino acids.

However, if we consider just the 19 chiral standard α-amino acids that undergo translation to form proteins, each exhibit the same absolute configuration and therefore form homochiral polypeptides (sequential stereocenters, regardless of the amino acid, all have the same configuration) as opposed to heterochiral polypeptides (sequential stereocenters have different configurations). Unless the mechanism that produced the mirror-symmetry breaking (Step 1) robustly induces the same handedness for all α-amino acids, then an additional relational mechanism is needed to explain why the predominant form of some α-amino acids are not D (*R*), and that polypeptides that contain them are not therefore heterochiral.

Typically, studies into chiral amplification have focused on single amino acids in isolation, though at least one study has indicated that various amino acids of the same configuration will preferentially co-crystallize [12]. The prevailing assumption in most work on chiral amplification is that the selection of handedness occurs before their polymerization or even covalent dimerization. However, the condensation of α-amino acids into dipeptides, oligopeptides, and polypeptides could have occurred concurrently with the chiral amplification processes and, through a relational mechanism in the growing polypeptides, the enantiomeric imbalance in one α-amino acid could influence and help amplify the enantiomeric imbalance in a completely different α-amino acid.

It could be argued that once the stereochemistry of a single α-amino acid (for example L-Tyr) was selected, it was a foregone conclusion that all of the standard α-amino acids would come to bear the same stereochemistry.

However, not all biological polypeptides with useful functions are homochiral. For example, most Gramicidins are heterochiral pentadecapeptides, composed of alternating L and D α-amino acids [13]. That being said, D amino acids found in Gramicidins and other polypeptides are installed through the same codon as their corresponding L amino acid and are epimerized post-translationally [14]. While this might imply that the similar and possible common ancestry of the 20 standard amino acid biosynthetic pathways is the cause for uniform homochirality, it is possible that homochiral selection process predated the cellular machinery to produce proteins. In this case, other factors would have to have dictated the stereochemical preferences.

DeGrado and Nanda have studied the effect of heterochirality in larger polypeptide structures [15, 16]. Recently, Nanda specifically modeled the difference between homochiral vs alternating heterochiral poly(alanine) and concluded that homochiral polypeptides were evolved in order to maximize the enthalpy of chain collapse [17]. Of course, if all the α-amino acids in a protein were replaced with their D analogs, they would be well suited to the enantiomeric substrates of a mirror-image Earth, as was shown synthetically with HIV-1 protease [18].

In biology, the polymerization of enantiopure α-amino acids into precise sequences results in exquisite control of three-dimensionality, self-assembly, and function. The α-amino acids in proteins achieve this control through communication of their steric and stereochemical information. This information is transfered locally through their covalent main-chain backbone, and also to adacent sequences or domains through specific and non-specific, non-covalent interactions. It typically requires an extended sequence of amino acids to achieve a regular secondary

structure. To study the origin of homochirality in such a system would therefore require the synthesis and structural analysis of vast arrays of stereoisomeric poly (peptide sequences).

This chapter, which serves as a substantial expansion of an earlier survey [19], will review the development of dendritic dipeptide porous protein mimics as a platform to study chiral amplification and chiral transmission in polypeptides composed of diverse α-amino acids.

2 Bioinspired Dendrons as a Self-Assembling Scaffold

Dendrons and dendritic topologies [20–22], if synthesized through appropriate iterative convergent [23, 24] or divergent strategies [25–27], are perfectly branched monodisperse macromolecules. Dendrons that also combine chemically dissimilar domains in their periphery and body have the potential to self-assemble in the bulk or in solvents that preferentially solvate one of the domains [28]. One such example, Percec-type dendrons, branched aryl-ether dendrons with aliphatic or semi-perfluorinated [29–31] periphery groups (Fig. 1) demonstrate an exceptional tendency toward spontaneous self-assembly into supramolecular dendrimers capable of self-organization into a remarkably diverse collection of periodic lattices and quasiperiodic arrays (Fig. 2).

While Percec-type dendrons look anything but biological in structure, they are in fact bio-inspired [33], mimicking [34–41] the self-assembly of tobacco mosaic virus (TMV) capsid proteins around the viral RNA core [42–44]. Since their initial discovery, several generational libraries of Percec-type dendrimers have been prepared including the benzyl [45] (Fig. 1), biphenylmethyl [46], propylphenyl [47], and propylbiphenyl [32] ether series, as well as related AB_4/AB_5 [48], hybrid [49], and deconstructed topologies [50]. The most common mechanisms of self-assembly for Percec-type dendrons include the packing of cone-shaped dendrons or crowns [51, 52] into spheres or polyhedral sphere-like objects [53] (Fig. 2, top right) or the stacking of supramolecular discs or crowns [51, 52] formed from wedge-like or disc-like dendrons into helical columns (Fig. 2, top left). Self-assembly through the helical columnar mechanism typically proceeds through self-organization into the *p6mm* hexagonal columnar (Φ_h) [54], *p2mm* simple rectangular ($\Phi_{r\text{-}s}$) [49], or *c2mm* centered rectangular ($\Phi_{r\text{-}c}$) [49] lattices. Likewise, self-assembly through the spherical mechanism typically proceeds through self-organization into the cubic *Pm3n* phase (*Cub*) [54–57], but sometimes into the cubic *Im3m* (BCC) [58] lattice, the tetragonal $P4_2/mnm$ (*Tet*) [59] lattice, or the 12-fold quasi-liquid crystalline (*QLC*) array [60, 61].

Retrostructural analysis of the generational libraries produced from the four classes of self-assembling Percec-type dendrons revealed that shape recognition through the dendrons' branching pattern is the primary determinant of the shape of the self-assembled structure [32]. As a relevant example, during self-assembly, the (3,5)-branching pattern of the second generation benzyl ether dendron [4-3,4-3,5]

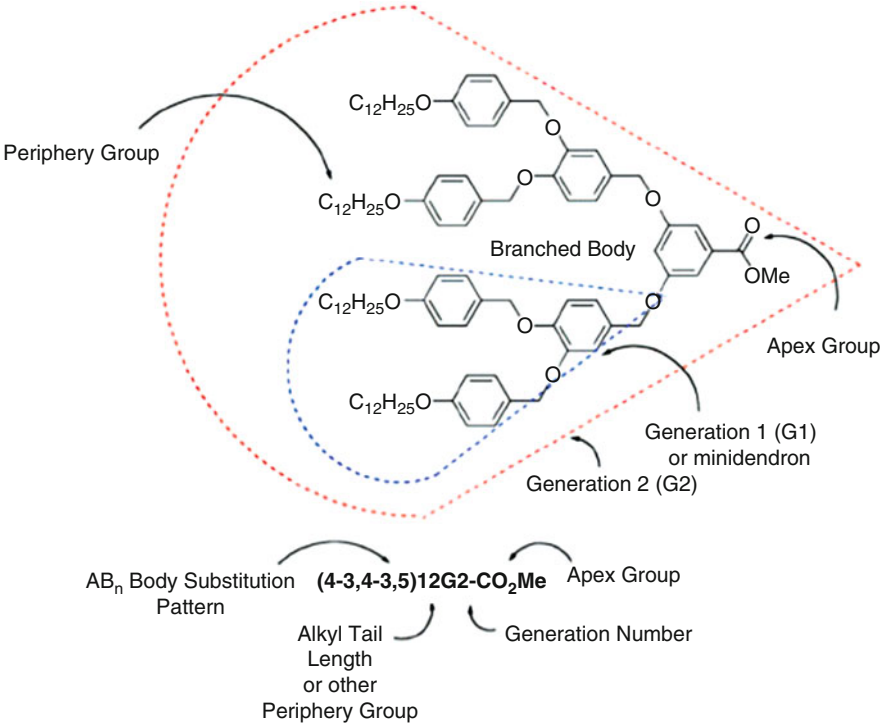

Fig. 1 Nomenclature for Percec-type dendrons. The *numbers inside the parentheses* represents the sequence of AB*n* branched building blocks from the periphery to the apex. The *number* indicates from which position of the phenyl unit the B branches emanate. The *number* or *descriptor following the parentheses* indicates the number of carbons in the aliphatic tail, or alternative periphery unit. Following the periphery descriptor is the generation number. The final segment identifies the apex moiety. Reprinted with permission from [28]. Copyright 2009 American Chemical Society

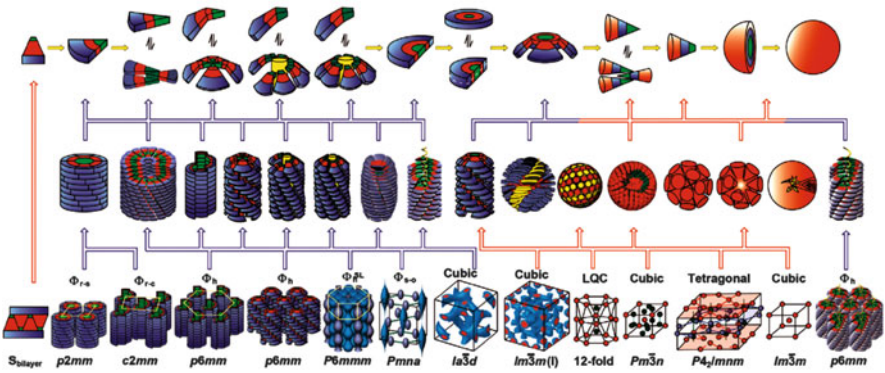

Fig. 2 Diversity of periodic lattices and quasi-periodic arrays formed via the self-assembly and self-organization of Percec-type dendrons. Reprinted with permission from [32]. Copyright 2009 American Chemical Society

12G2-CO_2CH_3 (Fig. 1) causes it to adopt a wedge-like conformation, forcing it to pack into a Φ_h lattice [45]. Each 4.7-Å [62] column stratum is composed of five quasi-equivalent dendritic building blocks that form a disc that spans a diameter of 56.7 Å. Substitution of the methyl ester apex functionality for a benzyl alcohol [4-3,4-3,5]12G2-CH_2OH or for a carboxylic acid [4-3,4-3,5]12G2-COOH does not alter the self-assembled structure except to reduce the columnar diameter to 53.1 Å and 52.8 Å, respectively. As illustrated with [4-3,4-3,5]12G2-CO_2CH_3, modifying the functionality from the apex of a dendron rarely results in significant alteration to the pattern of self-assembly, and dendrons with equivalent branching pattern but different apex functionality are typically capable of co-assembly [63]. Nevertheless, introduction of apex functionality with strong H-bonding such as hydroxyl or carboxylic acid groups can alter the dimensions and in some circumstances the structures formed.

3 Helical Pore Forming Dendritic Dipeptides

3.1 Discovery, Structure, and Function

A key difference between the self-assembling dendrons and the TMV capsid proteins that served as their inspiration [33] was their chirality. The dendrons that constitute the four generational libraries prepared are achiral, and though self-assembly of these dendrons can proceed through helical columns [64], these assemblies are racemic. From the perspective of developing a scaffold for probing the amplification, and transfer of chirality, this scenario is close to ideality: the building blocks themselves are achiral but the structures they form are chiral. As a result, in 2004, a new framework for studying the origin of α-amino acid homochirality was developed [65]. Here, the shortest possible α-amino acid sequence, a dipeptide, was coupled directly to the apex of a self-organizable Percec-type dendron.

To achieve a helical columnar structure, the wedge-like dendron [4-3,4-3,5]G2-CH_2OH was selected as the self-assembling sheath. To minimize the effect of the dendron on the peptide backbone, attachment is preferable on an α-amino-acid side chain. It was found that the phenol of tyrosine (Tyr) could be readily etherified to the apex benzyloxy group of [4-3,4-3,5]G2-CH_2OH via Mitsonubu coupling using PPh_3 and diisopropyl azodicarboxylate (DIAD). Boc-Tyr-Ala-OMe was selected as the simplest dipeptide with two stereocenters. Using this approach, the four stereoisomers [4-3,4-3,5]G2-CH_2-(L-Tyr-L-Ala) (L–L), [4-3,4-3,5]G2-CH_2-(L-Tyr-D-Ala) (L–D), [4-3,4-3,5]G2-CH_2-(D-Tyr-D-Ala) (D–D), and [4-3,4-3,5]G2-CH_2-(D-Tyr-L-Ala) (D–L) were prepared [63–66] (Fig. 3).

While the [4-3,4-3,5]12G2-CH_2OH dendritic sheath was able to enforce columnar self-assembly, a combination of the steric bulk and specific H-bonding interaction of the Tyr–Ala dipeptides resulted in a transformation of the self-assembled structure from filled racemic columns to chiral helical porous columns (Fig. 4).

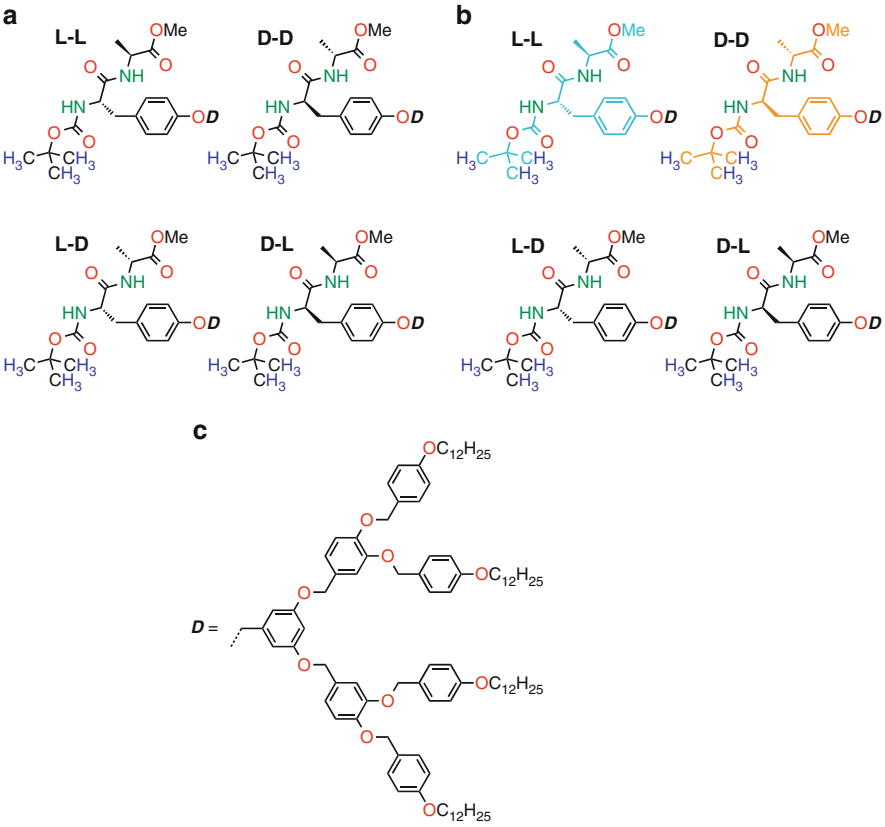

Fig. 3 The structures of homochiral and heterochiral dendritic dipeptides [4-3,4-3,5]12G2-CH_2-Boc-X-Tyr-Y-Ala-OMe and the color code of the dipeptides used in the molecular models illustrating the cross-section of the porous columns. (**a**) Color code of L–L, D–D, L–D, and D–L dipeptides used for molecular models to illustrate the cross-sections of the supramolecular columns self-assembled from enantiopure homo- and heterochiral dendritic dipeptides in Figs. 4 and 11 (–CH_3 from the Boc group of Tyr, *blue*; –CH_3 of the methylester and methyl of Ala, *white*; C, *gray*; O, *red*; N–H, *green*). (**b**) Color code of L–L, D–D, L–D, and D–L dipeptides used to illustrate the cross-sections of the supramolecular columns self-assembled from the different racemic variants L–DL, D–DL, DL–L, DL–D, and DL–DL in Figs. 12 and 13 (–CH_3 from Boc group of Tyr, *blue*; O, *red*; N–H, *green*; C in L–D and D–L, *gray*; C and –CH_3 groups of Ala in L–L and D–D, *light blue* and *orange*, respectively; –CH_3 groups of Ala in L–D and D–L, *white*). (**c**) Structure of the second generation dendron [4-3,4-3,5]12G2-. Reprinted with permission from [67]. Copyright 2011 American Chemical Society

Formation of the helical porous columns was determined through the combination of circular dichroism/UV–vis spectroscopy (CD-UV) and ^{1}H NMR in solution, as well as thin film CD-UV, differential scanning calorimetry (DSC), small-angle powder XRD, wide-angle oriented fiber XRD, transmission electron microscopy (TEM), electron diffraction (ED), and scanning force microscopy (SFM) in the bulk state [61–68]. Characterization of the four stereoisomers L–L, D–D, L–D, and D–L

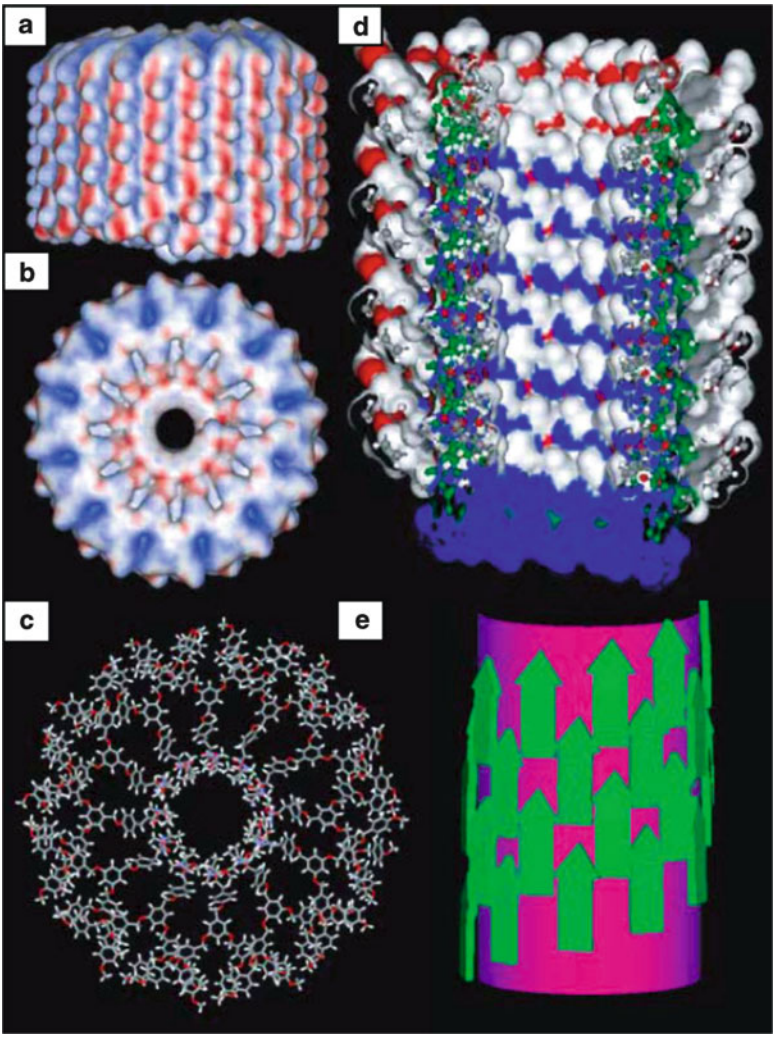

Fig. 4 (**a**) Side view of the column formed from [4-3,4-3,5]G2-CH_2-(L-Tyr-L-Ala). (**b**) Top view of the column formed from [4-3,4-3,5]G2-CH_2-(L-Tyr-L-Ala). (**c**) Top view of a single porous column stratum formed from [4-3,4-3,5]G2-CH_2-(L-Tyr-L-Ala). (**d**) Cross-section through the hydrophobic pore (without dendrons) (CH_3 of Ala is *white*, CH_3 of Boc are *blue*, O is *red*, C–N of dipeptide are *green*, aromatic groups are *gray*). (**e**) Schematic model for the self-assembly of the dipeptidic beta-barrel pore. The *green arrows* indicate the dipeptides main-chains. Reprinted with permission from [65]. Copyright 2004 Nature Publishing Group

showed that the stereochemistry of Tyr dictates the helical sense of the columns, while the stereochemistry of Ala plays a crucial role in the allosteric regulation of the assembly. The porous structure of the columns was further evidenced by the observation of proton transport through the pore. Thus, for this class of dendritic

dipeptides, the wedge-like dendritic sheath drives the self-assembly process into hexagonal columnar assemblies, but the structural and stereochemical information contained in the dipeptide tunes the finer structural details to generate helical porous columns that mimic the water transport function of Aquaporins [68].

3.2 *Cooperative Helical Supramolecular Polymerization Favors Homochiral Dendritic Tyr–Ala Dipeptides*

The relationship between dipeptide stereochemistry and self-assembled dendritic structure could not be fully elucidated by studying only stereopure dendritic dipeptides. In a subsequent study to understand more completely the role of the stereochemistry of Tyr and Ala in the self-assembly of dendritic dipeptides, all possible combinations of stereochemically pure and partially or fully racemized dipeptides were considered. A concise strategy was derived for the preparation of chiral dendritic dipeptides. A dipeptide Tyr–Ala was synthesized with *tert*-butoxycarbonyl (Boc) protection of the N-terminus and methyl ester protection of the C-terminus (Boc-Tyr-Ala-OMe). The phenolic group of the Tyr residue was attached to the benzylic position of [4-3,4-3,5]G2-CH_2OH via Mitsonobu coupling or via base-mediated displacement of the corresponding benzyl chloride [4-3,4-3,5]G2-CH_2Cl. Using this approach, the four stereoisomers [4-3,4-3,5]G2-CH_2-(L-Tyr-L-Ala) (L–L), [4-3,4-3,5]G2-CH_2-(L-Tyr-D-Ala) (L–D), [4-3,4-3,5]G2-CH_2-(D-Tyr-D-Ala) (D–D), and [4-3,4-3,5]G2-CH_2-(D-Tyr-L-Ala) (D–L) were prepared (Fig. 3) [65] as well as the five racemic variants [4-3,4-3,5]G2-CH_2-(L-Tyr-DL-Ala) (L–DL), [4-3,4-3,5]G2-CH_2-(D-Tyr-DL-Ala) (D–DL), [4-3,4-3,5]G2-CH_2-(DL-Tyr-D-Ala) (DL–D), [4-3,4-3,5]G2-CH_2-(DL-Tyr-L-Ala) (DL–L), and [4-3,4-3,5]G2-CH_2-(DL-Tyr-DL-Ala) (DL–DL) [67]. While the homochiral (L–L and D–D) and heterochiral (L–D and D–L) dendritic dipeptides were synthesized from enantiomerically pure D or L Tyr and Ala, the partially racemized (L–DL, D–DL, DL–D, and DL–L) and fully racemized (DL–DL) dendritic dipeptides were synthesized from racemic Ala and enantiopure Tyr, racemic Tyr and enantiopure Ala, or racemic Tyr and Ala, respectively. For example the partially racemized variant L–DL is an equimolar mixture of the L–D and the L–L stereoisomers, which was synthesized from enantiopure L-tyrosine and racemic alanine (red box in Fig. 5). The composition of the other partially racemized dendritic dipeptides is defined in a similar way: the D–DL variant is a 50:50 mixture of the D–D and D–L dendrons, synthesized from enantiopure D-tyrosine and racemic alanine (blue box); the DL–D variant is a 50:50 mixture of the D–D and L–D dendrons, synthesized from racemic tyrosine and enantiopure D-alanine (green box); and the DL–L variant is a 50:50 mixture of the D–L and L–L dendrons, synthesized from racemic tyrosine and enantiopure L-alanine (orange box). The fully racemized variant DL–DL is a 25:25:25:25 mixture of all four stereoisomers L–L, L–D, D–D, and D–L, synthesized from racemic tyrosine and racemic alanine (black box).

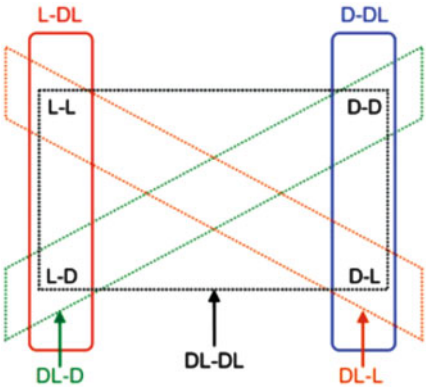

Fig. 5 The enantiomeric composition of racemized dendritic dipeptides. *Colored boxes* for each racemic mixture are composed of equimolar distributions of the enantiopure dipeptides that they enclose. Reprinted with permission from [67]. Copyright 2011 American Chemical Society

As mentioned above, the four enantiopure homochiral (L–L and D–D) and heterochiral (L–D and D–L) dendritic dipeptides self-assemble into helical porous columns in solution and in the solid state [66, 67]. Helical diffraction theory applied to the oriented fiber X-ray diffraction pattern provides information on the spatial disposition of the dendritic dipeptides in the columns [64]. Using a combination of XRD analysis, electron density maps, simulations of the XRD data, and molecular modeling [65], the structural and retrostructural analysis of the four stereoisomeric dendrimers was performed and gave access to their conformations in the supramolecular assembly, depicted in Fig. 6. As expected, the conformations of the homochiral enantiomeric pair L–L and D–D are mirror images. The same observation can be made for the heterochiral enantiomeric pair L–D and D–L. However, all other pairs, e.g., L–L and L–D, are diastereomers and have different conformations. All four dendritic dipeptides experience significant conformational changes upon self-assembly into helical columns compared to their lowest energy conformations as molecularly dissolved species. In all stereoisomers the hydroxyphenyl group of Tyr and the Boc group are in *anti* conformation. The orientations of the other substituents on the tetrahedral carbon atom of Tyr are imposed by its L or D stereochemistry, and thus the stereochemistry of Tyr determines the dendron sense and the handedness of the helix. The conformation of the Ala-OMe moiety varies in the different dendritic dipeptides. In the case of the homochiral L-Tyr-L-Ala and D-Tyr-D-Ala dipeptides the *methyl ester* group of Ala is located in the inner part of the pore, while in the case of the heterochiral L-Tyr-D-Ala and D-Tyr-L-Ala dipeptides the *methyl* group of Ala is located in the inner part of the pore, thus creating a larger pore. Overall the conformational analysis indicates that the stereochemistry of the dipeptide has an effect on the conformation of the dendron, which in turn allosterically controls the conformation of the Ala-OMe end group. The dipeptides are arranged in a parallel and partially interdigitated way in the pore, allowing the formation of hydrogen-bonding networks. The atoms indicated by *j*, *k*, *l*, and *m* (Fig. 6) participate in an in-layer hydrogen-bond network and form *j-k-j-k-j-k*... and *l-m-l-m-l-m*... helical patterns.

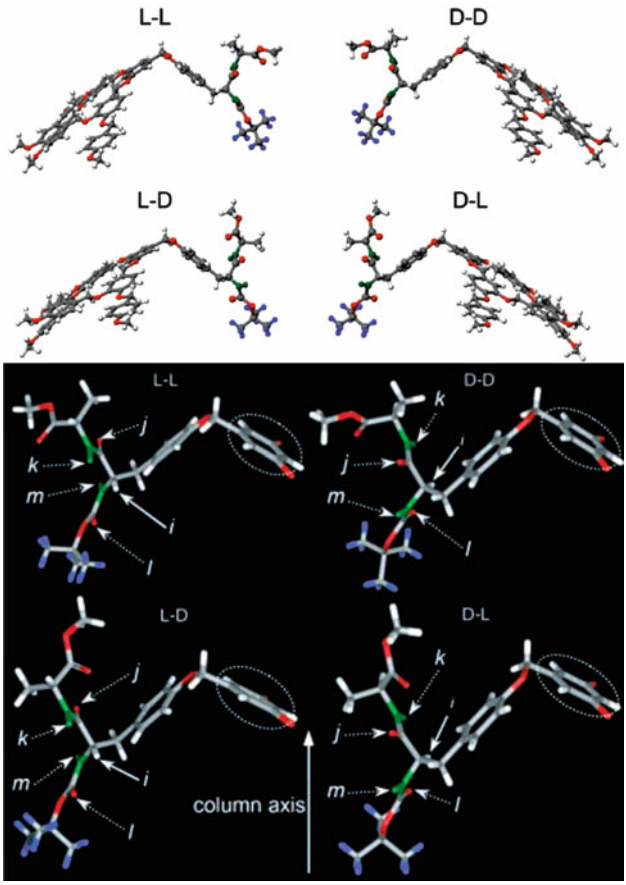

Fig. 6 Molecular models of the enantiopure dendritic dipeptides [4-3,4-3,5]G2-CH_2-(L-Tyr-L-Ala) (L–L), [4-3,4-3,5]G2-CH_2-(D-Tyr-D-Ala) (D–D), [4-3,4-3,5]G2-CH_2-(L-Tyr-D-Ala) (L–D), and [4-3,4-3,5]G2-CH_2-(D-Tyr-L-Ala) (D–L) in the supramolecular helical columns, obtained from structural and retrostructural analysis. Conformations of the full dendrons (peripheral alkyl chains were replaced with methyl groups for clarity) (*top*). Conformations of the apex end groups: dipeptide and first benzyl ether of the dendron (*dotted circle*) (*bottom*). *i* indicates the orientation of the L-Tyr or D-Tyr tetrahedral stereocenter, which determines the rotation sense; *j*, *k*, *l*, and *m* indicate the atoms that participate in the strong directional in-layer hydrogen-bonding networks *j-k-j-k-j-k*... and *l-m-l-m-l-m*... Reprinted with permission from [66, 67]. Copyright 2005 Wiley-VCH Verlag GmbH & Co. KGaA and 2011 American Chemical Society

The respective diameters of the column (d_{col}) and of the pore (d_{pore}) of the four dendritic dipeptide assemblies could be obtained from powder small-angle XRD at various temperatures [66]. All assemblies are essentially temperature-independent below $T_g = 57–60\ ^\circ C$, the temperature at which a glass transition is observed. The graphs in Fig. 7 show that the stereochemistry of the dipeptide influences both d_{col} and d_{pore} below T_g. The heterochiral dendritic dipeptides L–D and D–L form larger

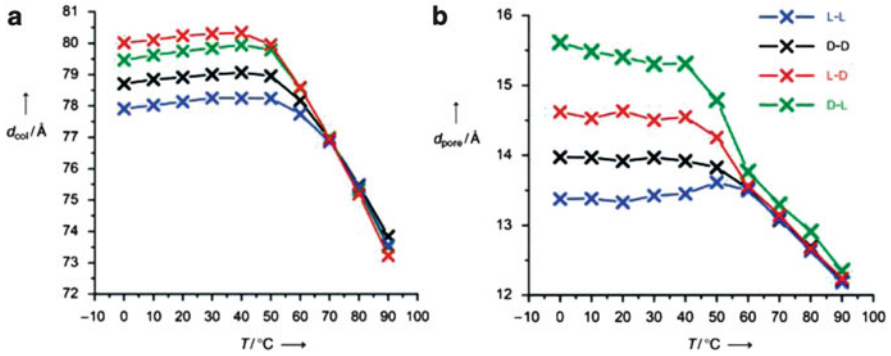

Fig. 7 Influence of the temperature and of the dipeptide stereochemistry on the (**a**) column diameter and (**b**) pore diameter of the self-assembly, determined by small- and wide-angle XRD. Reprinted with permission from [66]. Copyright 2005 Wiley-VCH Verlag GmbH & Co. KGaA

pores than the homochiral dipeptides L–L and D–D, which is consistent with the conclusions of the conformational analysis.

The self-assembly of the four stereochemically pure dendritic dipeptides L–L, D–D, L–D, and D–L in solution was studied by temperature-dependent CD/UV (Fig. 8) [66]. The CD spectra indicate that in all cases the dendrons are molecularly dissolved above 30 °C (insets in Fig. 8), since only a very weak Cotton effect at 232 nm, corresponding to the molecular solution of the dipeptide, is observed. Between 8 °C and 30 °C the self-assembly of the dendrons into helical columns is evidenced by the appearance of strong Cotton effects associated with the aromatic domain of the helical supramolecular dendrimer. Enantiomeric dipeptides form helical columns of opposite handedness, as evidenced by the mirror-imaged CD data of the L–L and D–D pair, or that of the L–D and D–L pair. Comparison of the sign of the Cotton effect for the four stereoisomers indicates the dominant role of Tyr in the handedness selection. The main Cotton effect at 225 nm is negative for the L–L and L–D dendritic dipeptides (where Tyr is L) and positive for the D–D and D–L dendritic dipeptides (where Tyr is D). However, the stereochemistry of Ala plays a significant role in the self-assembly process as well, as highlighted by the differences between the CD spectra of the L–L and L–D dipeptides, and the CD spectra of the D–D and D–L dipeptides, respectively. Different dipeptide stereochemistry leads to different dendron arrangements in the helical columnar structures. Comparison of the CD/UV data in solution with thin film CD/UV and fiber-oriented wide-angle XRD results suggests that the structures of the self-assembled columns formed in solution are essentially identical to the helical columns characterized in the bulk state.

Analysis of the CD/UV can also give an insight into the mechanism of self-assembly of the helical columns and into the thermodynamics of the helical supramolecular polymerization. Two models are usually considered to describe helical self-assembly mechanisms [69–72]. In the *isodesmic* mechanism each monomer association to the growing chain follows the same equilibrium constant

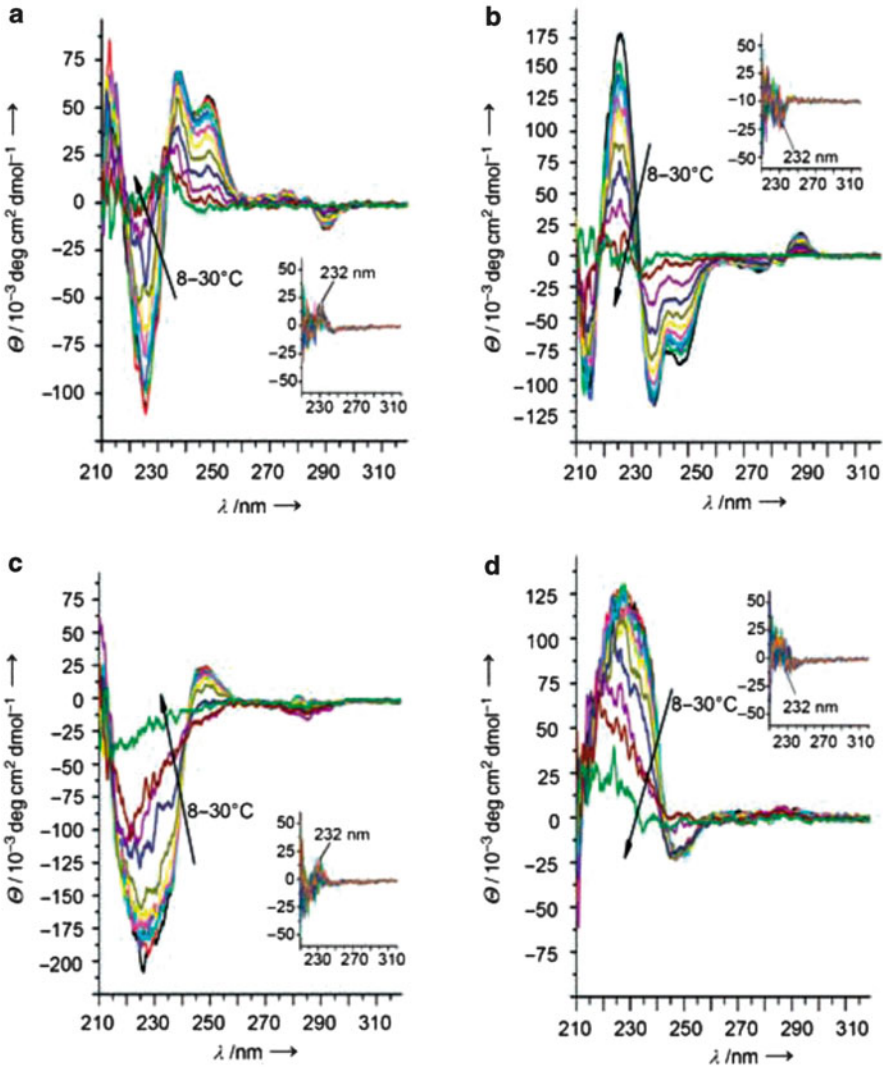

Fig. 8 CD spectra (1.6×10^{-4} M in cyclohexane) of the enantiopure homochiral and heterochiral dendritic dipeptides: (**a**) [4-3,4-3,5]12G2-CH_2-Boc-L-Tyr-L-Ala-OMe (L–L); (**b**) [4-3,4-3,5]12G2-CH_2-Boc-D-Tyr-D-Ala-OMe (D–D); (**c**) [4-3,4-3,5]12G2-CH_2-Boc-L-Tyr-D-Ala-OMe (L–D); (**d**) [4-3,4-3,5]12G2-CH_2-Boc-D-Tyr-L-Ala–OMe (D–L). The *arrows* indicate temperature increases. *Insets*: 30–60 °C. Reprinted with permission from [66]. Copyright 2005 Wiley-VCH Verlag GmbH & Co. KGaA

regardless of the degree of aggregation. In the *cooperative* mechanism the self-assembly consists of two steps, an unfavorable nucleation or activation step followed by growth or elongation. The activation and elongation processes in a cooperative self-assembly are governed by two distinct equilibrium constants K_a and K_e, respectively (Fig. 9).

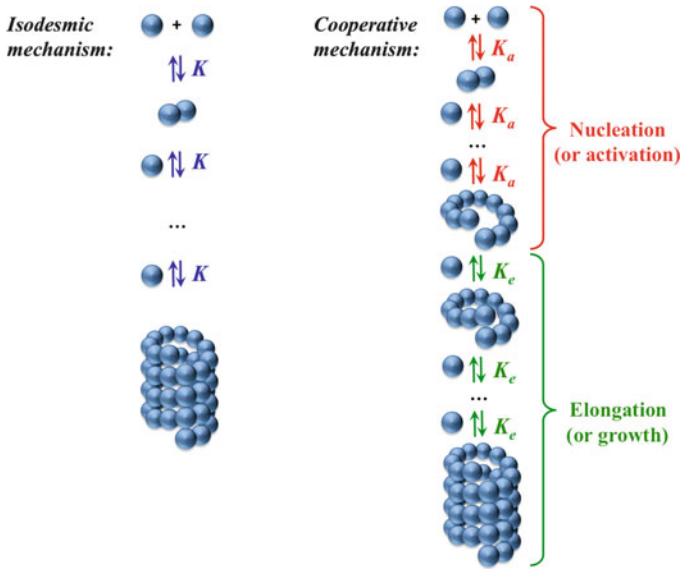

Fig. 9 Schematic representation of the isodesmic and cooperative mechanisms for helical supramolecular polymerizations. In the isodesmic model the same equilibrium constant K governs every monomer addition to the growing chain. In the cooperative model a nucleus forms first with an equilibrium constant K_a (nucleation step); formation of the nucleus is followed by elongation of the chain with an equilibrium constant K_e, with $K_e > K_a$

The assembly of the TMV capsid, which inspired the original design of Percec-type dendrons, is a classical biological example of cooperative helical polymerization [42]. Although self-assembly mechanisms have been studied extensively for proteins, these biological systems only provide information about homochiral structures. In contrast, the use of the dendritic dipeptide model allows for comparison of both homochiral, heterochiral and racemized species. Distinction between the isodesmic and the cooperative mechanisms can be achieved by following the CD or the UV signal at a given wavelength upon cooling or heating [72]. The CD/UV data can be rescaled between 0 and 1, and it then reflects the degree of aggregation Φ, assuming that aggregation is maximal at low temperature and non-existent at high temperature. The isodesmic mechanism should give rise to a sigmoidal relationship between the temperature and the degree of aggregation. In the case of a cooperative mechanism the curve profile should be non-sigmoidal with a sharp transition at an elongation temperature T_e, which corresponds to the formation of the first turn of the helix and the start of the growth from this nucleus. The slope of the curve below T_e is related to the thermodynamics of the elongation process and gives access to the molar enthalpy for polymerization h_e by fitting of the experimental data with (1).

$$\Phi = \Phi_{SAT}\left[1 - exp\left(-\frac{h_e}{RT_e^2}(T - T_e)\right)\right] \quad (1)$$

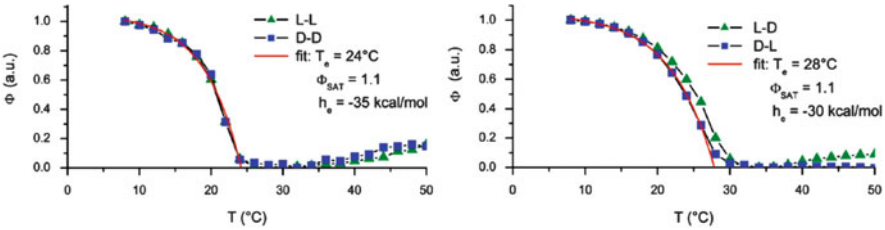

Fig. 10 Degree of aggregation as a function of temperature for homochiral (L–L and D–D, *left*) and heterochiral (L–D and D–L, *right*) dendritic dipeptides calculated from the UV–vis absorption at 230 nm; and fit with cooperative model (*red curve*). Reprinted with permission from [67]. Copyright 2011 American Chemical Society

The nucleation steps in cooperative self-assembly processes have not been as extensively studied as the elongation step. However, the equilibrium constant for the formation of the nucleus K_a can be estimated from the evolution of the degree of aggregation near the elongation temperature T_e:

The isodesmic/cooperative model was applied to the four homochiral and heterochiral dendritic dipeptides described above (Fig. 10) [67]. In all cases the dendrons self-assemble via a cooperative mechanism. The thermodynamics of the helical supramolecular polymerization was found to be virtually identical for enantiomeric pairs of dendritic dipeptides. The homochiral dendrons L–L and D–D assemble at $T_e = 24\ ^\circ C$ with a molar enthalpy for polymerization of -35 kcal mol^{-1}. The heterochiral dendrons L–D and D–L undergo transition from nucleation to elongation at a higher temperature of 28 °C, but with a lower molar enthalpy of -30 kcal mol^{-1}. Thus, all four enantiopure dendritic dipeptides undergo cooperative helical polymerization, but the elongation process is more enthalpically favorable in the case of homochiral dendrons.

The results of the helical self-assembly process in solution and in bulk are summarized in Fig. 11 for the four enantiomerically pure dendritic dipeptides. All stereoisomers undergo cooperative helical polymerization below a critical elongation temperature in solid state as well as in solution. As discussed more extensively in the preceding section, the stereochemistry of Tyr governs the helix handedness, while the stereochemistry of Ala determines the structural features of the columns. The homochiral supramolecular dendrimers were found to be more enthalpically favorable and to form slightly smaller pores than the heterochiral dendritic dipeptides [67].

If the self-assembly of dendritic dipeptides is cooperative, it should be possible to probe homochiral vs heterochiral selection by exploring the perturbation to observed h_e in stereochemically impure mixtures. To this end, the influence of chirality on the self-assembly process of dendritic dipeptides was further investigated by racemizing one of the α-amino acids of the dipeptide. As mentioned above (Fig. 5), the four partially racemized dendritic dipeptides L–DL, D–DL, DL–L, and DL–D, containing one chiral amino acid and one racemic amino acid, were prepared [67]. Each of these racemized structures is an equimolar mixture of diastereomeric homochiral and

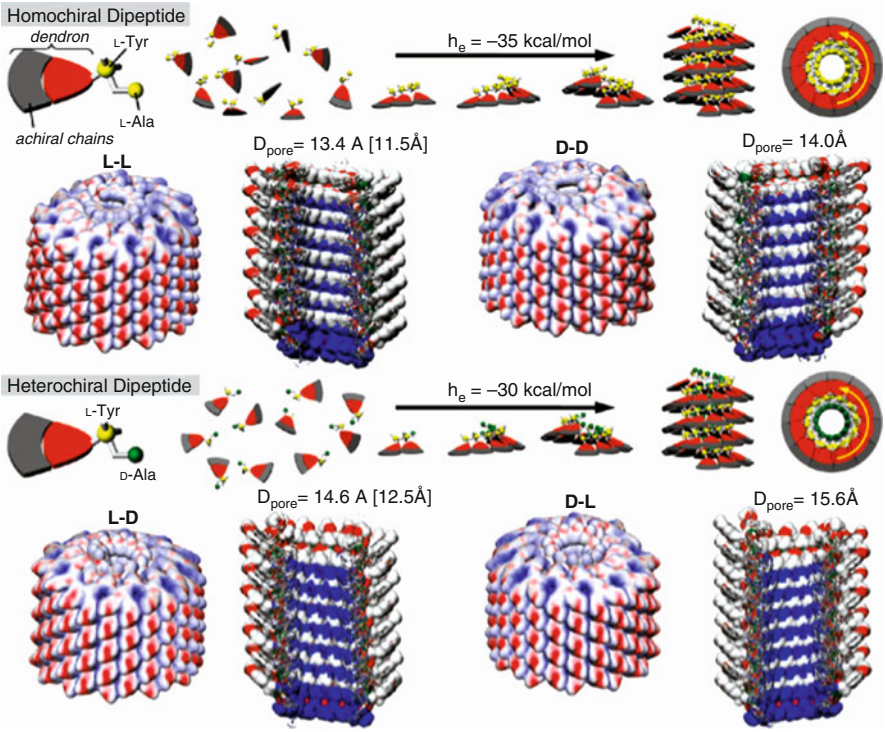

Fig. 11 Self-assembly of the homochiral (*top*) and heterochiral (*bottom*) dendritic dipeptides into supramolecular helical columns. The cooperative nucleation-and-growth mechanism, and the formation of right-handed helices, are schematically depicted in the case of the L–L and L–D dipeptides. The molar enthalpies for polymerization h_e, determined by temperature-dependent UV–vis studies in solution, are given. The side-views and cross-sections of the porous supramolecular columns were determined by XRD analysis in the solid state. (The color code of the dipeptides used in the cross-section of the columns is explained in Fig. 3a). Reprinted with permission from [67]. Copyright 2011 American Chemical Society

heterochiral dendritic dipeptides. The presence of an enantiopure Tyr in the dipeptide is sufficient to promote a preferred helicity in the self-assembled columns, as attested by the observation of a net ellipticity in the CD spectra of the L-Tyr-DL-Ala and D-Tyr-DL-Ala dipeptides in solution. However, no net ellipticity is observed when Tyr is racemized and Ala is chiral (DL-Tyr-L-Ala and DL-Tyr-D-Ala dipeptides). Two different self-assembly pathways can be anticipated for the partially racemized dendrons. For example, in the case of the L–DL dendron, the diastereomeric constituents L–L and L–D can either form two distinct columns or co-assemble into a single column (Fig. 12). In the former case the elongation temperature T_e and the molar enthalpy for polymerization h_e are expected to be an average of the values obtained for the enantiopure dipeptides L–L and D–D, i.e., T_e = 24–28 °C and h_e = −30 to −35 kcal mol^{-1}. Nevertheless, fitting of the experimental UV–vis data with

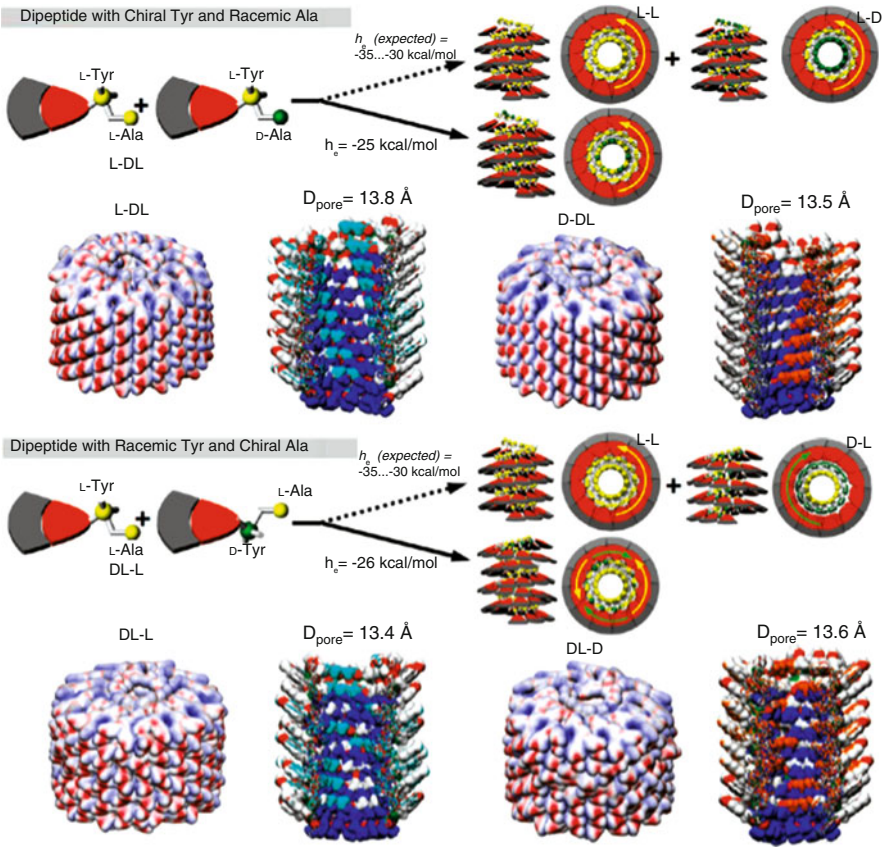

Fig. 12 Self-assembly of the partially racemized dendritic dipeptides into supramolecular helical columns: dipeptides with racemic Ala L–DL and D–DL (*top*) and dipeptides with racemic Tyr DL–L and DL–D (*bottom*). Two possible self-assembly pathways are presented for the L–DL and DL–L dendritic dipeptides. The experimental and expected molar enthalpies in solution are given for each pathway. The side-views and cross-sections of the porous supramolecular columns were determined by XRD analysis in the solid state. (The color code of the dipeptides used in the cross-section of the columns is explained in Fig. 3b). Reprinted with permission from [67]. Copyright 2011 American Chemical Society

the cooperative model gave a T_e of 21 °C and an h_e of −25 kcal mol^{-1}. These results suggest that the L–L and L–D dendrons co-assemble into single columns. The same conclusions were drawn from analysis of the UV–vis data of the D–DL, DL–L, and DL–D dendritic dipeptides: the D–DL dipeptide gave identical results to the L–DL dendron, and the DL–L and DL–D dipeptides co-assemble at $T_e = 19$ °C and $h_e = -26$ kcal mol^{-1}, below the expected values for assembly into two distinct columns (Fig. 12, bottom). All of the co-assembled columns obtained from partially racemized dendritic dipeptides are less enthalpically favorable than the helical columns assembled from the enantiopure dendrons.

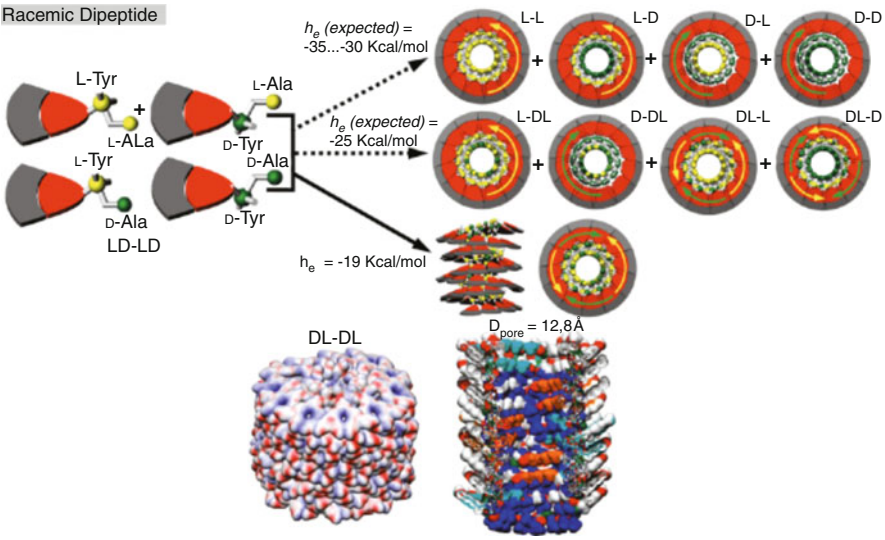

Fig. 13 Self-assembly of the fully racemized dendritic dipeptides into supramolecular helical columns: dipeptide DL–DL with racemic Tyr and racemic Ala. Three possible self-assembly pathways, with the corresponding expected or experimental molar enthalpies in solution, are presented. The side-views and cross-sections of the porous supramolecular columns were determined by XRD analysis in the solid state. (The color code of the dipeptides used in the cross-section of the columns is explained in Fig. 3b). Reprinted with permission from [67]. Copyright 2011 American Chemical Society

Co-assembly of the partially racemized dendrons, as observed by CD/UV analysis in solution, was confirmed by powder and fiber-oriented XRD experiments in the solid state. Porous columns were observed in bulk in each case, with no indication of the presence of distinct supramolecular objects, therefore excluding assembly of the diastereomeric dendrons into two distinct columns. As shown in Fig. 12, the L–DL and D–DL dendrons, which contain an enantiopure Tyr and a racemic Ala, form helical columns of opposite handedness. In contrast, the DL–L and DL–D dendrons, which contain a racemic Tyr and an enantiopure Ala, form less ordered columns without helicity over significant length scales. This confirms the preponderant role of Tyr in the selection of the helical sense.

The analysis of this family of dendritic dipeptides would be incomplete without examining the fully racemized DL–DL dendritic dipeptide. This dendron is an equimolar mixture of the four stereoisomers L–L, D–D, L–D, and D–L, as explained in Fig. 5. No net ellipticity was observed by CD analysis of the DL–DL dendron in solution, yet the UV–vis data supported the cooperative formation of a supramolecular column and allowed one to distinguish between three different self-assembly pathways [67]. As illustrated in Fig. 13, the homochiral and heterochiral constituents of the fully racemized dendritic dipeptide can assemble into four distinct enantiomerically and diastereomerically pure columns, assemble into two to four distinct columns composed of mixed diastereoisomers, or co-assemble into a single column. The low temperature of elongation T_e (20 °C) and molar enthalpy of monomer addition h_e

(-19 kcal mol^{-1}) obtained by analysis of the UV–vis data are consistent with co-assembly of all four stereoisomers into a single column and exclude the first two self-assembly pathways. The self-assembly process is driven by the dendritic part of the dendritic dipeptide, and the columns are further stabilized by hydrogen bonding between dipeptidic groups. Supramolecular polymerization in the bulk state occurs via a similar co-assembly pathway, as evidenced by the observation of a single type of columnar, less-ordered object from XRD experiments.

The aforementioned results elaborated the self-assembly process for equimolar mixtures of diastereomeric and enantiomeric dendritic dipeptides. However, in the context of the origin of biological homochirality, an evenly split mixture of the stereochemical permutations is statistically improbable. In order to elucidate further the self-assembly process for mixtures of enantiomeric dipeptides in different proportions, a majority-rules experiment [73–75] was performed. In this experiment, the net helicity is analyzed as a function of enantiomeric excess. A linear increase of net helicity indicates the absence of majority-rules behavior, whereas net helicity increases non-linearly and overcomes the enantiomeric excess in the case of a majority-rules effect. The majority-rules phenomenon typically depends on two factors: the monomer mismatch penalty, which represents the cost of placing the incorrect stereoisomer in a supramolecular assembly of opposite handedness, and the helix reversal penalty, which represents the energetic cost required to invert the helicity of a column. In the present system, mixtures of the enantiomeric L-Tyr-L-Ala and D-Tyr-D-Ala dendritic dipeptides in various proportions were prepared, and their CD spectra were measured in cyclohexane solution at 10 °C (where the dendrons are fully aggregated). A complex relationship between net helicity and enantiomeric excess was observed (Fig. 14) [67]. The relationship is non-linear, but the system does not exhibit a clear amplification of chirality. This may be explained by the conformational adaptability of both enantiomeric dendrons and by their ability to co-assemble into single supramolecular columns as discussed above. The conformations adopted by L–L and D–D dendrons in the helical columns are very different from their preferred conformations as molecularly dissolved species, and this flexibility also allows them to adapt their conformations so as to facilitate their incorporation into a mismatched column. Moreover, the entire structure of the assembly can change from enantiomerically pure, highly ordered helical columns to co-assembled, poorly ordered columns depending on the proportion between the enantiomers. Between 50% and 100% enantiomeric excess the long-range helical order will start getting disrupted by the minority dendron with mismatched handedness. Below 50% enantiomeric excess the helicity of the columns, and hence the amplification of chirality, will be reduced.

The supramolecular assemblies of the homochiral, heterochiral, and racemized dendritic dipeptides were further characterized in the solid state by DSC and fiber-oriented wide-angle XRD [67]. DSC traces upon heating indicate that all dipeptides undergo a glass transition from a glassy hexagonal phase $\Phi_{h,g}$ to a hexagonal columnar phase Φ_h around 50–60 °C, followed by isotropization at 94–96 °C (Fig. 15). Annealing experiments just below the isotropization transition led to intra- and inter-columnar crystallization of the homochiral dendritic dipeptide structures, and to partial crystallization of the heterochiral dipeptide structures,

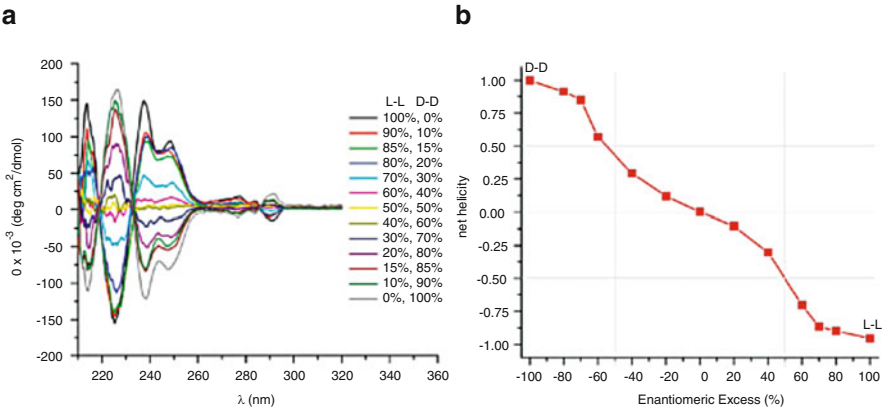

Fig. 14 CD spectra of mixtures of the L-Tyr-L-Ala and D-Tyr-D-Ala dendritic dipeptides in various proportions, collected at 10 °C in cyclohexane (1.6×10^{-4} M) (**a**); and net helicity as a function of the enantiomeric excess (majority-rules experiment) (**b**). Reprinted with permission from [67]. Copyright 2011 American Chemical Society

whereas no crystallization was observed in the cases of the partially and fully racemized dendritic dipeptides. Crystallization of the homochiral columnar structures was evidenced by the appearance of a second endothermic peak at higher temperature corresponding to a new isotropization transition from the ordered state to the isotropic melt. A complete shift in the isotropization, accompanied by a 125% increase in the enthalpy change associated with the transition, was observed after annealing for 2 h, indicating fast and complete crystallization of the structure. In the case of the heterochiral dendritic dipeptides both transitions are still observed even after annealing for 15 h, with a 38% increase in the enthalpy change associated with melting of the ordered phase. This evidences a slow and incomplete crystallization process. In the case of the partially and fully racemized dendritic dipeptides annealing did not result in the appearance of a higher-ordered phase or in a significant increase of the enthalpy change, which attests to the absence of crystallization.

The crystallization results obtained by DSC traces after annealing were confirmed by wide-angle XRD experiments. The XRD patterns of the homochiral dendritic dipeptides after annealing feature amplification of both short-range and long-range order, as indicated by the intensification of the 5.0-Å registry features and by the additional wide-angle features (blue arrows in Fig. 16) [67]. The fiber patterns collected for the heterochiral dendritic dipeptides exhibit amplification of the short-range order but only a slight increase of the long-range order following the annealing process, confirming the lesser extent of crystallization observed by DSC. Little change was observed in the XRD patterns of the racemized dendritic dipeptides upon annealing; these supramolecular dendritic dipeptides lack the intra- and intercolumnar order observed for enantiomerically pure dipeptides.

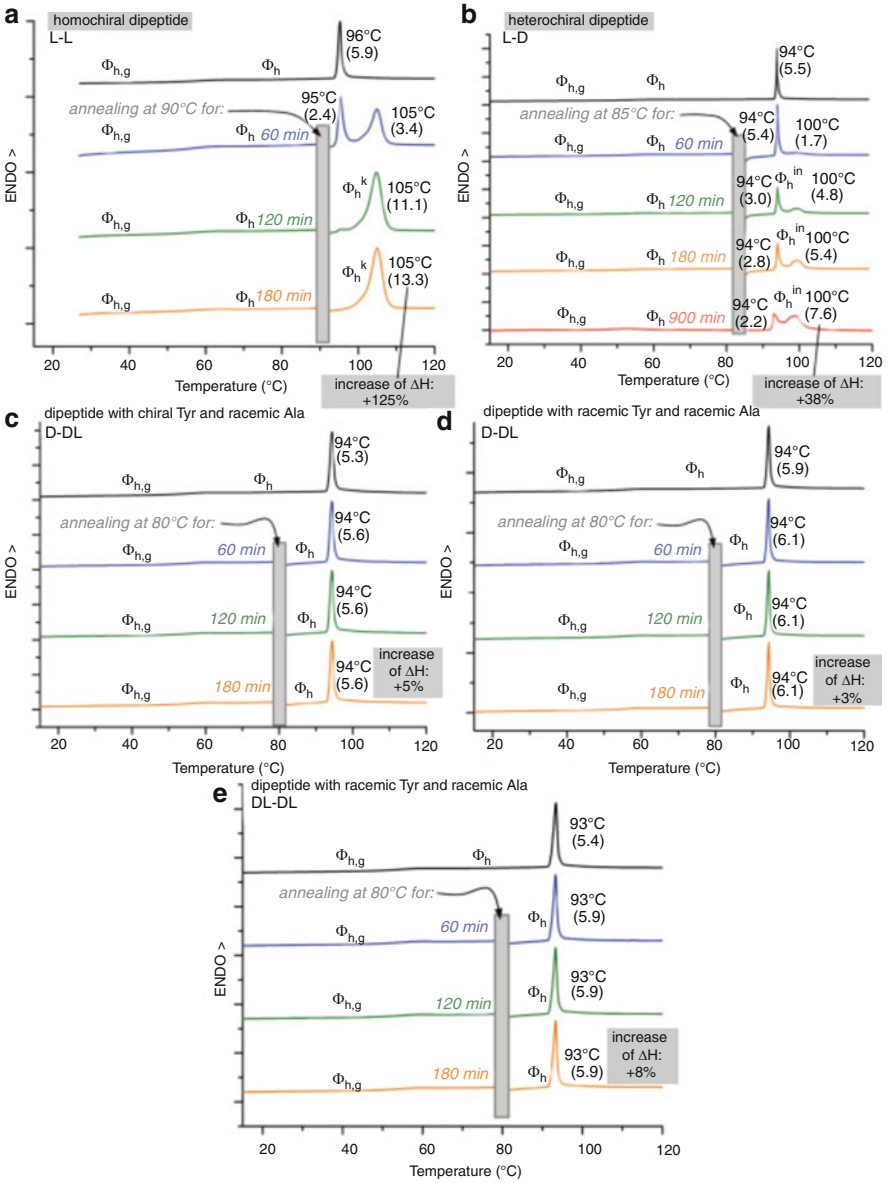

Fig. 15 DSC traces of dendritic dipeptides upon heating with various annealing times prior to isotropization: L–L (**a**), L–D (**b**), D–DL (**c**), DL–D (**d**), and DL–DL (**e**). The associated enthalpy changes are indicated in *parentheses* (kcal mol^{-1}). Reprinted with permission from [67]. Copyright 2011 American Chemical Society

Overall, the combination of solution and solid state analyses of dendritic dipeptides revealed critical relationships between the dipeptide stereochemistry and the self-assembly processes. All stereoisomers and mixtures of stereoisomers

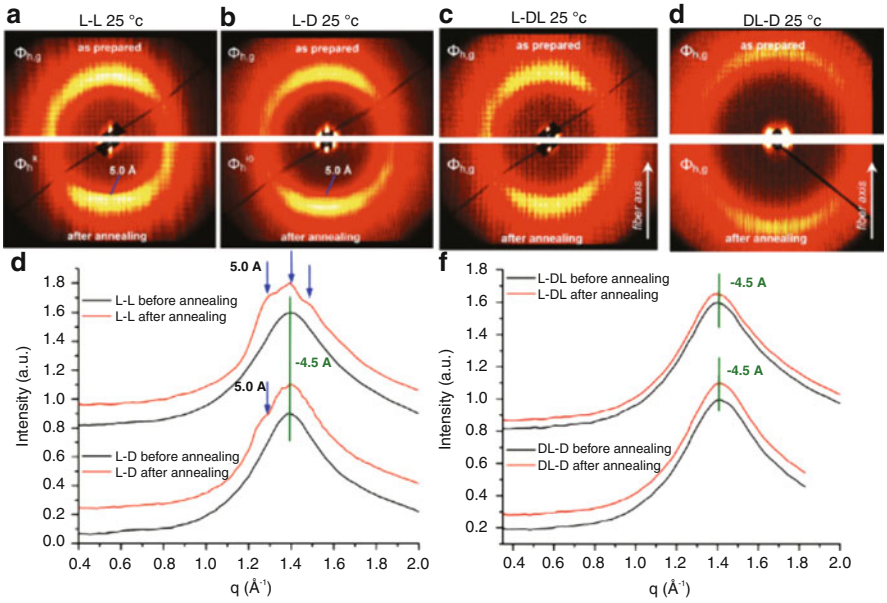

Fig. 16 Wide-angle XRD patterns collected from the oriented fibers of the dendritic dipeptides L–L (**a**), L–D (**b**), L–DL (**c**), and DL–D (**d**) before (*top*) and after annealing (*bottom*). Meridional plots of the XRD patterns of L–L and L–D (**e**) and L–DL and DL–D (**f**) before (*black curve*) and after annealing (*red curve*). *Blue arrows* indicate additional wide-angle features after annealing. Reprinted with permission from [67]. Copyright 2011 American Chemical Society

cooperatively assemble into columnar supramolecular structures. Formation of racemic helical columns from the achiral dendritic alcohol [4-3,4-3,5]12G2-CH_2OH shows that the self-assembly process is driven by the dendritic part of the molecule. When a Tyr–Ala dipeptide is covalently linked to the dendron the stereochemistry of Tyr governs the handedness of the helical columns, while the stereochemistry of Ala allosterically regulates the structural features of the columns. Helical self-assembly is more enthalpically favorable for the homochiral L–L and D–D dendritic dipeptides than for the heterochiral L–D and D–L dendritic dipeptides. Moreover, crystallization occurs readily in the solid state for homochiral dipeptides, but is slow and limited in the case of heterochiral dipeptides. These results suggest that in the present case homochirality leads to more ordered and more stable supramolecular structures and therefore they may enlighten nature's preference for homochirality. Diastereomeric and enantiomeric mixtures of dendritic dipeptides with one or two racemized α-amino acids co-assemble into single supramolecular columns with lower molar enthalpies for polymerization than those of stereoisomerically pure dipeptides. The co-assembly of mismatched stereoisomers disturbs the helical supramolecular polymerization process and induces loss of helicity when Tyr is racemized. None of the partially or fully

racemized dendritic dipeptides crystallizes in the bulk state, even after long annealing periods, which attests to the high level of disorder induced by the incorporation of a racemic α-amino acid in the structure of the dendritic dipeptide.

3.3 *Monitoring the Structure of Helical Supramolecular Dendritic Tyr–Ala Dipeptides Containing Different Dendrons and Protective Groups*

In Sect. 3.2 we detailed the influence of stereochemistry on self-assembly processes for a specific dendritic dipeptide system. However, in order to demonstrate that the stereochemical amplification is not limited to a single molecular system and that the conclusions can be generalized in the context of homochirality of biological molecules, our results must be confirmed by the study of other systems. Therefore, several analogues of the [4-3,4-3,5]12G2-CH_2-Boc-L-Tyr-L-Ala-OMe dipeptide described above were prepared [76]. These analogues contain the same homochiral protected dipeptide and have the same dendritic architecture as previously described, except for the alkyl chain lengths which vary from $n = 1$ to $n = 16$. The corresponding achiral dendritic alcohols without the peptidic apex were also synthesized for comparison (Fig. 17).

All achiral dendritic alcohols [4-3,4-3,5]12G2-CH_2OH and chiral dendritic dipeptides [4-3,4-3,5]12G2-CH_2-Boc-L-Tyr-L-Ala-OMe self-assemble into helical porous columns both in solution and in the bulk state. The diameters of the pores (D_{pore}) were calculated by simulation of the small-angle XRD diffractograms. Surprisingly, even the dendritic alcohols were found to form porous structures. As shown in Fig. 18 D_{pore} can effectively be tuned by modulating the length of the alkyl chain of the dendron. In the case of the dendritic dipeptides the pore size decreases when n increases from 6 to 16 whereas the diameter of the column shows the opposite trend.

Oriented-fiber XRD experiments demonstrated that all supramolecular columns self-assembled from the achiral dendritic alcohols and from the chiral dendritic dipeptides are helical. As expected, the achiral dendritic alcohols form racemic mixtures of helical columns with opposite handedness while the chiral dendritic dipeptides form enantiomerically pure helical columns. The helicity of the columns assembled from achiral alcohols confirms our previous hypothesis that the helicity is driven by the achiral dendritic part of the molecule. In the case of the chiral dendritic dipeptides the self-assembly process could be followed by temperature-dependent CD/UV in solution (Fig. 19). Helical self-assembly occurs upon cooling and is evidenced by the appearance of several positive and negative Cotton effects assigned to the aromatic part of the dendron, which indicate a transfer of chirality from the dipeptide to the dendritic core. Interestingly the Cotton effect at 237 nm depends on the length of the alkyl chain, which evidences that modulating the alkyl chain induces changes in the supramolecular conformations of the dendrons.

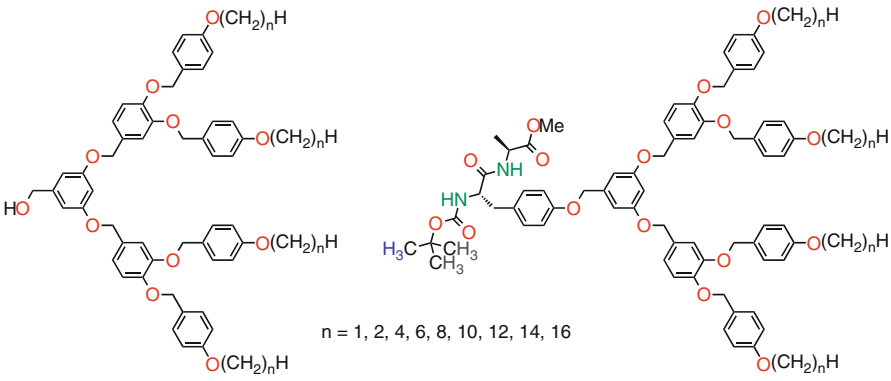

Fig. 17 Chemical structures of the achiral dendritic alcohols [4-3,4-3,5]nG2-CH_2OH and of the chiral dendritic dipeptides [4-3,4-3,5]nG2-CH_2-Boc-L-Tyr-L-Ala-OMe with alkyl chain lengths varying from $n = 1$ to $n = 16$

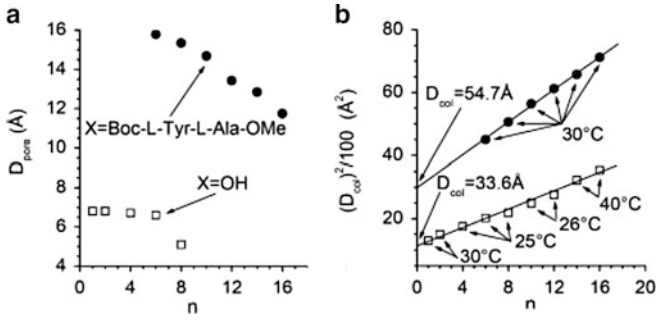

Fig. 18 Dependence of the pore diameter (D_{pore}) at 30 °C (**a**) and of the column diameter (D_{col}) (**b**) of the dendritic alcohols [4-3,4-3,5]nG2-CH_2OH and of the dendritic dipeptides [4-3,4-3,5] nG2-CH_2-Boc-L-Tyr-L-Ala-OMe on the alkyl chain length n. Reprinted with permission from [76]. Copyright 2006 PNAS

The conformations of the dendrons in the supramolecular assemblies were further investigated by molecular modeling based on the XRD data. These conformations give an insight into the dependence of the pore size on the structure of the dendron. D_{pore} is linked to μ, the number of dendrons forming a single turn of the helix, which in turn is linked to α', the projection of the solid angle of the dendron (Fig. 20) [54, 77, 78]. These relations explain the significant increase in pore size resulting from the attachment of a dipeptide to the apex of the dendron. Attaching the dipeptide to the dendron decreases α', which in turn increases μ and the diameter of the pore by 9 Å. Thus, we demonstrated in the last two sections that the structure and stability of helical pore-forming dendritic dipeptides depend on the length of the alkyl chain and on the stereochemistry of the second α-amino acid of the dipeptide.

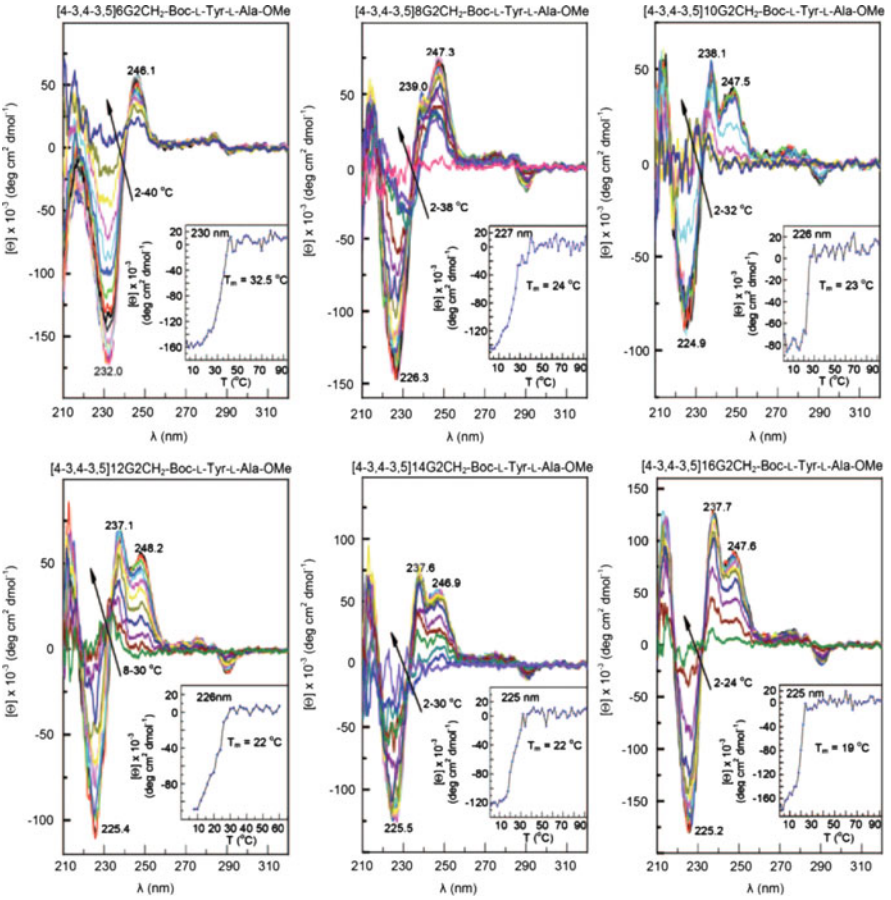

Fig. 19 Temperature-dependent CD spectra of the dendritic dipeptides [4-3,4-3,5]nG2-CH_2-Boc-L-Tyr-L-Ala-OMe (n = 6–16) in methylcyclohexane/cyclohexane solution (1.2×10^{-4} mol L^{-1}). *Arrows* indicate trends upon increasing temperature. *Insets*: dependence of molecular ellipticity on temperature at the wavelength at which the Cotton effect has maximum intensity. The melting temperatures (T_m) of the self-assemblies are also indicated. Reprinted with permission from [76]. Copyright 2006 PNAS

Moreover, complementary reports have shown that the structural features of the pore also depend on the protective groups of the dipeptide [79] and on the dendritic substitution pattern [80, 81] (Fig. 21). Varying the nature and the size of the protective group at the N-terminus of the dipeptide resulted in alteration of the thermal stability and size of the self-assembled helical pores [79]. Changes in the Cotton effects of the helical pores depending on the protective group further evidenced the influence of the end group at the N-terminus on the conformation of the dendrons in the self-assembly and hence on the structure and stability of the

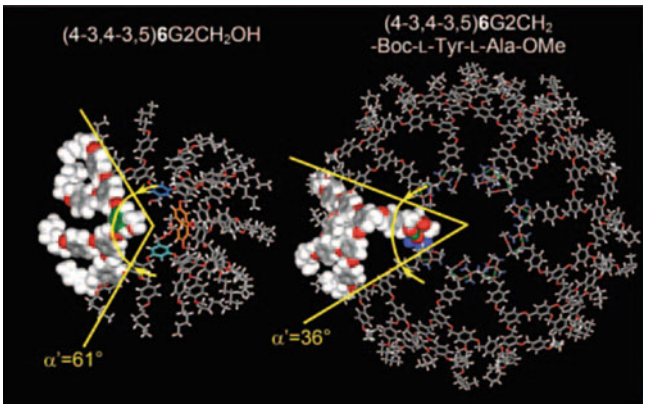

Fig. 20 Top view of one layer of the helical supramolecular pores assembled from [4-3,4-3,5] 6G2-CH_2OH and [4-3,4-3,5]6G2-CH_2-Boc-L-Tyr-X-OMe. The projections of the solid angles of each dendron (α') are indicated. Conformations obtained by molecular modeling of the XRD data together with experimental density. Reprinted with permission from [76]. Copyright 2006 PNAS

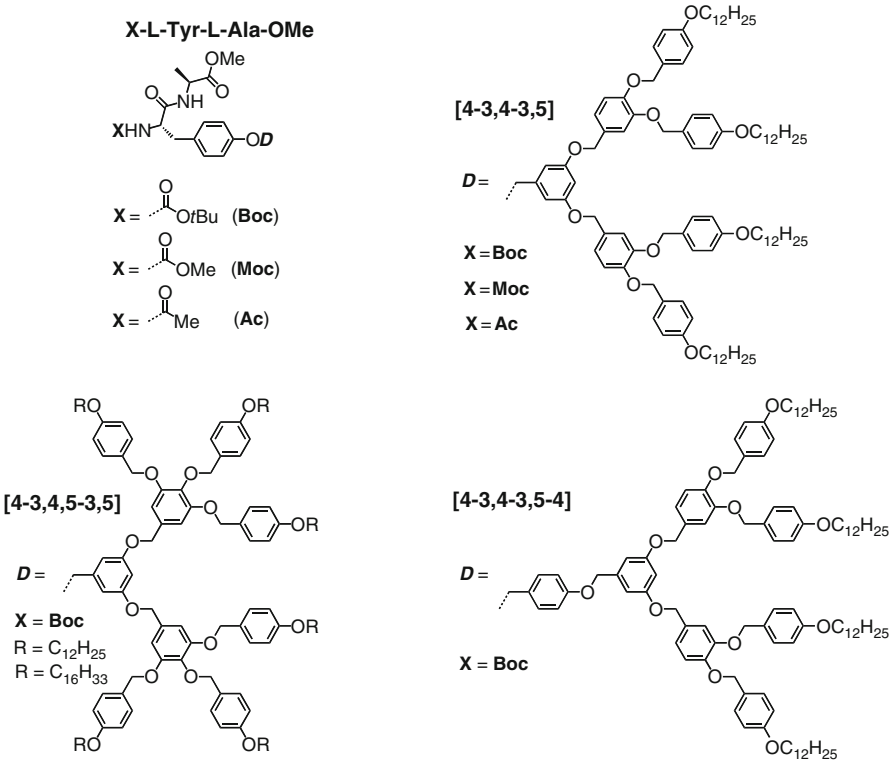

Fig. 21 Chemical structures of dendritic dipeptides with various protective groups at the N-terminus and various dendritic substitution patterns, which form circular or elliptic pores upon helical supramolecular polymerization

self-assembly. These observations combined with the effect of Ala in the pore formation suggest that allosteric regulation of the pore structure is bidirectional and occurs via the N-terminal amino acid as well as the C-terminal amino acid. Changing the dendritic substitution pattern from [4-3,4-3,5]12G2-CH_2- to [4-3,4,5-3,5]12G2-CH_2- on the protected dipeptide Boc-L-Tyr-L-Ala-OMe induces a reduction of the pore diameter [80]. The same protected dipeptide attached to a [4-3,4-3,5-4]12G2-CH_2- dendron forms helical pores that undergo reversible circular to elliptical shape changes [81]. In all the aforementioned studies transfer and amplification of chirality from the dipeptidic apex to the aromatic domain of the dendron were observed, thus demonstrating that the influence of stereochemistry in self-assembly processes can be generalized and linked to nature's inclination for homochirality. In addition, these studies provide powerful tools to design and program the internal structure and stability of synthetic helical pores, with potential applications in reversible encapsulation or stochastic sensing.

3.4 Beyond Tyr–Ala Dipeptides

In the previous sections the dendrons were constructed from the protected dipeptide Boc-Tyr-Ala-OMe, and the influence of the dipeptide stereochemistry and of the dendron architecture on the self-assembly process was determined by studying various combinations of Tyr and Ala stereochemistry and varying the length of the alkyl chain. Our results showed that the first α-amino acid, Tyr, selects the helical handedness, and suggested that the second α-amino acid, Ala, as well the dendron end chains, play an important role in the allosteric regulation of the structural features of the self-assembly (e.g., the diameters of the pore and of the column). Yet, nature possesses hundreds of amino acids, and 20 standard α-amino acids in abundance. In order to investigate further the influence of the second α-amino acid on the helical supramolecular polymerization, various dendritic dipeptides [4-3,4-3,5]12G2-CH_2-Boc-L-Tyr-X-OMe, in which X represents the non-polar α-amino acids Gly, L-Val, L-Leu, L-Ile, L-Phe, or L-Pro, were prepared (Fig. 22) [82]. The dendritic part of these compounds is the [4-3,4-3,5]12G2-CH_2- motif, which is identical to that used to build the Boc-Tyr-Ala-OMe dendritic dipeptides. It is covalently linked to the side chain of Tyr by etherification of the phenol group of Tyr as previously described for the Boc-Tyr-Ala-OMe dendrons.

All of the [4-3,4-3,5]12G2-CH_2-Boc-L-Tyr-X-OMe dendritic dipeptides self-assemble into helical porous columns in the solid state [82]. The helicity of the columns was confirmed by short-range helical order in the fiber-oriented XRD patterns, while the porous structure of the self-assembly was evidenced by powder small-angle XRD. In the solid state the columns are further organized into 2D or 3D columnar liquid crystal phases or columnar crystal phases. DSC experiments before and after annealing showed that the thermal stability of the periodic arrays and the

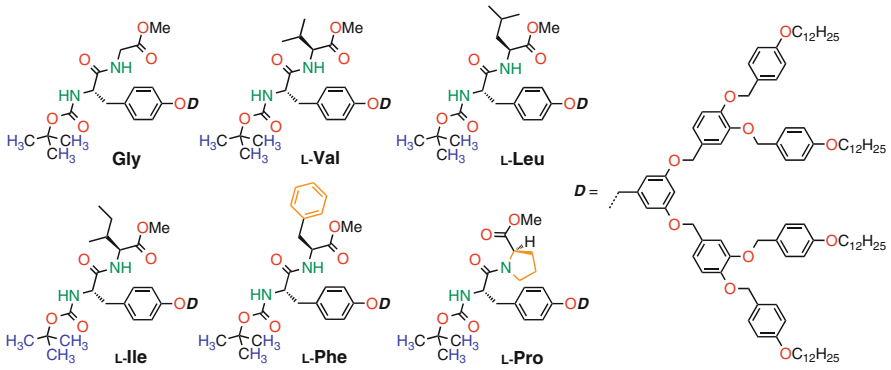

Fig. 22 Chemical structures of the dendritic dipeptides [4-3,4-3,5]12G2-CH_2-Boc-L-Tyr-X-OMe, where the second α-amino acid X is Gly, L-Val, L-Leu, L-Ile, L-Phe, or L-Pro, and color code used in the molecular models in Figs. 23 and 24

propensity for crystallization of the dendritic dipeptides in the solid state depend on the substituent of the second α-amino acid X. As a general trend the supramolecular dendrimers crystallize more readily when X contains a large hydrophobic substituent (L-Val, L-Leu, and L-Ile) or when X contains an aromatic substituent (L-Phe) that can stabilize the structure via π–π interactions. The dendritic dipeptides based on Gly and L-Pro do not crystallize, even after long annealing periods. The supramolecular dendrimer based on L-Pro also exhibits a lower thermal stability, which was explained by the limited stabilizing interactions of the conformationally restricted cyclic substituent of L-Pro.

Self-assembly of the dendritic dipeptides [4-3,4-3,5]12G2-CH_2-Boc-L-Tyr-X-OMe was studied in solution by CD/UV [82]. Except in the case of L-Pro, the CD spectra exhibit amplification of chirality upon cooling from 40 °C to 8 °C, which supports the formation of helical columns in solution. The dendritic dipeptide based on L-Pro must self-assemble at lower temperature in solution, in agreement with the lower thermal stability of its structure in the solid state. In all other cases self-assembly was observed and the signs of the Cotton effects in the CD spectra indicated that the stereochemistry of Tyr selects the helical sense of the column. Dendritic dipeptides with similar substituents at the X amino acid (e.g., the pairs L-Val, L-Ile and L-Leu, L-Phe) exhibit similar Cotton effects, which indicate that the substituent of X has an influence on the conformation of the dendron in the self-assembled structure. The presence of a large hydrophobic substituent on X also increases the thermal stability of the self-assembly in solution, in line with the DSC results in the solid state.

Structural and retrostructural analysis of the self-assembled dendritic dipeptides by means of XRD analysis on powder and oriented fibers, electron density maps, simulations of the XRD data, and molecular modeling gave access to the conformations of the dendrons in the helical columns (Figs. 23 and 24) [82].

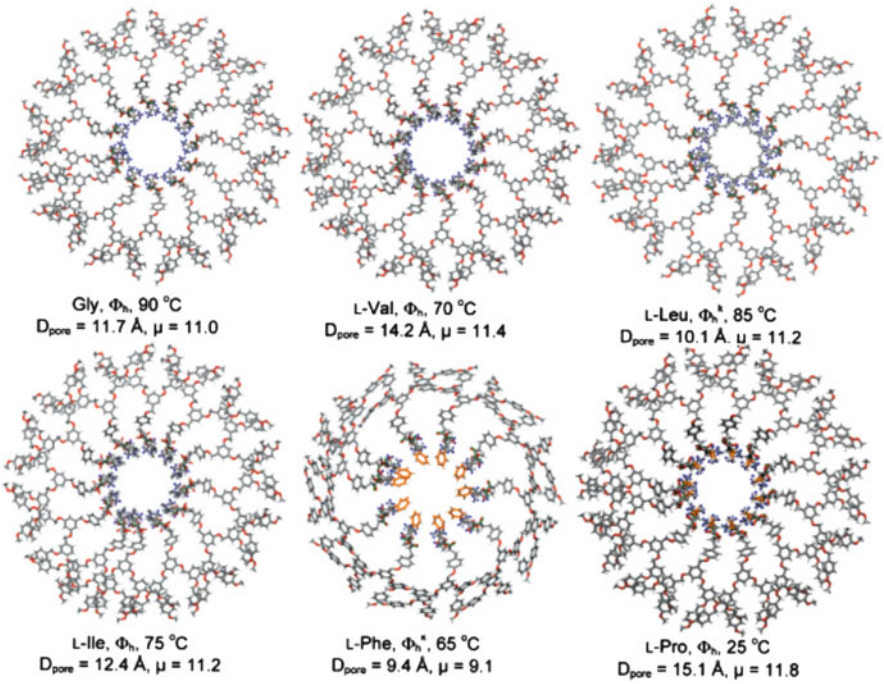

Fig. 23 Top view of one layer of the helical supramolecular pores assembled from [4-3,4-3,5] 12G2-CH_2-Boc-L-Tyr-X-OMe. The structure of the α-amino acid X of the dipeptide, lattice, temperature, pore diameter (D_{pore}) and number of dendrons forming one turn of the helix (μ) are indicated. The color code is the same as in Fig. 22. Reprinted with permission from [82]. Copyright 2011 American Chemical Society

Modifying the substituent of the X amino acid proves to be a powerful approach to monitor the size and the structure of the pore. In the solid state the diameter of the pore varies from 9.4 to 15.1 Å, and in all cases the substituent of the second amino acid is located in the inner part of the pore, thus altering the hydrophobicity of the pore. The molecular models also highlight the presence of several in-layer and inter-layer hydrogen-bonding networks between the dipeptide units. In the case of the tertiary peptide L-Pro the hydrogen-bond formation is limited by the bulky and conformationally restricted cyclic substituent, and the dipeptides do not display any other favorable intermolecular interactions, which explains the lower thermal stability of its supramolecular pore. In the case of L-Phe the inner part of the pore is stabilized by π–π stacking between the aryl substituents. This study revealed the key role of the second α-amino acid in dendritic dipeptides on the self-assembly, stability, and structure of porous helical columns.

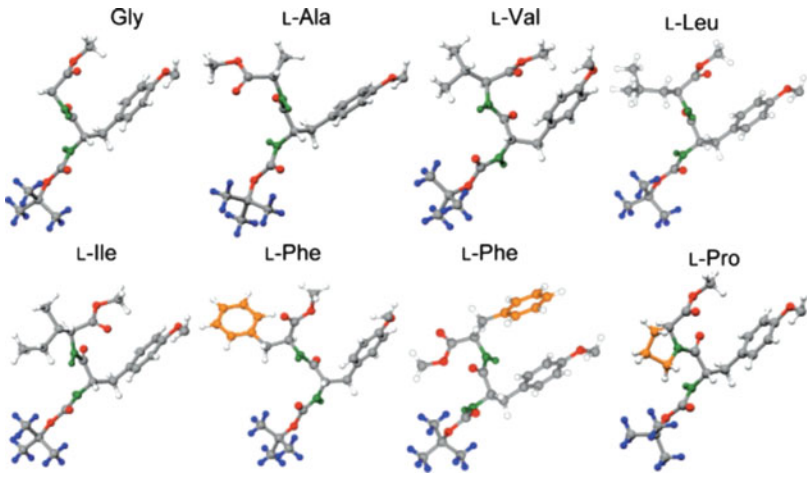

Fig. 24 Conformations of the dipeptidic apexes in the helical supramolecular pores assembled from [4-3,4-3,5]12G2-CH_2-Boc-L-Tyr-X-OMe. The conformations were obtained by molecular modeling generated from XRD experiments. Two possible models are presented in the case of L-Phe. The color code is the same as in Fig. 22. Reprinted with permission from [82]. Copyright 2011 American Chemical Society

4 Chiral Supramolecular Spheres

The conjugation of dipeptides to the apex of [4-3,4-3,5]12G2-CH_2OH provided immensely useful porous protein mimics that simultaneously provided potential insight into the origin of polypeptide homochirality. As described in Sect. 3, the topology of self-assembling Percec-type dendrons dictates the general shape of the self-assembling supramolecular dendrimer. The dendron [4-3,4-3,4]12G2-CH_2OH, the regioisomer of [4-3,4-3,5]12G2-CH_2OH where the innermost branching point is mutated from a 3,5 *meta*-dibenzyloxy geometry to a 3,4 *ortho*-dibenzyloxy geometry, produces exclusively *spherical* supramolecular dendrimers that typically pack into *Pm3n* lattices. When [4-3,4-3,4]12G2-CH_2OH is used to generate the chiral dendritic dipeptide [4-3,4-3,4]12G2-CH_2-Boc-L-Tyr-L-Ala-OMe, unprecedented hollow chiral spheres are generated (Fig. 25) [83].

While a library of dendrons with the [4-3,4-3,4] or hybrid [4-3,4-3,5-4^n] topologies and varying chiral or achiral periphery groups (Fig. 26) were able to generate hollow spherical structures, only the dendritic dipeptide [4-3,4-3,4]12G2-CH_2-Boc-L-Tyr-L-Ala-OMe was able to generate a Cotton effect attributable to the dendritic portion of the molecule (Fig. 27). The temperature-dependent CD-UV spectra collected on this hollow-sphere dendritic dipeptide exhibit similar features to those collected on helical porous column-forming dendritic dipeptide [4-3,4-3,5]12G2-CH_2-Boc-L-Tyr-L-Ala-OMe. The CD-UV spectra recorded in methyl

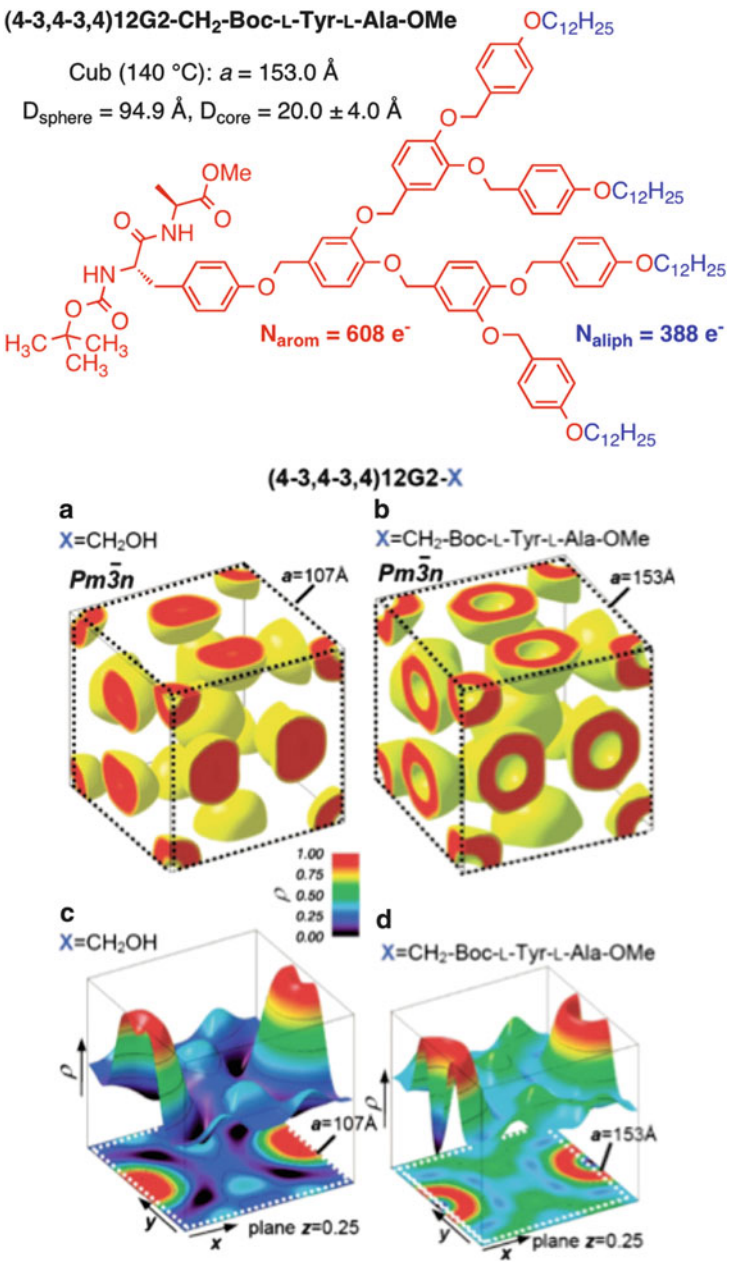

Fig. 25 Structure of [4-3,4-3,4]12G2-CH_2-Boc-L-Tyr-L-Ala-OMe (*top*). Reconstructed relative three-dimensional (**a**, **b**) and two-dimensional cross sections (**c**, **d**) of relative electron densities of [4-3,4-3,4]12G2-CH_2-X in the *Pm3n* cubic phase (*bottom*). In (**a**) and (**b**) only the high electron density regions are shown. Lattice parameter a, z-plane positions, and X-group are indicated. Reprinted with permission from [83]. Copyright 2008 American Chemical Society

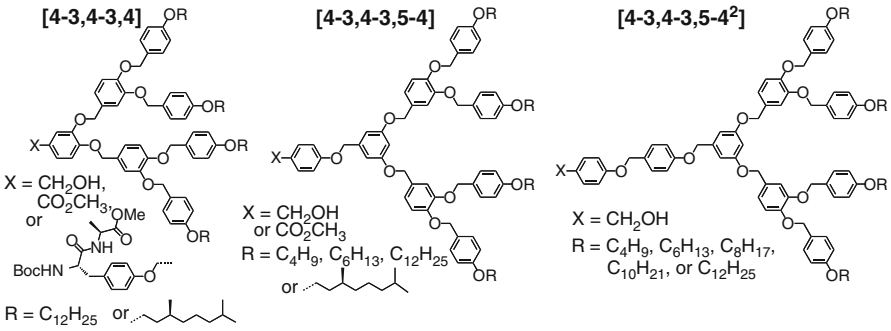

Fig. 26 Chemical structures of the dendrons with [4-3,4-3,4], [4-3,4-3,5-4] and [4-3,4-3,5-4^2] topologies that self-assemble into hollow supramolecular spheres

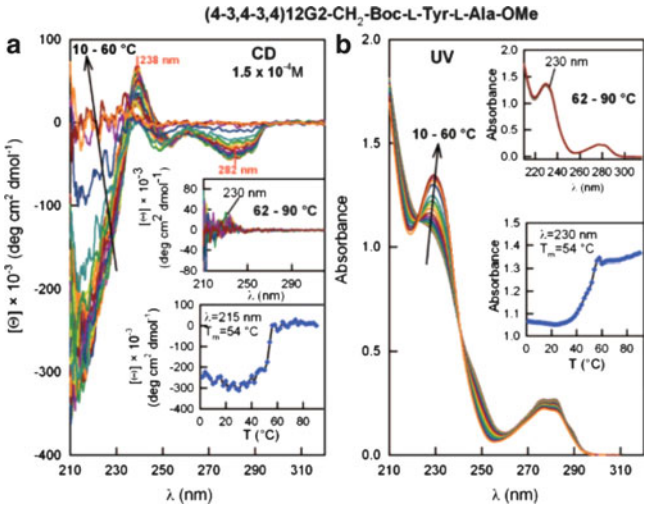

Fig. 27 (**a**) CD and (**b**) UV spectra of [4-3,4-3,4]12G2-CH_2-Boc-L-Tyr-L-Ala-OMe in methyl cyclohexane (1.5×10^{-4} M). *Arrows* indicate trends upon increasing temperature from 10 °C to 60 °C. *Upper insets*: Cotton effect associated with the molecular solution of the dendron above 60 °C. *Lower insets*: dependence of the ellipticity at 215 nm and of the absorbance at 230 nm on temperature. The *curve* profiles indicate a cooperative self-assembly mechanism. Reprinted with permission from [83]. Copyright 2008 American Chemical Society

cyclohexane solution were similar to those recorded by deposition of the dendritic dipeptide from solution into a thin-film. Therefore, it is concluded that the hollow spheres produced by the dendritic dipeptide in the solid state also exhibit helical chirality of the dendritic sheath.

Though the spherical representation is likely a simplification of a polygonal cluster structure, two models for the self-assembly of the conical dendritic dipeptides

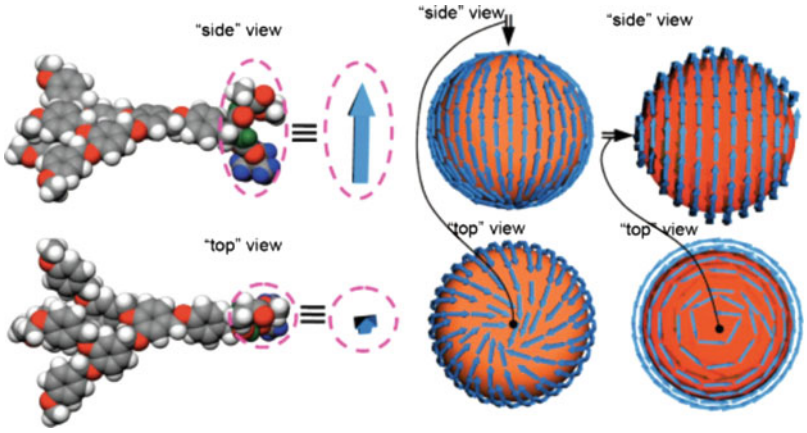

Fig. 28 Schematic of the two possible spherical helix (loxodrome) or apple peel contours created by the dipeptide on the hollow core of the supramolecular sphere assembled from [4-3,4-3,4] 12G2-CH_2-Boc-L-Tyr-L-Ala-OMe. The dipeptide is schematically represented by a *blue arrow*. Reprinted with permission from [83]. Copyright 2008 American Chemical Society

are presented (Fig. 28), where the orientation of the dipeptide and dendritic sheath vary along the surface like the spherical helix (also known as a loxodrome) generated by an apple peel.

Preliminary examination of the temperature dependent CD-UV spectra of [4-3,4-3,4]12G2-CH_2-Boc-L-Tyr-L-Ala-OMe suggests a cooperative self-assembly with transfer of chiral information from the dipeptide to the dendritic sheath below an elongation temperature (T_e) of 62 °C. Further analysis of the degree of aggregation of [4-3,4-3,4]12G2-CH_2-Boc-L-Tyr-L-Ala-OMe and all of its stereochemical permutations vs temperature would provide insight into the thermodynamics of this helical supramolecular polymerization and establish whether the same homochiral selection process is operating in this spherical chiral structure as in the case of the helical columnar structures. Such an analysis would be complementary to the reviewed studies on helical porous columns, as the spherical self-assembly process strictly limits the final degree of aggregation and incomplete aggregation would be thermodynamically disfavored. Such a self-assembly process may provide insight to homochiral selection in globular proteins' structures or their primitive micellar ancestors.

5 Conclusions and Outlook

Dendritic dipeptides show that in the right context the co-assembly of even simple dipeptides can be selective for homochiral configurations. In the case of Tyr–Ala, this allows the transmission of chirality from the tyrosine molecule to the alanine molecule and to the aromatic domain of the dendritic dipeptide. This means that it is possible that chiral transmission and uniformity of homochirality amongst all

standard amino acids could be the result of supramolecular structures of peptidic assemblies and not simply common biosynthetic machinery, for example. The helical self-assembly of the homochiral dipeptides is enthalpically more favorable than that of the heterochiral and racemized dipeptides, which provides insight into nature's general preference for homochiral biomolecules from primitive to contemporary biological systems. While our model does not predict any difference between the existing biological systems and their mirror images, it suggests that heterochiral or racemic biological systems would be far less ordered than homochiral systems and would not allow the assembly of complex molecular architectures in living organisms, hence leading to more primitive and less functional biomolecules. This hypothesis could be further assessed by studying the influence of stereochemistry on the self-assembly of longer peptidic systems (e.g., dendritic tripeptides) with greater resemblance to natural peptides and proteins.

Supramolecular dendritic dipeptides not only serve as models for the role of homochirality in living systems – they also highlight the general importance of chirality in self-assembly processes. Rod-like, columnar, and even spherical supramolecular assemblies are often helical, hence chiral. The first characterizations of chiral spherical supramolecular dendrimers [51, 52, 83] pose questions about the chirality of previously reported spherical dendritic structures. In particular, the formation of a spherical monodendron [84] raises a conceptually interesting issue: can an achiral molecule self-organize into a chiral three-dimensional structure? Further analyses would be needed to address this question. More generally, the chirality of helical supramolecular structures formed from achiral building blocks is often overlooked because racemic mixtures of helical objects are obtained. However, our dendritic dipeptide models suggest that chirality plays a critical role in determining the functional properties of helical supramolecular objects. Moreover, the systems discussed in this chapter show that these functional properties can be further modulated and controlled via the connection of (homo)chiral substituents to the supramolecular building blocks. This considerably extends the range of applications of helical supramolecular dendrimers, which has already proven extremely wide. Introduction of a chiral unit can be achieved either covalently or non-covalently, and both approaches are very promising. Thus, it was shown that supramolecular interactions of a chiral electron-acceptor molecule with a columnar supramolecular dendrimer selects the twist sense of the helical column [52], while the covalent attachment of a chiral alkyl chain at the periphery of a C_3-symmetric dendrimer mediates transfer, amplification, and thermal inversion of chirality in the corresponding supramolecular assembly [85]. Similarly, a homochiral unit could potentially be introduced in other electronic materials composed of donor/acceptor self-assembled dendrimers [30, 86, 87] in order to tune their structural and electronic properties. This strategy could also be used to monitor the structure and function of self-organizable dendronized polymers. These macromolecules possess self-assembling dendritic side chains on each repeat unit, which induce a helical conformation of the linear polymer backbone. Dendronized polymers typically self-organize into arrays composed of cylindrical [88] or spherical [89] objects, whose shape and structure are determined by the structure of the dendron and the length

of the polymer backbone [90, 91] and can be visualized by SFM [88, 92]. Their dendritic sheath modulates the reactivity and chemoselectivity of the polymeric backbone; for example, the thermal isomerization and electrocyclization of polyphenylacetylenes can be tuned depending on the presence and structure of dendritic side-chain substituents [93–98]. Moreover, the dendritic sheath generates completely new properties and functions: dendronized polyphenylacetylenes act as molecular gates [95] or as nanomechanical actuators that can displace objects by reversible extension and contraction [96, 97]. These properties could potentially be further monitored by the presence of stereocenters in the dendronized polymer. The wide scope of applications of chirality in covalent and supramolecular helical polymers will most certainly promote further studies about the influence of stereochemistry on self-assembly processes, both in synthetic and biological systems.

References

1. Coveney P, Highfield R (1995) Frontiers of complexity: the search for order in a chaotic world. Random House, New York
2. Sleep NH (2010) The Hadean-Archaean environment. CSH Perspect Biol 2:1–14
3. Umbarger HE (1978) Amino-acid biosynthesis and its regulation. Annu Rev Biochem 47:533–606
4. Miller SL (1953) A production of amino acids under possible primitive Earth conditions. Science 117:528–529
5. Guijarro A, Yus M (2009) The origin of chirality in the molecules of life. RSC Chemistry, Cambridge, UK
6. Cline DB (1996) Physical origin of homochirality in life. In: American Institute of Physics Conference Proceedings, Woodbury, New York
7. Bouchiat MA, Bouchiat C (1997) Parity violation in atoms. Rep Prog Phys 60:1351–1396
8. Viedma C, Cintas P (2011) On the chiral homogeneity of nature: from atoms to small molecules. Isr J Chem 51:997–1006
9. Quack M (2002) How important is parity violation for molecular and biomolecular chirality? Angew Chem Int Ed 41:4618–4630
10. Blackmond DG (2010) The origin of biological homochirality. CSH Perspect Biol 2:1–17
11. Weissbuch I, Leiserowitz L, Lahav M (2005) Stochastic "Mirror symmetry breaking" via self-assembly, reactivity and amplification of chirality: relevance to abiotic conditions. Top Curr Chem 259:123–165
12. Kojo S, Uchino H, Yoshimura M, Tanaka K (2004) Racemic D,L-asparagine causes enantiomeric excess of other coexisting racemic D,L-amino acids during recrystallization: a hypothesis accounting for the origin of L-amino acids in the biosphere. Chem Commun 2146–2147
13. Urry DW (1971) The Gramicidin-A transmembrane channel: a proposed π(L, D) helix. Proc Natl Acad Sci USA 68:672–676
14. Kreil G (1997) D-Amino acids in animal peptides. Annu Rev Biochem 66:337–345
15. Nanda V, DeGrado WF (2004) Simulated evolution of emergent chiral structures in polyalanine. J Am Chem Soc 126:14459–14467
16. Nanda V, DeGrado WF (2006) Computational design of heterochiral peptides against a helical target. J Am Chem Soc 128:809–816
17. Nanda V, Andrianarijaona A, Narayanan C (2007) The role of protein homochirality in shaping the energy landscape of folding. Protein Sci 16:1667–1675

18. Milton RCD, Milton SCF, Kent SBH (1992) Total chemical synthesis of a D-enzyme – the enantiomers of HIV-1 protease show demonstration of reciprocal chiral substrate-specificity. Science 256:1445–1448
19. Percec V, Leowanawat P (2011) Why are biological systems homochiral? Isr J Chem 51:1107–1117
20. Fréchet JMJ, Tomalia DA (2001) Dendrimers and other dendritic polymers. Wiley, Chichester
21. Newkome GR, Moorefield CN, Vögtle F (2004) Dendrimers and dendrons: concepts, syntheses, applications. Wiley-VCH Verlag GmbH & Co. KGaA, Weinheim
22. Vögtle F, Richardt G, Werner N (2009) Dendrimer chemistry: concepts, syntheses, properties, applications. Wiley-VCH Verlag GmbH & Co. KGaA, Weinheim
23. Hawker CJ, Fréchet JMJ (1990) Preparation of polymers with controlled molecular architecture – a new convergent approach to dendritic macromolecules. J Am Chem Soc 112:7638–7647
24. Grayson SM, Fréchet JMJ (2001) Convergent dendrons and dendrimers: from synthesis to applications. Chem Rev 101:3819–3867
25. Buhleier E, Wehner W, Vögtle F (1978) Cascade-chain-like and nonskid-chain-like syntheses of molecular cavity topologies. Synthesis-Stuttgart 155–158
26. Tomalia DA, Baker H, Dewald J, Hall M, Kallos G, Martin S, Roeck J, Ryder J, Smith P (1985) A new class of polymers – starburst-dendritic macromolecules. Polym J 17:117–132
27. Newkome GR, Yao ZQ, Baker GR, Gupta VK (1985) Micelles. 1. Cascade molecules – a new approach to micelles – a [27]-arborol. J Org Chem 50:2003–2004
28. Rosen BM, Wilson CJ, Wilson DA, Peterca M, Imam MR, Percec V (2009) Dendron-mediated self-assembly, disassembly, and self-organization of complex systems. Chem Rev 109:6275–6540
29. Percec V, Johansson G, Ungar G, Zhou JP (1996) Fluorophobic effect induces the self-assembly of semifluorinated tapered monodendrons containing crown ethers into supramolecular columnar dendrimers which exhibit a homeotropic hexagonal columnar liquid crystalline phase. J Am Chem Soc 118:9855–9866
30. Percec V, Glodde M, Bera TK, Miura Y, Shiyanovskaya I, Singer KD, Balagurusamy VSK, Heiney PA, Schnell I, Rapp A, Spiess HW, Hudson SD, Duan H (2002) Self-organization of supramolecular helical dendrimers into complex electronic materials. Nature 419:384–387
31. Percec V, Imam MR, Bera TK, Balagurusamy VSK, Peterca M, Heiney PA (2005) Self-assembly of semifluorinated janus-dendritic benzamides into bilayered pyramidal columns. Angew Chem Int Ed 44:4739–4745
32. Rosen BM, Wilson DA, Wilson CJ, Peterca M, Won BC, Huang CH, Lipski LR, Zeng XB, Ungar G, Heiney PA, Percec V (2009) Predicting the structure of supramolecular dendrimers via the analysis of libraries of AB_3 and constitutional isomeric AB_2 biphenylpropyl ether self-assembling dendrons. J Am Chem Soc 131:17500–17521
33. Percec V (2006) Bioinspired supramolecular liquid crystals. Philos T R Soc A 364:2709–2719
34. Percec V, Heck J (1989) Side-chain liquid-crystal polymers containing mesogenic units based on 1/2 disk and rod-like moieties. Abstr Pap Am Chem S 198:135-POLY
35. Percec V, Heck J (1992) Towards tobacco mosaic virus-like supramolecular synthetic polymers. Abstr Pap Am Chem S 203:6-POLY
36. Percec V, Heck J, Lee M, Ungar G, Alvarez-Castillo A (1992) Poly(2-vinyloxyethyl 3,4,5-tris [4-(N-dodecanyloxy)benzyloxy]benzoate) – a self-assembled supramolecular polymer similar to tobacco mosaic-virus. J Mater Chem 2:1033–1039
37. Percec V, Lee M, Heck J, Blackwell HE, Ungar G, Alvarez-Castillo A (1992) Reentrant isotropic-phase in a supramolecular disk-like oligomer of 4-[3,4,5-tris(normal-dodecanyloxy) benzoyloxy]-4'-[(2-vinyloxy)ethoxy]biphenyl. J Mater Chem 2:931–938
38. Percec V, Heck J, Tomazos D, Falkenberg F, Blackwell H, Ungar G (1993) Self-assembly of taper-shaped monoesters of oligo(ethylene oxide) with 3,4,5-tris(p-dodecycloxybenzyloxy) benzoic acid and of their polymethacrylates into tubular supramolecular architectures displaying a columnar mesophase. J Chem Soc Perkin Trans 1 2799–2811

39. Percec V, Heck J, Johansson G, Tomazos D, Kawasumi M, Chu P, Ungar G (1994) Molecular recognition directed self-assembly of supramolecular architectures. J Macromol Sci Pure Appl Chem A 31:1719–1758
40. Tomazos D, Out G, Heck JA, Johansson G, Percec V, Moller M (1994) Isomorphism within the hexagonal columnar mesophase of molecular and macromolecular self-assembled and co-assembled columns containing tapered groups. Liq Cryst 16:509–527
41. Percec V (1995) Molecular design of novel liquid crystalline polymers with complex architecture: macrocyclics and dendrimers. Pure Appl Chem 67:2031–2038
42. Klug A (1983) From macromolecules to biological assemblies (Nobel lecture). Angew Chem Int Ed 22:565–582
43. Lindsey JS (1991) Self-assembly in synthetic routes to molecular devices – biological principles and chemical perspectives – a review. New J Chem 15:153–180
44. Durham ACH, Finch JT, Klug A (1971) States of aggregation of tobacco mosaic virus protein. Nat New Biol 229:37–42
45. Percec V, Cho WD, Ungar G, Yeardley DJP (2001) Synthesis and structural analysis of two constitutional isomeric libraries of AB_2-based monodendrons and supramolecular dendrimers. J Am Chem Soc 123:1302–1315
46. Percec V, Holerca MN, Nummelin S, Morrison JL, Glodde M, Smidrkal J, Peterca M, Rosen BM, Uchida S, Balagurusamy VSK, Sienkowska MJ, Heiney PA (2006) Exploring and expanding the structural diversity of self-assembling dendrons through combinations of AB, constitutional isomeric AB_2, and AB_3 biphenyl-4-methyl ether building blocks. Chem Eur J 12:6216–6241
47. Percec V, Peterca M, Sienkowska MJ, Ilies MA, Aqad E, Smidrkal J, Heiney PA (2006) Synthesis and retrostructural analysis of libraries of AB_3 and constitutional isomeric AB_2 phenylpropyl ether-based supramolecular dendrimers. J Am Chem Soc 128:3324–3334
48. Percec V, Won BC, Peterca M, Heiney PA (2007) Expanding the structural diversity of self-assembling dendrons and supramolecular dendrimers via complex building blocks. J Am Chem Soc 129:11265–11278
49. Percec V, Mitchell CM, Cho WD, Uchida S, Glodde M, Ungar G, Zeng XB, Liu YS, Balagurusamy VSK, Heiney PA (2004) Designing libraries of first generation AB_3 and AB_2 self-assembling dendrons via the primary structure generated from combinations of $(AB)_y$-AB_3 and $(AB)_y$-AB_2 building blocks. J Am Chem Soc 126:6078–6094
50. Rosen BM, Peterca M, Huang CH, Zeng XB, Ungar G, Percec V (2010) Deconstruction as a strategy for the design of libraries of self-assembling dendrons. Angew Chem Int Ed 49:7002–7005
51. Percec V, Imam MR, Peterca M, Wilson DA, Heiney PA (2009) Self-assembly of dendritic crowns into chiral supramolecular spheres. J Am Chem Soc 131:1294–1304
52. Percec V, Imam MR, Peterca M, Wilson DA, Graf R, Spiess HW, Balagurusamy VSK, Heiney PA (2009) Self-assembly of dendronized triphenylenes into helical pyramidal columns and chiral spheres. J Am Chem Soc 131:7662–7677
53. Peterca M, Imam MR, Leowanawat P, Rosen BM, Wilson DA, Wilson CJ, Zeng XB, Ungar G, Heiney PA, Percec V (2010) Self-assembly of hybrid dendrons into doubly segregated supramolecular polyhedral columns and vesicles. J Am Chem Soc 132:11288–11305
54. Percec V, Cho WD, Ungar G (2000) Increasing the diameter of cylindrical and spherical supramolecular dendrimers by decreasing the solid angle of their monodendrons via periphery functionalization. J Am Chem Soc 122:10273–10281
55. Balagurusamy VSK, Ungar G, Percec V, Johansson G (1997) Rational design of the first spherical supramolecular dendrimers self-organized in a novel thermotropic cubic liquid-crystalline phase and the determination of their shape by X-ray analysis. J Am Chem Soc 119:1539–1555
56. Percec V, Cho WD, Mosier PE, Ungar G, Yeardley DJP (1998) Structural analysis of cylindrical and spherical supramolecular dendrimers quantifies the concept of monodendron shape control by generation number. J Am Chem Soc 120:11061–11070

57. Dukeson DR, Ungar G, Balagurusamy VSK, Percec V, Johansson GA, Glodde M (2003) Application of isomorphous replacement in the structure determination of a cubic liquid crystal phase and location of counterions. J Am Chem Soc 125:15974–15980
58. Yeardley DJP, Ungar G, Percec V, Holerca MN, Johansson G (2000) Spherical supramolecular minidendrimers self-organized in an "inverse micellar"-like thermotropic body-centered cubic liquid crystalline phase. J Am Chem Soc 122:1684–1689
59. Ungar G, Liu YS, Zeng XB, Percec V, Cho WD (2003) Giant supramolecular liquid crystal lattice. Science 299:1208–1211
60. Zeng XB, Ungar G, Liu YS, Percec V, Dulcey SE, Hobbs JK (2004) Supramolecular dendritic liquid quasicrystals. Nature 428:157–160
61. Ungar G, Percec V, Zeng XB, Leowanawat P (2011) Liquid quasicrystals. Isr J Chem 51:1206–1215
62. Ungar G, Abramic D, Percec V, Heck JA (1996) Self-assembly of twin tapered bisamides into supramolecular columns exhibiting hexagonal columnar mesophases. Structural evidence for a microsegregated model of the supramolecular column. Liq Cryst 21:73–86
63. Percec V, Smidrkal J, Peterca M, Mitchell CM, Nummelin S, Dulcey AE, Sienkowska MJ, Heiney PA (2007) Self-assembly of hybrid dendrons with complex primary structure into functional helical pores. Chem Eur J 13:3989–4007
64. Peterca M, Percec V, Imam MR, Leowanawat P, Morimitsu K, Heiney PA (2008) Molecular structure of helical supramolecular dendrimers. J Am Chem Soc 130:14840–14852
65. Percec V, Dulcey AE, Balagurusamy VSK, Miura Y, Smidrkal J, Peterca M, Nummelin S, Edlund U, Hudson SD, Heiney PA, Hu DA, Magonov SN, Vinogradov SA (2004) Self-assembly of amphiphilic dendritic dipeptides into helical pores. Nature 430:764–768
66. Percec V, Dulcey AE, Peterca M, Ilies M, Ladislaw J, Rosen BM, Edlund U, Heiney PA (2005) The internal structure of helical pores self-assembled from dendritic dipeptides is stereochemically programmed and allosterically regulated. Angew Chem Int Ed 44:6516–6521
67. Rosen BM, Peterca M, Morimitsu K, Dulcey AE, Leowanawat P, Resmerita AM, Imam MR, Percec V (2011) Programming the supramolecular helical polymerization of dendritic dipeptides via the stereochemical information of the dipeptide. J Am Chem Soc 133:5135–5151
68. Kaucher MS, Peterca M, Dulcey AE, Kim AJ, Vinogradov SA, Hammer DA, Heiney PA, Percec V (2007) Selective transport of water mediated by porous dendritic dipeptides. J Am Chem Soc 129:11698–11699
69. De Greef TFA, Smulders MMJ, Wolffs M, Schenning APHJ, Sijbesma RP, Meijer EW (2009) Supramolecular polymerization. Chem Rev 109:5687–5754
70. Jonkheijm P, van der Schoot P, Schenning APHJ, Meijer EW (2006) Probing the solvent-assisted nucleation pathway in chemical self-assembly. Science 313:80–83
71. Percec V, Ungar G, Peterca M (2006) Self-assembly in action. Science 313:55–56
72. Smulders MMJ, Nieuwenhuizen MML, de Greef TFA, van der Schoot P, Schenning APHJ, Meijer EW (2010) How to distinguish isodesmic from cooperative supramolecular polymerisation. Chem Eur J 16:362–367
73. Green MM, Garetz BA, Munoz B, Chang HP, Hoke S, Cooks RG (1995) Majority rules in the copolymerization of mirror-image isomers. J Am Chem Soc 117:4181–4182
74. Jin W, Fukushima T, Niki M, Kosaka A, Ishii N, Aida T (2005) Self-assembled graphitic nanotubes with one-handed helical arrays of a chiral amphiphilic molecular graphene. Proc Natl Acad Sci USA 102:10801–10806
75. van Gestel J, Palmans ARA, Titulaer B, Vekemans JAJM, Meijer EW (2005) "Majority-rules" operative in chiral columnar stacks of C_3-symmetrical molecules. J Am Chem Soc 127:5490–5494
76. Percec V, Dulcey AE, Peterca M, Ilies M, Nummelin S, Sienkowska MJ, Heiney PA (2006) Principles of self-assembly of helical pores from dendritic dipeptides. Proc Natl Acad Sci USA 103:2518–2523

77. Ungar G, Percec V, Holerca MN, Johansson G, Heck JA (2000) Heat-shrinking spherical and columnar supramolecular dendrimers: their interconversion and dependence of their shape on molecular taper angle. Chem Eur J 6:1258–1266
78. Percec V, Peterca M, Tsuda Y, Rosen BM, Uchida S, Imam MR, Ungar G, Heiney PA (2009) Elucidating the structure of the *Pm3n* cubic phase of supramolecular dendrimers through the modification of their aliphatic to aromatic volume ratio. Chem Eur J 15:8994–9004
79. Percec V, Dulcey AE, Peterca M, Ilies M, Sienkowska MJ, Heiney PA (2005) Programming the internal structure and stability of helical pores self-assembled from dendritic dipeptides via the protective groups of the peptide. J Am Chem Soc 127:17902–17909
80. Percec V, Dulcey A, Peterca M, Ilies M, Miura Y, Edlund U, Heiney PA (2005) Helical porous protein mimics self-assembled from amphiphilic dendritic dipeptides. Aust J Chem 58:472–482
81. Peterca M, Percec V, Dulcey AE, Nummelin S, Korey S, Ilies M, Heiney PA (2006) Self-assembly, structural, and retrostructural analysis of dendritic dipeptide pores undergoing reversible circular to elliptical shape change. J Am Chem Soc 128:6713–6720
82. Percec V, Dulcey AE, Peterca M, Adelman P, Samant R, Balagurusamy VSK, Heiney PA (2007) Helical pores self-assembled from homochiral dendritic dipeptides based on L-Tyr and nonpolar alpha-amino acids. J Am Chem Soc 129:5992–6002
83. Percec V, Peterca M, Dulcey AE, Imam MR, Hudson SD, Nummelin S, Adelman P, Heiney PA (2008) Hollow spherical supramolecular dendrimers. J Am Chem Soc 130:13079–13094
84. Percec V, Cho WD, Moller M, Prokhorova SA, Ungar G, Yeardley DJP (2000) Design and structural analysis of the first spherical monodendron self-organizable in a cubic lattice. J Am Chem Soc 122:4249–4250
85. Peterca M, Imam MR, Ahn CH, Balagurusamy VSK, Wilson DA, Rosen BM, Percec V (2011) Transfer, amplification, and inversion of helical chirality mediated by concerted interactions of C_3-supramolecular dendrimers. J Am Chem Soc 133:2311–2328
86. Percec V, Hudson SD, Peterca M, Leowanawat P, Aqad E, Graf R, Spiess HW, Zeng XB, Ungar G, Heiney PA (2011) Self-repairing complex helical columns generated via kinetically controlled self-assembly of dendronized perylene bisimides. J Am Chem Soc 133:18479–18494
87. Percec V, Peterca M, Tadjiev T, Zeng XB, Ungar G, Leowanawat P, Aqad E, Imam MR, Rosen BM, Akbey U, Graf R, Sekharan S, Sebastiani D, Spiess HW, Heiney PA, Hudson SD (2011) Self-assembly of dendronized perylene bisimides into complex helical columns. J Am Chem Soc 133:12197–12219
88. Percec V, Ahn CH, Cho WD, Jamieson AM, Kim J, Leman T, Schmidt M, Gerle M, Moller M, Prokhorova SA, Sheiko SS, Cheng SZD, Zhang A, Ungar G, Yeardley DJP (1998) Visualizable cylindrical macromolecules with controlled stiffness from backbones containing libraries of self-assembling dendritic side groups. J Am Chem Soc 120:8619–8631
89. Percec V, Ahn CH, Barboiu B (1997) Self-encapsulation, acceleration and control in the radical polymerization of monodendritic monomers via self-assembly. J Am Chem Soc 119:12978–12979
90. Percec V, Ahn CH, Ungar G, Yeardley DJP, Moller M, Sheiko SS (1998) Controlling polymer shape through the self-assembly of dendritic side-groups. Nature 391:161–164
91. Percec V, Schlueter D, Ungar G, Cheng SZD, Zhang A (1998) Hierarchical control of internal superstructure, diameter, and stability of supramolecular and macromolecular columns generated from tapered monodendritic building blocks. Macromolecules 31:1745–1762
92. Prokhorova SA, Sheiko SS, Ahn CH, Percec V, Moller M (1999) Molecular conformations of monodendron-jacketed polymers by scanning force microscopy. Macromolecules 32:2653–2660
93. Simionescu CI, Percec V, Dumitrescu S (1977) Polymerization of acetylenic derivatives. 30. Isomers of polyphenylacetylene. J Polym Sci Part A: Polym Chem 15:2497–2509
94. Simionescu CI, Percec V (1980) Thermal cis–trans isomerization of cis-transoidal polyphenylacetylene. J Polym Sci Part A: Polym Chem 18:147–155

95. Percec V, Rudick JG, Peterca M, Wagner M, Obata M, Mitchell CM, Cho WD, Balagurusamy VSK, Heiney PA (2005) Thermoreversible cis-cisoidal to cis-transoidal isomerization of helical dendronized polyphenylacetylenes. J Am Chem Soc 127:15257–15264
96. Percec V, Rudick JG, Peterca M, Heiney PA (2008) Nanomechanical function from self-organizable dendronized helical polyphenylacetylenes. J Am Chem Soc 130:7503–7508
97. Percec V, Imam MR, Peterca M, Leowanawat P (2012) Self-organizable veiscular columns assembled from polymers dendronized with semifluorinated Janus dendrimers act as reverse thermal actuators. J Am Chem Soc 134:4408–4420
98. Rudick JG, Percec V (2008) Induced helical backbone conformations of self-organizable dendronized polymers. Acc Chem Res 41:1641–1652

Top Curr Chem (2013) 333: 255–306
DOI: 10.1007/128_2012_369

Published online: 28 September 2012

Chirality and Protein Biosynthesis

Sindrila Dutta Banik and Nilashis Nandi

Abstract Chirality is present at all levels of structural hierarchy of protein and plays a significant role in protein biosynthesis. The macromolecules involved in protein biosynthesis such as aminoacyl tRNA synthetase and ribosome have chiral subunits. Despite the omnipresence of chirality in the biosynthetic pathway, its origin, role in current pathway, and importance is far from understood. In this review we first present an introduction to biochirality and its relevance to protein biosynthesis. Major propositions about the prebiotic origin of biomolecules are presented with particular reference to proteins and nucleic acids. The problem of the origin of homochirality is unresolved at present. The chiral discrimination by enzymes involved in protein synthesis is essential for keeping the life process going. However, questions remained pertaining to the mechanism of chiral discrimination and concomitant retention of biochirality. We discuss the experimental evidence which shows that it is virtually impossible to incorporate D-amino acids in protein structures in present biosynthetic pathways via any of the two major steps of protein synthesis, namely aminoacylation and peptide bond formation reactions. Molecular level explanations of the stringent chiral specificity in each step are extended based on computational analysis. A detailed account of the current state of understanding of the mechanism of chiral discrimination during aminoacylation in the active site of aminoacyl tRNA synthetase and peptide bond formation in ribosomal peptidyl transferase center is presented. Finally, it is pointed out that the understanding of the mechanism of retention of enantiopurity has implications in developing novel enzyme mimetic systems and biocatalysts and might be useful in chiral drug design.

Keywords Aminoacylation · Chirality · Peptide synthesis · Prebiotic · Protein

S. Dutta Banik and N. Nandi (✉)
Department of Chemistry, University of Kalyani, Kalyani 741235, India
e-mail: sindrila85@rediffmail.com; nilashisnandi@yahoo.com

Contents

1 Introduction

Chirality is an expression of nature, which is observed in its various forms. Traditionally, chirality is considered as a geometric property of various natural (as well as non-natural) objects that makes them non-identical and non-superposable with their own mirror images. This broad definition of chirality includes diverse macroscopic objects such as hands (the word *chirality* originated from the Greek word *cheir* meaning *hand*), animal organs, biological organisms, crystals and macromolecules as well as microscopic objects such as various molecules as chiral entities [1–3]. If the object lacks an improper or alternating axis of symmetry including a center of symmetry and a plane of symmetry, then it is chiral [4]. A necessary and sufficient condition for a molecule to be chiral is that it cannot be superimposed on its mirror image (as shown in Fig. 1). A molecule possessing an asymmetrically substituted carbon atom is a common example of a chiral molecule and lacks all symmetry elements (other than the identity E or C_1). According to this definition, objects of various length scales, starting from macroscopic objects mentioned before, mesoscopic objects (such as small to medium sized aggregates of molecules), as well as molecules of microscopic dimension, could be chiral entities. Chiral molecules such as amino acids and sugars are quite common natural biological basic subunits containing asymmetric center(s). However, as an exception, chiral molecules without asymmetric carbon atoms exist and instances of achiral molecules with more than one asymmetric carbon atoms are also well known. A detailed account of various aspects of molecular chirality is available in the standard literature [3–5]. Examples of chiral molecules are not only abundant among material systems such as organic and inorganic molecules but also plentiful among biotic systems.

The omnipresence of chirality can be seen in the plant and animal kingdoms as, for example, symmetry in patterns as well as shapes of leaves and structure of various animals, respectively. A closer look at the biomolecular level draws our attention to the fundamental and applied importance of chirality in life. Naturally, biochirality is an intriguing aspect of life from various perspectives [1, 2, 6, 7]. It is established that chirality plays a tremendously important role in biomimetic

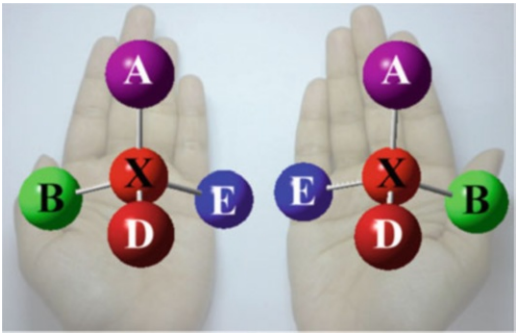

Fig. 1 General representation of a pair of enantiomeric molecules possessing an asymmetrically substituted carbon atom to which four different groups, *A*, *B*, *D*, and *E* are attached. This is a common example of a chiral molecule

systems and materials science [2, 8–13]. However, the detailed discussion about the fundamental aspects of chirality, its manifestation among biomimetic and material systems are beyond the scope of this review. We refer to the literature for such purposes [1–13].

The influence of chirality is observed at the molecular level in numerous biosynthetic pathways due to the omnipresence of different chiral molecules in biological systems. Qualitatively, this can be understood from the structure function relationship in biology. However, quantitative understanding of the origin of the chiral preference or discrimination and its importance in the progress of the specific process is challenging. The chirality dependent interactions in the reaction center within the respective enzyme, where such reactions takes place, are case specific and need to be understood in the perspective of the specific biological reaction. However, such influences are known to be decisive for the proper progress of the reaction. The relationship between biochirality and protein biosynthetic pathway is noteworthy. Though the relevance of chirality in this pathway seems obvious considering the involvement of a number of chiral molecules in various steps, several questions remain unanswered concerning the role of biochirality in the process.

A question arises why biochirality is relevant when racemization is rather common in chemical synthesis. How the enantiomers are discriminated in several important biochemical pathways and why? The answers to the fundamentally important questions of how life (or biomolecules) originated on Earth and how the homochirality in biological system evolved remain largely unresolved at present. The answer to the question "why so" also remains as an enigma. Since today's biochemical world is predominantly homochiral, how the biomolecules are developed at prebiotic time and the evolutionary mechanism towards the present day exclusiveness of homochirality have intrigued scientists over decades. The elementary questions of *why* the functional biological molecules are composed of homochiral basic subunits and *how* such an overwhelming predominance occurred in prebiotic times have fascinated scientists from diverse branches of science including biology, chemistry, mathematics, physics, and interdisciplinary areas such as biochemistry, biophysics, material science, astrobiology, geosciences, paleontology, and pharmaceutical science among others [6, 7].

A related question is: what is the implication of such homochirality in today's world? Not only the origin and development but the retention of biological homochirality at the present time is important for life processes. High level of stereospecificity of the biological reactions and its importance is well known [1]. Retention of the biological homochirality is vital for proper functionality of biological macromolecules. The incorporation of biological building blocks of wrong chirality might lead to dysfunctional biomolecules. The practical importance of the understanding of biochirality is immense. The understanding has utility in designing novel biomimetic materials and in developing chiral drugs. After the thalidomide disaster [14] it is recognized that the knowledge of effective chirality of a drug is must and now single enantiomeric drugs constitute a billion dollar industry [1]. Chirality is also important for agrochemicals and the perfume industry [1]. The relevance of chirality in the foregoing arenas implies the multifaceted nature of the importance of chirality in biology [1].

Chirality is expressed in various length scales in protein structure which are the workhorses of the kingdom of life. It is common knowledge that proteins are chiral at the length scale of the constituent amino acids (primary level), secondary, tertiary, and quaternary structural levels. In each case, both the basic building blocks and the architectures formed by such blocks are chiral. Only one enantiomer at the primary level makes the corresponding biological higher level structure as biologically active. Change in the enantiomeric form of the primary level is lethal for the functionality of the higher level structure of protein. Not only are protein molecules themselves chiral – most of the molecules involved in the process of protein synthesis are also chiral at the various levels of structural hierarchy. Protein biosynthesis is a multistep process and involves a number of small molecules such as amino acids, sugar, adenosine triphosphate (ATP), as well as large macromolecules such as synthetase, mRNA, and tRNA [15, 16]. It is tempting to conclude that chirality might have significance in the progress of the reaction. Molecular chirality influences the efficiency and accuracy of the process rather than remaining as a structural feature of the molecules developed merely by chance and without any specific purpose of nature. It is rather expected that the chiral structure of the protein as a macromolecule and its constituent primary structural elements influence its function, such as recognition of another molecule, and reactions performed by them. However, several gaps exist in the knowledge and understanding of the recognition of another molecule and reactions performed by them. Moreover, the origin of chirality of the protein structure, retention of enantiopurity (predominantly L-form of amino acid in the primary sequence) in protein structure, and relationship of the chiral structure of protein with its functionality are rather less explored.

Understanding the relationship between chirality and protein biosynthesis, which is a vital life process, is a longstanding problem. Recent years have witnessed progress in the molecular understanding of chirality in the process of protein biosynthesis. The present review attempts to consolidate the recent status of understanding. We first review the prebiotic pathway of synthesis of biomolecules and the origin of homochirality with a particular mention of protein synthesis.

This topic, however, has remained a matter of intense debate. We briefly mention a few significant propositions that are made to explain the issue. A brief description is presented of the existing pathway of protein biosynthesis and experimental studies confirming that the process of protein biosynthesis exhibits strong chiral specificity. This is followed by the recent molecular understanding of the mechanisms of the retention of biological homochirality in the various steps of protein synthesis. How the noncognate enantiomer can be discriminated within the active site of enzymes involved in protein synthesis such as aminoacyl tRNA synthetase (aaRS) (during aminoacylation step) and in peptidyl transferase center (PTC) (during peptide bond formation) in the course of protein synthesis is discussed. In the next section we examine the theories of prebiotic synthesis of basic building blocks of protein such as amino acids. We also mention the proposed mechanisms of the prebiotic synthesis of subunits which play a role in synthesizing proteins such as sugars in nucleic acids. This is followed by a discussion of the origin of homochirality.

2 Prebiotic Peptide Synthesis and Homochirality

In today's world the synthesis of protein enzymes is dependent on nucleic acids and the replication of nucleic acids is dependent on proteinous enzymes. This mutual dependence of the two most important biomolecules in the world today has led to the obvious and immensely debated question which came first, proteins or nucleic acids, often referred to as a "chicken and egg problem" [17]. This unresolved problem is further compounded by the fact that the basic building blocks of the biomolecules are overwhelmingly composed of homochiral units such as L-amino acids and D-sugars. Various theories proposed to explain "chirobiogenesis" is reviewed in recent literature [18]. The origins of biomolecules and homochirality are still open questions despite extensive studies.

It is expected that the early form of life must have been simpler than any of the simplest living thing of today's world but much more complicated than amino acids and nucleotides. The famous experiment by Stanley Miller triggered the concept that it is possible that amino acids were the first biological building blocks of life that are synthesised under prebiotic condition [19]. Using electrical discharge as a source of energy, Miller showed that amino acids can be produced in the laboratory from gases such as H_2, CO_2, N_2, and CH_4. This prompted the idea that gases such as H_2, CO_2, N_2, and CH_4 were present as starting material on Earth in the prebiotic era and amino acids were produced by lightning through the mixture of these gases [19–21]. However, the possibility remained that other forms of energy might act as energy source such as heat, solar radiation, X-rays, β and γ radiation [22–27]. It is also proposed that the Earth's atmosphere was not reducing and rather oxidizing and contained mainly CO, CO_2, N_2, H_2O gases. It is also proposed that such gases generate amino acids as well as other biomolecules when irradiated by cosmic rays [28, 29]. A completely different viewpoint is that the biomolecules might have arrived from space [30]. Early Earth was bombarded by comets and meteorites

when the solar system passed through interstellar clouds. All these extraterrestrial objects contain biologically important molecules and several molecules are found in these clouds using spectroscopic techniques [31–33]. However, there is no unequivocal hypothesis for the development of biomolecules in prebiotic times and which molecule developed first, protein or nucleic acid.

Once it is accepted that amino acids were synthesized during prebiotic times (by any of the aforesaid mechanisms), it may be hypothesized that the first form of life could be a protein molecule. The major limitation of this hypothesis is that proteins cannot self-replicate and fail to meet the major requirement of the propagation of life. On the other hand, RNA molecules satisfy the criteria for the ability to replicate and are able to catalyze biochemical reactions. Despite the acceptability of the RNA molecules as an early form of life, the synthesis of the basic units of RNA is much more difficult under prebiotic conditions. It is possible that the early molecule of life is a simpler pre-RNA type structure [20] which could be devoid of a ribose sugar ring and cytosine base. From the prebiotic point of view, the conditions under which amino acids and nucleobases could have been formed are more probable (less stringent) than the conditions required for the formation of ribose sugar and nucleosides. A number of hypotheses are made to understand how the RNA world might have developed on primitive Earth. Such hypotheses are based on experiments which are carried out to synthesize the basic building blocks of nucleosides. For example, adenine base can be produced by refluxing a solution of ammonium cyanide [34–37] and the pyrimidine base is synthesized by the reaction between cyanoacetylene (or its hydrolysis product, cyanoacetaldehyde) and cyanate ions (cyanogens or urea) [38–45]. In contrast, synthesis of ribose sugar under prebiotic conditions is more troublesome as it decays rapidly once produced. Another complication in assuming ribose sugar as a precursor in the prebiotic era is that it has two isomers and both might be produced during synthesis. A number of scientists are proponents of a pre-RNA molecule as precursor of biomolecules in the RNA world in view of these difficulties regarding the ribose sugar as a prebiotic unit. The advantage of this concept is that it conveniently excludes the problem of synthesizing ribose and cytosine from the RNA world. It is a prerequisite to understand how molecules are synthesized to complete one missing link in the "chicken and egg" problem, and is fairly complex. It was shown that a mixture of sugar is formed via the polymerization of formaldehyde in the presence of a simple minerals catalyst [46, 47]. It is also assumed that the prebiotic environment was enriched in one isomer of ribose. The synthesis of nucleosides from ribose and nucleoside base remained one of the weakest links in the chain of prebiotic reactions leading to oligonucleotides [17].

An equally challenging problem is the understanding of the origin of homochirality of amino acids and sugar. Both molecules are predominantly homochiral. Now it is possible that the homochirality originates during the prebiotic synthesis of these molecules or chiral discrimination occurred during the synthesis of RNA and protein molecules as shown in Fig. 2. Unfortunately, any of the propositions extended to explain the origin of biomolecules (as mentioned before) does not provide an indisputable account of the origin of homochirality. The naive

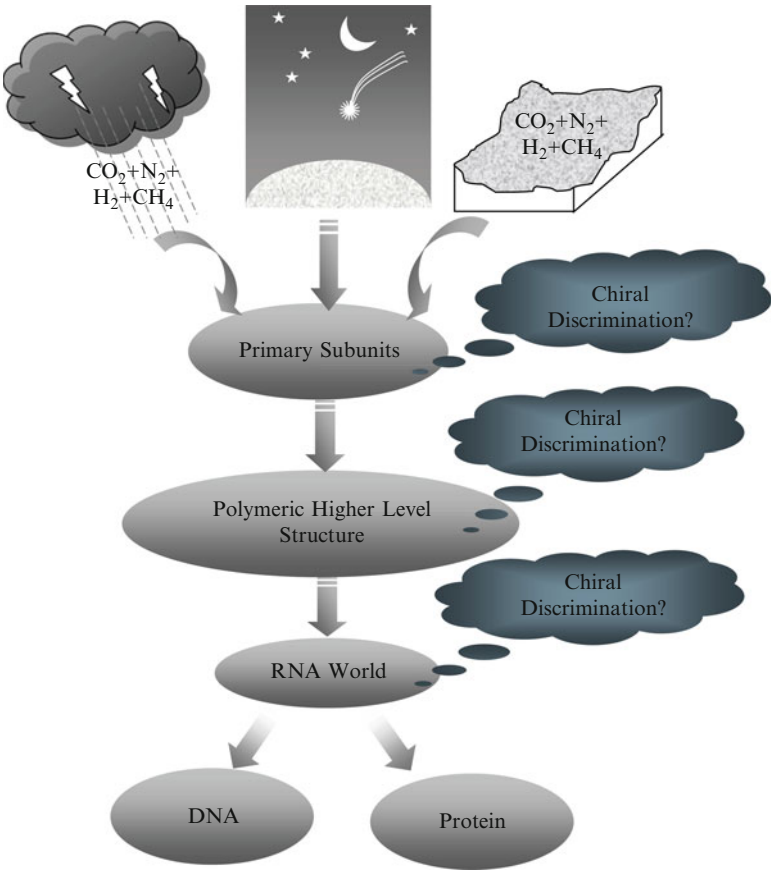

Fig. 2 Schematic representation of the prebiotic synthesis of biomolecules. In the beginning, various proposed ways of synthesis of amino acids, bases, and sugars are shown such as lightning through a mixture of gases, reaction of gases over a surface, and through meteor. Subsequently, the gradual evolution of polymeric higher level structures of biomolecules (such as peptides and nucleic acids) and RNA world leading to DNA and protein are shown. Various steps where homochirality of biomolecules may have originated are marked as question by "chiral discrimination"

proposition about the origin of homochirality of amino acids and sugars is that such development occurred just by chance. Thus, the homochirality could have been evolved by chance as chiral molecules were formed from achiral sources, grown autocatalytically and competing against each other for material resources [21, 48–50]. However, it remains a question as to how the current state of overwhelming predominance of L-amino acids and D-sugars happened from the starting (expectedly small) enantiomeric excess. Another proposition for the origin of homochirality is that it could also have been induced by asymmetric physical forces [21]. Absorption of biomolecules on asymmetric surfaces like quartz crystals may

have enhanced the homochirality. L-Amino acids are absorbed more on quartz crystal [51, 52]. Once it is accepted that the biomolecules came from space, it is suggested that the homochirality appeared from space [53–56]. Chiral symmetry breaking could have been triggered by low chiral interaction energy (within the range of parity violating weak-neutral-current interactions). Chiral interaction energies due to a combination of electric, magnetic, gravitational, and centrifugal fields, even when high field strengths are considered, are found to be rather small (less than 10^{-19} k_BT) [57]. A minute but systematic chiral interaction, no stronger than the weak-neutral-current interaction in amino acids, may lead to enantiomeric excess over a period of ~15,000 years [58]. Dynamic co-evolution of peptide as a possible mechanism of generation of homochirality is also proposed but yet to be verified [59]. Other models of chiral polymerization, relevant for understanding homochirality, are also proposed [60]. However, there are no indisputable arguments to favor any of the above.

The understanding of the evolution of the peptides and proteins is far from straightforward even if one assumes that L-amino acid and D-sugars are developed via any of the aforesaid mechanisms. Obviously, a question may arise as to how complex protein structures are evolved from simpler building blocks. It is proposed that evolution based on RNA replication preceded the appearance of protein synthesis [61]. RNA, as a single molecule, might be able to serve the purpose of genetic storage and as functional enzyme and this concept leads to the coining of the phrase of "RNA World" [62–65].

The next challenging question is how the protein is synthesized in the RNA World in the absence of proteinous enzymes. Aminoacylation of tRNA is an essential step in the protein synthesis process. Although protein enzymes (aaRS) play the major role in tRNA aminoacylation in the present biochemical world, RNA molecules could have catalyzed aminoacylation onto tRNA or tRNA-like molecules in the primitive translation system. Although such RNA enzymes are not yet identified from known organisms, in vitro selection has generated such RNA catalysts from a pool of random RNA sequences [66]. It is proposed that the first catalysts that made aa-RNAs for coded protein synthesis probably appeared long before any protein aaRS, to serve a preexisting translation system. It seems that this ancestral translation system relied on a molecule like RNA [67]. The ability of RNA to catalyze reactions with aminoacyl esters expands the catalytic versatility of RNA and suggests that the first aaRS could have been an RNA molecule [68]. It is proposed that the primitive protein synthesis machinery was such that the growing polypeptide chain was switched from the 2′OH to the 3′OH of a unique ribose molecule. Each elongation step necessitates two catalytic events, one for the aminoacylation of the ribose (either 2′OH or 3′OH) and one for the transferase activity. The mechanism described is actually one of the simplest ways to achieve a binary code and necessitates only two different sites on the RNA, one for class I amino acids and one for class II amino acids. The aminoacylation reaction on two different chiral centers (2′OH and 3′OH) imposes the existence of two types of reaction centers which could be the ancestors of our present classes of synthetases [69]. It is suggested that aaRSs are developed from ancient common ancestors [67]

which took a prolonged period to develop. If this is true, then a preexisting class of catalysts for aminoacyl-tRNA (aa-tRNA) synthesis must have been present. Due to the limited number of aaRSs (maybe one or two) available for the protein synthesis, other amino acids (noncognate to the aforesaid one or two aaRSs) must have been activated by ancestral aaRSs [67] which acted in unison. Thus, the ancestral enzymes catalyzing the aa-tRNA synthesis remained a subject of intensive investigation [67]. Of course, details of the active site of early aaRS remains a puzzle.

Peptide nucleic acids (PNA) are an attractive alternative to ribonucleic acid and are strongly relevant as the precursor of present day biomolecules in the context of prebiotic chemistry [70–73]. The PNA is an uncharged, achiral analog of RNA or DNA in which the ribose-phosphate backbone of the nucleic acid is replaced by a backbone held together by amide bonds. Pairs of complementary PNA oligomers form Watson–Crick base paired double helices. The chemical transfer of genetic information from PNA to another PNA and to RNA (or DNA) is feasible, since homocytosine PNA oligomers can direct template-dependent synthesis of a complementary homoguanine PNA oligomer or RNA oligonucleotide. Furthermore, PNA being achiral, it indicates nature's choice of chirality to a later stage in evolution. Eschenmoser and coworkers have undertaken a systematic study of the properties of analogs of nucleic acids in which ribose is replaced by some other sugar or in which the furanose form of ribose is replaced by the pyranose form [74]. The polynucleotides based on the pyranosyl analog of ribose (p-RNA) from Watson–Crick paired double helices are more stable than the RNA [75, 76].

If it is assumed that the homochiral preference did not occur during the prebiotic development of amino acids, the preference of L-amino acid over the D-enantiomer may also have arisen as a consequence of the properties of the RNA molecule during protein synthesis in the RNA world. Aminoacylation of RNA is the primary reaction for selection of amino acids during protein synthesis. While this reaction is not predictably stereoselective (for either L- or D-enantiomers of amino acid) in solution with no rotational constraints, the reaction with the aid of the constrained environment of the RNA structure becomes selective for L-enantiomer. It has been indicated in the literature that steric interference with the α-amino group prevents the incorporation of D-isomer [77]. It has been shown recently that the restriction of degrees of freedom of reacting amino acids leading to the formation of peptide bond within the ribosomal active site leads to significant chiral discrimination preferring incorporation of L-enantiomer and exclusion of D-enantiomer [78].

Not only have the aforesaid problems concerning the origin and development of biochirality remained a subject of intense investigation and debate, the enhancement of homochirality after the initial chiral symmetry breaking and retention of the preferred chirality are also a puzzle. One proposition about the enrichment of chirality is that the absorption of biomolecules on asymmetric surfaces like quartz crystal may have enhanced homochirality. It has been shown that L-amino acids are absorbed more on quartz crystal and recently that restriction of rotation of enantiomeric molecules (amino acids) enhances the chiral discrimination [78]. The intermolecular interaction between enantiomeric molecules and that between racemic molecules as a function of mutual separation and orientation are different when the

degrees of freedom of molecules are restricted. However, this discrimination vanishes once the molecules are free to rotate and translate (when the molecules are not confined). More recently it has been shown that confinement of enantiomeric molecules within a nanodimensional space significantly enhances the chiral discrimination [1, 79, 80].

It has been pointed out that the evolution of present day ribosomal architecture with its complex functionality from simpler, primitive RNA structures is correlated with the evolution of the process of protein synthesis [81–84]. However, there remained several gaps in the knowledge concerning the origin of ribosome and coevolution of the subdomains of tRNA and rRNA. Future explorations might resolve the problem of understanding the origin of the RNA world and lead to a better understanding of how the protein biosynthesis mechanism, as it occurs in present day, has developed.

3 Protein Biosynthesis in Today's World and Chiral Specificity

The present day mechanism of protein biosynthesis is a fairly complex process. The process takes place in successive stages in vivo. Major steps of protein synthesis are initiation, elongation, termination, release, folding, and posttranslational processing [15, 16] as shown in Fig. 3. The initiation step is the aminoacylation reaction and this step is followed by the elongation step which involves the peptide bond formation. The relationship between an amino acid (AA) and its cognate tRNA is established via the aminoacylation reaction. Once the aminoacyl tRNA is formed via the aminoacylation reaction, the polypeptide chain is lengthened by peptide bond formation between successive activated amino acid units. The elongation step takes place in the active site of ribosome (PTC). Subsequently, the termination codon of mRNA terminates the polypeptide chain synthesis and newly formed polypeptide is released. Finally the newly formed polypeptide chain folds into its functional (biologically active) conformation [15, 16].

The aminoacylation reaction links the realm of the protein with the RNA world. Faithful translation of the genetic information is carried out in this step with surprising speed and accuracy [15, 16, 82–93]. The reaction occurs in two steps. The first step is the amino acid activation with the formation of aminoacyl adenylate and release of inorganic pyrophosphate. In the second step, the 2′OH or 3′OH (hydroxyl group) (depends on the class to which the aaRS belongs) of the terminal adenosine of tRNA (A76) nucleophilically attaches to the carbonyl carbon atom of the aminoacyl-adenylate. This results in the 2′ or 3′-esterification of the tRNA with the AA moiety and generation of AMP as the leaving group. Subsequently the product is released. The reaction scheme for the two step aminoacylation reaction is shown in Fig. 4.

Both activation and charging steps of 20 natural amino acids are catalyzed by 20 aaRSs. Each member of the aaRS family is specific for its cognate natural amino acid. The aaRSs are partitioned into two classes (class I and class II) based on exclusive

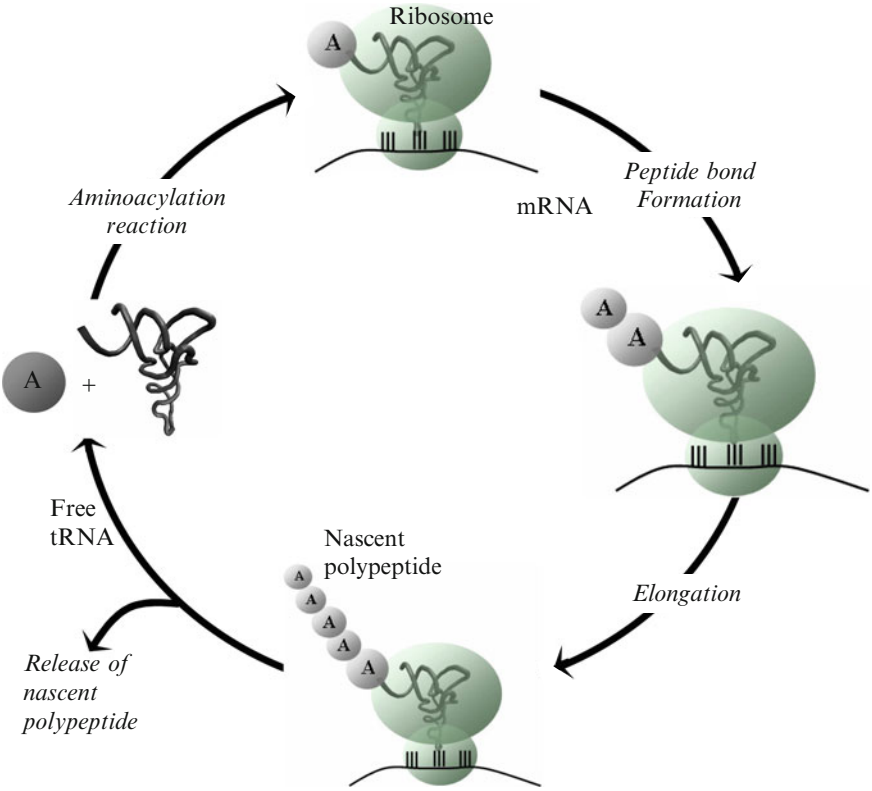

Fig. 3 Representation of the present day pathway of protein biosynthesis. The major steps involved in the cycle are aminoacylation, peptide bond formation, elongation, and release of nascent peptide

motifs [82–93]. The enzymes of the two classes are different in many respects starting with their primary sequences to higher level structural organization. The aaRSs not only recognize the substrates (AA and ATP) but also properly place and orient them for progress of reaction as well as lowering the activation energy barrier. The structure and the function of the 20 aaRSs have been extensively studied by crystallographic analysis [94–141], molecular dynamics simulations [142–149], and other experimental techniques such as biochemical and kinetic methods [77, 150–169].

The subsequent step of protein synthesis after aminoacylation is the peptide bond formation occurring in the ribosome (a large and complex macromolecule). Pioneering studies revealed detailed organization at the molecular level of this functional molecular machine [170–179]. The active site of the ribosome is known as PTC. It accelerates peptide bond formation by 10^7-fold relative to the uncatalyzed reaction [170–179]. A scheme of the peptide bond formation as occurs within the PTC is shown in Fig. 5. In this process, the α-amino group of the amino acid at A-site tRNA makes a nucleophilic attack at the carbonyl carbon of the ester

Step 1: AA activation:

AA (aa) + Adenosine triphosphate (ATP) + aminoacyl-tRNA synthetase (aaRS)
= aminoacyl-adenylate (aa-AMP) + PPi

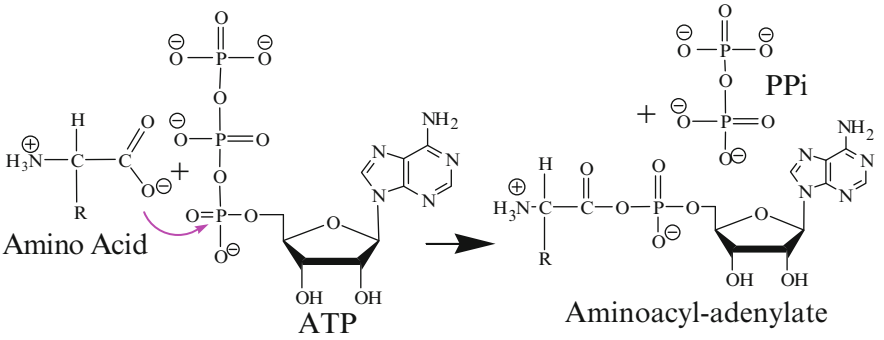

Step 2: tRNA charging:

aa-AMP•aaRS + tRNA = aminoacyl-*t*RNA (aa-tRNA) + Adenosine monophosphate (AMP)

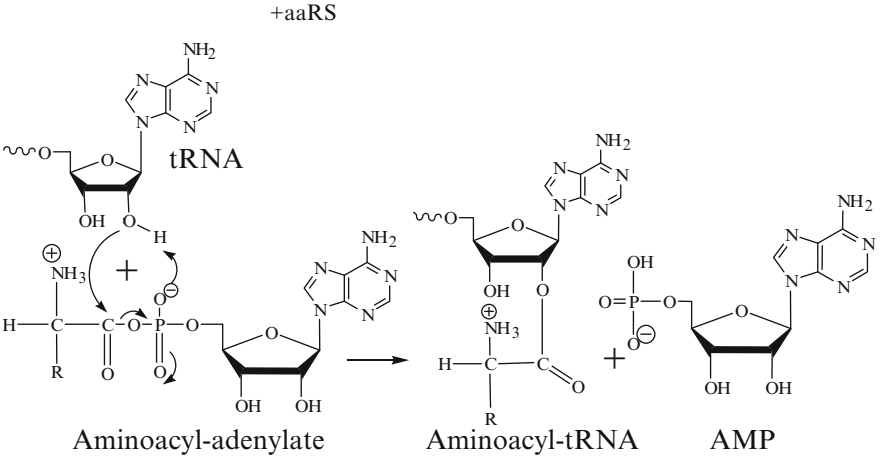

Fig. 4 The reaction scheme for the two steps of aminoacylation reaction at the active site of aminoacyl tRNA synthetase. The first step is the amino acid activation with the formation of aminoacyl adenylate and release of inorganic pyrophosphate. In the second step of the reaction, the 2′OH or 3′OH (hydroxyl group) of the terminal adenosine of tRNA (A76) makes a nucleophilic attack to the carbonyl carbon atom of the aminoacyl adenylate

bond connecting nascent peptide to P-site tRNA and forms an intermediate. The aminoacyl moiety attached to A76 of the tRNA in the A-site accepts the growing polypeptide from the tRNA in the P-site during peptidyl transfer. The new peptidyl-tRNA is subsequently translocated from the A-site to the P-site. The deacylated tRNA is translocated from the P-site to the exit (E)-site. Both concerted and

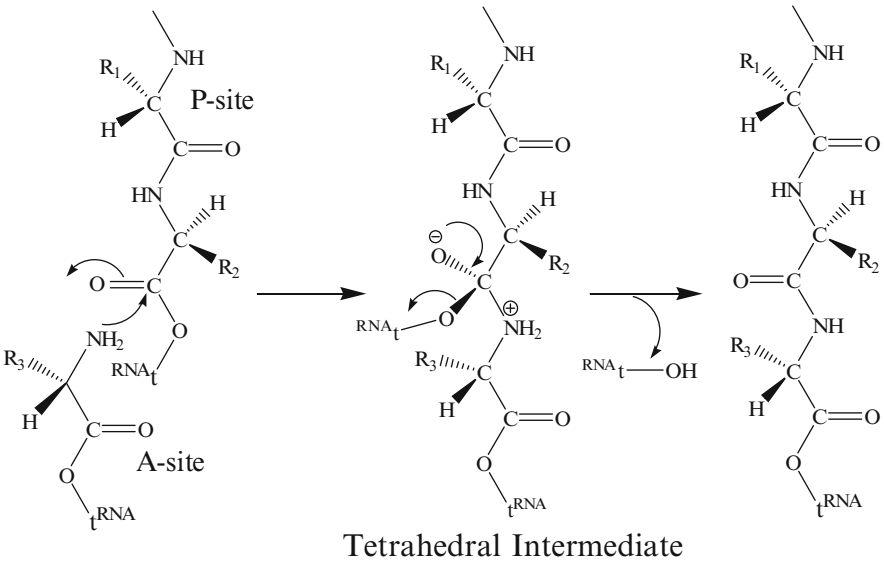

Fig. 5 The reaction scheme of peptide bond formation at the peptidyl transferase center in ribosome

stepwise mechanisms are proposed for the peptide synthesis. The two mechanisms are competitive and are studied in detail using experimental and computational methods. The stepwise mechanism takes place through a tetrahedral intermediate.

Both aminoacylation reaction and peptide bond formation exhibit strong chiral discrimination. The specificity of the aaRSs to incorporate a specific amino acid and its ability to discriminate between several competing substrates is well known. Synthetase ensures that only cognate substrates are selected from the large cellular pool of similar amino acids or tRNA. The ability to discriminate between amino acids is one of the major requirements for accurate translation of the genetic code because the structure of the cognate and noncognate amino acids may differ only in a subtle way in terms of charge distribution or spatial arrangements of groups attached to the chiral center. The frequency of misincorporation of noncognate amino acid is 1 in 10,000, which reflects a surprising accuracy of the mechanism. It was proposed earlier that there may be a succession of discriminating processes. It was also suggested that a number of intricate contacts between aaRS and amino acids, which are favorable for cognate but unfavorable for noncognate amino acids, make the successful recognition and concomitant discrimination. Most of the aa-tRNA contains an editing site in addition to an acylation site. These complementary pairs of sites act as a double filter to ensure that noncognate amino acids are rejected. It is proposed in the literature that the acylation site rejects amino acids larger than the correct one because there is insufficient space for them. On the other hand the smaller amino acids are cleaved by the hydrolytic editing site. However, this size or volume based mechanism is not able to discriminate the enantiomeric

species of the cognate amino acid as the D- and L-enantiomers occupy identical total volume. Each synthetase can specifically recognize the correct pair of substrates from the pool of amino acids and tRNA molecules. The discrimination of cognate and noncognate amino acids is achieved by a number of intermolecular interactions between aaRS and substrates (amino acid and tRNA). Several workers have explored how a particular aaRS recognizes its cognate amino acid by various methods such as crystallographic analysis, biochemical methods, mutation experiments, as well as computational analysis.

Experimental evidence concerning the stringent chiral specificity in both aminoacylation and peptide bond formation is plentiful. The reactions have specificity at a level sufficient to discriminate the enantiomeric species. Early studies indicated that when D-isomer is tested as substrate with particle free supernatant of pancreas homogenate containing synthetase, no activity has been observed [180]. In an early study, Calender and Berg observed that D-tyrosine could be esterified to $tRNA^{Tyr}$ and could then be incorporated into peptides [158, 160]. D-Tyrosine was incorporated into the peptide in an assay for the protein synthesizing system. However, the L-tyrosine incorporation is 114 μmol and D-tyrosine incorporation is only 19 μmol. The reduced (about one-sixth of the L-isomer) incorporation of D-tyrosine indicates that the protein synthetic system is unfavorable towards the incorporation of D-amino acids into peptides. Overall rate of dipeptide formation is 30-fold higher for the L-enantiomer compared to the D-enantiomer. It is noted that 75–90% of D-Tyr-tRNA dissociates from the ribosome while less than 30% of L-Tyr-tRNA is lost through this pathway. These early experiments draw attention to the homochiral preference in peptide bond formation. Barely detectable amounts of D-phenylalanyl tRNA are seen to be formed using phenylalanyl tRNA synthetases and this was only ~6×10^{-5} the rate found for L-phenylalanyl tRNA. Yamane and coworkers studied the stereoselectivity of peptide chain elongation [181].

Bergmann and coworkers tested the specificity of the L- and D-isomers of valine, isoleucine, and leucine for aminoacyl adenylate formation with valyl, isoleucyl, leucyl, and methionyl tRNA synthetases [157]. In all cases, formation of the D-aminoacyl adenylate is negligible or nil compared to the corresponding L-aminoacyl adenylate. Similar chiral specificity is noted for aspartyl tRNA synthetase of *Lactobacillus arabinosus* [182]. Hopfield observed that both L- and D-tyrosine can be esterified by tyrosine-tRNA synthetase [183]. This conclusion corroborates the study by Calendar and Berg. The amounts of ATP hydrolyzed per tRNA acylated are practically identical for both enantiomers. Tyrosyl tRNA synthetase is known to be nonspecific with respect to the acylating position (2′ or 3′ position of hydroxyl group of adenosine moiety) and it is suggested that it may lack the 2′ hydrolytic activity of other synthetases. This may also explain the existence of D-Tyr tRNA deacylase and absence of enzymatic deacylation of D-Tyr-tRNA [183].

Soutourina and coworkers concluded that, in addition to D-tyrosine, D-enantiomers of other amino acids could be incorporated based on an investigation of *Escherichia coli* and *Saccharomyces cerevisiae* systems [154]. It is also pointed out that the deacylase activity might have a broader implication in retaining enantiopurity. The deacylase recognizes very different D-aminoacyl moieties like

the acidic aspartate or the bulky aromatic tryptophan. The authors discuss another important pathway of removal of the toxic D-amino acid in addition to the proofreading mechanism during the aminoacylation step. In the case of auxotrophic bacteria, the lack of many biosynthetic pathways might result in low levels of endogenous D-amino acids. The deacylase activity would be redundant in such bacteria. However, D-aminoacyl-tRNA deacylase activity would be necessary in other cells to reduce the harmful effect of D-amino acid transfer to tRNA. More studies are required in this direction.

Tamura and Schimmel studied the plausibility of chiral selectivity during the second step of aminoacylation using an RNA minihelix that recapitulates the amino acid attachment site within tRNA [151]. A bridging oligonucleotide, and 5′-[^{14}C]-L-Ala-p-dT$_6$dA$_2$ as well as 5′-[^{14}C]-D-Ala-p-dT$_6$dA$_2$, are mixed together to achieve aminoacylation of minihelix^{Ala}. Formation of the [^{14}C]-L-Ala-minihelix is preferred over that of [^{14}C]-D-Ala-minihelix by a ratio of about 4:1. Both stereoisomers of Leu-p-dT$_6$dA$_2$ and of Phe-p-dT$_6$dA$_2$ are also tested for chiral selectivity. A clear preference for L- over D-leucine (or phenylalanine) was observed. Chiral preference appears to occur during aminoacyl transfer from the 5′-phosphate to the minihelix. It might be noted that the mutual spatial orientation and distance between reacting molecular segments in the model system studied by Tamura and Schimmel could be different from a corresponding biological system which might influence the observed ratio of selectivity. Tamura and Schimmel also synthesized the aminoacyl phosphate oligonucleotide, bridging oligonucleotide and minihelix^{Ala}, which contain L-ribose (in contrast with natural D-ribose). Minihelix^{Ala}, bridging oligonucleotide, and either 5′-[^{14}C]-L-Ala-p-dT$_6$dA$_2$ or 5′-[^{14}C]-D-Ala-p-dT$_6$dA$_2$ (both containing L-deoxyribose), were combined and analyzed for aminoacylation of minihelix^{Ala}. Formation of [^{14}C]-D-Ala minihelix was preferred over that of [^{14}C]-L-Ala minihelix at a ratio of 1:3.6, about the reciprocal of that determined when RNA containing D-ribose is used. This result again points out the complementary heterochiral relationship between L-amino acid and D-sugar which seems to play also a role in the aminoacylation reaction.

In a subsequent study, Tamura and Schimmel attempted to address whether the free amino group attached to the asymmetric α-carbon of the amino acid played a role in the chiral selectivity of aminoacylation [152]. To address the question, the amino group of Ala was acetylated and *N*-acetyl-L- or D-Ala-aminoacyl oligonucleotide was used for the aminoacylation reaction. Acetylation of Ala was performed with more than 70% of both L-[^{14}C]Ala and D-[^{14}C]Ala being acetylated. While the CH_3 of D-Ala crowds the 3′-OH of A, the CH_3 of L-Ala is distal to the same 3′-OH. Based on such model building, a dT:G pair was introduced to create a potential clash of the CH_3 of L-Ala with that of dT. This substitution sharply reduced the yield of L-Ala-minihelix^{Ala} without altering production of D-Ala-minihelix^{Ala}. These results suggested that the chiral preference for L-Ala in these constructs depends on avoiding a sugar-pucker sensitive steric clash between a pendant group of a base with the CH_3 of L-Ala. It is pointed out that the chiral preference can arise during the process of aminoacyl transfer from the 5′-phosphate of the oligonucleotide to the minihelix or from a difference in template (bridging oligonucleotide) hybridization efficiency between

the L-amino acid- and D-amino acid-oligonucleotides. Nearly fourfold preference of L-Ala-minihelix^{Ala} to D-Ala-minihelix^{Ala} was observed. An energetic difference of <1 kcal mol^{-1} in the rate-determining step of the transition state is sufficient to give the observed fourfold preference for chiral specificity in the aminoacylation process.

In a series of detailed studies, Hecht and coworkers examined the extent of incorporation of D-amino acid into ribosome [184–187]. Misacylated tRNAs like *N*-acetyl-D-phenylalanyl-tRNA^{Phe}, *N*-acetyl-L-tyrosyl-tRNA^{Phe}, *N*-acetyl-D-tyrosyl-tRNA^{Phe}, and *N*-acetyl-β-phenylalanyl-tRNA^{Phe} are used to study the peptidyl (P-site) binding and peptide bond formation in a cell free system involving *E. coli* ribosome programmed with poly-uridylic acid [185, 186]. Unlike the tRNA^{Phe} activated with L-phenylalanine and L-tyrosine, the *N*-acetyl-D-phenylalanyl-tRNA^{Phe} and *N*-acetyl-D-tyrosyl-tRNA^{Phe} performed poorly for dipeptide formation when L-phenylalanyl-tRNA^{Phe} acts as acceptor (A-site) tRNA. Another study confirms the foregoing results [185]. The relative yield of dipeptide synthesis for D-analogue is only 7% and 13% for *N*-acetyl-D-tyrosyl-tRNA^{Phe} relative to the L-*N*-acetyl phenylalanyl-tRNA^{Phe}. The small amount of dipeptide produced indicates that the D-isomer incorporation is severely inhibited compared to the natural isomer [185]. Further influence of the chiral structure of the amino acid moiety is noted for the *N*-acetyl-(D, L) β-phenylalanyl-tRNA^{Phe} system. The relative yield of dipeptide synthesis for the analogue is 110–130% relative to the L-*N*-acetyl phenylalanyl-tRNA^{Phe} system. The studies by Hecht and coworkers confirm the earlier studies of Calendar and Berg as well as that of Yamane and Hopfield that the incorporation of D-amino acids into a peptide is unfavorable relative to the incorporation of natural enantiomer. Hecht and coworkers have used aa-tRNA analogues bearing noncognate aminoacyl moieties [186]. Two tRNA^{Phe}s bearing noncognate amino acids (*N*-pyroglutamyl-L-*O*-methyltyrosyl-tRNA^{Phe} and *N*-pyroglutamyl-L-phenylglycyl-tRNA^{Phe}) are also able to participate as acceptors in the peptidyltransferase reaction. In contrast, neither *N*-pyroglutamyl-D-phenylalanyl-tRNA^{Phe} nor *N*-pyroglutamyl-D-tyrosyl-tRNA^{Phe} acted as an acceptor in the peptidyltransferase reaction following treatment with pyroglutamate aminopeptidase and *N*-pyroglutamyl-D, L-β-phenylalanyl-tRNA^{Phe} produced dipeptide only to the extent of 8%. Profy and Usher studied the aminoacylation of diinosine monophosphate (inosinylyl-(3′-5′)-inosine) which is a model system with both 2′ and 3′ hydroxyl groups [150]. When the acylating agent was the imidazolide of *N*-(*tert*-butoxycarbonyl)-DL-alanine, a 40% enantiomeric excess of the L-isomer was incorporated at the internal 2′ site. The positions of equilibrium for the 2′–3′ migration reaction differed for the D- and L-enantiomers. In contrast, reaction of IpI with the imidazolide of unprotected DL-alanine led to an excess of the D-isomer at the internal 2′ site, while reaction with the *N*-carboxy anhydride of DL-alanine proceeded without detectable stereoselection.

Chamberlin and coworkers also noted the diminished activity of D-isomer [188]. In an alternative approach, in the presence of nonsense codons incorporated in mRNA (codons which effect termination of peptide synthesis as there is no corresponding tRNAs) like 5′UAG, 5′UAA, and 5′UGA, a compensatory DNA

mutation can lead to the production of mutated tRNA (called suppressor tRNA) after activation with a normal amino acid. The presence of the suppressor tRNA during in vitro cell-free translation of mRNA containing a nonsense suppression site can incorporate non-natural amino acids. While tRNAs activated with iodotyrosine, *N*-methylphenylalanine, or glycine functioned well in suppression, D-phenylalanyl-tRNA did not. The result that D-amino acid fails to be incorporated is further confirmed by both normal rapid assay method and direct analysis of the isolated HPLC fraction.

Significant influence of the chirality of the sugar ring involved in the CCA moiety is also noted [184]. This result is important in understanding the heterochiral relationship of D-sugar and L-amino acid in peptide synthesis, where the former is present as a part of the tRNA structure. While the *N*-acetyl-D-phenylalanyl-$tRNA^{Phe}$ and *N*-acetyl-D-tyrosyl-$tRNA^{Phe}$ produced only small amounts of dipeptide, the 2′ and 3′ deoxyadenosine analogues (L-*N*-acetyl phenylalanyl-$tRNA^{Phe}$-CC2′dA and L-*N*-acetyl phenylalanyl-$tRNA^{Phe}$-CC3′dA) produced no detectable dipeptide formation. The results indicate that the effect of the sugar ring chirality is decisive over the peptide bond formation and alteration of the chirality of the same is unfavorable for the synthesis. Suppression efficiency of misacylated D-phenylalanyl-$tRNA_{CUA}^{Gly}$-dCA is nil compared to other misacylated phenylalanyl-$tRNA_{CUA}^{Gly}$-dCA.

Chiral discrimination is also studied in different model systems. Puromycine [9-{3′-deoxy-3′-[(4-methoxy-phenylalanyl)amino]-β-D-ribofuranosyl}-6(*N*,*N*′-dimethylamino) purine] is a small molecule mimic of aa-tRNA and acts as a translation inhibitor by entering the ribosomal A-site and participating in the peptide bond formation with the nascent peptidyl chain. Puromycin blocks protein synthesis by acting as an analogue of the charged tRNA. It substitutes for an incoming aa-tRNA as the acceptor of the carboxyl activated peptide and forms peptidyl-puromycin. While peptidyl-tRNA in ribosome is normally transferred to the amino group of the next aa-tRNA, the carboxyl activated peptide is transferred to puromycin. This causes the ending of the sequential extension of peptide and stops the growth of the nascent peptide chain [189, 190]. Note that the orientational degrees of freedom of A- and P-terminals in such analogues are in principle different from those within the ribosomal active site. Hence the mechanism and extent of discrimination might be different in these two cases.

While it is virtually impossible to incorporate D-amino acid into proteins without modifying the chemical structure of the PTC of naturally occurring tRNA, it is possible to perform the corresponding D–L peptide bond formation in the model puromycin system. It may be noted that the alignment and surrounding environment of the amino terminals in the two cases are different. The attachment of the amino acid moieties at the CCA end of amino and peptidyl terminals restricts their free rotation. The available orientational degrees of freedom (which is restricted compared to bulk) changes from one system to the other as studied experimentally. Examples are different tRNAs, puromycin, or other analogues. Consequently, the degrees of freedom available and the extent of confinement do vary and these factors affect the interaction and discrimination in the respective cases.

Starck et al. used a series of synthetic puromycin analogues to measure the activity of D-amino acid and β-amino acids in an intact eukaryotic translation system (rabbit reticulocyte ribosome) [191]. The puromycin derivatives differ in amino acid stereochemistry and amino acid moiety as well as number of carbon units in the amino acid backbone. The activity of the model compounds are measured in a high dynamic range IC_{50} potency assay using the rabbit reticulocyte protein synthesis system. While the L-puromycin inhibits globin mRNA translation with an IC_{50} value of 1.8 μm, the corresponding D-puromycin or 9-{3′-deoxy-3′-[(4-methoxy-D-phenylalanyl)amino]-β-D-ribofuranosyl}-6(*N*,*N*′-dimethylamino) purine inhibits globin translation giving an IC_{50} value of 280 μm. The difference is 150-fold. The activity of a modified puromycin derivative (9-{3′-deoxy-3′-[(4-methyl-L-phenylalanyl) amino]-β-D-ribofuranosyl}-6(*N*,*N*′-dimethylamino) purine or L-(4-Me)-Phe-PANS) is found to be highest, giving an IC_{50} value of 1.0 μm. However, its D-amino acid isomer has an IC_{50} value of 2,400 μm which is even lower than D-puromycin and 2,400-fold less potent than the corresponding L-isomer. Alanine analogues show little difference (approximately threefold) between the L- and D-isomers. The size and geometry of the side chain is suggested to play an important role in the synthesis with larger hydrophobic side chains having improved function. It is also indicated that the structural basis of the stereoselectivity could not be addressed due to the unavailability of the high resolution structure of the rabbit reticulocyte ribosome. Modeling of the placement of D-puromycin in the active site of *Haloarcula marismortui* 50S subunit is attempted for which the high resolution structure is available. U2620 residue is found to be the closest nucleotide to the D-side chain. This view is supported by the structural analysis which suggested that the steric hindrance of the molecular segments of the D-amino acid make the incorporation of D-isomer unfavorable. The role of the surrounding environment of the active site and particularly the role of U2620 in the discrimination in the peptide synthesis were recently studied using computational methods and will be discussed later.

While the foregoing studies indicated that D-amino acid incorporation into proteins is practically impossible, Hecht and coworkers pointed out that alteration of the PTC might lead to enhanced D-amino acid incorporation [192]. Mutations in the 23SrRNA in the region of PTC and helix 89 leads to a conformational change in ribosome that alters its behavior in the protein synthesis. Modified ribosomes with mutations in regions 2447–2450 (belongs to the PTC region) and 2457–2462 (belongs to helix 89 region) of *E. coli* 23S rRNA and cell free protein synthesizing systems were prepared from mutant ribosomes. A high level of suppression in the presence of D-methionine (23%) and D-phenylalanine (12%) is observed. This indicates that ribosome active site structure is, at least partly, responsible for the discriminating mechanism against D-aminoacyl-$tRNA_{CUA}$s in the ribosomal A site. Putative alterations may lead to enhanced incorporation of D-amino acid. The results indicate that the surrounding of PTC has major influence on the process of synthesis. This result is supported by recent computational studies where it is shown that the removal of a residue can reduce the chiral discrimination and will be discussed later.

The possibility of incorporation of D-isomer in a biosynthetic pathway or development of a racemic mixture cannot be ruled out due to the presence of D-amino acid in several organisms [193]. The protein active site is complementary to substrate. With double composition of proteins it would be too cumbersome to maintain life. This could be a reason why evolution did not supported the coexistence of protein composed of L-amino acid and protein composed D-amino acid. Equally, the development of protein structures composed of both L-and D-amino acids is unexpected. However, the foregoing view does not identify the mechanism of rejection of D-enantiomer when the presence of the same are well known. The presence of D-amino acids in several biological organisms are known, for example, in the non-ribosomal peptide synthesis and posttranslational modification therein [193–198]. A large number of biological molecules exhibit strong preference for one of the enantiomeric forms out of the two (for each chiral center) nearly equal possible isomers. While the incorporation of D-amino acids is a hallmark of peptide synthetase-based non-ribosomal peptide synthesis [194, 195, 198, 199] and posttranslational modification [193, 196, 197], the RNA-dependent ribosomal synthesis of peptides and proteins exclusively incorporates only the 20 natural amino acids and selenocysteine with their natural chirality (L-form). Incorporation of D-amino acids into an organism can be toxic if it does not naturally occur in the same [200–208]. D-amino acid which naturally occurs in selected systems like peptidoglycans of bacterial cell walls (D-Ala- and D-Glu-), peptide antibiotics, and in the human brain (D-Asp and D-Ser are present at high concentrations). Transformation of L-enantiomer by a racemase can also lead to the development of D-enantiomer. Conversion of the L- to the D-stereoisomer of tryptophan was observed in the presence of tryptophan synthetase. The D-tyrosine might arise at the step of the addition of an amino group to 4-hydroxyphenylpyruvate. Moreover, D-amino acids are likely to be non-specifically formed as side reaction products in the presence of pyridoxal phosphate-containing enzymes or of pyridoxal phosphate alone.

Dedkova et al. [192] pointed out that alteration of the peptidyltransferase center might lead to enhanced D-amino acid incorporation. Mutations in the 23S rRNA in the region of PTC and helix 89 leads to conformational change in the ribosome that alters its behavior in the protein synthesis. Modified ribosomes with mutations in regions 2447–2450 (belongs to PTC region) and 2457–2462 (belongs to helix 89 region) of *E. coli* 23S rRNA and cell-free protein synthesizing systems were prepared from mutant ribosomes. These systems were analyzed for their ability to incorporate D-Met and D-Phe into protein in vitro in terms of UAG codon suppression. A high level of suppression in the presence of D-methionine (23%) and D-phenylalanine (12%) is observed. This indicates that in ribosome, active-site structure is, at least partly, responsible for the discriminating mechanism against D-aminoacyl-$tRNA_{CUA}$s in the ribosomal A-site. Putative alterations may lead to enhanced incorporation of D-amino acid. The results indicate that the surrounding of the PTC has a major influence on the process of synthesis. This result is supported by recent computational studies where it is shown that the removal of a residue can reduce the chiral discrimination and will be discussed in the following section.

The presence of D-enantiomers only in some specific organisms and almost complete exclusion of them in the natural biosynthetic pathway of protein synthesis in today's world is now well established. This raises the question about the mechanism of chiral discrimination in different organisms. Since the racemic compound in the crystalline state is more stable than the corresponding enantiomeric form, it is questionable how the chances of racemization are avoided throughout the course of evolution in the biosynthetic pathways. The answer to the question of why the basic blocks of life are not being scrambled and retain enantiomeric purity is challenging as many biological systems incorporate D-amino acids as well as racemize in other cases as mentioned before. In the following section computation analysis of the chiral discrimination in protein biosynthesis pathway are discussed. These studies provided molecular understanding of the mechanism of chiral discrimination.

4 Retention of Chirality and Exclusion of Non-cognate Enantiomer in Protein Biosynthesis

Amino acids with natural chirality (L-amino acids) are incorporated into peptides leading to the formation of functional proteins. Several mechanisms effectively discriminate D-amino acid incorporation and racemization in this pathway. In the present section we discuss the mechanisms of chiral discrimination in aminoacylation and peptide bond formation.

4.1 Chiral Discrimination in Aminoacylation Reaction

The aaRSs are highly specific about the incorporation of the cognate enantiomer of the amino acid as mentioned before in Sect. 3. The aaRSs ensure that only cognate substrates as well as tRNA are selected from the large cellular pool of similar amino acids or other tRNAs. The frequency of misincorporation of noncognate amino acid is 1 in 10,000, which reflects a surprising accuracy of the mechanism. It is proposed earlier that there may be a succession of discriminating processes [156, 182]. It is also suggested that a number of intricate contacts between aaRS and amino acid, which are favorable for cognate but unfavorable for noncognate amino acids, makes the successful recognition and concomitant discrimination.

Most of the aaRSs contain an editing site in addition to an acylation site. These complementary pairs of sites act as a double filter to ensure that noncognate amino acids are rejected. It is proposed in the literature that the acylation site rejects amino acids larger than the correct one because there is insufficient space for them. On the other hand the smaller amino acids are cleaved by the hydrolytic editing site. However, this size or volume based mechanism is not able to discriminate the

enantiomeric species of the cognate amino acid as the D- and L-enantiomers occupy identical total volumes. Recent computational studies have shown that the discrimination of cognate and noncognate enantiomers of amino acids is controlled by a network of intermolecular interactions between aaRS and substrates (amino acid and ATP). This is discussed below.

Electronic structure based studies are carried out to understand the chiral discrimination in the first step of aminoacylation reaction in histidyl-tRNA synthetase (HisRS) (a class II aaRS). A combined quantum mechanical: semi-empirical calculation level of theory is applied to study the discrimination between L-His and D-His using a model of the corresponding active site [209]. The crystal structure of the oligomeric complex of HisRS complexed with ATP and histidinol as well as histidyl-adenylate from *E. coli* are used to model the active site. This initial study showed that the substrate amino acid (His) is located within a network of interactions within the nanospace enclosed by the active site residues. The network of interaction is perturbed when the D-amino acid is incorporated. The transition state geometry corresponding to the activation by D-His is also unfavorable due to the lack of stabilizing interactions which are present in the transition state structure corresponding to the activation by L-His [210]. Comparison of the reactant and the product geometry shows that the reacting moieties (amino acid and ATP) undergo a change in mutual separation and orientation during the course of the activation. The resulting variation in the energy is unfavorable for the D-His (as substrate) compared to L-His and this factor contributes to the chiral discrimination. The restriction of the degrees of freedom enhances the chiral discrimination. The spatial reorganization required for going to the product state for L-amino acid is effectively without any significant energy barrier. The approach of L-His to form product is favored relative to the same process for the corresponding D-amino acid. The results indicate that the incorporation of the D-form of amino acid is strongly unfavored.

Despite the limitations of the simplified model used, the above-mentioned preliminary study pointed out a few factors responsible for the chiral discrimination. First, the distance and orientational changes involved in the approach of D-amino acid towards the ATP is unfavorable within the active site leading to the high level of stereospecificity observed in aminoacylation reaction. Second, the charge distribution is important for discrimination and it is shown that the removal of the charges in the model drastically reduces the discrimination. The third factor contributing to the discrimination is the restricted nature of the mutual orientation within the cavity of the active site where the His and ATP are located during the change in orientation for the approach to form the adenylate. The restricted rotation does not allow averaging out of the differences in energy profiles of L-His, ATP and of D-His, ATP. Hence the chiral discrimination is exhibited. Fourth, the stereochemistry of D-His is such that unfavorable electrostatic interaction of the D-enantiomeric structure with the surrounding residues destabilizes the transition state relative to the L-enantiomeric case.

The chiral discrimination is studied in further detail in a subsequent study. It is pointed out in the foregoing study that a change in the distance and orientation of

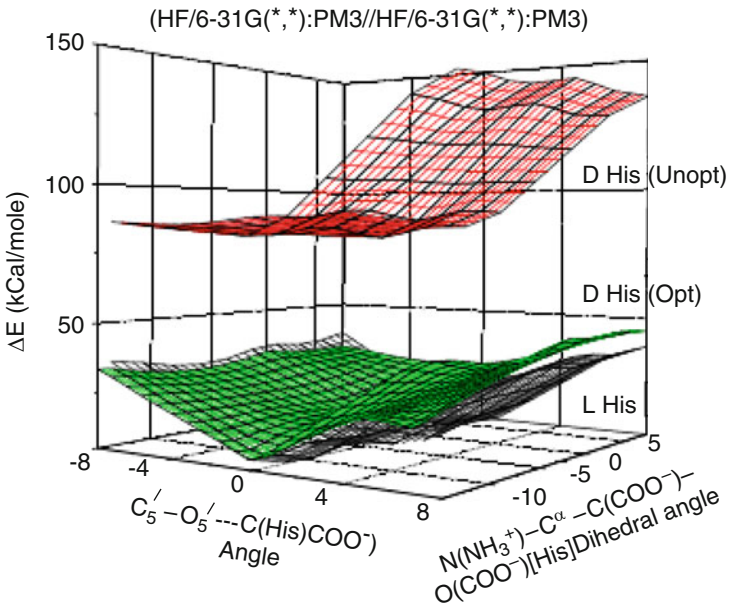

Fig. 6 Comparison of the variation of the interaction energy as a function of the orientation of the His moiety (expressed in degrees) and the orientation of the carboxylic acid group of His relative to the ATP (expressed in degrees) for optimized model of reactant containing L-His (indicated by L His), D-His (indicated by D His Unopt), that is the D-His is placed within the active site without optimization and optimized model containing D-His. The variation in the energy is computed using two level ONIOM (HF/6-31G**:PM3//HF/6-31G**:PM3) All calculations are performed by the Gaussian 03W suite of programs [211] (reprinted with permission from the American Chemical Society. © American Chemical Society)

the amino acid moiety relative to the ATP occurs during the course of the reaction. The energy variation of the mutual approach of L-His and ATP and that corresponding to D-His and ATP are shown to be strikingly different using electronic structure based theory. The variation in the interaction energy as a function of the coordinates which are changing during the progress of the reaction is shown in Fig. 6 for both L-His and D-His. The result shows that the surrounding nanospace of synthetase confines the L-His and ATP in the global minima of the plot and proximally places the reactants in geometry suitable for the in-line nucleophilic attack. The energy surface becomes highly unfavorable when the D-His is placed within the active site [indicated as D His (Unopt) in Fig. 6]. The reorganization of the surrounding nanospace can lower the unfavorable nature of the intermolecular energy surface of D-His and surrounding residues [indicated as D His (Opt) in Fig. 6]. However, such a rearrangement requires large-scale structural reorganization of the synthetase structure and is unfavorable. Notably, the rearranged geometry is still higher in energy compared to the structure containing L-His (shown in Fig. 6). This indicates that the arrangement of the active site of synthetase to allow the incorporation of D-His is ruled out by energy cost to be paid for

such misincorporation. The active site of the synthetase needs large scale structural reorganization in order to reduce the unfavorable nature of the energy profile of the model of active site including D-His. In all the cases studied, the reorganization is disruptive to the overall structure of the synthetase. This is another reason why the first step of the aminoacylation is highly specific for the enantiomeric form of His and the active site cavity of aaRS is highly specific for L-enantiomer.

The variations in the interaction energy as a function of intermolecular variables between substrates (His and ATP) and the respective surrounding residues (such as Glu83, Arg113, Arg259, and Tyr264) and concomitant effect on discrimination are also studied. The details are as follows. Variation in the interaction energy as a function of relative distance between nitrogen atom of α-amino group of His and δC of Glu83 (Å) as well as the relative distance between the chiral center of His and δC of Glu83 (Å) for L-enantiomer as well as D-enantiomer with rigid geometry is shown in Fig. 7a. Starting from the mutual arrangement of His and Glu83 (as present in the crystal structure), mutual separation is varied as present in the product state $\text{Model}_{\text{Product (L)}}$. Variation in interaction energy as a function of relative distance between the α phosphorus atom of ATP and ξC of Arg113 (Å) as well as the relative distance between the chiral center of His and ξC of Arg113 (Å) for L-His as well as D-His with rigid geometry is shown in Fig. 7b. Starting from the mutual arrangement of His or ATP and Arg113 (as present in the crystal structure), mutual separation is varied as present in the product state $\text{Model}_{\text{Product (L)}}$. The variation in interaction energy as a function of relative distance between the carbon atom of α carboxylic acid group of His and ξC of Arg259 (Å) as well as the relative distance between the chiral center of His and ξC of Arg259 (Å) for both cognate L-enantiomer and non-cognate D-enantiomer with rigid geometry is shown in Fig. 7c. Starting from the mutual arrangement of His and Arg259 as in the crystal structure, mutual separation is varied as present in the product state $\text{Model}_{\text{Product (L)}}$. Finally, variation in interaction energy as a function of relative distance between δN of His and ηO of Tyr264 (Å) as well as the relative distance between the chiral center of His and ηO of Tyr264 (Å) for L-His and D-His with rigid geometry is shown in Fig. 7d. Starting from the mutual arrangement of His and Tyr264 as in the crystal structure, mutual separation is varied as present in the product state $\text{Model}_{\text{Product (L)}}$. All computations are performed using two level ONIOM method (HF/6-31G**:PM3) with respective active site residues (Glu83, Arg113, Arg259, and Tyr264) at the HF/6-31G**.

The variations in energies in respective cases reveal the relative stability of the cognate amino acid (L-His) compared to the D-His as a function of the separation between the surrounding residues and His. The results emphasize the role of the active site residues in controlling the fidelity of the reaction. The variation of the potential energy as a function of intermolecular variables between substrate (His) and active site residues Glu83 is shown in Fig. 7a for both enantiomers.

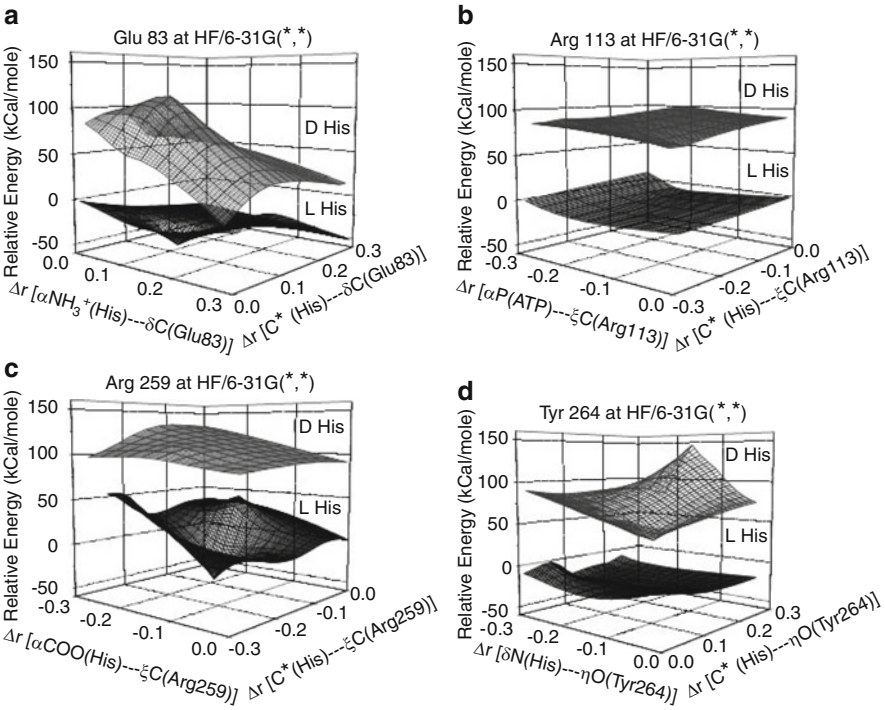

Fig. 7 The computed energy surfaces for the variations in the interaction energy as a function of intermolecular variables between substrates (L-His or D-His and ATP) and the respective surrounding residues: (**a**) Glu83, (**b**) Arg113, (**c**) Arg259, and (**d**) Tyr264. Starting from the mutual arrangement of His and the respective residues in the crystal structure, the mutual separation is varied as present in the product state $\text{Model}_{\text{Product (L)}}$ [209]. Details are given in the text. Computations are performed using two level ONIOM method (HF/6-31G**:PM3) with respective active site residues (Glu83, Arg113, Arg259, and Tyr264) at the HF/6-31G**. All calculations are performed by the Gaussian 03W suite of programs [211] (reprinted with permission from the American Chemical Society. © American Chemical Society)

The difference in energy between the two enantiomers is due to the difference in the separation of the positively charged amino group of His and the negatively charged carboxylic acid group of Glu83 in the respective cases. The unfavorable nature of the energy surface of the D-His indicates that the electrostatic interaction of Glu83 with His protects against the activation by the wrong enantiomer. Figure 7c shows the variation of interaction energy as a function of intermolecular variables between substrate (His) and active site residues Arg259 for L-His and D-His. The corresponding energy surface of the D-His is largely unfavorable due to the unfavorable electrostatic interaction of the positively charged amino group of His with positively charged guanidinium group of Arg259.

The foregoing analysis indicates that the L-His is located in a network of favorable interactions created by active site residues such as Glu83, Arg113, Arg259, and Tyr264 which is highly unfavorable for noncognate D-His. The study of the variation in the

energy during the mutual approach of the His and ATP to form adenylate shows that the surrounding nanospace of synthetase confines the L-His and ATP to proximally place the reactants in a geometry suitable for the in-line nucleophilic attack. The confinement of reacting moieties placed within the nanometer regime of an active site drives the corresponding reaction very precisely with remarkable discrimination capacity. The significantly higher energy of the energy surface of the model containing D-His is due to unfavorable interaction of D-His with surrounding residues. Interaction of L-His and the surrounding residues is more favorable than the interaction of the same residues with D-His. The foregoing result shows that the set of active site residues confine the amino acid and ATP in a potential well using intricate interaction which is selective of the (natural) L-His for adenylation.

The above-mentioned conclusions concerning the influence of the surrounding active site residues on the chiral discrimination is not limited to a particular aaRS (HisRS) or a particular species (such as *E. coli*). Computational analyses have shown that the mechanism of chiral discrimination is common in other species studied [212, 213]. Crystallographic and biochemical studies revealed that a number of active site residues are conserved in different species for a given aaRS. Comparison of the primary sequence and architecture of the active site of HisRS in three different species shows that the residues which are responsible for creating a network of important and favorable interactions with the substrate His and ATP are conserved in *E. coli*, *Thermus thermophilus*, and *Staphylococcus aureus* [212]. The relative arrangement of the conserved residues with respect to the substrate His is unchanged in three organisms. The analysis indicates that the arrangement of residues in controlling the stringent chiral discrimination is developed through evolution and retained thereafter. Essentially these active site residues and their architectonics control the mechanism of the reaction which is remarkably accurate. This accuracy is developed through evolution to make the process of protein synthesis as error-free as possible. The active site structure, so perfected, is possibly retained further till date.

Similar chiral discrimination is also expected to be observed in another aaRS belongs to class I (namely GlnRS). A negatively charged residue (Asp66) is located within the active site of GlnRS which is in close proximity to the positively charged amino group of substrate amino acid. The favorable interaction present between the active site residues Asp66 and positively charged amino group of substrate L-amino acid is lost as the spatial arrangement of the amino group is different in D-Gln. It is expected that the Asp66 of GlnRS interacts with substrate amino acid (via electrostatic interaction) and plays a similar role to Glu83 of HisRS in chiral discrimination.

Crystal structure analysis shows that organization of active site and pattern of intermolecular interaction between active site residues and substrates of all aaRSs is such that the L-enantiomer of amino acid complements the active site but not the D-enantiomer. Negatively charged residues as well as polar residues (which can act as hydrogen bond acceptor) are present in close proximity to the positively charged amino group of substrate amino acid for all aaRSs (both belong to class I and class II aaRSs) [1, 213]. These active site residues create favorable interaction with the amino group of cognate enantiomer of substrate amino acid. In summary,

crystal structure analysis indicates that active site residues of all aaRSs create a perfectly complimentary binding pocket for the cognate L-amino acids and the cavity is highly unfavorable for the non-cognate D-enantiomer. However, such a proposition is only qualitative.

Computational studies such as simulation and electronic structure based computations (ab initio) are useful in analyzing the network of electrostatic interaction within the active site of aaRS which controls the chiral discrimination. Thompson et al. investigated the preference for acylation of L-Asp over D-Asp by Aspartyl-tRNA synthetase (AspRS) using classical molecular dynamics simulations. The study points out that the influence of the network of electrostatic interaction present in aaRS protects AspRS against most binding errors. Discrimination against D-Asp can be explained by the unfavorable binding with the D-Asp. Component analysis indicates that Coulomb interactions with the protein are the major favorable factor to the L-Asp binding [145]. It is pointed out that the proofreading of Asp is difficult for AspRS as it must protect not only against D-Asp but also against an inverted orientation where the two substrate carboxylates are swapped. Discrimination against D-Asp can be explained by unfavorable binding with the inverted D-Asp binding being slightly better than D-Asp binding in the regular orientation. For both TyrRS and AspRS, a moderate binding free energy difference between the L- and D-amino acids is noted which is in agreement with their known ability to misacylate their tRNAs. It is predicted that AspRS is strongly protected against inverted L-Asp binding. The study points out that the networks of electrostatic interaction present is the major influence that protects AspRS against most binding errors.

Recent computational study shows that the stereochemistry of the oxygen atom of the carboxylic acid group of substrate amino acid participating in the first step of aminoacylation reaction is different for class I and class II aaRSs [214]. The *syn* oxygen atom with respect to the amino group of substrate amino acid participate in the reaction in case of class I aaRSs and the *anti* oxygen atom participate in the reaction for class II aaRSs. The subtle difference in the reaction mechanism is guided by the relative arrangement of the substrates in the active sites of respective aaRSs. Further the organization of the active site controls the relative arrangement of the substrates in the active site. The study shows that active site residues are not only involved in proper placement and orienting the substrates but also form a network of interaction with the substrates to facilitate the reaction. This network is highly specific for the cognate enantiomer of the substrate amino acid. Any attempt to incorporate the wrong enantiomer (such as D-amino acid) perturbs the network of interaction and is not favored. Another reason for the chiral specificity in aaRSs is noted [214]. The reduction of unfavorable electrostatic potential at the reaction center (between the attacking oxygen atom of the carboxylic acid group of substrate amino acid and αP atom of ATP) is an important prerequisite for the nucleophilic attack during the first step of aminoacylation reaction. The positively charged amino group of substrate amino acid (and the active site residues close to the reaction center) plays a major role in reducing the aforesaid unfavorable electrostatic potential. Alteration of the chirality of substrate amino acid to the D-enantiomeric structure would change the spatial arrangement of the amino group.

The resulting arrangement of groups is ineffective in reducing the potential. The incorporation of D-amino acid is thereby unfavored for a number of reasons as mentioned above.

4.2 Chiral Discrimination in Peptide Bond Formation Reaction

Out of the several partial reactions of protein biosynthesis, peptidyl transferase reaction is one of the most intensively studied. Peptidyl transferase is an aminoacyl transferase enzyme in ribosome and is essentially a ribozyme. The peptide bond formation occurs in the ribosome which is a large and complex macromolecule (approximately 2.5 MDa in bacteria) and consists of two subunits (small subunit 30S and large subunit 50S). The active site is termed as PTC. Out of the five steps in protein synthesis, the PTC performs the elongation of the protein chain after the activation of amino acid and formation of initiation complex. The mechanism of the process is described in Sect. 3. Although ribosome is made up of RNA and proteins, the PTC is essentially composed of nucleic acid with no protein present within 1.5 nm distance of active site. The active site of the large subunit of the ribosome is composed of layers of conserved nucleotides [215]. This is in contrast with the more common occurrence of the amino acid residues rather than nucleotides in the active sites of various enzymes.

It is an important question as to how chiral discrimination is carried out by PTC and how the ribosomal pathway makes the exclusion of amino acids other than the L-enantiomer. It has been mentioned before that the mechanism of retention of enantiopurity is not straightforward to understand since D-amino acid is involved in non-ribosomal peptide synthesis, post-translational modifications, and is present in bacterial cell walls and human brain. Despite the reaction being remarkably fast, the chance of incorporation of wrong (D-enantiomer, for example) amino acid is only 10^{-4} per amino acid for a 1,000 residue protein in the ribosomal pathway. It is also noted that the modification of active site structure (mutation) is necessary to enhance D-amino acid incorporation during elongation. Several experimental studies, as discussed in Sect. 3, suggested that the accuracy in chiral discrimination in ribosomal peptide synthesis is controlled by the chiral amino acid terminals, chiral sugar rings involved, and structure of the PTC including the achiral bases as discussed below.

Before we proceed to discuss the computational analysis of the chiral discrimination in peptide synthesis, it must be pointed out that various experimental results on chiral discrimination in the reaction must be interpreted with caution. The states of the reacting amino acid segments (their degrees of freedom, proximity, the mutual orientation of the amino and peptidyl terminals, and interaction with the surrounding residues) might differ from one experimental situation to the other. Different relative spatial arrangements of the reacting moieties and the proximities with neighboring residues as well as varying degrees of confinement during the reaction may give rise to variations in intermolecular interaction and the resulting discriminations are different.

For example, various results concerning the peptide bond formation reaction are obtained using different analogues in the in vitro experiments. The substrate specificity of the peptide synthesis process, especially as regards the structural nature and spatial orientation of the aminoacyl moiety, has been investigated using analogs of puromycin, aminoacylated nucleotides structurally related to the 3′ terminus of tRNA [216–219], and tRNA analogs in which the cognate amino acid was maintained in a "defined" spatial orientation [220–222]. The reason for using the mimics is that the incorporation of D-amino acid by aminoacylation (which is a prerequisite for the formation of aa-tRNA) is difficult or even impossible in many cases. As the D-amino acid could not be incorporated as a reacting terminal in the tRNA or its analogue, the synthesis of D–L peptide could not be performed in such cases. Hence, for the foregoing reasons, the experimental results concerning chiral discrimination in peptide synthesis must be judged with caution.

Few features of the reaction relevant to chiral discrimination are qualitatively understood from the experimental studies. First, the intermolecular energy profile of the reaction is expected to be orientation dependent. Consequently, chiral discrimination may not be averaged out for all possible orientational degrees of freedom as in the case of the same reaction in a solvent. Further, molecular segments involved in reaction (L-amino acid and D-sugar), being chiral, their chirality should influence the nature of the corresponding energy surface. Confinement within a nanodimension must have an influence on the discrimination exhibited by the reaction as also observed in biomimetic systems. It is pointed out in the literature that the preorganization of the active site residues and their proximity is important for effective catalysis during the progress of the reaction [223]. All of these factors have recently been explored using computational methods to discover the molecular mechanism of the discrimination and are discussed as follows.

Peptide bond formation is studied using ab initio methods for L-alanine dipeptide formation considering both concerted and stepwise mechanisms [224]. In this study, the reacting amino acids are not covalently linked to any part of a larger structure unlike that present in the CCA terminal in tRNA during peptide synthesis in PTC. The amino acid moieties are not surrounded by the active site moieties. It is unlikely that chiral discrimination will be exhibited in such a system as the reacting moieties are free to assume various mutual arrangements without being constrained as they are not covalently linked to a larger structure (RNA) and neighboring residues (composing the PTC). As a result, discrimination is not expected to be observed which is averaged out over all possible mutual orientations. However, the reacting segments in PTC in tRNA are constrained as they are covalently linked with A- and P-terminals and are located within nanometer range proximity. The A- and P-terminals are surrounded by nucleic acid residues which are also within nanoscale separation. Consequently, significant and observable chiral discrimination in the reaction within the PTC is expected to be observed due to the influence of restricted rotation, confinement, and interaction with neighboring residues. These factors are important for chiral discrimination as noted in biomimetic systems like monolayers and bilayers [2].

Orientation dependence of the interaction between substrates in the reaction is also important for chiral discrimination. During the peptide bond formation, the 3′ end of the A-site arrives at the P-site by a process of mutual rotation within the active site [225]. The discrimination in the intermolecular energy surfaces of a pair of alanine molecules in the restricted orientational state (a model of the A- and P-site terminals during their restricted rotation in PTC) is investigated [226]. Starting from the optimized structures of the nonbonded homochiral (L–L) and heterochiral (D–L) pairs of molecules, the energy surfaces are studied with rigid geometry by varying the distance and orientation. The potential energy surface is scanned with rigid geometry of the residues as a function of distance and orientation starting from the optimized geometry. The justification of such variation is that the peptide bond formation is possible only when the corresponding $-NH_2$ group of amino terminal is in the proper orientation suitable for the nucleophilic attack at the carbonyl carbon of carboxyl group. As the orientation dependence of the proximity effect of the peptide bond formation is important, the variation in energy of the L–L and D–L pair with the dihedral angle will reveal the chiral discrimination of the corresponding pairs. The resulting energy profile is expected to provide information about the energetic advantage (if any) of the approach of an L-alanine (with varying orientation and distance) to another L-alanine compared to the corresponding process where a D-alanine molecule approaches the L-alanine molecule.

The energy difference between the L–L-pair and D–L-pair at given intermolecular orientation and separation for the same value of both variables for both pairs is defined as the chiral discrimination energy and is denoted by $\Delta E_{\text{LL–DL}}$. The difference in the nature of the energy surfaces of the respective pairs can be understood from $\Delta E_{\text{LL–DL}}$ as a function of orientation. Homochiral preference is observed when $\Delta E_{\text{LL–DL}}$ is negative and when $\Delta E_{\text{LL–DL}}$ is positive a heterochiral preference is noted. The discrimination is computed for both neutral and zwitterionic states. It is ensured that the discrimination observed is not artificially generated by basis set superposition error (BSSE) [227]. The energy surfaces are calculated by MP2/6-311++G** level of theory. BSSE is further corrected at the same (MP2/6-311++G**) level using the counterpoise method. The energy profile of the naturally available achiral amino acid, glycine in the zwitterionic state, is also investigated to compare better the effect of chirality of the alanine. The orientation and distance dependence is investigated as described before for a pair of alanine molecules.

The result shows that the interaction energy of the L–L pair and the corresponding interaction energy of the D–L pair are not identical neither with the variation of the distance nor with the variation of the mutual orientation of two molecules. The potential energy surfaces of the L–L and D–L pairs are found to be dissimilar and reflect the underlying chirality of the homochiral pair and racemic nature of the heterochiral pair. The plot of the L–L pair is dissymmetric, revealing the underlying chirality of the molecules. In contrast, the plot of the D–L pair is symmetric around 180° orientation, revealing the racemic state of the neutral pair where the charge dissymmetry is also absent. Unlike the neutral case, the asymmetric charge distribution of the neighboring molecules (starting geometry) breaks the

symmetry of the energy profile of the D–L zwitterionic pair, which can be observed in the corresponding dissymmetric nature of the energy profile. The conformational energy differences between the D- or L-molecules themselves are negligibly small (the energies are identical for their optimized structures) and the observed difference in the intermolecular potential ($\Delta E_{\text{LL–DL}}$) is not due to any conformational difference. The deviation in energies for the zwitterionic case between the L–L pair and D–L pair is due to the difference in the position of the proton between the amide groups and the carboxyl groups in the respective cases.

It is pointed out that the very large difference between the energy surfaces of L–L and D–L pairs at specific orientations at same distances between the corresponding pairs is due to short range repulsive interactions. In general, the short range repulsive part of both van der Waals and electrostatic (Coulombic, dipolar, or multipolar) interaction varies more sharply than the corresponding long range attractive part of the intermolecular interaction [228, 229]. The energy profile of L–L at a given short range separation is less unfavorable than the corresponding energy profile of the D–L pair at the same intermolecular separation. However, the variations in intermolecular interaction energy are large at such short range intermolecular distance and this causes the large discrimination observed (which is the major source of the discrimination for neutral molecules). Favorable electrostatic interaction further contributes to the large homochirality of the $\Delta E_{\text{LL–DL}}$ for the zwitterionic pair in addition to the short-range steric repulsion. The BSSE corrected results show enhanced discrimination. Use of the higher-level Møller–Plesset perturbation theory (MP2) and further BSSE correction do not change the conclusions made at the Hartree–Fock (HF) level. It is seen that BSSE correction enhances the discrimination at the HF level. The $\Delta E_{\text{LL–DL}}$ is also calculated using MP2/6-311++G** theory and further corrected with BSSE using the same level of theory. The major conclusions based on HF and MP2 level calculations agree with the results from the B3LYP/6-311++G** level of density functional theory (DFT) calculations.

The chiral discrimination exhibited by a pair of alanines arises when their mutual rotatory path is orientationally restricted. Such discrimination in the intermolecular interaction is relevant to the process of peptide biosynthesis where the A- and P-terminals undergo restricted rotation during their paths of approach to carry out the reaction. It is obvious that there would be little or no energetic advantage of L–L synthesis over D–L synthesis provided the interaction energy profile for the rotational motion of the A to the P site is independent of the mutual orientation of the concerned chiral species. The chiral discrimination observed could influence the preferred L-amino acid incorporation. It is interesting to note that the maximal value *of* $\Delta E_{\text{LL–DL}}{}^{\text{Homochiral}}$ (observed homochiral preference) is larger than the maximal value of $\Delta E_{\text{LL–DL}}{}^{\text{Heterochiral}}$ in the same plot (observed heterochiral preference) for both neutral and zwitterionic pairs of alanine using both the HF and the DFT level of theoretical calculations. Short range steric overlap in the case of the D–L pair is a major reason for the preferred homochirality, which does not occur for the L–L pair. The electrostatic interaction at close separation further augments the homochirality in the case of the zwitterionic pair.

It is observed in the plot of $\Delta E_{\text{LL–DL}}$ for zwitterionic alanine pairs that the largest discrimination is not at the orientation corresponding to the optimized geometry of the respective pairs as in neutral alanine. The rise in energy due to short-range steric repulsion is highest when the hydrogen atom of the second amino group of D-alanine comes in steric hindrance with the oxygen atom of the second carboxylic group of L-alanine. This is due to the strong short-range overlap of atoms in the zwitterionic D–L pair. In the case of the L–L zwitterionic pair, on the other hand, the second carboxyl of the L-molecule and second amine of the D-molecule are at close proximity at the same relative orientation. This gives rise to the short range electrostatic attraction. Thus, the favorable electrostatic interaction contributes further to the large homochirality of the $\Delta E_{\text{LL–DL}}$ for the zwitterionic pair in addition to the short-range steric repulsion (which is the major source of the discrimination for neutral molecules).

Experimental studies indicated that the 3′ ends of the A- and P-site tRNA have to face each other in order to form the proper stereochemistry related to peptide bond formation. A process of spiral rotation of the 3′ end of the tRNA achieves this. The outcome of this spiral motion is that a P-site carbonyl carbon atom faces the A-site nucleophilic amine. This occurs without any significant conformational alterations of the 3′ end. During the A–P rotatory motion, the L–L and D–L pairs of A- and P-terminals have to pass through orientations which are different from the intermolecular mutual orientation corresponding to the optimized geometry of the pair of molecules (while the individual molecules may remain in their respective optimized geometries). This passage is easier for the L–L pair than the D–L pair. In other words, during the A–P rotatory movement, the L–L pair will pass through relatively low energy regions of the intermolecular energy surface compared to the D–L pair. The intermolecular energy surface of the L–L pair is more favourable than the corresponding energy surface of the D–L pair. The study suggests a possible way of D-amino acid exclusion. This is due to the larger degree of steric hindrance between D- and L-amino acids themselves than the L–L pair and concomitant homochiral preference. The electrostatic interaction of the homochiral pair further augments the homochirality in the case of the zwitterionic pair. The results indicate that chiral discrimination in peptide synthesis can arise, at least partly, from the interaction between amino acids themselves as a function of intermolecular separation and orientation when the two amino acids are restricted to follow a rotatory path as occurs during peptide synthesis when A- and P-terminals are covalently linked to the tRNA structure and are not allowed to assume all possible mutual orientations. The result can also be correlated with the observed discrimination noted in model systems like puromycin where the amino acids undergo restricted rotation but are not confined by surrounding residues.

The effect of surrounding the PTC on the chiral discrimination is studied in a model of PTC from crystal structure of *H. marismortui* using hybrid quantum chemical studies [227]. The crystal structure of CCA-Phe-cap-biotin bound simultaneously at half occupancy to both the A-site and P-site of the 50S ribosomal subunit [230] is used to generate the molecular segments used in the theoretical calculation. Residues located in close proximity to A- and P-terminals during rotation are as follows (all numberings corresponds to the scheme as in

H. marismortui): phenylalanine at A-terminal, phenylalanine at P-terminal, A2485, A2486, C2487, A2488, U2620, A2637, G2540, U2451, and C2452. Phenylalanine at A-terminal has either L-(natural) or D-configuration and phenylalanine at P-terminal has L-configuration in calculations.

The study shows that the interaction of the L–L pair can happen at significantly lower energy and without any steric constraint over the range of orientation. The interaction between the D–L pair is relatively unfavorable and the corresponding energy profile has two minima only at a limited range of orientations. The orientational space for the D–L pair is limited which leads to more steric clash with surrounding residues compared to the L–L pair. This is clear evidence of homochiral preference. In order to understand the origin of the observed discrimination, different surrounding residues are removed and the influence on the ease of the rotatory path is studied. Exclusion of the U2620 from the surrounding residues drastically diminishes the discrimination. This indicates that the U2620 has preferential nonbonded interaction with A- and P-terminals in the L–L form rather than the D–L form. However, homochiral preference still remains significant. Entire preferred homochirality, as observed in experiment and calculated, is not due to U2620 and the residual discrimination is non-negligible. All other residues are successively removed (A2485, A2486, C2487, A2488, A2637, G2540, U2451, and C2452) in order to identify the origin of residual discrimination and this is noted to change little from that when U2620 was removed. It may be noted that the removal of backside residues such as A2485, A2486, C2487, and A2488 gradually diminish the repulsive steric constraint but discrimination remained effectively unchanged from that observed in Fig. 8. Finally, all residues are removed and two phenylalanine groups are rotated without any surrounding residues in the same specified range of rotation. Interestingly, the discrimination is non-vanishing. Strong homochiral preference is still noted which is entirely determined by the amino acid side chains. Comparison of the relative energy gap of L–L and D–L pair plots including all surrounding residues except U2620 and the relative energy gap of L–L and D–L pair with all surrounding residues removed clearly shows that the residual discrimination (as remaining after removal of U2620) stayed the same in the specified range of orientation and is independent of other residues.

This conclusion corroborates the results of previous study based on ab initio and DFT based studies on interaction of alanine molecules where homochiral preference is noted as a function of mutual orientation [226]. The study shows quantitatively that the observed homochiral preference is due to U2620 residue as well as the amino acid side chain at the A- and P-terminals. A major part of the discrimination comes from the variation of nonbonded interaction of rotating A-terminal with U2620 during approach of the former towards the P-terminal. Significant discrimination is due to the difference in the side chain interaction of A- and P-terminals themselves during the rotatory motion even when no surrounding residues are present.

It is important to state how important is the chirality of the D-sugar in the context of the long-length scale structural organization of the PTC and, explicitly, whether

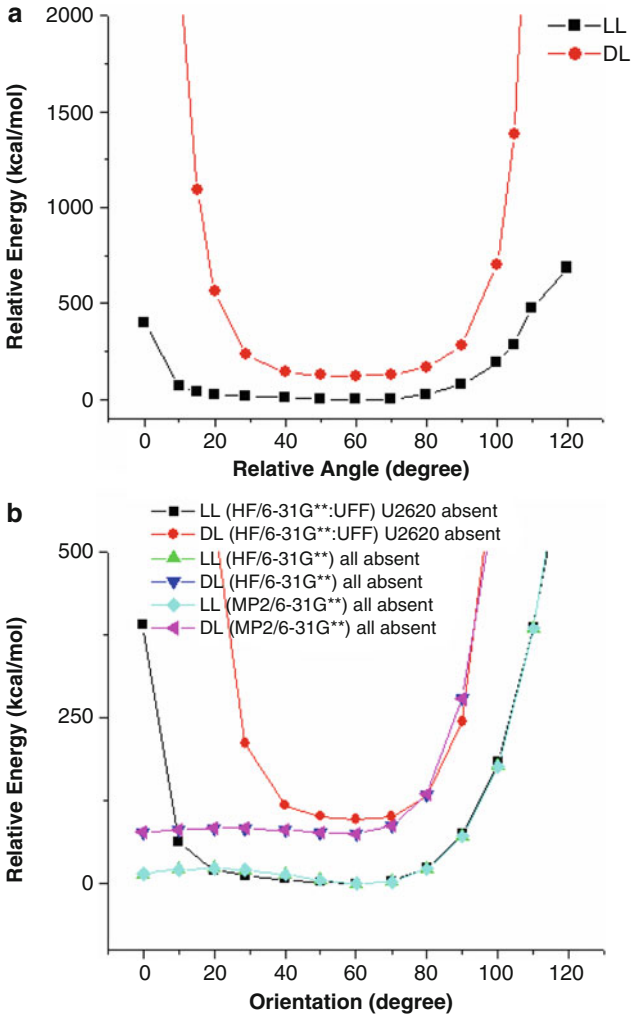

Fig. 8 (**a**) Variation in interaction energy as a function of orientation of phenylalanine at A-terminal and phenylalanine at P-terminal in presence of A2485, A2486, C2487, A2488, U2620, A2637, G2540, U2451, and C2452 residues for L–L and D–L pair combinations of two terminals [227]. Starting from the mutual arrangement of A- and P-terminals in crystal structure, the A-terminal is oriented clockwise by 60° and anticlockwise by 60° with 10° increments covering a total range of orientation of 120°. (**b**) Comparison of the relative energy gap of L–L and D–L pairs with all surrounding residues included except U2620 and the relative energy gap of L–L and D–L pairs with all surrounding residues removed [227] (reprinted with permission from the American Chemical Society. © American Chemical Society). All calculations are performed by the Gaussian 03W suite of programs [211]

the possible heteropairs and homopairs (other than the D-sugar and L-amino acid) can perform the peptide synthesis with similar efficiency in the natural biological surrounding (PTC). As the enantiomers differ only in the mutual spatial

arrangement of groups, the changes in the spatial interactions in other hetero- and homopair combinations within the PTC may be negligible for discrimination. It is questionable whether such changes in spatial orientation have any influence on the effective peptide synthesis. Several complementarities of the sugar chirality with amino acid and the surrounding bases can exist which might have a favorable contribution with the D-sugar ring to the process of chiral discrimination in the peptide synthesis. As mentioned earlier (Sect. 2 and in the present section), the molecular understanding of the origin of the chiral specificity of the sugar ring (the D-form rather than the L-form) in nucleic acid structure and its role in controlling the fidelity of the peptide synthesis is important. Experimental studies of Hecht and coworkers [184] indicated that, while the *N*-acetyl-D-phenylalanyl-$tRNA^{Phe}$ and *N*-acetyl-D-tyrosyl-$tRNA^{Phe}$ produced only small amount of dipeptide, the 2′ and 3′ deoxyadenosine analogues produced no detectable dipeptide formation.

The possibility that the discrimination in peptide synthesis might be coupled with the D-form of sugar has been investigated recently [78]. First, it is possible that the D-form of sugar ring might have favorable stereochemistry related to the structural organization of the tRNA itself. Second, the sugar ring might have the proper stereochemistry that can make the rotatory path (through which the A-site tRNA 3′-end flips into the P-site by rotating around the bond connecting the single strand 3′-end) leading to the optimal orientation for peptide bond formation easier. Third, the hydroxyl group attached to 2′ can catalytically lower the transition state barrier (related to the formation of the peptide bond) when positioned in a favorable stereochemical orientation.

Modeling studies show that the alterations in the chiral centers of the ribose sugar ring brings about large scale structural changes in the tRNA structure. Such structural modifications are unfavorable for the peptide synthesis process [78]. Model building indicates that the unnatural combinations of amino acid and sugar (L-amino acid: L-sugar, D-amino acid: D-sugar, and D-amino acid: L-sugar) are unfavorable to make proper stereochemistry to form a peptide bond within the PTC as well as creating steric hindrance. Large scale structural rearrangement is required to accommodate these unnatural pairs [78]. Exchanging the C_5' with any other atom or group leads to a change in the orientation of the phosphodiester backbone. This is energetically unfavorable. Similarly, change in the chirality at C_1' will lead to a change in the orientation of the bases and will affect the base-pairing. The results indicate that the naturally available PTC is highly specific concerning the chiralities of the amino acid and sugar ring and can accommodate only the natural heterochiral pair of sugar and amino acid without any large scale structural change in tRNA.

The influence of the ribose sugar ring on the rotatory path of the approach of the two terminals towards each other has also been studied [78]. The results show that the presence of sugar ring in both terminals makes the rotatory path more favorable compared to the case when the sugar ring is removed (Fig. 9). Since rotation of the A-terminal occurs around the 3′ bond, the rotatory process is a mutual orientational motion of the amino terminal with respect to the A-site sugar ring. As a result,

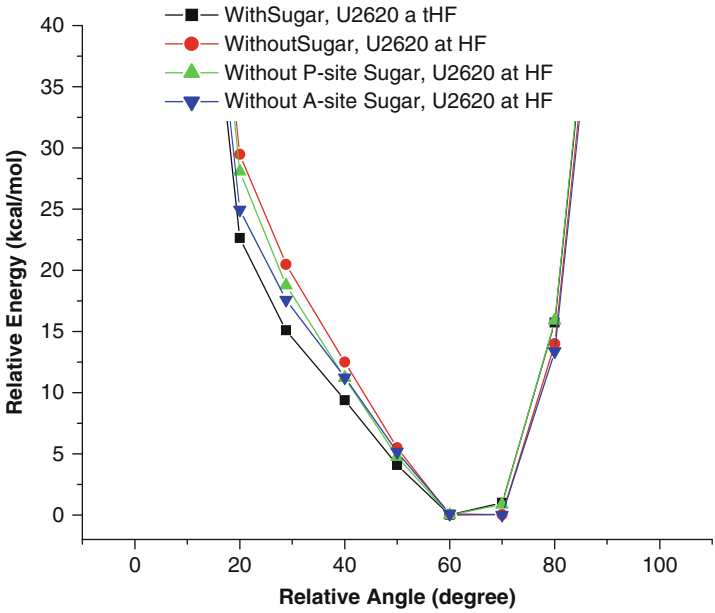

Fig. 9 The variation in interaction energy as a function of orientation of phenylalanine at A-terminal and phenylalanine at P-terminal in presence and in absence of sugars attached to A-76 attached to both terminals and within a model of the peptidyl transferase center. Starting from the mutual arrangement of A- and P-terminals in crystal structure, the A-terminal is oriented clockwise by 60° and anticlockwise by 60° with 10° increments covering a total range of orientation of 120°. The ONIOM calculation is performed at (HF/6-31G**:UFF). The phenylalanine at A-terminal, P-terminal, and U2620 is considered at QM level. The residues other than U2620 included in the model are considered at UFF level. The variation in interaction energy as a function of orientation of phenylalanine at A-terminal and phenylalanine at P-terminal in presence and in absence of sugars of only A-site and P-site, respectively (reprinted with permission from the American Chemical Society. © American Chemical Society). All calculations are performed by Gaussian 03W suite of programs [211]

removal of the A-site sugar ring raises the energy due to the loss of favorable interaction. The contribution of the P-site sugar ring in stabilizing the process is more than the A-site sugar ring. This result is consistent with the fact that as the A-site approaches the P-site, the amino group of the A-site interacts with the peptidyl terminal and sugar ring of the P-site. This contributes to the orientation dependent interaction which is lost with the removal of the ring and energy rises further. The results show that the A- and P-site sugar rings have a significant favorable influence in the rotatory path. It further indicates that the combined presence of D-sugar and L-amino acid makes the rotatory path more favorable compared to the structure in which the D-sugar is absent.

The ribose sugar ring also has another influence on the peptide bond formation process. The role of the microscopic chirality of the sugar ring and specifically that of the 2′ chiral carbon of the A76 seems important. Its catalytic role in the peptide synthesis has been studied [78]. Experimental studies indicate that the hydroxyl

group is responsible for the significantly high rate of the peptide synthesis in ribosome compared to that of an uncatalyzed one (in absence of ribosome). The catalytic mechanism of the involvement of the 2′ OH group of the sugar ring remains questionable. A role for 2′ OH in the peptide synthesis has long been suggested [231]. A comparison of the activities of 2′ deoxy derivative of AcLeuAMP and AcLeuAMP derivatives with either a second AcLeu at the 2′ OH or with a 2′ OCH_3 at the 2′ position of ribose indicates that the activity of the deoxy substrate is at least 100-fold lower than the substrates containing active 2′ hydroxyl group [232]. Substitution of the P-site tRNA A76 2′ OH with 2′ H or 2′ F resulted in a 10^6-fold decrease in peptide bond formation [233]. It is noted that the rate effect is inconsistent with the pH dependent catalytic mechanism and the role of the 2′ OH could be orienting the nucleophile, stabilizing the transition state, or inducing a favorable catalytic conformation of the PTC [234]. It is proposed that it facilitates the peptide bond formation by substrate positioning and acting as a proton shuttle between the amino group of A-site tRNA and the A76 3′ oxygen atom of the ester bond of the peptidyl tRNA. A study of modified substrates and mimics of intermediates indicates that 2′ OH can serve as a proton shuttle [233]. A proton shuttle is proposed in which the 2′ OH receives a proton from attacking amino group and simultaneously donates the proton to the neighboring 3′ OH as the transition state is decomposed into product [235].

It is proposed that the catalytic effect is due to the stable hydrogen bond network observed in the reaction. However, other catalytic pathways involving 2′ OH are possible. First, it is possible that the amino group attacks the ester carbon to yield the tetrahedral intermediate, which breaks down to deacylated tRNA and elongated peptidyl tRNA. Second, it is possible that the zwitterionic intermediate may break down through a proton shuttle via the 2′ OH of A76 in the P site in a stepwise or concerted pathway and, finally, the proton shuttle may involve water molecules that interact with 2′ and 3′ hydroxyl of A76 [236]. Recent detailed quantum mechanical calculation of the transition state also emphasized the role of the increase in the hydrogen bonding between the transition state geometry and the ribosomal components in stabilizing the transition state [237]. It is suggested that the 2′ OH group of the sugar ring remains in close interaction with the A-site amine and carbonyl group during the rotatory path leading to peptide bond formation through substrate assisted catalysis. This mechanism is different from the proton shuttle mechanism. The role of the 2′ OH group into the rate enhancement produced by ribosome based on entropic contribution is proposed [238, 239]. These studies indicate that the stereochemistry of the 2′ chiral carbon facilitates the reaction by a catalytic mechanism using the 2′ OH group despite the fact that the two mechanisms are found to be competitive.

The barrier heights of the transition states for the formation of peptide bonds and the influence of the 2′ OH group is studied for two different mechanisms (proton shuttle and anchoring mechanism) and the difference in the barrier heights is attributed to the absence of the 2′ OH group which results in removal of the chirality of the 2′ carbon of the sugar ring [78]. The transition state geometry of the reaction in the absence of the 2′ OH of the sugar ring and the respective transition state

geometry when 2′ OH is present (as in the natural form of sugar ring) are calculated from the models built from ribosomal parts of *H. marismortui* using the HF level of theory [78] and from DFT theory based on a model from the crystal structure of a 50S large ribosomal subunit from *Deinococcus radiodurans* complexed with a tRNA acceptor stem mimic. Although the theoretical methods employed and the species studied are different (*H. marismortui* and *D. radiodurans*), the results obtained show no significant differences in the mechanisms proposed in the respective cases [78]. It is noted that the reactant geometry contains a cycle of hydrogen bonds and the hydrogen bond distances are further shortened in the transition state geometry. Several of these hydrogen bonds are absent when the 2′ OH is removed. The corresponding transition state (in the absence of the 2′ OH) contains a hydrogen bond of distance 1.37 Å between the A-site α-amine hydrogen and P-site 3′ oxygen atom of the ester bond. The results indicate that all catalyzing bonds present in the transition state structure containing the P-site 2′ OH are missing in the corresponding transition state structure when the 2′ center is made achiral. While the proton shuttle and anchoring mechanisms differ substantially, both lower the transition state energy compared to the case when the chirality of the 2′ carbon is either altered or removed. This can be followed from the geometries of the corresponding transition states (where the OH group is taking part in a proton shuttle and where the OH group acts as anchor).

The results indicate that the change in the stereochemistry of the 2′ center can alter the progress of the synthesis by several orders of magnitude. The observation corroborates the experimental data that the substitution of P- site tRNA 2′ OH by 2′ H and 2′ F results in 10^6-fold reduction in the rate of peptide bond formation [233]. A comparison of the transition states in the two cases indicates that the anchoring role of the 2′ OH group is responsible for lowering the barrier height compared to the case when the 2′ OH group is removed. The result strongly suggests that the chirality of the 2′ carbon is vital for rate enhancement.

If the proper orientation of the 2′ OH and its role as an anchor in the transition state are responsible for the effective catalysis, then it is possible that the change in the orientation of the group will lead to a diminishing rate. Alteration of the stereochemistry at the 2′ center of sugar ring results in a rise of the barrier height. The results indicate that the change in the stereochemistry of the 2′ OH makes the process as unfavorable. The rate is diminished less than the case when the OH group is completely removed. This indicates that the proper positioning of the group as well as the natural chirality (with respect to the 2′ center, at least) is vital for the reaction. The stereochemical orientation of the hydroxyl group is changed when the chirality at 2′ carbon is either altered or removed. This affects the proximal geometry for the catalytic process and leads to a reduction in the rate of peptide synthesis which is consistent with the experimental studies [233].

The surrounding residues present in the PTC (which are at a distance on the nanometer scale from the D-sugar) also influence the rotatory path and the discrimination. Although the bases are achiral, their interaction with the sugar ring can be orientation dependent and can influence chiral discrimination. It is pointed out earlier that when achiral moieties have restricted orientational freedom, their interaction

profile with a chiral moiety can have orientation dependence [240]. The orientation dependence can be different for the L- and D-forms of the chiral moiety and might give rise to discrimination. The influence of various surrounding residues such as C2104, C2105, A2485, A2486, C2487, U2541, C2542, C2608, G2618, U2619, U2620, and A2637 on the rotatory path and their interaction with the sugar ring related to the A-site and P-site of the 50S ribosomal subunit of *H. marismortui* has been investigated recently [78]. The removal of the surrounding residues affect the nonbonded interaction with the amino acid: sugar heteropair of natural chirality. The removal of the U2620 diminished the discrimination, indicating that U2620 has favorable interaction with the L-terminal rather than the D-form of the terminal. The removal of U2620 affects the rotatory path to form a peptide bond. The removal produces a loss of interaction between sugar ring and U2620 for a certain range of orientation and hence the energy rises in the absence of U2620. A computational study of the effect of removal of A2486 on the rotatory path has been made [78]. The results show a loss of favorable intermolecular interaction in the range of orientation in which the rotating A-site is in proximity to the base when the latter is removed. Similar loss of intermolecular interaction is noted by removing the G2618. On the other hand, removal of C2487, U2541, C2104, C2105, A2485, C2542, C2608, U2619, A2637, and U2541 shows no significant loss of intermolecular interaction. These results indicate that while a set of surrounding residues have a favorable influence on the peptide bond formation between A- and P-terminals within PTC, a number of other residues might have less influence on the same process. However, more detailed study using higher level theory and basis set is necessary to understand the influence of the nucleotides on chiral discrimination in PTC.

The computational studies described earlier reveal that the molecular mechanism of the chiral discrimination involves the A- and P-amino acids, D-sugar ring, and surrounding bases of the PTC. Several factors are noted to be responsible for discrimination and explain the high level of stereospecificity of the process. The factors can be summarized as follows. The chiralities of the amino acids at A- and P-terminals are most important. The rotatory path for the approach of D-amino acid towards the L-terminal is unfavorable due to steric hindrance between the amino acids themselves. Their nanoscale separation is important for discrimination and at larger separation no discrimination is noted. The second factor is the restricted nature of the range of mutual orientation of the terminals during the rotatory path for the approach to form the peptide bond. This factor makes the resultant interaction profiles for L–L and D–L pairs different which is the origin of chiral discrimination. Natural chirality (D-form) of the sugar ring has favorable influence on the long length scale organization of the tRNA structure and is another factor for influencing discrimination. Alteration of the chirality of the sugar ring is unfavorable as it requires large structural rearrangements of tRNA. Favorable influence of the D-sugar ring is noted on the rotatory path for the process of approach to form the peptide bond. The removal of the sugar ring makes the rotatory path for approach to form the peptide bond unfavorable which indicates that the interactions of the D-sugar with the amino acids are more favorable than other homo- or heteropair combinations of the sugar amino acid pair. The stereochemistry of the 2′ center of the D-sugar has a

vital influence as it catalyzes the peptide bond formation by ensuring proper placement of the OH group which is involved in the catalysis. The analysis of the transition state structure revealed that the alteration and removal of chirality of the 2′ center destabilize the transition state and makes the formation of peptide bond unfavorable. Finally, the nanoscale proximity of some of the surrounding bases present in PTC with the A- and P-terminals and their restricted orientation have an influence on the discrimination. Thus, multiple factors control the discrimination in the peptide synthesis in PTC and allow accurate retention of the biological homochirality in the reaction.

5 Concluding Remarks

In the present review we first presented an introduction about biochirality and its relevance to protein biosynthesis. We discussed a few important propositions about the prebiotic origin of biomolecules with particular reference to proteins and nucleic acids. The problem of the origin of homochirality is also mentioned. There is no unequivocal hypothesis concerning these two fundamental problems. However, given that homochirality of the proteins and nucleic acids originated by any proposed hypotheses, questions remain pertaining to the mechanism of the retention of biochirality which is essential for keeping the life process ongoing. We discussed the experimental evidence which shows that it is virtually impossible to incorporate D-amino acids in protein structure via any of the two major steps of protein synthesis, particularly aminoacylation and peptide bond formation in current biosynthetic pathways. The molecular level explanations of the stringent chiral specificity in each step are extended based on computational analysis.

Computational studies on the aminoacylation reaction in aaRS indicate that an intricate network of electrostatic interaction is present in the active site of aaRS which can favorably incorporate the L-enantiomer and is highly unfavorable for the D-enantiomer. Restriction of the degrees of freedom within the active site is another reason for enhancement of chiral discrimination. The capacity to exhibit stringent chiral discrimination is critically dependent on the conserved active site residues in close proximity to the reactants, each of which performs a specific role. The various roles are catalyzing the reaction, reducing the unfavorable electrostatic charges to facilitate the reaction, and positioning of substrate in a suitable orientation for reaction. However, these roles are common in different species. Although few residues in close proximity to the reaction center play a significant catalytic role, other conserved residues also influence the nature of the transition state. Comparison of the transition state barrier heights in the presence and absence of different active site surrounding residues in the case of HisRS shows that the barrier height abruptly increases as the conserved active site residues are removed from the model. This indicates very large differences in the rates of the aminoacylation reaction in the presence and the absence of the active site residues. The results clearly indicate that the conserved active site residues (like Glu83, Arg113, Gln127,

and Arg259 in the case of HisRS) play more important roles than merely anchoring the reactants at suitable orientation in the reaction and are responsible for the stabilization of transition state as well as retention of enantiopurity. The factors responsible for the retention of enantiopurity seem to be common in all aaRSs. However, the networks of interactions protecting the incorporation of non-cognate enantiomer differ from one aaRS to the next. However, recent studies showed some commonality in the role of active site residues between the members of class I and class II aaRSs.

The factors controlling the discrimination and the high level of stereospecificity of the peptide bond formation can be summarized as follows. The chiralities of the amino acids at A- and P-terminals are most important. The rotatory path for the approach of D-amino acid towards the other terminal is unfavorable due to steric hindrance between the amino acids themselves. Their nanoscale separation is important for discrimination and at larger separation no discrimination is noted. The second factor is the restricted nature of the range of mutual orientation of the terminals during the rotatory path for the approach to form the peptide bond. This factor makes the resultant interaction profiles for L–L and D–L pairs as different exhibiting discrimination. Natural chirality (D-form) of the sugar ring has favorable influence on the long length scale organization of the tRNA structure and is another factor for influencing discrimination. Alteration of the chirality of the sugar ring is unfavorable as it requires large structural rearrangements of tRNA. Favorable influence of the D-sugar ring is noted on the rotatory path for the process of approach to form the peptide bond. The removal of the sugar ring makes the rotatory path for approach to form the peptide bond unfavorable which indicates that the interactions of the D-sugar with the amino acids are more favorable than other homo- or heteropair combinations of the sugar amino acid pair. The stereochemistry of the 2′ center of the D-sugar has a vital influence as it catalyzes the peptide bond formation by ensuring proper placement of the OH group which is involved in the catalysis. The analysis of the transition state structure revealed that the alteration and removal of chirality of the 2′ center destabilize the transition state and makes the formation of peptide bond unfavorable. Finally, the nanoscale proximity of some of the surrounding bases present in PTC with the A- and P-terminals and their restricted orientation have an influence on the discrimination. Thus, multiple factors control the discrimination in the peptide synthesis in PTC and allow accurate retention of the biological homochirality in the reaction.

At the beginning, questions are posed as to what could be the correlation between the omnipresence of chirality in naturally occurring molecules and their functionality. Enzymes are molecular machines, where stringent chiral discrimination occurs within the active site. Recent computational studies reviewed in the present chapter prove that the analyses of the molecular organization of the active site structure and of the related interactions are useful to understand the chiral specificity of enzymatic reactions.

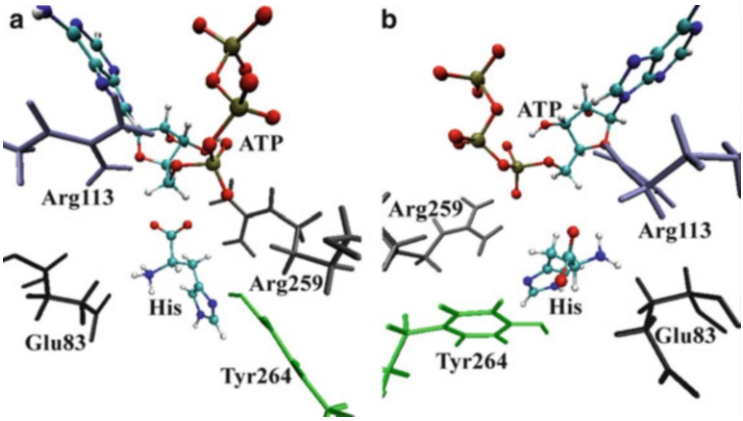

Fig. 10 The simulated structure of the active site surrounding the substrates in reactant state of (**a**) natural HisRS and (**b**) "inverted" HisRS at 500 ps of the trajectory. The substrates are (**a**) L-His and ATP containing D-sugar, and (**b**) D-His and ATP containing L-sugar. For details, see text. The simulation is carried out in NPT ensemble with a time step of 2 fs. Initially the system is minimized for 500 steps using steepest descent and conjugate gradient algorithm at the beginning of the simulation. Subsequently, the system was heated from 0 K to 300 K for 20 ps followed by equilibration at constant temperature ($T = 300$ K) and pressure ($P_{ext} = 1$ atm.) for about 500 ps under NPT conditions and the volume of the system was allowed to fluctuate during the run. The production run under NPT conditions continued at 300 K for 500 ps. The SHAKE algorithm was used to restrain the bonds linking hydrogen atoms. All constant temperature calculations used the Langevin thermostat with a collision frequency of 1.0 ps^{-1}. Calculations with pressure regulation used a relaxation time of 2.0 ps

One may wonder that, if the chiral symmetry breaking (at prebiotic era) occurred in favor of D-amino acid and L-sugar, what would have been the fate of biosynthetic pathways thus developed. The corresponding higher level structures of the biomolecules containing D-amino acids and L-sugars might have structures which are mirror symmetric to the structures composed of L-amino acids and D-sugars. A naive view is that the biochemical pathways in that case should involve the inverted structures of related biomolecules and the life processes should have progressed accordingly. In order to test such a hypothesis, the structure of HisRS (including the L-amino acid and ATP as substrate) is inverted through a mirror plane (Dutta Banik S, Nandi N, unpublished data). The substrate and amino acids of aaRS have D-configuration in the resultant structure. The sugar of the ATP has L-configuration. The structure is termed "inverted." The inverted HisRS (Fig. 10) is subjected to classical molecular dynamics simulation using the AMBER suite of programs [241]. Analysis of the simulated trajectory (over 500 ps) shows that the substrates (D-amino acids and ATP with L-sugar) in the "inverted" structure fail to have favorable and stabilizing interaction with the active site residues and hence fail to lead to the product state. Explicitly, the residues such as Glu83, Arg113, Arg259, and Tyr264 lose their interactions with the substrates (compared to the interactions present in the natural aaRS as shown in Fig. 7). The separations

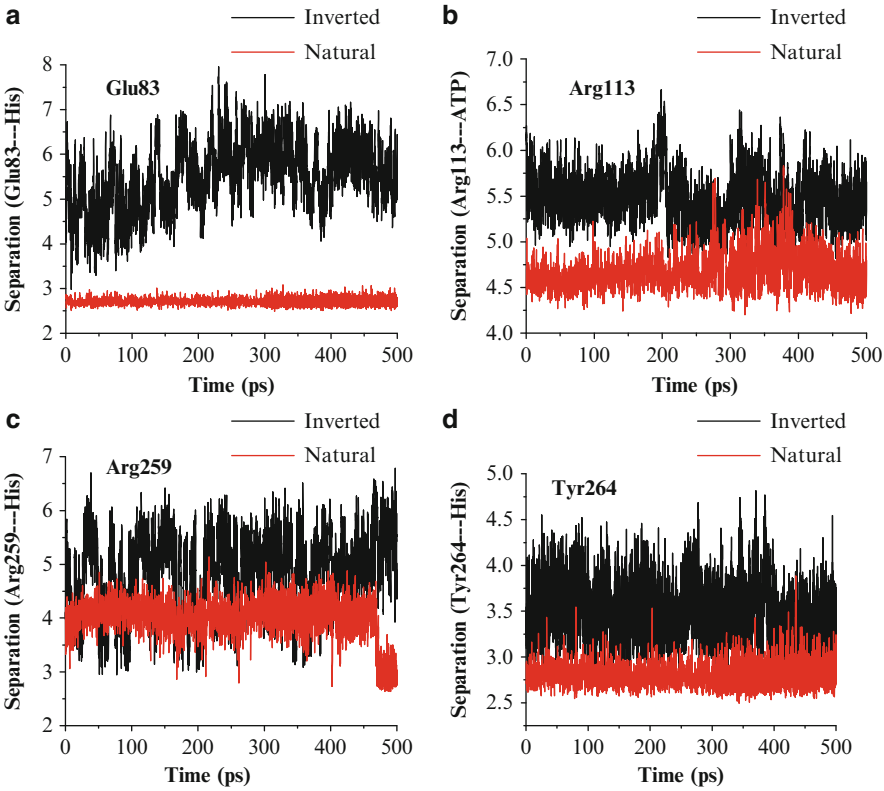

Fig. 11 The variation in separation (Å) between substrates (amino acid and ATP) and active site residues (**a**) Glu83, (**b**) Arg113, (**c**) Arg259, and (**d**) Tyr264 as a function of time (ps) for natural HisRS as well as "inverted" HisRS. The separations are larger in the inverted structure compared to the corresponding separations in natural HisRS indicating weaker interaction in the case of inverted HisRS. The larger fluctuations in the separations in the inverted structure around the average position indicate greater structural flexibility in the inverted active site. This is suggestive of diminished discrimination capacity

between the substrates and the active site residues such as Glu83, Arg113, Arg259, and Tyr264 are shown in Fig. 11 for natural and inverted HisRS. The separations are significantly larger in the inverted structure compared to the corresponding separations in natural HisRS, indicating weaker interaction in the case of inverted HisRS. In many cases the separations in the inverted structure have large fluctuation around the average position which indicates greater structural flexibility in the inverted active site and is suggestive of diminished discrimination capacity [1, 2]. The simulation study points out that the process of protein synthesis involving inverted structures (D-amino acid and L-sugars) may not progress exactly in a mirror-symmetric fashion of the current biosynthetic pathway. It will be worthwhile to compare the efficiency of the biochemical reactions relevant to protein synthesis with natural and inverted structure in more detail. A point to note is that

the structure of the protein with D-amino acids and resultant stability of the same is an open question. Limited studies are available in this direction [242]. The structural differences between the natural proteins and the proteins containing D-amino acids might pose further complicacy in understanding how life might have been progressed in an "inverted" biochemical world. Further studies are ongoing in this direction (Dutta Banik S, Nandi N, unpublished data).

Crystallographic analysis has provided a clear insight into the microscopic organization of the enzymatic structures. Electronic structure based computations and molecular dynamics studies provided complementary views about the enzymatic reactions. The wealth of information now provides a platform for analysis of the origin of the chiral preferences exhibited by various enzymes. Active sites are nanoflasks where such reactions occur and it is instructive to look into the molecular processes therein so that one can learn about the generic mechanisms used by these natural devices to utilize the cognate substrate and reject the others in a fast and accurate way. Although different enzymes and even enzymes in a given class can catalyze reactions of bewildering variety, studies so far are very promising for understanding the role of chirality in the biological reactions and for following the fundamental correlation between chirality and life. Notably, the mechanism of discrimination of one substrate from another is the key of the ability of enzymes to act as efficient biocatalysts. The efficiency of biocatalysts is hard to match by synthetic design. This surprising observation provides further impetus for the study.

The lessons learned from the active site structural features can be utilized in making the process of enzyme engineering more effective. If the principles of stereoselectivity and fidelity of the enzyme catalysis are understood then it will be possible to develop new enzymes using either minimal modification of natural enzymatic structure or developing de novo scaffolds. An understanding of the conserved structural scaffolds, particularly near the reaction center in the active site, is important in this regard. Efficient preparation of template enzymes and identification of most suitable candidates are two important steps in enzyme engineering. Preparation of the desired enzyme can be achieved either by random trial and error (a stochastic method in which the random changes of amino acids are made without caring about their position or function) or through rational design. Part of the rational design is the combination of crystal structure analysis and modeling. Various methods such as random methods, semi-rational design, or quantitative structure activity relationship studies are also applied to the design of effective enzymes. The decision to choose certain amino acids is often based on a judged guess rather than a rational decision. Analysis of the pattern of interaction between the active site residues and chiral substrates can be useful in making the tailored enzyme. Applications of computational methods in developing model enzymes with increased catalytic activity and better turnover are known [243, 244]. Considering the biotechnological activity and related utility of diverse natural products produced from organisms from all kingdoms of life, it has long been realized that pharmaceuticals can be developed by mimicking the related natural products. Interactions of chiral drugs with enzymes are important and hence the development of understanding how chiral substrates interact within an enzymatic

active site is very important. A combination of structural analysis based on crystallographic information and electronic structure based computation should be a useful tool for such future developments. Since a number of antibiotics target the ribosomal architecture [245] and these drugs often have a chiral center, it is worthwhile exploring the relationship between the chirality of the drug and enzymatic structure.

The principles learned can be extended to the tunable synthesis of useful materials. We have discussed in this review some of the issues concerning the principles behind nature's technique in retention of the chiral structure of its functional molecules and replication of these structures without allowing incorporation of non-cognate building blocks through evolution as well as the accurate performance of the corresponding life processes. Combining these principles with the technological advancements already made might lead to the possible development of new synthetic architecture with desired functionality. The basic units of known materials of technological interests such as diverse polymers, crystals, liquid crystals, and gels are rather simple in structure. Biological functional architectures are much more sophisticated. Nature has always been superior in designing the world through molecules on which the very existence of life depends. The immensely efficient and orchestrated synthesis of a vast number of biomolecules uses biophysical principles to achieve this. The confinement of biomolecules in a nanoscale dimension and their chirality seem to be utilized in biosynthetic reactions to enhance fidelity. Thus, gaining the control over the methods of confinement of chiral moieties in a nanospace has a vast potential in building up newer functional structures with the desired physico-chemical characteristics. Knowledge about the chiral discrimination in active sites has implications in building usable materials. Such principles are already known for biomimetic systems [246, 247].

With this end in view, it can be stated that understanding the role of biochirality in protein biosynthesis has tremendous importance. The origin of biomolecules and homochirality has remained an enigma and how the present day biosynthetic pathway is predominantly homochiral seems not to be answered so easily. However, one should not waver in exploring the influence of molecular chirality within the enzymatic structures where the biochemical reactions of various steps of protein synthesis occur. These studies are promising in facilitating an understanding of the principles of the organization of molecular machines such as aaRSs and ribosomes which have unmatched biosynthetic capacity.

Acknowledgements The authors thank the Department of Science and Technology for partial support of this research. One of the authors (SDB) is grateful to University of Kalyani for a research fellowship.

References

1. Nandi N (2011) Chirality in biological nanospaces: reactions in active sites. CRC/Taylor & Francis Group, New York
2. Nandi N (2009) Int Rev Phys Chem 28:111
3. Eliel EL, Wilen SH, Mander LN (1994) Stereochemistry of organic compounds. Wiley, New York
4. Jacques J, Collet A, Wilen SH (1981) Enantiomers, racemates, and resolutions. Wiley, New York
5. Flapan E (2000) When topology meets chemistry: a topological look at molecular chirality. Cambridge University Press, Cambridge
6. Pályi G, Zucchi C, Caglioti L (1999) Advances in biochirality. Elsevier Science, Oxford
7. Pályi G, Zucchi C, Caglioti L (2004) Progress in biological chirality. Elsevier Science, Oxford
8. Guerra G, Cavallo L, Corradini P (2003) Chirality of catalysts for stereospecific polymerizations. In: Green M, Nolte RJM, Meijer EW (eds) Materials chirality, vol 24 of Topics in stereochemistry series, and Denmark SE, Siegel J (series eds) Wiley Interscience/ Wiley, New York, pp 1–69
9. Rosa CD (2003) Chain conformation, crystal structures, and structural disorder in stereoregular polymers. In: Green M, Nolte RJM, Meijer EW (eds) Materials chirality, vol. 24 of Topics in stereochemistry series, and Denmark SE, Siegel J (series eds) Wiley Interscience/ Wiley, New York, pp 71–155
10. Okamoto Y, Yashima E, Yamamoto C (2003) Optically active polymers with chiral recognition ability. In: Green M, Nolte RJM, Meijer EW (eds) Materials chirality, vol 24 of Topics in stereochemistry series, Denmark SE, Siegel J (series eds) Wiley Interscience/Wiley, New York, pp 157–207
11. Fujiki M, Nakashima H, Toyoda S, Koe JR (2003) Chirality in polysilanes. In: Green M, Nolte RJM, Meijer EW (eds) Materials chirality, vol 24 of Topics in stereochemistry series, Denmark SE, Siegel J (series eds) Wiley Interscience/Wiley, New York, pp 209–279
12. Amouri H, Gruselle M (2008) Chirality in transition metal chemistry: molecules, supramolecular assemblies and materials. Wiley, Chichester
13. Capiro V, Williams MJJ (2009) Catalysis in asymmetric synthesis. Wiley, Chichester
14. Silverman RB (2004) The organic chemistry of drug design and drug action. Academic/ Elsevier, London
15. Nelson DL, Cox MM (2002) Lehninger principles of biochemistry. W.H. Freeman & Co, New York
16. Berg JM, Tymoczko JL, Stryer S (2002) Biochemistry. W.H. Freeman & Co, New York
17. Orgel LE (2004) Crit Rev Biochem Mol Biol 39:99–123
18. Gleiser M, Walker SI (2011) Plenary talk delivered at the Sao Paulo Advanced School of Astrobiology, Sao Paulo, December 2011. Int J Astrobio, arXiv:1202.5048v2 [q-bio.BM] 2 Mar 2012 (in press)
19. Miller SL (1953) Science 117:528
20. Larralde R, Robertson MP, Miller SL (1995) Proc Natl Acad Sci USA 92:8158
21. Hajdu C, Keszthelyi L (2004) Origin of biomolecules – origin of homochirality. In: Palyi G, Zucchi C, Caglioti L (eds) Progress in biological chirality. Elsevier Science, Oxford
22. Bahadur K (1954) Nature 173:1141
23. Dose K, Rajewsky B (1957) Biochim Biophys Acta 25:225
24. Hasselstrom T, Henry MC, Murr B (1957) Science 125:350
25. Paschke R, Chang RWH, Yong D (1957) Science 125:881
26. Fox SJ, Harada K (1960) J Am Chem Soc 82:3745
27. Brooks J, Shaw G (1973) Origin and development of living systems. Academic, New York
28. Kasting JM (1990) Orig Life Evol Biosph 20:199
29. Kobayashi K, Tsuchija M, Oshima T, Yanagawa H (1990) Orig Life Evol Biosph 20:99

30. Oro J (1961) Nature 190:389
31. Tielens AGGM, Charley SB (1997) Orig Life Evol Biosph 27:23
32. Ehrenfreund P, Charmley SB (2000) Annu Rev Astron Astrophys 38:427
33. Engel MH, Nagy B (1982) Nature 296:837
34. Oro J (1961) Nature 191:1193
35. Oro J, Kimball AP (1960) Biochem Biophys Res Commun 2:407
36. Oro J, Kimball AP (1961) Arch Biochem Biophys 94:217
37. Oro J, Kimball AP (1962) Arch Biochem Biophys 96:293
38. Ferris JP, Sanchez RA, Orgel LE (1968) J Mol Biol 33:693
39. Ferris JP, Zamek OS, Altbuch AM, Freiman H (1974) J Mol Evol 3:301
40. Robertson MP, Miller SL (1995) Nature 375:772
41. Robertson MP, Miller SL (1995) Nature 377:257
42. Nelson KE, Robertson MP, Levy M, Miller SL (2001) Orig Life Evol Biosph 31:221
43. Sanchez RA, Ferris JP, Orgel LE (1966) Science 154:784
44. Sanchez RA, Ferris JP, Orgel LE (1967) J Mol Biol 30:223
45. Orgel LE (2002) Orig Life Evol Biosph 32:279
46. Butlerow A (1861) Compt Rend Acad Sci 53:145
47. Mizuno T, Weiss AH (1974) Synthesis and utilization of formose sugars. In: Horton D, Tipson RW (eds) Advance in carbohydrate chemistry and biology. Academic, New York, pp 173–227
48. Avetisov VA, Goldanskii VI (1996) Phys Usp 39(8):819
49. Avetisov VA, Goldanskii VI (1996) Proc Natl Acad Sci USA 93:11435
50. Soai K, Sato I, Shibata T, Hayashi S, Matsueda Y, Inamura H, Hayashi T, Morioka H, Tabira H, Yamamoto J, Kowata Y (2003) Tetrahedron Asymmetry 14:185
51. Keszthelyi L (1995) Q Rev Biophys 28:437
52. Bonner WA (1991) Orig Life Evol Biosph 21:59
53. Rubinstein E, Bonner WA, Noyes HP, Brown GS (1983) Nature 306:118
54. Bonner WA, Rubinstein E (1987) Biosystems 20:99
55. Greenberg JM, Kouchi A, Niessen W, Irth H, van Paradijs J, de Groot M, Hermsen W (1994) J Biol Phys 20:61
56. Bonner WA, Greenberg JM, Rubinstein E (1999) Orig Life Evol Biosph 29:215
57. Kondepudi DK, Nelson GW (1984) Physica 125A:465
58. Kondepudi DK, Nelson GW (1985) Nature 314:438
59. Commeyras A, Taillades J, Collet H, Boiteau L, Vandenabeele-Trambouze O, Pascal R, Cottet H, Plasson R, Biron JP, Souaid E, Garrel L, Lagrille O, Danger D, Rossi JC, Selsis F, Dobrijevic M, Martin H (2004) Molecular origins of life: homochirality as a consequence of the dynamic co-emergence and co-evolution of peptides and chemical energetics. In: Palyi G, Zucchi C, Caglioti L (eds) Progress in biological chirality. Elsevier, Amsterdam
60. Gleiser M, Walker SI (2008) arXiv:0802.2884v1 [q-bio.BM] 20 Feb 2008
61. Joyce GF, Orgel LE (1999) Prospects for understanding the origin of the RNA world. In: Gesteland RF, Cech TR, Atkins JF (eds) The RNA world. Cold Spring Harbor Laboratory Press, Cold Spring Harbor, pp 49–77
62. Woese C (1967) The genetic code. The molecular basis for genetic expression. Harper & Row, New York
63. Crick FHC (1968) J Mol Biol 38:367
64. Orgel LE (1968) J Mol Biol 38:381
65. Benner SA, Kim H-J, Carrigan MA (2012) Acc Chem Res, DOI: 10.1021/ar200332w
66. Suga H, Hayashi G, Terasaka N (2011) Phil Trans R Soc B 366:2959
67. Yarus M, Illangasekare M (1999) Aminoacyl-tRNA synthetases and self-acylating ribozymes. In: Gesteland RF, Cech TR, Atkins JF (eds) The RNA world. Cold Spring Harbor Laboratory Press, New York, pp 183–196
68. Piccirilli JA, McConnell TS, Zaug AJ, Noller HF, Cech TR (1992) Science 256:1420
69. Delarue M, Moras D (1993) Bioessays 15:675

70. Egholm M, Buchardt O, Nielson PE, Berg RH (1992) J Am Chem Soc 114:1895
71. Egholm M, Buchardt O, Christensen L, Behrens C, Freier SM, Driver DA, Berg RH, Kim SK, Norden B, Nielson PE (1993) Nature 365:566
72. Wittung P, Nielson PE, Buchardt O, Egholm M, Norden B (1994) Nature 368:561
73. Nielsen PE (1999) Acc Chem Res 32:624
74. Eschenmoser A (1997) Orig Life 27:535
75. Pitsch S, Wendeborn S, Jaun B, Eschenmoser A (1993) Helv Chim Acta 76:2161
76. Pitsch S, Krishnamurthy R, Bolli M, Wendeborn S, Holzner A, Minton M, Lesueur C, Schlönvogt I, Jaun B, Eschenmoser A (1995) Helv Chim Acta 78:1621
77. Bailey JM (1998) FASEB J 12:503
78. Thirumoorthy K, Nandi N (2008) J Phys Chem B 112:9187
79. Nandi N, Vollhardt D (2007) Acc Chem Res 40:351
80. Nandi N, Vollhardt D (2008) Curr Opin Colloid Interface Sci 13:40
81. Noller HF (1999) On the origin of the ribosome: coevolution of subdomain of tRNA and rRNA. In: Gesteland RF et al (eds) The RNA world. Cold Spring Harbor Laboratory Press, Cold Spring Harbor, pp 197–219
82. Eriani G, Delarue M, Poch O, Gangloff J, Moras D (1990) Nature 347:203
83. Moras D (1992) Trends Biochem Sci 17:159
84. Arnez JG, Moras D (1997) Trends Biochem Sci 22:211
85. Ibba M, Söll D (2000) Annu Rev Biochem 69:617
86. Jasin M, Regan L, Schimmel P (1983) Nature 306:441
87. Eriani G, Caverelli J, Martin F, Ador L, Rees B, Thierry J-C, Gangloff J, Moras D (1995) J Mol Evol 40:499
88. Vasil'eva IA, Moor NA (2007) Biochemistry 72:247
89. Ataide SF, Ibba M (2006) ACS Chem Biol 1:285
90. Sankaranarayanan R, Moras D (2001) Acta Biochim Pol 48:323
91. Szymañski M, Deniziak M, Barciszewski J (2000) Acta Biochim Pol 47:821
92. Mucha P (2002) Acta Biochim Pol 49:1
93. Wolf YI, Aravind L, Grishin NV, Koonin EV (1999) Genome Res 9:689
94. Francklyn C, Musier-Forsyth K, Martinis SA (1997) RNA 3:954
95. Cusack S (1997) Curr Opin Struct Biol 7:881
96. Martinis SA, Plateau P, Cavarelli J, Florentz C (1999) Biochimie 81:683
97. Szymanski M, Barciszewski J (1999) Nucleic Acids Res 27:332
98. Perona JJ, Rould MA, Steitz TA (1993) Biochemistry 32:8758
99. Rath VL, Silvian LF, Beijer B, Sproat BS, Steitz TA (1998) Structure 6:439
100. Gruic-Sovulj I, Uter N, Bullock T, Perona JJ (2005) J Biol Chem 280:23978
101. Nureki O, O'Donoghue P, Watanbe N, Ohmori A, Oshikane H, Araiso Y, Sheppard K, Soll D, Ishitani R (2010) Nucleic Acids Res 38:7286
102. Deniziak M, Sauter C, Becker HD, Paulus CA, Giege R, Kern D (2007) Nucleic Acids Res 35:1421
103. Newberry KJ, Hou YM, Perona JJ (2002) EMBO J 21:2778
104. Delagoutte B, Moras D, Cavarelli J (2000) EMBO J 19:5599
105. Cavarelli J, Delagoutte B, Eriani G, Gangloff J, Moras D (1998) EMBO J 17:5438
106. Nakama T, Nureki O, Yokoyama S (2001) J Biol Chem 276:47387
107. Sekine S, Nureki O, Dubois DY, Bernier S, Chenevert R, Lapointe J, Vassylyev DG, Yokoyama S (2003) EMBO J 22:676
108. Cusack S, Yaremchuk A, Tukalo M (2000) EMBO J 19:2351
109. Yaremchuk A, Kriklivyi I, Tukalo M, Cusack S (2002) EMBO J 21:3829
110. Brick P, Bhat TN, Blow DM (1988) J Mol Biol 208:83
111. Fersht AR, Knill-Jones JW, Bedouelle H, Winter G (1988) Biochemistry 27:1581
112. Retailleau P, Huang X, Yin Y, Hu M, Weinreb V, Vachette P, Vonrhein C, Bricogne G, Roversi P, Ilyin V, Carter CW Jr (2003) J Mol Biol 325:39

113. Fukai S, Nureki O, Sekine S, Shimada A, Tao J, Vassylyev DG, Yokoyama S (2000) Cell 103:793
114. Arnez JG, Harris G, Mitschler DC, Rees B, Francklyn CS, Moras D (1995) EMBO J 14:4143
115. Arnez JG, Augstine JG, Moras D, Francklyn CS (1997) Proc Natl Acad Sci USA 94:7144
116. Åberg A, Yaremchuk A, Tukalo M, Rasmussen V, Cusack V (1997) Biochemistry 36:3084
117. Qiu X, Janson CA, Blackburn MN, Chhohan IK, Hibbs M, Abdel-Meguid SS (1999) Biochemistry 38:12296
118. Cusack S, Berthet-Colominas C, Hartlein M, Nassar N, Leberman R (1990) Nature 347:249
119. Biou V, Yaremchuk A, Tukalo M, Cusack S (1994) Science 263:1404
120. Belrhali H, Yaremchuk A, Tukalo M, Berthet-Colominas C, Rasmussen B, Bosecke P, Diat O, Cusack S (1995) Structure 3:341
121. Cavarelli J, Eriani G, Rees B, Ruff M, Boeglin M, Mitschler A, Martin F, Gangloff J, Thierry JC, Moras D (1994) EMBO J 13:327
122. Eiler S, Dock-Bregeon AC, Moulinier L, Thierry JC, Moras D (1999) EMBO J 18:6532
123. Moulinier L, Eiler S, Eriani G, Gangloff J, Thierry JC, Gabriel K, McClain WH, Moras D (2001) EMBO J 20:5290
124. Briand C, Poterszman A, Eiler S, Webster G, Thierry J-C, Moras D (2000) J Mol Biol 299:1051
125. Goldgur Y, Mosyak L, Reshetnikova L, Ankilova V, Lavrik O, Khodyreva S, Safro M (1997) Structure 5:59
126. Colominas CB, Seignovert L, Hartlein M, Grotli M, Cusack S, Leberman R (1998) EMBO J 17:2947
127. Sekine S, Nureki O, Shimada A, Vassylyev DG, Yokoyama S (2001) Nat Struct Biol 8:203
128. Arnez JG, Dock-Bregeon AC, Moras D (1999) J Mol Biol 286:1449
129. Logan DT, Mazauric MH, Kern D, Moras D (1995) EMBO J 14:4156
130. Desogus G, Todone F, Brick P, Onesti S (2000) Biochemistry 39:8418
131. Onesti S, Desogus G, Brevet A, Chen J, Plateau P, Blanquet S, Brick P (2000) Biochemistry 39:12853
132. Yaremchuk A, Tukalo M, Grøtli M, Cusack S (2001) J Mol Biol 309:989
133. Torres-Larios A, Sankaranarayanan R, Dock-Bregeon AC, Moras D (2003) J Mol Biol 331:201
134. Kamtekar S, Kennedy WD, Wang J, Stathopoulos C, Soll D, Steitz TA (2003) Proc Natl Acad Sci USA 100:1673
135. Arnez JG, Steitz TA (1996) Biochemistry 35:14725
136. Xie W, Nangle LA, Zhang W, Schimmel P, Yang XL (2007) Proc Natl Acad Sci USA 104:9976
137. Forster C, Mankowska M, Furste JP, Perbandt M, Betzel C, Erdmann VA (2008) Biochem Biophys Res Commun 368:996
138. Nameki N, Tamura K, Asahara H, Hasegawa T (1997) J Mol Biol 268:640
139. Bonnefond L, Frugier M, Touze E, Lorber B, Florentz C, Giege R, Sauter C, Thirion JR (2007) Structure 15:1505
140. Nureki O, Vassylyev DG, Tateno M, Shimada A, Nakama T, Fukai S, Konno M, Hendrickson TL, Schimmel P, Yokohama S (1998) Science 280:578
141. Lincecum TL Jr, Tukalo M, Yaremchuk A, Mursinna RS, Williams AM, Sproat BS, Eynde WVD, Link A, Calenbergh SV, Grøtli M, Martinis SA, Cusack S (2003) Mol Cell 11:951
142. Hughes SA, Tanner JA, Miller AD, Gould IA (2006) Proteins Struct Funct Bioinf 62:649
143. Arnez JG, Flanagan K, Moras D, Simonson T (1998) Proteins Struct Funct Genet 32:362
144. Archontis G, Simonson T, Moras D, Karplus M (1998) J Mol Biol 275:823
145. Thompson D, Lazennec C, Plateau P, Simonson T (2007) J Biol Chem 282:30856
146. Thompson D, Simonson T (2006) J Biol Chem 281:23792
147. Archontis G, Simonson T (2001) J Am Chem Soc 123:11047
148. Ul-Haq Z, Khan W, Zarina S, Sattar R, Moin ST (2010) J Mol Graph Model 28:401
149. Ghosh A, Vishveshwara S (2007) Proc Natl Acad Sci USA 104:15711

150. Profy AT, Usher DA (1984) J Mol Evol 20:147
151. Tamura K, Schimmel P (2006) Proc Natl Acad Sci USA 103:13750
152. Tamura K, Schimmel P (2004) Science 305:1253
153. Tamura K (2008) Biosystems 92:91
154. Soutourina J, Plateau P, Blanquet S (2000) J Biol Chem 275:32535
155. Soutourina J, Blanquet S, Plateau P (2000) J Biol Chem 275:11626
156. Yamane T, Hopfield JJ (1977) Proc Natl Acad Sci USA 74:2246
157. Bergmann FH, Berg P, Dieckmann M (1961) J Biol Chem 236:1735
158. Calendar R, Berg P (1966) Biochemistry 5:1690
159. Berg P (1956) J Biol Chem 222:1025
160. Calendar R, Berg P (1967) J Mol Biol 26:39
161. Long LL, Huang YQ (2011) J Mol Model 17:555
162. Hansia P, Ghosh A, Vishveshwara S (2009) Mol Biosyst 5:1860
163. Guth E, Connolly SH, Bovee M, Francklyn CS (2005) Biochemistry 44:3785
164. Francklyn CS, First EA, Perona JJ, Hou Y (2008) Methods 44:100
165. Guth EV, Francklyn CS (2007) Mol Cell 25:531
166. Xin Y, Li W, Donard DS, First EA (2000) J Mol Biol 303:287
167. Trezeguet V, Merle M, Gandar JC, Labouesse B (1983) FEBS Lett 157:210
168. Airas RK (2006) Biochim Biophys Acta 307:1764
169. Airas RK (2007) Biophys Chem 131:29
170. Yonath A, Leonard KR, Wittmann HG (1987) Science 236:813
171. Ban N, Nissen P, Hansen J, Moore PB, Steitz TA (2000) Science 289:905
172. Carter AP, Clemons WM Jr, Brodersen DE, Morgan-Warren RJ, Hartsch T, Wimberly BT, Ramakrishnan V (2001) Science 291:498
173. Bashan A, Agmon I, Zarivach R, Schluenzen F, Harms J, Berisio R, Bartels H, Franceschi F, Auerbach T, Hansen HAS, Kossoy E, Kessler M, Yonath A (2003) Mol Cell 11:91
174. Bashan A, Yonath A (2008) Trends Microbiol 16:326
175. Yonath A, Mussig J, Tesche B, Lorenz S, Erdmann VA, Wittmann HG (1980) Biochem Int 1:428
176. Clemons WM, Brodersen DE Jr, McCutcheon JP, May JL, Carter AP, Morgan-Warren RJ, Wimberly BT, Ramakrishnan V (2001) J Mol Biol 310:827
177. Clemons WM, May JL Jr, Wimberly BT, McCutcheon JP, Capel MS, Ramakrishnan V (1999) Nature 400:833
178. Ban N, Freeborn B, Nissen P, Penczek P, Grassucci RA, Sweet R, Frank J, Moore PB, Steitz TA (1998) Cell 93:1105
179. Weinger JS, Strobel SA (2007) Blood Cells Mol Dis 38:110
180. Davie E, Konigsberger V, Lipman F (1956) Arch Biochem Biophys 65:21
181. Yamane T, Miller L, Hopfield JJ (1981) Biochemistry 20:7059
182. Norton S, Ravel J, Lee C, Shive W (1963) J Biol Chem 238:269
183. Hopfield JJ (1974) Proc Natl Acad Sci USA 71:4135
184. Hecht SM (1992) Acc Chem Res 25:545
185. Heckler TG, Zama Y, Naka T, Hecht S (1983) J Biol Chem 258:4492
186. Roesser JR, Xu C, Payne RC, Surratt CK, Hecht S (1989) Biochemistry 28:5185
187. Heckler TG, Roesser JR, Xu C, Chang PI, Hecht S (1988) Biochemistry 27:7254
188. Bain JD, Diala ES, Glabe CG, Wacker DA, Lyttle MH, Dix TA, Chamberlin AR (1991) Biochemistry 30:5411
189. Nathans D (1964) Proc Natl Acad Sci USA 51:585
190. Nathans D, Neidle A (1963) Nature (Lond) 197:1076
191. Starck SR, Qi X, Olsen BN, Roberts RW (2003) J Am Chem Soc 125:8090
192. Dedkova LM, Fahmi NE, Golovine SY, Hecht SM (2003) J Am Chem Soc 125:6616
193. Kreil G (1997) Annu Rev Biochem 66:337
194. Marahiel MA, Stachelhaus T, Mootz HD (1997) Chem Rev 97:2651
195. von Döhren H, Keller U, Vater J, Zocher R (1997) Chem Rev 97:2675

196. Fuji N (2002) Orig Life Evol Biosph 32:103
197. Torres AM, Tsampazi M, Kennett EC, Belov K, Geraghty DP, Bansal PS, Alewood PF, Kuchel PW (2007) Amino Acids 32:63
198. Stachelhaus T, Walsh CT (2000) Biochemistry 39:5775
199. Challis GL, Naismith JH (2004) Curr Opin Struct Biol 14:748
200. Friedman M (1999) J Agric Food Chem 47:3457
201. Ohnishi E, Macleod H, Horowitz NH (1962) J Biol Chem 237:138
202. Champney WS, Jensen RA (1970) J Bacteriol 104:107
203. Cosloy SD, McFall E (1973) J Bacteriol 114:685
204. Rytka J (1975) J Bacteriol 121:562
205. Harris CL (1981) J Bacteriol 145:1031
206. Tsuruoka T, Tamura A, Miyata A, Takei T, Iwamatsu K, Inouye S, Matsuhashi M (1984) J Bacteriol 160:889
207. Caparros M, Torrecuadrada JLM, de Pedro MA (1991) Res Microbiol 142:345
208. Capparos M, Pisabarro AG, de Pedro MA (1992) J Bacteriol 174:5549
209. Dutta Banik S, Nandi N (2010) J Phys Chem B 114:2301
210. Dutta Banik S, Nandi N (2009) Colloids Surf B Biointerfaces 74:468
211. Frisch MJ et al (2004) Gaussian 03, Revision C.02. Gaussian, Inc., Wallingford
212. Dutta Banik S, Nandi N (2011) Biophys Chem 158:61
213. Dutta Banik S, Nandi N (2012) Architectonics of active sites: life processes at nanodimension. In: Ariga K (ed) Materials nanoarchitectonics. Royal Society Publication Cambridge, UK
214. Dutta Banik S, Nandi N (2012) Biomol Struct Dyn http://dx.doi.org/10.1080/07391102.2012.689701
215. Youngman EM, Brunelle JL, Kochaniak AB, Green R (2004) Cell 117:589
216. Monro RE, Marcker KA (1967) J Mol Biol 25:347
217. Monro RE, Cerna J, Marcker KA (1968) Proc Natl Acad Sci USA 61:1042
218. Bhuta A, Quiggle K, Ott TW, Ringer D, Chladek S (1981) Biochemistry 20:8
219. Quiggle K, Kumar G, Ott TW, Ryu EK, Chladek S (1981) Biochemistry 20:3480
220. Hecht SM (1977) Tetrahedron 33:1671
221. Sprinzl M, Cramer F (1979) Prog Nucleic Acid Res Mol Biol 22:1
222. Harris RJ, Pestka S (1977) In: Weissbach H, Pestka S (eds) Molecular mechanisms of protein biosynthesis. Academic, New York, pp 413–422
223. Sharma PK, Xiang Y, Kato M, Warshel A (2005) Biochemistry 44:11307
224. Thirumoorthy K, Nandi N (2007) J Mol Struct (Theo Chem) 818:107
225. Zarivach R, Bashan A, Berisio R, Harms J, Auerbach T, Schluenzen F, Bartels H, Baram D, Pyetan E, Sittner A, Amit M, Hansen HAS, Kessler M, Liebe C, Wolff A, Agmon I, Yonath A (2004) J Phys Org Chem 17:901
226. Thirumoorthy K, Nandi N (2006) J Phys Chem B 110:8840
227. Thirumoorthy K, Nandi N (2007) J Phys Chem B 111:9999
228. Israelachvili JN (1985) Intermolecular and surface forces: with applications to colloidal and biological systems. Academic, London
229. Maitland GC, Rigby M, Smith EB, Wakeham WA (1981) Intermolecular forces: their origin and determination. Clarendon, Oxford
230. Hansen JL, Schmeing MT, Moore PB, Steitz TA (2002) Proc Natl Acad Sci USA 99:11670
231. Chamberlin SI, Merino EJ, Weeks KM (2002) Proc Natl Acad Sci USA 99:14688
232. Dorner S, Polacek N, Schulmeister U, Panuschka C, Barta A (2002) Biochem Soc Trans 30:1131
233. Weinger JS, Parnell KM, Dorner S, Green R, Strobel S (2004) Nat Struct Mol Biol 11:1101
234. Rodnina MV, Beringer M, Bieling P (2005) Biochem Soc Trans 33:493
235. Trobro S, Åqvist J (2005) Proc Natl Acad Sci USA 102:12395
236. Schmeing TM, Huang KS, Kitchen DE, Strobel SA, Steitz TA (2005) Mol Cell 20:437

237. Gindulyte A, Bashan A, Agmon I, Massa L, Yonath A, Karle J (2006) Proc Natl Acad Sci USA 103:13327
238. Sievers A, Beringer M, Rodnina MV, Wolfenden R (2004) Proc Natl Acad Sci USA 101:7897
239. Schweet RS, Allen E (1958) J Biol Chem 233:1104
240. Nandi N (2004) J Phys Chem B 108:789
241. Case DA et al (2010) AMBER11. University of California, San Francisco
242. Demizu Y, Yabuki Y, Doi M, Sato Y, Tanakac M, Kuriharaa M (2012) J Pept Sci 18:466
243. Rőthlisbeger D, Khersonsky O, Wollacott AM, Jiang L, DeChancie J, Betker J, Gallaher JL, Althoff EA, Zanghellini A, Dym O, Albeck S, Houk KA, Tawfik DS, Baker D (2008) Nature 453:190
244. Jiang L, Althoff EA, Clemente FR, Doyle L, Rőthlisbeger D, Zanghellini A, Gallaher JL, Betker J, Tanaka F, Barbas CF III, Hilvert H, Houk KA, Stoddard BL, Baker D (2008) science 319:1387
245. Ramakrishnan V (2008) Biochem Soc Trans 36:567
246. Ariga K, Michinobu T, Nakanishi T, Hill JP (2008) Curr Opin Colloid Interface Sci 13:23
247. Ariga K, Nakanishi T, Hill JP (2006) Soft Matter 2:465

Top Curr Chem (2013) 333: 307–308
DOI: 10.1007/128_2012_401

Published online: 11 January 2013

Erratum to: Synthesis and Chirality of Amino Acids Under Interstellar Conditions

Chaitanya Giri, Fred Goesmann, Cornelia Meinert, Amanda C. Evans, and Uwe J. Meierhenrich

In Sect. 5.3, the second paragraph should read [. . .] Kondepudi et al. [112, 113] have established this concept within a number of autocatalytic systems to demonstrate its effectiveness (Fig. 9). The reductive Zn-mediated alkylation reported by Soai et al. in 1995 was the first truly autocatalytic asymmetric amplification, with greater than 99.5% ee observed [114]. Both Breslow [115] and Blackmond [116, 117] have reported successful enantiomeric enhancements of amino acids in the context of asymmetric amplification. One study describes an ee amplification achieved via the conversion of one enantiomer to the other under racemizing conditions [118].

C. Giri
Max Planck Institute for Solar System Research, Max-Planck-Str. 2, 37191 Katlenburg-Lindau, Germany

Institut de Chimie de Nice, University of Nice-Sophia Antipolis, UMR 7272 CNRS, 28 Avenue Valrose, 06108 Nice Cedex 2, France

F. Goesmann
Max Planck Institute for Solar System Research, Max-Planck-Str. 2, 37191 Katlenburg-Lindau, Germany

C. Meinert and U.J. Meierhenrich (✉)
Institut de Chimie de Nice, University of Nice-Sophia Antipolis, UMR 7272 CNRS, 28 Avenue Valrose, 06108 Nice Cedex 2, France
e-mail: Uwe.Meierhenrich@unice.fr

A.C. Evans
Institut de Chimie de Nice, University of Nice-Sophia Antipolis, UMR 7272 CNRS, 28 Avenue Valrose, 06108 Nice Cedex 2, France

University of Cambridge, Murray Edwards College, Cambridge CB3 0DF, UK

Top Curr Chem (2013) 333: 309–310
DOI: 10.1007/128_2012_396

Published online: 11 January 2013

Erratum to: Stochastic Mirror Symmetry Breaking: Theoretical Models and Simulation of Experiments

Celia Blanco and David Hochberg

Erratum to: Top Curr Chem
DOI: 10.1007/128_2012_362

In Sect. 2.1.3, in conformity with chemical equilibrium, the simulation leading to Fig. 2 (and for Fig. 5 in Sect. 2.2.3) is now performed with the value $k_{-1} = 5 \times 10^{-5}\ s^{-1}$. We thank Donna Blackmond for pointing this out. Section 4.2.2: the relative R:S mixtures should read 3:7 in the inset for the lower halves of Figs. 19 and 20.

The online version of the original chapter can be found under
DOI: 10.1007/128_2012_362

C. Blanco and D. Hochberg (✉)
Centro de Astrobiología (CSIC-INTA), Carretera Ajalvir Kilómetro 4, 28850 Torrejón de Ardoz, Madrid, Spain
e-mail: hochbergd@cab.inta-csic.es

Index